Double Layers
in Astrophysics

NASA

Double Layers in Astrophysics

Edited by
Alton C. Williams and Tauna W. Moorehead
NASA George C. Marshall Space Flight Center
Marshall Space Flight Center, Alabama

PREFACE

An international symposium with the theme "Double Layers in Astrophysics" was held at Marshall Space Flight Center in March 1986. The symposium was sponsored by NASA and the Universities Space Research Association (USRA). Participants from six countries came together for 3 days to discuss their latest research efforts in the experimental, theoretical, and astrophysical application aspects of double layers.

This was the third such symposium. The other two were held at Riso National Laboratory in Roskilde, Denmark, and at the University of Innsbruck in Innsbruck, Austria, in 1982 and 1984, respectively. Whereas, the first two symposia concentrated on laboratory and numerical simulation studies of double layers, this symposium placed emphasis on astrophysical application of double layers.

Most of the applications involved the magnetosphere-ionosphere plasma environment of the Earth because of its accessibility to direct observatories. However, other astrophysical applications were discussed. These included the heliospheric circuit, double radio sources, the solar prominence circuit, magnetic substorms, x-ray and gamma ray bursts, cosmic ray acceleration, x-ray pulsars, and the critical velocity phenomenon.

It is widely felt by the participants that much more work in double layer research needs to be done, especially in the theoretical aspect. A particular area of concern are the effects of physical boundaries and boundary conditions on the formation and nature of double layers.

A recommendation was made by the participants to adopt a standard symbol for the double layer when shown in an electric circuit. This is discussed in more detail in the Recommendations Section of this report.

ORGANIZING COMMITTEE

H. Alfvén
L. Lyons
T. Moore
M. Weisskopf
A. Williams

TABLE OF CONTENTS

III. SPACE APPLICATIONS

AGENDA

Monday, March 17

Chairman, A. Williams

W. Lucas	Welcome from MSFC
A. Dessler	Welcome from Space Science Laboratory
H. Alfvén	Keynote Address
	Summary of the Two Previous Symposia
J. Borovsky	Theory
N. Hershkowitz	Laboratory
T. Moore	Space Observations

Chairman, K. Wright

H. Hora	A New Hydrodynamic Analysis of Double Layers
C. Chan	Formation Mechanisms of Laboratory Double Layers
T. Carpenter	Double Layers in a Triple Plasma Device
N. Hershkowitz	Pumping Potential Wells
P. Leung	Formation of Potential Double Layers
Y. C. Saxena	Ion-Acoustic Double Layers in Laboratory Plasma

Tuesday, March 18

Chairman, T. Moore

H. L. Pécseli	Phase Space Structures in Turbulent Plasmas
R. L. Lysak	Double Layers in Magnetosphere-Ionosphere Coupling
G. Chanteur	Nonlinear Ion Hole Instability and Weak Double Layers

Chairman, J. H. Waite

N. Singh	Double Layer Formation and Dynamics
W. Lotko	Electron Acceleration in Stochastic Double Layers
R. A. Smith	Double Layers in a Model Auroral Circuit
M. K. Hudson	Weak Double Layers in the Ionospheric Plasma
B. L. Smith	Particle Simulation of Auroral Double Layers

Wednesday, March 19

Chairman, J. Horwitz

L. R. Lyons   Why Double Layers in the Earth's Auroral Regions?
W. Lennartsson   Double Layers in a Magnetic Mirror Constrained Plasma
D. S. Evans   Electric Potential Between Plasmasheet Clouds
M. Temerin   Double Layers Above the Aurora

Chairman, R. Bussard

R. Epstein   Beamed Emission from Gamma Ray Burst Sources
J. E. Borovsky   Double Layers and Extragalactic Jets
A. Williams   X-Ray Pulsars and the Critical Velocity Phenomenon
H. Alfvén   Concluding Remarks

ATTENDEES

Hannes Alfvén
Royal Institute of Technology
10044 Stockholm, Sweden

Joseph Borovsky
Mail Stop D438
Los Alamos National Lab.
Los Alamos, NM 87545

Roger W. Bussard
Space Science Lab./ES65
NASA Marshall Space Flight Center, AL 35812

Tom Carpenter
University of Iowa
Iowa City, Iowa 52242

Gérard Chanteur
CNET/CRPE
38-40 rue du General Leclerc
92131 Issy-les-Moulineaux, France

Chung Chan
ECE Dept.
Northeastern University
Boston, MA 02115

Richard H. Comfort
Physics Dept.
The University of Alabama in Huntsville
Huntsville, AL 35899

Wesley Darbro
Space Science Lab./ES65
NASA Marshall Space Flight Center, AL 35812

William Dent
Space Science Lab./ES65
NASA Marshall Space Flight Center, AL 35812

James H. Derrickson
Space Science Lab./ES62
NASA Marshall Space Flight Center, AL 35812

A. J. Dessler
Space Science Lab./ES01
NASA Marshall Space Flight Center, AL 35812

R. F. Elsner
Space Science Lab./ES65
NASA Marshall Space Flight Center, AL 35812

Richard Epstein
Los Alamos National Lab.
Mail Stop D436
Los Alamos, NM 87545

David Evans
SEL/NOAA
325 Broadway
Boulder, CO 80303

Carl-Gunne Fälthammar
Dept. of Plasma Physics
Royal Institute of Tech.
10044 Stockholm, Sweden

Gerald J. Fishman
Space Science Lab./ES62
NASA Marshall Space Flight Center, AL 35812

Heinrich Hora
553A Van Allen Hall
Iowa City, IO 52242

Noah Hershkowitz
Dept. of Nucl. Eng.
Univ. Wisconsin-Madison
1500 Johnson Dr.
Madison, WI 53706

James L. Horwitz
Dept. of Physics
The University of Alabama in Huntsville
Huntsville, AL 35899

Mary K. Hudson
Physics & Astron. Dept.
Dartmouth College
Hanover, NH 03755

Craig Kletzing
CASS C-011
UCSD
La Jolla, CA 92093

Walter Lennartsson
Lockheed Palo Alto Res. Lab.
D/91-20, B/255
3251 Hanover St.
Palo Alto, CA 94304

Philip Leung
MS144-218
Jet Propulsion Lab.
Pasadena, CA 91109

William Lotko
Thayer School of Engineering
Dartmouth College
Hanover, NH 03755

Larry Lyons
Space Sciences Lab. M2-260
The Aerospace Corp.
P.O. Box 92957
Los Angeles, CA 90009

Robert L. Lysak
School of Physics & Astronomy
University of Minnesota
Minneapolis, MN 55455

Shigeki Miyaji
Space Science Lab./ES65
NASA Marshall Space Flight Center, AL 35812

Thomas E. Moore
Space Science Lab./ES53
NASA Marshall Space Fligh Center, AL 35812

Hans L. Pécseli
Riso National Lab.
Physics Dept.
P.O. Box 49
DK-4000 Roskilde, Denmark

David L. Reasoner
Space Science Lab./ES53
NASA Marshall Space Flight Center, AL 35812

Y. C. Saxena
Physical Res. Lab.
Navrangpura
Ahmedabad 380009
India

N. Singh
CASS, UMC 3400
Utah State University
Logan, UT 84322

L. L. Smalley
Space Science Lab./ES65
NASA Marshall Space Flight Center, AL 35812

Bruce L. Smith
Princeton Plasma Physics Laboratory
Princeton, NJ 08544

Robert A. Smith
SAIC, Div. 157
1710 Goodridge Dr.
McLean, VA 22102

Nobie H. Stone
Space Science Lab./ES53
NASA Marshall Space Flight Center, AL 35812

E. A. Tandberg-Hanssen
Space Science Lab./ES01
NASA Marshall Space Flight Center, AL 35812

Michael A. Temerin
Space Sci. Lab.
Univ. of Calif.
Berkeley, CA 94720

Roy R. Torbert
D4A-RI
The University of Alabama in Huntsville
Huntsville, AL 35899

M. C. Weisskopf
Space Science Lab./ES65
NASA Marshall Space Flight Center, AL 35812

A. C. Williams
Space Science Lab./ES65
NASA Marshall Space Flight Center, AL 35812

K. H. Wright, Jr.
Dept. of Physics
The University of Alabama in Huntsville
Huntsville, AL 35899

KEYNOTE ADDRESS

H. Alfvén

Department of Plasma Physics, Royal Institute of Technology
Stockholm, Sweden
and
Department of Electrical Engineering and Computer Sciences
University of California, San Diego, California

ABSTRACT

As the rate of energy release in a double layer with voltage ΔV is $P = I\Delta V$, a double layer must be treated as part of a circuit which delivers the current I.

As neither double layer nor circuit can be derived from magnetofluid models of a plasma, such models are useless for treating energy transfer by means of double layers. They must be replaced by particle models (Lyons and Williams, 1985) and circuit theory (Alfvén, in Chapter III of *Cosmic Plasma*, 1981, hereafter referred to as CP).

A simple circuit (Fig. 1) is suggested which is applied to the energizing of auroral particles, to solar flares, and to intergalactic double radio sources. Application to the heliographic current system leads to the prediction of two double layers on the Sun's axis which may give radiations detectable from Earth.

Double layers in space should be classified as a new type of celestial object (one example is the double radio sources). It is tentatively suggested that x-ray and gamma ray bursts may be due to exploding double layers (although annihilation is an alternative energy source).

M. Azar has studied how a number of the most used textbooks in astrophysics treat important concepts like double layers, critical velocity, pinch effects and circuits. He has found that students using these textbooks remain essentially ignorant of even the existence of these, in spite of the fact that some of them have been well known for half a century [e.g., double layers (Langmuir, 1929) and pinch effect (Bennett, 1934)]. The conclusion is that astrophysics is too important to be left in the hands of the astrophysicists. The billion-dollar telescope data must be treated by scientists who are familiar with laboratory and magnetospheric physics and circuit theory, and of course with modern plasma theory. At least by volume the universe consists of more than 99 percent of plasma, and electromagnetic forces are 10^{39} times stronger than gravitation.

I. GENERAL PROPERTIES OF DOUBLE LAYERS

A. Double Layers as a Surface Phenomenon in Plasmas

Since the time of Langmuir, we know that a double layer is a plasma formation by which a plasma — in the physical meaning of this word — protects itself from the environment. It is analogous to a cell wall by which a plasma — in the biological meaning of this word — protects itself from the environment.

If an electric discharge is produced between a cathode and an anode (Fig. 2) there is a double layer, called a cathode sheath, produced near the cathode that accelerates electrons which carry a current through the plasma. A positive space charge separates the cathode sheath from the plasma. Similarly, a double layer is set up near the anode, protecting the plasma from this electrode. Again, a space charge constitutes the border between the double layer and the plasma. All these double layers carry electric currents.

The lateral limitation of the plasma is also produced by double layers which reduces and slows down the escape of the rapid electrons and accelerates the positive ions outwards so that an ambipolar diffusion is established (no net currents). If the plasma is enclosed in a vessel, its walls get a negative charge and a positive space charge is set up which, again, is the border between the double layer and the plasma. If the discharge constricts itself, the walls can be taken away (without removing the space charge they carry). In these double layers the net electric current is zero.

If the cathode itself emits electrons; e.g., if it is a thermionic or photoelectric emitter, the sign of the cathode fall may be reversed, so that the double layer is limited by a negative space charge which acts as a "virtual cathode." The anode fall may also be reversed.

The lateral double layers may also change sign. This occurs in a dusty plasma if the dust is negatively charged (e.g., by absorbing most of the electrons). In this case we have a "reversed plasma" in which the ions form the lighter component. A magnetized plasma in which the Larmor radius of the ions is smaller than that of the electrons may also be a reversed plasma.

If a plasma is inhomogeneous so that the chemical composition, density, and/or electron temperature differs in different parts of the plasma, the plasma may set up double layers which split the plasma into two or more regions, each of which become more homogeneous. For example, a Birkeland current flowing between the ionosphere and the magnetosphere may produce one or more double layers in this way when they flow through regions with different densities.

There are innumerable variations and complications of the simple case we have discussed, in the same way as biological cell walls show innumerable variations. If we try to increase the current by increasing the applied voltage, the plasma may produce a double layer (see Fig. 2) which takes up part of the voltage so that the plasma current density does not exceed a certain value. Hence, the plasma divides itself into two cells, analogous to what a biological cell does when it gets a large energy input.

The voltage difference ΔV over a double layer is usually of the order 5 to 10 times the equivalent of the temperature energy kT_e/e. However, if there are two independent plasmas produced by different sources, the double layer which is set up at the border between them may be 100 or 1000 k T_e/e or even larger (see Torvén and Andersson, 1979).

B. Noise in Double Layers

There is one property of a double layer which often is neglected: a double layer very often (perhaps always) produces noise. By this we mean irregular rapid variations within a broad band of frequencies. Lindberg (1982) studied the noise in a stationary fluctuating double layer and demonstrated what a profound influence it has. It broadens the energy spectrum of the electrons and the plasma expands perpendicular to the magnetic field. The electrons in the beam which is produced in the double layer are scattered much more by the noise than by collisions. (Some people claim that noise is essential for the formation and sustenance of a double layer. This is actually a "chicken-egg" problem.)

An analogy to this is that the "critical velocity" phenomenon also seems to be associated with noise. Noise production is often associated with strong currents through plasmas.

The noise is such an important property of plasmas that theories which do not take it into consideration run some risk of being irrelevant. It is difficult to include noise in numerical simulations of double layers, which means

that we should also regard the simulations with some scepticism. It is claimed that supercomputers are powerful enough to treat a noisy plasma. With so many prominent theoreticians present, I believe that the noise problem will be clarified.

C. Theoretical and Experimental Approaches

Since thermonuclear research started with Zeta, Tokamaks, Stellarators (not to forget the Perhapsotron!), plasma theories have absorbed a large part of the energies of the best physicists of our time. The progress that has been achieved is much less than was originally expected. The reason may be that from the point of view of the traditional theoretical physicist, a plasma looks immensely complicated. We may express this by saying that when, by an immense number of vectors and tensors and integral equations, theoreticians have prescribed what a plasma must do, the plasma — like a naughty child — refuses to obey. The reason is either that the plasma is so silly that it does not understand the sophisticated mathematics, or it is that the plasma is so clever that it finds other ways of behaving, ways which the theoreticians were not clever enough to anticipate. Perhaps the noise generation is one of the nasty tricks the plasma uses in its IQ competition with the theoretical physicists. I am confident that the prominent theoreticians and the plasma will be reconciled before the end of this meeting.

One way out of this difficulty is to ask the plasma itself to integrate the equations; in other words, to make plasma experiments. Confining ourselves to cosmic plasmas, presently there are two different ways of doing this.

1. By performing scale model experiments in the laboratory. This requires a sophisticated technique, which in part we can borrow from the thermonuclear plasma physicists. It also requires methods to "translate" laboratory results to cosmic situations (see CP, I.2; Alfvén, 1986). Great progress has been made in this respect, but much remains to be done.

2. By using space as a laboratory and performing the experiments in space. This is a fascinating new technology which is most promising, but somewhat more expensive. We shall shortly discuss the laboratory experiments in later sections. There are a number of good surveys on the program of this meeting.

D. Field and Particle Aspects of Plasmas

Space measurements of magnetic fields are relatively easy; whereas, direct measurements of electric currents are very difficult and in many cases impossible. (Roy Torbert is now developing a technique which makes direct measurements of space currents possible.) Hence, it is natural to present the results of space exploration (from spacecrafts and from astrophysical observations) with pictures of the magnetic field configuration. Furthermore, in magnetohydrodynamic theories, it is convenient to eliminate the current (i = current density) by curl B. This method is acceptable in the treatment of a number of phenomena (see Fig. 3).

However, there are also a number of phenomena which cannot be treated in this way, but which require an approach in which the electric current is taken account of explicitly. The translation between the magnetic field description and the electric current description is made with the help of Maxwell's first equation

$$\nabla \times B = \mu_0 \left(i + \frac{\partial D}{\partial t} \right)$$

3

in which the displacement current can usually be neglected. (However, it is sometimes convenient to account for the kinetic energy of a magnetized plasma by introducing the permittivity $\epsilon = \epsilon_o[1 + (c/V_{MH})^2]$, where c and V_{MH} are the velocities of light and of hydromagnetic waves (Alfvén, 1950, 3.4.4). If this formalism is used, the displacement current is often large.)

Phenomena which cannot be understood without explicitly accounting for the current are:

1. Formation of double layers.

2. Energy transfer from one region to another.

3. The occurrence of explosive events such as solar flares, magnetic substorms, possibly also "internal ionization" phenomena in comets (Wurm et al., 1963; Mendis, 1978), and stellar flares.

4. Double layer violation of the Ferraro corotation. Establishing "partial corotation" is essential for the understanding of some features of the solar system.

5. Formation of filaments in the solar atmosphere, in the ionosphere of Venus, and in the tails of comets and in interstellar nebulae.

6. Formation of current sheets which may give space a "cellular structure."

Exploration of those plasma properties which can be described by the magnetic field concept has in general been successful. However, this is not the case for those phenomena which cannot be understood by this approach.

E. Recent Advances

There is a rapidly growing literature concerning double layers and their importance for different cosmic situations. Of special interest is the work of Knorr and Goertz (1974), Block (1978), and Sato and Okuda (1980, 1981). A balanced review of these achievements is given by Smith (1983). Further, to judge from the abstracts of this present symposium, we can look forward to important new results.

As indicated by the title of the present lecture, I will concentrate my attention on the astrophysical applications of double layer theory. The development of the theory of double layers, including numerical simulation, is covered by a number of other papers.

II. LABORATORY EXPERIMENTS

A. Electrical Discharges in Gases

Toward the end of the nineteenth century electric discharges in gases began to attract increased interest. They were studied in Germany and in England; and, as there were few international conferences, the Germans and the English made the same discoveries independently. Later, a strong group in Russia was also active. The best survey of the early development is Engel-Steenbeck, *Theorie der Gasentladungen*; see also Cobine (1958). Some modern textbooks are those by Loeb (1961), Papoular (1963), and Cherrington (1974).

B. Birkeland

At the turn of the century geophysicists began to be interested in electrical discharges, because it seemed possible that the aurora was an electrical discharge. Anyone who is familiar with electrical discharges in the laboratory and observes a really beautiful aurora cannot avoid noting the similarity between the multi-colored flickering light in the sky and in the laboratory. Birkeland was the most prominant pioneer. He made his famous terrella experiment in order to investigate this possibility (Birkeland, 1908). Based on his experiments and on extensive observations of aurora in the auroral region, he proposed a current system which is basically the same as is generally accepted today. However, the theory of electric discharges was still in a very primitive state, and the importance of double layers was not obvious.

When Sydney Chapman began his investigations on magnetic storms and aurora one or two decades later, he proposed a current system [the Chapman and Vestime system (Chapman and Vestine, 1938)] which was located entirely in the ionosphere. His most important argument against Birkeland's current system was that above the atmosphere there was a vacuum, and hence there could be no electrons or ions which could carry any currents. [The relation between Chapman and Birkeland is analyzed by Dessler (1983)].

C. Langmuir and Plasma

The interest in double layers made a great leap forward when Langmuir began his investigaitons. He introduced the term "plasma" in his paper "Oscillation in Ionized Gases" (Langmuir and Tonks, 1929a; see also Langmuir and Tonks, 1929b). Curiously enough, he does not give any motivation for choosing this word, which was probably borrowed from medical terminology. He just states: "We shall use the name 'plasma' to describe this region containing balanced charges of ions and electrons." His biographers do not give any explanation either. Langmuir also made the first detailed analyses of double layers (Langmuir, 1929).

Irving Langmuir was probably the most fascinating man of the plasma pioneers. As his biographers describe him, he was far from being a narrow-minded specialist. His curiosity was all-embracing, his enthusiasm indiscriminate. He liked whatever he looked upon, and he looked everywhere. He was not far from the ideal which Roederer, in a recent paper (1985), contrasts with the insulated specialists that dominate science today (see Section VIII).

Langmuir once wrote, "Perhaps my most deeply rooted hobby is to understand the mechanism of simple and familiar phenomena..." and the phenomena might be anything from molecules to mountains. One of his friends said, "Langmuir is a regular thinking machine: put in facts and you get out a theory." And the facts his always active brain combined were anything from electrical discharges and plasmas to biological and geophysical phenomena. Science as fun was one of his cardinal tenets.

From this one gets the impression that he was very superficial. This is not correct. He got a Nobel prize in chemistry because he was recognized as the father of surface chemistry. He knew enough of biology to borrow the term plasma from this science, and the mechanism of double layers from surface chemistry. Langmuir's probes were of decisive value for the early exploration of plasmas and double layers, and they are still valuable tools.

All magnetospheric physicists must regret that as far as is known, he probably never saw a full-scale auroral display. Schenectady, where he spent most of his life, is rather far from the auroral zone, and he seems never to have traveled to the auroral zone. If he had, his passion for combining phenomena in different fields might very well have made him realize that the beautiful flickering multi-colored phenomenon in the sky was basically the same as the beautiful flickering multi-colored phenomenon he had observed so many times in his discharge tubes. At a time

when Birkeland was dead he might have saved magnetospheric physics from half a century when it was a credo that the road to magnetic storms and aurorae should go through a jungle of misleading mathematical formulae where trees and trees prevented you from seeing the woods — but you can never reconstruct history.

In 1950 I published a monograph, *Cosmical Electrodynamics* (Alfvén, 1950), in which Chapter III deals with electrical discharges in gases. Essential parts of this is devoted to plasma physics; I mention Langmuir only in passing because a quarter of a century after his breakthrough the results were considered as "classical": all experimental physicists were familiar with his works on plasmas, double layers, probes, etc. However, many theoreticians were not; they had no knowledge of Langmuir's work. They do not mention the word "plasma" and had no idea that experiments in close contact with theory had shown that plasmas were drastically different from their "ionized gases." I tried to draw the attention to this by pointing out: "What is urgently needed is not a refined mathematical treatment (referring to Chapman-Cowling) but a rough analysis of the basic phenomena" (referring to the general knowledge of plasmas).

Today, 60 years after Langmuir, most astrophysicists still have no knowledge of his work. The velocity of the spread of relevant knowledge to astrophysics seems to be much below the velocity of light (compare Section VIII).

D. The Energy Situation in Sweden and Exploding Double Layers

In Sweden the waterpower is located in the north, and the industry in the south. The transfer of power between these regions over a distance of about 1000 km was first done with a.c. When it was realized that d.c. transmission would be cheaper, mercury rectifiers were developed. It turned out that such a system normally worked well, but it happened now and then that the rectifiers produced enormous over-voltages so that fat electrical sparks filled the rectifying station and did considerabl harm. In order to get rid of this, a collaboration started between the rectifier constructors and some plasma physicists at the Royal Institute of Technology in Stockholm.

An arc rectifier must have a very low pressure of mercury vapor in order to stand the high back voltages during half of the a.c. cycle. On the other hand, it must be able to carry large currents during the other half-cycle. It turned out that these two requirements were conflicting, because at a very low pressure the plasma could not carry enough current. If the current density is too high, an exploding double layer may be formed. This means that in the plasma a region of high vacuum is produced: the plasma refuses to carry any current at all. At the sudden interruption of the 1000 km inductance produces enormous over-voltages, which may be destructive.

In order to clarify this phenomenon, a series of laboratory experiments were made, in close contact with theoretical work on the same phenomenon. Nicolai Herlofson was the leader of this activity.

At low current densities, a drift motion $v_d \ll v_T$ is superimposed on the thermal velocity v_T of the electrons in the plasma. If the current density increases so that $v_d > v_T$ the motion becomes more similar to a beam, and an instability sets in which is related to the two-beam instability. This produces a double layer which may be relatively stable (although it often is noisy and may move along the tube.) If the voltage over the tube is increased in order to increase the current, the higher voltage is taken up by the double layer and the current is not increased. However, under certain conditions the double layer may explode.

6

A simple mechanism of explosion is the following. The double layer can be considered as a double diode, limited by a slab of plasma on the cathode side and another slab on the anode side. Electrons starting from the cathode get accelerated in the diode and impinge upon the anode slab with a considerable momentum which they transfer to the plasma. Similarly, accelerated ions transfer momentum to the cathode slab. The result is that the anode and cathode plasma columns are pushed away from each other. When the distance between the electrodes in the diodes becomes larger the drop in voltage increases. This run-away phenomenon leads to an explosion.

Today the mercury arc rectifiers are long since replaced by semiconductors, but our work with them led to an interesting spin-off in cosmic physics. We had since long been interested in solar physics and had interpreted solar prominences as caused by pinching electric currents. With this as background, Jacobsen and Carlqvist (1964) suggested that the violent explosions called solar flares were produced by the same basic mechanism as made the mercury arc rectifiers explode. It drew attention to the fact that every inductive circuit carrying a current is intrinsically explosive.

Further consequences were:

1. The obvious connection between laboratory and space plasma led to a long series of plasma experiments planned to clarify cosmic phenomena.

2. It inspired Carlqvist (1969; 1982a,b,c) to work out a detailed theory of solar flares, and later to develop a theory of relativistic DL's.

3. It inspired Boström (1974) to develop a theory of magnetic substorms which, in important respects, is similar to Akasofu's theory (Akasofu, 1977).

In general, the connection between a technical difficulty and an astrophysical phenomenon led to what Roederer (1985) calls an "interdisciplinarification," which turned out to be very fruitful.

E. Extrapolation to Relativistic Double Layers

In most of the DL's in the magnetospheres and those studied so far in the laboratory, the electrons and ions have such low energies that relativistic effects are usually not very important. However, in solar flares, DL's with voltages of 10^9 V or even more may occur, and in galactic phenomena we may have voltages which are several orders of magnitude larger.

Carlqvist (1969, 1982a,c) finds that in a relativistic double layer the distribution of charges $Zn_+(x)$ and $n_-(x)$ can be divided into three regions: two density spikes near the electrodes and one intermediate region with almost constant charge density. The particles are mainly accelerated in the spikes; whereas, they move with almost constant velocity in the intermediate region. Examples are given of possible galactic DL voltage differences of 10^{12} V. This means that by a straightforward extrapolation of what we know from our cosmic neighborhood, we can derive acceleration mechanisms which brings us up in the energy region of cosmic radiation.

III. DOUBLE LAYERS AND FROZEN-IN MAGNETIC FIELD LINES

A. Frozen-In Field Lines — A Pseudo-Pedagogical Concept

In *Cosmical Electrodynamics,* I tried to give a survey of a field in which I had been active for about two decades. In one of the chapters, I treated magnetohydrodynamic waves. I pointed out that in an infinitely conductive magnetized fluid the magnetic field lines could be considered as "frozen" into the medium — under certain conditions — and this concept made it possible to treat the waves as oscillations of the frozen-in medium.

The "frozen-in" picture of magnetic field lines differs from Maxwell's views. He defined a magnetic field line as a line which everywhere is parallel to the magnetic field. If the current system which produced the field changes, the magnetic field changes and field lines can merge or reconnect. However, if the current system is constant the magnetic field is also constant. To speak of magnetic field lines moving perpendicular to the field makes no sense. They are not material.

In a detailed analysis of the motion of magnetic lines of force, Newcomb (1958) has demonstrated that "it is permissible to ascribe a velocity $\vec{v}$ to the line of force if and only if $\nabla \times (\vec{E} \times \vec{v} \times \vec{H})$ vanishes identically."

I thought that the frozen-in concept was very good from a pedagogical point of view, and indeed it became very popular. In reality, however, it was not a good pedagogical concept but a dangerous "pseudo-pedagogical concept." By pseudo-pedagogical I mean a concept which makes you believe that you understand a phenomenon whereas in reality you have drastically misunderstood it.

I never totally believed in it myself. This is evident from the chapter on "Magnetic Storms and Aurora" in the same monograph. I followed the Birkeland-Störmer general approach; but, in order to make that applicable to the motion of low-energy particles in what is now called the magnetosphere, it was necessary to introduce an approximate treatment (the "guiding-center" method) of the motion of charged particles. (As I have pointed out in *CP*, III.1, I still believe that this is a very good method for obtaining an approximate survey of many situations and that it is a pity that it is not more generally used.) The conductivity of a plasma in the magnetosphere was not relevant.

Some years later criticism by Cowling made me realize that there was a serious difficulty here. According to Spitzer's formula for conductivity, the conductivity in the magnetosphere was very high. Hence the frozen-in concept should be applicable and the magnetic field lines connecting the auroral zone with the equatorial zone should be frozen-in. At that time ($\sim$1950) we already knew enough to understand that a frozen-in treatment of the magnetosphere was absurd, but I did not understand why the frozen-in concept was not applicable. It gave me a headache for some years.

In 1963 Carl-Gunne Fälthammar and I published the second edition of *Cosmical Electrodynamics* (Alfvén and Fälthammar, 1963). He gave a much higher standard to the book and new results were introduced. One of them was that a non-isotropic plasma in a magnetic mirror field could produce a parallel electric field $E_{\parallel}$. We analyzed the consequences of this in some detail and demonstrated with a number of examples that in the presence of an $E_{\parallel}$, the frozen-in model broke down. On page 191 we wrote:

"In low density plasmas the concept of frozen-in lines of force is questionable. The concept of frozen-in lines of force may be useful in solar physics where we have to do with high- and medium-density plasma, but may be *grossly misleading if applied to the magnetosphere of the earth.* To plasma in interstellar space it should be applied with some care."

B. Magnetic Merging — A Pseudo-Science

Since then I have stressed in a large number of papers the danger of using the frozen-in concept. For example, in a paper "Electric Current Structure of the Magnetosphere" (Alfvén, 1975), I made a table showing the difference between the real plasma and "a fictitious medium" called "the pseudo-plasma," the latter having frozen-in magnetic field lines moving with the plasma. The most important criticism of the "merging" mechanism of energy transfer is due to Heikkila (1973) who with increasing strength has demonstrated that it is wrong. In spite of all this, we have witnessed at the same time an enormously voluminous formalism building up based on this obviously erroneous concept. Indeed, we have been burdened with a gigantic pseudo-science which penetrates large parts of cosmic plasma physics. The monograph *CP* treats the field-line reconnection (merging) concept in I.3, II.3, and II.5. We may conclude that anyone who uses the merging concepts states by implication that no double layers exist.

A new epoch in magnetospheric physics was inaugurated by L. Lyons and D. Williams' monograph (1985). They treat magnetospheric phenomena systematically by the particle approach and demonstrate that the fluid dynamic approach gives erroneous results. The error of the latter approach is of a basic character. Of course there can be no magnetic merging energy transfer.

I was naive enough to believe that such a pseudo-science would die by itself in the scientific community, and I concentrated my work on more pleasant problems. To my great surprise the opposite has occurred; the "merging" pseudo-science seems to be increasingly powerful. Magnetospheric physics and solar wind physics today are no doubt in a chaotic state, and a major reason for this is that some of the published papers are science and part pseudo-science, perhaps even with a majority for the latter group.

In those parts of solar physics which do not deal with the interior of the Sun and the dense photospheric region (fields where the frozen-in concept may be valid), the state is even worse. It is difficult to find theoretical papers on the low density regions which are correct. The present state of plasma astrophysics seems to be almost completely isolated from the new concepts of plasma which the in situ measurements on space plasma have made necessary (see Section VIII).

I sincerely hope that the increased interest in the study of double layers — which is fatal to this pseudo-science — will change the situation. Whenever we find a double layer (or any other $E_{\parallel} \neq 0$) we hammer a nail into the coffin of the "merging" pseudo-science.

IV. DOUBLE LAYER AS A MECHANISM FOR ENERGY RELEASE

A. Double Layer as a Circuit Element

It is a truism to state that a DL which releases a power $P = I\Delta V$ is part of a circuit in which a current I flows. We shall investigate the properties of such a circuit by starting with a conventional simple circuit and step by step adopt it to cosmical conditions.

Figure 1 depicts a simple circuit which, besides the double layer DL, contains an inductance in which is stored an energy ("circuit energy").

$$W_L = \frac{1}{2}LI^2 = \frac{1}{2\mu_o}\int B_I^2 d\tau \qquad (1)$$

where B_I is the magnetic field produced by the current I and $d\tau$ is a volume element.

If a magnetized plasma (field B_o) moves with velocity $\vec{v}$ in relation to the circuit it produces an emf

$$V = \int \vec{v} \times \vec{B}_o \cdot \vec{ds}$$

(2)

where $\vec{ds}$ is a line element in the direction of $\vec{I}$.

If $V > 0$ we have a generator transferring plasma energy $I\Delta V$ into the circuit; if $V < 0$ we have a motor transferring circuit energy into kinetic energy of the plasma. In Figure 1 we have introduced a symbol ⊖ with the arrow parallel to I to represent a generator and a similar ⊖, but with the arrow antiparallel to I, to represent a motor. Finally, the circuit may contain a resistance R which dissipates energy $1/2RI^2$ into heat, etc.

An electrotechnical circuit like Figure 1 consists essentially of metal wires. Is it realistic to use this for cosmic plasma problems? Apparently not. There are no metal wires in space. Further, if we want to use the circuit in connection with a cosmic problem, most or all the circuit elements are distributed over cosmic distances. There have been many detailed studies made concerning the relations between kinetic energy of a plasma and currents which give a deeper understanding of these processes than our circuit approach.

However, our purpose is not to study the detailed problems but to get a general survey of energy transports in cosmical physics. Is the circuit approach useful as a first approximation to such problems? Maybe.

A map of a city is useful in spite of the fact that it does not describe all the houses, or rather because it does not attempt to do so. For calculating the motion of charged particles the guiding center method is often preferable to the Störmer method even if it does not give the exact position of a particle at a certain moment, or rather because it does not.

In space, charged particles move more easily parallel to B than perpendicular, and parallel currents are often pinched to filaments. A wire is not too bad an approximation to a pinched filament. Moreover, the generators-motors as well as the double layer are often confined to relatively small volume. Hence, with all these reservations in mind we are going to apply the simple circuit of Figure 1 to a number of cosmical problems in Section VI.

However, the circuit representation could — and must — be developed in many respects. For example when a current flows in large regions, the simple inductance L should be replaced by a transmission line (see Fig. 4).

We should also observe that a theory of certain phenomena need not necessarily be expressed in the traditional language of different equations, etc. It could also be expressed as an equivalent circuit. The pioneer in the field is Boström who summarized his theory of magnetic substorms in the circuit shown in Figure 11. If this method is developed, it is quite possible that it will be recognized as the best way to represent energy transfer in cosmic plasmas.

B. Properties of the Circuit

Every circuit which contains an inductance L is intrinsically explosive (cf. Section II.D). The inductive energy $W_l = 1/2 LI_o^2$ can be tapped at any point of the circuit. If we try to interrupt the current I_o, the inductance tends to supply its energy to the point of interruption where the power $P = I\Delta V$ is delivered (ΔV = voltage over the point of interruption and I the current at this point). This means that most of the circuit energy may be released in a double layer, and if large, cause an explosion of the DL. (If the inductance is distributed over a considerable region, there are transient phenomena during which I is not necessarily the same over the whole circuit.)

In electro-technical literature in general, the resistors and inductances in the circuit may often be non-linear and sometimes distributed over larger volumes. Similarly, the DL symbol may mean one double layer but also a multiple DL. We should also allow this circuit element to represent other types of $E_{\parallel}$; for example, mirror-produced fields. Hasagawa and Uberoi (1982) have shown that under certain conditions a hydromagnetic wave produces a magnetic field-aligned electric field, which also should be included as DL. This means that DL stands for any electric field parallel to the magnetic field.

C. Local Versus Global Plasma Theories

Consider a long, homogeneously magnetized uniform plasma. It is confined laterally by tube walls or by a magnetic field. It carries no longitudinal current. Information/energy is transmitted in a time T from one end to the other by sound waves or diffusion. Phenomena with a time constant $<<$ T can be treated by local theories (because one end does not know what happens in the other). The Chapman-Cowling (1970) theory may be valid. However, if a longitudinal current I flows through the plasma and returns through an outer wire (or circuit), the situation is different. Except for rapid transients the current must be the same in the whole tube and in the wire. If the current is modulated in one end, this information is rapidly transferred to the other end and to the wire. The current may produce double layers which accelerate electrons (and ions) to kV, MV, GV, etc. It may pinch the plasma, producing filaments. These effects also produce coupling between the two ends of the plasma column and reduce the coupling to its local environment.

Electrons accelerated in a DL in the plasma column may travel very rapidly from one end of the plasma column to the other.

Hence, if there is a current through a plasma, we must use global theories, taking account of all the regions through which the current through the plasma column flows. Local theories are not valid (except in special cases).

The theoretical treatment of a current-carrying plasma must start with locating the whole region in which the current flows. It is convenient to draw the circuit and determine the resistances, the inductances, the generators, and DL's. These elements ae usually distributed and non-linear, and the circuit theory may be rather complicated.

The return current need not flow through a wire. It could very well flow through another plasma column. An example of this is the auroral current system. As pointed out in Section VI.A the energy is transferred from the cloud C to DL not by high energy particles nor by waves (and of course, not by magnetic reconnection!). It is a property of the circuit. A global theory is necessary which takes account not only of the plasma cloud in the equatorial but also of the ionosphere and double layers which may be found in the lower magnetosphere. Another still more striking example is given in Section VI.C.

V. TRANSFER OF KNOWLEDGE BETWEEN DIFFERENT PLASMA REGIONS

In *CP* it is pointed out that the basic properties of a plasma are likely to be the same in different regions of cosmic plasmas. This is represented by Figure 5, called the Cosmic Triple Jump.

The linear dimensions of plasma vary by 10^{27} in three jumps of 10^9: from the laboratory plasmas ~ 0.1 m, to magnetospheric plasmas $\sim 10^8$ m, to interstellar plasmas $\sim 10^{17}$ m, up to the Hubble distance $\sim 10^{26}$. Including laser fusion experiments, brings us up to 10^{27} orders of magnitude. New results in laboratory plasma physics and in situ

measurements by spacecraft in the magnetospheres (including the heliosphere) make sophisticated plasma diagnosis possible out to the reach of spacecraft ($\sim 10^{13}$ m). Plasmas at larger distances should to a large extent be investigated by extrapolation. This is possible because of our increased knowledge of how to translate results from one region to another.

The figure shows us an example of how cosmogony (formation of the solar system) can be studied by extrapolation from magnetospheric and laboratory results, supplemented by our knowledge about interstellar clouds. When better instruments for observing the plasma universe in x rays and gamma rays are developed, we may get more information from these than from visual observations.

Figure 6 contains essentially the same information as Figure 5. It demonstrates that plasma research has been based on highly idealized models, which did not give an acceptable model of the observed plasma. The necessary "paradigm transition" leads to theories based on experiments and observations. It started in the laboratory about 20 years ago. In situ measurements in the magnetospheres caused a similar paradigm transition there. This can be depicted as a "knowledge expansion," which so far has stopped at the reach of spacecraft. The results of laboratory and magnetospheric research should be extrapolated further out. When this knowledge is combined with direct observations of interstellar and intergalactic plasma phenomena, we can predict that a new era in astrophysics is beginning, largely based on the plasma Universe model.

VI. EXAMPLES OF COSMIC DOUBLE LAYERS

In order to demonstrate the usefulness of the equivalent circuit methods, we shall apply it here to a variety of different cosmical problems.

A. Auroral Circuit

The auroral circuit is by far the best known. It is derived from a large number of measurements in the magnetosphere and in the ionosphere which were pioneered by the Applied Physics Laboratory at Johns Hopkins.

Zmuda and Armstrong (1974) observed that the average magnetic field in the magnetosphere had superimposed on it transverse fields which they interpreted as due to hydromagnetic waves. Inspired by discussions with Fälthammer, Dessler suggested that the transverse field components instead indicated electric currents essentially parallel to the magnetic field lines (Cummings and Dessler, 1967).

This means that it was Dessler who discovered the electric currents which Birkeland had predicted. Dessler called them "Birkeland currents," a term which is now generally accepted and sometimes generalized to mean all currents parallel to the magnetic fields. I think that it is such a great achievement by Dessler to have interpreted the magnetospheric data in what we now know is the correct way that the currents should be called Birkeland-Dessler currents.

In the auroral current system the central body (Earth and ionosphere) maintains a dipole field (Fig. 7). B_1 and B_2 are magnetic field lines from the body. C is a plasma cloud near the equatorial plane moving in the sunward direction (out of the figure) producing an electromotive force

$$V = \int_{C_1}^{C_2} (\vec{v} \times \vec{B}) \cdot \vec{ds}$$

12

which gives rise to a current in the circuit C_1, a_1, a_2, C_2 and C_1. The circuit may contain a double layer DL with the voltage ΔV, in which the current releases energy at the rate $P = I\Delta V$ which essentially is used for accelerating auroral electrons. The energy is transferred from C to DL not by high energy particles or waves (and, of course, not by magnetic merging or field reconnection). It is a property of the electric circuit (and can also be described by the Poynting vector, see Fig. 7).

B. Heliospheric Current

In a way which is described in *CP*, II.4.2, we go from the auroral circuit to the heliospheric circuit (Fig. 8).

The Sun acts as a unipolar inductor (A) producing a current which during odd solar cycles goes outward along the axes (B_2) in both directions and inward in the equatorial plane B_1. The current closes at large distances (B_3), but we do not know where. The equatorial current layer is often very inhomogeneous. Further, it moves up and down like the skirt of a ballerina. In even solar cycles the direction of the current is reversed.

By analogy with the magnetospheric circuit we may expect the heliospheric circuit to have double layers. They should be located at the axis of symmetry, but only in those solar cycles when the axial current is directed away from the Sun.

No one has yet tried to predict how far from the Sun they should be located. They should produce high energy electrons directed toward the Sun, and synchrotron radiation from these should make them observable as radio sources. Further, they should produce noise. They may be observable from the ground, but so far no one has cared to look for such objects.

C. Double Radio Sources

If in the heliospheric circuit we replace the rotating magnetized Sun by a galaxy, which is also magnetized and rotating, we should expect a similar current system, but magnified by about 9 orders of magnitude (Fig. 9, *CP*, II.4). This seems to be a very large extrapolation, but in fact a number of successful extrapolations from the laboratory to the magnetosphere are by almost the same ratio. (Of course all theories of plasma phenomena in regions which cannot be investigated by in situ measurements are by definition speculative!)

The emf is given by equation (2), taken from the galactic center out to a distance where the current leaves the galaxy, which may be the outer edge. Inside the galaxy the current may flow in the plane of symmetry similar to the current sheet in the equatorial plane of the Sun, but whether the intragalactic picture is correct or not is not really important to our discussion here. The emf which derives from the galactic rotation is applied to two circuits in parallel, one to the "north" and one to the "south" (see Fig. 9). As galaxies in general are highly north-south symmetric, it is reasonable that the two circuits are similar. Hence, we expect a high degree of symmetry in the current system (at least under idealized conditions).

In the magnetosphere, the current flowing out from the ionosphere produces double layers (or magnetic mirror induced fields) at some distance from the Earth. Because of the similarity of the plasma configuration, we may expect double layers at the axis of a galaxy and a large release of energy in them. It has been suggested that the occurrence of such double layers is the basic phenomenon producing the double radio sources.

In the galactic circuit, the emf is produced by the rotating magnetized galaxy acting as a homopolar inductor, which implies that the energy is drained from the galactic rotation, but from the interstellar medium, not from the stars. By the same mechanisms as in the auroral circuit, it is transferred first into circuit energy and then to the

double layers where the power $P = I\Delta V$ is released. In a single DL or a series of DL's on each side of the galaxy, an acceleration of charged particles takes place. From the magnetosphere, we know that layers are produced when the current flows outward. (Whether double layers can be formed when the current flows inward is still an open question.) If the same is true in the galactic case, there is a flow of thermal electrons to the layer from the outside and when passing a series of double layers, the electrons are accelerated to very high energies. Hence, a beam of very high energy electrons is emitted from the double layer along the axis toward the central galaxy. This process is the same as the one which produces auroral electrons, only scaled up enormously both in size and energy. In analogy with the current in the magnetotail, the current in the equatorial plane of a galaxy may also produce double layers, which may be associated with large releases of energy.

Figure 9 shows a radio astronomy picture of a double radio source. It is essential in our model that the emf of the galaxy has such a direction that the axial currents flow outward. The DL's they produce should be located at the outer edges of the strong radio source. When electrons conducting the currents outside the double layer reach the double layer, they are accelerated to very high energies. Similarly, ions reaching the double layer on their outward motion from the central galaxy will be accelerated outward when passing the double layers. The strong axial current produces a magnetic field, which pinches the plasma, confining it to a cylinder close to the axis.

Although the electrons are primarily accelerated in the direction of the magnetic field, they will be scattered by magnetic inhomogeneities and spiral in such a way that they emit synchrotron radiation. The accelerated electrons will be more like an extremely hot gas than a beam. With increasing distance from the double layer the electrons will spread and their energy, and hence their synchrotron emission, will decrease. This is in agreement with observations. It is possible that some of them will reach the central galaxy and produce radio emission there. It is also possible that the observed radio emission from the central galaxy is due to some other effect produced by the current (there are several mechanisms possible). Such phenomena in the central galaxy will not be discussed here.

The ions passing the double layer in the outward directionn will be accelerated to the same energy as the electrons. Because of their larger rest mass, they will not emit much synchrotron radiation, but there are a number of other mechanisms by which they may produce the observed radio emission from the regions farther away from the central galaxy.

It should be stressed again that, just as in the magnetosphere and in the laboratory, the energy released in the double layer derives from circuit energy and is transferred to it by electric currents which essentially consist of relatively low-energy particles. There is no need for a beam of high energy particles to be shot out from the central galaxy (or plasmons). On the contrary, the central galaxy may be bombarded by high energy electrons which have obtained their energy from the double layer.

A quantitative analysis of the double radio galaxies is given in CP. It is possible that some modifications are needed.

D. Solar Prominence Circuit. Solar Flares

The circuit consists of a magnetic flux tube above the photosphere and part of photosphere (see Fig. 10). The generator is in the photosphere and is due to a whirl motion in sunspot magnetic field.

Generator output increases circuit energy which can be dissipated in two different ways: (1) When current density surpasses critical value, an exploding DL is produced in which most of the circuit energy is released. This causes a solar flare. Hénoux (1985) has recently given an interesting study of solar flares and concludes that a current disruption by DL's is an appealing explanation of solar flares. (2) Under certain circumstances the electromagnetic pressure of the current loop may produce a motor which gives rise to a rising prominence (Alfvén and Carlqvist, 1967; Carlqvist, 1982b).

14

E. Magnetic Substorms

According to Boström (1974) and Akasofu (1977), an explosion of the transverse current in the magnetotail gives an attractive mechanism for the production of magnetic substorms (see Fig. 11). Boström has shown that an equivalent magnetic substorm circuit is a way of presenting the substorm model. The onset of a substorm is due to the formation of a double layer, which interrupts the cross-tail current so that it is redirected to the ionosphere.

F. Currents and Double Layers in Interstellar Space

As it is relatively easy to measure magnetic fields, it is natural that the first description of the electromagnetic state of interstellar and intergalactic space is based on a magnetic field description. However, as no one claims — at least not explicitly — that the magnetic fields are curl-free, we must have a network of currents. As investigations of DL's (and quite a few other phenomena) require explicit pictures of electric currents, it is essential to apply these pictures.

Filamentary structures were quite generally observed long ago, and may be observed everywhere where sufficient accurate observations can be made. There are a number of processes by which they are generated. For example, the heliospheric current system must close at large distances (cf. Fig. 8), and it is possible — perhaps likely — that this is done by a network of filamentary currents. Many such filaments may produce DL's, and some of these may explode.

G. Double Layers as a New Class of Celestial Objects

The general structure and evolution of such a network of currents, including their production of DL's, has not yet been investigated. It is possible that under certain circumstances the final destiny of a set of currents is DL's, perhaps exploding DL's. DL's may be considered as a new class of celestial objects. We have already given an example of this in the interpretation of double radio sources as DL's.

H. X-Ray and Gamma Ray Bursts

When a number of explosions are observed, such as gamma ray and x-ray bursts, one may try to explain them as exploding DL's. However, another possible source of energy is annihilation (CP, VI.3). There is also a possibility that they may be due to double layers in a baryon symmetric universe.

I. Double Layers as a Source of Cosmic Radiation

As pointed out in Section II.E, relativistic DL's in interstellar space may accelerate ions up to cosmic ray energies (see Carlqvist, 1969; 1982a,c).

VII. DOUBLE LAYERS IN TEXTBOOKS

As has been pointed out many times (see e.g., *CP* I; Alfvén, 1982) in situ measurements in the magneto-spheres and progress in laboratory plasma physics have caused a "paradigm transition" which means that a number of old concepts have to be abandoned and a number of new phenomena must be taken into account. Michel Azar has gone through some of the most generally used textbooks in astrophysics and listed in which of these the new concepts have been presented to the student in astrophysics. The results are shown in Table 1. The table gives the surprising and depressing result that the students in astrophysics still are kept ignorant of what has happened in plasma physics.

Double layers were analyzed in detail by Langmuir (1929). The development described in Section III.A demonstrated that there must be "double layers" in a generalized sense (= magnetic field-aligned electric field) so the first decisive evidence for their existence in the magnetosphere dates from 1962. The real discovery of double layers in the magnetosphere is due to Gurnett (1972), but still there are only 2 out of 17 textbooks which even mention that anything like that could exist.

The critical velocity was postulated in 1942 in order to explain the band structure of the solar system. In a series of experiments especially designed to clarify this and other cosmic plasma phenomena, the critical velocity phenomenon was confirmed in the laboratory by Fahleson (1961), by Angerth et al. (1962), by Eninger (1965), and by Danielsson (1973).

The use of "equivalent circuits" is discussed in Alfvén and Fälthammar (1963) and further in a number of papers. Boström (1974) has given the most interesting account of their use. Still, Akasofu is the only one in the list who has understood the value of this in cosmic physics.

That parallel currents attract each other was known already at the times of Ampere. It is easy to understand that in a plasma, currents should have a tendency to collect to filaments. In 1934, it was explicitly stated by Bennett that this should lead to the formation of a pinch. The problem which led him to the discovery was that the magnetic storm producing medium (solar wind with present terminology) was not flowing out uniformly from the Sun. Hence, it was a problem in cosmic physics which led to the introduction of the pinch effect.

Today everybody who works in fusion research is familiar with pinches. Indeed, several big multimillion dollar thermonuclear projects are based on pinches. Pinches in cosmical physics are discussed in detail in Alfvén and Fälthammer (1963) and further in a large number of papers; see *CP*, II.4. However, to most astrophysicists it is an unknown phenomenon. Indeed, important fields of research, e.g., the treatment of the state in interstellar regions, including the formation of stars, are still based on a neglect of Bennett's discovery more than half a century ago. As shown in the table, present-day students in astrophysics hear nothing about it. A recent survey article in *Science* described some "mysterious" threads which were claimed to be different from anything earlier discovered (Waldrop, 1985). Published photographs indicated that these phenomena are likely to be common filamentary structures; indeed, they have been well known since 1934.

In conclusion, it seems that astrophysics is too important to be left in the hands of theoretical astrophysicists who have gotten their education from the listed textbooks. The multibillion dollar space data from astronomical telescopes should be treated by scientists who are familiar with laboratory and magnetospheric physics, circuit theory, and, of course, modern plasma physics. More than 99 percent of the Universe consists of plasma, and the ratio between electromagnetic and gravitational forces is 10^{39}.

VIII. ROEDERER'S INTERDISCIPLINARIFICATION

A. The Roederer Syndrome

In his article "Tearing Down Disciplinary Barriers," Juan G. Roederer (1985) points out the conflict between the demand for "increased specialization on one hand and the pursuit of an increasingly interdisciplinary approach on the other."

This is important. Indeed, in the present state of science specialization is favored to such an extent that science is split up into a number of increasingly small specialties. We lack the global view. This is evident from the preceding section.

We should remember that there once was a discipline which was called "Natural Philosophy" ("reine Naturwissenschaft"). Unfortunately this discipline seems not to exist today. It has been renamed "science," but science of today is in danger of losing much of the Natural Philosophy aspect.

Roederer further discusses the psychological and structural causes for the loss of the global view, and points out that one syndrome of cause is the "territorial dominance, greed, and fear of the unknown." Scientists tend to "resist interdisciplinary inquiries into their own territory...In many instances, such parochialism is founded on the fear that intrusion from other disciplines would compete unfairly for limited financial resources and thus diminish their own opportunities for research."

B. Microscale Example

All this agrees with my own experience. When running a lab I found that one of my most important activities was to go from room to room and discuss in depth the problems which a certain scientist or a group of scientists was trying to understand. It often happened that one group reported that in their field they had a special problem which they could not possibly understand. I told them that if they cared to open the door to the next room — it was not locked! — just this special problem had been solved half a year ago, and if they injected the solution into their own field, this would take a great leap forward. Often they were not at all happy for this suggestion, probably because of the syndrome which Roederer has discussed, but when faced with "tearing down the disciplinary barriers" within the laboratory they realized how important such action is for progress (cf. Section II.D). This may be considered a mild case of the Roederer syndrome.

Such an example from the microscale structure of science supports Roederer's general views, but examples from the macroscale structure are much more important. Large parts of this lecture have been a series of examples of the malady which Roederer describes.

The lack of contact between Birkeland's and Langmuir's experimental-theoretical approach on the one hand and the Chapman-Cowling mathematical-theoretical approach on the other had delayed progress in cosmic plasma physics by perhaps half a century. The many new concepts which came with the space age begin to be understood by magnetospheric physicists but have not yet reached the textbooks in astrophysics, a delay of one or two decades, often more as seen in the preceding section. Very few if any deny that (at least by volume) more than 99 percent of the Universe consists of plasma but students in astrophysics are kept ignorant even of the existence of important plasma phenomena like those listed in Table 1.

Dr. Roederer's prescription for curing this serious disease is "tearing down disciplinary barriers," indeed "interdisciplinarification" of science. This seems to be wise. However, we must suspect that to many astrophysicists this is bitter medicine. Can we find ways to sweeten it?

REFERENCES

Akasofu, S-I., *Physics of Magnetospheric Substorms,* D. Reidel Publ. Co., Dordrecht, Holland, 1977.

Alfvén, H., *Cosmical Electrodynamics,* Oxford University Press, London, 1950.

Alfvén, H., in *Physics of the Hot Plasma in the Magnetosphere,* edited by B. Hultqvist and L. Stenflo, Plenum Press, New York, p. 1, 1975.

Alfvén, H., *Cosmic Plasma,* D. Reidel Publ. Co., Dordrecht, Holland, 1981.

Alfvén, H., *Physica Scripta, T2,* 10 (1982).

Alfvén, H., Plasma Universe, preprint, 1986.

Alfvén, H., and P. Carlqvist, *Solar Phys., 1,* 220 (1967).

Alfvén, H., and C.–G. Fälthammar, *Cosmical Electrodynamics,* Second Edition, Oxford University Press, London, 1963.

Angerth, B., L. Block, U. V. Fahleson, and K. Soop, *Nucl. Fusion Suppl., 3,* 9 (1962).

Bennett, W. H., *Phys. Rev., 45,* 840 (1934).

Birkeland, K., in *The Norwegian Aurora Polaris Expedition, 1902-1903,* Vol. 1, Section 1, H. Aschehoug and Co., Christiana, p. 1, 1908.

Block, L. P., *Astrophys. Space Sci., 55,* 59 (1978).

Boström, R., in *Magnetospheric Physics,* edited by B. M. McCormac, D. Reidel Publ. Co., Dordrecht, Holland, p. 45, 1974.

Carlqvist, P., *Solar Phys., 7,* 377 (1969).

Carlqvist, P., in *Symposium on Plasma Double Layers,* edited by P. Michelsen and J. Juul Rasmussen, June 16-18, 1982, Riso National Laboratory, Roskilde, p. 71, 1982a.

Carlqvist, P., in *Symposium on Plasma Double Layers,* edited by P. Michelsen and J. Juul Rasmussen, June 16-18, 1982, Riso National Laboratory, Roskilde, p. 255, 1982b.

Carlqvist, P., *Astrophys. Space Sci., 87,* 21 (1982c).

Chapman, S., and T. G. Cowling, *The Mathematical Theory of Nonuniform Gases,* Cambridge University Press, London, 1970.

Chapman, S., and F. H. Vestine, *Terr. Mag., 43,* 351 (1938).

Cherrington, B. E., *Gaseous Electronics and Gas Lasers,* Pergamon Press, Oxford, 1974.

Cobine, J. D., *Gaseous Conductors,* Dover Publications, Inc., New York, 1958.

Cummings, V. D., and A. J. Dessler, *J. Geophys. Res., 72,* 1007 (1967).

Danielsson, L., *Astrophys. Space Sci., 24,* 459 (1973).

Dessler, A. J. in *Magnetospheric Currents,* edited by T. A. Potemra (Proceedings of the Chapman Conference on Magnetospheric Currents, Tides Inn, Irvington, Virginia, April 5-8, 1983), p. 22, 1983.

Eninger, J., *Proc. 7th Int. Conf. Phenom. Ionized Gases, 1,* p. 520, 1965.

Fahleson, U. V., *Phys. Fluids, 4,* 123 (1961).

Gurnett, D. A., in *Critical Problems of Magnetospheric Physics,* edited by E. R. Dyer, p. 123 (Proceedings of Joint COSPAR, EAGA, URSI Symposium, Madrid, May 1972), UCSTP, Washington, D.C., 1972.

Hargrave, P. J., and N. Ryle, *Roy. Astron. Soc. Mon. Not., 166,* 305 (1974).

Hasegawa, A., and C. Uberoi, *The Alfvén Wave,* Chapter V, p. 18, Technical Information Center, U.S. Department of Energy, U.S. Printing Office, Washington, D.C., 1982.

Heikkila, W. J., *Astrophys. Space Sci., 23,* 261 (1973).

Hénoux, J. C., Dynamo Theories of Solar Flares, SMA Workshop on Solar Flares, Irkutsk, June 1985.

Jacobsen, C., and P. Carlqvist, *Icarus, 3,* 270 (1964).

Knorr, G., and C. K. Goertz, *Astrophys. Space Sci., 31,* 209 (1974).

Langmuir, I., *Phys. Rev., 33,* 954 (1929).

Langmuir, I., and L. Tonks, *Phys. Rev., 33,* 195 (1929a).

Langmuir, I., and L. Tonks, *Phys. Rev., 34,* 876 (1929b).

Lindberg, L., in *Symposium on Plasma Double Layers,* edited by P. Michelsen and J. Juul Rasmussen, p. 164, June 16-18, 1982, Riso National Laboratory, Roskilde, 1982.

Loeb, L., *Basic Processes of Gaseous Electronics,* Cambridge University Press, London, 1961.

Lyons, L., and D. Williams, *Quantitative Aspects of Magnetospheric Physics,* D. Reidel Publ. Co., Dordrecht, Holland, 1985.

Mendis, A., *Moon and Planets, 18,* 361 (1978).

Newcomb, W. A., *Annals of Physics, 3,* 347 (1958).

Papoular, R., *Electrical Phenomena in Gases,* American Elsevier Publ. Co., New York, 1963.

Roederer, J. G., *EOS, 66,* 681 (1985).

Sato, T., and H. Okuda, *Phys. Rev. Lett., 44,* 740 (1980).

Sato, T., and H. Okuda, *J. Geophys. Res., 86,* 3357 (1981).

Smith, R. A., in *Proc. 107th International Astronomical Union Symposium,* edited by M. R. Kundu and G. Holman, p. 113, College Park, Maryland, 1983.

Torvén, S., and S. Andersson, *J. Phys. D. Appl. Phys., 12,* 717 (1979).

Waldrop, M. M., *Science, 230,* 652 (1985).

Wurm, in *The Moon Meteorites and Comets,* edited by B. M. Middehurst and G. P. Kuiper, p. 573, University of Chicago Press, Chicago, 1963.

Zmuda, A. J., and J. C. Armstrong, *J. Geophys. Res., 74,* 4611 (1974).
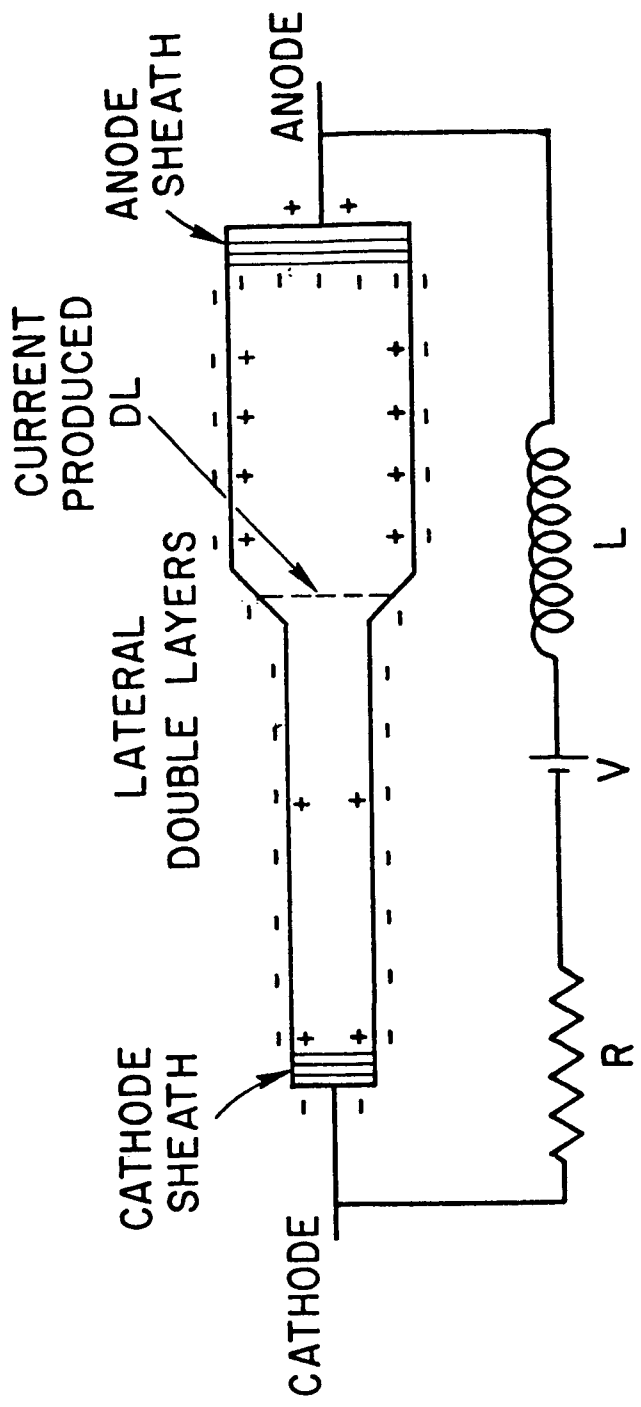
Figure 1. Example of a simple electric circuit where the double layer symbol suggested by Carlqvist (1982c) is used. The double layer is connected in series with a voltage source V, an inductance L., and a resistance R. A current I flows in the circuit. The usual symbol for an emf (which is derived from a galvanic element) is replaced by the suggested symbol for a "generator." The arrow points in the direction of the current I. The same symbol with the arrow antiparallel to I represents a "motor" in which circuit energy is used to accelerate the plasma.

DUALISM IS COSMIC PLASMA PHYSICS

TRANSLATION FORMULA

$$\nabla \times B = \mu_0 i$$

MAGNETIC FIELD DESCRIPTION

MAGNETIC FIELDS ARE:
MEASURED RATHER EASILY
BASIC FOR PLASMA ANISOTROPY
INCLUDING HIGH ENERGY PARTICLE MOTION
GIVES A GOOD DESCRIPTION OF SOME
WAVES IN PLASMAS

ELECTRIC CURRENT DESCRIPTION

ELECTRIC CURRENTS ARE:
DIFFICULT TO MEASURE DIRECTLY BUT
ESSENTIAL FOR UNDERSTANDING:
DOUBLE LAYERS
TRANSFER OF ENERGY FROM ONE REGION
TO ANOTHER
CURRENT SHEET DISCONTINUITIES
CELLULAR STRUCTURE OF SPACE
MAGNETIC SUBSTOMS, SOLAR FLARES

THE PLASMA DUALISM IS SOMEWHAT ANALOGOUS TO THE GENERAL PARTICLE-FIELD DUALISM IN PHYSICS.

THE CURRENT DESCRIPTION REQUIRES A NEW FORMALISM WITH DOUBLE LAYER AND ELECTRIC CIRCUITS

AS IMPORTANT INGREDIENTS.

Figure 2. Plasma produced by an electric discharge. In case the plasma is inhomogeneous, either because its cross section varies or its chemical composition or its density varies, one or more double layers may be produced between the electrodes (cf. Lindberg, 1982).

SIMPLE CIRCUIT
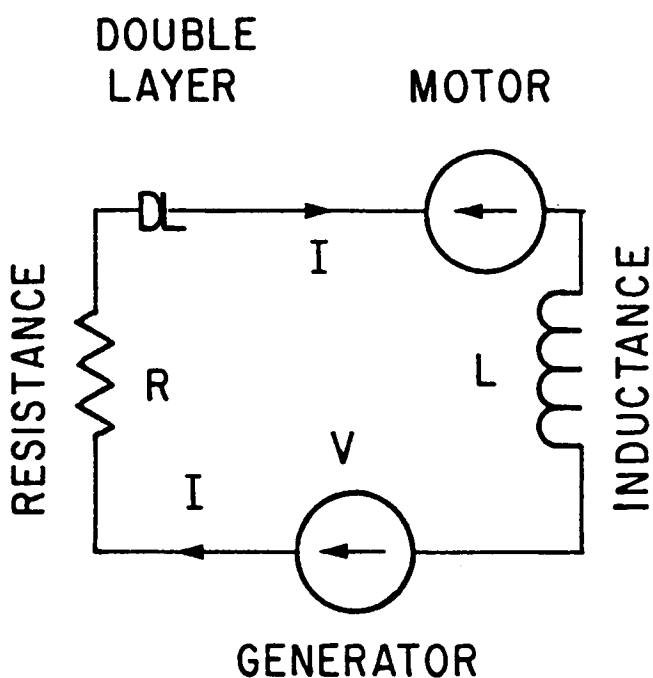
$$\text{CIRCUIT ENERGY} \quad W_C = 1/2 \ L \ I^2$$

$$\text{GENERATOR VOLTAGE} \ V_G = \int_{GEN} \vec{v} \times \vec{B} \cdot \vec{ds}$$

$$\text{MOTOR VOLTAGE} \quad V_M = \int_{MOT} \vec{v} \times \vec{B} \cdot \vec{ds}$$

$$\text{GENERATOR POWER} \quad P_G = I V_G$$

$$\text{MOTOR POWER} \ P_M = I V_M$$

$$\text{DOUBLE LAYER VOLTAGE} \ \Delta V$$

$$\text{POWER DELIVERED TO PARTICLES BY DL} \ P_0 = I \Delta V$$

$$\text{ENERGY LOSSES IN RESISTANCES ETC.} \ P_R = 1/2 \ R \ I^2$$

Figure 3. Dualism in plasma physics (cf. *CP*, I.3).

OTHER SYMBOLS

IF INDUCTANCE IS DISTRIBUTED L SHOULD BE REPLACED
BY TRANSMISSION LINE.
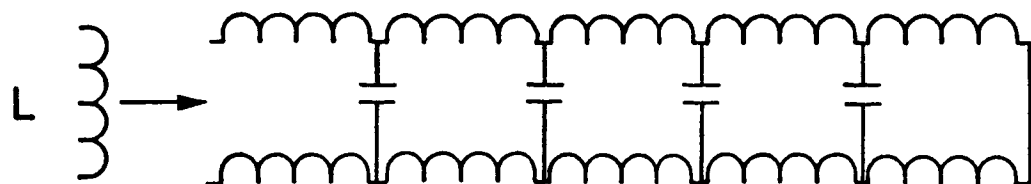
MAGNETIZED CELESTIAL
BODY ACTING AS
HOMOPOLAR INDUCTOR
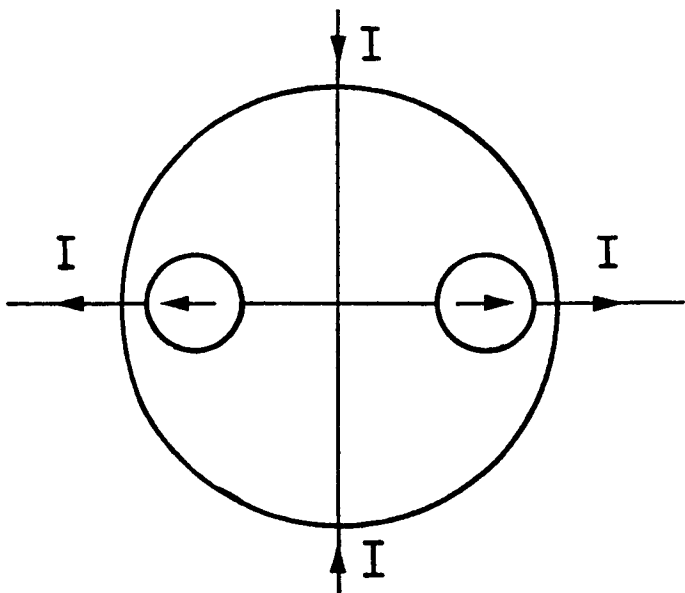
Figure 4. (Upper) In certain cases, e.g., if the circuit has large dimensions, the simple inductance L should be replaced by a transmission line. (Lower) A rotating magnetized celestial body often acts as a homopolar inductor.
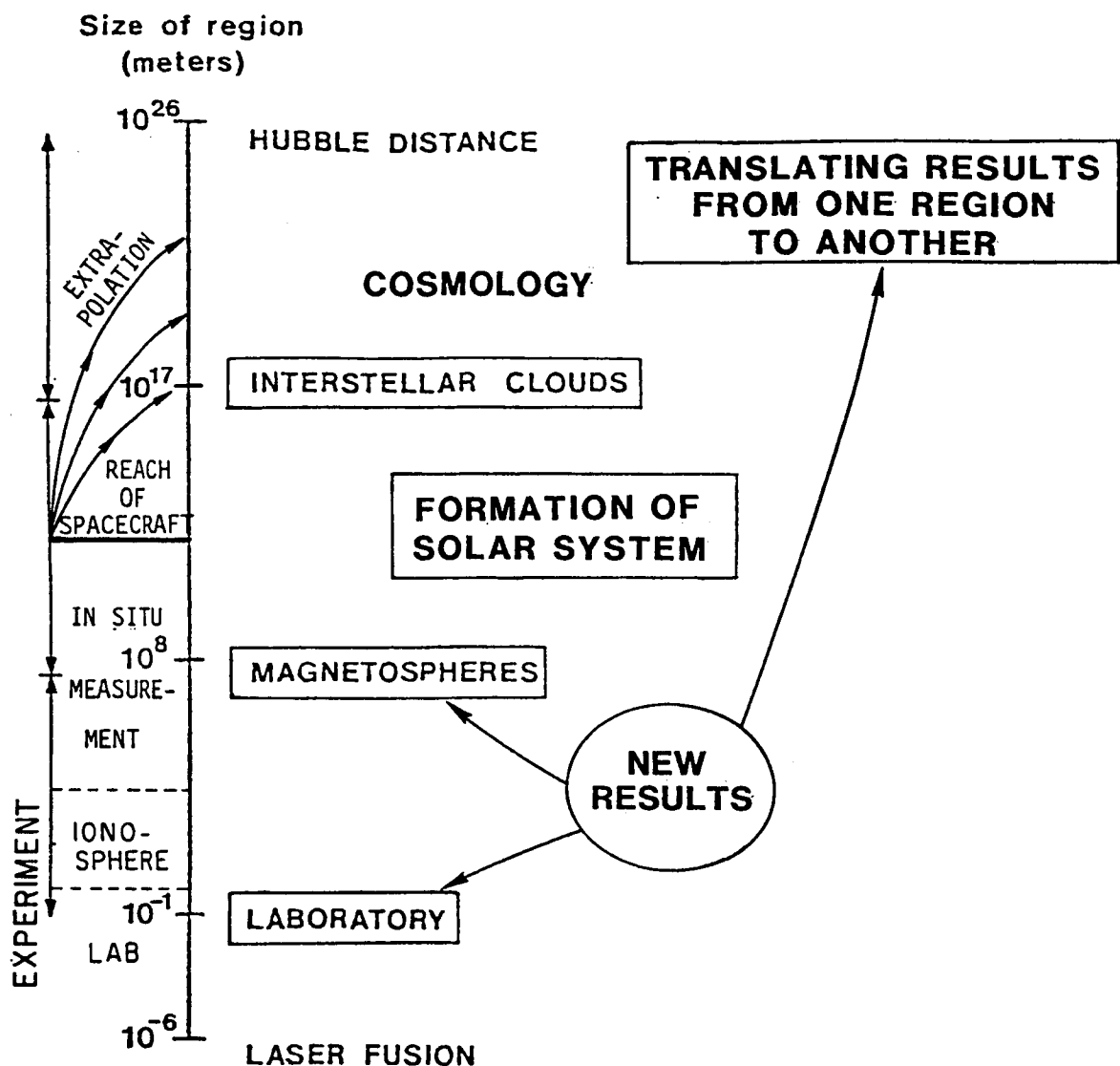
Figure 5. Cosmic triple jump.

PLASMA UNIVERSE

Logarithmic Scale (linear in Lab)
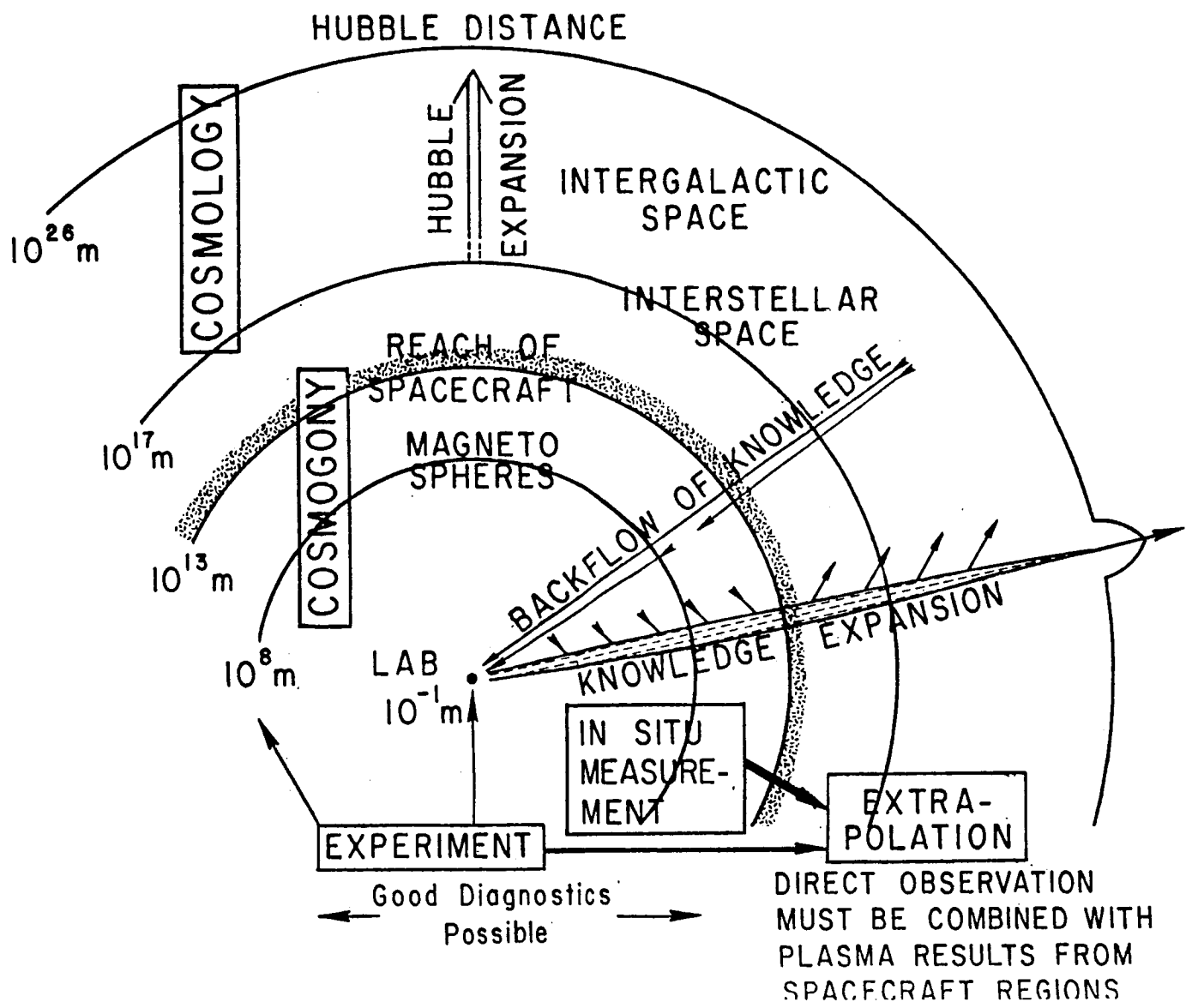
Figure 6. The plasma Universe and knowledge expansion.
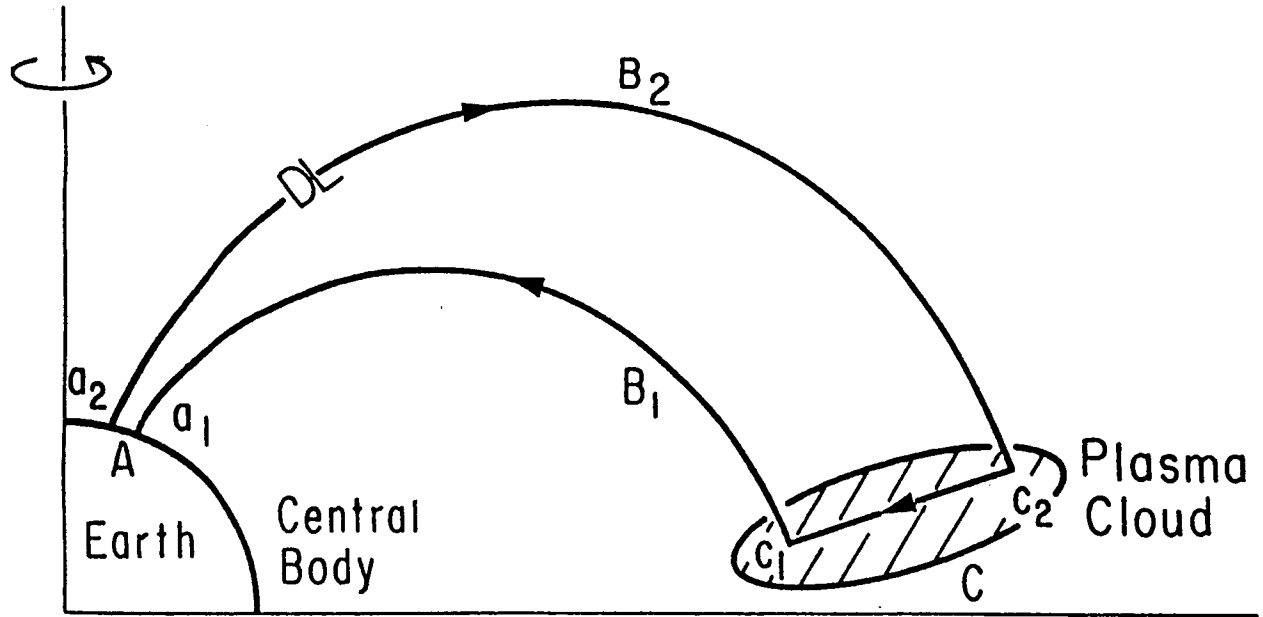
Figure 7. Auroral circuit (seen from the Sun) (cf. *CP*, Figure II:17).
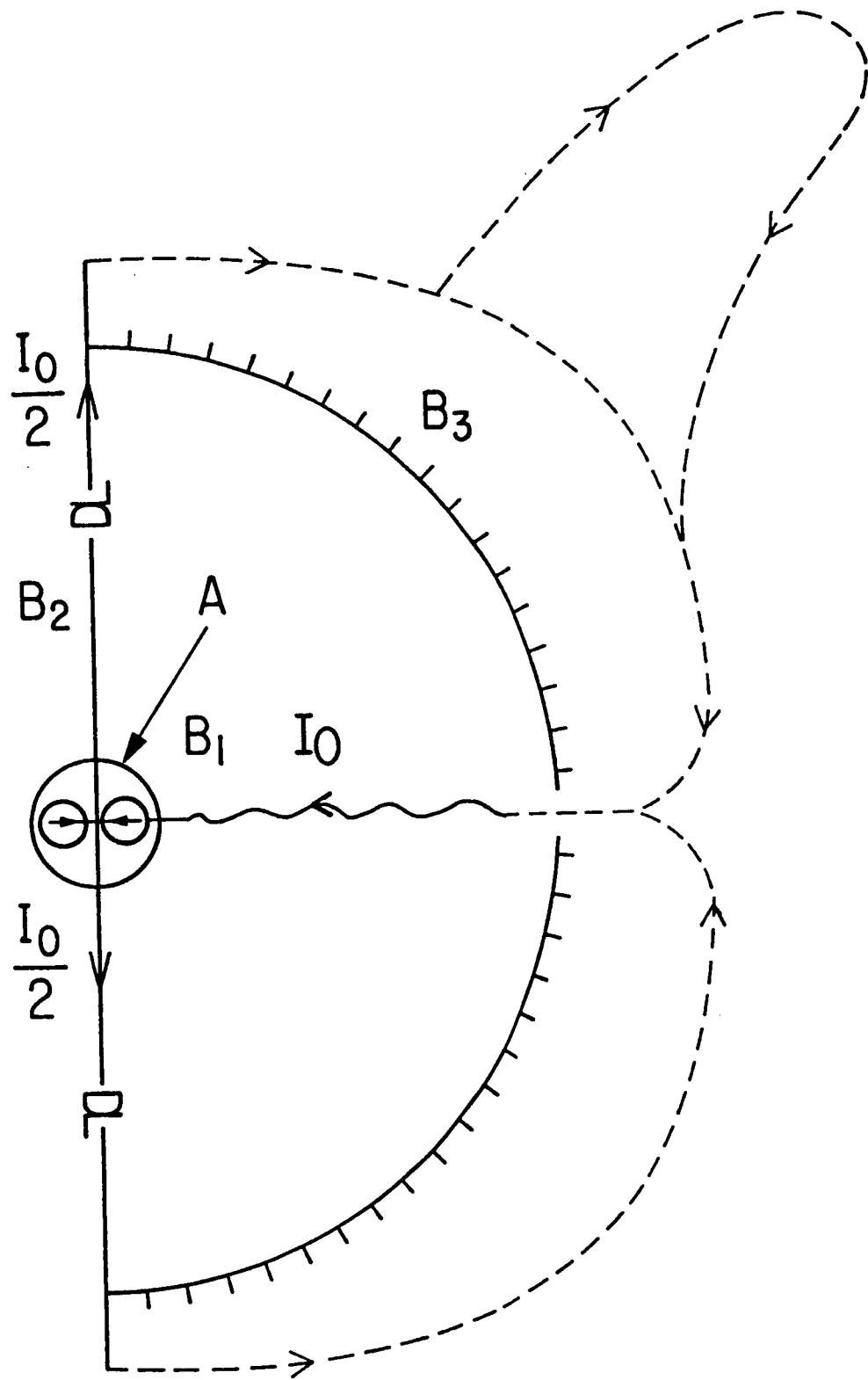
Figure 8. Heliospheric circuit. The Sun acts as a unipolar inductor (A) producing a current which goes outward along both the axes (B_2) and inward in the equatorial plane C_1 and along the magnetic field lines B_1. The current must close at large distances (B_3), either as a homogeneous current layer, or — more likely — as a pinched current. Analogous to the auroral circuit, there may be double layers which should be located symmetrically at the Sun's axes. Such double layers have not yet been discovered.

a)   b)
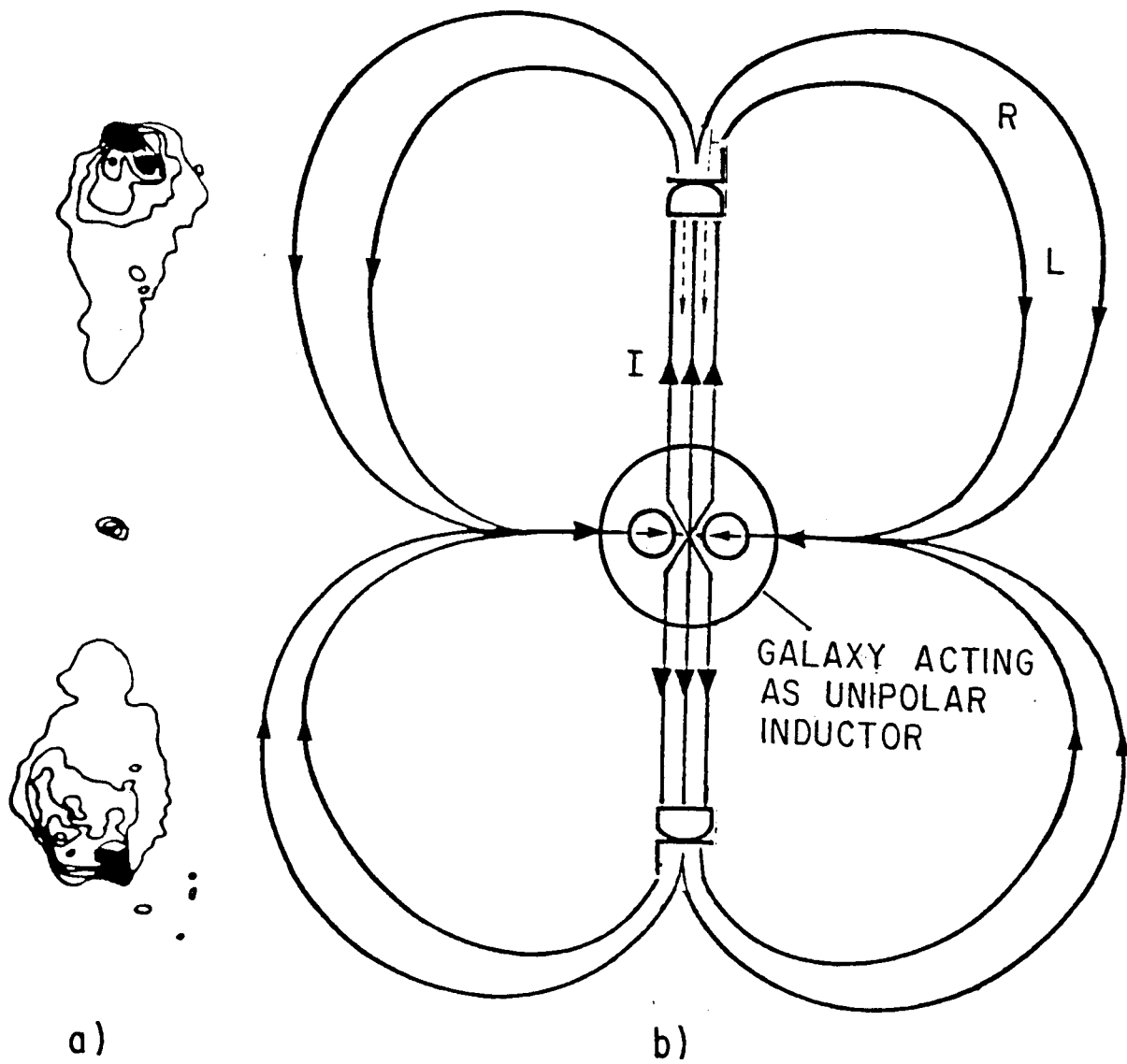
Figure 9. Galactic Circuit. (a) Observed radio emission of Cygnus A (by Hargrave and Ryle,1974) is attributed to synchrotron emission by electrons accelerated in the double layer. (b) The heliospheric circuit is scaled up by a factor 10^9 and the Sun replaced by a galaxy located almost exactly between the radio sources (cf. *CP*, III.4.4).
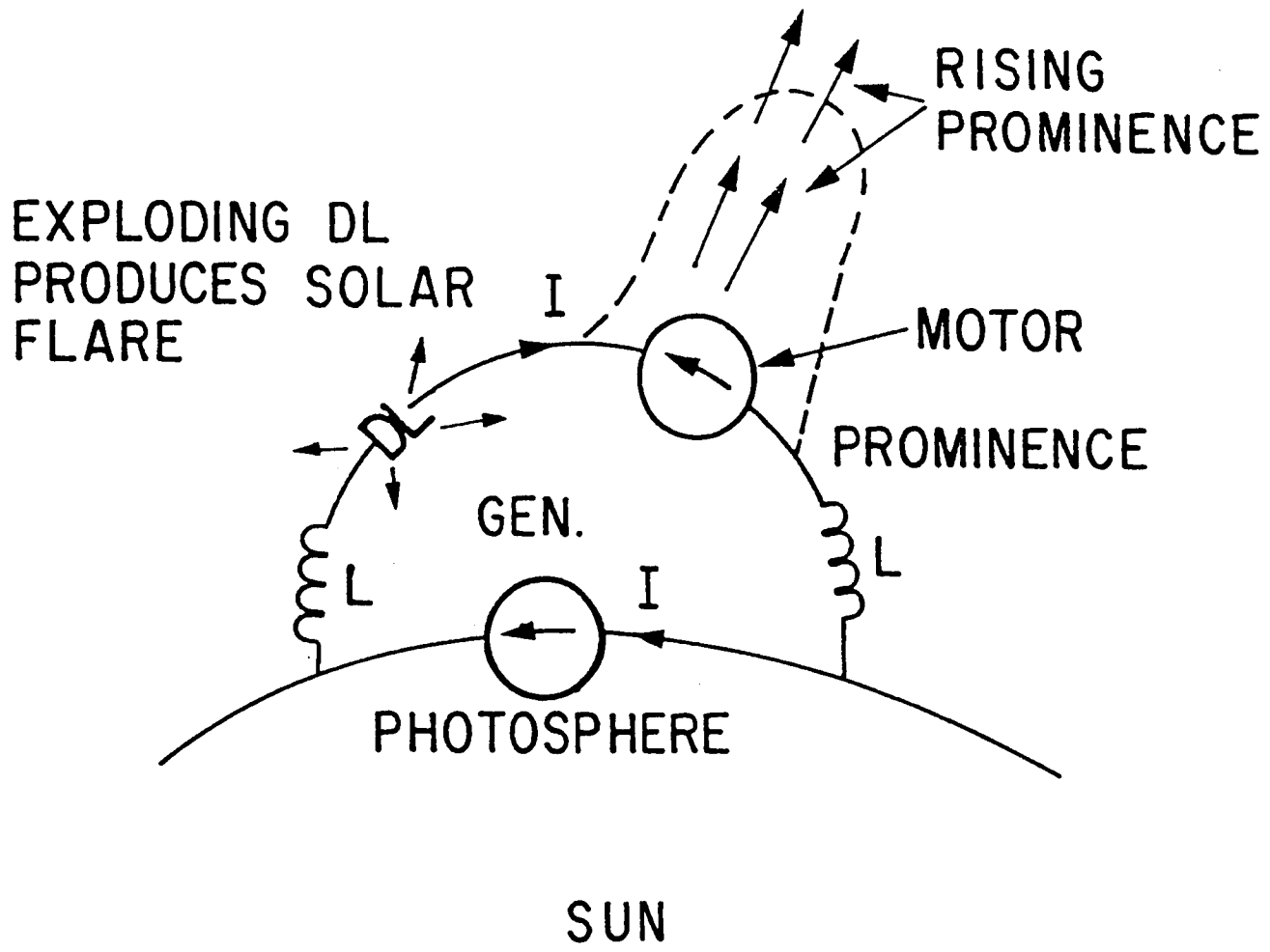
Figure 10. Prominence-solar flare circuit. Whirling motions in the photosphere act as a generator, feeding energy into the circuit (which is similar to Figure 1). The circuit energy can be released either as a solar flare produced by an exploding double layer and/or as a kinetic energy in a rising prominence.
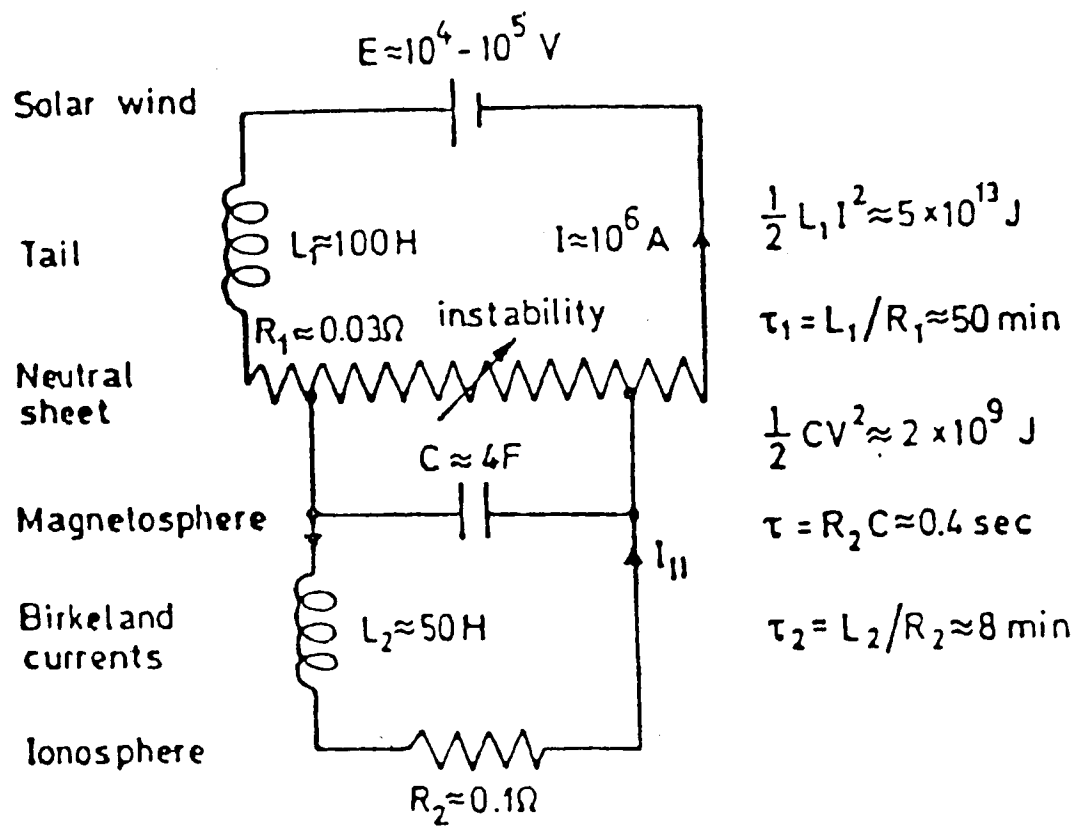
Figure 11. Boström (1974) has given a summary of his theory of magnetic substorms in the form of a circuit. Solar wind energy produces a cross-tail current in the neutral sheet. The arrow indicates that this current can give rise to a very large voltage. (In our terminology, it should be replaced by the DL symbol.) This causes the circuit energy to be discharged over the ionosphere, where it is observed as a magnetic substorm. At substorm onset, the resistance of the neutral sheet increases because a DL is produced and the tail current is redirected to the ionosphere.

TABLE 1. CURRENT TEXTBOOKS DEALING WITH DOUBLE LAYERS AND RELATED PHENOMENA*

	Double Layers	Critical Velocity	Pinch Effect	Circuits
Astrophysical Concepts M. Harwit, 1973 (New York: John Wiley & Sons)				
Theoretical Astrophysics Ambartsumian, 1958 (New York: Pergamon Press)				
Astrophysics: The Atmospheres of the Sun and Stars L. H. Aller, 1963 (New York: The Ronalet Press)				
Plasma Astrophysics Kaplan and Tystovich, 1973 (New York: Pergamon Press)				
Astrophysics and Space Science A. J. McMahon, 1964 (Englewood Cliffs, NJ: Prentice-Hall)				
Plasma Astrophysics, Vol. 2 D. B. Melrose, 1980 (New York: Gordon and Breach, Science Publ.)	X			
Astrophysics and Stellar Astronomy T. L. Swihart, 1968 (New York: John Wiley & Sons)				
General Astrophysics with Elements of Geophysics J. S. Stodolkiewiecz, 1973 (New York: Amer. Elsevier Publ.)				
Astrophysics W. K. Rose, 1973 (New York: Holt, Rinehart & Winston, Inc.)				
Cosmic Electrodynamics J. H. Piddington, 1964 (New York: John Wiley & Sons)				
Astrophysics I and II Bowers and Deeming, 1984 (Boston: Jones and Bartlett Publ.)				
Solar Flare Magnetohydrodynamics E. R. Priest, 1982 (Dordrecht, Holland: D. Reidel Publ. Co.)				
Physics of the Solar Corona L. S. Shkloviskii, 1965 (New York: Pergamon Press)				
Solar Terrestrial Physics S. I. Akasofu and S. Chapman, 1972 (London: Oxford University Press)	X			X
Introduction to Space Science Haymes, 1971 (New York: John Wiley & Sons)				
Introduction to the Physics of Space Rossi and Albert, 1970 (New York: McGraw-Hill Book Co.)				
Physics of Magnetospheric Substorms S. I. Akasofu, 1977 (Dordrecht, Holland: D. Reidel Publ. Co.)	X			X

* X means that the field of research is at least mentioned. Blank squares mean that the student is kept ignorant of the fact that such a field exists.

I. DOUBLE LAYERS IN THE LABORATORY

FORMATION MECHANISMS OF LABORATORY DOUBLE LAYERS

Chung Chan

Center for Electromagnetics Research

and

Department of Electrical and Computer Engineering

Northeastern University

Boston, Massachusetts 02115, U.S.A.

ABSTRACT

The evolution processes of double layers have been studied in a series of laboratory experiments. It was found that the existence of virtual cathode-type potential wells at the electron injection boundary was the dominant triggering mechanism. The rapid growth of the potential well led to collisionless ion trapping and the establishment of the necessary trapped ion population. For double layers with small potential drops, collisionless ion trapping actually induced ion-ion streaming instabilities and the formation of ion phase-space vortices. In this regime, the system often exhibited relaxation-type oscillations which corresponded to the disruption and the recovery of the double layers.

I. INTRODUCTION

Much of our recent understanding of double layers has come from laboratory experiments and numerical simulations which had rather limited system dimensions. The system boundaries are often in close proximity with the double layer electric field, thus affecting almost all aspects of double layer physics. The situation is obviously different in space plasmas where boundaries are not well defined and often far away from the regions of possible double layer formation. In order to extrapolate the results from laboratory and computer experiments to the space context, it is important to understand the role of the system boundaries on the formation of double layers.

Most double layers experiments (Quon and Wong, 1976; Leung et al., 1980; Singh and Schunk, 1983; Iizuka et al., 1979; Saeki, et al., 1980) have utilized the injection of a drifting electron species to trigger the formation process. It was found that a necessary condition for double layer formation is that the electron drift velocity v_d exceed the thermal velocity v_{te} of the ambient electrons. This condition results in the belief that the Buneman instability with an instability threshold of $v_d \geq v_{te}$ was the triggering mechanism for double layers. However, double layers with potential drops $\Phi > T_e/e$, the electron temperature divided by the electron charge, have been observed (Hollenstein et al., 1980) experimentally with v_d as small as $0.2\ v_{te}$. Ion-acoustic turbulence instead of the Buneman instability was expected to be the triggering mechanism for double layer formation in that experiment.

Numerical simulation (Sato and Okuda, 1980) of double layers with $v_d \leq v_{te}$ have found different results. No double layers with $\phi > T_e/e$ were found. Rather, a new class of double layers with non-montonic potential profiles and $\phi \leq T_e/e$ was found. These double layers were always preceded by negative potential pulses and associated with current-driven, ion-acoustic turbulence. As such, these double layers have been identified as "ion acoustic" in order to distinguish them from the conventional double layers. Since an electron drift velocity of $v_d > v_{te}$ may not exist in space (e.g., the auroral plasma), the ion-acoustic double layers have also become a subject of considerable interest.

In this talk, we will discuss previous (Hershkowitz et al., 1981) as well as new experimental results in order to identify the formation mechanism of double layers in our triple plasma device. We begin with the roles of the

boundaries on the steady state characteristics of double layers. It is shown that the drifting electrons provide the initial space charge for double layer formation, while the trapped ions determine the evolution process and the shape of the potential profile. It is also shown that the growth of virtual cathode-type potential wells at the electron injection boundary is the triggering mechanism for double layers. Collisionless ion trapping by the potential well is found to be the main process for the establishment of the necessary trapped ion population.

Furthermore, double layers with $\phi \leq T_e/e$ are shown to be unstable to the evolution of ion phase-space vortices from ion-ion streaming instabilities. In this regime, the double layer potential profile has a strong resemblance to ion-acoustic double layers. This result may represent an alternative explanation of the small electric field signatures observed in the auroral plasma.

II. STEADY STATE EXPERIMENT

It is useful to first describe the operational characteristics of the triple plasma device in order to get some insights into the sources of particles that support the double layer. The triple plasma device consists of two source plasmas bounding a target plasma. Each source is separated from the target chamber by two grids. Plasma potential in each chamber is determined by the bias voltages of the grid and the internal anode. The source plasmas are created by filament discharge in argon gas (operating pressure $P_o \leq 1 \times 10^{-4}$ Torr) with density $n_s = 10^9 \rightarrow 10^{10}$ cm^{-3} and $T_e \approx 2$ eV. The ionizing electrons are trapped by surface multidipole magnetic fields in the region closed to the filaments so that they cannot reach the target chamber and produce plasma there directly. We have also confined our study on double layers with $\phi \leq 10$ V. These procedures ensure that ionization effects are minimized in our double layer experiment. A schematic of the triple plasma device is shown in Figure 1.

Stable double layers with $\phi \leq 5$ T_e/e can routinely be achieved using the boundary conditions shown in Figure 2. We chose to investigate these smaller double layers in order to limit the accelerated electron beam energy to below the ionization potential of argon. From the boundary conditions shown in Figure 2, we expect ions to only come from the high potential source. These ions are usually pre-accelerated into the target chamber by the potential difference between the high potential source plasma and the target plasma. These ions are further accelerated by the double layer into the low potential side. These beam ions either exit the target chamber at the left boundary or they charge exchange with neutrals and form cold ions ($T_i \sim 0.3$ eV). The cold ions, once formed, are confined electrostatically by the potentials of grids B and C. Although the charge exchange reaction rate is relatively low at our operating neutral pressure, the cold ion density accumulates to a significant fraction of the beam ion density due to their long confinement times.

Electrons which enter the target chamber from the high potential source are those in the tail of the Maxwellian source distribution function. These electrons have almost no drift energy, thus becoming the thermal electron species in the target plasma. This contrasts with the situation at the low potential end. There the tail of the source distribution function, which is energetic enough to get over the barrier provided by grid A, is accelerated into the target plasma. This results in an electron drift with the drift energy determined by the potential difference between grid A and the target plasma.

The boundary conditions in this experiment are believed to play the following roles:

1. The high potential side boundary ensures that the ions will enter the target chamber with a flow velocity $u_o > C_s$. This situation is quite similar to that of a sheath at a plasma boundary. Downward curvature of the plasma potential requires an ion drift velocity $u_o > C_s$. Since the high potential side electrons can be treated as approximately isothermal, the "Bohm sheath criteria" applies in this case for the double layer as well.

2. Grid B acts as a potential barrier for the low potential source ions as well as for the charge exchange cold ions which formed between the double layer and grid B. Since the height of the potential barrier of grid B is roughly 20 times the ion temperature ($T_i \approx 0.3$ eV), no low potential source ions are expected to enter the target chamber. On the other hand, the high potential source ions are at a much higher energy than grid B and can exit through grid B into the low potential source. As such the only source of thermal ions in the target plasma appears to be that of the charge exchange ions.

3. The low potential side boundary allows only electrons to drift in from the left. Such excess electron space charge may be neutralized only by the ion beam and the charge exchange ions.

4. There is no externally applied electric field across the target plasma since grids B and C are at roughly the same potential. The formation of double layers is a result of the particle flow rather than that of an external electric field.

Using the experimental boundary conditions and the particle distributions at the sources, it is possible to determine the potential profile across the target chamber by solving the Vlasov-Poisson equations. The details of such calculations have been described in an earlier paper (Hershkowitz et al., 1981) and will not be repeated here. Rather we will point out some results which are relevant to our present discussion. A typical solution of the target plasma potential profile and the boundary conditions employed is shown in Figure 3. The model has grid potentials similar to those shown in Figure 2. The double layer is formed in the region $x_L \leqslant x \leqslant x_R$ where $\phi(x_L) = 0$ and $\phi(x_R) = \phi_D$. Using the dimensionless variable $\psi = e\phi/T_e$, the density of the free ions n_{if} and trapped electrons n_{et} entering from the high potential source are, respectively:

$$n_{if}(\psi) = \frac{N}{2} e^{(T_e/T_i)(\psi_2 - \psi)} \, \text{erfc} \sqrt{\frac{T_e}{T_i}(\psi_2 - \psi)} \tag{1}$$

and

$$n_{et}(\psi) = N \, e^{(\psi - \psi_2)} (1 - \text{erfc}\sqrt{\psi - \psi_A}) \qquad . \tag{2}$$

The density of the free electrons entering from the low potential source is:

$$n_{ef}(\psi) = \frac{N}{2} e^{\psi - \psi_1} \, \text{erfc}\sqrt{\psi - \psi_A} \tag{3}$$

where ψ_1, ψ_2 and ψ_A are, respectively, the low potential source, high potential source, and grid A potentials normalized to the electron temperature. Both source particles are assumed to be Maxwellian distributed with equal density N.

The density of the charge exchange ions cannot be calculated from the boundary conditions, thus it can be treated as a variable or:

$$n_{it}(\psi) = \beta\, n_e(0)\, e^{-(T_e/T_i)\psi} \tag{4}$$

and

$$\beta = 1 - \frac{n_{if}(0)}{n_e(0)} \quad . \tag{5}$$

β is a parameter which depends on the density ratio of the trapped ions to the beam ions and $n_e(0)$ is the total electron density at $\psi = 0$.

We show the dependence of the double layer on the trapped ion density with β varying from 0 to 0.35 in Figure 4. As the trapped ion density increases, the double layer becomes more detached from the low potential side boundary. Since $\beta = 0.35$ corresponds closely to the potential profile in the experiment, it is possible that a significant amount of charge exchange ions are trapped by the double layer at the low potential side; i.e., $\beta = 0.35$ corresponds to a trapped ion/beam ion density ratio of 54 percent. The trapped ions neutralize the excess negative space charge created by the drifting electrons, thus maintaining a uniform plasma potential at the low potential region of the double layer.

The contributions of the various particle species on the double layer space charge are shown clearly in Figures 5a and 5b where the charge density profile and particle density profiles are plotted versus axial distance. As discussed earlier, the ion beam provides the positive charge density for the downward curvature of the double layer at the high potential side, while the drifting electrons supply the negative charge density for the upward curvature of the double layer at the low potential side.

III. THE FORMATION MECHANISM

In order to understand the triggering mechanism for the double layers in our experiment, we examine the temporal evolution of the target plasma potential profile with $v_D \leq v_{te}$ and $v_D > v_{te}$. An extra grid is installed at the low potential side to facilitate the pulsing of the drifting electrons. The boundary conditions for this experiment are shown in Figure 6. A steady state target plasma with $n_e \cong 10^7$ cm^{-3} is extracted from the high side source, and the target plasma potential is quite uniform axially with $\phi_T = 4$ V. Low side source electrons and ions are normally excluded from the target plasma by the potential barriers of grid B (biased at -30 V) and grid C (biased at +12 V), respectively.

At time t = 0, grid B is switched to the ground potential and the low side source electrons are accelerated into the target plasma by the potential difference between ϕ_T and ground, i.e.,

$$v_D \cong \sqrt{\frac{e\,\phi_T}{T_e}}\; v_{te} \qquad . \qquad\qquad (6)$$

When the un-neutralized electron stream enters the target plasma, the entire target potential decreases rapidly from 4 to 3 V in 10 μs which results in v_D = 1.2 v_{te}. The temporal evolution of the target plasma potential profiles, as obtained with an emissive probe using Boxcar interferometer averaging technique, is shown in Figure 7. A potential well begins to form near the electron injection boundary at t = 50 μs. The potential well grows deeper and widens into a double layer at t > 400 μs. The amplitude of the double layer is ϕ = 1.1 T_e/e and appears to be quite stable. This result can be interpreted as follows.

Electron injection from the low side source creates excess space charge at the injection boundary, and a virtual cathode-type potential well is formed to limit the injected current. The growth of the potential well is accompanied by ion trapping in the potential well. As the density of the trapped ions increases, the double layer becomes detached from the electron injection boundary, in agreement with our earlier result on the effects of trapped ions (see Figure 3). Notice the double layer formation time of $T_{DL} \lesssim 400$ μs is considerably shorter than the charge exchange time of $T_{cx} \cong 1$ ms in this experiment. At such, the trapped ion population cannot come entirely from the charge exchange ions which fall into the potential well. A more possible source is the neighborhood ions which fall into the well during its growing phase. These ions will actually get accelerated down the potential well with energies depending on their locations in the potential well.

We further decrease the drift velocity of the injected electrons by decreasing the target plasma potential to ϕ_T $\cong$ 3 V. When the un-neutralized electron stream enters the target plasma, ϕ_T decreases from 3 to 1.5 V in 10 μs. As shown in Figure 8, a potential well is once again formed near the electron injection boundary at t = 50 μs when v_D $\cong$ 0.7 v_{te}. At t > 75 μs, a small double layer with ϕ $\cong$ 0.5 T_e/e has formed. However, in contrast with the earlier experiment, the double layer decays into an ion hole-like potential well. Note the similarity between the potential profile at t = 150 μs and an ion-acoustic double layer.

The time history of the plasma potential (ϕ_L) at an axial distance of x = 10 cm, the electron current flow across the target chamber from the low potential source (I_{eH}), and the ion saturation current (I_{iL}) at x = 15 cm are shown in Figure 9 in order to illustrate the double layer formation processes. At t > 50 μs, ϕ_T = 1 V, and v_D $\cong$ 0.7 v_{te}, the growth of the potential well corresponds to the abrupt decrease of ϕ_L. On the other hand, I_{eH} continues to increase due to the injected electron current until ϕ_L becomes negative where I_{eH} begins to decrease rapidly. As ϕ_L reaches a minimum at -1.0 V, I_{eH} returns almost to the level at t < 0. ϕ_L subsequently becomes slightly more positive, and an intense low frequency noise appears in I_{iL} which corresponds to the evolution of the ion hole-like pulse.

A similar evolution process is observed when we increase v_D just slightly. As shown in Figure 10, the double layer breaks into one or more ion hole-like pulses. The long time history of this experiment is shown in Figure 11. The ion saturation current exhibits relaxation-type oscillations in time with a period roughly characterized by the transit time of the ion hole-like pulses across the target plasma. The relaxation oscillation corresponds to the evolution of the double layer from virtual cathode potential well and the subsequent decay into ion hole-like pulses. When the pulses reach the high side boundary (e.g., the ion-hole velocity is the order of the ion thermal velocity), the process repeats itself.

The breaking of the double layer into the ion hole-like pulses can be understood as follows. The magnitude of the virtual cathode potential well ϕ_w is formed to limit the injected current. Since the potential well must become a potential barrier to the injected electrons in order to limit the current, $\phi_w \cong (v_D/v_{te})^2 \, T_e/e$. The potential drop of the double layer $\phi \cong \phi_w$; also, we have $\phi = (v_D/v_{te})^2 \, T_e/e$.

As shown in Figure 9c, the injected current I_{eH} and v_D are reduced to very small values as a result of the formation of the double layer. We believe the growth of the potential well and the double layer formation also triggered bursts of counterstreaming ions which are accelerated down each side of the potential well with an average velocity:

$$ v_b < \sqrt{\frac{2\,e\,\phi}{T_e}} \; C_s \; . \tag{7} $$

This results in a counterstreaming or "tuning fork" ion phase space configuration at the double layer front. As reported in many numerical and experimental studies (Pécseli and Trulsen, 1984; Chan et al., 1984) of ion-acoustic shocks and ion holes, the ion-ion two-stream region becomes unstable when $v_b \leq C_s$ and evolves into one or more ion phase-space vortices.

As we have observed double layer formation with $v_D \leq v_{te}$, it is doubtful that the Buneman instability plays any roles in triggering the formation of double layers in these experiments. When $v_D < v_{te}$, no steady double layer exists as a result of the ion two-stream instability and the evolution of ion phase-space vortices.

IV. DISCUSSION

We have reviewed results from a series of laboratory experiments concerning the formation of double layers in a triple plasma device. In steady state, the double layer electric field is sustained by the negative space charge of the drifting electrons and the positive space charge of the ion beam. The low potential boundary condition permits the injection of an un-neutralized electron species which space charge is crucial for the initiation of the virtual cathode potential well. The ion reflecting grid (grid B in Fig. 2) plays two roles; first, to prevent the low potential source ions from entering the double layer and second, to confine the charge exchange cold ions in the low potential side of the double layer. The charge exchange (trapped) ions are needed to neutralize part of the drifting electrons, thus allowing the double layer to move away from the low potential boundary.

The formation phase of the double layers is associated with the growth of virtual cathode-type potential wells at the electron injection boundary. The formation of the virtual cathode potential well is a result of the lack of neutralizing ions at the electron injection boundary. As long as the injected electron density is sufficiently high, the potential well will form independent of v_D and it need not be associated with instabilities. We have clearly shown the formation of double layers with $v_D < v_{te}$ which is below the threshold of the Buneman instability.

The movement of the double layer electric field away from the electron injection boundary is probably caused by the accumulation of the trapped ion density at the low potential side of the double layer as demonstrated by Figure 3. Since the double layer formation time is much shorter than the charge exchange time, the source of trapped ions is more likely coming from ions in the neighborhood of the potential well during the growth of the well. As such, these ions are accelerated down the potential well with a maximum velocity of:

$$v_b \overset{\leq}{=} \sqrt{\frac{2\, e\, \phi_w}{T_e}} \ C_s \quad .$$

(8)

When the magnitude of the potential well $\phi_w < T_e/e$, the ions become two stream unstable because $v_b < C_s$. As such, the double layer decays into ion phase space vortices with potential structures that resemble ion acoustic double layers. This situation is similar to the auroral plasma condition where small electric signatures (Temerin et al., 1982) are often observed along with counterstreaming ions.

For the case of $v_D > v_{te}$, the depth of the potential well $\phi_w > T_e/e$ and results in a stable double layer formation. For the stable double layers, the charge exchange ions will be the main fueling source for the trapped ion population in steady state. In that case, the main loss mechanism for the trapped ions is radial diffusion to the side walls.

REFERENCES

Chan, C., M. H. Cho, N. Hershkowitz, and T. Intrator, *Phys. Rev. Lett., 52,* 1782 (1984).
Hershkowitz, N., G. Payne, and C. Chan, *Plasma Phys. 23,* 910 (1981).
Hollenstein, Ch., M. Guyot, and E. S. Weibel, *Phys. Rev. Lett., 45,* 2110 (1980).
Iizuka, S., K. Saeki, N. Sato, and Y. Hatta, *Phys. Rev. Lett., 43,* 1404 (1979).
Leung, P., A. Y. Wong, and B. H. Quon, *Phys. Fluids, 23,* 992 (1980).
Pécseli, H. L., and J. Trulsen, *Phys. Rev. Lett., 48,* 1355 (1982).
Pécseli, H. L., R. J. Armstrong, and J. Trulsen, *Phys. Rev. Lett., 81A,* 386 (1980).
Quon, B. H., and A. Y. Wong, *Phys. Rev. Lett., 37,* 1393 (1976).
Saeki, K., S. Iizuka, and N. Sato, *Phys. Rev. Lett., 45,* 1853 (1980).
Sato, T., and H. Okuda, *Phys. Rev. Lett., 44,* 740 (1980).
Singh, N., and R. W. Schunk, *Phys. Fluids, 26,* 2781 (1983).
Temerin, M., K. Cerny, W. Lotko, and F. S. Mozer, *Phys. Rev. Lett., 48,* 1175 (1982).
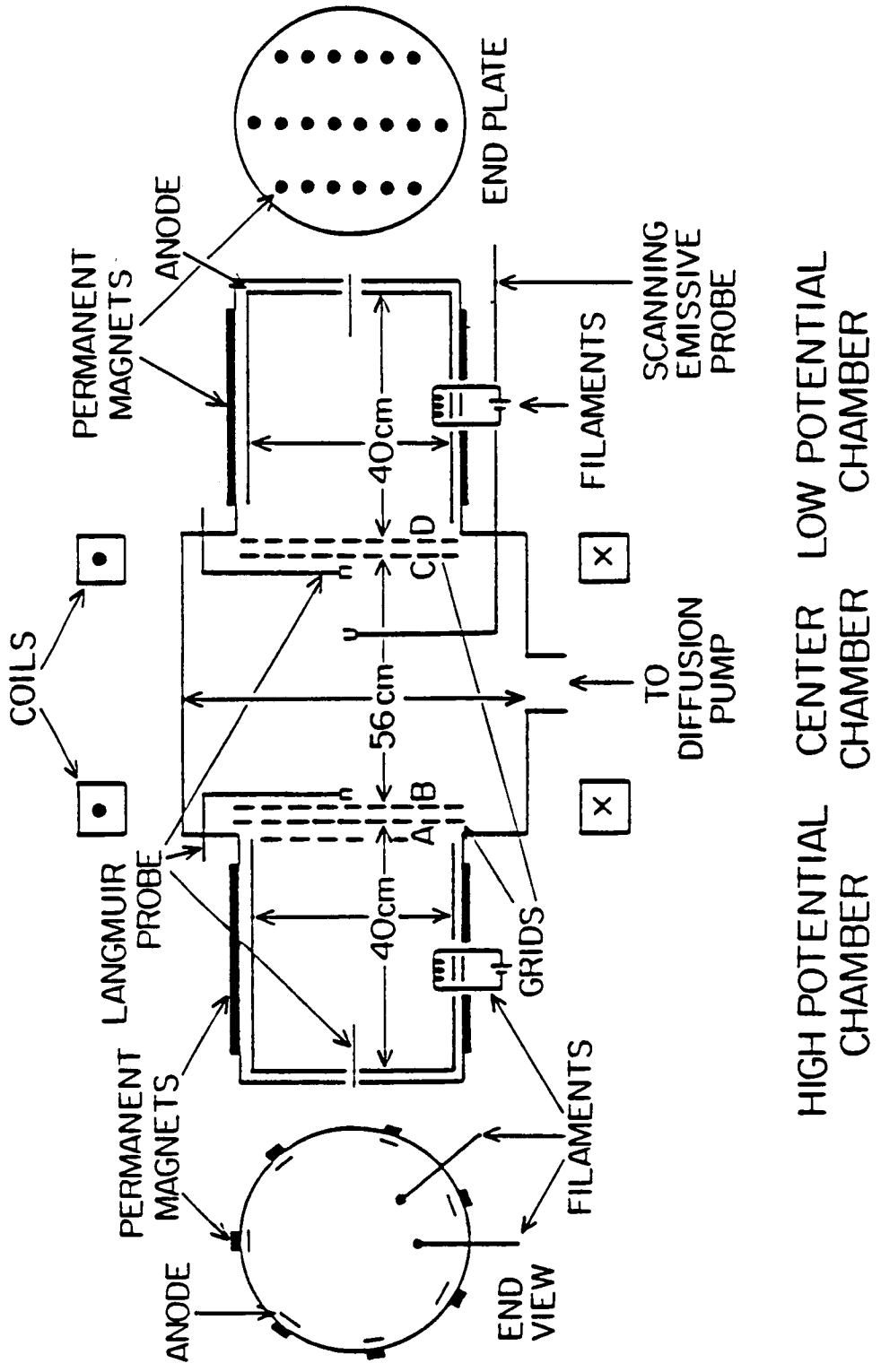
Figure 1. A schematic of the triple plasma device.
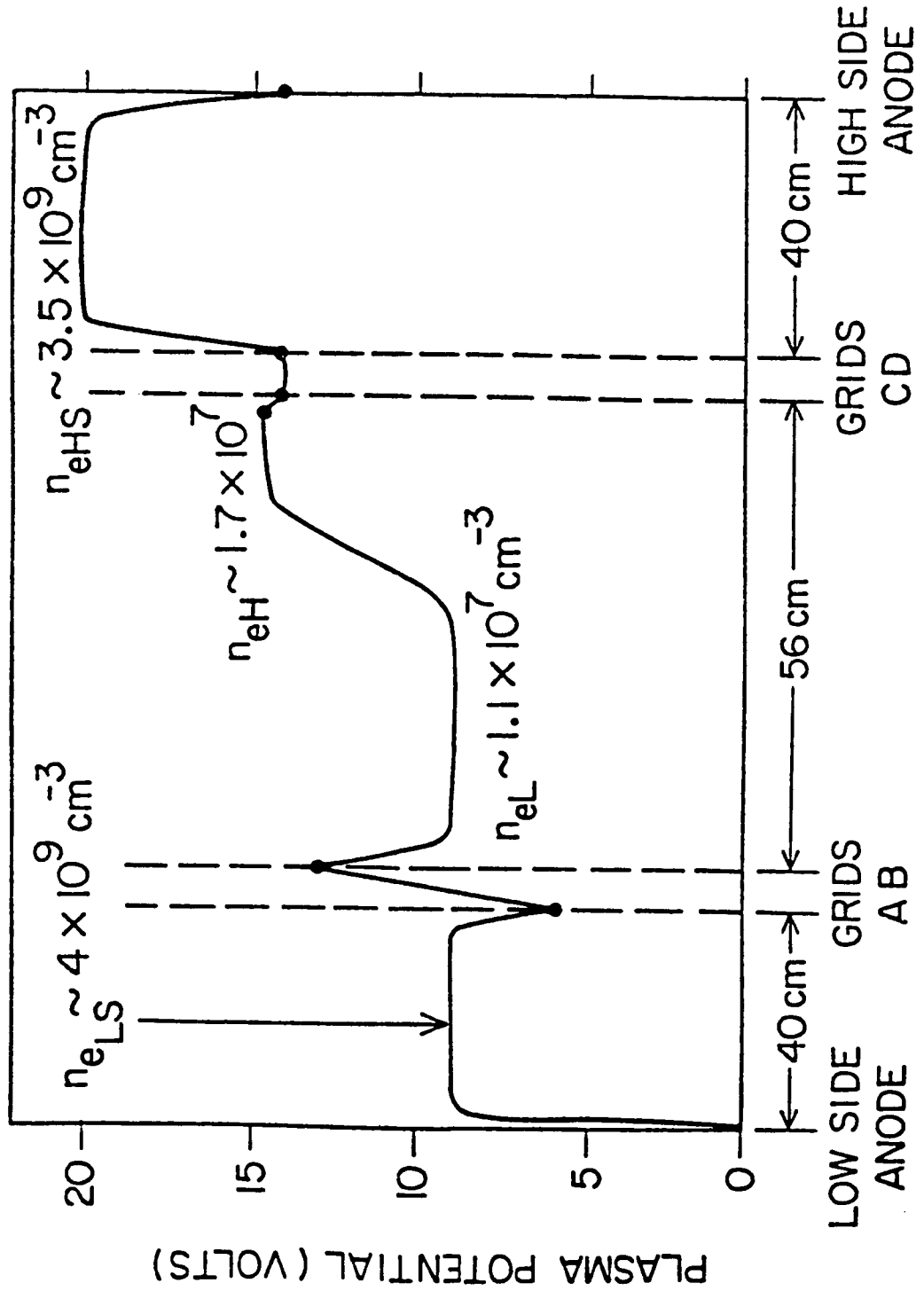
Figure 2. Axial potential profile of the laboratory double layer including the boundary condition.
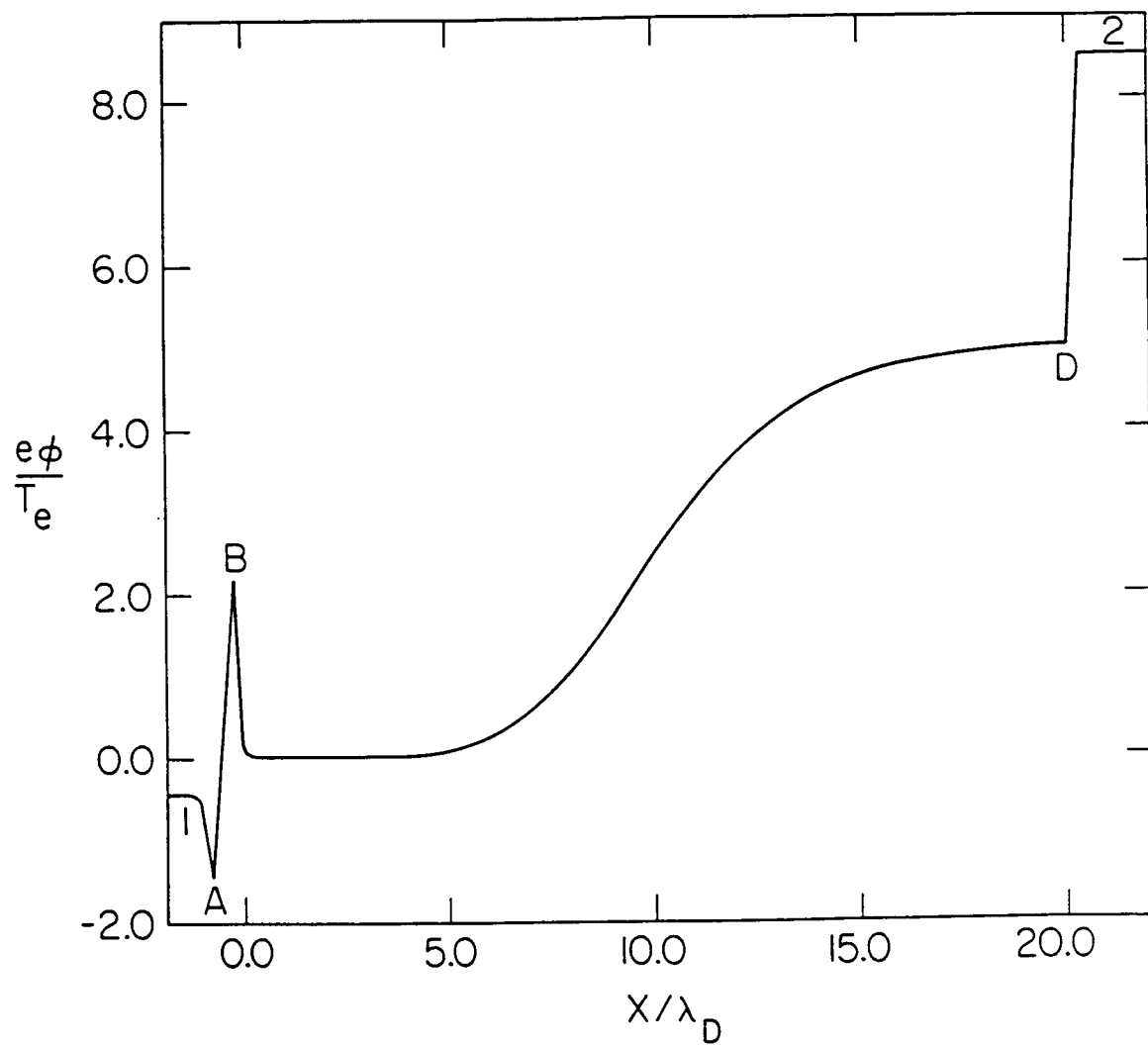
Figure 3. A solution of Poisson's equation $d^2\psi/dx^2 = n_{ef}(\psi) + n_{et}(\psi) - n_{if}(\psi) - n_{it}(\psi)$ where $\psi = e\phi/T_e$; $x = x/\lambda_D$; n_{if}, n_{et}, n_{ef}, and n_{it} are given by equations (1) through (4), respectively.
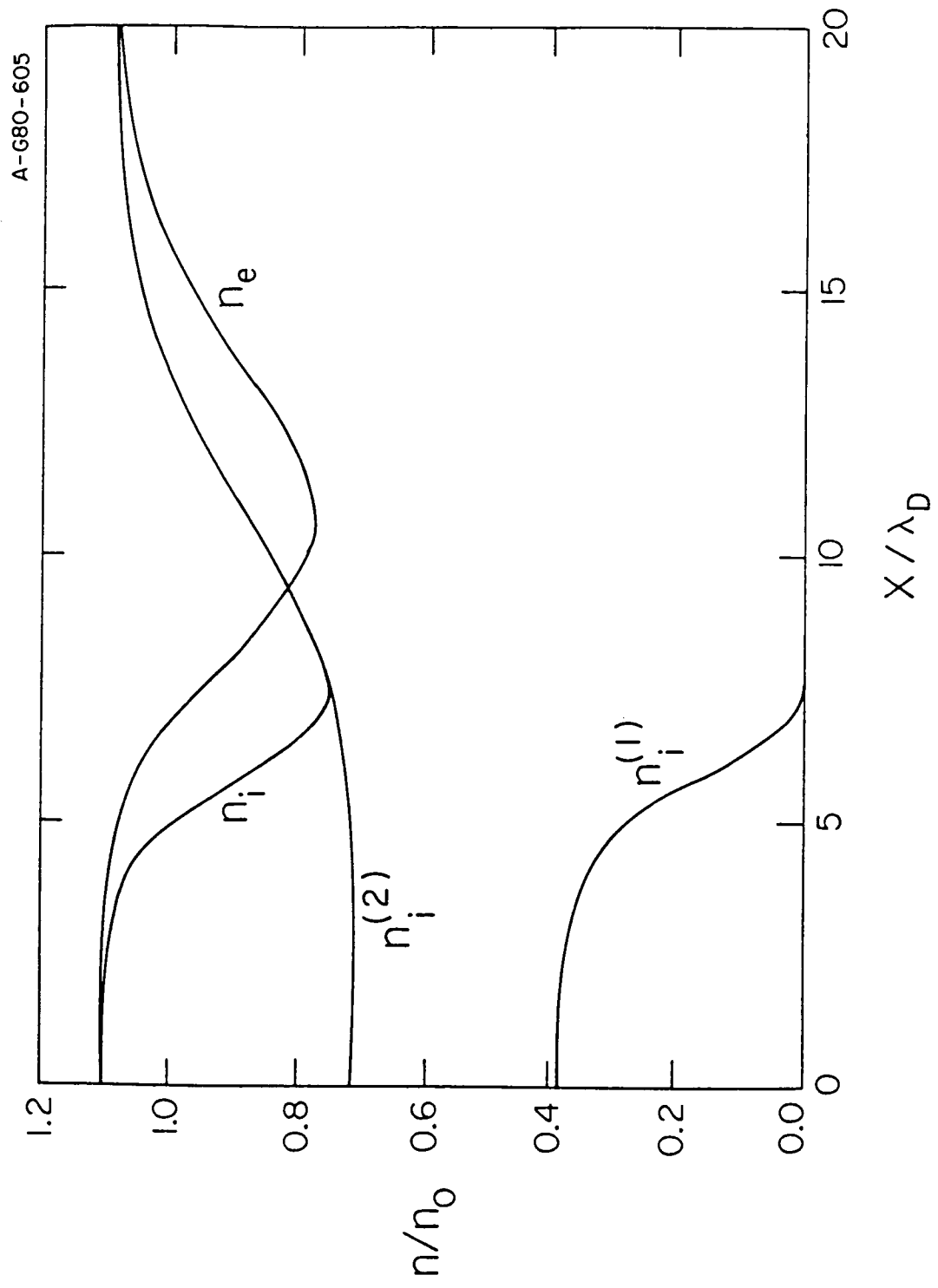
Figure 4a. The total ion and electron density profiles for the model double layer.

A-G8O-6O8
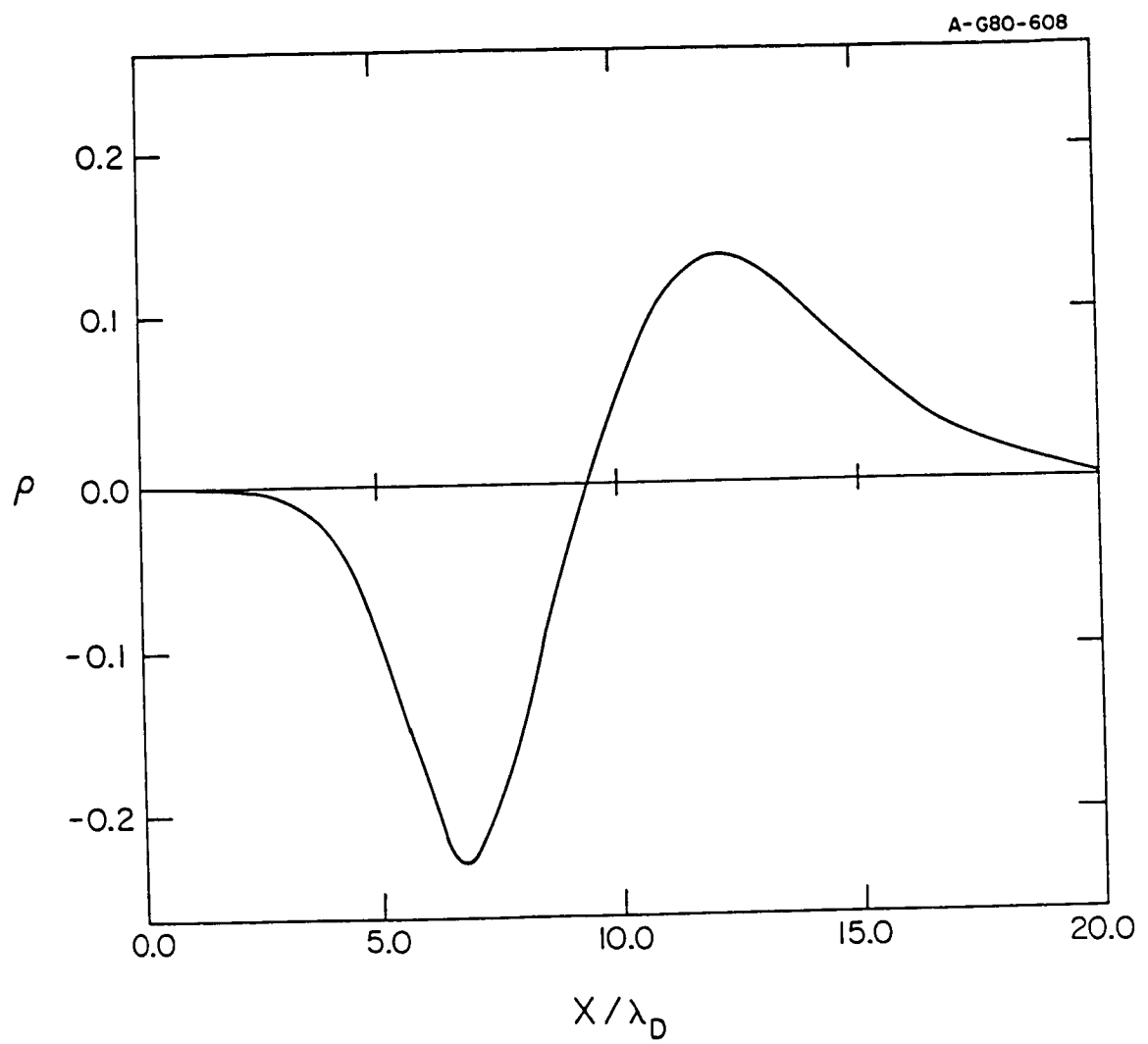
Figure 4b. Total charge density profile for the model double layer.
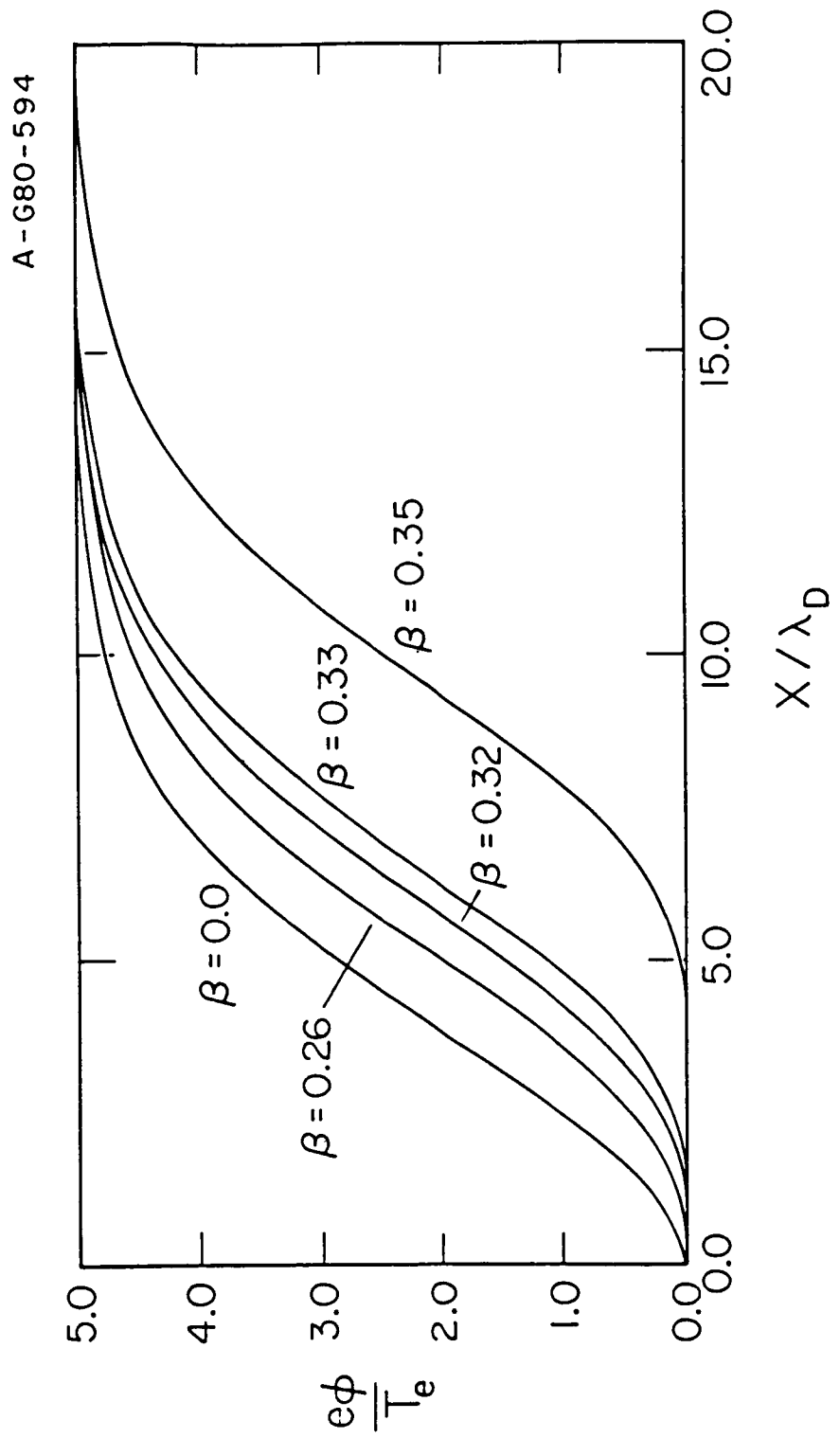
Figure 5. Illustration of the dependence of double layer position on the density of trapped ions. The curve labeled β = 0.0 has no trapped ions.
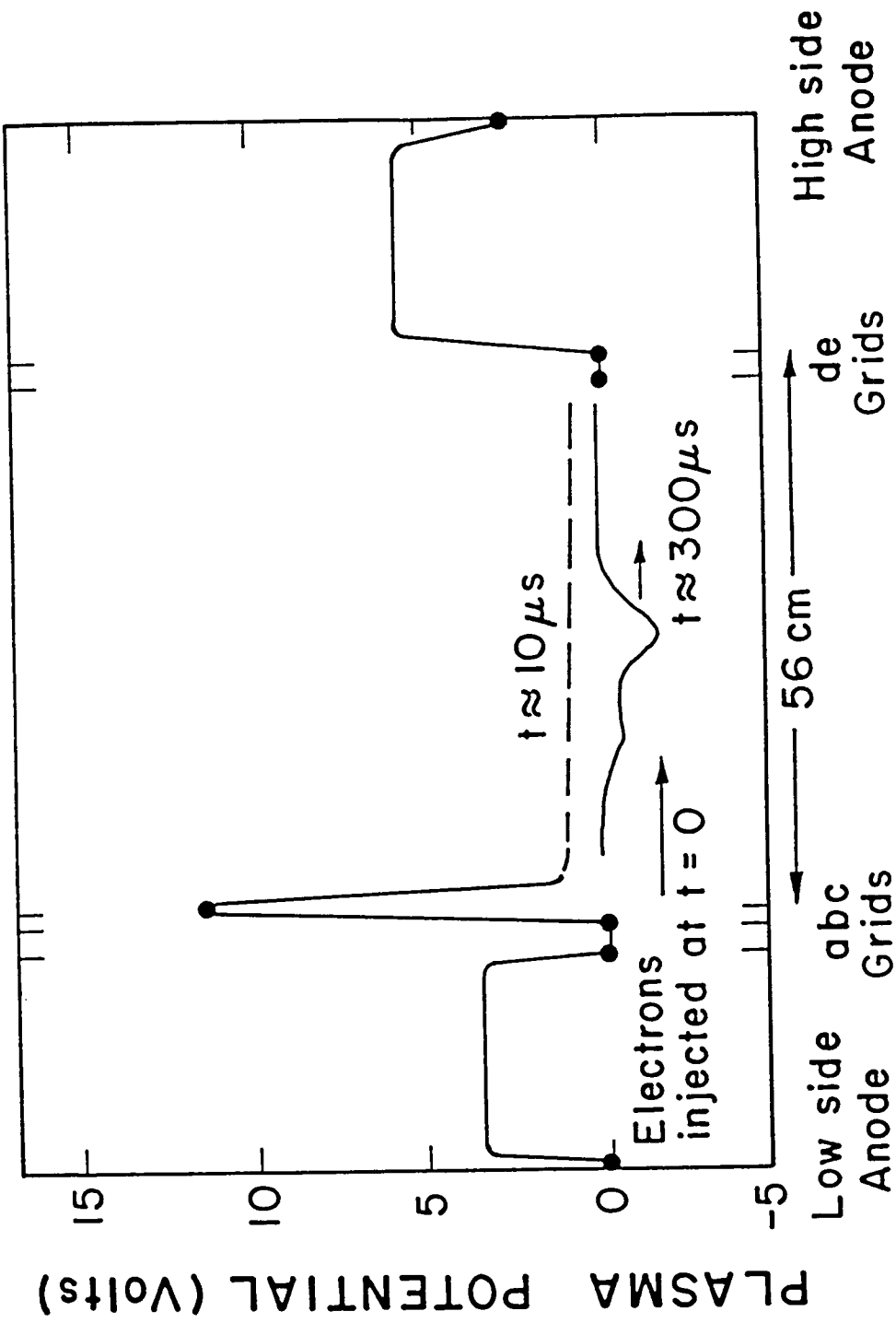
Figure 6. Axial potential profile along the axis of the device. Grid B was switched from -30 V to ground at t = 0.
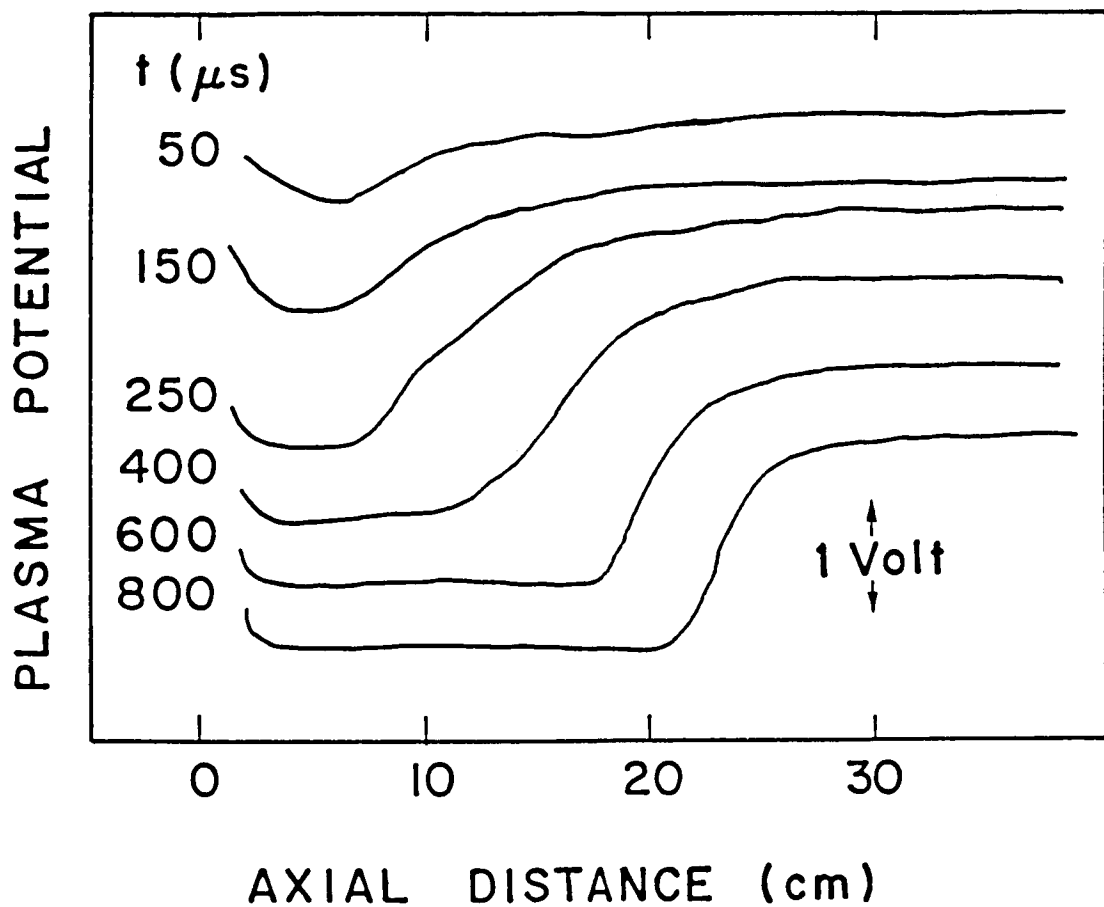
Figure 7. Temporal evolution of the target plasma potential profile when $v_D > v_{te}$. Each profile is displaced for clarity.
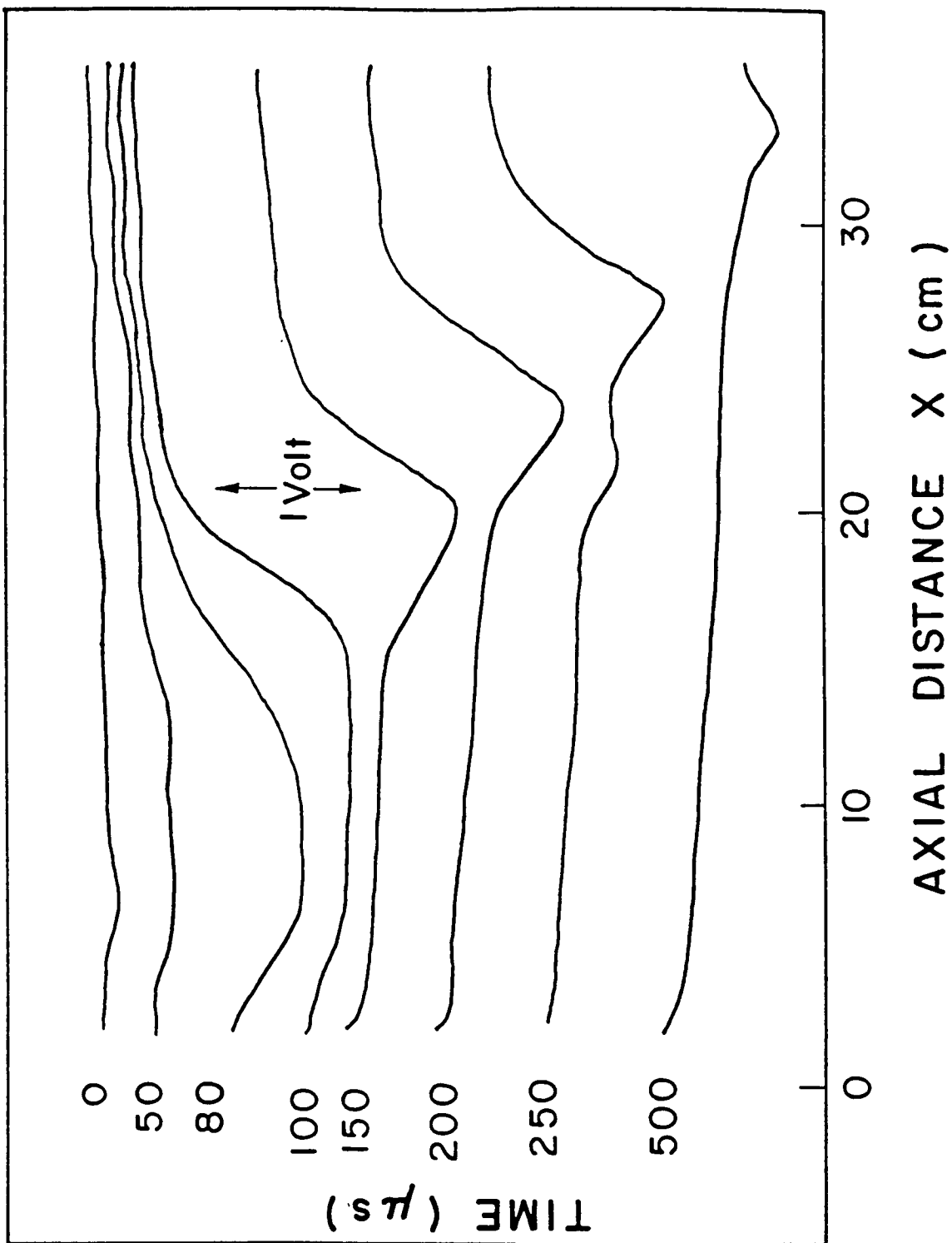
Figure 8. Temporal evolution of the target plasma potential profile when $v_D > v_{te}$.

50
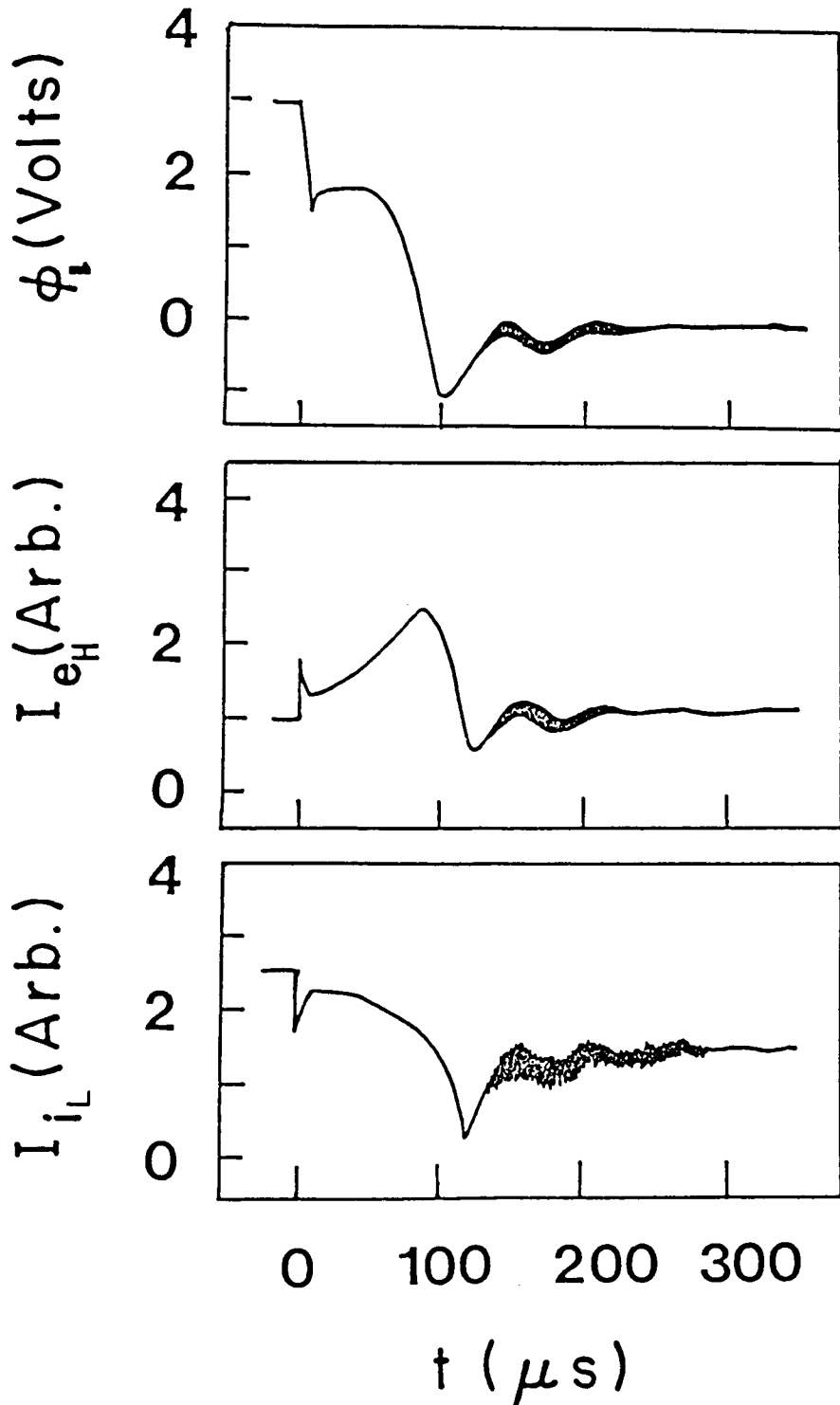
Figure 9. Time history of (a) the target plasma potential (ϕ_L) as measured by an emissive probe at 10 cm away from grid C; (b) the electron current (I_{eH}) collected by a single-sided Langmuir probe facing the low potential source; and (c) the ion saturation current (I_{iL}) collected by a wire probe at 15 cm away from grid C.
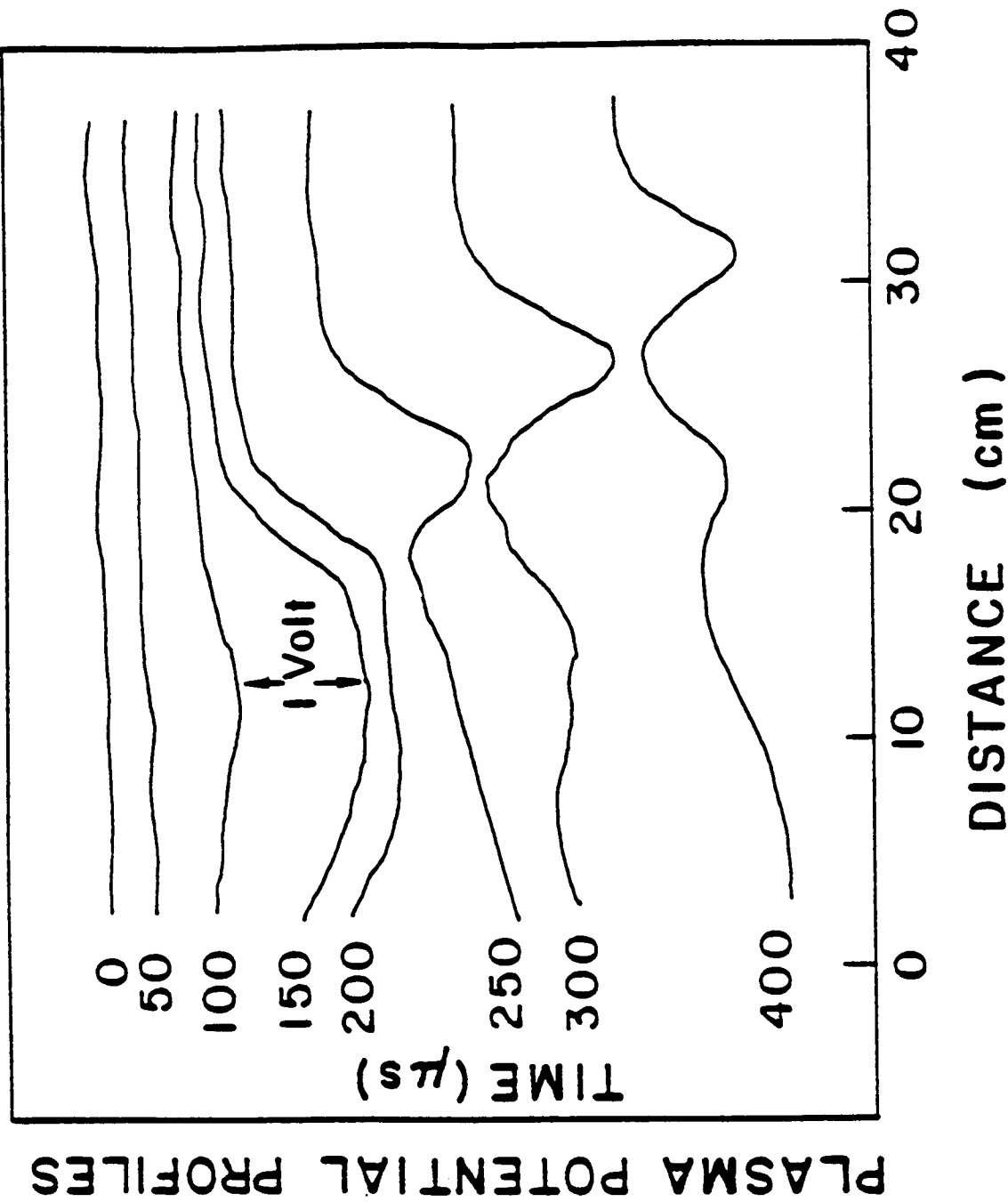
Figure 10. Temporal evolution of the target plasma potential with $v_D < v_{te}$ and the double layer decays into more than one ion hole-like pulses.
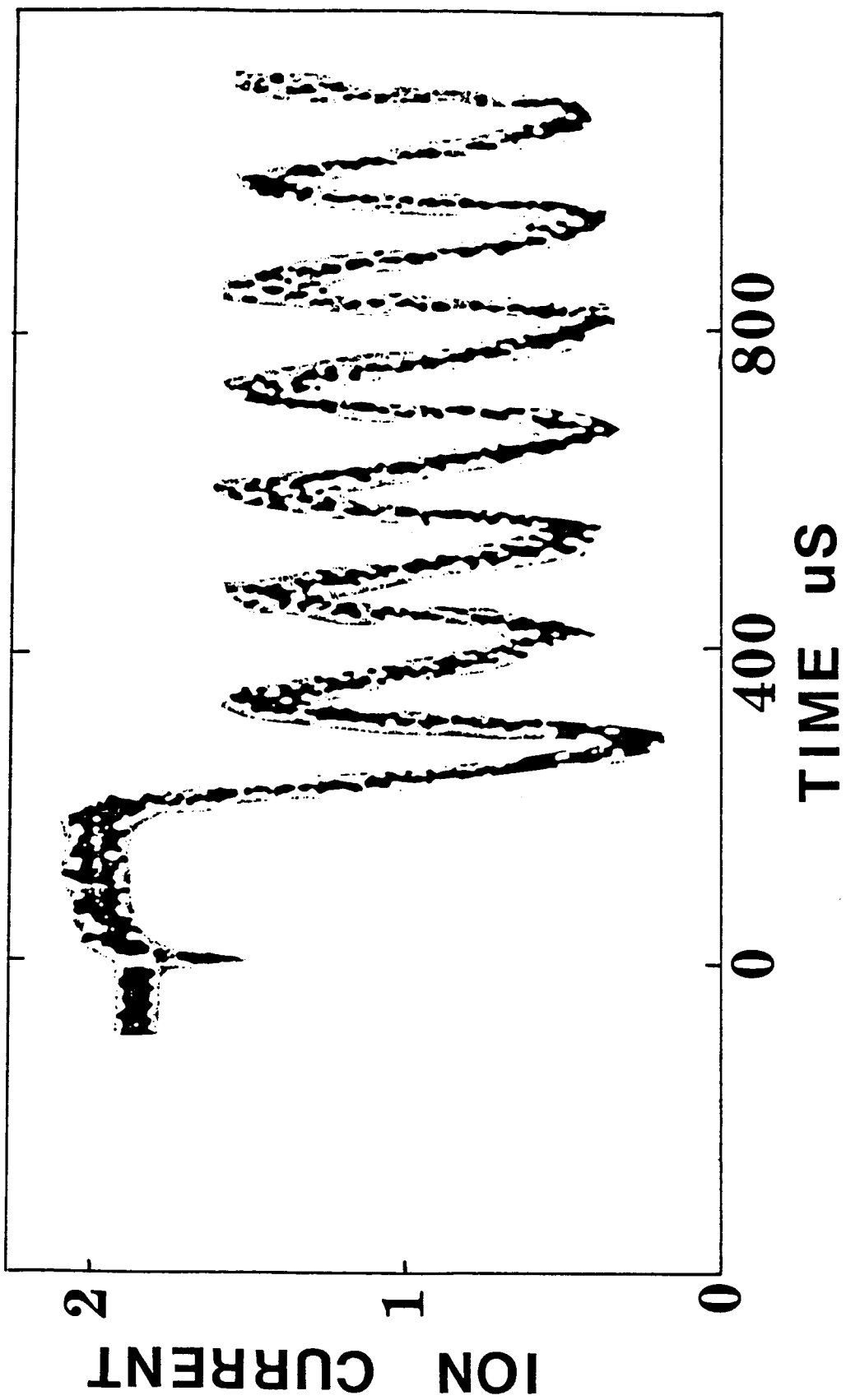
Figure 11. Long time history of the ion saturation current when the system exhibits relaxation oscillation.

SOME DYNAMICAL PROPERTIES OF VERY STRONG DOUBLE LAYERS
IN A TRIPLE PLASMA DEVICE

T. Carpenter
Department of Physics
University of Iowa
Iowa City, Iowa 52242, U.S.A.

N87-23315

and

S. Torvén
Department of Plasma Physics, Royal Inst. of Technology, Stockholm, Sweden

I. INTRODUCTION

Since double layers observed in space and in simulations are rarely if every static, considerable attention has been given to studies of motions of double layers in the laboratory. Extensive reviews have recently been published of the dynamical properties of very strong double layers ($eV/kT_e \sim 1000$) in a Q machine (Sato et al., 1983; Iizuka et al., 1983) and strong double layers ($eV/kT_e \sim 10$) in a triple plasma device (Hershkowitz, 1985). In both cases the double layers were essentially planar. We report here on some of the dynamical properties of very strong double layers ($eV/kT_e \sim 200$) seen in a differentially pumped triple plasma device (Torvén, 1982). These double layers are V-shaped. In particular, we discuss the following findings: (1) Disruptions in the double layer potential and in the plasma current occur when an inductance is placed in series with the bias supply between the sources in the external circuit. These disruptions, which can be highly periodic, are the result of a negative resistance region that occurs in the I-V characteristic of the device. This negative resistance is due to a potential minimum which occurs in the low potential region of the double layer, and this minimum can be explained as the self-consistent potential required to maintain charge neutrality in this region. (2) When reactances in the circuit are minimized, the double layer exhibits a jitter motion in position approximately equal to the double layer thickness. The speed of the motion is approximately constant and is on the order of 2 times the ion-sound speed. The shape of the double layer does not change significantly during this motion. (3) When the bias between the sources is rapidly turned on, the initial phase in the double layer formation is the occurrence of a constant electric field (uniform slope of the potential) for the first few microseconds. The potential then steepens in the region where the double layer will eventually be formed and flattens in regions above and below this. The double layer is completely formed after about 100 microseconds and then engages in the jitter motion discussed above.

In the following we discuss first the apparatus used in all of the work and then consider each of the three phenomena mentioned above. In the first case it is believed that the phenomenon is rather completely understood and the situation is discussed at some length. The same cannot be said for the last two cases and limited discussion is included. However, these two phenomena have characteristics which differ qualitatively from what is seen in Q machines and these differences are identified.

II. EXPERIMENTAL DETAILS

The experiment was performed in a triple plasma device (Torvén, 1982) consisting of a central chamber with coaxial plasma sources located on either side as shown in Figure 1. Plasma was produced in the sources by discharges in argon between heated tungsten filaments and the source chamber walls. The electrodes B1 and B2 can also be used as anodes; but, for the present investigation, they were left floating. They, therefore, acquired potentials approximately equal to the respective filament potentials. The sources were independent in the sense that

discharge voltages and currents and gas flow rates could be varied independently in either source with unmeasurably small effects on the plasma parameters in the other source. The potential between the anodes of the two sources was determined by U_0, which was also taken as the difference in the plasma potentials in the sources. This assumption was tested several times during the course of the experiments using collecting probes in the sources to measure the potentials there and was found to be satisfied within the accuracy with which the potentials could be determined from the probe characteristics, or about ± 0.5 volt, over a variation of U_0 by more than 200 volts. Plasma diffused into the central chamber from the sources through apertures A1 and A2 in the end plates of the central chamber. These apertures determined the diameter of the plasma column (3.0 cm) which was radially confined by a homogeneous magnetic field of up to 20 mT. Because of the small diameter of the apertures compared to the diffusion pump (25 cm), it was possible to maintain sufficient pressure in the sources for their proper operation (10 to 100 mPa) while restricting the pressure in the central chamber to about 1 mPa, thereby minimizing the importance of ionizing processes in the chamber. It is this property that allows the production of very strong double layers (potential drops up to 3 kV) in this device (Torvén, 1982).

Electric potentials were measured with electron emitting probes which could be moved both radially and axially with electric motors. For low frequency measurements (from d.c. up to about 10 kHz), the probes were operated essentially at their floating potential, which was measured using 100 mohm frequency-compensated voltage dividers. For a.c. signals which are not too large (cf. Torvén et al., 1985), the frequency response of the probe is determined by the product of the dynamic resistance of the plasma near the floating potential and the distributed capacitance of the probe and its heating circuit. This capacitance (about 100 pf) is dominated by the capacitance to ground of the feed wires to the movable probe inside the vacuum chamber. The dynamic resistance of the plasma, defined as the reciprocal of the slope of the probe characteristic, depends on the plasma density and the probe wire temperature. For the present experiment it was on the order of 10 kohm.

III. DISRUPTIONS WITH AN INDUCTIVE EXTERNAL CIRCUIT

When an inductor of sufficient size is placed in series with the bias source U_0, it is observed that periodic disruptions of the plasma current and of the double layer potential occur. These disruptions have been previously reported in detail (Torvén et al., 1985) and we review here only those aspects pertinent to the present work.

Figure 2 shows an example of the disruptions when the inductance was 0.1 Hy. The top oscilloscope trace shows that the potential measured on the positive source varied from zero to 400 volts. For these runs U_0 was 100 volts so there was a 300-volt inductive overvoltage. This overvoltage was given exactly by L dI/dt, where I is the current flowing through the inductor. This current is shown by the bottom trace in Figure 2. The other traces are of potentials measured by probes at fixed positions in the plasma and show that the potential drop does occur over a limited spatial region, that is, in a double layer.

The disruptions are thus seen to be completely explained in terms of variations in the plasma current. The plasma current, in turn, is controlled by the potential structure between the two sources. Figure 3 shows the potential measured in the low potential region for various times during the disruption cycle. There is clearly qualitative agreement between the minimum value of the potential, which should be the only feature of the potential structure that influences the plasma current, and the plasma current. To test the quantitative sufficiency of this mechanism, a series of experiments were performed with the inductance removed and with U_0 varied slowly over the voltage range of interest. Preliminary reports of these results have appeared (Carpenter and Torvén, 1984; Carpenter et al., 1984), and a detailed account will appear (Carpenter and Torvén, 1986), but we will review the pertinent results here.

To obtain I-V characteristics of the device, the potential U_0 between the sources was slowly varied, either by hand or by using a function generator to control the power supply with voltage-control programming, and the resulting plasma current measured using precision 1 ohm shunts. The data were taken using a calibrated X-Y plotter, or a calibrated two-parameter transient digitizer. The emitting probes were used to measure both axial and radial potential profiles for different values of U_0. An example of the axial potential structure observed between the sources is shown in Figure 4. For these data U_0 was 150 volts. A minimum in the potential is clearly seen at about 15 cm from the left aperture. That the minimum is in fact quite well defined is seen more clearly with the expanded scale. The magnitude of the minimum potential, V_m, was determined for values of U_0 between zero and 200 volts. For details of how this was accomplished see Carpenter and Torvén (1986). An example of such a measurement is shown in the lower half of Figure 5. The corresponding I-V characteristic is shown as the solid curve in the upper half of this figure.

The purpose of these measurements, as mentioned above, was to test whether or not the variations in V_m could quantitatively explain the variations in the plasma current. For purposes of this discussion, consider only the case where the right source is biased positive with respect to the left source. Plasma from both sources diffuses into the central chamber. Since a potential minimum exists between the sources, the ion flow will not be affected, but the electron current between the sources will be reduced because of reflection of electrons from both sources by an amount that depends only on the differences between the minimum potential V_m and the plasma potentials in the sources. These potential differences can be obtained from the data, and the I-V characteristics can accordingly be calculated if the electron distribution functions are known.

Assume that the plasmas in the sources are Maxwellian with temperatures T_p and T_n and densities n_p and n_n, where the subscripts p and n refer to the positive and negative sources, respectively. These symbols refer to the electrons only. (Ion currents can be easily included, but they contribute much less than 1 percent of the total current and so are ignored in order to simplify the notation.) Then the distribution function at a point where the potential is $V(x)$ is generally given by

$$f(x,v) = n_0 \left(\frac{2m}{\pi kT}\right)^{\frac{1}{2}} \exp\left[-\frac{mv^2}{2kT} - \frac{e(V_0 - V(x))}{kT}\right] \quad \text{for} \quad a < v < \infty$$

$$= 0 \quad \text{for velocities outside this range} \quad .$$

(1)

Here n_0 is the plasma density at a point where the potential is V_0, e is the magnitude of the electronic charge, m is the electron mass, and k is the Boltzman constant. The lower velocity limit a is negative for points between the source and the minimum, since reflected electrons exist in this region, and positive for points beyond the minimum. It is exactly zero at the minimum, so the lower limit is the velocity such that the energy, which is constant, is just equal to V_m. Thus,

$$a = \pm \left\{\left(\frac{2e}{m_e}\right) \left[V(x) - V_m\right]\right\}^{\frac{1}{2}} \quad .$$

(2)

The current is of course independent of the point x where it is evaluated. However, it is convenient to evaluate the contributions to the total current from each source at the position of the potential minimum, since at this point the distribution functions take on their simplest forms. The result is

$$I = Ae \left\{\left(\frac{2k}{\pi m_e}\right)^{\frac{1}{2}} \left[n_n T_{en}^{\frac{1}{2}} \exp\left(-\frac{V_n - V_m}{kT_{en}}\right) - n_p T_{ep}^{\frac{1}{2}} \exp\left(-\frac{V_p - V_m}{kT_{ep}}\right)\right]\right.$$

$$\left. + \left(\frac{2k}{\pi m_i}\right)^{\frac{1}{2}} \left[n_p T_{ip}^{\frac{1}{2}} \exp\left(-\frac{V_p - V_n}{kT_{in}}\right)\right]\right\} \quad .$$

(3)

Here V_p and V_n are the plasma potentials in the sources and the other quantities have been defined previously. As the applied voltage U_0 is increased, the current increases at first because of the decrease in the magnitude of the second term. That is, V_p approximately follows U_0 and V_n stays approximately at ground. After U_0 increases to several times kT_p, the second term will become negligible, and further changes in I can only occur if V_m changes relative to V_n.

In order to test the sufficiency of this picture, we have used the measured variation of V_m with U_0 and determined the values of the temperatures and densities that best fit the data with equation (3). That is, the value of V_m observed at $U_0 = V_p - V_n$ is used in equation (3) to calculate I_{fit} and the results compared with the corresponding observed currents I_{exp}. The parameters in equation (3) are varied in order to minimize the sum

$$\psi = \sum (I_{exp} - I_{fit})^2 \quad . \tag{4}$$

The result of a typical fit is shown by the dashed line in the upper part of Figure 5. The main features of the data are certainly rather well explained. However, the temperatures that give acceptable fits are larger than those observed with probes in the sources. For example, the temperatures that give the fit shown in Figure 5 are 12.3 eV for the left source and 21.5 eV for the right source. Measured values for the temperatures were about 8 eV in both sources. However, the probe characteristics showed high energy tails of the type usually seen in discharge sources corresponding to a significant population of ionizing electrons. If distributions corresponding to such electrons were included in the model, the best-fit temperatures of the Maxwellian populations would certainly be reduced. However, the number of parameters to be fit would be doubled, thereby reducing the significance of the small improvement in the fit that might be expected. It is felt that the appropriateness of the model has been adequately demonstrated without this refinement. Data were taken and fits performed in the manner described for 12 different combinations of source parameters, such that the plasma density in both sources varied by an order of magnitude. No unusual characteristics were observed and the fits obtained were in all cases comparable to that described above.

The model can also be used to provide some insight into the role of the potential minimum and its behavior. The basic feature of the region of space below the double layer is its charge neutrality. That is, even though there are variations in the potential here, they occur over many hundreds, even thousands, of Debye lengths, so the departure of the ratio of electron-to-ion densities from unity is expected to be vanishingly small. Therefore, since the electron and ion charge densities depend in different ways on the voltage applied between the sources, some self-adjusting potential is needed between the sources in order to keep the region quasineutral. Mathematically, the requirement that the net charge density at the minimum be zero will insure quasineutrality over a broad region near this point. The electron densities were obtained by integrating the distribution functions given in equation (1) over the appropriate velocity intervals. The ion densities were obtained in a similar way. The form of the distribution functions was the same, but the velocity intervals were different since the ions were accelerated from the sources. The equation giving zero net charge at the minimum is

$$n_{ep} \exp\left(-\frac{V_p - V_m}{T_{ep}}\right) + n_{en} \exp\left(-\frac{V_n - V_m}{T_{en}}\right) = n_{if} \exp\left(\frac{V_p - V_m}{T_{ip}}\right)$$

$$\times \left[1 - \mathrm{erf}\left(\sqrt{\frac{V_p - V_m}{T_{ip}}}\right)\right] + n_{in} \exp\left(\frac{V_n - V_m}{T_{in}}\right)$$

$$\times \left[1 + \mathrm{erf}\left(\sqrt{\frac{V_p - V_m}{T_{in}}}\right) - 2\,\mathrm{erf}\left(\sqrt{\frac{V_n - V_m}{T_{in}}}\right)\right] \quad , \tag{5}$$

58

where the new subscripts i and e refer to the ions and electrons. This equation was solved by simply stepping V_m, in successively smaller steps each time zero was crossed, until the step size was smaller than the accuracy desired. The results are sensitive to the ion temperatures, about which we have little experimental information. Examples showing how V_m varies as $U_0 = V_p - V_n$ is changed are shown in Figure 6 for three different sets of ion temperatures. The plasma parameters used were typical of those observed experimentally in the two sources. It seems clear that a rather good fit to the experimental curve of V_m versus U_0 could be obtained by adjusting the ion parameters, with possibly some small adjustment of the electron parameters, but in view of the number of parameters involved and the fact that the charge exchange ions have been neglected, such an effort hardly appears justified. However, the agreement with the data of the trends shown in Figure 6 provides some confidence in the following explanation: As U_0 is first increased, the biggest change is the reduction in the number of electrons reaching the minimum region from the positive source. To compensate, the minimum becomes less negative so more electrons from the negative source are admitted. This continues until all electrons from the positive source are reflected. Competing with this effect is the reduction of ion density from the positive source due to increasing ion velocity as U_0 increases and when the electrons are eliminated, this effect becomes dominant. Thus, the minimum increases in depth to reduce the flow of electrons from the negative source. It is exactly this last process that gives rise to the negative resistance region according to this model.

The main features of the variation of V_m with U_0 are obviously rather well explained by these considerations, at least for cases where U_0 varies slowly with time. Thus, the negative-resistance region in the I-V characteristic is explained, and it can be said that the low frequency disruptions are understood. It should be emphasized that in order to observe disruptions of low enough frequency that this explanation applies without modification, additional lumped capacitance must be added in parallel with the distributed capacitance between the sources (Carpenter et al., 1984). At higher frequencies ion-transit times become significant and there is some delay in the charge neutrality condition that can be expected to affect V_m. Although these effects have not been included, it seems clear that careful consideration of the potential structure in the low potential region must be included in any complete theory of double layers.

IV. JITTER MOTION

When the potential indicated by the emissive probe is monitored by a device capable of following high frequency variations, such as an oscilloscope, it is observed that the signal fluctuates wildly when the probe is in the vicinity of the double layer. Observations as the probe moves through the double layer lead quickly to the conclusion that the fluctuations are due to the random motion of the entire potential structure around its equilibrium position. The effect is shown in Figure 7. These data were recorded by plotting single sweeps obtained with a transient digitizer on the same graph. Also shown is an overlay of the double layer obtained with an X-Y plotter during this run. The sweeps were obtained with the probe fixed at the three positions marked A, B, and C on the double layer. For all three sets of sweeps, horizontal lines are shown that correspond to the variation in potential which results when the double layer makes an excursion with a total extent of 1.2 cm centered at each of the three points. Clearly the various amplitudes of the fluctuations which are observed as the probe moves through the double layer are all explained by movements of the structure by a constant amount. Also evident in these data are regions where the potential changes with a constant slope for several microseconds. The velocity of the structure is apparently constant during these times. Since the double layer provides a convenient conversion factor — distance required for a given potential change — the velocity of the motion can be determined if we can determine the change in shape of the double layer (the calibration constant) as it undergoes its random motion.

The X-Y plotter provides a potential profile which is time-averaged over the rapid jitter motion. To obtain instantaneous profiles, a second stationary probe was mounted in the double layer slightly off-axis. The signal from

this probe provided a trigger which gated the output of the moving probe used to map the potential structure. The varying signal from the trigger probe corresponded to varying positions of the structure. Thus, different double layer positions could be selected by choosing different trigger levels. Data obtained with three different levels are shown in Figure 8. If any of the curves is displaced horizontally, it is seen to closely overlap the other two curves. We conclude that the double layer moves with little, if any, change in shape. Another interesting implication of this result should be mentioned. The fact that double layer shapes that have been previously reported are time averages has been invoked by some authors to explain the apparent broadness of laboratory double layers. However, the widths of the instantaneous profiles reported here, defined for example as the distance required for a change from 10 percent to 90 percent of the full height, are not significantly different from those obtained with an X-Y plotter. This is the expected result if the structure between the 10 percent and 90 percent points was a straight line, the velocity was constant, and the maximum excursion was equal to the double layer width, which seems to be approximately the case.

The data in Figure 7 indicate that motion toward the negative source, corresponding to an increasing potential, occurs with a higher velocity than motion toward the positive source. However, this apparent difference is entirely due to experimental effects associated with the distributed capacitance of the emissive probe to ground. This was first suspected when it was noticed that the apparent difference was reduced when the emissive probe was shunted with an external resistor. The distributed capacitance can easily be charged more positively by simply emitting electrons. However, to become more negative it must collect electrons and it has insufficient area to do this rapidly enough. Put another way, the time response of the probe is determined by its RC time constant, where C is the distributed capacitance and R is the dynamic resistance of the plasma, defined as the reciprocal of the slope of the probe's I-V characteristic. The distributed capacitance is on the order of 100 pF and the dynamic resistance of the probe normally is on the order of 10 kohms. Thus, RC is on the order of 1 microsecond and the probe can respond to changes on the order of 1 MHz. However, when the probe is collecting electron saturation current, which would happen if the plasma potential suddenly dropped, the dynamic resistance is on the order of a few megohms, giving RC on the order of a tenth of a millisecond.

In order to overcome this effect, a special emissive probe was constructed in which the heating circuit, which contributed almost all of the distributed capacitance, was mechanically disconnected from the potential measuring circuit during the measurement time. The distributed capacitance during the measuring time was reduced to 10 pF which gives an RC value of 10 microseconds even in the worse case. Some traces of the fluctuating potential taken with this probe are shown in Figure 9. There is still a slight difference between the maximum rates of increase and decrease, but it is small enough that it can be explained as a residual effect of the distributed capacitance of the probe. The details of this probe and a further discussion of the effect of distributed capacitance on probe measurements will appear elsewhere (Torvén, private communication, 1986).

The maximum rates of increase and decrease shown by overdrawn lines in Figure 8 are 36 and 24 volts per microsecond, respectively. The central portion of the double layer observed for this case had a slope of 50 volts per centimeter. Thus, the indicated velocities are 7.2 and 4.8 $\times$ 10^5 cm/s. As a comparison, the electron temperature observed for this run was 7 eV so the ion-acoustic speed was 4.1 $\times$ 10^5 cm/s.

Fluctuations are observed also in double layers formed in Q machines (Iizuka et al., 1983; Sato et al., 1981). In the case of double-ended operation, the mode most comparable to the triple plasma machine, nearly stationary double layers are observed. The fluctuation consists of a more or less periodic variation of the slope of the double layer with the knee at the high potential side remaining approximately fixed. Thus, the knee at the low potential side shows a sort of roughly periodic motion which has been termed a "foot-point oscillation."

V. INITIAL FORMATION

In order to study the initial formation of the double layer, U_0 was replaced by a transistor-switched power source capable of supplying 100 volts with a rise time on the order of 1 microsecond. Standard boxcar sampling techniques were then used to measure the potential structure at various times after the bias voltage was switched on. Typical results are shown in Figure 10. There is a small structure near the low potential source that seems to propagate toward the high potential source, but the striking feature of the potential structure is that at early times the slope is essentially a constant. As time progresses the slope steepens in the vicinity of the place where the double layer will eventually form while it flattens in regions above and below this. The structure is nearly formed after 50 microseconds and completely formed after 100 microseconds. If one wants to think of the low potential foot-point as propagating toward the high potential source, then its velocity of propagation is about 50 cm in say 100 microseconds or 5 × 10⁵ cm/s, a speed which is somewhat supersonic and which seems to be typical of the propagation velocity of the double layers in this device.

The initial formation of double layers has also been studied in a double-ended Q machine (Iizuka et al., 1983). In this work it was observed that immediately following the application of the bias voltage the potential rose to the positive source potential over nearly all of the column, forming an ion-rich sheath near the cathode. This condition persisted for about 100 microseconds, after which the double layer detached itself from the cathode and propagated, as a completely formed structure, toward its final position. The velocity of propagation was approximately 3 times the ion-sound speed.

It has been suggested that the motion of laboratory double layers represents a sort of "hunting" for that position where the Langmuir criterion (the square of the electron-to-ion current ratio equals the ion-to-electron mass ratio) is satisfied (Iizuka et al., 1983; Torvén, 1982). The basis for this explanation is that the ion flux at the double layer should decrease as the length of the high potential region increases because of radial losses of ions along the part of the column at high potential. It should be expected, then, that the larger these losses are, the smaller should be the excursions from the equilibrium position. This may explain why the double layers seen with relatively weak magnetic fields are more stable than those seen in the Q machines. It may also explain the lack of stability of double layers seen in simulations where the use of periodic boundary conditions at the sides is equivalent to the total removal of radial ion losses. In order to investigate this question, a systematic investigation should be made of the motion of double layers as a function of the strength of the magnetic field and the planarity of the plasma column.

REFERENCES

Carpenter, R. T., and S. Torvén, *Proc. Int. Conf. on Plas. Phys.*, Lausanne, P14-3, 1984.

Carpenter, R. T., S. Torvén and L. Lindberg, in *Second Symposium on Double Layers and Related Topics*, edited by R. Schrittwieser and G. Eder, p. 159, University of Innsbruck, 1984.

Carpenter, R. T., and S. Torvén, to be published, 1986.

Hershkowitz, N., *Space Sci. Rev., 41,* 351, (1985).

Izuka, S., P. Michelsen, J. Juul Rasmussen, R. Schrittwieser, R. Hatakeyama, K. Saeki, and N. Sato, Riso National Laboratory Report RISO-M-2414, 1983.

Sato, N., R. Hatakeyama, S. Iizuka, T. Mieno, K. Saeki, J. Juul Rasmussen, and P. Michelsen, *Phys. Rev. Lett., 46,* 1330 (1981).

Sato, N., R. Hatakeyama, S. Iizuka, T. Mieno, K. Saeki, J. Juul Rasmussen, P. Michelsen, and R. Schrittwieser, *J. Phys. Soc. Jpn., 52,* 875 (1983).

Torvén, S., *J. Phys. D., Appl. Phys., 15,* 1943 (1982).

Torvén, S., L. Lindberg, and R. T. Carpenter, *Plasma Phys., 27,* 143 (1985).
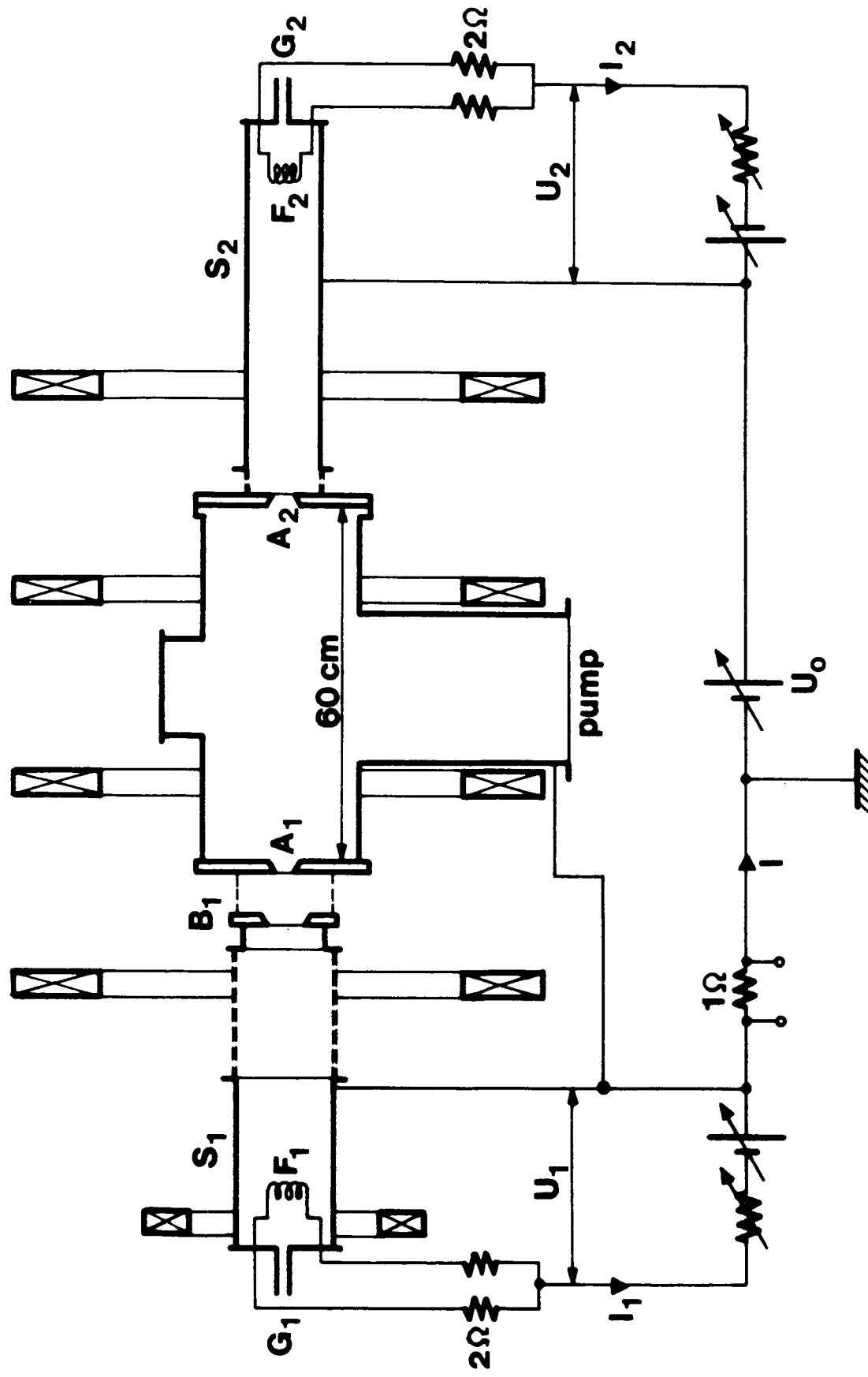
Figure 1. Schematic of the triple plasma machine.
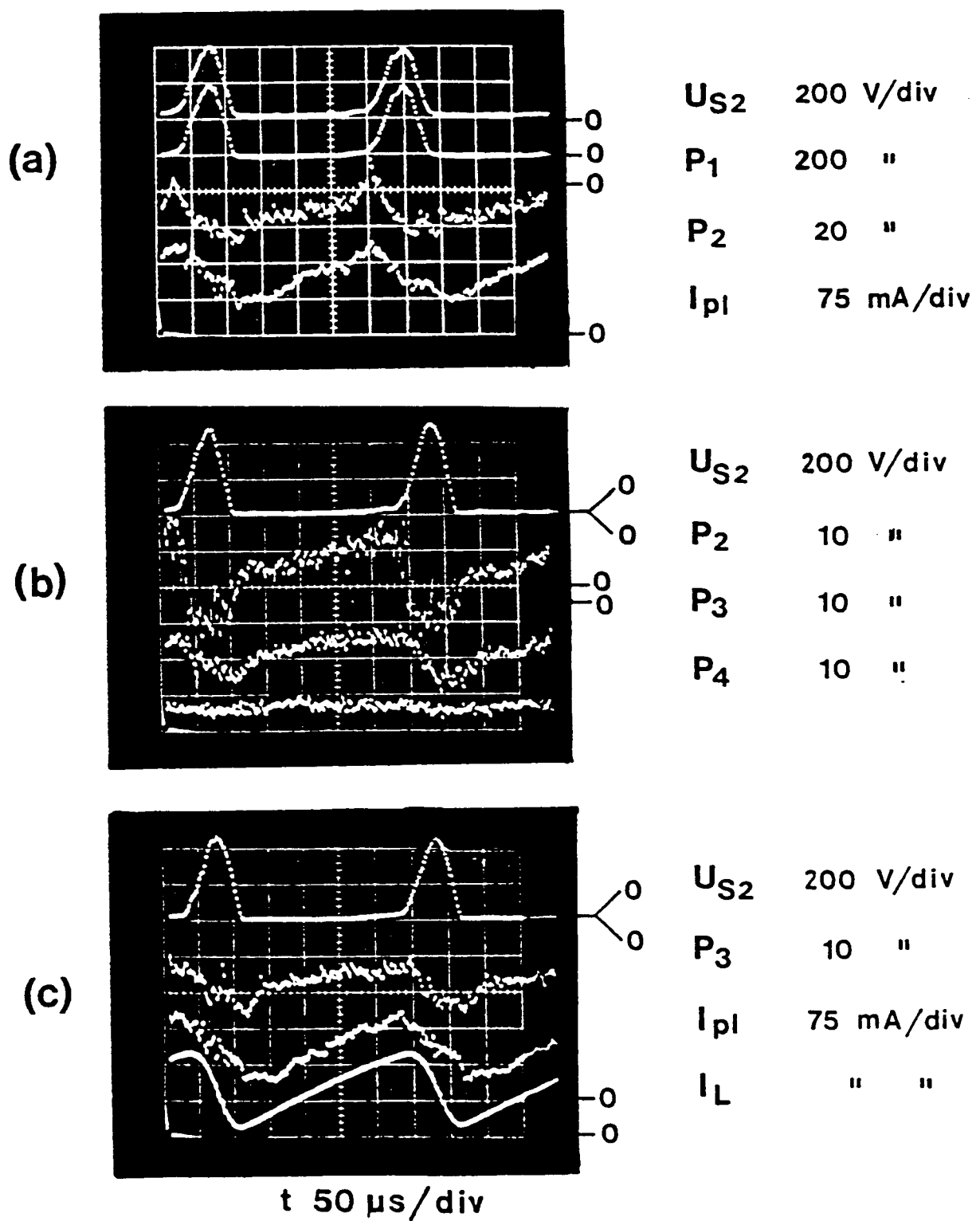
Figure 2. Oscilloscope traces during the disruptions. Probes P1, P2, P3, and P4 were located at 55, 45, 20 and 6 cm from aperture A1. The gain settings and zero levels are different for the various sweeps and are indicated to the right of each trace.
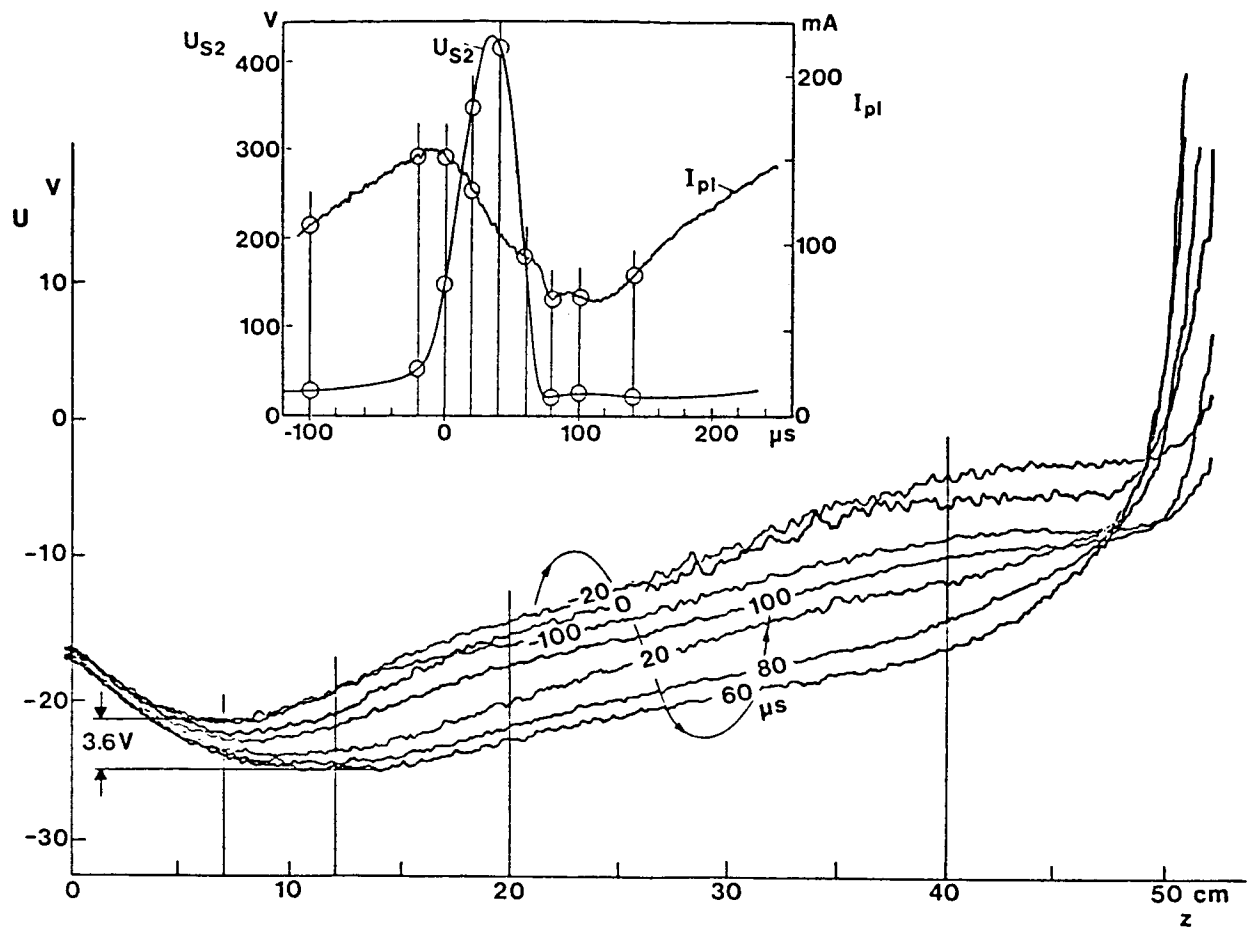
Figure 3. Potential structure in the low potential region sampled at various times, indicated by circles in the inset, during the disruption cycle. The serpentine line shows the timing sequence and the inset shows the time variation of the plasma current and the positive source potential.
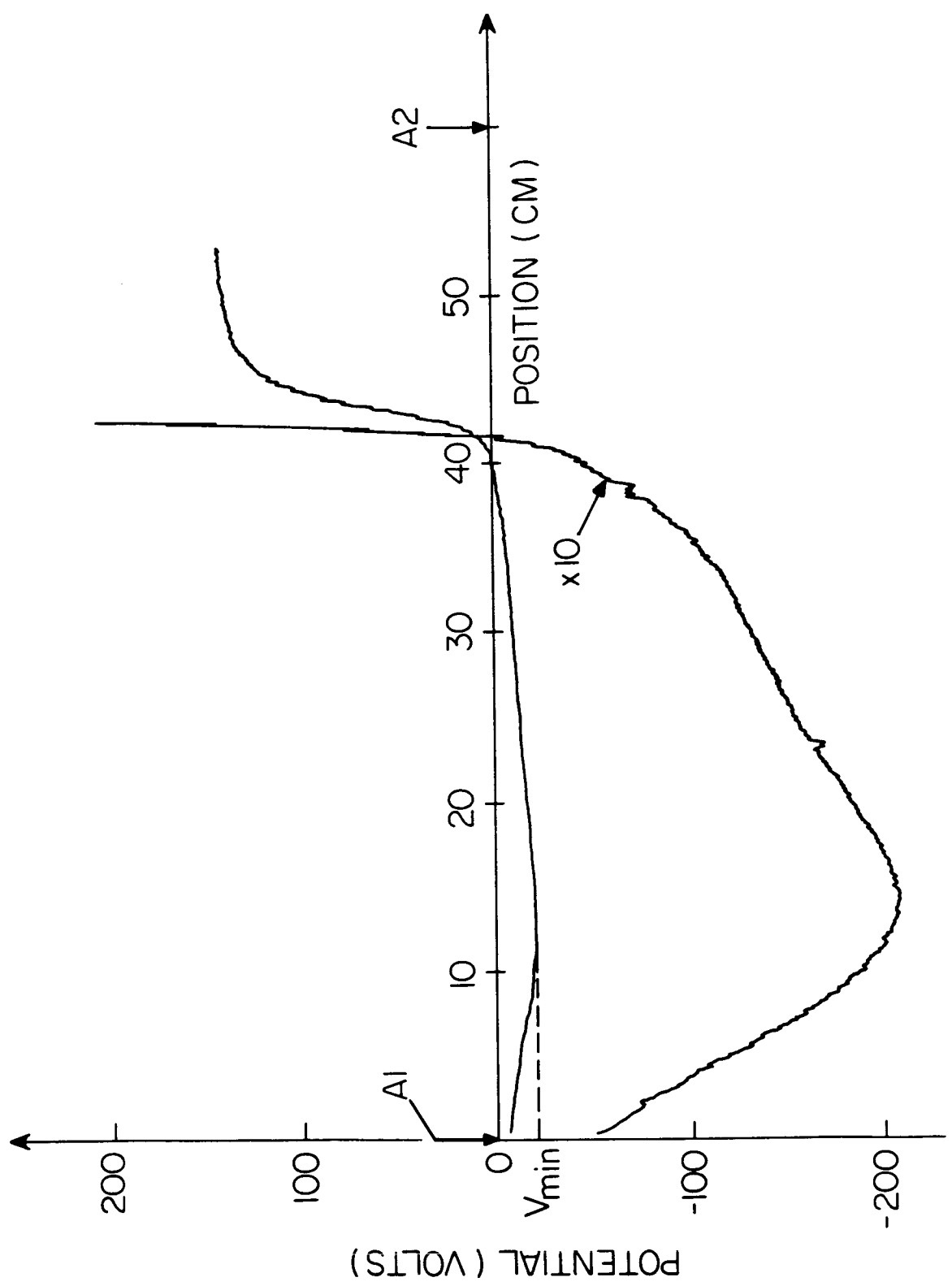
Figure 4. Steady state double layer showing the potential minimum in the low potential region.
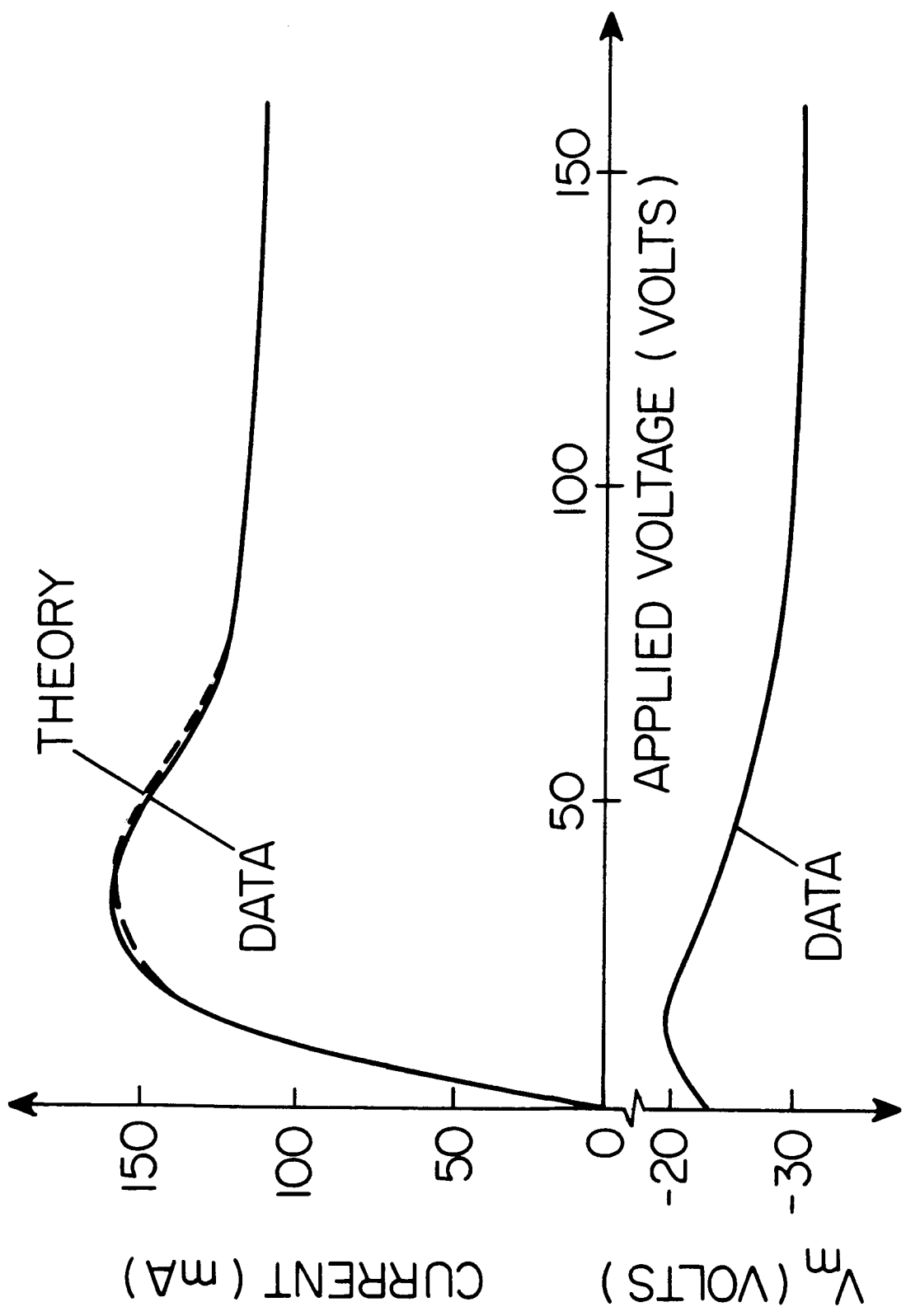
Figure 5. I-V characteristic for the double layer (upper curve) and the variation of the current-limiting minimum (lower curve). A fit to the I-V chracteristic, using the data in the lower curve and assuming Maxwellian distributions in the sources, is shown by the dashed curve.
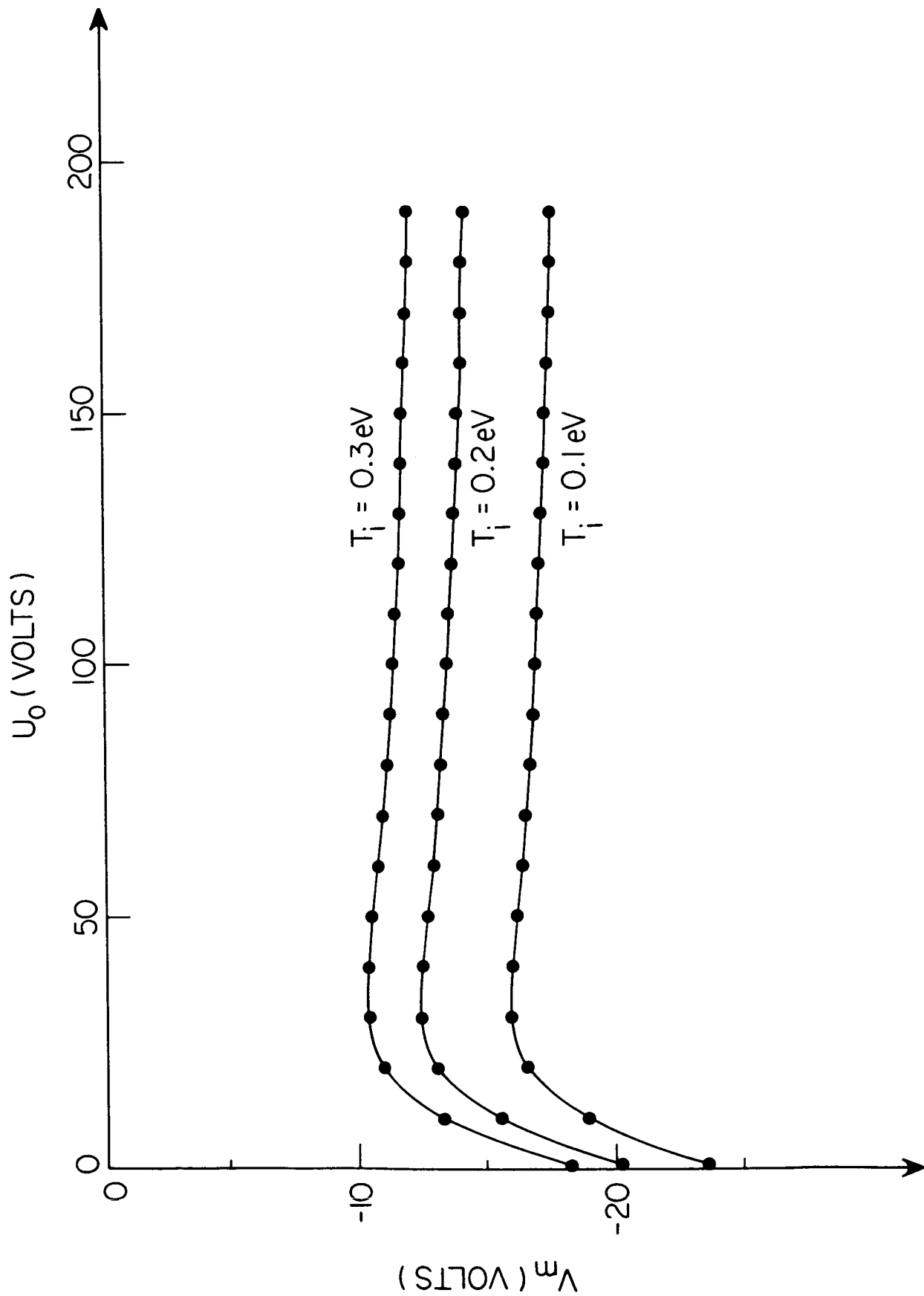
Figure 6. Examples of the calculated variation of the potential minimum V_m required to produce charge neutrality at the minimum. The ion temperatures were assumed to be the same in both sources.

68
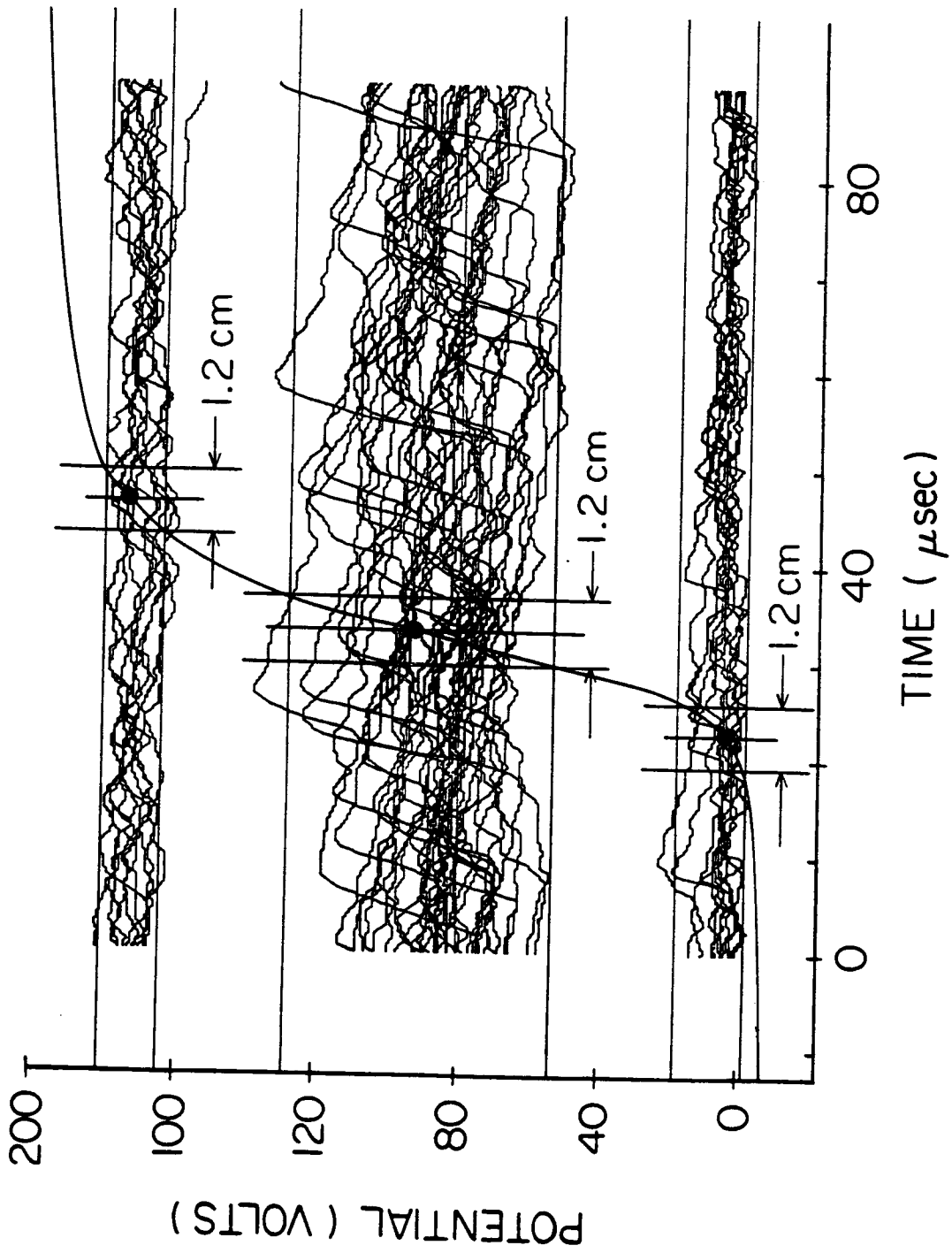
Figure 7. Oscilloscope traces, obtained with a digital transient recorder, of the potential indicated by an emissive probe when the probe was located at three different positions in the double layer. The positions chosen are shown on the overdrawn double layer which also shows potential variations corresponding to excursions in the double layer position by a total of 1.2 cm, centered at the indicated points.

69
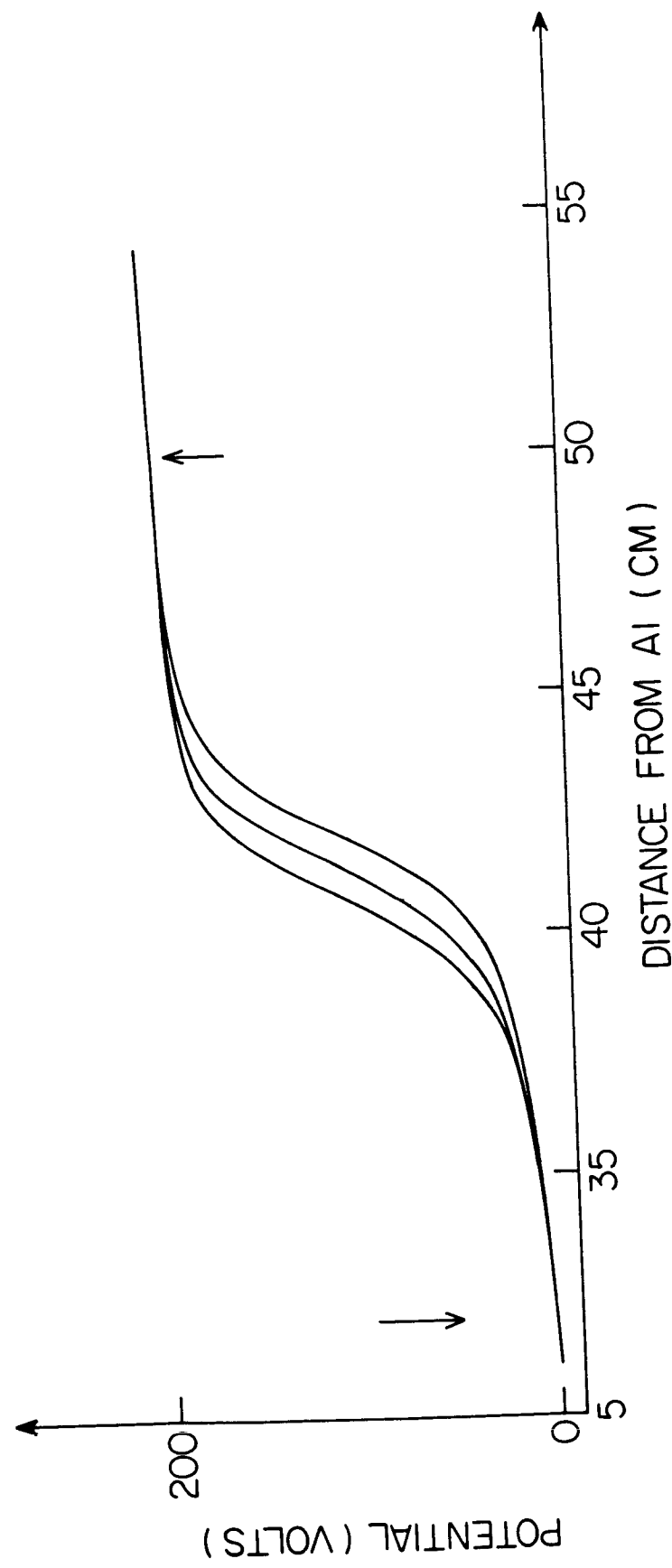
Figure 8. Potential structures obtained using a fixed probe to provide a gate, when the potential reached certain preset values, for the signal from the moving probe. Results for three different trigger levels are shown.
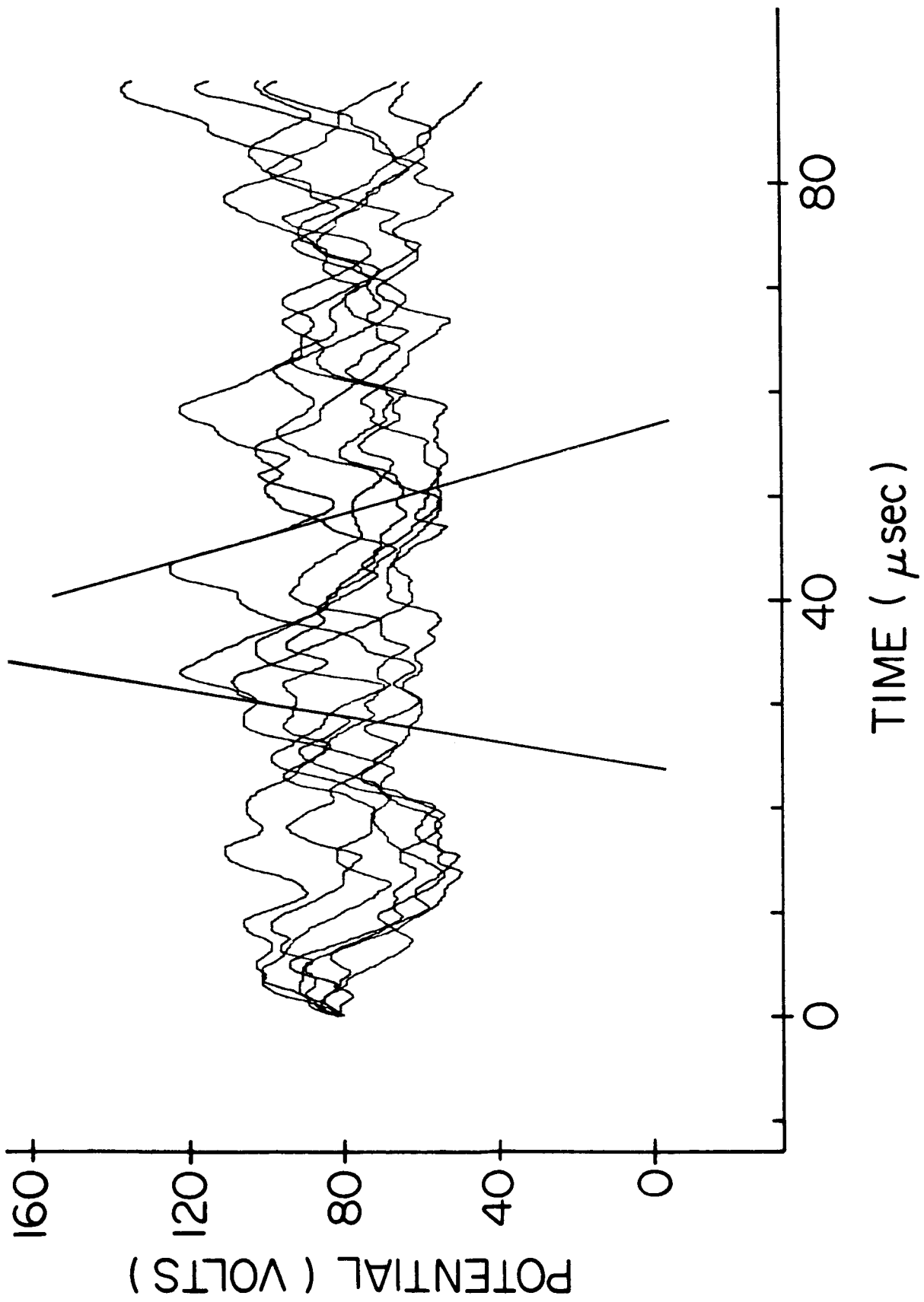
Figure 9. Oscilloscope traces similar to those shown in Figure 8 but taken with a probe with greatly reduced distributed capacitance.

71
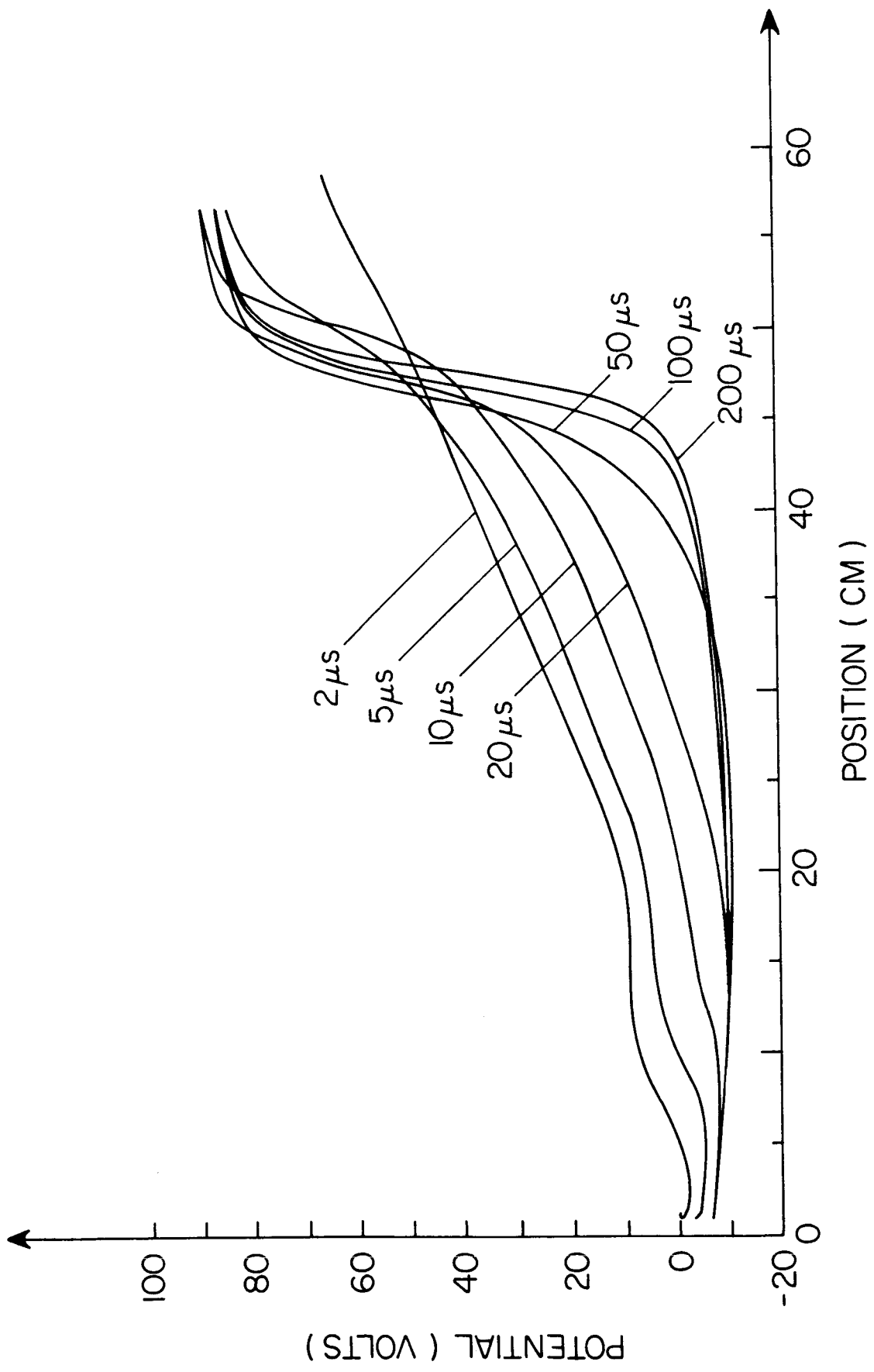
Figure 10. Measured potential structure at various times after the high voltage was switched on. The double layer forms quickly from an initial state where the structure is nearly that of a vacuum capacitor.

PUMPING POTENTIAL WELLS

N. Hershkowitz, C. Forest, E. Y. Wang,* and T. Intrator
Department of Nuclear Engineering
University of Wisconsin-Madison
Madison, Wisconsin 53706, U.S.A.

ABSTRACT

Nonmonotonic plasma potential structures are a common feature of many double layers and sheaths. Steady state plasma potential wells separating regions having different plasma potentials are often found in laboratory experiments. In order to exist, all such structures must find a solution to a common problem. Ions created by charge exchange or ionization in the region of the potential well are electrostatically confined and tend to accumulate and fill up the potential well. The increase in positive charge should eliminate the well. Nevertheless, steady state structures are found in which the wells do not fill up. This means that it is important to take into account processes which "pump" ions from the well. As examples of ion pumping of plasma wells, we consider potential dips in front of a positively biased electron collecting anode in a relatively cold, low density, multidipole plasma. Pumping is provided by ion leaks from the edges of the potential dip or by oscillating the applied potential. In the former case the two-dimensional character of the problem is shown to be important.

I. INTRODUCTION

A variety of experimental measurements of double layer and double layer related phenomena have demonstrated the presence of steady state plasma potential dips, at least in one dimension. Experiments range from glow discharge plasmas (Biborosch et al., 1984), to unmagnetized collisionless laboratory plasmas (Leung et al., 1980), to Q machine experiments (Sato et al., 1981), to fusion experiments (Hershkowitz, 1984). The general problem with all such structures is the question — what prevents the dip from filling up with ions either by charge exchange or by some kind of scattering? This problem has been identified as a key issue in maintaining "thermal barriers" in tandem mirrors (Baldwin and Logan, 1979) for which several techniques have been proposed for "pumping" out trapped ions. The only technique so far tested has been "neutral beam pumping" (Inutake et al., 1985; Grubb et al., 1984) — they use charge exchange of trapped ions on energetic neutral beams injected into the thermal barriers.

Although a dip may be present in one-dimensional data, it is not immediately apparent that ions are electrostatically confined in the dip in the perpendicular dimensions. Many structures have been found to have only minima in the potential in one dimension, while, in the other dimension the potential might be a relative maximum. In this case ions are not confined, pumping is not an issue, and potential variations in the perpendicular dimension can dominate the self-consistent solution to the problem. It is clear that the double layer is the wrong structure upon which to concentrate. This paper considers the problem of pumping steady state and slowly time varying potential dips in a multidipole laboratory plasma.

Representative double layers with dip structures that have been previously reported are shown in Figures 1 through 4. The data in Figure 1 (Coakley et al., 1978) were obtained in a triple plasma device for which $T_i = 0.2$ eV. The various steady state structures were obtained by varying the bias on a boundary grid on the low potential

---

*On leave from Southwestern Institute of Physics, Leshan, Sichuan, China.

side. Note that potential dips as deep as 5 V, equal to 25 T_i/e, were achieved. For these data the pumping mechanism was later identified to be ion leaks in the perpendicular dimension. Another example is a discharge tube double layer shown in Figure 2 (Maciel and Allen, 1984). Examination of the associated radial potential profile also showed that the potential minimum was a relative maximum in the perpendicular dimension and that ions could again leak out.

While the first two examples are ones for which the ions can easily leak out, the data shown in Figure 3 (Suzuki et al., 1984) give a different situation. In that case a double layer was found at a B field minimum in a magnetized plasma. Ions trapped in the dip had to cross the magnetic field. In addition it was also found that the dip was an absolute minimum in potential in the radial direction. As the neutral pressure was incresed to 7×10^{-6} from 10^{-7} Torr, the dip was substantially reduced and eventually disappeared (as seen in Figure 4) (Suzuki et al., 1984). The pumping mechanism of this dip is not yet understood, but it is possible that instabilities provided wave energy which energized the trapped ions or that trapped ions were lost to the diagnostic used to determine the dips presence.

II. EXPERIMENTAL RESULTS

Consider the potential near a positively biased plate (Forest and Hershkowitz, 1986). A copper plate, radius = 3 cm, coated with a ceramic insulator on the back side and support, was introduced into an argon plasma with plasma density $n = 10^8$ cm^{-3} and electron temperature $T_e = 3.5$ eV. The plate was biased to $+20$ V and the chamber walls were grounded. The plasma was produced in a conventional multidipole device (Leung et al., 1975).

The plasma potential measured with an emissive probe along the axis of the plate is given in Figure 5. Note that a potential dip equal to $\Delta\phi \approx 1.7$ V is found a distance d_{MIN} from the plate and that the potential far from the plate is only 3 V compared to the plate bias potential of 20 V.

We have also achieved a similar result (Wang et al., 1986) by looking at the potential on the axis of a set of parallel plates mounted in the same device. One was grounded and one biased to an oscillating potential at 100 kHz whose amplitude was approximately 12 V. The resulting plasma potential profiles at the maximum and minimum part of the cycle are shown in Figure 6. Note that once again a potential dip is also apparent in front of the positively biased electrode. In this case the backs of the plates were not insulated. The data shown in Figure 6 were taken using a new technique based on differentiated time-averaged emissive probe I-V characteristics which has been described elsewhere (Wang et al., 1986).

We can separate the interpretation of the results shown in Figures 5 and 6 into two issues. The first is the dip characteristics and the second is the question of why the dip does not fill in. Figure 7a shows that the size of the potential dip in Figure 5 scales linearly with electron temperature and is approximately equal to $T_e/2$. In Figure 7b it is also shown that the dip separation d_{MIN} from the plate decreases as the plasma density is increased. In Figure 8 we compare the dip separation to the predictions of the Child-Langmuir law and show that there is good agreement. This indicates that the self-consistent potential is established to make the electron loss from the plasma consistent with space charge limited emission as only electrons from the plasma are present near the front of the plate.

The question of why the dip does not fill in requires a look at the two-dimensional equipotential contours for a somewhat different case (shown in Figure 9) which also exhibits a dip (labeled 16). For that particular case, contours are apparent (indicated by $+4 \rightarrow +14$) which are negative with respect to the potential dip. These were identified as being associated with a fingerprint on the plate. These suggest that the presence of an insulator on the surface could provide the necessary ion leaks. A careful examination of the contours near a cleaned plate is given in Figure 10. The potential dip is still present. Note that the dip contours terminate on the edges of the plate at the insulator which coats the back of the plate. The pumping is clearly provided by these leaks. Note also that the contours are quite one-dimensional near the center of the plate and that the radius of the plate is equal to approximately 30 Debye lengths.

We investigated the spatial profile near the plate as a function of neutral pressure and found that the dip is reduced as the neutral pressure increased (as shown in Figure 11). This can be understood as the leaks out of the end of the dips not being able to keep up with the charge exchange filling of the dip.

We believe that ion pumping is a necessary condition for the presence of the dip. We can test this conjecture by removing the pumping from the system. For the static case, we removed the source of the pumping, i.e., the insulator from the back of the plate. This resulted in a very different plasma potential axial profile shown in Figure 12. These data correspond to the same conditions as those shown in Figure 5. The only difference is that the insulator on the back of the plates was not present for the data in Figure 12 but was present for the data in Figure 5. It is apparent that when pumping is not present, the plasma potential is everywhere more positive than the plate. This means that the self-consistent solution that the plasma finds is determined by the coating on the back of the plate, 30 Debye lengths from the center of the plate. This result strongly suggests that double layer potential profiles may be determined by the presence of, for example, an insulating boundary on the edge of the device. We demonstrated that the insulator must be in a location where it can pump the dip by removing the insulator from the plate while still locating it within the plasma volume. In this case the plasma potential also remained more positive than the plate.

The data shown in Figure 7 indicate that a similar potential dip can also occur in front of a capacitor plate during the part of the cycle that it is biased positively. However, in that case there is no problem with trapped ions because such ions empty out during the part of each cycle when the plate is negatively biased.

III. SUMMARY

We have shown that a plasma potential dip can exist in front of positively biased plates because of "ion pumping" of trapped ions from the dip. The dips were located in front of a steady state positively biased plate and also when the maximum positive bias was applied during an oscillating potential. Pumping was achieved by providing ion leaks, i.e., decreasing potential contours leading far from the structure that is usually measured, and indicates that boundary conditions far from the axes of experimental devices may play key roles in determining measured structures. A similar plasma potential structure was found when an oscillating potential was applied to a plate and no insulator was present. In that case ions were emptied from the dip by the time varying potential.

REFERENCES

Baldwin, D. E., and B. G. Logan, *Phys. Rev. Lett.*, *43*, 1318 (1979).

Biborosch, L., G. Popa, and M. Sanduloviciu, in *Second Symposium on Double Layers and Related Topics*, edited by R. Schrittwieser and G. Eder, p. 154, University of Innsbruck, 1984.

Coakley, P., N. Hershkowitz, R. Hubbard, and G. Joyce, *Phys. Rev. Lett.*, *40*, 230 (1978).

Forest, C., and N. Hershkowitz, *Journal of Applied Physics*, in press, (1986).

Grubb, D. P. S. et al., *Phys. Rev. Lett.*, *53*, 783 (1984).

Hershkowitz, N., in *Second Symposium on Double Layers and Related Topics*, edited by R. Schrittwieser and G. Eder, p. 55, University of Innsbruck, 1984.

Inutake, M. et al., *Phys. Rev. Lett.*, *55*, 939 (1985).

Leung, K. N., T. K. Samec, and A. Lamm, *Phys. Lett.*, A51, 490 (1975).

Leung, P., A. Y. Wong, and B. H. Quon, *Phys. Fluids*, *23*, 992 (1980).

Maciel, H. S., and J. E. Allen, in *Second Symposium on Double Layers and Related Topics*, edited by R. Schrittwieser and G. Eder, p. 218, University of Innsbruck, 1984.

Sato, N., R. Hatakeyama, S. Iizuka, T. Mieno, K. Saeki, J. Juul Rasmussen, and P. Michelsen, *Phys. Rev. Lett.*, *45*, 1330 (1981).

Suzuki, Y., R. Hatakeyama, and N. Sato, in *Second Symposium on Double Layers and Related Topics*, edited by R. Schrittwieser and G. Eder, p. 243, University of Innsbruck, 1984.

Wang, E. Y., N. Hershkowitz, T. Intrator, and C. Forest, *Rev. of Sci. Instrum.*, submitted, 1986.
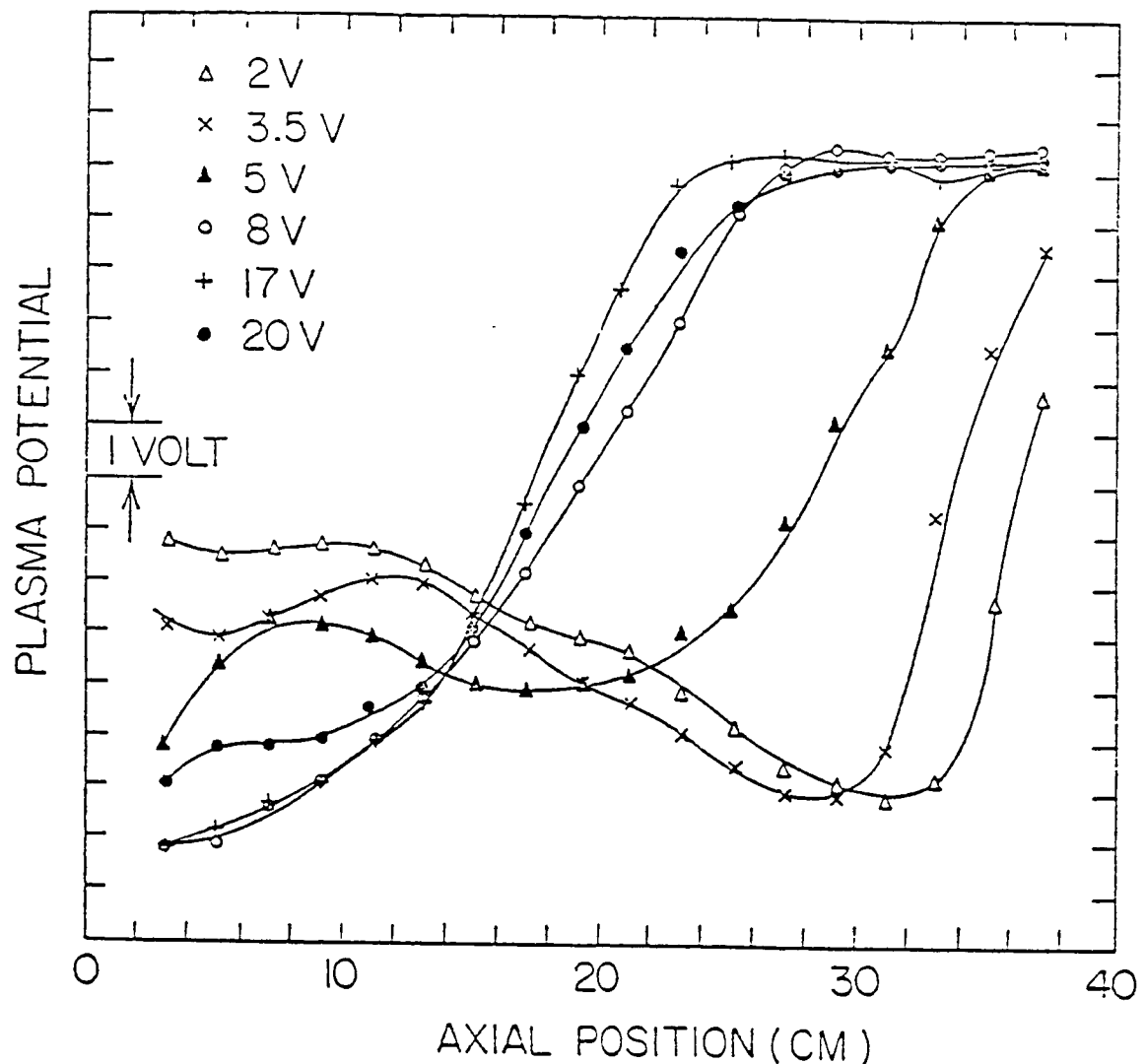
Figure 1. Stationary double layers showing potential dips on the low potential side. Axial potential profiles are given as a function of the bias of a grid on the low potential boundary. Multidipole double layers are apparent for bias voltages of 2-5 V. A bias voltage of 18 V was applied across the two source chambers.
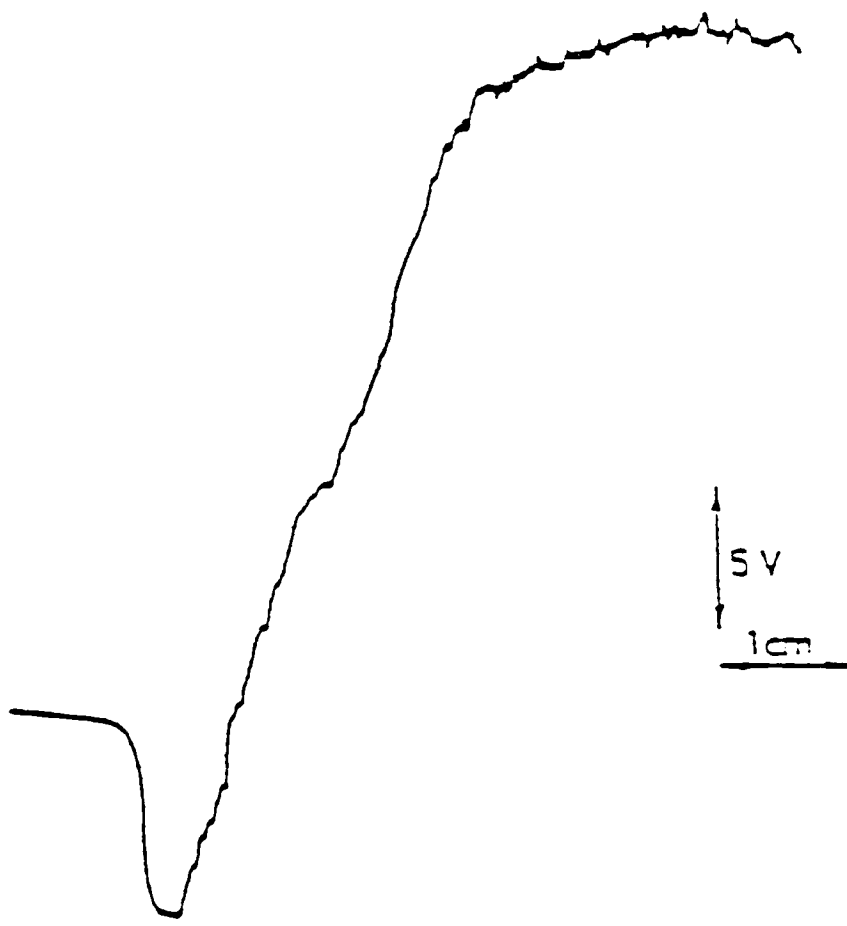
Figure 2. Triple layer axial potential profile obtained in a low pressure Hg arc discharge. This solution was identified to depend only on the boundary conditions; i.e., it was found to be a BGK solution.
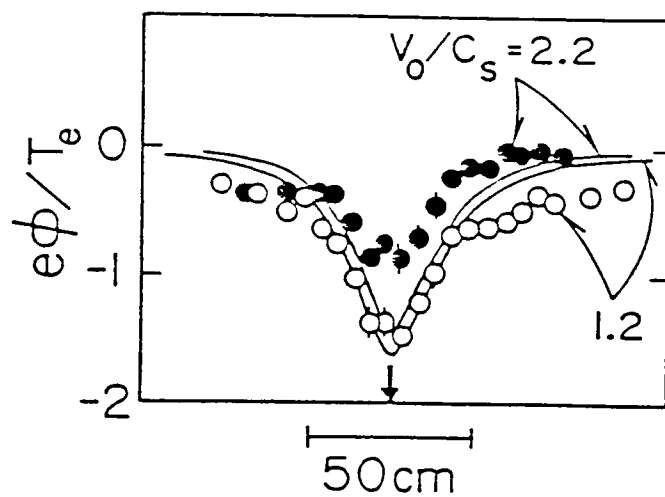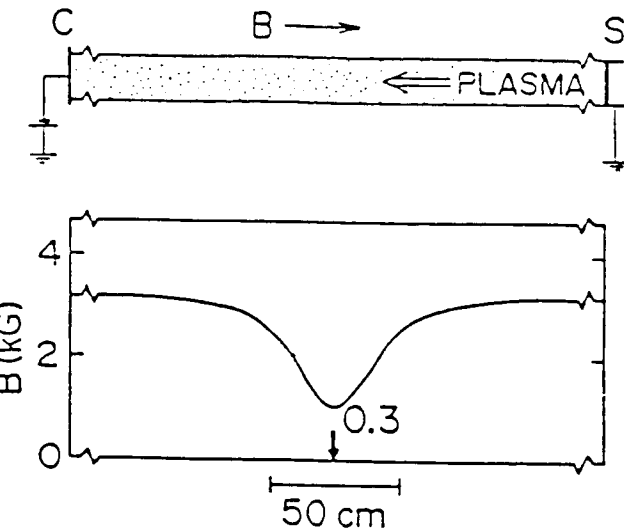
Figure 3. Schematic of the Q machine setup used by Suzuki et al. (1984) and the corresponding axial magnetic field profile. The axial potential profiles corresponding to two ion flow speeds are also shown.
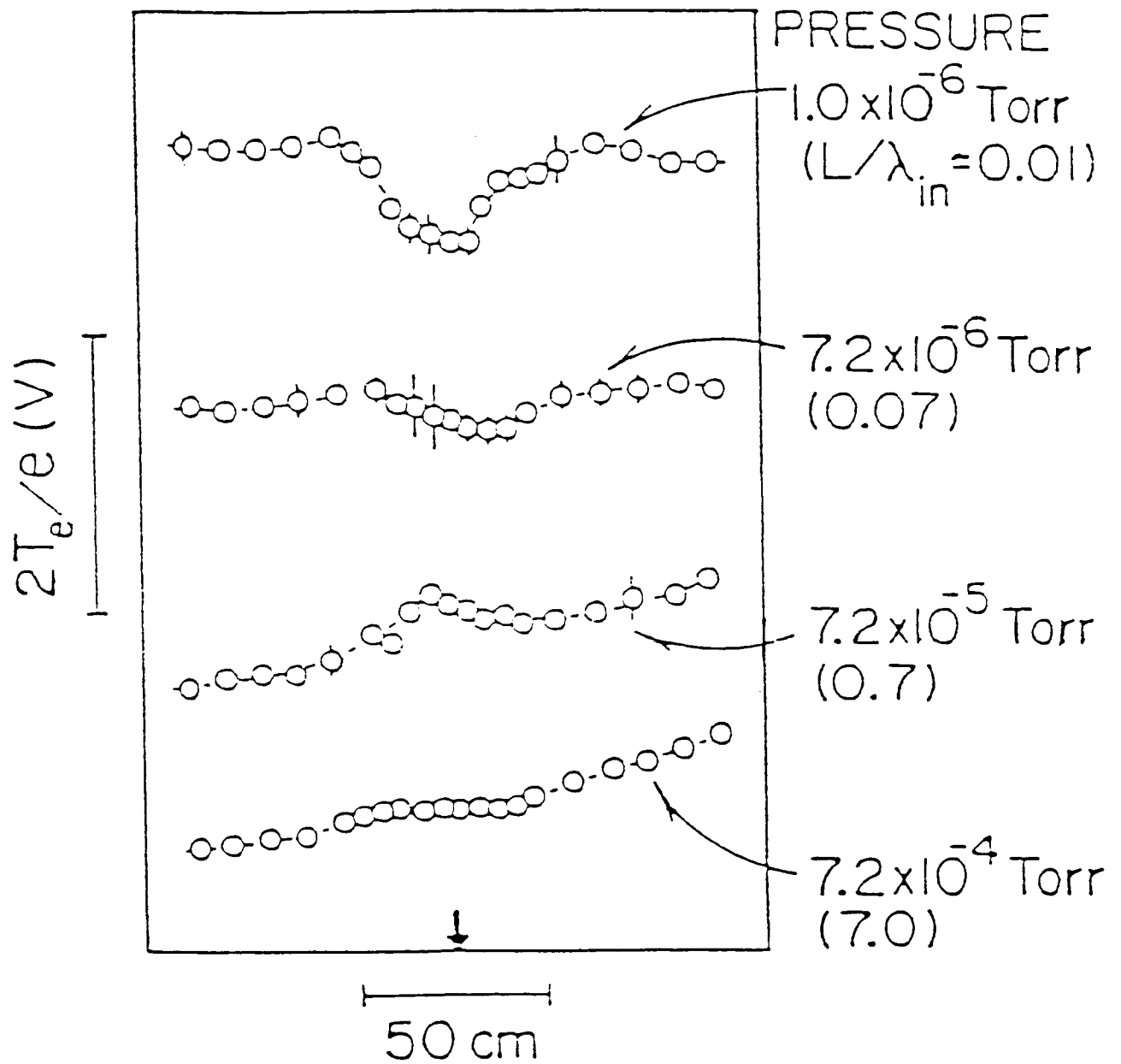
Figure 4. Axial potential profiles as a function of neutral gas pressure in the magnetic well (R_m = 0.3).
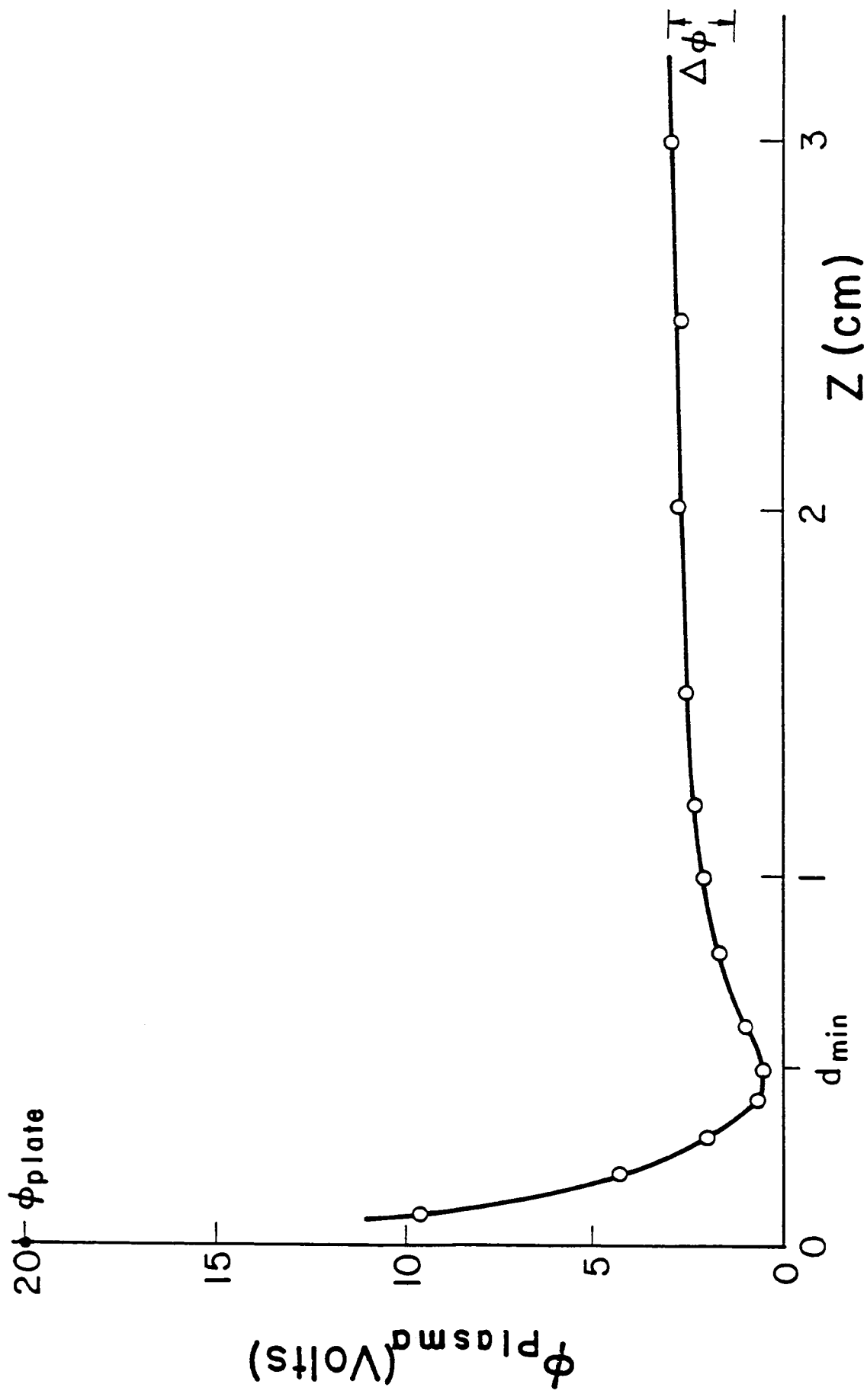
Figure 5. The plasma potential, measured with an emissive probe on-axis of a circular plate biased at + 20 V. The electron temperature was measured to be T_e = 3.5 eV.
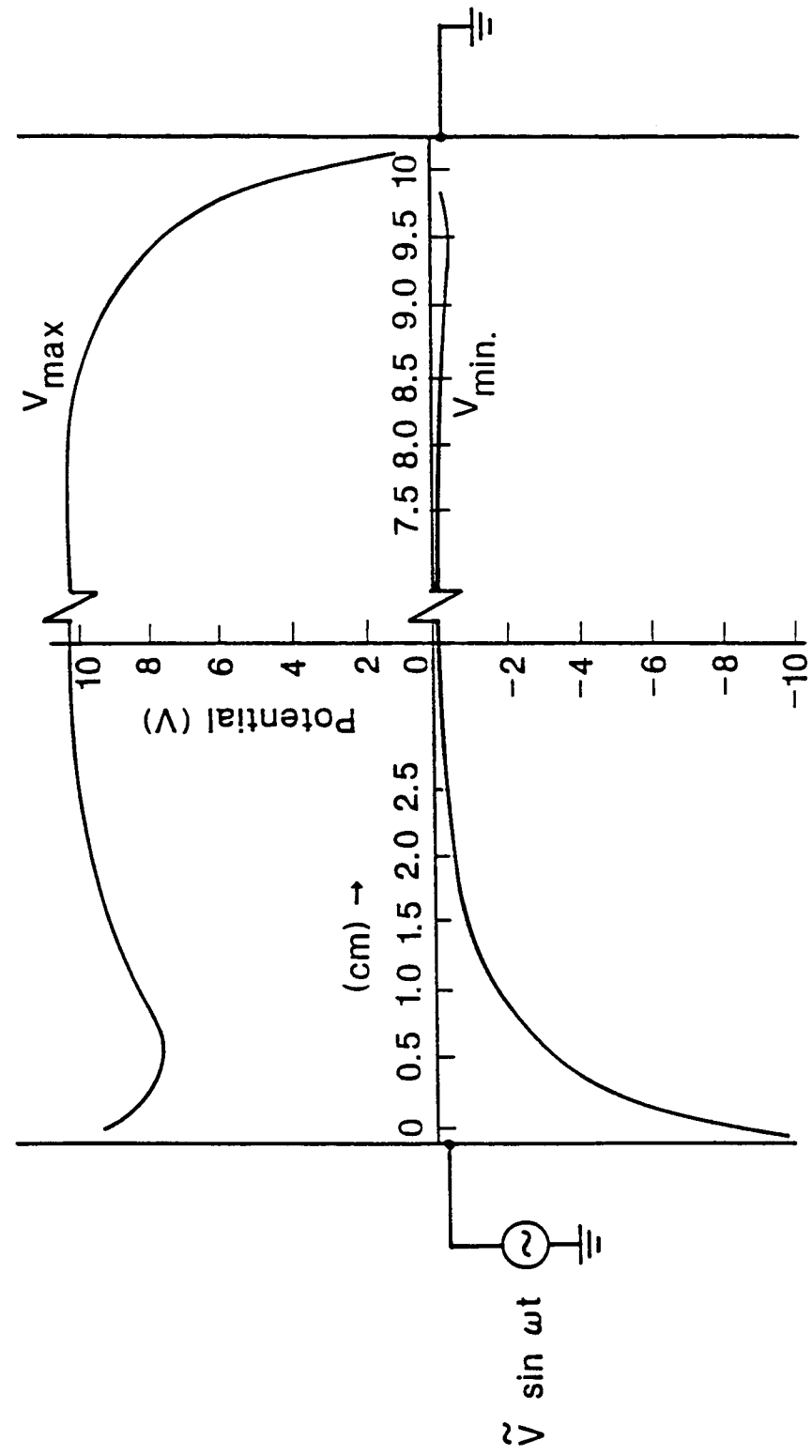
Figure 6. The maximum and minimum potential profiles between two parallel plates; a 100 kHz potential was applied between the plates. Data were obtained using emissive probes and a time-averaging method.
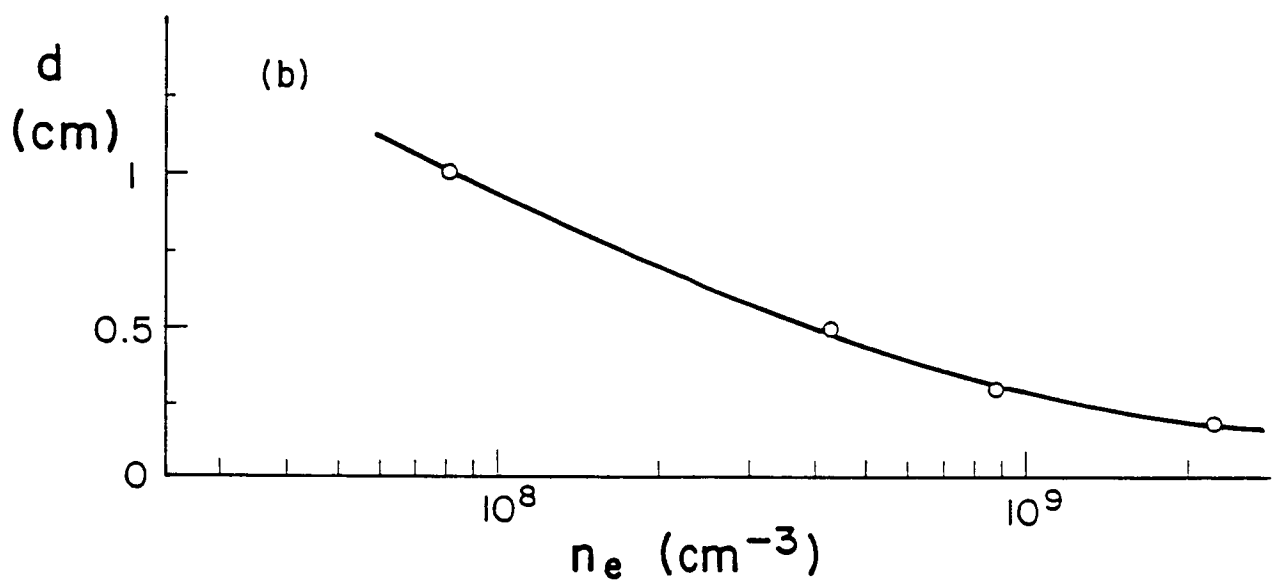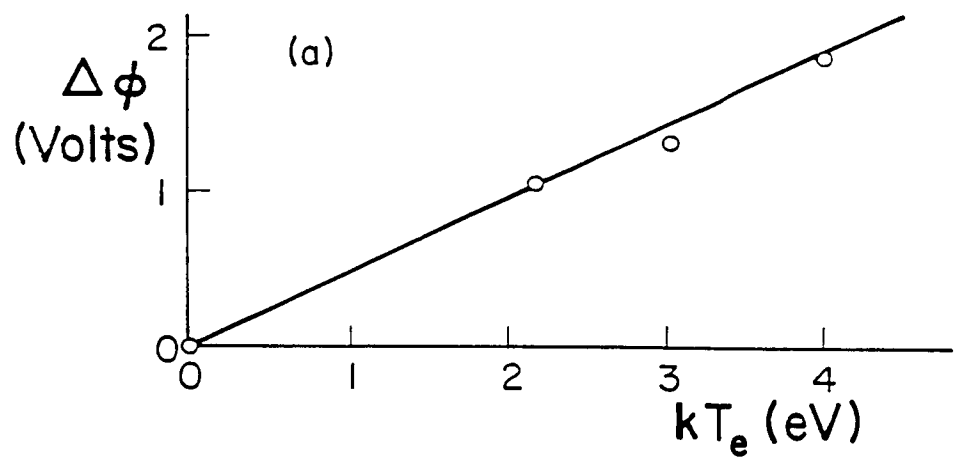
Figure 7. (a) The potential difference $\Delta\phi$ between the plasma and the inflection point of the dip, as a function of electron temperature. A straight line is drawn through the data. (b) The penetration of the dip (d) as a function of plassma density. A smooth curve is drawn through the data.
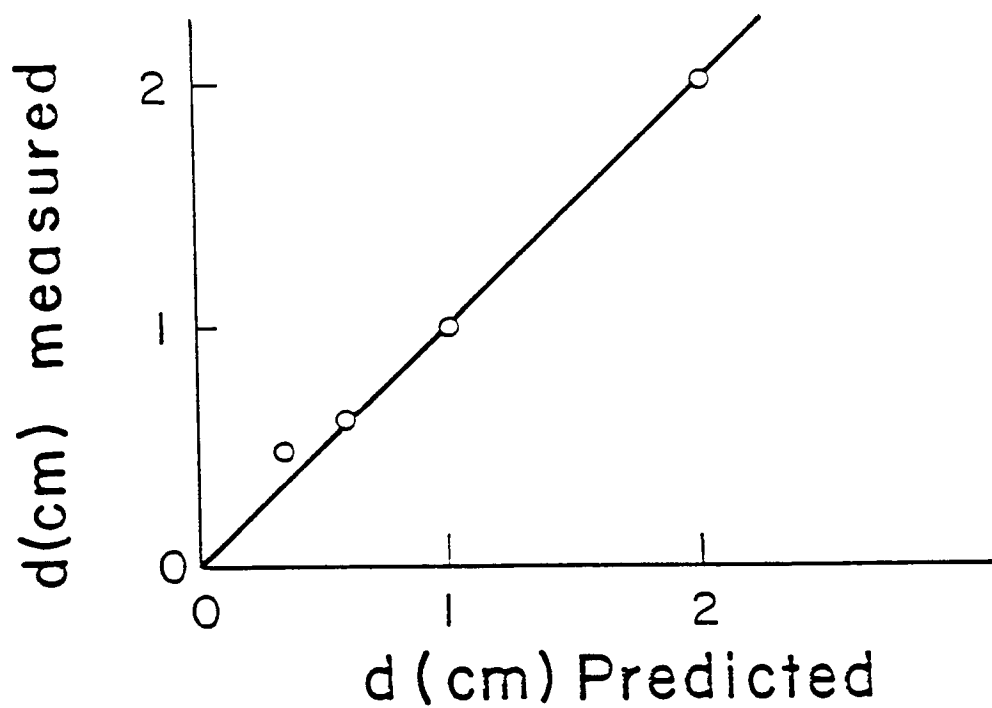
Figure 8. A comparison between measured values of d_{min} and values predicted by using space charge limited electron flow to the plate.
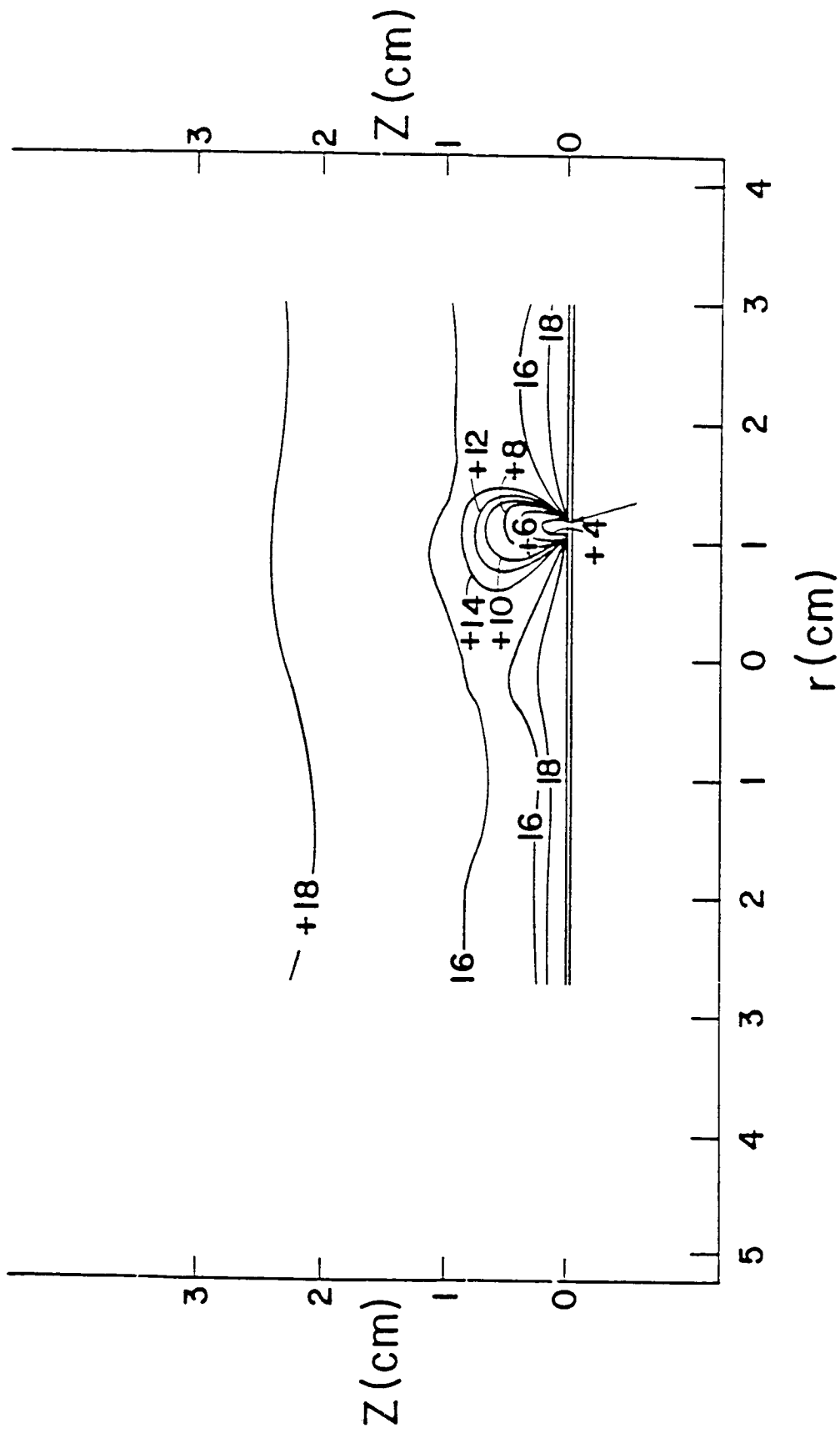
Figure 9. The equipotential contours near a circular brass plate (r = 3.5 cm, 2 mm thick). Note the contours near a grease fingerprint (labeled by the arrow). The plate is in the center of the multidi-pole soup pot device, 10 cm from one end.
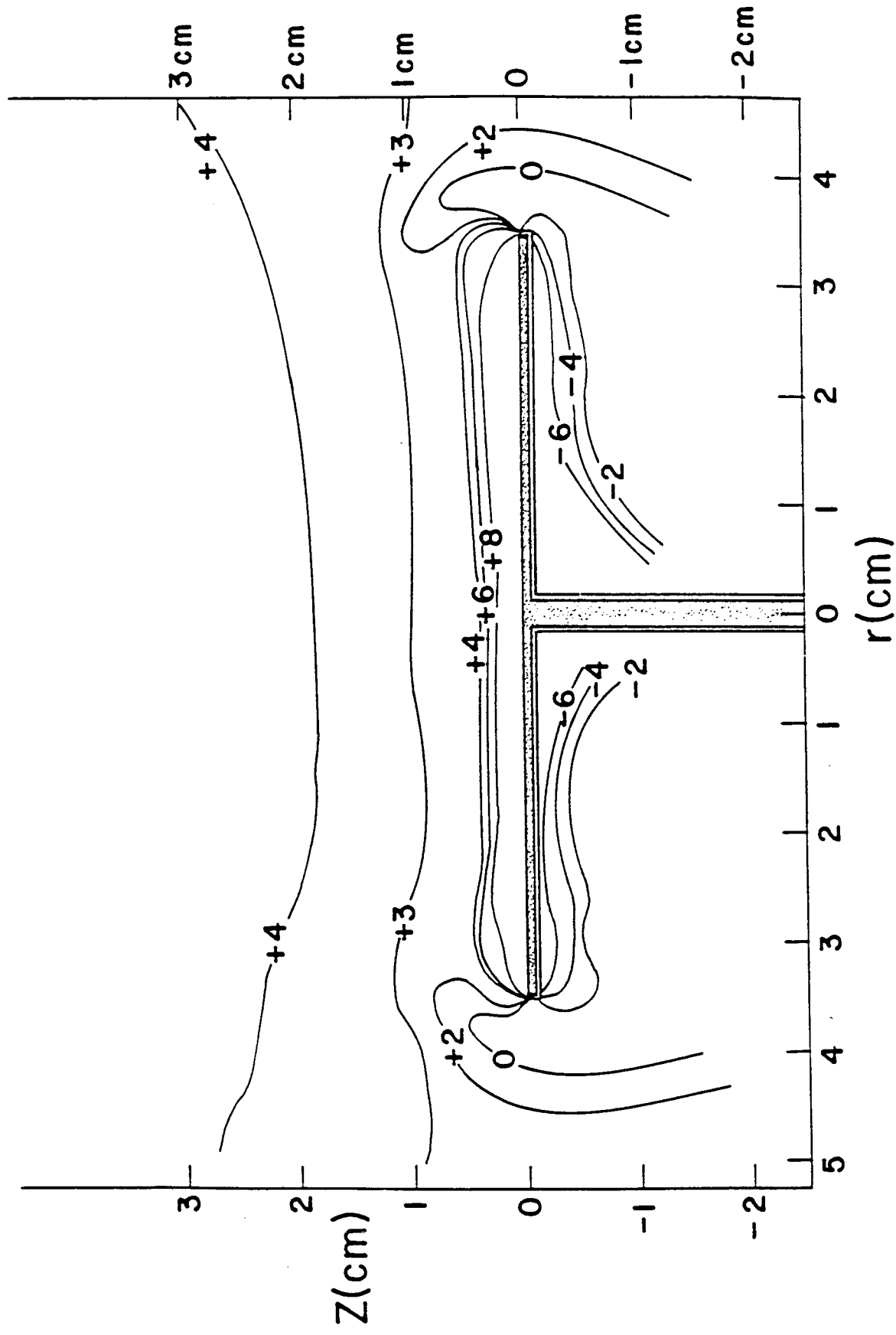
Figure 10. The equipotential contours near a clean plate. The back of the plate, the edges of the plate, and the support are covered with ceramic.
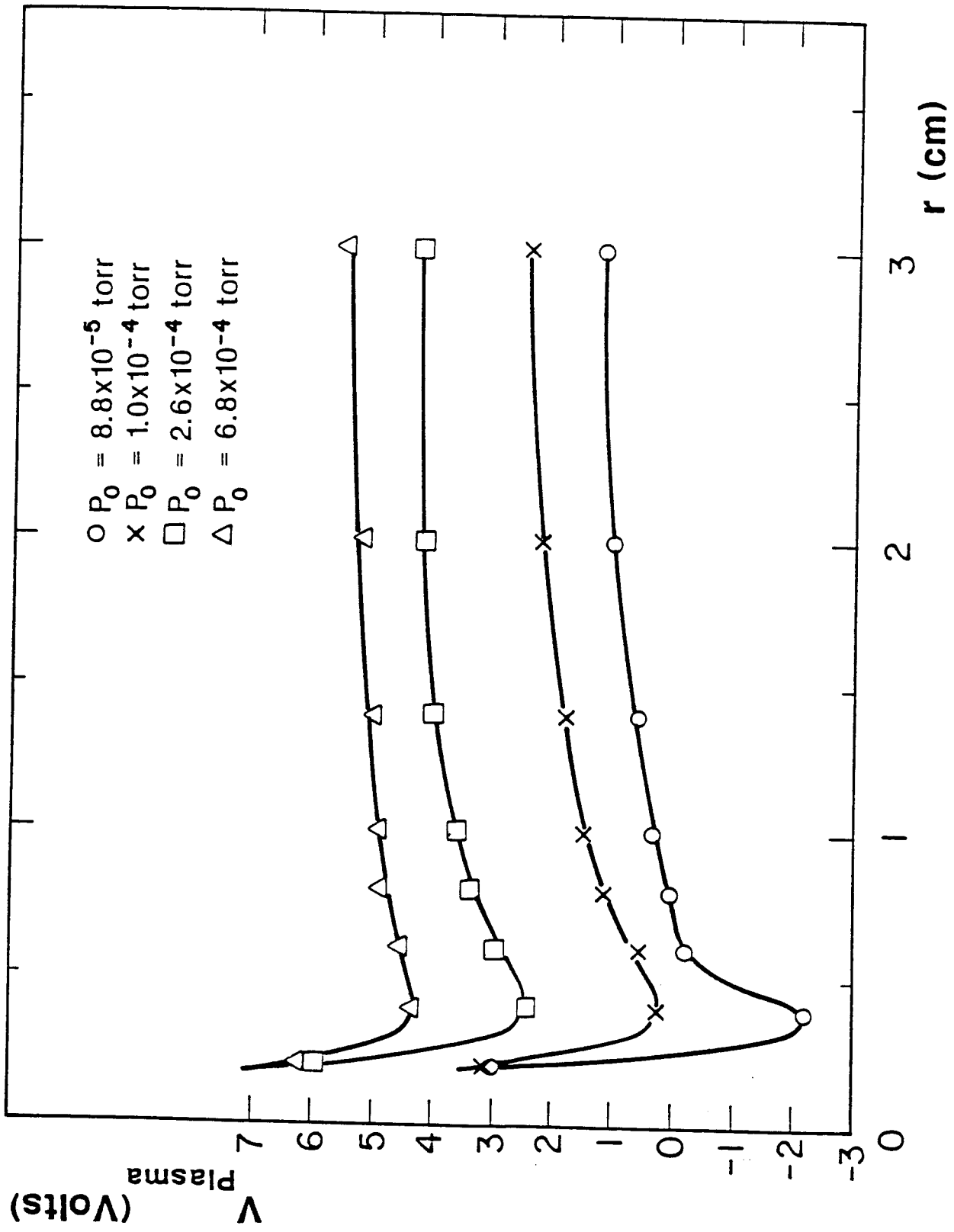
Figure 11. Axial potential profiles, near the positively biased disc, at several neutral pressures. As the neutral pressure is increased, the size of the dip $\Delta\phi$ is seen to be reduced.
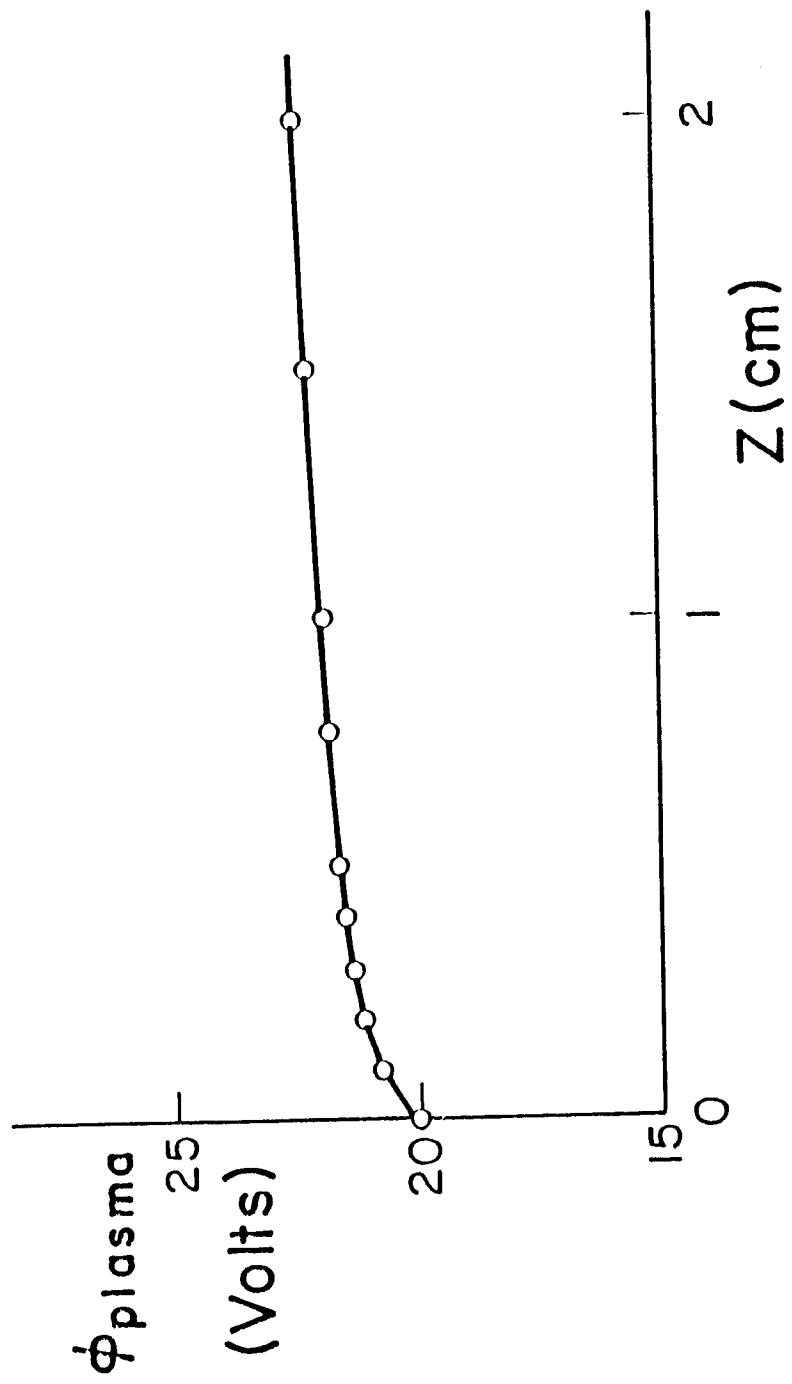
Figure 12. The plasma potential measured on the axis of the plate with ceramic removed from the back.

A LABORATORY INVESTIGATION OF POTENTIAL DOUBLE LAYERS

Philip Leung
Jet Propulsion Laboratory
California Institute of Technology
Pasadena, California 91109, U.S.A.

ABSTRACT

In a triple plasma device, the injection of electron current from the source chamber to the target chamber causes the formation of a potential double layer. At a low current density, the space charge of the injected current produces a virtual cathode-type potential double layer. This double layer is stable, and various wave instabilities are observed to associate with this double layer. As the current density is increased, the double layer becomes unstable, and a moving double layer results. As the current density is increased further, the enhanced ionization causes the neutralization of the space charge of the electron beam, and the "beam plasma discharge" is ignited.

I. INTRODUCTION

The importance of potential double layers in astrophysical phenomena is well known (Alfvén, 1958). Theoretical work on potential double layers has indicated that wave instabilities may be responsible for the formation of potential double layers. However, different theoretical models have predicted different instabilities in order for a double layer to form. These instabilities include ion-acoustic (Sato and Okuda, 1980), ion hole (Schamel and Bujarbarua, 1983), Langmuir turbulence (Levine and Crawford, 1978), and Buneman (Iuzuka et al., 1979) instabilities. This paper presents experimental measurements of the characteristics of instabilities associated with a potential double layer. The double layers were produced in a conventional triple plasma device by the injection of an electron current from the source chamber to the target chamber. Different types of wave turbulences were observed to be associated with a stable double layer. Despite the presence of these wave instabilities, the virtual cathode-type mechanism (Leung et al., 1980) associated with the space charge of the injection electron current was found to be the single most important mechanism responsible for the double layer formation. Experimental data on the transition of the double layer phenomenon into the beam plasma discharge phenomenon (Bernstein et al., 1978) will also be discussed. This transition was due to the transition from space charge-limited electron current flow to source temperature-limited electron current flow. This transition further illustrates the importance of space charge effects in the stability and formation of potential double layers.

Part II of this paper describes the experimental setup, part III presents the measurements of wave instabilities associated with a stable double layer, part IV discusses the transition of a stable double layer into the beam plasma discharge phenomenon, and part V is the conclusion.

II. EXPERIMENTAL SETUP

The experiments were performed in a modified triple plasma device. The details of this setup have been described elsewhere (Leung et al., 1980). In most of the experiments, the system was operated as a double plasma device. The diagnostics consist of a two-sided Langmuir probe and an emissive probe, both mounted on the same

✳ C-2

probe shaft. This permits measurements of plasma potential and plasma electron distribution function simultaneously. An electron gun (5-9 keV, 100 nA) is available for electric field measurements. This gun provides a nonperturbative diagnostic to verify the existence of a double layer. The ion dynamics are measured by an electrostatic energy analyzer.

A shielded RF probe is used to measure the unstable wave spectrum. Wavelength measurements are made by two probe correlational methods. In this series of experiments, the frequency of unstable waves ranges from 50 kHz to 100 MHz.

III. RESULTS

A steady state double layer is produced by operating the system in a double plasma device configuration. The potential profile and the grid biases are shown in Figure 1. The plasma parameters associated with this double layer are shown in Figure 2. In the high potential side, the electron distribution function is in the form of a bump-on-tail distribution. In the low potential region, the electron distribution function is a modified drifting Maxwellian. In the low potential region, counterstreaming ion beams are present; whereas, in the high potential region, only thermal ions are present. These particle distributions are very important for the understanding of a potential double layer since they are responsible for both the self-consistent potential profile and the wave instabilities.

The typical frequency spectrum associated with a stable double layer is shown in Figure 3. The frequency spectrum can be divided into two regions: (1) the high frequency spectrum around the electron plasma frequency and (2) the low frequency spectrum in the vicinity of the ion plasma frequency. The unstable waves at ω_{pe} only have significant amplitude at the high potential side. This is because the bump-on-tail electron distribution on the high potential side excites beam plasma instabilities. The cross-spectral intensity obtained by a two-probe correlation method is shown in Figure 4a. The value of the wavelength derived from this interferometer trace indicates that the waves propagate at approximately the same velocity as the electron beam that is present in the high potential region. Consequently, the waves are excited by the beam-plasma (Schmidt, 1979) instabilities.

The waves around the ion plasma frequency range from $0.1\ \omega_{pi}$ to $3\ \omega_{pi}$, where ω_{pi} is the ion plasma frequency. The amplitudes of these waves are significant only in the low potential region. Figure 4b shows a typical cross-spectral density function obtained by the two-probe correlation measurement technique. The dispersion relationship of these low frequency waves is shown in Figure 5. The data displayed in Figure 5 show that the phase velocity of most waves is faster than V_b, where V_b is the ion beam velocity associated with the stable double layer. Due to their fast phase velocity and the fact that the unstable waves are present above the ion plasma frequency, the waves cannot be excited by the ion-beam plasma instabilities.

A theoretical model was developed to interpret the dispersion relationship shown in Figure 5. The details of this model are discussed in a previous publication (Leung, 1980). The model indicates that the waves around the ion plasma frequency are excited by a modified Buneman-type (Buneman, 1959) instability. The main interaction mechanism is operating between the drifting electrons and the ion beam that is propagating at the same velocity as the electron drift. In the stationary frame of the ion beam, the excited waves have Buneman-type properties. The observed dispersion relationship is just the Buneman dispersion relationship after a transformation from the stationary frame of the ion beam to the stationary frame of the laboratory. The drifting electrons should also interact with the ion beam that propagates in the opposite direction; however, the resulting unstable waves will be subjected to strong Landau damping. This is because the phase velocity of this unstable wave in the laboratory frame will be very close to the velocity of the preceding (rightward in Figure 2) ion beam. Consequently, this mode was not observed in the measurements. The theoretical model discussed in Leung (1980) predicts a very high growth rate. In our measurements, the growth of the Buneman-type waves was not observed. This could be due to the fact that the high growth rate caused the waves to saturate near the grid.

90

IV. TRANSITION OF A STABLE DOUBLE LAYER INTO THE BEAM PLASMA DISCHARGE

The current that flows from the source to the target region can be increased by increasing the grid bias. As the grid bias is increased, the potential drop across the double layer also increases. This trend continues until the potential drop reaches 14 V, which is approximately the first ionization potential of argon. Beyond this point, a sudden increase in the grid bias causes an abrupt increase in the current; and, at the same time, the double layer potential profile collapses (Fig. 6). The plasma density in the target chamber increases by more than an order of magnitude and the "beam plasma discharge" (Bernstein et al., 1978) is excited. The ignition of the beam plasma discharge (BPD) phenomenon is characterized by abrupt increases in the following plasma parameters: (1) optical emission, (2) plasma density, (3) plasma current (Fig. 7), and (4) wave turbulence (Fig. 8).

It should be noted that before the ignition of BPD, the double layer becomes unstable, and large amplitude potential fluctuations are observed. Figure 9a shows the fluctuations in the local electric field as measured by the diagnostic electron beam. The electric field fluctuates at a frequency of approximately 1 kHz. Figure 9b shows the signal detected by the Langmuir probe. The fluctuation in the probe current was due to the change in local plasma potential induced by the moving double layer. The temporal change in potential profile was obtained by performing a time sampling of the emissive probe trace. Figure 10 shows the time development of the potential profile. In this figure, t = 0 is chosen arbitrarily. The data show that the double layer is no longer stable but is moving toward the end of the chamber, i.e., away from the source. The velocity of propagation varies, but under most conditions it is faster than the ion-acoustic speed. The data presented in Figure 10 indicate the significance of the space charge of the electron current in double layer formation. At t = 150 μs, the normalized potential of the low potential region has a value of 2, and the amount of electron current that can flow from source chamber to target chamber is very large (Figs. 11a,b). At t = 200 μs, the normalized potential has a value of 6, the flow of current from source to target is severely limited, and the potential double layer is not well defined. The cycle for the formation and disappearance of a potential double layer repeats itself. This is responsible for the observed fluctuation in the potential profile. A detailed model (Leung et al., 1980) on double layer formation has been discussed elsewhere and will not be discussed in this article.

Referring again to Figure 10, at t = 150 μs, the current limitation by the space charge effect is at its minimum. If the absolute potential of the low potential region is further reduced, the current flow is significantly increased (Figs. 11a,b). This increase in current increases the rate of ionization in the high potential region. The increase in the ion fluxes further reduces the space charge in the low potential region, and eventually the space charge limitation of the electron current flow is eliminated. The uninhibited flow of current leads to the ignition of the beam plasma discharge.

It should be noted that the transition from double layer (DL) to BPD is not a reversible process. By lowering the bias, the BPD will not transform back to a DL immediately. A DL is formed only when the bias voltage is lowered to a value such that the ionization cross-section is substantially reduced.

The injection of electron current from the source to the target chamber is very similar to the injection of an electron beam from a rocket to the ionosphere. BPD has been observed in several rocket experiments (Hallinan et al., 1978). In some of the beam injection experiments, large amplitude fluctuations (Winckler, 1980) in the electron return current and in the optical emission were also observed. This type of fluctuation could be due to the excitation of moving double layer-type potential structures in the ionosphere. The space shuttle and the future Space Station, with its diverse sophisticated diagnostic instruments, should be able to provide a test bed for beam-excited double layer structures in the ionosphere.

V. CONCLUSIONS

This paper has discussed the instabilities associated with a stable double layer. The unstable wave spectrum around the electron plasma frequency is due to the excitation of the beam plasma instabilities by the electron beam that is present in the high potential region. The unstable waves around the ion plasma frequency are due to the excitation of the Buneman-type waves by the electron current.

The data in our experiments show that as the grid bias is increased, there is a transition from a stable double layer to a moving double layer, followed by the ignition of beam plasma discharge. This transition shows that the space charge of the injected electron current plays a very important role in double layer formation. The role of instabilities is not evident in our experimental measurements. Since wave instabilities are always associated with double layers, their role in modifying the characteristics of DLs is undeniable and should be further investigated.

REFERENCES

Alfvén, H., *Tellus, 10,* 104 (1958).

Bernstein, W., et al., *Geophys. Res. Lett., 5,* 127 (1978).

Buneman, O., *Phys. Rev., 115,* 503 (1959).

Hallinan, T., H. C. Stenbaek-Nielsen, and J. R. Winckler, *J. Geophys. Res., 83,* 3263 (1978).

Iizuka, S., K. Saeki, N. Sato, and Y. Hatta, *Phys. Rev. Lett., 43,* 1404 (1979).

Levine, J., and F. Crawford, SU-IPR Report 78-7, Stanford University, CA, 1978.

Leung, P., "Interaction Between Particle Beams and Nonlinear States," Ph.D. Thesis, University of California, Los Angeles, 1980.

Leung, P., A. Wong, and B. Quon, *Phys. Fluids, 23,* 992 (1980).

Sato, T., and H. Okuda, *Phy. Rev. Lett., 44,* 740 (1980).

Schamel, H., and S. Bujarbarua, *Phys. Fluids, 26,* 190 (1983).

Schmidt, G., *Physics of High Temperature Plasmas,* Academic Press, 1979.

Winckler, J. R., *Rev. Geophys. Space Phys., 18,* 659 (1980).
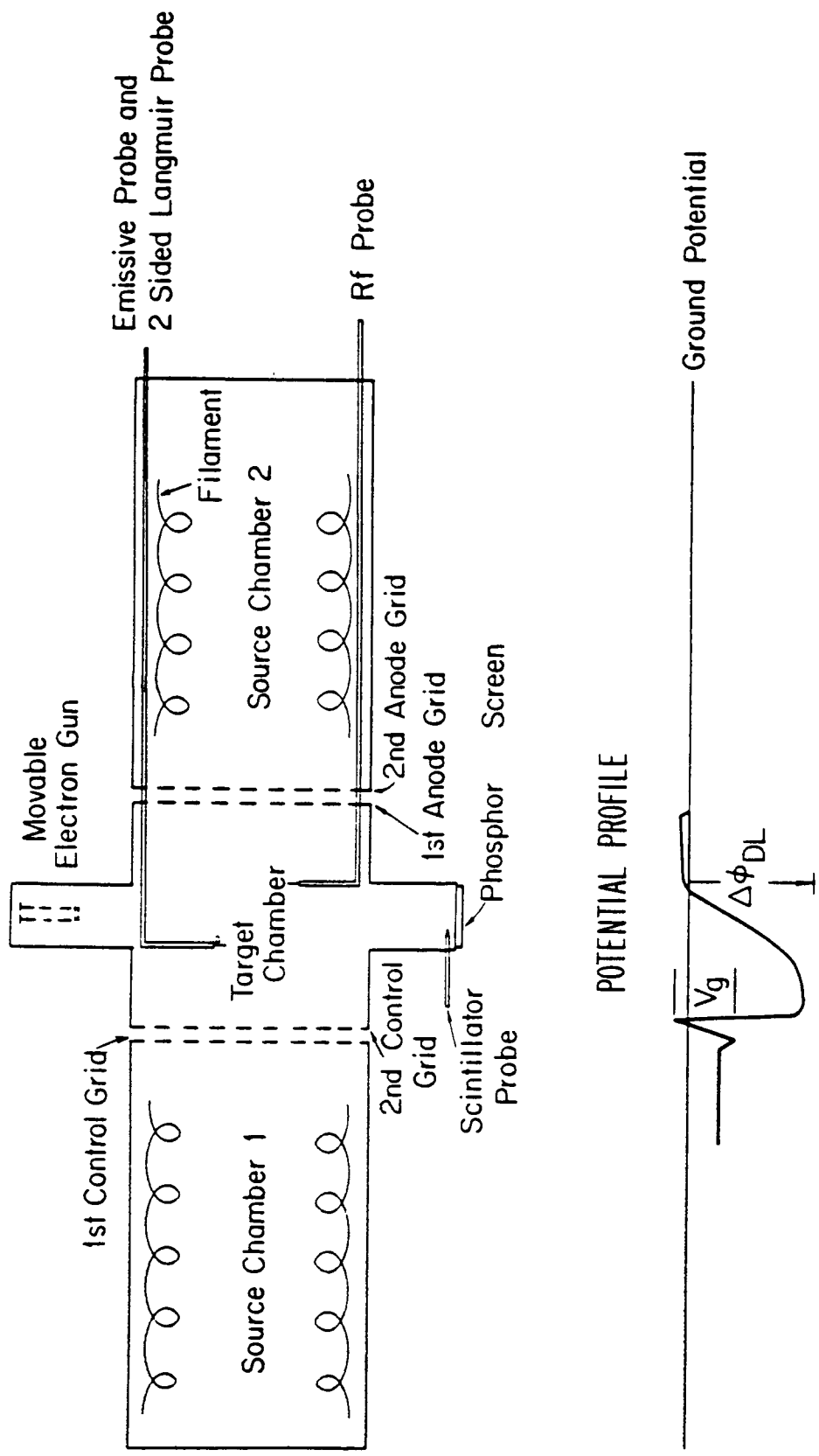
Figure 1. Schematics of the triple plasma device.
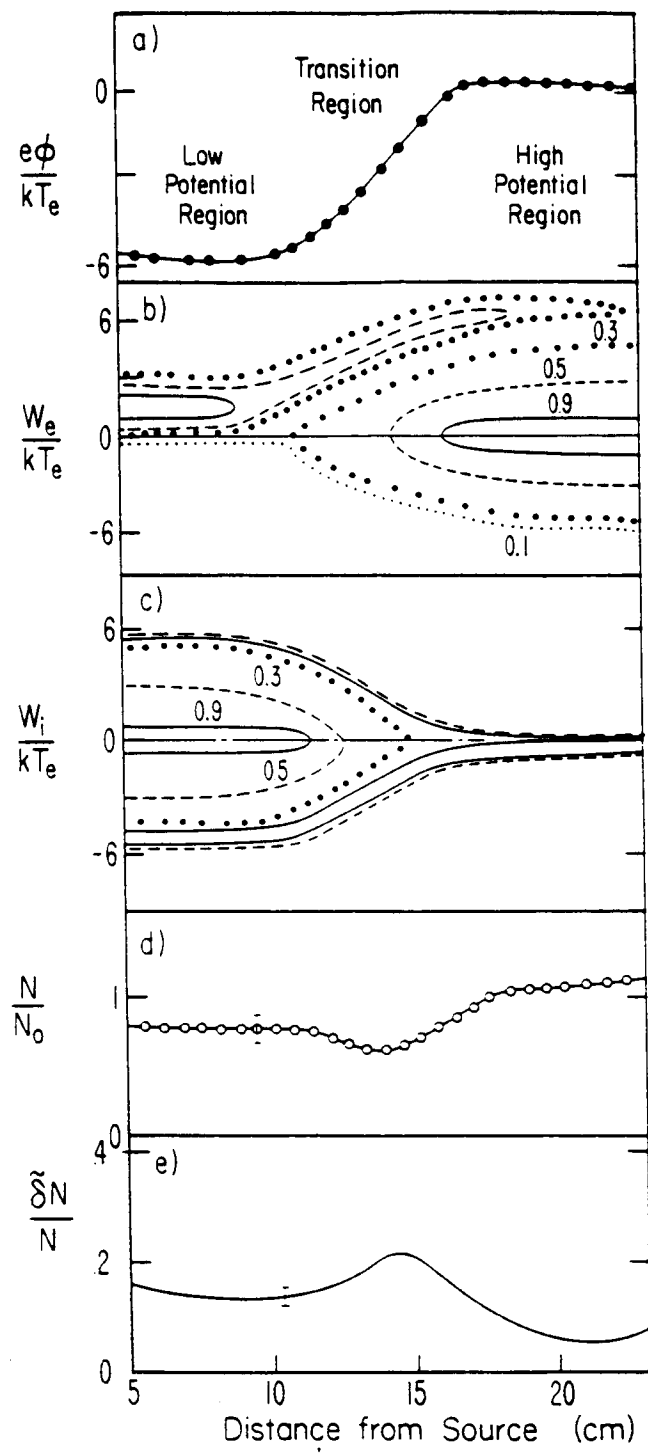
Figure 2. The plasma parameters associated with a potential stable double layer. The plasma parameters are normalized with respect to electron temperature T_e and the electron density at the high potential side. (a) Plasma potential profile. (b) One-dimensional phase-space representation of electron distribution, $W_c = 1/2\ m_c v^2$, where W_e is the normalized electron energy. The numbers on the curves indicate the normalized height of the distribution function. The negative values of W_e/kT_e represent velocity in the opposite direction. (c) Phase representation of the ion distribution function, $W_i = 1/2\ M_i v^2$. (d) Relative electron density. N is the spatial density in the target region. (e) Relative peak-to-peak density fluctuation.
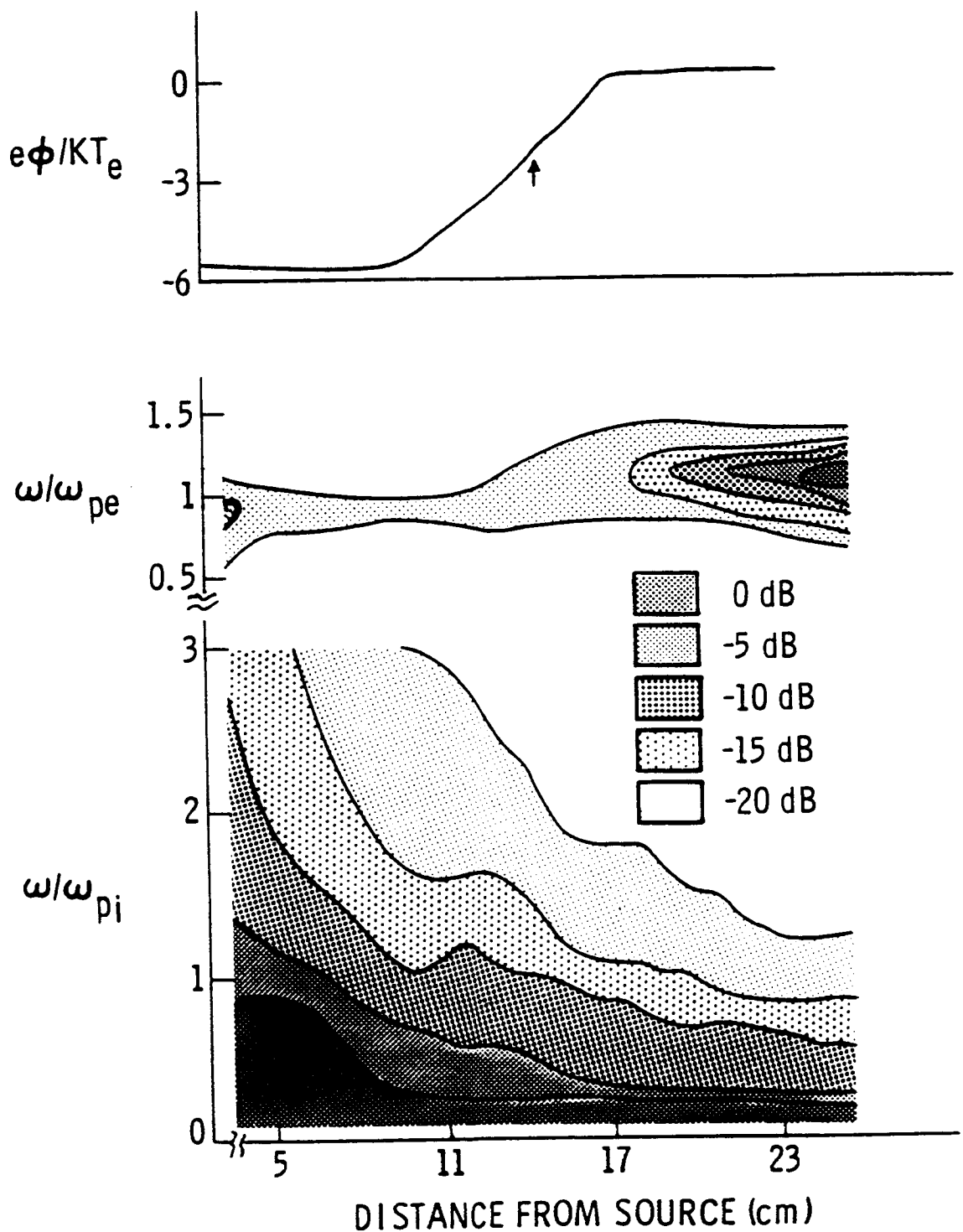
Figure 3. The power spectrum of unstable waves associated with a stable double layer, showing the power level of different frequencies present at different points along the potential profile (top). The power levels are divided into five arbitrary levels. The frequencies of unstable waves are normalized to electron plasma frequency (ω_{pe}) and ion plasma frequency (ω_{pi}).
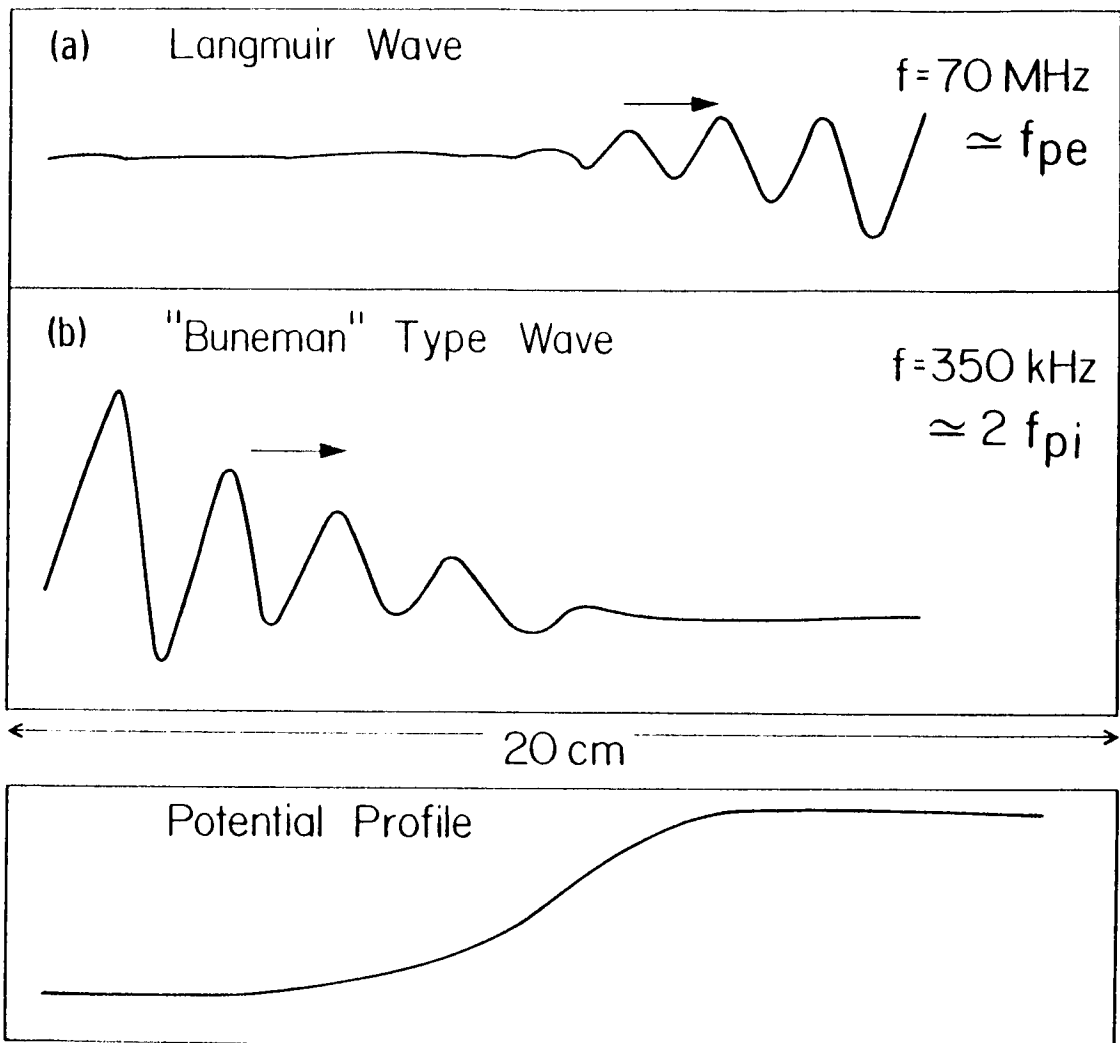
Figure 4. The cross power spectral density of the Langmuir wave and Buneman-type waves. The potential profile is also shown here for reference.
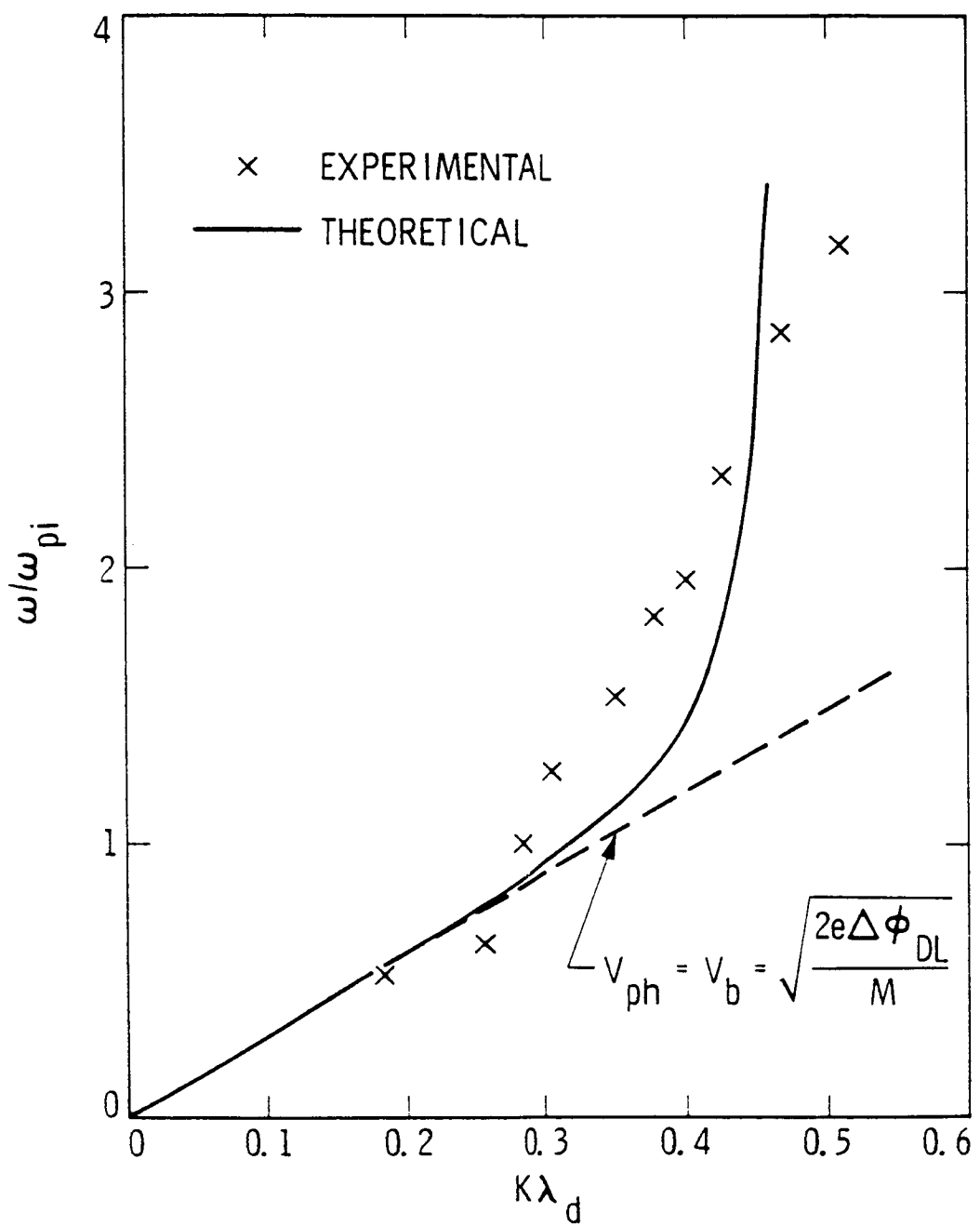
Figure 5. The dispersion relationship of the Buneman-type wave: x represents the experimental data, and the solid line is the theoretical dispersion relationship.
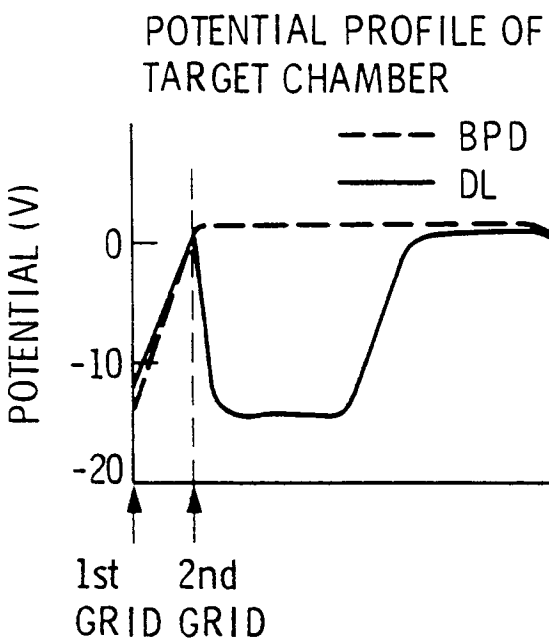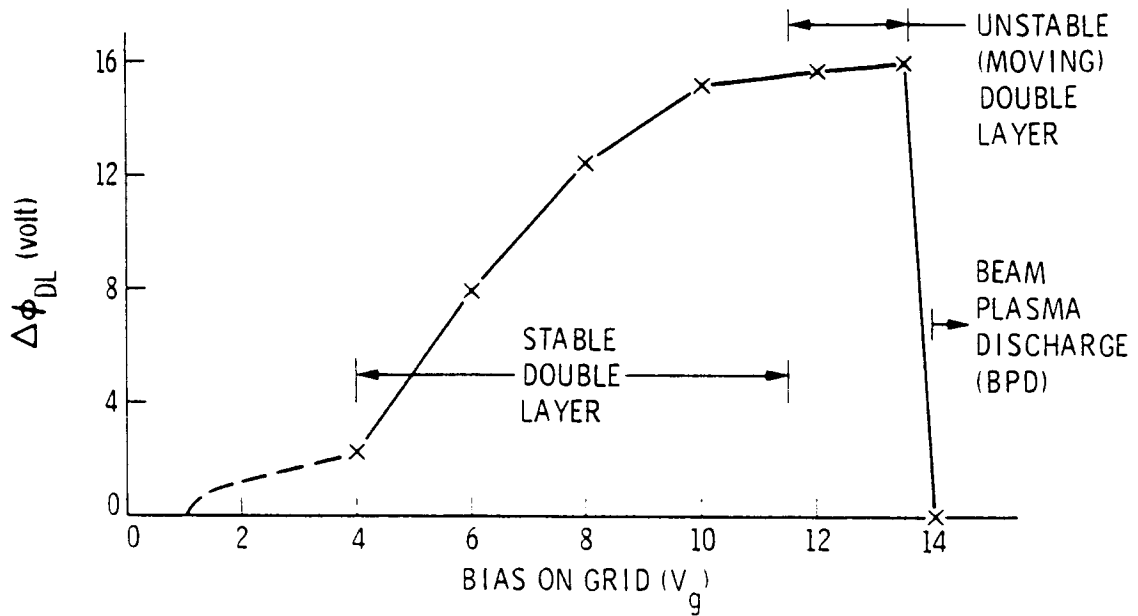
Figure 6. The change in potential drop of the double layer as the grid bias is increased. The beam plasma discharge is ignited when the grid bias exceeds 13 V. The potential profile of the target chamber before and after the ignition of the BPD is shown in the lower diagram.
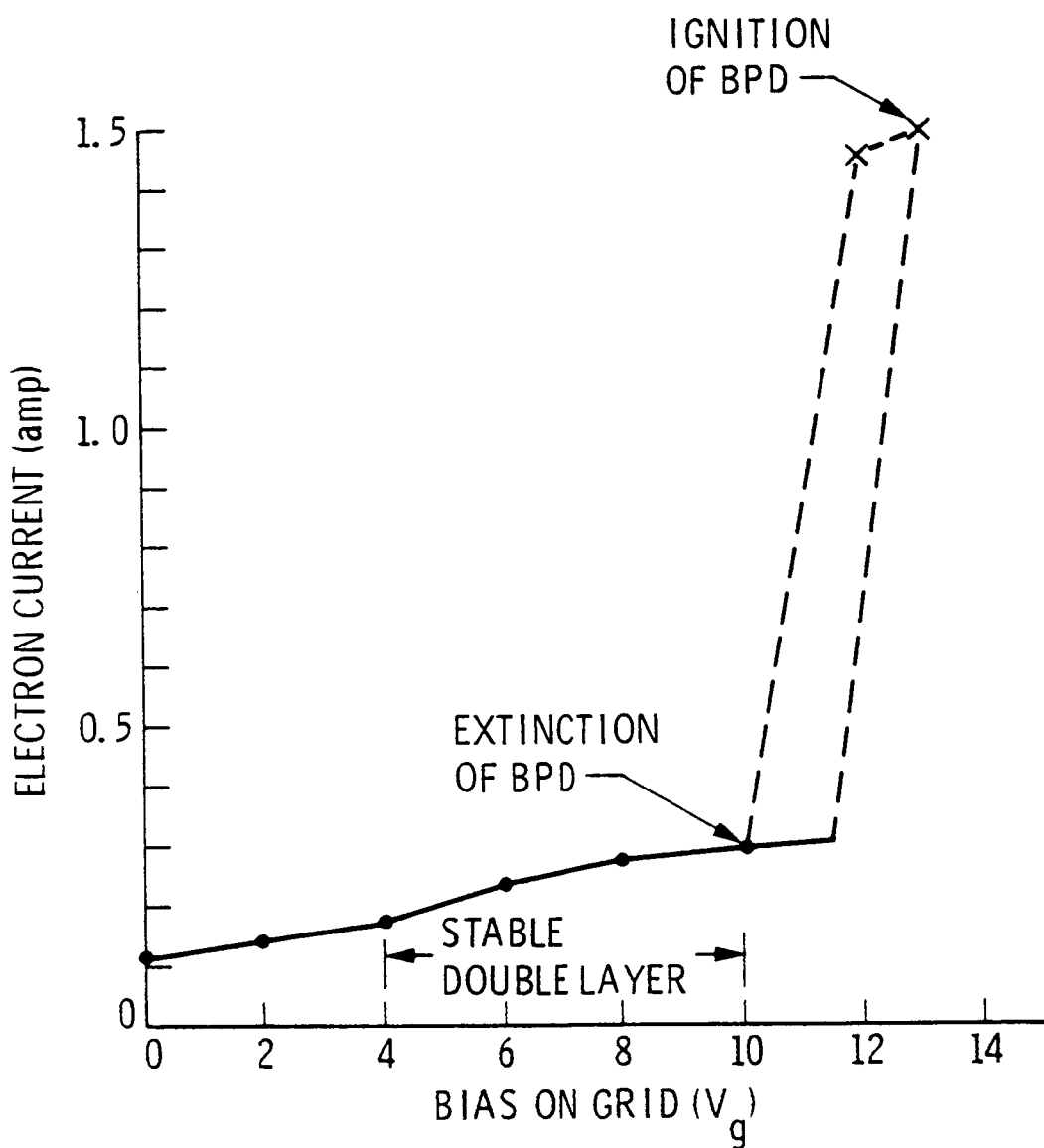
Figure 7. The injected electron current as a function of the grid bias showing the ignition of the BPD.
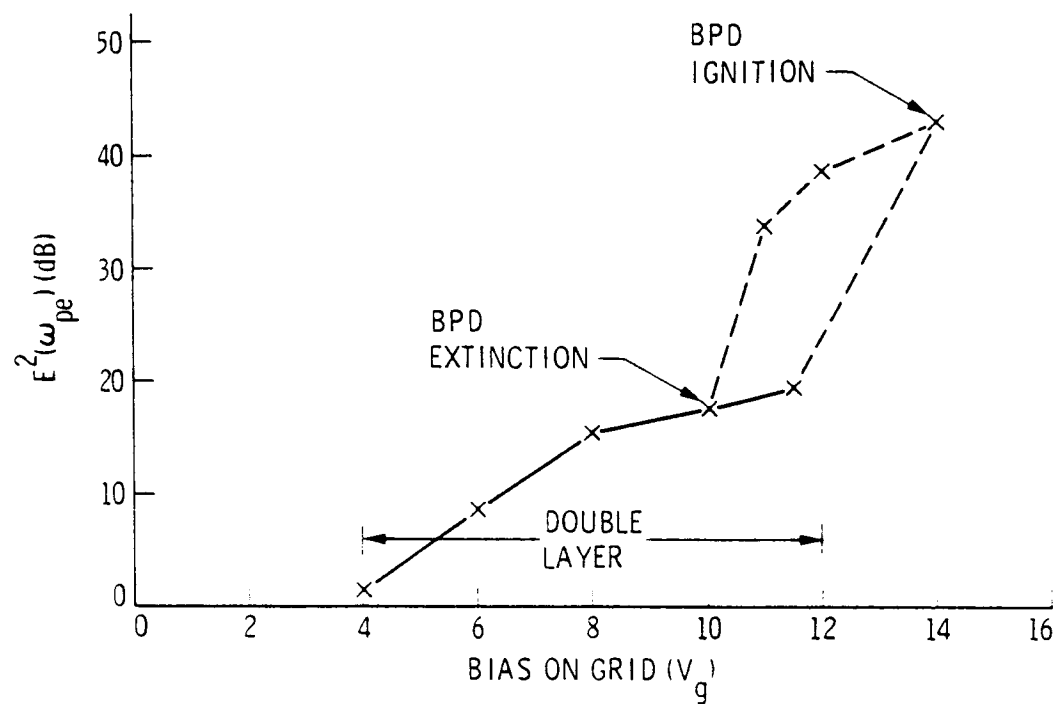
Figure 8. The wave turbulence level as a function of grid bias showing the igniton of BPD. When the BPD is ignited, the electron distribution function is a bump-on-tail distribution.
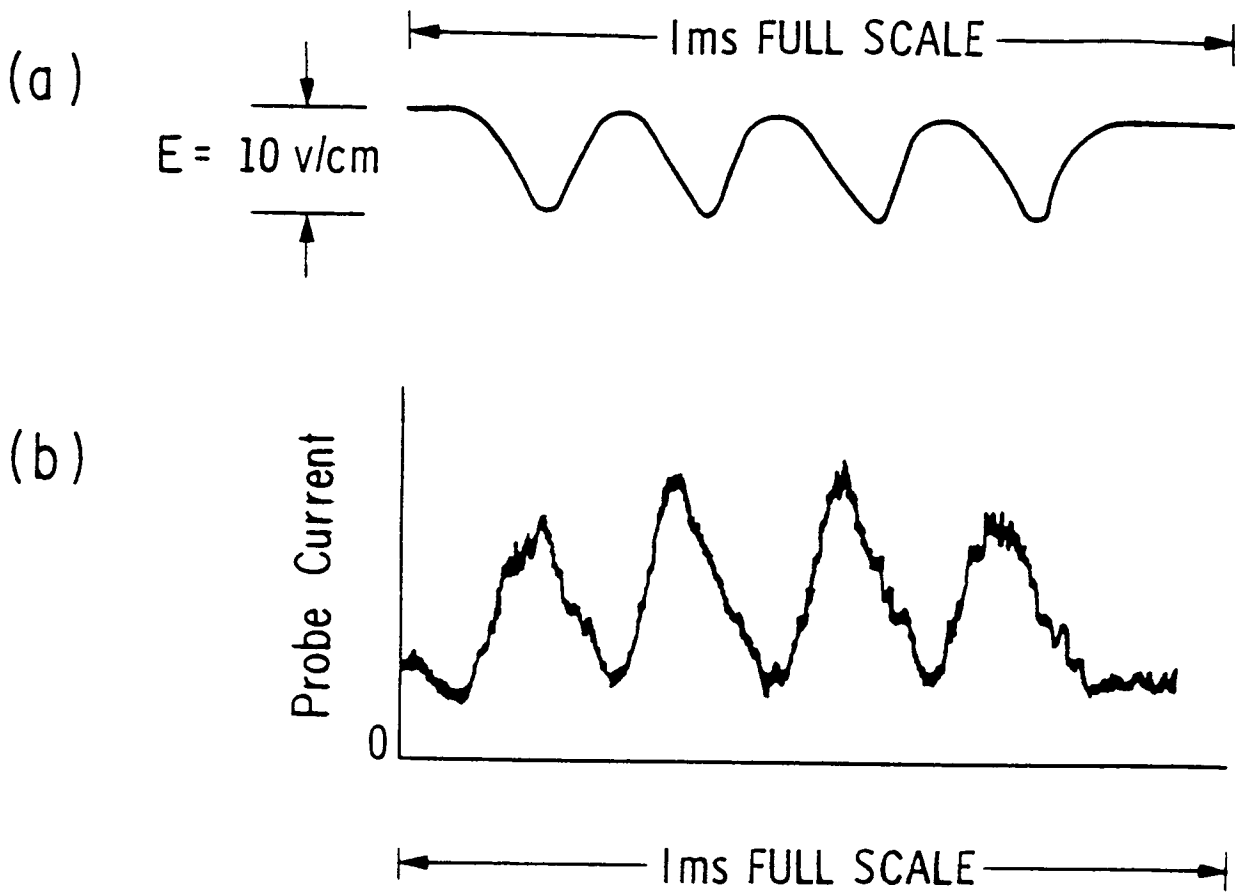
Figure 9. The top trace (a) shows the fluctuation in the local electric field as measured by the diagnostic electron beam. The fluctuation is due to the motion of the double layer. The corresponding fluctuation in the Langmuir probe current is shown in the bottom trace (b).
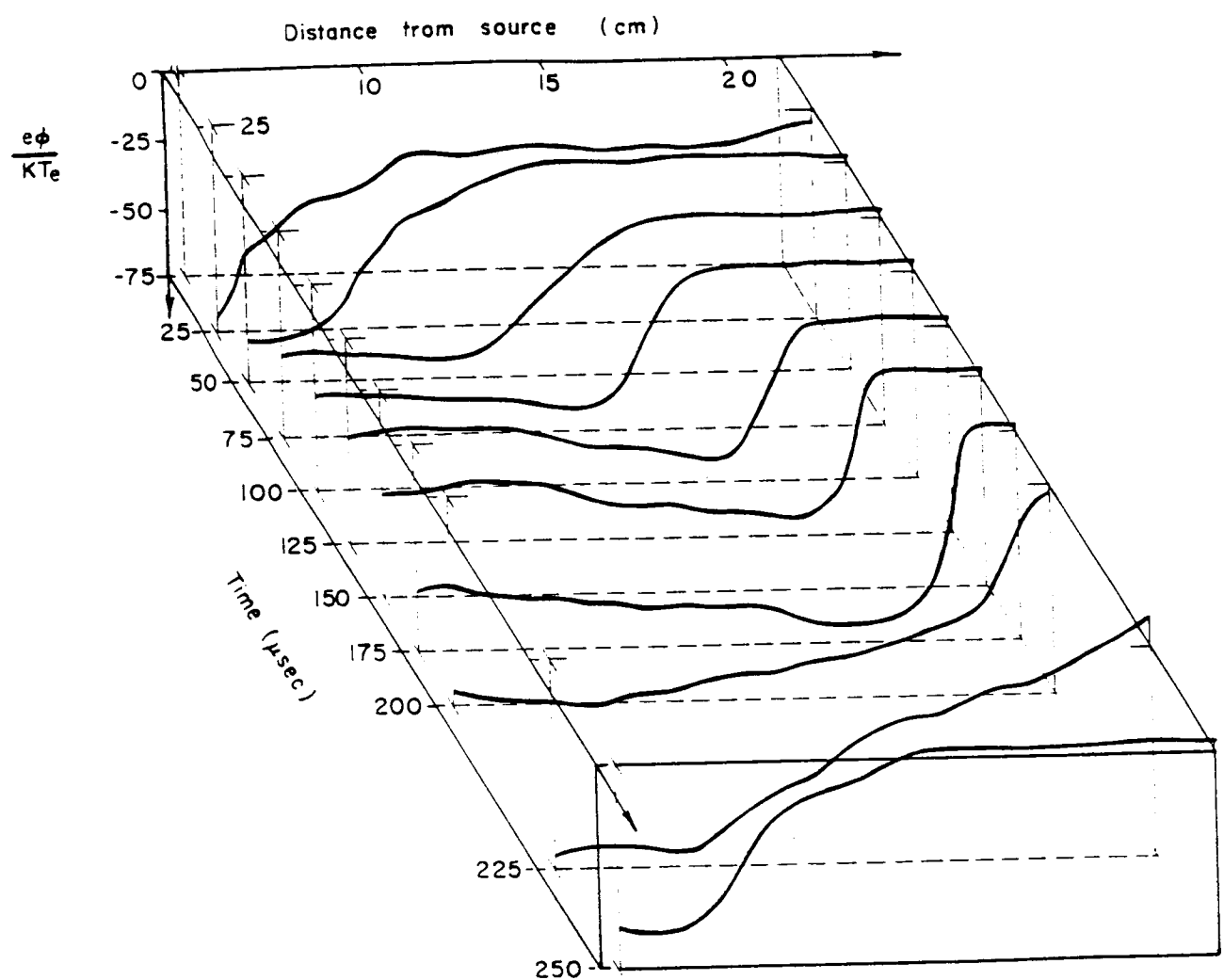
Figure 10. Time development of moving double layers.
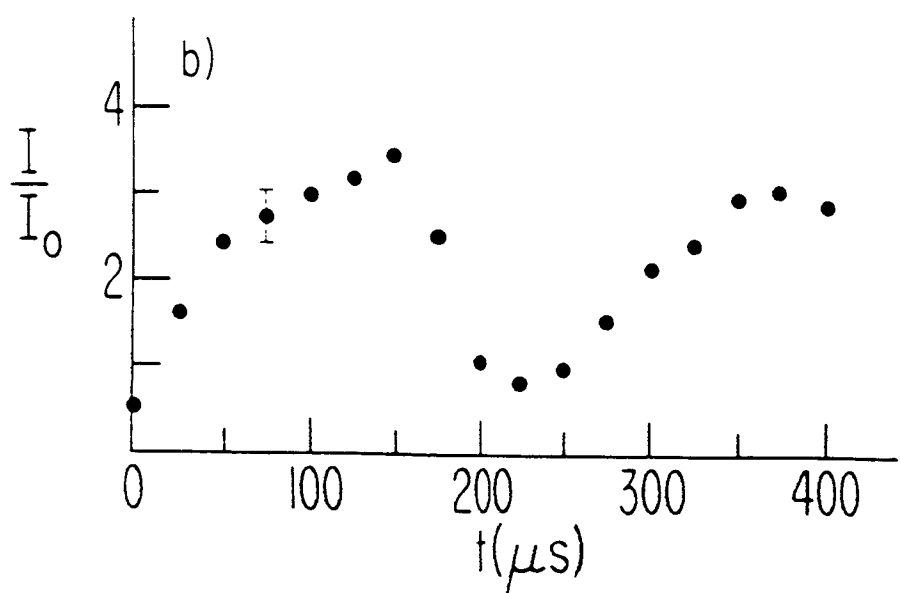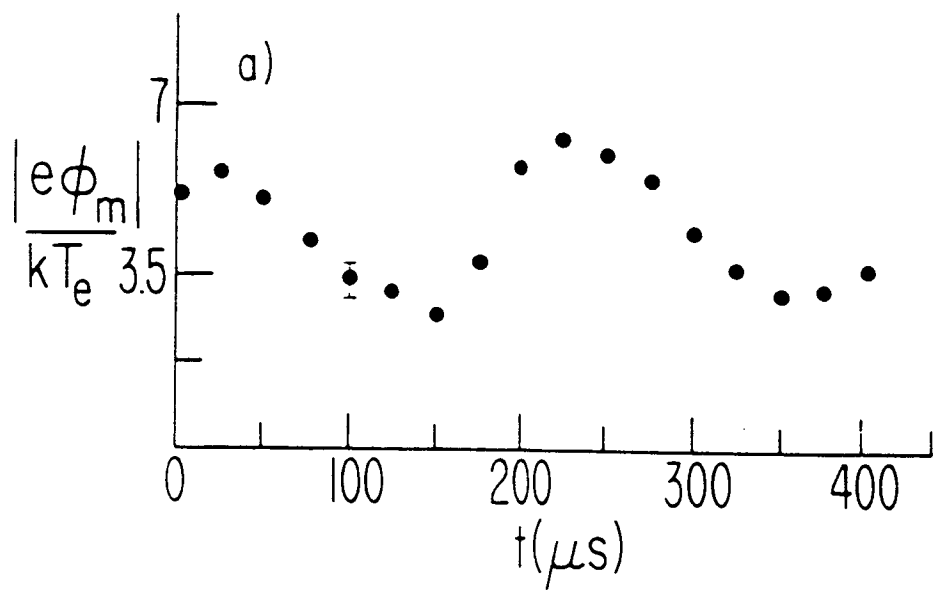
Figure 11. The two important parameters that control the moving double layers: (a) the potential of the low potential region and (b) the injection current as a function of time.

EXPERIMENTAL OBSERVATION OF ION-ACOUSTIC DOUBLE LAYERS IN LABORATORY PLASMA

Y. C. Saxena
Plasma Physics Programme
Physical Research Laboratory
Ahmedabad 380009, India

ABSTRACT

Computer simulations indicate existence of weak, electrostatic potential structure with $e\Delta\phi/kT_e \lesssim 1$, having a negative potential dip on low potential side in a current carrying plasma (DeGroot et al., 1977; Sato and Okuda, 1980). These types of structures, known as ion-acoustic double layers, have been analytically correlated with the ion-holes which are known to be nonlinear extensions of normally damped slow ion-acoustic modes (Schamel, 1979; Hasegawa and Sato, 1982). Ion-acoustic double layers have also been evoked for explaining recent satellite observations (Hudson et al., 1983).

In this paper we present experimental results on the observation of ion-acoustic double layers in laboratory plasma. In a double-plasma device, modified suitably to inject electron beam into the target plasma, modulation of the beam through a step potential leads to excitation of ion-acoustic fluctuations. The fluctuations, growing away from the separating grids, develop into weak asymmetric ion-acoustic double layers. The observations are compared with the scenario emerging out of the computer simulations and analytical results on ion-acoustic double layers.

REFERENCES

DeGroot, J. S., C. Barnes, A. E. Walstead, and O. Buneman, *Phys. Rev. Lett.*, *38*, 1283 (1977).
Hasegawa, A., and T. Sato, *Phys. Fluids*, *25*, 632 (1982).
Hudson, M. K., W. Lotko, I. Roth, and E. Witt, *J. Geophys. Res.*, *88*, 916 (1983).
Sato, T., and H. Okuda, *Phys. Rev. Lett.*, *44*, 740 (1980).
Schamel, H., *Physica Scripta*, *20*, 336 (1979).

PRECEDING PAGE BLANK NOT FILMED

II. THEORY AND SIMULATION OF DOUBLE LAYERS

A NEW HYDRODYNAMIC ANALYSIS OF DOUBLE LAYERS

Heinrich Hora
Department of Physics and Astronomy
and
Iowa Laser Facility
The University of Iowa
Iowa City, Iowa 52242, U.S.A.

ABSTRACT

A genuine two-fluid model of plasmas with collisions permits the calculation of dynamic (not necessarily static) electric fields and double layers inside of plasmas including oscillations and damping. For the first time a macroscopic model for coupling of electromagnetic and Langmuir waves was achieved with realistic damping. Starting points were laser-produced plasmas showing very high dynamic electric fields in nonlinear force-produced cavitous and inverted double layers in agreement with experiments. Applications for any inhomogeneous plasma as in laboratory or in astrophysical plasmas can then be followed up by a transparent hydrodynamic description. Results are the rotation of plasmas in magnetic fields and a new second harmonics resonance, explanation of the measured inverted double layers, explanation of the observed density-independent, second harmonics emission from laser-produced plasmas, and a laser acceleration scheme by the very high fields of the double layers.

I. INTRODUCTION

There is a close similarity between the double layers in the surface of laser-produced plasmas and a wide class of astrophysical plasmas (Hora, 1975). In both cases a high temperature plasma is produced which expands into vacuum or into gases of much less density. During this dynamic process, a separation of space charges will happen at the plasma surfaces when the equithermal electrons with their much higher velocity than that of the ions will expand much faster generating first a negatively charged cloud followed by a positively charged cloud of the ions. Then the more or less homogeneous and space charge quasi-neutral plasma follows. The separation of the electrons and ions with a net neutral charge is a double layer (DL) in which electric fields persist within these plasma areas (Fig. 1). These fields were suggested for explaining phenomena in extraterrestric plasmas by Alfvén (1958) not without hefty opposition of other plasma theoreticians. Even the more advanced presentation (Alfvén, 1981) was commented by Kulsrud (1983) as "Alfvén's electric fields whose origin is intuitively not clear." These fields and double layers were also suggested to be involved with the solar atmosphere (Alvén and Carlqvist, 1967; Carlqvist, 1979, 1982; Torvén et al., 1985), in the ionosphere and magnetosphere of the Earth and the magnetosphere of Jupiter (Shawhan, 1976), and with the striated structure of the barium clouds when expanding in the ionosphere (Haerendel et al., 1976).

In laser-produced plasmas, these double layers in the surface of the expanding plasma were thought to be involved with the measured speeding up of the ions to multi-kiloelectronvolt energies as measured by Linlor (1963) while the particle temperatures were 100 eV or less. However, the analysis of the double layer (Hora et al., 1967) with a derivation of its thickness being of a Debye length (Hora, 1975) arrived at a number of accelerated ions which was 10^5 times less than measured. A completely different acceleration mechanism had to be derived by nonlinear forces (as a generalization of the ponderomotive forces) of nonthermal electrodynamic interaction of the laser radiation with the plasma (Hora, 1969).

The direct experimental proof of the double layer and high electric fields in laser-produced plasmas was given by Mendel and Olson (1975) where the bending of an ion beam passing the double layer led to the measurement of electric fields of 10 kV/cm. The generation of electrostatic potentials was measured by Pearlman and Dahlbacka (1977), and a more detailed study using Rogowski coils (Eliezer and Ludmirsky, 1983), Figure 2, with a high temporal resolution to 50 psec or less (Ludmirsky et al., 1985; Eliezer et al., 1986) arrived at the discovery of the inverted double layers and spatially oscillating behavior of the double layers (Hora et al., 1984).

The first measurement of the double layers in space plasmas was not before 1977 (Mozer et al., 1977; Temerin et al., 1982; Temerin and Mozer, 1984) using S3-3 satellite data. These results, together with the laboratory experiments on double layers as reviewed by Hershkowitz (1985), emerged from the initial theory on plasma double layers by Langmuir (1929), Bohm (1949), Bernstein et al. (1957), and Knorr and Goertz (1974), and from computer simulations by DeGroot et al. (1977) and Sato and Okuda (1980). Turbulence theory by Yabe et al. (1981) arrived at electric fields inside of these turbulence areas and may be interpreted as some sort of a double layer behavior. The laboratory experiments showed double layers in mercury discharges (Torvén, 1981; Stangeby and Allen, 1973), Q machines (Sato et al., 1976), and triple devices where two plasmas at different electric potential are connected through grids by a plasma which has then a double layer according to the difference of the voltages plus the difference of the temperatures between the two outer plasmas (Coakley and Hershkowitz, 1981; Quon and Wong, 1976; Leung et al., 1980). The geometry can be one-dimensional (Hershkowitz et al., 1981), two-dimensional (Baker et al., 1981), or three-dimensional (Merlino et al., 1984).

A special motivation for studying the double layer in laser-produced plasma was given from the theory of the nonlinear force (Hora, 1969, 1974, 1981; Lindl and Kaw, 1971; Peratt and Watterson, 1977; Peratt, 1979). The electrodynamic, dielectrically caused acceleration of plasma by laser radiation is based on the force acting on the high density electron gas in the plasma being pushed or pulled and the ion gas has to follow then by the electric fields generated between the two fluids. When the essential properties of the nonlinear force were derived from the space charge quasi-neutral plasma model (Hora, 1969), the mentioned fields were disguised by the presumptions of the model. However, the existence of the fields of the description of the single electron motion (Hora, 1971) was evident, and a search was overdue since the beginning of the work on the nolinear force in 1965.

While the treatment of the double layers and the high electric fields is essentially no problem on the basis of the kinetic theory with the Vlasov equation (Knorr and Goertz, 1974), the inclusion of collisions for the conditions of the high density laser-produced plasmas would have been necessary for which the complications of the collision processes for the kinetic theory would be a problem. How important the collision processes are in laser-produced plasma can be seen from several examples. Simply, the classical optical constants (Hora, 1981) can be evaluated only by carefully watching the numerical problems close to a pole of the related functions where the change of the real part or the imaginary part of the optical constant can be by a factor 10^3 or much more for a change of the plasma temperature or the plasma density by less than 1 percent. Another drastic example is the theory of Denisov's resonance absorption (to distinguish from a new resonance found by Hora and Ghatak, 1985) where the derivation based on the electric field by White and Chen (1974) arrived at a negative infinite pole of the function for the effective dielectric function of the plasma was collisionless. Introducing a tiny little bit of absorption (collisions), however, caused a swap of the pole from minus infinity to nearly plus infinity (Hora, 1979). Collisions are therefore essential in laser-produced plasmas.

The use of N-particle simulation of the plasma (with $N = 10^6$) by computers could again not be used as the physics of the collisions could be covered yet only in a limited way and only first attempts have been done to correctly treat Coulomb collisions now in a simplified way by using supercomputers (Yabe, 1985). The difficulties in this macroscopic theory, however, are in the presumptions of space charge quasi-neutrality that could not at all be used to treat the electric fields or double layers in plasmas. It even could not describe the coupling of the longitudinal ("electrostatic") Langmuir waves with transversal electromagnetic waves in plasma (Schamel, 1979).

II. THE GENUINE TWO-FLUID MODEL

The macroscopic hydrodynamic theory for the consequent description of the double layers and the generated electric fields required the use of the complete two fluids for electrons and ions including collisions, viscosity, equipartition of temperatures between ions and electrons, optical constants with the correct nonlinear dependence on the laser intensity (about an incorrect formula, see e.g., Duderstadt and Moses, 1983), and including the general expression of the nonlinear force apart from the thermokinetic force given by the gas dynamic pressure (Hora, 1969, 1981, 1985a). In one spatial dimension, the problem was then to solve the following seven quantities depending on the spatial coordinate x and the time t for given initial and boundary values: the density, temperature and velocity (in the x-direction) for electrons, the same for ions (n_e, T_e, v_e, n_i, T_i, v_i) and the electric field E (in the x-direction) differing from the external electric and magnetic fields E_L and H_L of the incident laser radiation. For the seven functions, seven differential equations are available: the equations of continuity for electrons and ions, the equations of motions for electrons and ions, the equations of energy conservation for electrons and ions, and the Poisson (or better Gaussian) equation (Lalousis and Hora, 1983). For the whole three-dimensional description there have to be added the two variables for the other components of the electron velocity and the same for the ion velocities for which the four further velocity components of the equation of motion are accounted. Instead of the longitudinal electric field component E of the one-dimensional case, all three components of E and that of the magnetic field H generated in the plasma during the complex dynamics have to be included for which instead of the Gaussian law in one dimension, the six components of the Maxwellian equations have to be used. All together, there are 16 equations for the 16 quantities to be determined in space and time, automatically also reproducing the complete development of the so-called spontaneous magnetic fields in the laser-produced plasmas.

The solution of the one-dimensional problem allowed for numerics is very complicated in this general property of the plasma because the time steps have to be very much shorter than the shortest plasma oscillation time. For the plasmas at irradiation with neodymium glass laser radiation, the time steps have then to be shorter than 0.1 fs. In order to arrive at physically detectable results in the picosecond scale, long computer runs have to go on, where for each time step the Maxwellian equations also have to be solved for the incident laser radiation with the correct conditions for the reflected wave. For the treatment of the reflection field, a very quick computation by a matrix procedure was invented (Lalousis, 1983). The whole computation had to be using a very unusual Eulerian code instead of the usual Lagrangian codes because of the appropriate inclusion of the description of the electric fields produced inside the plasma. The basic problem of the boundary conditions in this case ran into instabilities, and a special new method for a stable solution had to be discovered as derived by numerical experiments (Lalousis, 1983; Lalousis and Hora, 1984).

The results described in the following were attained by using a CD 7600 computer and a Cray 1. The stability of the computation and the correctness of the output was confirmed after the runs up to the picosecond range by checks of the conservation of energy. Also the fact that the gain or loss of energy of relativistic electrons, fired through the then not longer static and conservative electric fields with potentials, but having the dynamic electric fields E where

$$\oint E \cdot dx \neq 0 \tag{1}$$

resulted in reasonable numbers of the gain or loss of electron energies (Green et al., 1986), was a proof of the correct computations.

III. ELECTRIC FIELDS, DL'S, AND OSCILLATIONS IN PLASMA WITHOUT LASER INTERACTION

When using the genuine two-fluid code, the appearance of strong electric oscillations was marked. For a plasma without laser irradiation, the following initial condition was chosen; a fully ionized hydrogen plasma slab of 10 μm thickness with a linear increase of the electron density from 5×10^{20} cm^{-3} at $x = 0$ to 10^{21} cm^{-3} at $x = 10$ μm was taken at time $= 0$ with same ion density and an electron and ion temperature $T_e = T_i = 10^3$ eV at $t = 0$. The initial velocities were $v_e = v_i = 0$ everywhere at $t = 0$ and, consequently, the electric field $E = 0$ at $t = 0$. Working with time steps of 1.5×10^{-16} s ($1/30$ of the shortest plasma period of 5×10^{-15} s) at $x = 10$ μm, expanding plasma showed a very strong oscillation of the electric field displayed by electrons moving down the ramp and being returned. The field was always negative, never positive, because the electron cloud went back to the initial position within the ions or less. At later times an "ambipolar" oscillation field was noted (Figs. 3 to 5) which decayed faster when the initial plasma temperature was lower (higher collision frequency). The oscillations were damped out and a bent profile of the electric field resulted, nearly unchanged along the whole expanding plasma profile. The field had the highest negative values at $x = 0$ of 2.6×10^6 V/cm. This value was interpreted for a temperature of 10^3 eV and a length of 10^{-3} cm, reaching a value of 3×10^6 V/cm, of a "potential" of 10^3 kT was assumed. As we have a time-dependent evaluation of the field E due to the plasma dynamics, we have no longer a conservative field and therefore no potential. These fields are then, strictly speaking, no longer electrostatic fields, and the generated double layer is, strictly speaking, not an electrostatic double layer, though the result is close to the picture of one.

An analytical description of the numerically very general result is possible with some approximations: The Poisson equation, which was formulated for a potential as an inhomogeneous differential equation to the homogeneous Laplace differential equation, is then only an approximation as the fields are, strictly speaking, no longer conservative. The following Gauss law was used where n_e and n_i have to be considered as time-dependent. The non-conservative character of these fields, equation (1), can be used to produce an acceleration or a stopping of charged particles by manipulating the time dependence of n_e and n_i. From the time-dependent electric field, we get the Gauss law by time differentiation, substitution of the equations of continuity, and integration over the spatial coordinate (without discussing the integration constant),

$$\frac{\partial}{\partial t} E = 4\pi e(n_e v_e - Z v_i n_i) \quad . \tag{2}$$

Further time differentiation, substitution by the equations of motion and re-arrangement of the terms with the collision frequency ν results in

$$\frac{\partial^2 E}{\partial t^2} + \nu \frac{\partial E}{\partial t} + \omega_{po}^2 E = E_0 \omega_{po}^2 + \frac{4\pi e}{m_e} \frac{\partial}{\partial x} (E_L^2 + H_L^2)/8\pi + 4\pi e \nu (n_e v_i - Z_n{}^i v_e) \tag{3}$$

where

$$E_0 = \frac{4\pi e}{\omega_{po}^2} \left[\frac{\partial}{\partial x} \left(\frac{3 n_i k T_i}{m_i} + 2 n_i v_i^2 \right) - \frac{\partial}{\partial x} \right] \frac{3 n_3 k T_e}{m_e} + n_e v_e^2 \tag{4}$$

and

$$\omega_{po}^2 = 4\pi e^2 \frac{n_e}{m_e} + \frac{Z^2 n_i}{m_i}$$ (5)

The driving laser field E_L and H_L were used for the following section. Neglecting (3) for $\nu << \omega_p$ and assuming a vanishing laser field ($E_L = H_L = 0$), the local solution of (3) results in an electric field,

$$E = E_0 \left\{ 1 - \exp\left(-\frac{\nu}{2} t\right) \left[\cos\left(\sqrt{\omega_{po}^2 - \nu^2} t\right) + \frac{\nu}{2\sqrt{\omega_{po}^2 - \nu^2}} \sin\left(\sqrt{\omega_{po}^2 - \nu^2} t\right) \right] \right\}$$ (6)

which oscillates with a frequency close to the plasma frequency. These oscillations, however, are damped (exponentially decaying) by the collision frequency such that after a time $t >> 2/\nu$ a nearly constant electric field E remains, as seen numerically (Fig. 5). This field E is determined by the spatial gradients of the enthalpy of the ions and electrons given in the brackets within the square bracket of equation (4) divided by the particle masses.

The (nearly static) electric field has an understandable order of magnitude at least for the early time of the damping processes of an initially stationary inhomogeneous plasma where any electron and ion velocity is small and from the big ratio of the ion to the electron mass. It follows,

$$E \approx \frac{4\pi e}{\omega_{po}^2 m_e} \frac{\partial}{\partial x} 3 n_e k T_e \quad ,$$ (7)

or

$$eE \approx \frac{1}{n_e} \frac{d}{dx} 3 n_e k T_e \quad .$$ (8)

We see that the electric field E is simply caused by the gradients of the electron density and/or the temperature temporally changing. Therefore the expression "inhomogeneity field" or "dynamic electric field" has been used. In the stationary approximation (8) the inhomogeneity field corresponds to the (thermionic) work function for the electrons that moved from the plasma interior to the vacuum (or an electrode) outside corresponding to the spread Debye sheath (Hora, 1983).

This result of a quasi-potential value $eE_i \ell = eV_c = 3kT_e$ corresponds to the measured 600 volts in a tokamak of a maximum temperature of 200 eV where the missing factor 3 was mentioned as an unexplained result (Razumova, 1983). If there are experimental conditions where, instead of a factor 3, a factor 10 (Eliezer and Ludmirsky, 1983) has been measured from the electric fields in laser-produced plasmas with (spread) Debye lengths over 10 to 100 times of its usual value, this may be explained for the more general conditions of the time developing enthalpy in (4) which was simplified in (8). Higher values than a factor 3 were also measured in cases of double layer experiments.

IV. ELECTRIC FIELDS AND DL'S WITH LASER INTERACTIONS

For the case of incident laser radiation, the computer output of the following cases will be discussed (Hora et al., 1984). A 25 μm thick plasma slab of initial 10^3 eV temperature and zero velocity with an ion and electron density of symmetric parabolic shape very close to the value in Figure 6 for t = 0.5 ps is given. No laser interaction occurs during the first 0.5 ps such that the minor thermal expansion does not change much of the initial density profiles while this time is long enough to damp down the fast electric oscillations. At t = 0.5 ps, a neodymium glass laser field incident from the left-hand side is switched on with a vacuum amplitude of 10^{16} W/cm^2. The resulting electric field density $\overline{E_L^2}/8\pi$ averaged over a laser period is given in Figure 7 showing an exponential decay for x > 8 μm because of superdense plasma there. At several time steps up to 1.5 ps, the resulting densities (Fig. 6) and ion velocity (Fig. 8) are given. The density (Fig. 6) shows a strong minimum (caviton) at x = 5 μm indicating the predominance of the nonlinear force-driven ponderomotion. Plasma blocks with ion velocities up to 10^7 cm/s are created in agreement with simplified estimates of the strong acceleration densities.

The resulting differences of the ion and electron densities are given in Figure 9. They cause fast changing electric fields E given in Figure 10 reaching values beyond 10^8 V/cm. This value corresponds to the expected numbers: the dielectrically swollen laser field E_L in the plasma can be up to 10^{11} V/cm decaying to zero within 10^{-3} cm.

Using similar simplifying approximations as in equation (6), including the oscillating laser field, the longitudinal (dynamic electric) field E from (3) is given by

$$
E = 4\pi e \left[\frac{\partial}{\partial x} \left(\frac{3n_i kT_i}{m_i} + Zn_i v_i^2 \right) - \frac{\partial}{\partial x} \left(\frac{3n_e kT_e}{m_e} + n_e v_e^2 \right) + \frac{1}{m_e} \frac{\partial}{\partial x} (E_L^2 \right.
$$

$$
\left. + H_I^2)/8\pi \right] \left[1 - \exp\left(-\frac{\nu}{2} t \right) \cos \omega_p t \right] + \frac{\omega_p^2 - 4\omega^2}{(\omega_p^2 - 4\omega^2)^2 + \nu^2 \omega^2} \tag{9}
$$

$$
\times \frac{4\pi e}{m_e} \frac{\partial}{\partial x} \overline{(E_L^2 + H_L^2)} \cos 2\omega t + \frac{2\nu\omega}{(\omega_p^2 - 4\omega^2)^2 + \nu^2 \omega^2} \frac{4\pi e}{m_e} \frac{\partial}{\partial x} (E_L^2 + H_L^2) \sin 2\omega t \quad ,
$$

where the first term represents the former quasi-static field E, (4) with its damped-fast oscillations but modified by the amplitude of the fast time-averaged laser field density $E_L^2 + H_L^2$ which is dominant before the gas dynamic pressure $n_e kT_e$ acts. As $E_L^2 + H_L^2$ changes fast (still very slow compared to the laser oscillation time), a quite complicated result for E_s can be seen in Figure 12, in which the exact result is given without the simplification of equation (9). Considering the complicated time dependence of n_i, n_e, T_i, T_e, E_L and H_L, the term "potential" is no longer applicable and E is a dynamic electric field following equation (1). Only at stationary conditions, the pressure may be a potential or one may consider a ponderomotive potential.

The second and last terms in equation (9) oscillate quickly with twice the laser frequency. As E_s is directed to the x-direction, i.e., perpendicular to the E_L of the laser field, we have — obviously for the very first time — the coupling of the transverse electromagnetic wave with the longitudinal plasma waves which is made possibly only by overcoming the restriction of the quasi-neutrality of the earlier two-fluid theory, and without the artificial inclusions of microscopic model assumptions. The last term in equation (9) has a resonance denominator, causing a very steep increase of the oscillation amplitude at $2\omega = \omega_p$. As we consider a case of purely perpendicular incidence without

114

any surface rippling and no self-focusing, we have here a new type of resonance mechanism acting in the evanescent part of the wave in a depth of 4 times the critical density, if there is still sufficient laser intensity. This resonance is basically different from Denisov's reesonance absorption which works at oblique incidence for p-polarization only (Denisov, 1957). The new type of perpendicular incidence resonance can be significant (Hora and Ghatak, 1985) as will be discussed in Section V with other phenomena.

The numerical result of Figure 9 can explain the inverted double layers in laser-produced plasmas if cavitons are produced by the nonlinear forces. The existence of the electric fields in plasma surfaces had been shown directly by electron beam probes and from electrostatic acceleration of a small number of the nonlinear force-accelerated ions. A more systematic experiment was done by Eliezer and Ludmirsky (1983), Ludmirsky et al. (1985), and Eliezer et al. (1986) where the temporal dependence of charge of the expanding plasma and the temporal change of the target potential were measured. A very unexpected observation was that the plasma leaving the target was first positively charged and then negatively charged. This was in contrast to the general expectation that an electron cloud should first leave the plasma. The picture changes, however, if we look at all fields at the surface and in the interior of the plasma in the genuine two-fluid model if a nonlinear force-driven caviton is generated. Figure 9 shows, near $x = 25$ μm, where no laser light acts, that a negatively charged plasma expands before the positively charged plasma follows. Near $x = 0$, one sees that first a strong positively charged plasma is emitted and then a negatively charged plasma before a nearly neutral plasma follows. This is the result of the caviton generation. Though the experiment (Eliezer and Ludmirsky, 1983) was on the nanosecond time scale, the comparison with the picosecond processes should be justified not only by the correct polarity of the plasma charges but also from other experiments that showed the picosecond buildup of the cavitons (Briand et al., 1985). The experiment of Eliezer and Ludmirsky (1983) is an indirect proof that they had also generated cavitons.

A further experiment which can be explained is the energy upshift of alpha particles from laser fusion pellets. It was observed (Gazit et al., 1979) that the DT-alpha particles from laser fusion pellets had not the expected maximum energy of 3.56 MeV but showed an upshift by $\Delta\epsilon$ of up to 0.5 MeV. The exact description of the interaction of the alphas with the spatially and temporally varying electric field $E(x,t)$ in the (one-dimensional) plasma corona is very complicated as the field is non-conservative. The velocity of the alpha particle, v, with an initial velocity, v_o and mass, m_α is given by the complex integral equation,

$$v(x) = v_o + \frac{2e}{m_\alpha} \int_{t_1}^{t_2} E[x(t),t]\, dt \quad ; \quad x = v(t)dx \quad .$$ (10)

For a very simplified estimate we use,

$$d\left(\frac{m_\alpha}{2}\, v^2\right) = 2eE[x,t(x)]\, dx \quad ,$$ (11)

with an average value $\overline{E}$ of E to give the increase of the alpha energy,

$$\Delta\epsilon = 2\overline{eE}\, \Delta x \quad ,$$ (12)

after acceleration along a length Δx of the plasma corona. In order to reach $\Delta\epsilon = 0.5$ MeV for $\Delta x = 10$ μm, we find $\overline{E} = 2.7 \times 10^3$ V/cm. Such fields for Nd glass laser pulses of 10^{16} W/cm² are possible only if the nonlinear force-produced cavitons (Fig. 10) are present, since lengths very much larger than 10 μm are not realistic. Thermally produced fields of up to 10^6 V/cm could not produce the measured upshifts of 0.5 MeV. Our results, therefore, are

not only a rough explanation of the alpha upshift by the large electric fields in the cavitons but are also a clear indication that no thermal electric field can cause the measured upshifts.

We have preliminary results on the exact numerical solution of equation (10) from E-values derived from laser plasma dynamics (Green et al., 1985). It was discovered that broad E-maxima move within 0.3 to 0.9 of the speed of light (Fig. 10). The correct phasing of the charged particles in the field does lead to an acceleration by multiples of the estimate of equation (12). It can be shown how today available CO_2 lasers (Antares) with 80 TW short laser pulses and a sequence of several pulses can shift electron clouds of GeV energy to TeV electron energy. The caviton (nonlinear force) fields of the type in Figure 12 of 10^{11} V/cm act like the (non-conservative) pump fields in the microwave cavities of an accelerator. The phasing of the nonlinear force field electron acceleration is an extension of the concept based on many years of work on the nonlinear force and the then recent results on high electric fields in plasmas (Clark et al., 1985).

V. DISCUSSION AND FURTHER RESULTS

Against all prior assumptions of space charge quasi-neutrality of plasmas, our analysis of genuine two-fluid hydrodynamics has shown very high electric fields inside of plasmas. These are simply given by gradients of density and/or temperature (inhomogeneity fields) modified by plasma oscillations due to changes in mechanical motion for free expansion or due to the nonlinear force-produced block motion or cavitons. A consequence for laser fusion of the resonance at perpendicular incidence may be significant, but it is only one of numerous anomalous and nonlinear phenomena known. A more important consequence, however, is the fact that the electric fields in the double layers change the thermal conductivity drastically. In order to fit experiments with too low temperatures of the interior of the plasma-irradiated pellet and the low fusion neutron emission with the computations, fitting factors f for reduction of the thermal conduction were used since 1979 (Ding et al., 1983; Richardson et al., 1986) which were around 1/100. The results of the double layers offer a quantitative theory for this reduction. This and further consequences of the reviewed results will be discussed in this section (Hora, 1985b).

A. Double Layers and Reduction of Thermal Conduction

The generation of electric fields and double layers inside of plasmas at gradients of density and/or temperature can cause the inhibition (reduction) of thermal conductivity below the Spitzer-value for the plasma electrons. This inhibition was detected indirectly from laser fusion experiments when the interior of the compressed pellet did not reach the temperatures expected from electronic thermal conduction (Cicchitelli et al., 1984), expressed by a reduction factor f. This can be understood simply from Figure 11 where a double layer is produced between a hot laser-irradiated corona and the cold pellet interior.

The energetic electrons have left the positive area (causing a mostly negligible preheat), and the following electrons are returned by the positive charges. If a total disconnection of the electron transport through the double layer is considered because fo the return current of the electrons, only the ions can transport the heat. The thermal conductivity κ is then that of the ions, κ_i given by that of the electrons κ_e,

$$\kappa = \kappa_i = \kappa_e (m/m_i)^{1/2} \ ,$$

(13)

where m is the electron mass and m_i is the ion mass. This gives the factor $\kappa/\kappa_e = 1/70$ for the ion mass of deuterium and tritium used in the experiments where a computation fit with a factor 1/100 was shown (Ding et al., 1983; Richardson et al., 1986).

116

This explanation of the reduced thermal conduction by the double layer does not take into account that the electrons in the hot plasma may have a Maxwellian equilibrium distribution of their energy with a small number of very fast electrons penetrating the double layer. The factor f of the thermal conduction by the fast electrons through the double layer is given by the ratio of the energy flux density of the electrons (of temperature T) in the x-direction E_{out} at $x = x_2$ in Figure 11 over the energy flux density E_{in} of the electrons incident from the left-hand side at $x = x_1$,

$$f = E_{out}/E_{in} \tag{14}$$

Based on an equilibrium distribution n of the electrons with the velocity $v = (v_x; v_y; v_z)$

$$n(v_x, v_y, v_z) = \left(\frac{m}{2kt}\right)^{1/2} n_0 \exp\left(-\frac{mv^2}{2kT}\right) \quad , \tag{15}$$

where n_0 is the (spatial) electron density, we find,

$$E_{in} = \int_{-\infty}^{+\infty} v_x \frac{m}{2} v^2 n \, dv_x dv_y dv_z = 4\pi n_0 m(kT/2\pi n)^{3/2} \quad . \tag{16}$$

The flux density E_{out} must take into account the fact that the energy of the electrons beyond the double layer is reduced by the electric potential eV_0 of the layer and only electrons with a velocity component in the x-direction $v_x > v_{xo} = (2eV_o/m)^{1/2}$ will be transmitted. This results in,

$$E_{out} = \int_{+\infty}^{+\infty} \int_{+\infty}^{+\infty} dv_y dv_z \int_{v_{xo}}^{\infty} v_x(mv^2/2 - eV_0)n \, dv_x \tag{17}$$

$$= 4\pi n_0 m(kT/2 \, m)^{3/2} \exp(-\alpha) \quad , \tag{18}$$

where

$$\alpha = eV_0/(kT) . \tag{19}$$

The final result

$$f = \exp(-eV_0/kT) \tag{20}$$

is then a simple Boltzmann factor.

From the experiments (Eliezer et al., 1985) there may be good reasons that eV_0 is more than 5 kT up to at least 10 kT. In this case f is less than 1/70 given from the thermal ion conduction for D-T plasma. If we, however, work with the simple (one-dimensional) adiabatic relation $eV_0 = 3kT$, the factor f is 1/20, showing a well reduced but electronically dominated thermal conduction.

117

We conclude that the reduction of the thermal conductivity by the electrostatic double layer between hot and cold plasma does not necessarily drop down to the low value of the ion conductivity, and a reduced electronic thermal conduction by the energetic tail of the electron energy distribution may remain. For the analysis of future experiments, these variables of thermal conductivity factors have to be taken into account if no further competitive mechanisms (e.g., turbulence, classical thermal conductivity in inhomogeneous media) are taken into account. With respect to the energetic (so-called "hot") electrons in laser-produced plasmas, it has been found that there does not exist a fast Maxwellian tail of the energy distribution (McCall, 1983) proving that these energies are due to nonthermal quiver motion. These electrons would not be able to contribute to the thermal conduction mechanism discussed here. Another indication that these energetic electrons are not of a thermal nature (very probably representing the coherent quiver motion) is the very anistropic "butterfly" directivity of the x-ray emission.

The reduced thermal conductivity in the double layers at steep thermal or density gradients, as given by the dynamic electric field strength E (inhomogeneity field), equation (9), is an important consideration in pellet ablation-compression computations whether the driving is by particle beams or by lasers. As long as no nonlinear forces, nonlinear optical response (absorption), and parametric effects are involved, there is a lot of similarity to the laser driving where the computer evaluation of the hydrodynamics automatically results in a compression of the plasma below the driver heated ablating corona. As a sufficient temperature is needed for the compressed plasma in the pellet core, the heat transport between corona and core is essential. If the classical electronic conductivity is used (without change by the inhomogeneity fields or the space charges of the double layers), it is no surprise that the laser ablation resulted in high core densities well after the mechanical recoil, but the temperatures were too low (Yaakobi et al., 1984) and the neutron gains from fusion were 10^4 times less than expected at this ablation mode (Hora, 1981).

It should be noted that the inhibition of electron transport by the double layer (Fig. 11) is valid also for the energetic (erroneously called "hot") electrons. Even if their energy is some 100 keV as in CO_2 laser-irradiated fusion pellets, the number of electrons to produce a Debye layer only can move to the pellet interior to preheat the plasma. The following electrons, especially if they have no fast Maxwellian tail of a distribution, cannot pass the 100 keV DL. The usual electron preheat in pellets is then only a few mJ at some 100 J absorption of laser radiation.

B. New Resonance at Perpendicular Incidence

The only resonance phenomenon (to be distinguished from parametric instabilities) at laser-plasma interaction is Denisov's (1957) resonance absorption which only may work at oblique incidence of laser radiation for p-polarization. White and Chen (1974) published the first derivation with the electric field description for a collisionless plasma, showing a resonance maximum of the electric field component of the laser field in the direction perpendicular to the surface at the critical density for laser light which is obliquely incident and p-polarized. The resonance in this case is in the evanescent field region below the reflection point of the propagating radiation. When generalizing this derivation (Hora, 1979) to the case with collisions, the pole of the effective dielectric constant suddenly changes from minus infinity to a high positive value and the width of Denisov's resonance maximum can be directly calculated in a transparent way (Hora, 1981).

In difference to this, a resonance was found (Hora and Ghatak, 1985) at perpendicular incidence of the (laser driven) longitudinal dynamic plasma field E (not the laser field) of such magnitudes that some phenomena at perpendicular incidence may be explained now where Denisov resonance was mentioned hoping that density ripple provides the necessary oblique incidence. This was questionable with respect to the low angle of incidence.

While the results on the numerical theory of the genuine two-fluid model were most general, the simplified analytical evaluation of the equations was possible by neglecting terms because of the electrons to ion mass ratios,

dropping discussions of integration constants and reducing to local differentiations and by coupling with Maxwell's equations. In a laser-irradiated plasma for perpendicular incidence, an inhomogeneous oscillation equation is then derived (with driving terms) for the (longitudinally oscillating dynamic) electric field E which is perpendicular to the driving laser field E_L (and H_L). The solution of the differential equation resulted in equation (9).

The last term in equation (9) significantly indicated a resonance of $\omega_p = 2\omega$ (4 times the critical density). This was noted approximatively before and evaluated roughly numerically (Hora et al., 1984; Hora and Ghatak, 1985). The more precise evaluation was performed by Goldsworthy et al. (1986). It is stressed again that in evaluating the last term in equation (9) before time averaging, the whole nonlinear force needs to be strong enough such that the term proportional to $\sin(2\omega t)$ resonantly dominates. The coefficient of this term is

$$E_R = \frac{2\nu\omega}{(\omega_p^2 - 4\omega^2)^2 + 16\nu^2\omega^2} \frac{e}{2m} \frac{\partial}{\partial x} (E_L^2 + H_L^2) \ . \tag{21}$$

In order to get the solutions E_L and H_L from the inhomogeneous plasma we especially select the condition that the electron density is increasing linearly in the region of the evanescent field. In this case, the wave equation can be solved by Airy functions (Lindl and Kaw, 1971; Goldsworthy et al., 1986). The full resonance amplitude given in equation (21) can now be evaluated numerically for any slope of the linear density profile and a constant temperature (collision frequency) by numerically solving E_L, deriving H_L from Maxwell's equations and calculation ñ, and using these values to compute the resonance amplitude E_R.

Numerical evaluation of the resonance phenomenon described in the previous sections was carried out for a plasma irradiated by neodymium glass laser light.

In Figure 12 the value of E_R of the resonant field amplitude is plotted as a function of depth x where the zero of the depth axis represents the critical layer. Noting that the resonant field depends linearly on the incident laser intensity, only the results of the realistic case, an initial intensity of 10^{16} W/cm^2, are discussed.

The electron collision frequency ν is density dependent and is given by

$$\nu = 2.72 \times 10^{-5} \frac{n_e}{T^{3/2}} \ \ell n \, \Lambda \tag{22}$$

where n_e is the electron density per cubic centimeter, T_e is the electron temperature in electron volts (eV), and $\ell n \, \Lambda$ is the Coulomb logarithm.

Results have been obtained for several different plasma temperatures, of which the case for 1 keV is given in Figure 12. The gradient of the density profile was varied as a parameter of the curves. The gradient is determined by α,

$$\alpha^2 = (\partial n_e / \partial x)^{-1} \omega / c \ \ , \tag{23}$$

where the maximum of each curve is at such depth x where the density has reached 4 times the critical density. Figure 12 shows the results for the conditions $T_e = 1$ keV for different depths of the maxima. The density gradients α^2 range from 140 to 240. T_e is the effective temperature (chaotic plus coherent motion of the electrons) which can well have the values of 10^4 eV at high laser intensities. Figure 13 evaluates the maximum field E_{max} of E_R as E_{max}/E_L related to the amplitude of the laser field in vacuum for various plasma temperatures.

Figure 13 shows that any strong resonance effect can be expected only when the profile has a very high steepening such that 4 times the density is reached at one wavelength or less below the critical density. This high steepening, however, is not unusual in cases where the nonlinear force is dominating the plasma dynamics (Ahlstrom, 1982; and Montes and Willi, 1982).

For laser-plasma interaction at perpendicular incidence a resonance is analyzed which produces high electric fields oscillating with the second harmonic perpendicular to the plasma surface (longitudinal oscillations). These fields are found in the application of a new genuine two-fluid hydrodynamic theory which is not restricted by space charge quasi-neutrality. For linear density profiles beyond the critical density, the resonance maxima are evaluated on the basis of the Airy functions and reach considerably high values for such profiles which can be generated by nonlinear force driving of the laser-plasma dynamics. Even the necessary high temperatures (appearing then as quiver energy as in the theory of the optical constants) seem to be reasonable. This perpendicular resonance mechanism may possibly be distinguished from the ordinary nonlinear force acceleration by the appearance of electron bursts.

C. Density Independent Second Harmonics Emission

A rather surprising phenomenon was reported by Mayer et al. (1982). Irradiating a plane target in vacuum by a neodymium glass laser, a side-on time-integrated picture in the second harmonic frequency showed the large plasma plume in nearly constant 2ω intensity though the plasma density has been lower by orders of magnitudes in the outermost parts of the plasma than in the focus. A similar observation was detected more precisely (Aleksandrova et al., 1985) from a 400 μm diameter pellet irradiated by a 2 ns rectangular neodymium glass laser pulse (Delfin), where a nearly constant 2ω radiation from a sphere of 2 mm diameter (to which the pellet corona had expanded during the laser irradiation) was detected. The fact that the very low peripheric plasma density emits the same 2ω radiation as the inner part of the cut-off density can be explained by the middle term of equation (9). The factor is nearly density-independent at low ω_p ($\omega_p \ll \omega$), and the standing wave pattern may result in a constant nonlinear force factor; therefore, this term of equation (9) should produce a spatially constant term of the dynamic electric field E_s as long as the laser is shining.

While this gives a qualitative explanation of the observation, a quantitative evaluation of the transfer of the dipole oscillation of E into emission of electromagnetic radiation results in an emission power of about 10^6 watts (Goldsworthy et al., 1986). The experimental evaluation of the calibration of the experimental results in a 2ω-power of about 10^5 watts (Fedotov et al., 1985).

D. E x B Rotation of Plasmas

Since the dynamic electric fields, e.g., (9), in plasmas are (apart from the oscillations, damping, and transient effects of internal and/or external plasma dynamics) in a simplified way due to gradients of electron density and/or temperature, their $\mathbf{E} \times \mathbf{B}$ interaction with external magnetic fields $\mathbf{B}$ may cause drift motion or rotation of plasmas. We shall first discuss this as examples with plasmas without laser irradiation, e.g., with tokamaks and stallarators, and then consider the extremely high E-fields by the nonlinear forces in laser-produced plasmas that describe fast block acceleration of plasma. There is a similarity to the simple ambipolar field effects.

The consequences for dynamic inhomogeneity electric fields in tokamaks are not only the modification of the thermal conduction but also the resulting basic change in the dynamics. The radial decay of density and temperature in any plasma column produces an inhomogeneity field in the radial direction which under stationary conditions is given by equation (9)

$$E_s = \frac{3}{en_e} \frac{d}{dx} n_e kT_e \quad \bullet \tag{24}$$

This field combines with the toroidal magnetic field B and causes a drift with the velocity of the poloidal plasma rotation in meters/second (Fig. 14)

$$v_{rot} = 3T/rB \quad , \tag{25}$$

where the electron temperature is in electronvolts, the radius r of the plasma column is in meters, and B is in Tesla.

Measurements from tokamaks fully agree with the result of equation (25). Bell (1979) measured rotation velocity $v = 2 \times 10^3$ m/s for $r = 2 \times 10^{-2}$ m, B = 0.5 T, $T_e = 50$ eV for which case equation (25) results in $v = 2.4 \times 10^3$ m/s. These plasma rotations were detected from the Doppler shift of Hα-lines, with similar agreement with equation (25), by Sigmar et al. (1974) who did not interpret them as plasma rotation, but as an anomaly of hot protons in the banana and plateau regimes. The agreement with equation (25), however, favors an interpretation of a simple rotation.

The same is with the experiment at the stellarator W7, where the result of 1980 agrees with a rotation according to equation (25). As this experiment was with tangential neutral beam injection, one would have had to exclude the rotation of these neutrals, which is difficult. Recent measurements at W7 without neutral beam injection but with plasma production by intensive microwave irradiation and heating (Thumm, 1985) result in exactly the same rotation given by equation (25).

REFERENCES

Ahlstrom, H. G., *Physics of Laser Fusion*, National Technical Service, Springfield, Virginia, 1982.

Aleksandrova, I. V., W. Brunner, S. I. Fedotov, R. Guther, M. P. Kalashnikov, G. Korn, A. M. Maksimchuk, Y. A. Mikhailov, S. Ploze, R. Riekher, and G. V. Shlizkov, *Laser and Particle Beams, 3*, 197 (1985).

Alfvén, H., *Tellus, 10*, 104 (1958).

Alfvén, H., *Cosmic Plasmas*, Reidel Publ. Co., Dordrecht, Holland, 1981.

Alfvén, H., and P. Carlqvist, *Solar Phys., 1*, 220 (1967).

Baker, K. D., N. Singh, L. P. Block, R. Kist, W. Kampa, and H. Thiemann, *J. Plasma Phys., 26*, 1 (1981).

Bell, M., *Nucl. Fusion, 13*, 33 (1979).

Bernstein, I. B., J. M. Green, and M. D. Kruskal, *Phys. Rev., 108*, 546 (1957).

Bohm, D., *Characteristics of Electric Discharges in Magnetic Fields*, edited by A. Guthrie and R. K. Wakerling, McGraw Hill, New York, 1949.

Briand, J., V. Adrian, M. El Tamer, A. Gomes, Y. Quemener, J. P. Dinguirared, and J. C. Kieffer, *Phys. Rev. Lett., 54*, 38 (1985).

Carlqvist, P., *Solar Phys., 63*, 353 (1979).

Carlqvist, P., *Astrophys. Space Sci., 87*, 21 (1982).

Cicchitelli, L., S. Eliezer, J. S. Elijah, A. K. Ghatak, M. P. Godsworthy, H. Hora, and P. Lalousis, *Laser and Particle Beams, 2*, 467 (1984).

Clark, P. J., S. Eliezer, F. J. M. Farley, M. P. Goldsworthy, F. Green, H. Hora, J. C. Kelly, P. Lalousis, B. Luther-Davies, R. J. Stening, and J. C. Wang. *Laser Acceleration of Particles*, AIP Conf. Proc. 130, edited by C. Joslin et al., p. 380, AIP, New York, 1985.

Coakley, P. G., and N. Hershkowitz, *Phys. Lett. 83A,* 131 (1981).

DeGroot, J. S., C. Barnes, A. E. Walstead, and O. Buneman, *Phys. Rev. Lett., 38,* 1283 (1977).

Denisov, N. G., *Sov. Phys. JETP, 4,* 544 (1957).

Ding, L. M., T. W. Hai, and W. R. Wen, *Plasma and Nuclear Fusion in China, 1,* 187 (1983).

Duderstadt, J. J., and G. A. Moses, *Laser and Particle Beams, 1,* 216 (1983).

Eliezer, S., and A. Ludmirsky, *Laser and Particle Beams, 1,* 251 (1983).

Eliezer, S., A. D. Krumbein, H. Szichman, and H. Hora, *Laser and Particle Beams, 3,*207 (1985).

Eliezer, S. et al., *Laser Interaction and Related Plasma Phenomena,* edited by H. Hora and G. H. Miley, Vol. 7, p. 345, Plenum, New York, 1986.

Fedotov, S. J., Y. A. Mikhailov, and G. V. Sklizkov, Private Communication, 1985.

Gazit, Y., J. Delettrez, T. C. Bristow, A. Entenberg, and J. Soures, *Phys. Rev. Lett., 43,* 1943 (1979.

Goldsworthy, M. P., H. Hora, and R. J. Stening, *Phys. Fluids,* to be published, 1986.

Green, F., G. W. Kentwell, H. Hora, and S. Tapalaga, *International Conference on Laser Sciences,* AIP Conf. Proc. 146, edited by W. C. Stwalley, p. 386, AIP, New York, 1985.

Haerendel, G., E. Rieger, A. Valenzuela, H. Föppl, H. Stenback-Nielsen, and E. M. Wescott, *European Space Programmes on Sounding-Rocket and Balloon Research in the Aurural Zone,* Report ESA SP-115, European Space Agency, Neuilly, France, 1976.

Hershkowitz, N., *Space Sci. Rev., 41,* 351 (1985).

Hershkowitz, N., G. L. Payne, C. Khan, and J. K. Dekock, *Plasma Phys., 23,* 903 (1981).

Hora, H., *Phys. Fluids, 12,* 182 (1969).

Hora, H., *Laser Interaction and Related Plasma Phenomena,* edited by H. Schwarz and H. Hora, Vol. 1, p. 383, Plenum, New York, 1971.

Hora, H., *Phys. Fluids, 17,* 939 (1974).

Hora, H., *Laser Plasmas and Nuclear Energy,* Plenum, New York, 1975.

Hora, H., *Nonlinear Plasma Dynamics,* Springer, Heidelberg, 1979.

Hora, H., *Physics of Laser Driven Plasmas,* Wiley, New York, 1981.

Hora, H., *Laser and Particle Beams, 1,* 151 (1983).

Hora, H., *Phys. Fluids, 28,* 3705 (1985a).

Hora, H., *Laser and Particle Beams, 3,* 87 (1985b).

Hora, H., and A. K. Ghatak, *Phys. Rev., 31A,* 3473 (1985).

Hora, H., D. Pfirsch, and A. Schlüter, *Z. Naturforsch, 22A,* 278 (1967).

Hora, H., P. Lalousis, and S. Eliezer, *Phys. Rev. Lett., 53,* 1650 (1984).

Knorr, G., and C. Goertz, *Astrophys. Space Sci., 31,* 309 (1974).

Kulsrud, A., *Phys. Today, 36*(4), 54 (1983).

Lalousis, P., Ph.D. Thesis, Univ. New South Wales, 1983.

Lalousis, P., and H. Hora, *Computational Techniques and Application,* CTAC-83, edited by J. Noye and C. Fletcher, p. 699, Elsevier, North-Holland, 1984.

Langmuir, I., *Phys. Rev., 33,* 954 (1929).

Leung, P., A. Y. Wong, and B. H. Quon, *Phys. Fluids, 23,* 992 (1980).

Lindl, J., and P. Kaw, *Phys. Fluids, 14,* 371 (1971).

Linlor, W. I., *Appl. Phys. Lett., 3,* 210 (1963).

Ludmirsky, A., S. Eliezer, B. Arad, A. Borowitz, Y. Gazit, S. Jackel, A. D. Krumbein, D. Salzmann, and H. Szichman, *IEEE Trans. Plasma Sci., 13,* 132 (1985).

Mayer, F. J. et al., *Abstracts, European Conference on Laser Interaction with Matter,* Schliersee, Germany, 1982.

McCall, G., *Phys. Fluids, 26,* 1943 (1983).

Mendel, C. W., and J. N. Olson, *Phys. Rev. Lett., 34,* 859 (1975).

Merlino, R., S. Cartier, M. Alport, and G. Knorr, *Second Symposium on Double Layers and Related Topics,* edited by R. Schrittwieser and G. Eder, p. 224, University of Innsbruck, 1984.

Montes, A., and O. Willi, *Plasma Phys., 24,* 671 (1982).

Mozer, F. S., C. W. Carlson, M. K. Hudson, R. B. Torbert, B. Parady, and J. Yatteau, *Phys. Rev. Lett., 38,* 292 (1977).

Pearlman, J. S., and G. H. Dahlbacka, *Appl. Phys. Lett., 31*, 414 (1977).

Peratt, A. L., *Phys. Rev. A, A20*, 2555 (1979).

Peratt, A. L., and R. L. Watterson, *Phys. Fluids, 20*, 1911 (1977).

Quon, B. H., and A. Y. Wong, *Phys. Rev. Lett., 37*, 1393 (1976).

ʼ Razumova, K. A., *Plasma Phys., 26*, 37 (1983).

Richardson, M. C. et al., *Laser Interaction and Related Plasma Phenomena*, edited by H. Hora and G. H. Miley, Vol. 7, p. 624, Plenum, New York, 1986.

Sato, T., and H. Okuka, *Phys. Rev. Lett., 44*, 740 (1980).

Sato, N., G. Popa, E. Märk, E. Mravlag, R. Schrittwieser, *Phys. Fluids, 19*, 70 (1976).

Schamel, H., *Physica Scripta, 20*, 336 (1979).

Shawhan, S. D., *J. Geophys. Res., 81*, 3373 (1976).

Sigmar, D. J., J. F. Clarke, R. V. Neidigh, and K. L. Vander-Sluis, *Phys. Rev. Lett., 33*, 1376 (1974).

Stangeby, P. C., and J. E. Allen, *J. Phys., D6*, 224 (1973).

Temerin, M., K. Cerny, W. Lotko, and F. S. Mozer, *Phys. Rev. Lett., 48*, 1175 (1982).

Temerin, M., and F. S. Mozer, *Second Symposium on Double Layers and Related Topics*, edited by R. Schrittwieser and G. Eder, p. 119, University of Innsbruck, 1984.

Thumm, M., Private Communication, 1985.

Torvén, S., *Phys. Rev. Lett., 47*, 1053 (1981).

Torvén, S., L. Lindberg, and R. T. Carpenter, *Plasma Phys., 27*, 143 (1985).

White, R. B., and F. F. Chen, *Plasma Phys., 16*, 565 (1974).

Yaakobi, B., J. Delettrez, R. F. McCrory, R. Marjoribanks, M. C. Richardson, D. Shvarts, J. M. Soures, C. Verdon, D. M. Villeneuve, T. Boehly, R. Hutchinson, and S. Letzring, *Laser Interaction and Related Plasma Phenomena*, edited by H. Hora and G. H. Miley, Eds., Vol. 6, p. 731, Plenum, New York, 1984.

Yabe, T., K. Mima, K. Yoshikawa, H. Takabe, and M. Hamano, *Nucl. Fusion, 21*, 803 (1981).

Yabe, T., Private Communication, 1985.
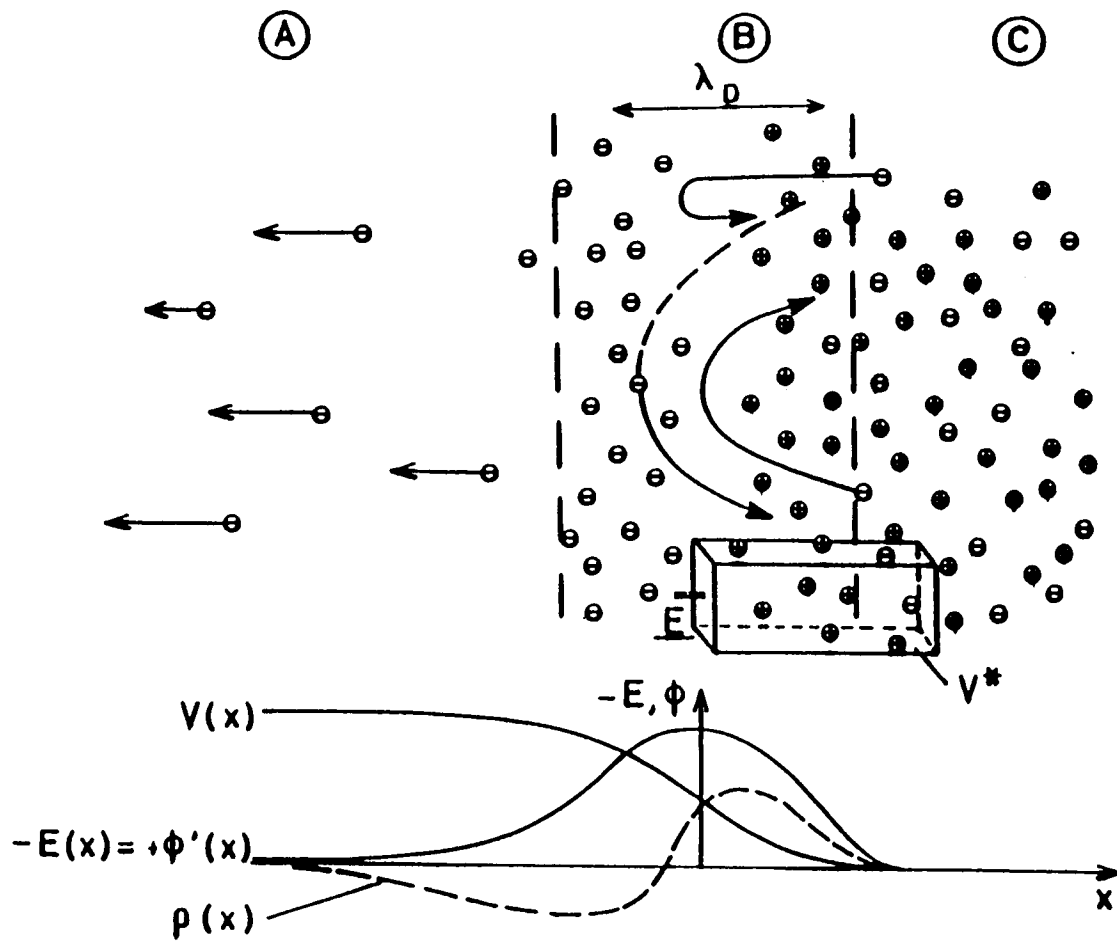
Figure 1. Between the vacuum range A and the space charge neutral interior of homogeneous plasma C, the plasma surface sheath is depleted by the escape of fast electrons until such a strong space charge is built up that the following fast electrons from the plasma C are electrostatically returned into C. The electric field E(x), due to the space charge density $\rho(x)$, and the resulting potential V are given schematically (Hora, 1975).

124
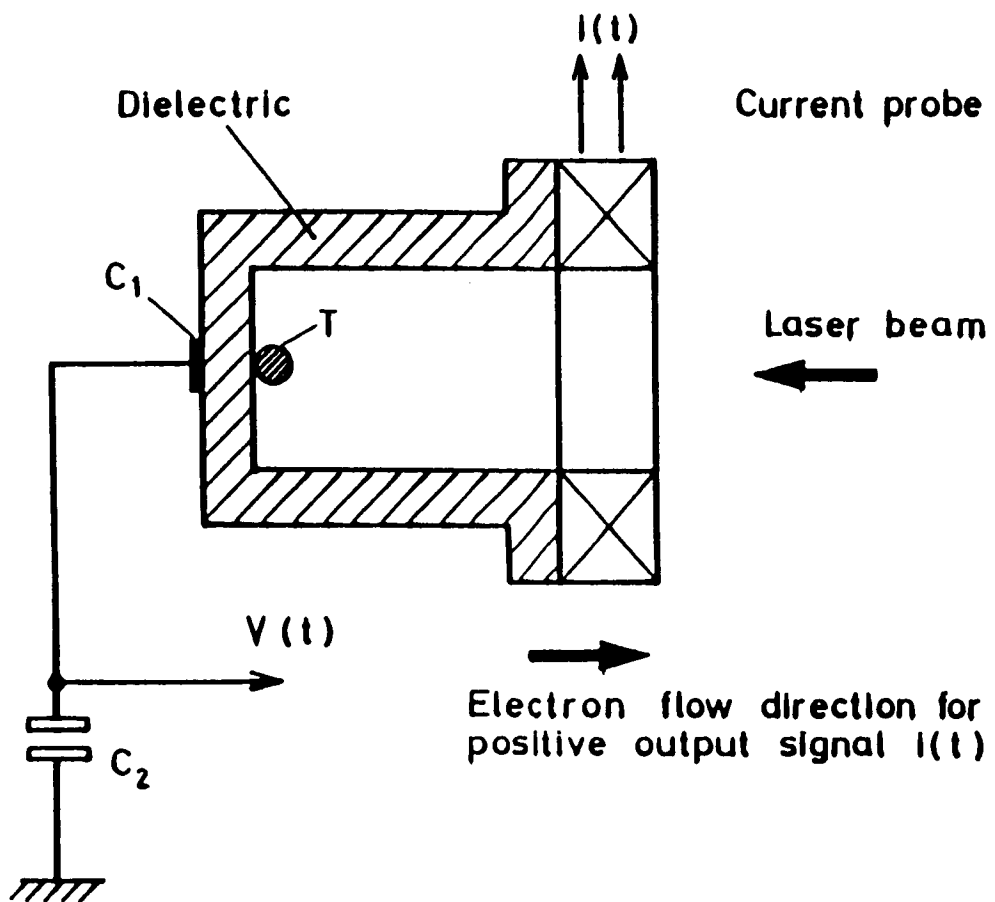
Figure 2. Experiment for a laser-irradiated pellet whose potential and the field [by the Rogowski coil I(t)] are measured.
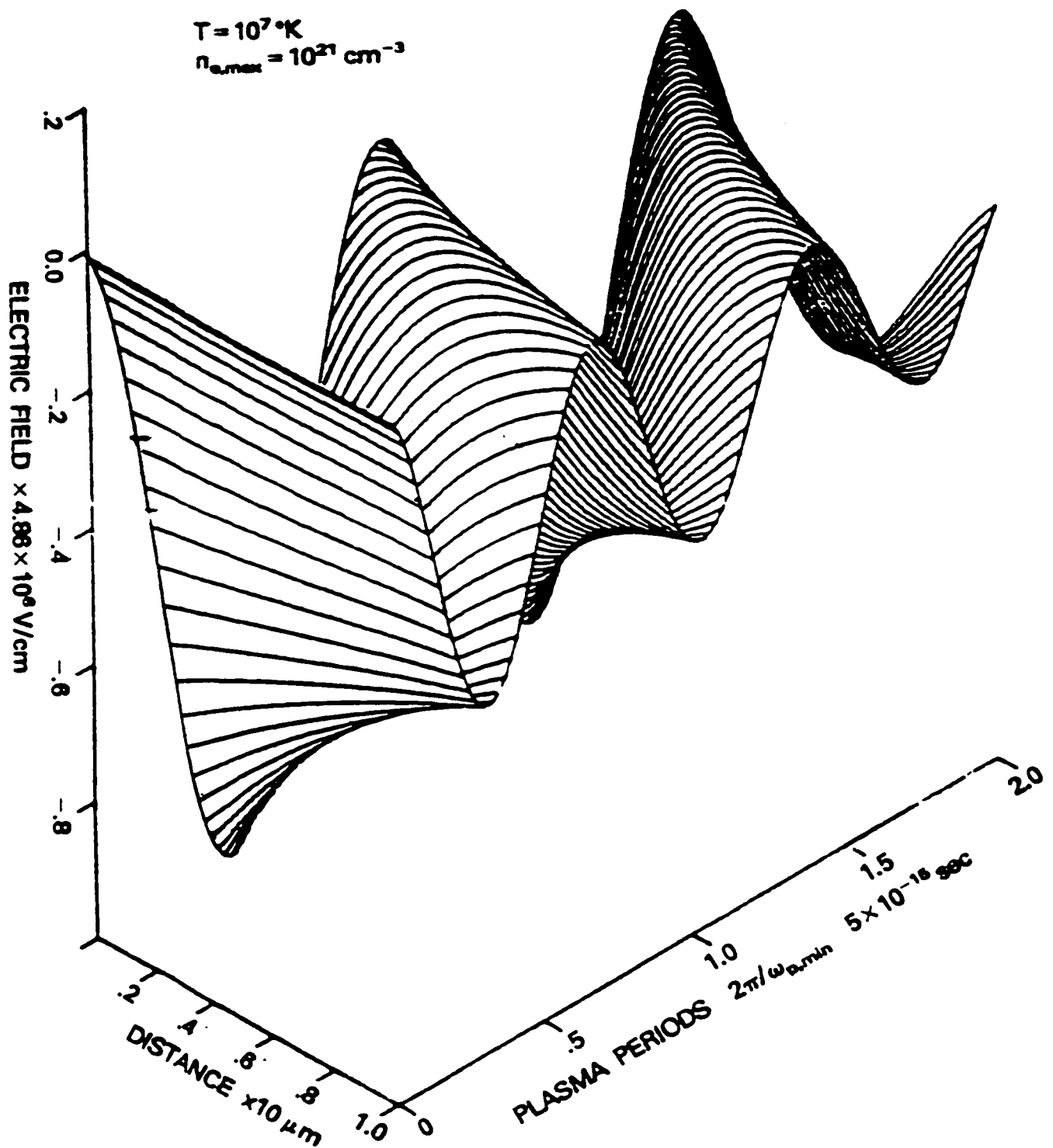
Figure 3. Time-dependent development of the longitudinal dynamic electric field E_s along the density with an initial ramp of linear plasma of initial temperature 10^7 K of 5×10^{20} cm^{-3} at x = 0 and 10^{21} cm^{-3} at x = 10 μm (Lalousis and Hora, 1983).
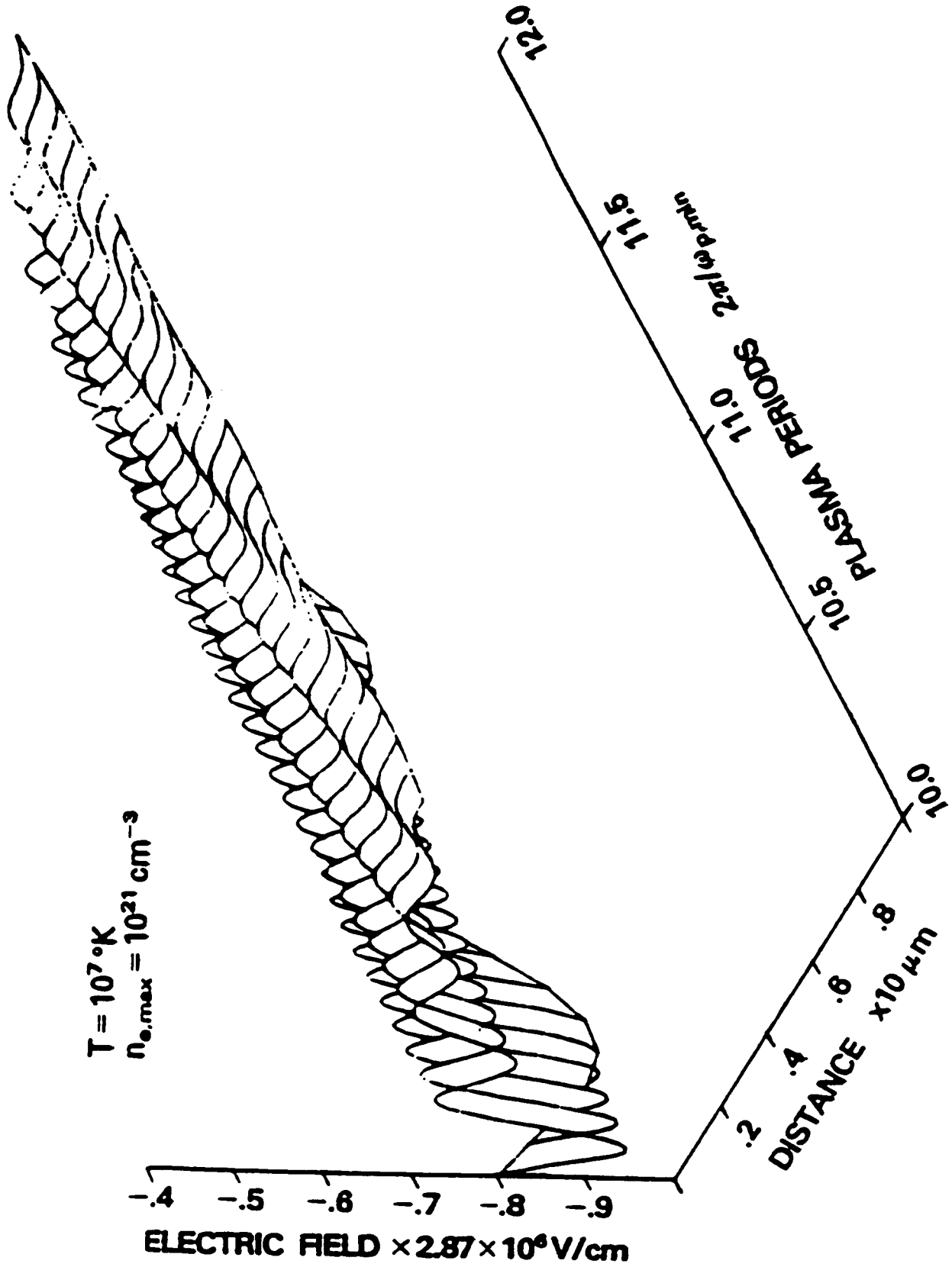
Figure 4. Same as Figure 3 for times of 10 and 12 plasma oscillation period (Lalousis nad Hora, 1983).

127
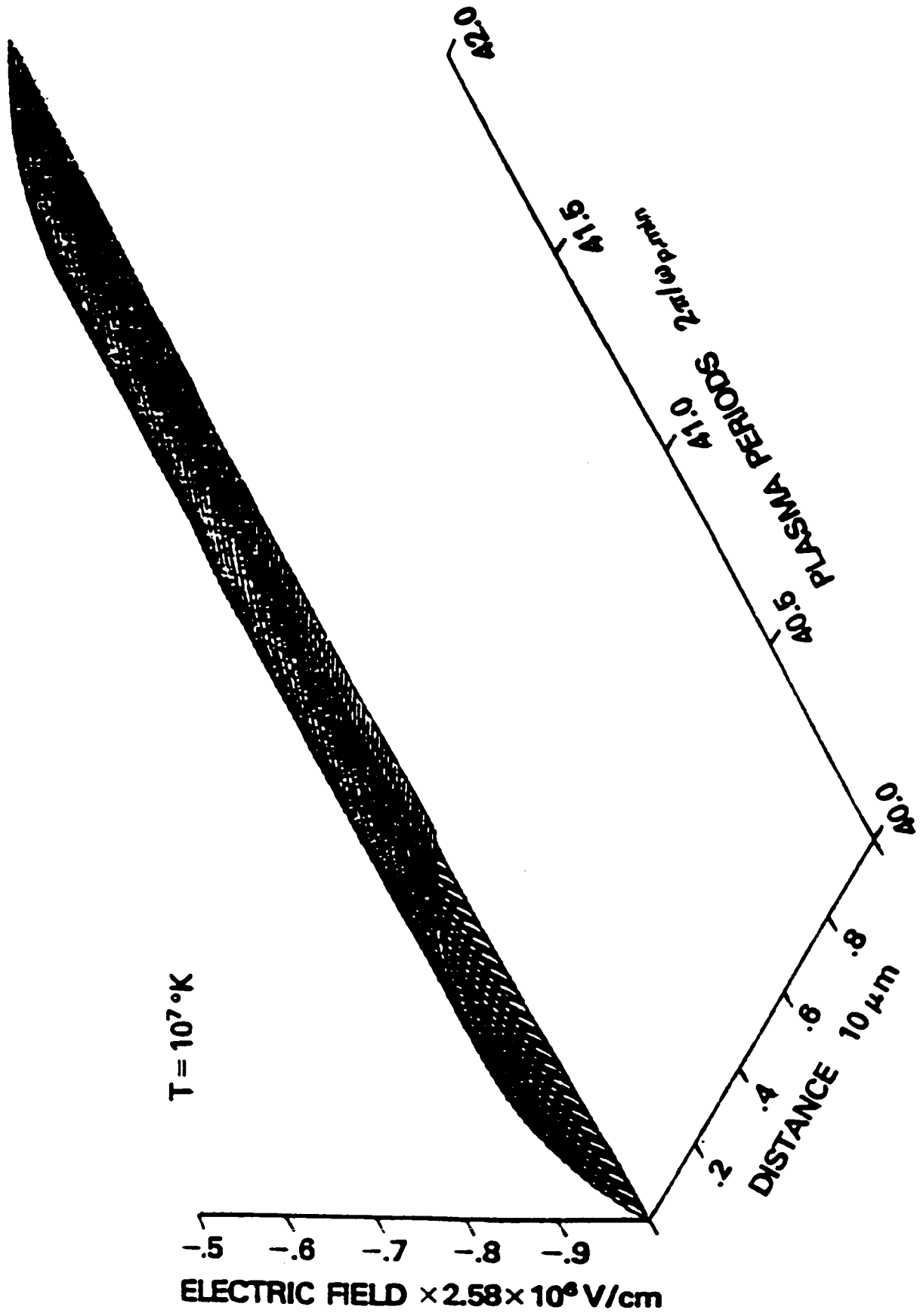
Figure 5. Same as Figure 3 for times of 40 to 42 periods (Lalousis and Hora, 1983).
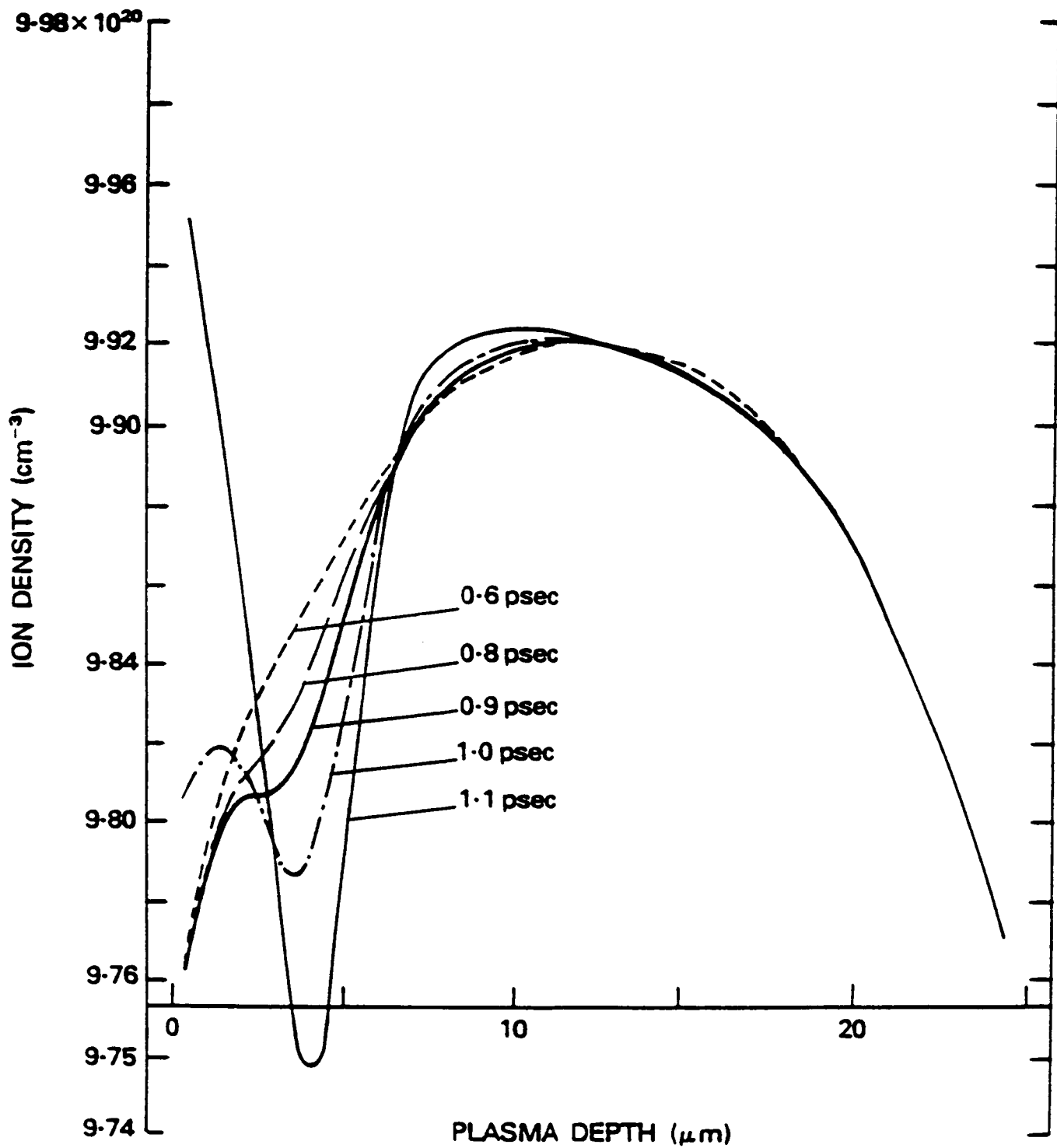
Figure 6. Ion density of a 25 μm thick hydrogen plasma slat initially at rest and 1 keV temperature irradiated from the left-hand side by a 10^{16} W/cm^2 Nd glass laser. At t = 0.6 ps the density is very similar to its initial value. The energy maximum near x = 4 μm produces a caviton by nonlinear forces.
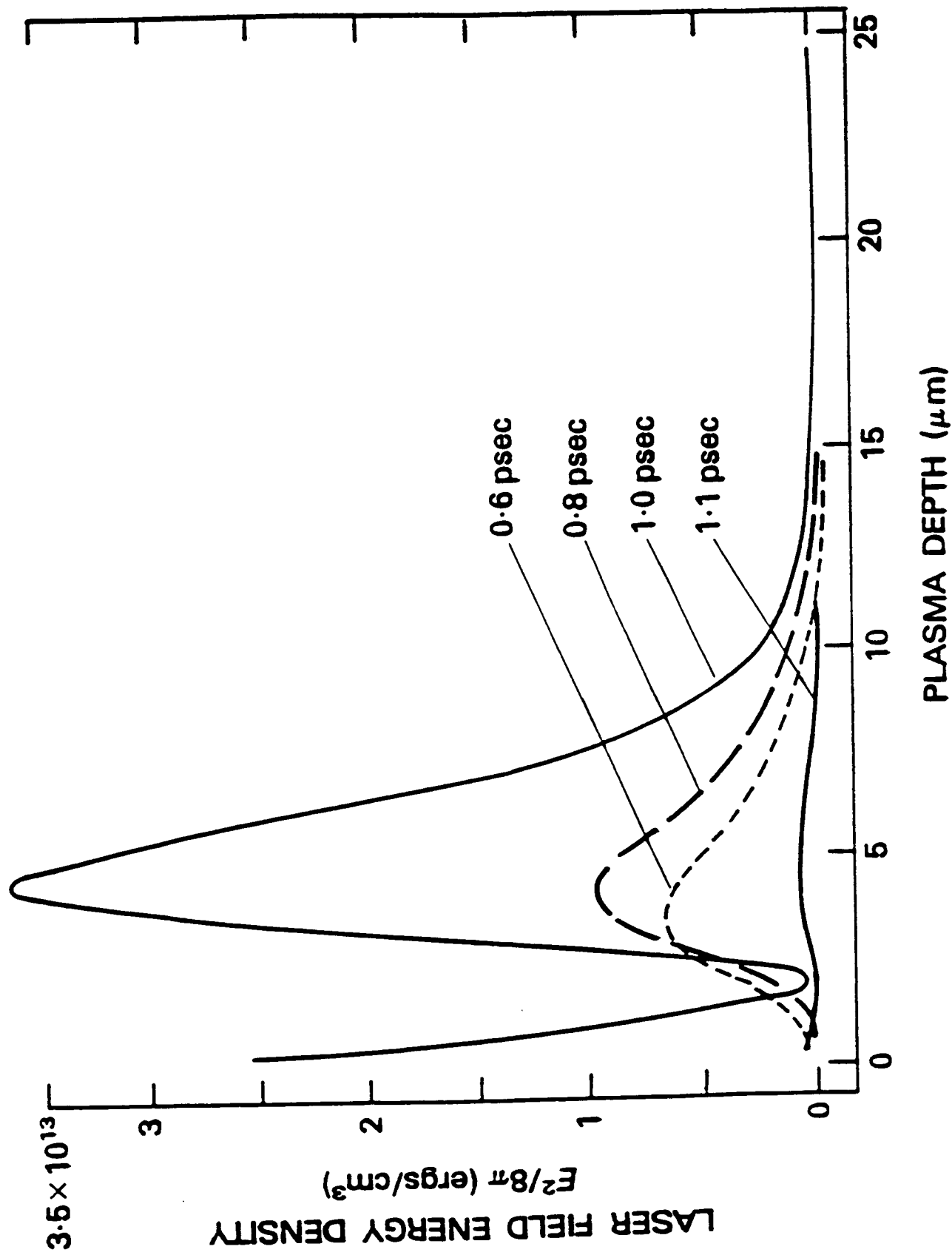
Figure 7. Density of the electric field energy of the laser (without the electrostatic fields generated within the plasma).
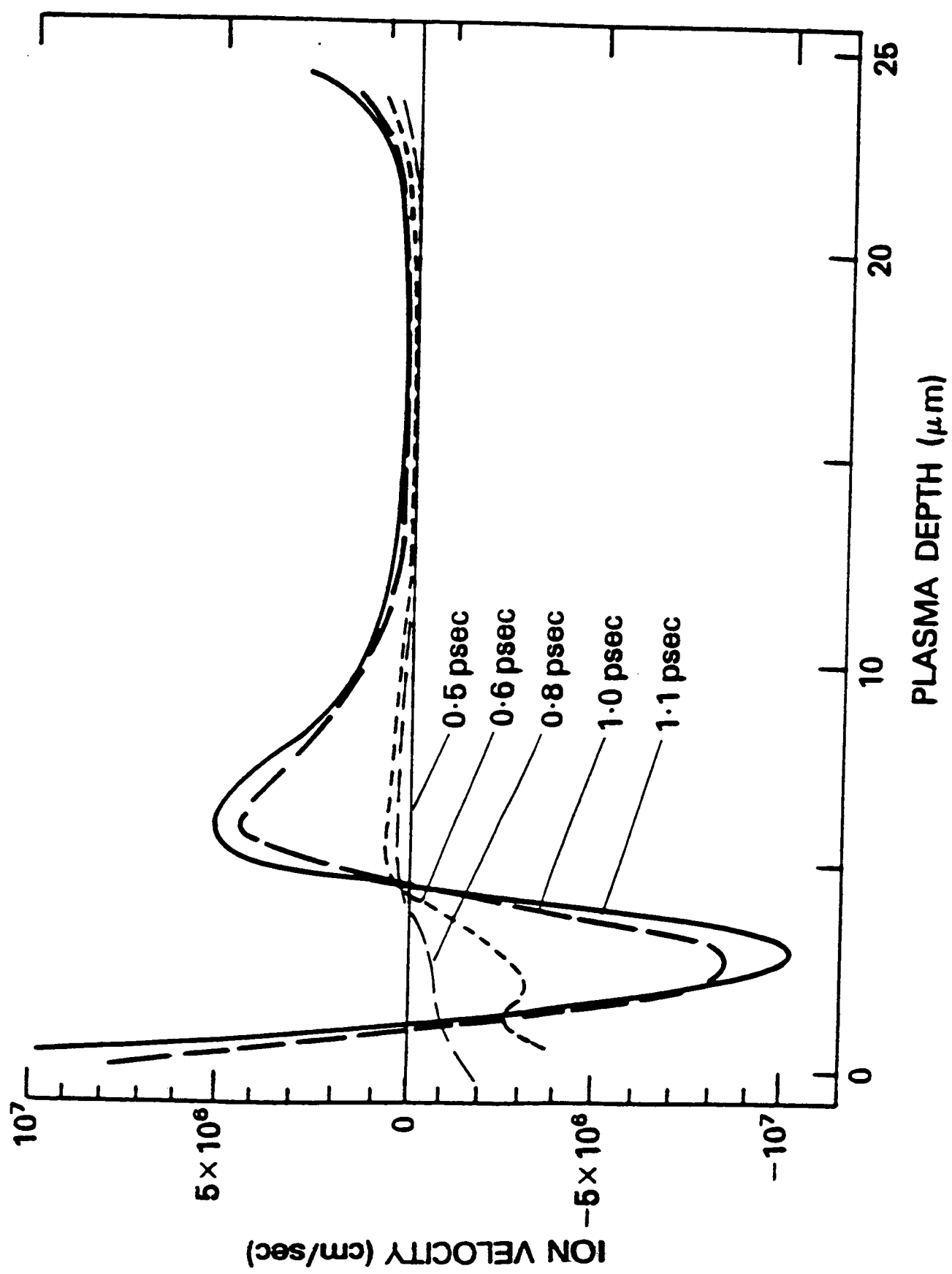
Figure 8. Ion velocity v_o at several time steps for a plasma, as in Figure 3. A block of plasma is generated with a velocity up to 10^7 cm/s.
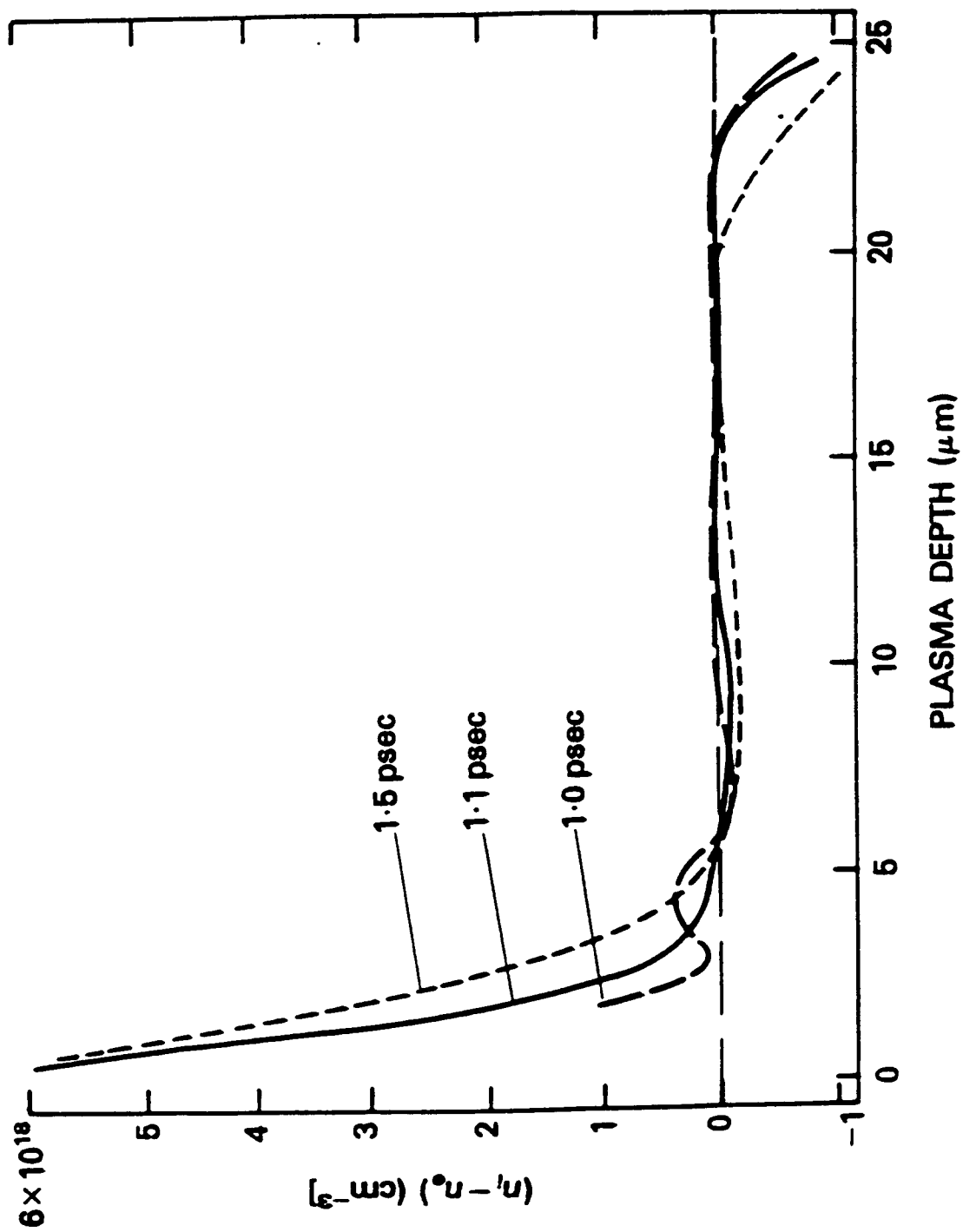
Figure 9. The genuine two-fluid model shows the difference between ion density n_i and electron density n_e with the surprising result of a positive difference (space charge) before the caviton and a negative region behind the caviton (inverted double layer as observed by Eliezer and Ludmirsky, 1983). Near $x = 25$ μm the laserless plasma expands normally with a negative periphery.
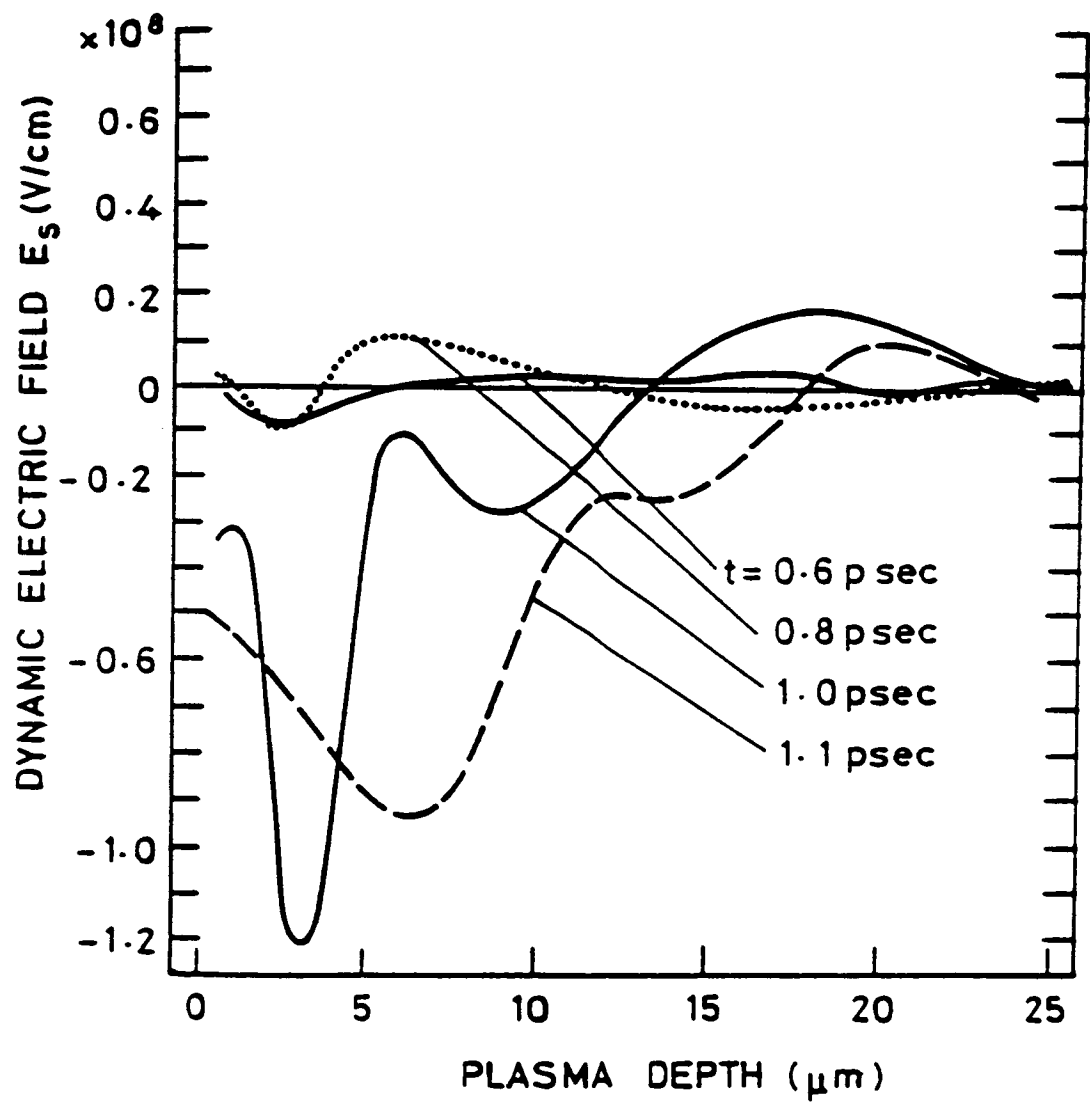
Figure 10. Electric field $E = E_s$ inside the plasma of Figure 3 dynamically evolving with absolute values beyond 10^8 V/cm near the caviton produced by the nonlinear laser forces at times (in picoseconds) 0.6-; 0.8...; 1.0-; 1.1... .
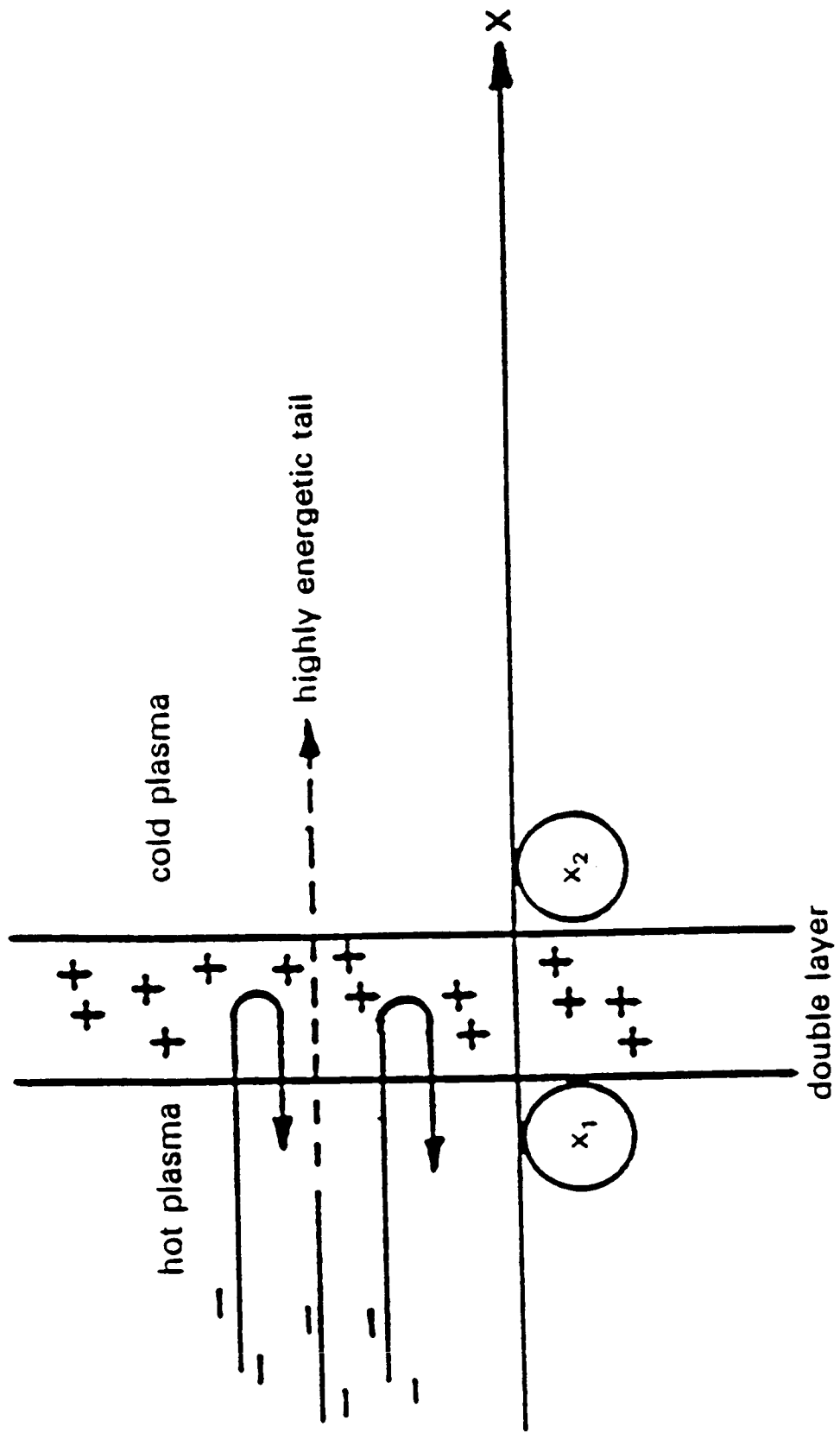
Figure 11. The positive charge of the double layer between the hot and the cold plasma causes a return of the electrons to the hot plasma with the exception of the electrons from the energetic tail of the energy distribution (Cicchitelli et al., 1984).

134
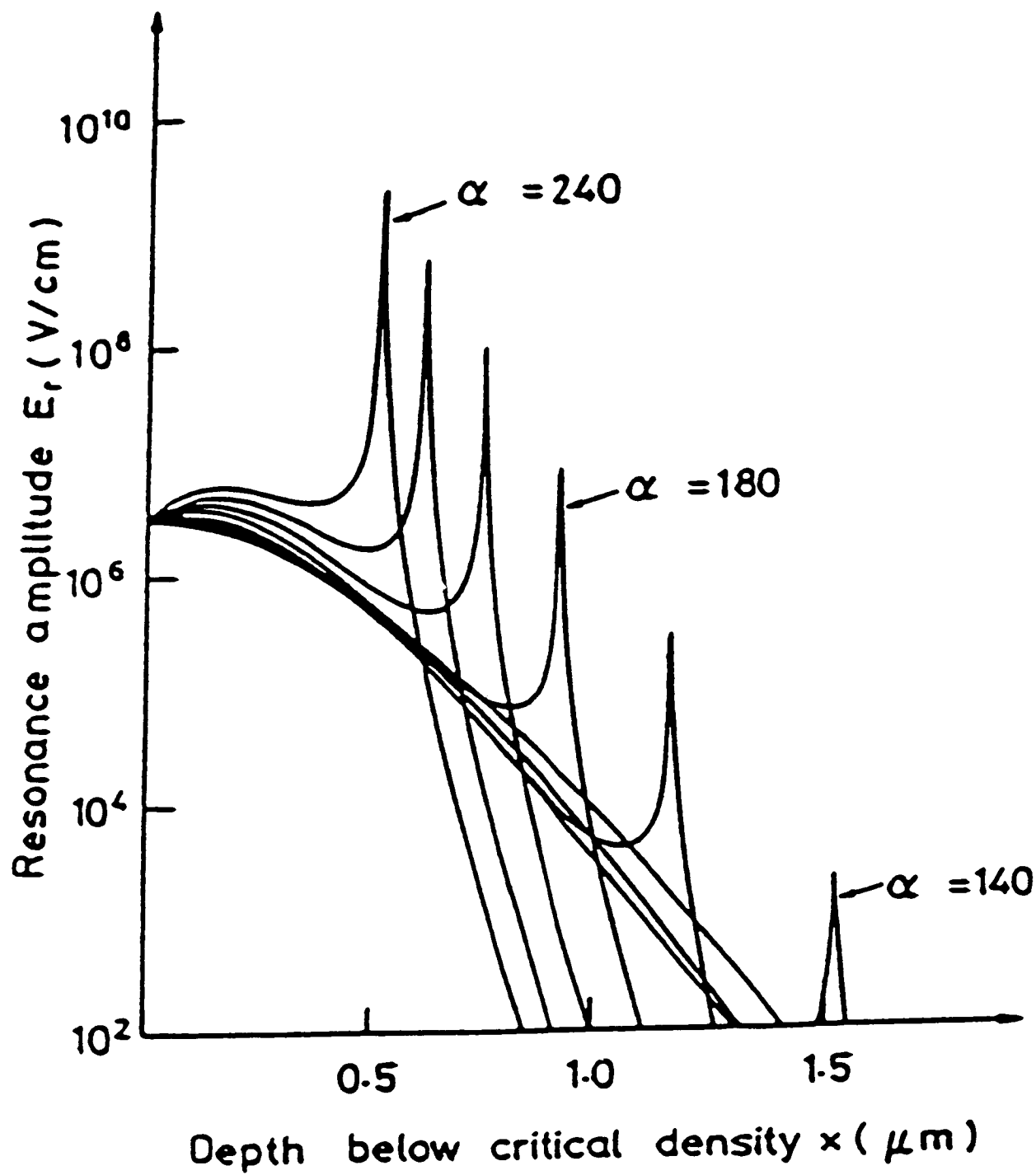
Figure 12. Resonance amplitude E_R of the longitudinal electric field, as a function of the depth x below the critical density, for neodymium glass laser irradiation of 10^{16} W/cm^2 into plasma with a temperature of 1 keV. The parameter for profile steepening α^2 ranges from 100 to 240. The critical density n_e corresponds to the axis x = 0.
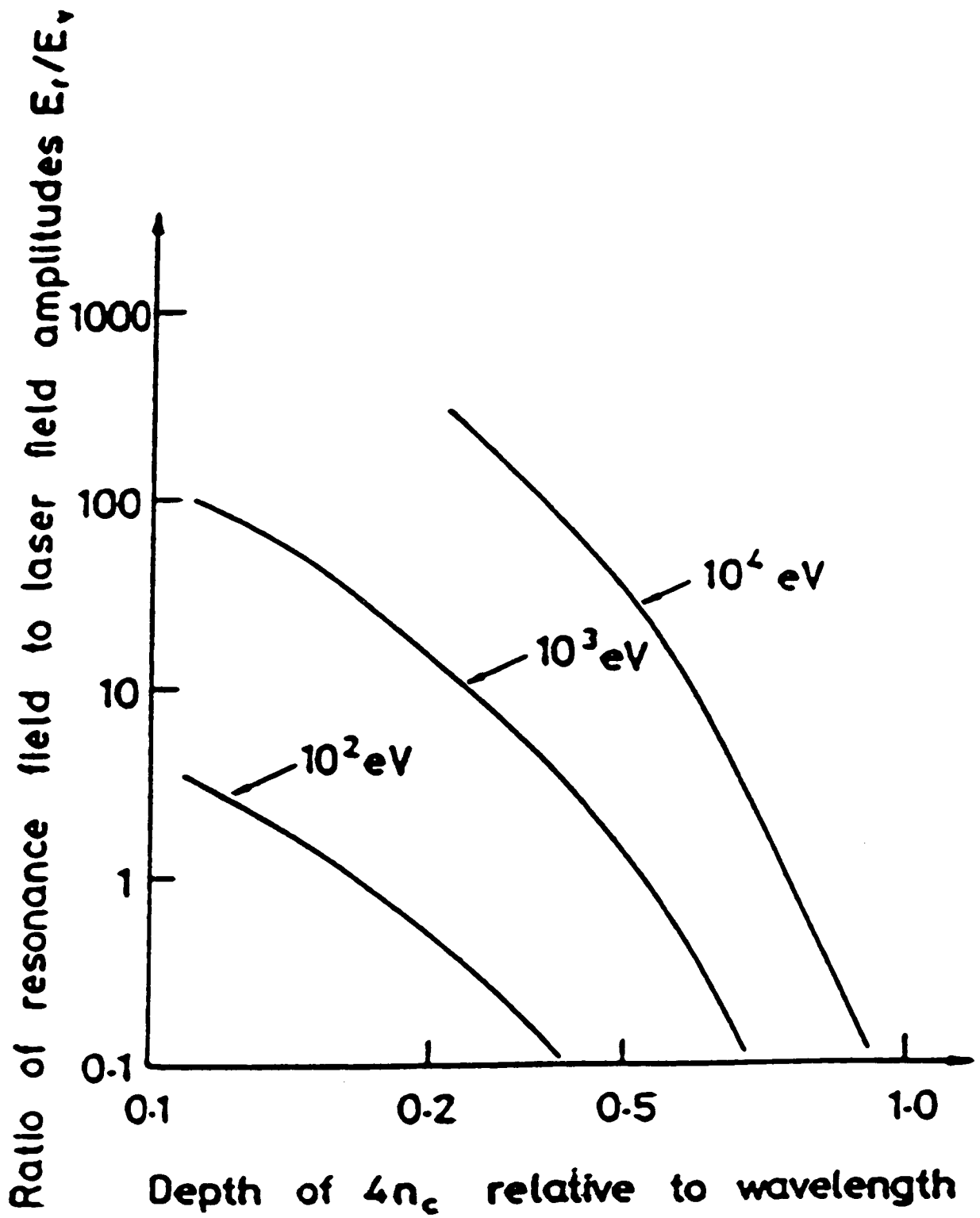
Figure 13. Combining the resonacne maxima of Figure 12 and for other temperatures given as ratio to the incident laser amplitude for various plasma temperatures in electron volts depending on the depth x below the critical density for neodymium glass laser radiation.
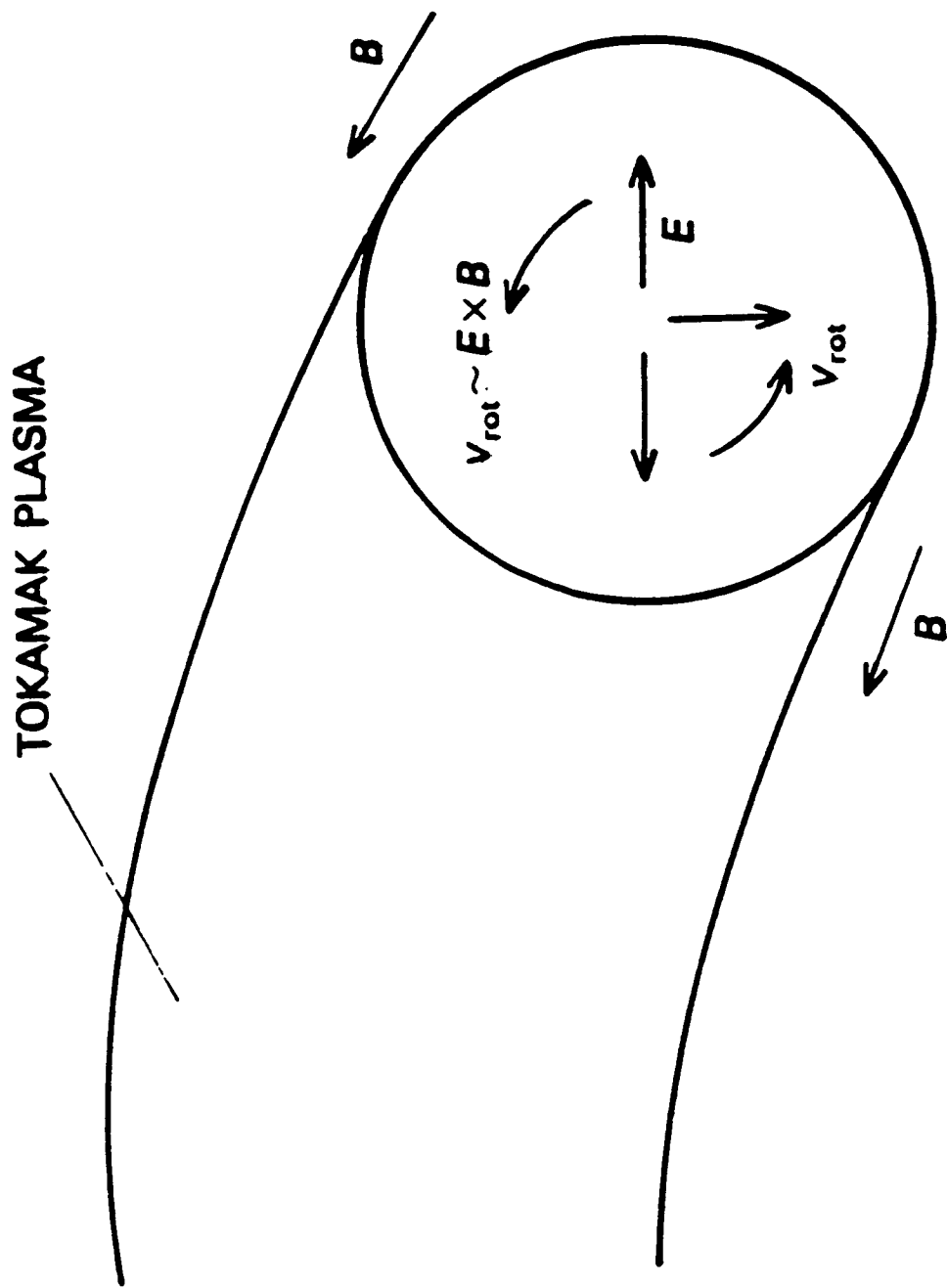
Figure 14. Poloidal rotation of tokamak plasma by $\mathbf{E} \times \mathbf{B}$ forces where the electric field E is the inhomogeneity field.

ION PHASE-SPACE VORTICES AND THEIR RELATION
TO SMALL AMPLITUDE DOUBLE LAYERS

Hans L. Pécseli
Association EURATOM-Riso National Laboratory
Physics Department, Riso National Laboratory
P.O. Box 49, DK-4000 Roskilde, Denmark

ABSTRACT

The properties of ion phase-space vortices are reviewed with particular attention to their role in the formation of small amplitude double layers in current-carrying plasmas. In a one-dimensional analysis, many such double layers simply add up to produce a large voltage drop. A laboratory experiment is carried out in order to investigate the properties of ion phase-space vortices in three dimensions. Their lifetime is significantly reduced as compared with similar results from one-dimensional numerical simulations of the problem.

I. INTRODUCTION

A plasma can support a large variety of stationary (or quasi-stationary) double-layer-like structures. The proceedings (Michelsen and Rasmussen, 1982; Schrittwieser and Eder, 1984) of the first two double layer sumposia at Riso and in Innsbruck contain an extensive summary of theoretical, numerical, and experimental investigations. A number of these investigtions, however, refer to conditions with very carefully chosen initial or boundary conditions imposed on the plasma. These conditions may often be highly idealized, or even unrealistic representations of those met in, for example, ionospheric conditions. However, not all examples have this shortcoming. One of these seems to be small amplitude double layers occurring in current-carrying plasmas. One possible mechanism for their generation is reflection of electrons by a negative potential dip associated with an ion plasma-space vortex, which consequently acts as a "seed" for the double layer (Sato and Okuda, 1980; Hasegawa and Sato, 1982; Nishihara et al., 1982; Berman et al., 1985, Pécseli, 1984). This is a spatially localized process and thus independent of any boundary conditions. The potential drop associated with one such double layer will be rather small. If, however, the system is large and the ion phase-space vortices sufficiently frequently occur, many of these small double layers may be generated and will eventually add up to a significant potential drop. With this scenario in mind, we found it worthwhile to investigate the properties of the ion phase-space vortices in detail. These properties will be summarized in the following paragraphs.

II. ION PHASE-SPACE VORTICES IN ONE-DIMENSIONAL SYSTEMS

The properties of ion phase-space vortices are discussed in some detail in Berman et al., 1985, Pécseli, 1984, Burjarbarua and Schamel, 1981, Pécseli et al., 1984, 1984, and Trulsen, 1980. They represent one particular type of Bernstein-Green-Kruskal (BGK) equilibria (Bernstein et al., 1957) which appear to be very stable. An ion phase-space vortex thus represents a careful balance between trapped and untrapped particles maintaining a local potential dip, resulting in a corresponding plasma density depletion. It was demonstrated (Bujarbarua and Schamel, 1981) that a simple analytical model, characterized by only three parameters, can be constructed for the ion velocity distribution function. The electrons were assumed to be Boltzmann-distributed. In spite of its simplicity, this model accounts very well for the properties of ion vortices. The analysis is formally very similar to that of electron holes

(Bujarbarua and Schamel, 1981; Lynov et al., 1979, 1985) especially if electron modes in a strongly magnetized plasma waveguide are considered (Pécseli, 1984). A particularly important result of the analysis (Bujarbarua and Schamel, 1981) predicts that ion vortices cease to exist (i.e., their amplitude goes to zero) as the electron-to-ion temperature ratio T_e/T_i becomes smaller than ~ 3.5. This result was confirmed in a numerical particle simulation (Pécseli et al., 1981, 1984; Trulsen, 1980).

The dynamic properties of ion phase-space vortices can be most conveniently accounted for by considering them as quasi-particles. A simplified analysis demonstrates that an ion vortex can be assigned a negative charge and a negative mass (Pécseli, 1984; Dupree, 1983). Numerical simulations (Pécseli, 1984; Bujarbarua and Schamel, 1981; Pécseli et al., 1981, 1984; Trulsen, 1980) demonstrated that two ion vortices may coalesce into one when they are sufficiently close in phase space, very much like electron vortices (Lynov et al., 1979, 1980). A detailed parameter study of this process remains to be carried out. Isolated ion holes, on the other hand, appeared to be very stable (Pécseli et al., 1981, 1984; Trulsen, 1980) in a description where the electron component is assumed to be in Boltzmann equilibrium at all times. This simplification becomes inappropriate in current-carrying plasmas, where the interaction between ion vortices and individual electrons becomes important. In this case, the reflected electrons give up a net momentum to the ion vortex, which consequently decelerates, since its effective mass is negative. However, as its velocity is decreased, it can move into regions of increasing ion phase-space density. The result is a slow increase in amplitude of the phase-space vortex, which consequently becomes more efficient in reflecting electrons. The process is thus accelerated. The charge distribution of the reflected electrons gives rise to localized double-layer-like structures. Eventually, the phase-space vortex is destroyed. The very simplified physical picture outlined here is elaborated in more detail by Berman et al. (1985) and Dupree (1983) and also by Nishihara et al., (1982) and Pécseli (1984). In particular, Berman et al. (1985) describe very spectacular one-dimensional numerical particle simulations, showing the slow time evolution of ion phase-space vortices under conditions like those discussed here. It is important to emphasize that the unstable growth of the ion vortices is due to a slowly growing nonlinear instability, which can be excited for bulk electron flow velocities well below those giving the linear two-stream instability. The only criterion for the nonlinear instability seems to be that long-lived ion vortices are formed. In the simulations reported in Berman et al. (1985), this formation occurred for a rather wide class of initial phase-space distributions of simulation particles. The formation of large ion vortices was investigated by Pécseli et al. (1981, 1984) and Trulsen (1980). It could be analytically demonstrated that such vortices are formed in the saturated stage of the one-dimensional ion-ion, two-stream instability of Pécseli and Trulsen (1982). Alternatively, the formation could be due to ion bursts (which after all can be considered as a segment of an ion beam).

III. ION PHASE-SPACE VORTICES IN THREE DIMENSIONS

The properties of ion phase-space vortices described in the previous section referred mainly to one-dimensional investigations. The experimental investigation reported in Pécseli et al. (1981, 1984) and Trulsen (1980) is of course three-dimensional, but it refers to very carefully chosen initial and boundary conditions. Numerical investigations (Morse and Nielson, 1969) of electron phase-space vortices demonstrated that an ensemble of these was very stable in one dimension, while the phase-space structures were very rapidly eroded in two or, in particular, three spatial dimensions. In order to investigate the properties of ion vortices in three dimensions, we performed a laboratory experiment where the vortices were generated by the ion-ion beam instability, which gives linear instability for wave directions in a cone around the beam velocity.

Our investigations were carried out in the double-plasma device at the University of Tromso (Johnsen, 1986; Johnsen et al., 1985). The vacuum vessel has an inner diameter of 60 cm and is divided into source and target parts (length 40 cm and 80 cm, respectively) by a fine meshed grid. The device was operated at a typical neutral argon pressure of 1.5×10^{-4} Torr, with plasma densities in the range 2 to 10×10^8 cm^{-3}. The electron temperature was $T_e \approx 2.5$ eV, while $T_i \approx 0.15$ eV in the absence of a beam. By adjusting the bias of the source, an ion beam was injected into the target plasma. Typical beam energies were 4-8 eV. The density ratio between beam and background ions is

adjustable in the setup and was chosen to be around one. The fluctuation level increases along the direction of beam propagation (Z axis in the following, with Z = 0 corresponding to the position of the separating grid) and saturates roughly at a distance of Z = 9 cm, with a density fluctuation level of $\tilde{n}/n_0 \sim$ 1-5 percent. The increase in noise level is accompanied by a significant scattering of the incoming ion beam, as observed by using both conventional three-grid and the novel directional electrostatic energy analyzers. It is not experimentally possible to obtain information about spontaneously generated individual ion vortices. Instead, we performed a statistical analysis of the experimental data. The turbulent plasma fluctuations in the frequency range 10 kHz to 1 MHz were investigated by the fluctuations in electron saturation current to two movable Langmuir probes with an exposed spherical tip of 1 mm in diameter. Realtime signal sequences of 800 μs duration were recorded with a sample rate of 2.5 MHz. At each combination of probe positions, five such sequences formed the basis of a statistical analysis. With the realtime signals available, we thus performed a statistical analysis on a conditional basis. The signal n_A from the fixed probe (A) at position $\vec{r}'$ was chosen as a reference. Choosing a certain value of the density perturbation, say n_i, the corresponding time records are subsequently searched for times t', where the signal takes a value within the narrow interval $(n_1, n_1 + \Delta)$, where Δ is taken as the minimum amplitude resolution of the record. Each time this condition on signal A is satisfied, the signal from the movable probe B is recorded in a certain prescribed time interval $(t' - \tau, t' + \tau)$. These conditionally chosen time series are then considered as independent realizations for the ensuring statistical analysis. The analysis is repeated for varying positions $\vec{r}$ of probe B. The result is most conveniently expressed in terms of the electrostatic potential by the relation $\tilde{n}/n_0 \sim e\tilde{\phi}/T_e$, which is adequate for the relatively low fluctuation level in the experiment. A record of 800 μs duration is sufficiently long to give an adequate representation of many realizations in the ensemble. By the procedure outlined above, we thus obtained the conditional ensemble average, where t' is just a dummy variable for time stationary turbulence

$$\bar{\phi} = \langle \phi(\vec{r}, t+t') | \phi(\vec{r}', t') = \phi_1 \rangle .\tag{1}$$

This quantity has the following rather self-evident physical interpretation: given that a particle is located in a potential ϕ_1 at a position $\vec{r}'$ at time t', then $\bar{\phi} = \bar{\phi}(\vec{r}, t+t')$ is the average potential variation it will experience in the vicinity of $\vec{r}'$ at the same or at different times.

One important question to be discussed in the following is the lifetime τ_L of a conditional structure (or eddy for simplicity) described by equation (1), compared to the average bounce time τ_B of a charged particle derived from $\bar{\phi}$. Thus, if $\tau_B \lesssim \tau_L$, a small cloud of test particles released at $(\vec{r}', t')$ will be likely to stay together with the trajectories being correlated for a substantial time. Ions with velocities close to that of the eddy will, if $\phi_1 < 0$, be trapped, on average, by the (average) potential, thus exhibiting the features of three-dimensional ion phase-space vortices. On the other hand, if τ_L is very short, the particles will disperse rapidly with a large probability, and vortex or "clump-like" features will be immaterial for the description of the turbulent fluctuations in question. In our case, we find $\tau_L \approx \tau_B$. In Figures 1a,b we show equipotential contours for ϕ in a rectangular cross-section of the plasma for two different values of the reference potential ϕ_1. The position of the reference probe is indicated by ●. The full spatial variation is obtained by rotating the figure around the Z axis. This symmetry was explicitly verified in the experiment. For the region of measurements, we may consider the turbulence to be homogeneous and isotropic in the plane perpendicular to the axis of the device. In particular we note that since full time records are available, it is perfectly feasible to let t be negative, i.e., to consider the formation of the conditional eddy. Evidently the eddy rapidly assumes a roughly spherical shape and propagates in the direction of the ion beam. A lifetime of 60 μs for the eddy is estimated for the present plasma conditions. By fitting a parabola to the local minimum of the conditional spatial potential profile, we obtain an inverse angular ion bounce frequency $\omega_B^{-1} \approx 8$ μs for the largest eddy, indicating that the trapping of ions is a significant dynamic process. The observed structures corresponding to large negative values of ϕ_1 can thus be considered as evidence for quasi-static three-dimensional ion holes. Using the electrostatic energy analyzer, we verified (Johnsen et al., 1985) that there was indeed a significant number of ions in the velocity range where they can be trapped by the conditional eddy. From measurements such as those summarized in Figure 1, it is easy to deduce the eddy velocity.

An eddy described by equation (1) and shown in Figure 1 is an average quantity. In each individual realization we may find eddies which may deviate significantly from the average. However, we expect these to have little statistical weight. This statement can be given support by a theoretical analysis.

Being particularly interested in ion-hole formation, we concentrated on negative values for ϕ_1 in the present summary of our results. Of course, positive values of ϕ_1 can be chosen as well, where now the electrons can be trapped. We found that the evolution of conditional structures corresponding to $\phi_1 > 0$ was somewhat similar to the overall features given in Figure 1, with some deviations in the actual shapes and velocities. A more general account of these results is in preparation.

IV. CONCLUSIONS

In this work we discussed experimental observations of conditional structures in ion beam driven turbulence, presenting the actual variation of the average potential deduced from a conditional analysis of measured fluctuations. Given the propagation velocity and lifetime of these structures, we obtained evidence for the formation of quasi-stationary, ion phase-space vortices. We find it worthwhile to emphasize that the conditionally averaged potential need not coincide with the most probably conditional potential variation. An analysis of this problem requires investigations of the conditional amplitude probability distribution of potential in each spatial point as a function of time. This (rather lengthy) investigation was also carried out. However, the differences between the resulting spatial potential variations and those shown in Figure 1 were not sufficiently pronounced to necessitate a separate figure here. Although we have obtained evidence for the formation of three-dimensional ion phase-space vortices, it seems conclusive that their lifetime is much shorter than for those found in one-dimensional numerical simulations (Pécseli et al., 1981, 1984; Trulsen, 1980, Pécseli et al., 1982). In particular, we find that the vortex lifetime is too short to manifest coalescence of two vortices, which is a relatively slow process in units of bounce time. Several reasons for this difference between one and higher dimensions can be found. First of all, a stability analysis (Schamel, 1982) has demonstrated that one isolated vortex is unstable with respect to transverse perturbations in three dimensions, although the growth rate of this instability is rather small for realistic conditions. Probably more important, however, is the possibility of two or many such vortices colliding at an angle in three dimensions, thus destroying the simple trapped particle orbits. Finally, the interaction between ions and potential structures is rather different in one and in higher spatial dimensions, as illustrated in Figure 2. Thus, in one dimension (Fig. 2a), an ion coming in from infinity may give up momentum to an isolated positive quasi-stationary potential structure (top trace) while it only gives a transient perturbation to a negative potential variation (lower trace). In two or three dimensions, an ion may give up momentum to both polarities of a potential variation as indicated in Figure 2b. We see no obvious method to discriminate between these effects in our experiment. Numerical simulations such as those reported in, for example, DeGroot et al. (1977) and Barnes et al. (1985) may provide some insight into these features. It is rather evident that the experimental conditions discussed here do not exactly match those met in current-carrying plasmas. It seems fair, however, to assume that the properties of ion phase-space vortices are, at least in a first approximation, independent of a small electron drift. The conclusion based on the results summarized here will consequently be that the lifetime of ion vortices in three-dimensional unmagnetized systems is not sufficiently long to allow an analysis in terms of quasi-particles interacting with individual electrons, in contrast to the one-dimensional investigations discussed in Berman et al. (1985) and Dupree (1983). The growth of very small vortices, or holes, from an initial low-level noise is thus improbable for a small electron drift. If, however, the electron drift exceeds the threshold for the linear current-driven instability, a rapid growth of negative potential spikes may occur (Barnes et al., 1985) which subsequently form ion vortices by particle trapping (Nishihara et al., 1982). The instability may then evolve nonlinearly as described in Section II. Although the ion vortices have a relatively short lifetime, they have in this case a large amplitude and are thus effective local barriers for the slow electrons. One might expect that these conclusions should be modified for magnetized plasmas with electron drifts

along B-field lines. However, the two-dimensional numerical simulations in Barnes et al. (1985) do not reveal any particular variations of the results with the intensity of an externally applied magnetic field. Unfortunately, practical limitations imply that most numerical simulations are restricted to at most two spatial dimensions.

Although ion phase-space vortices were discussed here with reference to one particular plasma phenomenon, it may be worth mentioning that they present a nonlinear plasma mode which may be interesting also in a different context [see, for instance, the discussion by Hershkowitz (1984)].

REFERENCES

Barnes, C., M. K. Hudson, and W. Lotko, *Phys. Fluids, 28,* 1055 (1985).

Berman, R. H., D. J. Tetrault, and T. H. Dupree, *Phys. Fluids, 28,* 155 (1985).

Bernstein, I. B., J. M. Green, and M. D, Kruskal, *Phys. Rev., 108,* 546 (1957).

Bujarbarua, S., and H. Schamel, *J. Plasma Phys., 25,* 515 (1981).

DeGroot, J. S., C. Barnes, A. E. Walstead, and O. Buneman, *Phys. Rev. Lett., 38,* 1283 (1977).

Dupree, T. H., *Phys. Fluids, 26,* 2460 (1983).

Hasegawa, A., and T. Sato, *Phys. Fluids, 25,* 632 (1982).

Hershkowitz, N., in *Second Symposium on Double Layers and Related Topics,* edited by R. Schrittwieser and G. Eder, p. 55, University of Innsbruck, 1984.

Johnsen, H., *Physica Scripta, 33,* 84 (1986).

Johnsen, H., H. L. Pécseli, and J. Trulsen, *Phys. Rev. Lett., 55,* 2297 (1985).

Lynov, J. P., P. Michelsen, H. L. Pécseli, J. J. Rasmussen, K. Saéki, and V. A. Turikov, *Physica Scripta, 20,* 328 (1979).

Lynov, J. P., P. Michelsen, H. L. Pécseli, and J. J. Rasmussen, *Phys. Lett., 80A,* 23 (1980).

Lynov, J. P., P. Michelsen, H. L. Pécseli, J. J. Rasmussen, and S. H. Sorensen, *Physica Scripta, 31,* 596 (1985).

Michelsen, P., and J. J. Rasmussen (editors), *Symposium on Plasma Double Layers,* Riso National Laboratory, Roskilde, Denmark, 1982.

Morse, R. L., and C. W. Nielson, *Phys. Rev. Lett., 23,* 1087 (1969).

Nishihara, K., H. Sakagami, T. Taniuti, and A. Hasegawa, in *Symposium on Plasma Double Layers,* edited by P. Michelsen and J. J. Rasmussen, p. 41, Riso National Laboratory, Roskilde, Denmark, 1982.

Pécseli, H. L., in *Second Symposium on Double Layers and Related Topics,* edited by R. Schrittwieser and G. Eder, p. 81, University of Innsbruck, 1984.

Pécseli, H. L., and J. Trulsen, *Phys. Rev. Lett., 48,* 1355 (1982).

Pécseli, H. L., R. J. Armstrong, and J. Trulsen, *Phys. Lett., 81A,* 386 (1981).

Pécseli, H. L., J. Trulsen, and R. J. Armstrong, *Physica Scripta, 29,* 241 (1984).

Sato, T., and H. Okuda, *Phys. Rev. Lett., 44,* 740 (1980).

Schamel, H., *Phys. Lett., 89A,* 280 (1982).

Schrittwieser, R., and G. Eder (Editors), *Second Symposium on Double Layers and Related Topics,* University of Innsbruck, 1984.

Trulsen, J., University of Tromso Report, 1980.

$$\Phi_1 = -1.5\,\Phi_{RMS} \qquad\qquad \Phi_1 = -0.5\,\Phi_{RMS}$$
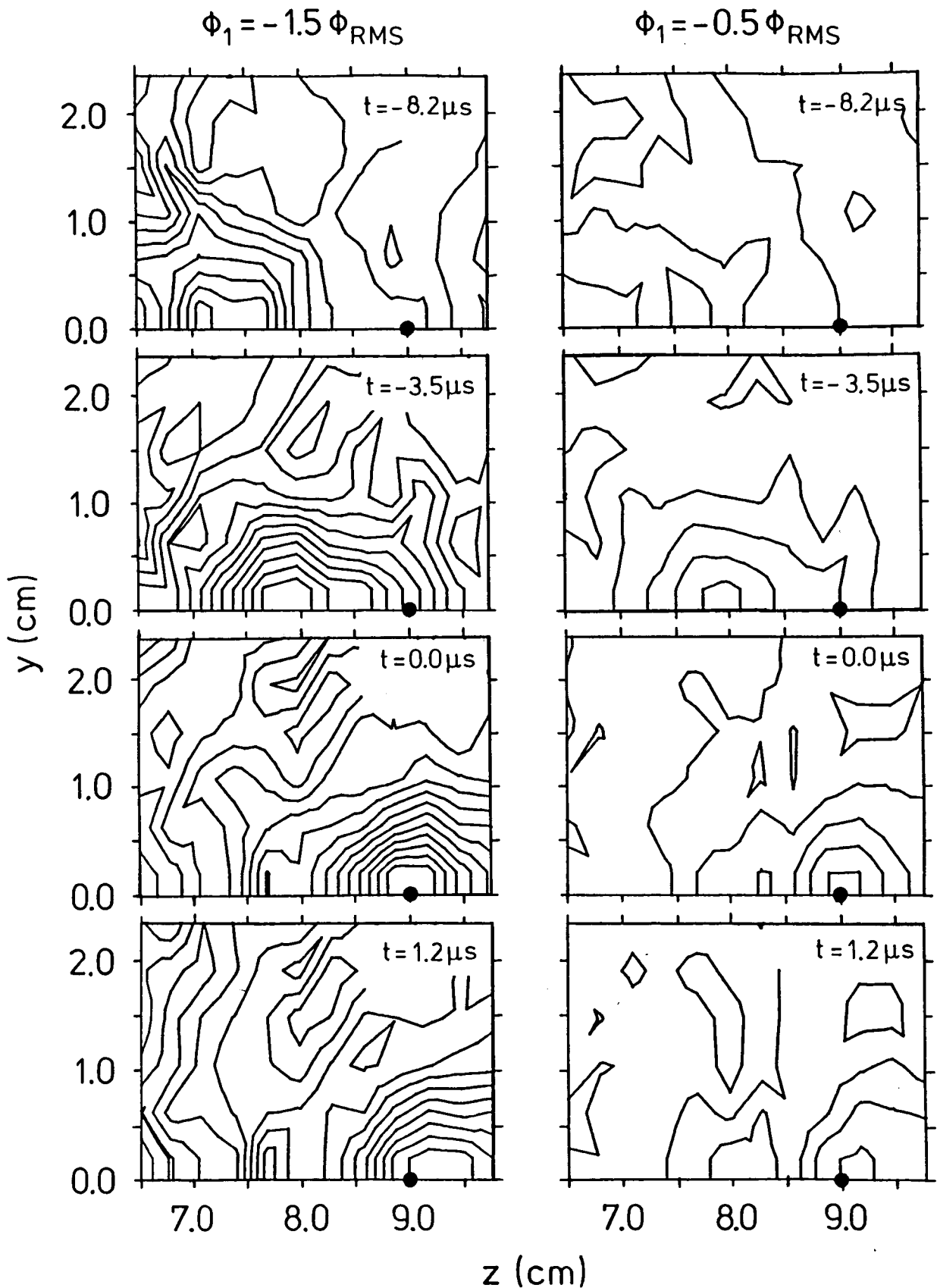
Figure 1. Contour plots of conditional eddies for two different reference values ϕ_1 in equation (1) measured in units of the rms value of the potential fluctuations ϕ_{rms}. The position of the reference probe is Z = 9 cm measured from the separating grid of the double-plasma device. The spacing between contours is 0.1 ϕ_{rms}.

144
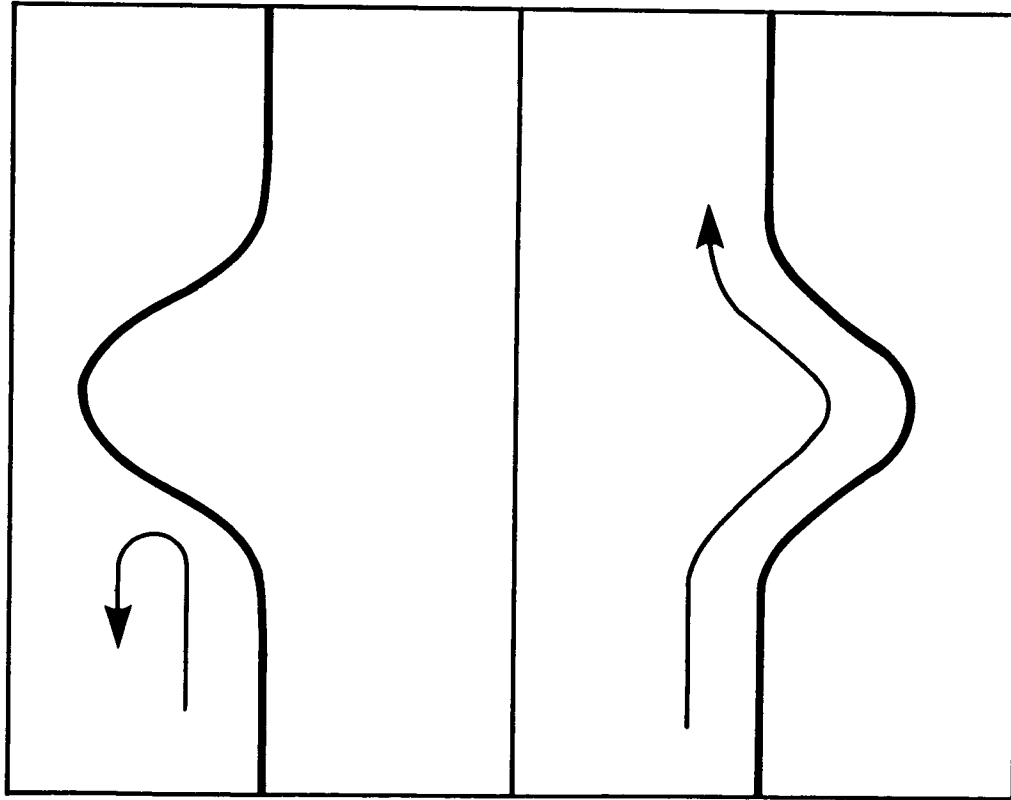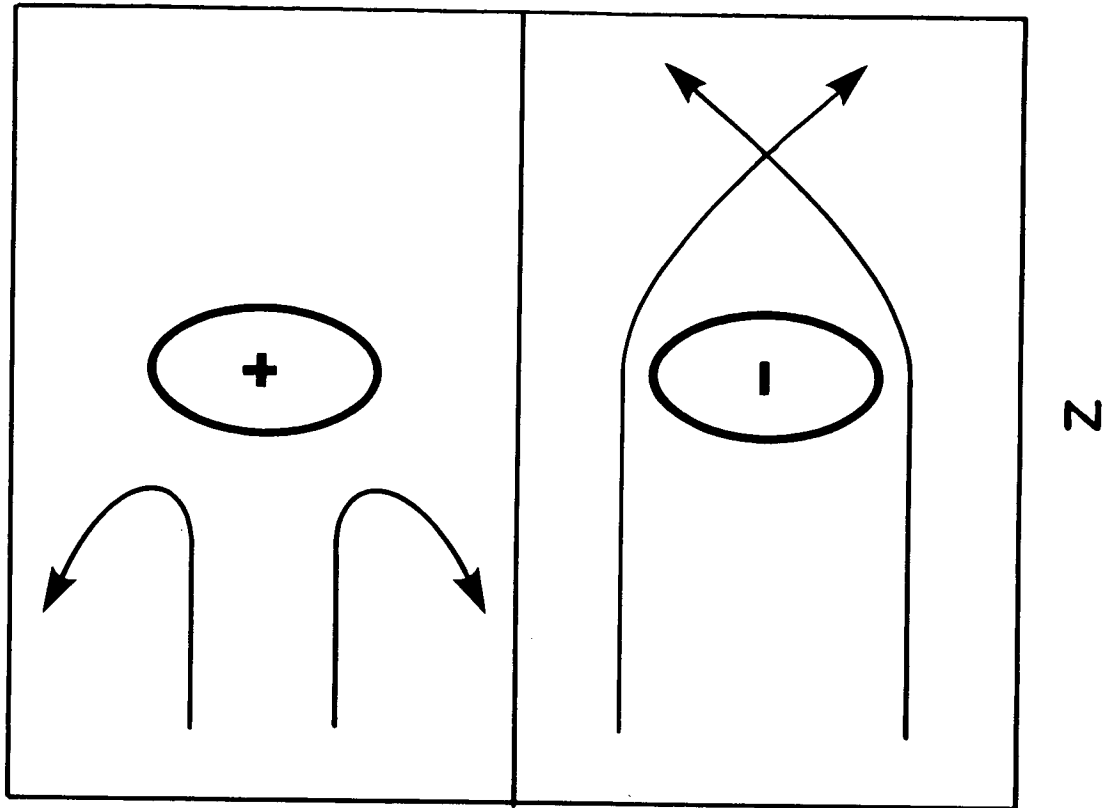
Figure 2. Schematic diagram for discussing the difference between particles interacting with localized potential variations in one and in higher dimensions.

EFFECT OF DOUBLE LAYERS ON MAGNETOSPHERE-IONOSPHERE COUPLING

Robert L. Lysak
School of Physics and Astronomy, University of Minnesota
Minneapolis, MN 55455, U.S.A.

Mary K. Hudson
Department of Physics and Astronomy, Dartmouth College
Hanover, NH 03755, U.S.A.

N87-23321

ABSTRACT

The Earth's auroral zone contains dynamic processes occurring on scales from the length of an auroral zone field line (about 10 R_E) which characterizes Alfvén wave propagation to the scale of microscopic processes which occur over a few Debye lengths (less than 1 km). These processes interact in a time-dependent fashion since the current carried by the Alfvén waves can excite microscopic turbulence which can in turn provide dissipation of the Alfvén wave energy. This review will first describe the dynamic aspects of auroral current structures with emphasis on consequences for models of microscopic turbulence. In the second part of the paper a number of models of microscopic turbulence will be introduced into a large-scale model of Alfvén wave propagation to determine the effect of various models on the overall structure of auroral currents. In particular, we will compare the effect of a double layer electric field which scales with the plasma temperature and Debye length with the effect of anomalous resistivity due to electrostatic ion cyclotron turbulence in which the electric field scales with the magnetic field strength. It is found that the double layer model is less diffusive than in the resistive model leading to the possibility of narrow, intense current structures.

I. INTRODUCTION

Auroral arcs and the auroral current structures which produce them occur in a variety of scale sizes and time scales. While electrostatic models of auroral electrodynamics (Lyons et al., 1979; Fridman and Lemaire, 1980; Chiu and Cornwall, 1980) have had success at describing the overall current-voltage relationship of the auroral zone and in defining the scale size of the inverted-V precipitation signature, they are not well suited to describing the dynamics of small-scale auroral arcs, multiple auroral arcs, and time-dependent auroral structures. In this realm a fluid picture of auroral electrodynamics has advantages and can describe a number of auroral processes (Sato, 1978; Goertz and Boswell, 1979; Miura and Sato, 1980; Lysak and Dum, 1983; Lysak, 1985, 1986). The difficulty with the fluid models is that the kinetic processes which play an important part in defining the auroral potential drop must be described by means of assumed transport coefficients which should be determined by a consideration of the microscopic plasma processes.

The formation of parallel potential drops in laboratory and computer simulated plasmas has been covered in many of the reviews in this workshop. The problem with applying most of these results to the auroral zone is the high sensitivity of the results to the initial and boundary conditions which are imposed. In the auroral plasma, there are no grids to be set to a certain voltage and, perhaps more fundamentally, the scale of the system is vastly larger than the sizes of a thousand Debye lengths or so which are typical in laboratory and computer studies. Therefore a description of the auroral potential drop should consider the large-scale dynamics of the auroral zone as well as the microscopic processes which can directly produce parallel electric fields.

The remainder of this review will consist of two major sections. In the first, we will consider some of the time-dependent aspects of auroral current structures and the implications these structures have for models of microscopic plasma turbulence. In particular, we will argue that auroral currents are closely associated with Alfvén wave

147

signatures that tend to define the current which flows along auroral field lines and that include a transient parallel electric field which can set up the particle distributions necessary to support double layer structures. In the second part of the review, we will discuss some numerical experiments in which the form of the parallel electric field is changed. We will consider two extreme cases. In the first, we assume a double layer model in which a potential drop that scales with the electron temperature is distributed over distances which scale with the Debye length when the current exceeds a threshold. We will compare this model with a model of nonlinear resistivity due to electrostatic ion cyclotron turbulence in which the effective resistivity increases with the current over a threshold. These models produce rather different overall current structures, since in the resistive model the current diffuses across the magnetic field producing broader structures, while in the double layer model narrow current structures can persist.

II. A BRIEF REVIEW OF AURORAL ELECTRODYNAMICS

The Earth's auroral zone is a region in which the ionosphere and the outer magnetosphere are coupled by means of magnetic field-aligned currents which flow between the two regions. These currents must close across field lines in the ionosphere and also somewhere in the outer magnetosphere. Ionospheric current closure is described by the current continuity equation, which is generally integrated along the field line over the thin layer (about 50 km) in which the ionospheric currents flow. To simplify the description, we will consider a two-dimensional geometry in which variations in longitude are ignored. This assumption is well justified on the dawn and dusk flanks of the magnetosphere, although it should be modified to take into account the more complicated current structures at noon and midnight. With these approximations ionospheric current continuity can be expressed as follows:

$$j_z = \frac{\partial I_x}{\partial_x} = \frac{\partial}{\partial_x} [\Sigma_P E_x] \quad , \tag{1}$$

where Σ_P is the height integrated Pedersen conductivity and the geometry is defined in Figure 1. Note that here a positive current is parallel to the magnetic field line, i.e., downward in the northern hemisphere.

In the steady state and in the absence of parallel electric fields, the north-south electric field E_x simply maps along the field line, which, in the dipolar coordinates of Figure 1, means that it stays constant. (More details on the dipolar coordinate system can be found in Lysak, 1985.) However, if we assume that a linear relationship exists between the parallel current and the parallel potential drop:

$$j_z = -K(\Phi_i - \Phi_e) \quad , \tag{2}$$

where Φ_i and Φ_e represent the potential in the ionosphere and in the equatorial plane, respectively, the perpendicular field must change along the field line so that the curl of the total electric field vanishes. In this case, we can combine equations (1) and (2) to relate the potential in the ionosphere to the equatorial potential:

$$\left[1 - \frac{\Sigma_P}{K} \frac{\partial^2}{\partial x^2} \right] \Phi_i = \Phi_e \quad . \tag{3}$$

This relationship indicates that large-scale potential structures in the equatorial plane, with sizes large compared to $L = \sqrt{\Sigma_P/K}$, will pass unattenuated to the ionosphere with no potential drop along the field line. On the other hand, equatorial structures with sizes less than L will not be mapped to the ionosphere, and the resulting difference will

148

appear as a parallel potential drop. For auroral zone parameters, this scale length L is about 100 km. This scale size is appropriate for the largest scale auroral structures, but is large compared to the sizes of individual auroral arcs which have a scale of about 1 km.

Consequences of this type of model in the steady state have been considered by Lyons et al. (1979), Chiu and Cornwall (1980), and others. Two critical assumptions are made in these models. First, it is assumed that a linear current-voltage relationship as in equation (2) is present. These authors associate such a relationship with plasma sheet particle motion in the dipolar magnetic field, as was shown by Fridman and Lemaire (1980). As we shall see below, such an approximate linear relationship is not restricted to these adiabatic models. A second assumption is that the driving force in the outer magnetosphere is characterized by a fixed potential as a function of position represented by the right-hand side of equation (3). Such a potential could be related to the E × B motion of the equatorial plasma, in which case treating it as constant implies that the equatorial convection is not affected by conditions on the field line which connects it to the ionosphere.

On the other hand, it has been known for some time that the ionosphere exerts a frictional influence on magnetospheric convection due to the dissipation caused by the finite Pedersen conductivity (e.g., Vasyliunas, 1970; Sonnerup, 1980). Information on ionospheric conditions is transmitted to the equatorial region by means of shear mode Alfvén waves which can propagate along the field line between the two regions, which have a travel time from the ionosphere to the equator of about 30 s in the auroral zone, as is evidenced by the existence of Pi2 pulsations with periods of about 2 min (Southwood and Hughes, 1983), which would correspond to the travel time from one ionosphere to the conjugate ionosphere and back.

The presence of Alfvén waves on auroral field lines should cause one to rethink the steady state model presented above. For one thing, the steady state model assumes that currents perpendicular to the magnetic field only exist at the ionosphere and in the equatorial plane, while Alfvén waves carry with them a polarization current which depends on the rate of change of the perpendicular electric field. In a static structure, these currents will vanish, but the possibility exists that a standing wave structure could be set up in which the polarization currents could persist. Such a situation is shown in Figure 2, which shows results from a time-dependent, two-dimensional MHD model of auroral currents (Lysak and Dum, 1983; Lysak, 1985). The contours in this figure represent flow lines of the current for a case in which a potential structure is propagated across the field line. Alternatively, this figure could be viewed as the current pattern produced by a potential structure in the presence of a north-south component of plasma convection in the auroral zone. As can be seen, the multiple reflections of the Alfvén wave pulses give rise to wave structure in which interference occurs between up- and downgoing waves. This wave interference decouples the field-aligned currents which connect to the ionosphere from those which flow up to the equatorial plane. In a structure such as this, which may be typical of multiple auroral arc structures, the steady state model is clearly inappropriate.

This structure can be described by a generalization of the model given above by replacing the assumption that a fixed equatorial potential structure is present by a more general assumption that a relation exists between the electric field and the perpendicular currents. For the case of polarization currents, this relation involves the so-called Alfvén conductance (Mallinckrodt and Carlson, 1978), $\Sigma_A = c^2/4\pi V_A$, where V_A is the Alfvén speed. If it is assumed that the ionospheric currents close via these polarization currents, a relation with the form of equation (3) results but with the scale length becoming:

$$L = \left[\frac{\Sigma_P \Sigma_A}{K (\Sigma_P + \Sigma_A)} \right]^{1/2}.$$

(4)

The Alfvén conductance Σ_A is plotted along an auroral field line in Figure 3, where it can be seen that its value over the field line is generally less than the Pedersen conductivity, which is typically over 1 mho. For the Case $\Sigma_A \ll \Sigma_P$, equation (4) shows that the scale length depends on the Alfvén conductance rather than the Pedersen conductivity, leading to smaller scales than those predicted by equation (2). Thus, the 1-km scale size of discrete auroral arcs may in fact be a result of current patterns such as those shown in Figure 2.

Another process which violates the steady state assumption is the enhancement of the ionospheric conductivity due to the enhanced energetic electron precipitation produced by the parallel electric field. This can give rise to a feedback instability (Sato, 1978; Rothwell et al., 1984; Lysak, 1986) in which traveling enhancements of the conductivity and the field-aligned current occur (Fig. 4). Numerical modeling of this instability (Lysak, 1986) shows periods of about 1 s which appear to be due to Alfvén wave reflections at altitudes of 2 R_E or less, so these currents also close well before they reach the equatorial region. The structures shown in Figure 4 have scale sizes of about 10 km, approaching the size of the discrete aurora.

The discussion above indicates that while the steady state model can describe the large-scale properties of the aurora, time-dependent effects may be important at creating short-scale current structures on auroral field lines. Parallel electric fields thus form in a current environment which can fluctuate on time scales as quickly as 1 s. On these time scales, Alfvén waves carry changes in the field-aligned currents. Parallel electric fields form as a result (Goertz and Boswell, 1979) of the current required to flow because of the magnetic perturbation associated with the Alfvén wave. Plasma turbulence will form when the current exceeds the threshold for instabilities. The effect of this turbulence will be examined in the following section.

III. MACROSCOPIC EFFECTS OF PLASMA TURBULENCE

If plasma turbulence does develop, it can affect the development of the current structure which produced it. Lysak and Carlson (1981) showed that the introduction of parallel resistivity modified the Alfvén wave dispersion relation, producing a reflection and dissipation of the wave which reduces the current. From the point of view of the MHD equations, this is the result of the well-known magnetic diffusion equation in the presence of resistivity. Plasma turbulence in a strong magnetic field will most likely give rise to a non-isotropic conductivity. In the case of double layer formation of electrostatic ion cyclotron turbulence, the dominant effect is that of parallel resistivity (Lysak and Dum, 1983). It can be shown that this term gives rise to diffusion across the magnetic field:

$$\frac{\partial B_y}{\partial x} = \frac{\partial}{\partial x}\left[\eta_\| \frac{\partial B_y}{\partial x}\right] \quad , \tag{5}$$

in the geometry of Figure 1 with gradients in y ignored. Thus, the presence of plasma turbulence will in general lead to a broadening of current structures and the reduction in the current strength.

In this section, we will compare three models of parallel electric fields caused by current-driven turbulence. In order to incorporate these effects into a MHD model, a simple relationship between the fluid properties of the plasma, such as density, drift velocity and temperature, and the parallel electric field, must be introduced. Clearly, a satisfactory model of this type has not yet been found and, indeed, it is likely that the complexities of plasma turbulence cannot be so easily parameterized. Nevertheless, some simple models of this type can be considered and will serve to indicate some of the relevant effects.

The first model we will consider will be based on simulations of current driven double layers (e.g., Sato and Okuda, 1981; Kindel et al., 1981; Barnes et al., 1985). When the drift velocity in these models is about half the electron thermal speed, double layers with amplitude $e\Phi/T_e \simeq 1$ are produced and, in long enough systems, will recur at intervals of the order of 1000 Debye lengths, where a Debye length is the order of a few meters in the auroral plasma. Since the MHD model has a grid size along the magnetic field of about 500 km, it is appropriate to consider the average electric field, which for the above numbers leads to:

$$E_z = 0.001 \ [4\pi n T_e]^{1/2} \qquad . \tag{6}$$

Although the drifts in excess of the threshold cause these double layers to grow and decay more quickly (Barnes et al., 1985), the average electric field over the time step of the MHD model (about 0.01 s) may remain roughly constant. To avoid a discontinuity in the electric field, the parallel field is increased linearly [using the linear resistivity given by equation (9) below] until the double layer electric field given above is reached. It should be noted that double layer electric fields are not present when the plasma frequency exceeds the electron cyclotron frequency (Barnes et al., 1985). This effect has not been explicitly included in the model; however, in the region in which the critical current is the lowest, the plasma frequency remains below the cyclotron frequency.

As an alternate to the double layer model, we consider a model for electrostatic ion cyclotron (EIC) turbulence due to resonance broadening (Dum and Dupree, 1970; Lysak and Dum, 1983). In this model, a resistive potential drop is introduced whenever the current exceeds the threshold for the EIC instability, i.e., about 0.3 of the electron thermal speed for $T_e = T_i$. The amplitude of the fluctuating electric field, and thus the effective resistivity, increases quadratically as the current increases. Thus, the electric field becomes:

$$E_z = \frac{m\nu^*}{ne^2} \ (j_z - j_{crit}) \quad , \tag{7}$$

where the effective collision frequency is:

$$\nu^* = 0.4 \ \Omega_i \left[1 + 0.1 \left(\frac{j_z - j_{crit}}{j_{crit}} \right)^2 \right] \qquad . \tag{8}$$

Note that in this case the parallel electric field will scale with the strength of the background magnetic field through the ion gyrofrequency $\Omega_i = eB/m_i c$, in contrast to the double layer model described by equation (6).

These two models have very differing behavior in that the double layer model is electric field-saturated in the sense that once the critical current is reached, the parallel electric field does not increase further. The nonlinear resistive model described by equations (7) and (8) is in a sense current-saturated since the electric field rises very rapidly after the critical current is reached. This enhances the diffusion of the current and reduces it to a lower level. The third model that will be considered will be one in which an effective collision frequency is assumed as in equation (7) but the collision frequency is independent of the current once the threshold is reached. Thus, equation (8) is replaced by:

$$\nu^* = 0.4 \ \Omega_i \quad , \tag{9}$$

when the drift velocity exceeds 0.3 of the electron thermal speed. This model will be referred to as the linear resistivity model.

In order to assess the macroscopic consequences of these models, a series of runs were done with the MHD model described earlier. In these runs, a current loop of a fixed magnitude and width is introduced on the field line, propagates toward the ionosphere, and enters a region of parallel electric field described by one of the three models. The ionospheric conductivity is taken to be fixed at 1 mho, and the density profile is of the form:

$$ n(r) = 10^5 \, e^{-(r-r_o)/h} + 5 \, (r - 1)^{-1.5} \quad , \tag{10} $$

where n is measured in cm^{-3}, r is in R_E, the base altitude for the ionosphere is $r_o = 1.05 \, R_E$, and the scale height h = 0.1 R_E. The electron temperature is 1 eV and the upper boundary condition is taken to absorb Alfvén waves which are incident upon it after being reflected from lower altitudes (Lysak, 1985). As the runs proceed, the maximum potential drop and the field-aligned current at the ionosphere are monitored, as the system approaches a steady state. Since the ionosphere is a very good conductor, the current of a reflected Alfvén wave is in the same direction as that of the incident wave (Mallinckrodt and Carlson, 1978); thus, the final value of the current will be twice the injected current in the limit of infinite ionospheric conductivity ($\Sigma_P >> \Sigma_A$) and no parallel electric field. Such a case is shown in Figure 5 in which the injected current was 20 $\mu A/m^2$ and the final current of 36 $\mu A/m^2$ is nearly double this value. Because of the diffusion associated with the parallel electric field, the current reaching the ionosphere is reduced when a parallel electric field is present. This effect is shown for the double layer model and the nonlinear resistivity model in Figures 6 and 7, respectively. In these figures the injected current was 20 $\mu A/m^2$. It can be seen that the double layer model is much less diffusive than the resistive model, with the final currents being 30 $\mu A/m^2$ and 6 $\mu A/m^2$ for the two runs.

The final current-voltage characteristics for a series of runs are shown in Figure 8. First of all, note that each of the models produces potentials in the kilovolt range for currents of a few microamps per square meter. This is significant since the parameters of the parallel electric field model were determined purely from the local properties of the auroral plasma without any requirement that the global current-voltage relation come out right. Therefore, none of the models can be ruled out on this basis.

Turning to differences in the models, we see that the double layer model exhibits the voltage-saturation effect referred to earlier. As the current increases, more of the field line can support the formation of double layers, leading to an increased total potential drop. Since it is assumed that the parallel electric field does not increase further as the current increases, the addition of more current does not further increase the total potential drop.

The linear resistivity model produces a linear current-voltage characteristic. At first glance this may appear obvious, but actually the situation is complicated by the scaling of the fields and currents along the field line. It was shown by Lysak and Dum (1983), however, that these factors cancel when the resistivity scales with the magnetic field strength, preserving the linear relationship between the total potential and the field-aligned current at the ionosphere. The approximate linear relationship has been invoked by Lyons (1980) to support the nonlocal current-voltage relationship based on adiabatic particle motions (e.g., Fridman and Lemaire, 1980). However, the present argument shows that this interpretation is not unique.

The current limiting effect of the nonlinear resistivity model is apparent from Figure 8. Here an attempt to increase the current simply causes an enhancement in the diffusion, leading to large potentials and a broader current structure as is seen in Figures 9 and 10, which compare the field and current profiles for the double layer and non-linear resistivity models. Here the enhanced diffusion due to the nonlinear resistivity is evident.

152

Figure 11 shows the effective diffusion in the entire set of runs by plotting the ratio between final and input currents against the input current. As discussed above, the maximum value of this ratio is 2 for the case of infinite Pedersen conductivity. The open squares represent runs with no parallel electric field and a Pedersen conductivity of 1 mho. The small reduction from 2 in these cases represents the effect of ionospheric dissipation. Note that the linear and nonlinear resistive models have comparable diffusion for small currents where the nonlinear part of the resistivity is not important; but, at larger currents, the nonlinear model is more diffusive. The double layer model is comparable to the other models at low currents, but an increase in the current decreases the effective diffusion since the potential drop does not increase for increasing current.

In summary, the three models for a local current voltage relation produce results consistent with the observed global relationship. Thus, this type of model cannot be distinguished from the kinetic models of parallel potential drop on this basis. The double layer model allows for very strong currents to flow in a narrow channel since the potential drop and thus the effective diffusion do not increase much as the current increases. The nonlinear resistive model has the opposite effect in that the strong increase in the potential drop for an increase in the current causes an enhanced diffusion which broadens the current channel, in effect causing the current to flow around the region of parallel electric field.

IV. SUMMARY AND CONCLUSIONS

The simplified models of parallel electric fields presented here have provided some insight into the development of the auroral potential drop, but are clearly limited in their applicability to the auroral plasma. Auroral conditions can be quite varied, and the presence of turbulence along the field line can result in the heating of the plasma as well as a decrease in the plasma density as transversely heated ions are expelled from the acceleration region. Therefore, there is more to auroral dynamics than can be found in the simple cold plasma model used here.

Density decreases in the auroral zone serve to decrease the critical current necessary for the generation of microscopic turbulence, and therefore will increase the total potential drop for a given level of current. Numerical results indicate that this result is more important in the double layer model because of the "switch-on" nature of the double layer electric field. Since the double layer electric field scales with the plasma pressure, the potential drop is localized at the lowest altitudes at which the critical current is exceeded. This is in contrast with the resistive electric field which depends on the excess current over the critical current, and thus maximizes at the point where the critical current is lowest. A set of runs in which a current of 10 μA/m^2 is injected showed that the potential drop increased by 25 percent in the double layer model when the ionospheric scale height [see equation (10)] is reduced to 0.05 R$_E$ from the value of 0.1 R$_E$ used in the other runs, while in the nonlinear resistivity model the increase was only 18 percent. Thus, the effect of a density cavity would be to produce an increase in the potential drop, especially in the double layer model.

The temperature of the topside ionosphere can also vary under auroral conditions, and may be expected to increase as the result of microscopic turbulence. Increases in the temperature will tend to decrease the extent of the turbulent region since the critical current scales as the electron thermal speed. Thus, potential drops due to nonlinear resistivity would be expected to decrease. A similar result is true in the double layer model; however, this effect is counteracted by the increase of the average electric field due to double layers since this field scales with the square root of the temperature. Runs at 10 μA/m^2 indicate that the potential drop in the nonlinear resistivity model decreased by 35 percent when the temperature was raised by a factor of 10, while in the double layer model the potential increased by 12 percent. Thus, the increase of temperature favors the double layer model, at least until the point at which the current becomes sub-critical.

In the actual auroral zone, these two effects will be necessarily connected. The transverse heating of ions observed in the auroral zone can create density cavities since the heated ions are subject to the magnetic mirror force that expels them from the low-altitude auroral zone. One can imagine a scenario in which the increase of the current magnitude excites turbulence, leading to the heating of ions and the creation of the density cavity. This hot, low density plasma would lead to conditions under which the formation of double layers could further accelerate electrons into the atmosphere and ions out of the atmosphere. This would result in the density cavity progressively extending to lower and lower altitudes, with a corresponding increase in the total potential drop along the field line. While the existing numerical model is too crude to account for all these effects, this scenario seems plausible based on the results above. A more complete model including the effects of the thermal evolution of the plasma will be the subject of future work.

In conclusion, this work has shown first of all that models of the auroral potential drop based on microscopic turbulence, whether due to double layrs or a nonlinear resistivity, can account for the correct magnitude of the auroral potential drop for typical auroral currents. The two models differ in that the nonlinear resistivity model limits the current density by spreading the current over a broader area. In contrast, the double layer model proposed above has a limit to its total potential drop and can sustain currents with a high density. At such high current densities, however, this model will most likely be too simplified, since plasma heating and the formation of a density cavity, effects not included in the cold plasma model presented here, will likely change the nature of the current-voltage relation.

The oversimplified models presented here represent an attempt to incorporate kinetic effects of the plasma into a fluid model. In order to model the global structure of the auroral zone, some such approximation must be made since particle-in-cell or Vlasov models of any large volume of the auroral zone are technically not feasible with present or anticipated computer resources. The question of a satisfactory parameterization of the kinetic effects for use in a fluid model remains an open question, which can only be answered by a combination of fluid modeling and kinetic modeling, as well as analytic theory of the auroral current region.

154

REFERENCES

Barnes, C., M. K. Hudson, and W. Lotko, *Phys. Fluids, 28,* 1055 (1985).

Chiu, Y. T., and J. M. Cornwall, *J. Geophys. Res., 85,* 543 (1980).

Dum, C. T., and T. H. Dupree, *Phys. Fluids, 13,* 2064 (1970).

Fridman, M., and J. Lemaire, *J. Geophys. Res., 85,* 664 (1980).

Goertz, C. K., and R. W. Boswell, *J. Geophys. Res., 84,* 7239 (1979).

Kindel, J. M., C. Barnes, and D. W. Forslund, in *Physics of Auroral Arc Formation, American Geophysical Union Geophysical Monograph 25,* edited by S.-I. Akasofu and J. R. Kan, p. 296, 1981.

Lyons, L. R., *J. Geophys. Res., 85,* 17 (1980).

Lyons, L. R., D. S. Evans, and R. Lundin, *J. Geophys. Res., 84,* 457 (1979).

Lysak, R. L., and C. W. Carlson, *Geophys. Res. Lett., 8,* 269 (1981).

Lysak, R. L., and C. T. Dum, *J. Geophys. Res., 88,* 365 (1983).

Lysak, R. L., *J. Geophys. Res., 90,* 4178 (1985).

Lysak, R. L., *J. Geophys. Res.,* accepted for publication, 1986.

Mallinckrodt, A. J., and C. W. Carlson, *J. Geophys. Res., 83,* 1426 (1978).

Miura, A., and T. Sato, *J. Geophys. Res., 85,* 73 (1980).

Rothwell, P. L., M. B. Silevitch, and L. P. Block, *J. Geophys. Res., 89,* 8941 (1984).

Sato, T., *J. Geophys. Res., 83,* 1042 (1978).

Sato, T., and H. Okuda, *J. Geophys. Res., 86,* 3357 (1981).

Sonnerup, B.U.O., *J. Geophys. Res., 85,* 2017 (1980).

Southwood, D. J., and W. J. Hughes, *Space Sci. Rev., 35,* 301 (1983).

Vasyliunas, V. M. in *Particles and Fields in the Magnetosphere,* edited by B. McCormac, p. 29, D. Reidel, Hingham, Massachusetts, 1970.
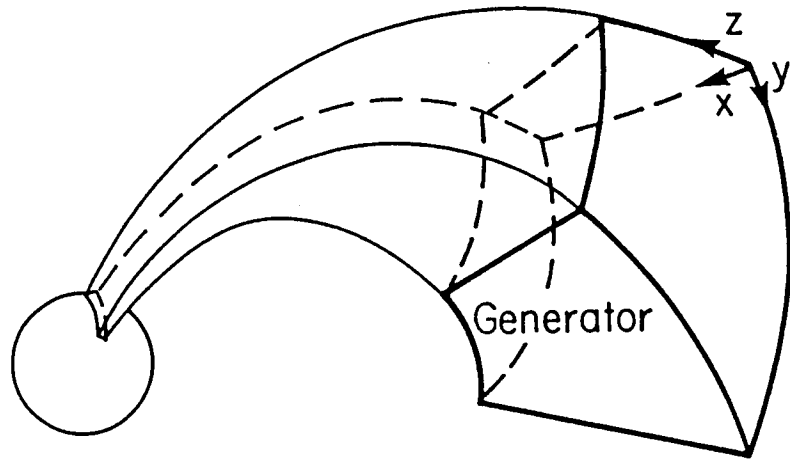
Figure 1. A sketch of the dipolar coordinate system used in this paper. Here z is the coordinate along the geomagnetic field, y is the longitude, and x is a coordinate proportional to the inverse of the L value of the field line.
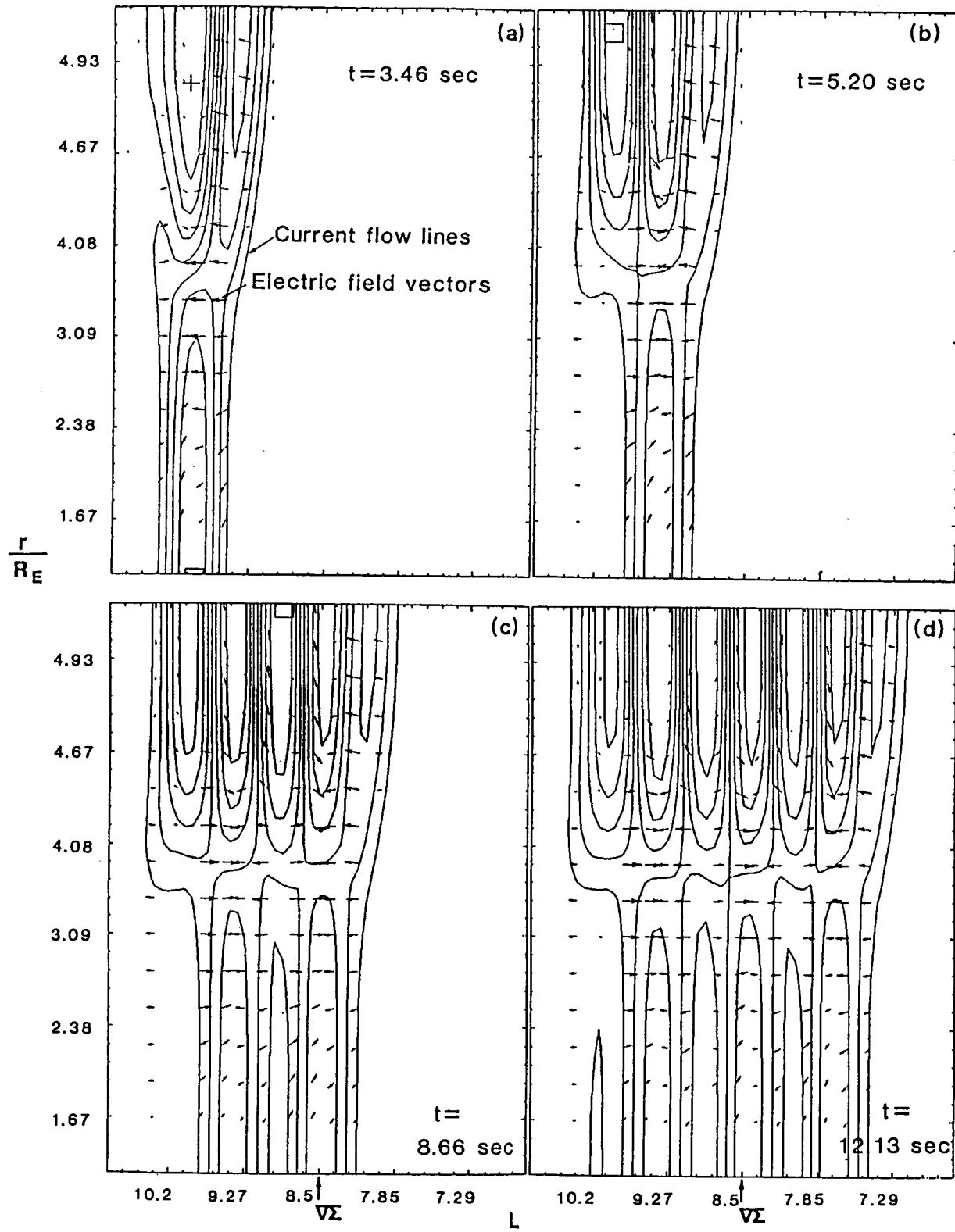
Figure 2. A set of snapshots showing the evolution of a run in which a moving voltage pulse travels across field lines (Lysak, 1985). The contour lines represent current flow lines ni the xz plane of Figure 1. Note that the currents which reach the ionosphere close in the region between 3 and 4 R_E where up- and downgoing waves interfere.

157
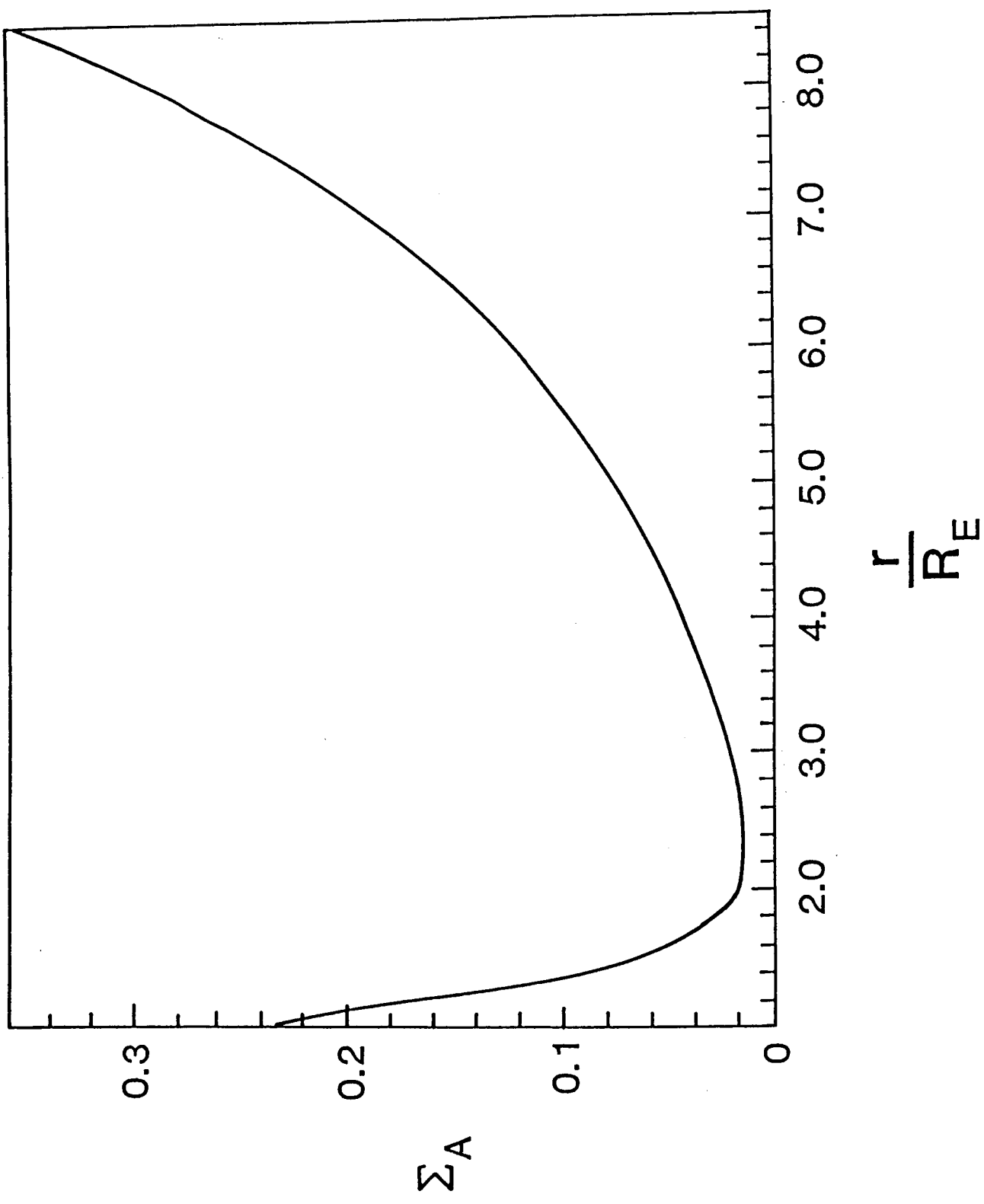
Figure 3. A sketch of the Alfvén wave admittance Σ_A (in mho) as a function of radial distance for the density profile given by equation (10).
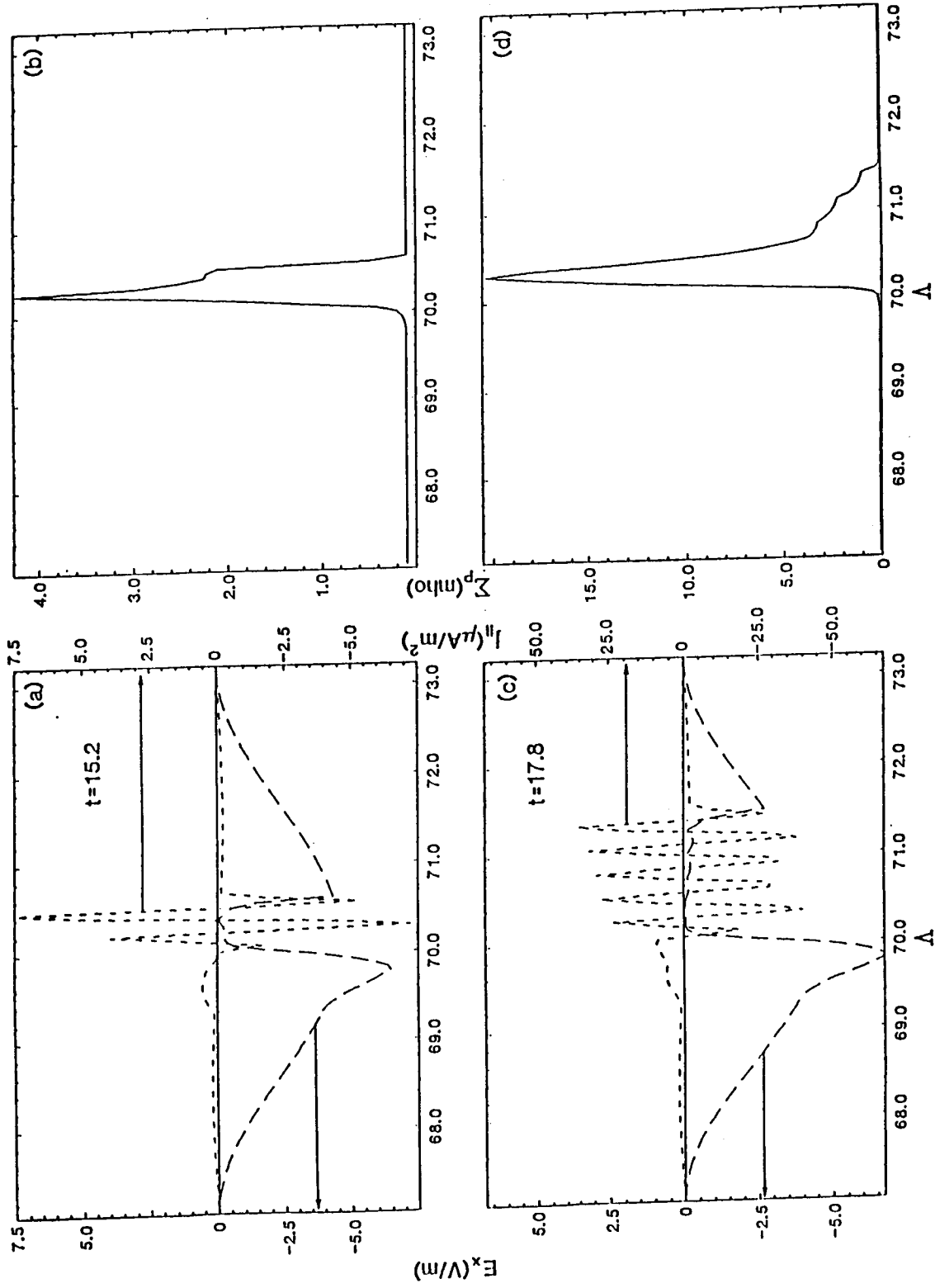
Figure 4. Ionospheric electric field, field-aligned currents, and Pedersen conductivity for a run in which the conductivity increases due to electron precipitation and a feedback instability results (Lysak, 1986). The oscillations in the current have a wavelength of about 20 km and a frequency of near 1 Hz, indicative of wave reflection from the region of minimum wave admittance.
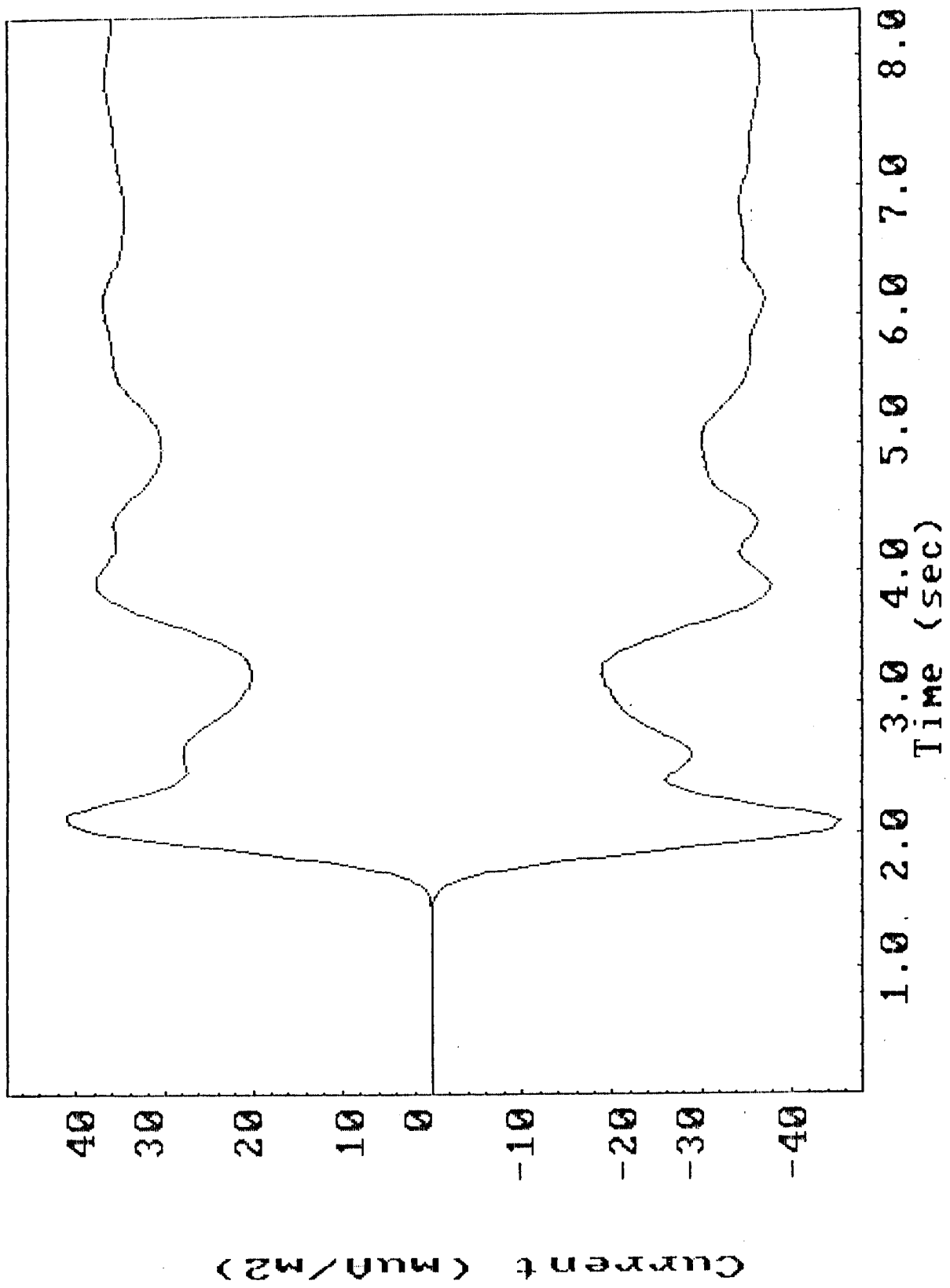
Figure 5. Maximum and minimum field-aligned currents at the ionosphere for a run with a Pedersen conductivity of 1 mho, an injected current of 20 $\mu A/m^2$, and no parallel electric field. The maximum current attainable in this system is 40 $\mu A/m^2$, and the final value of 36 $\mu A/m^2$ is due to losses in the ionosphere.
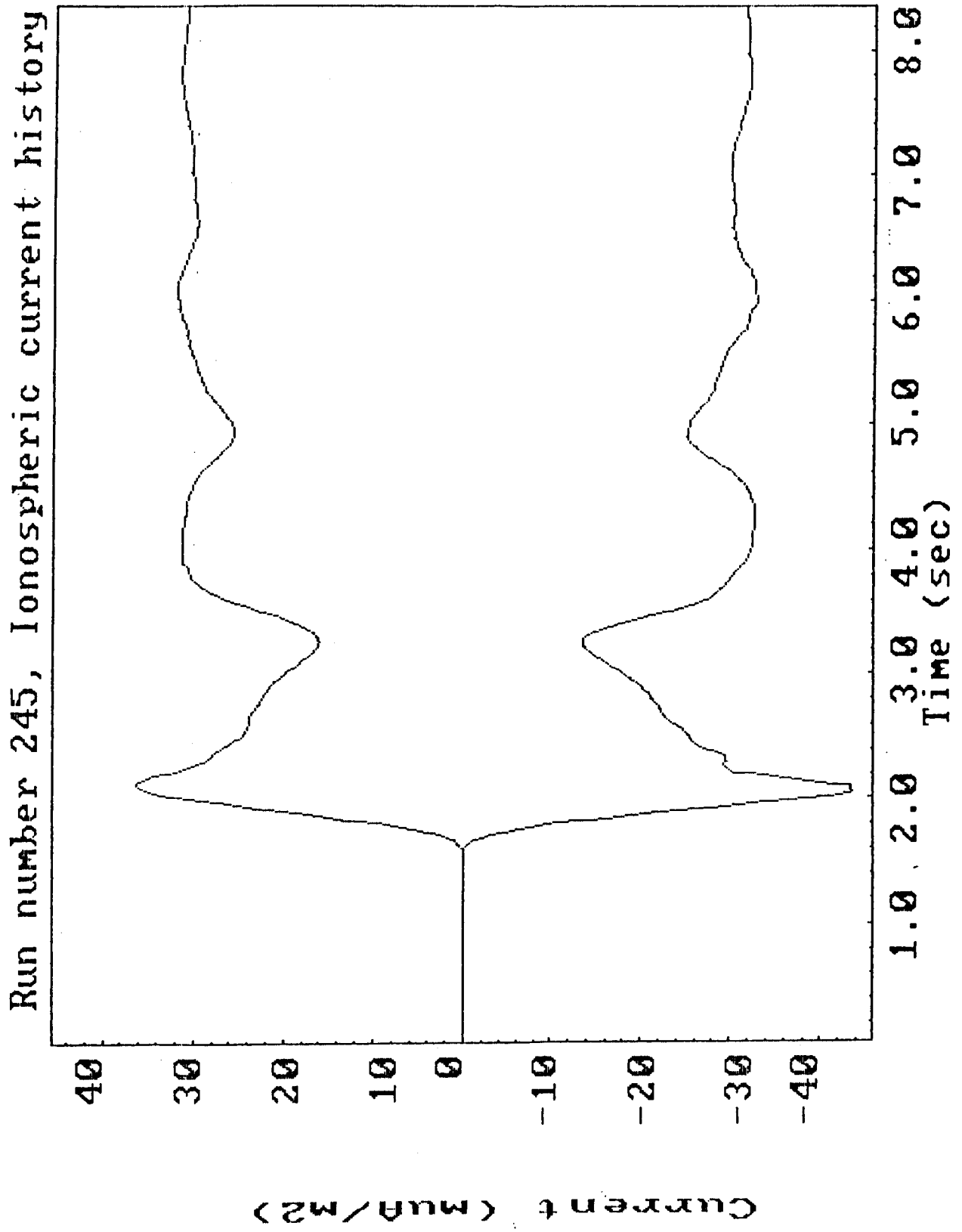
Figure 6. Similar to Figure 5 except that a double layer electric field has been included. The maximum current is reduced to 30 μA/m² in this case.
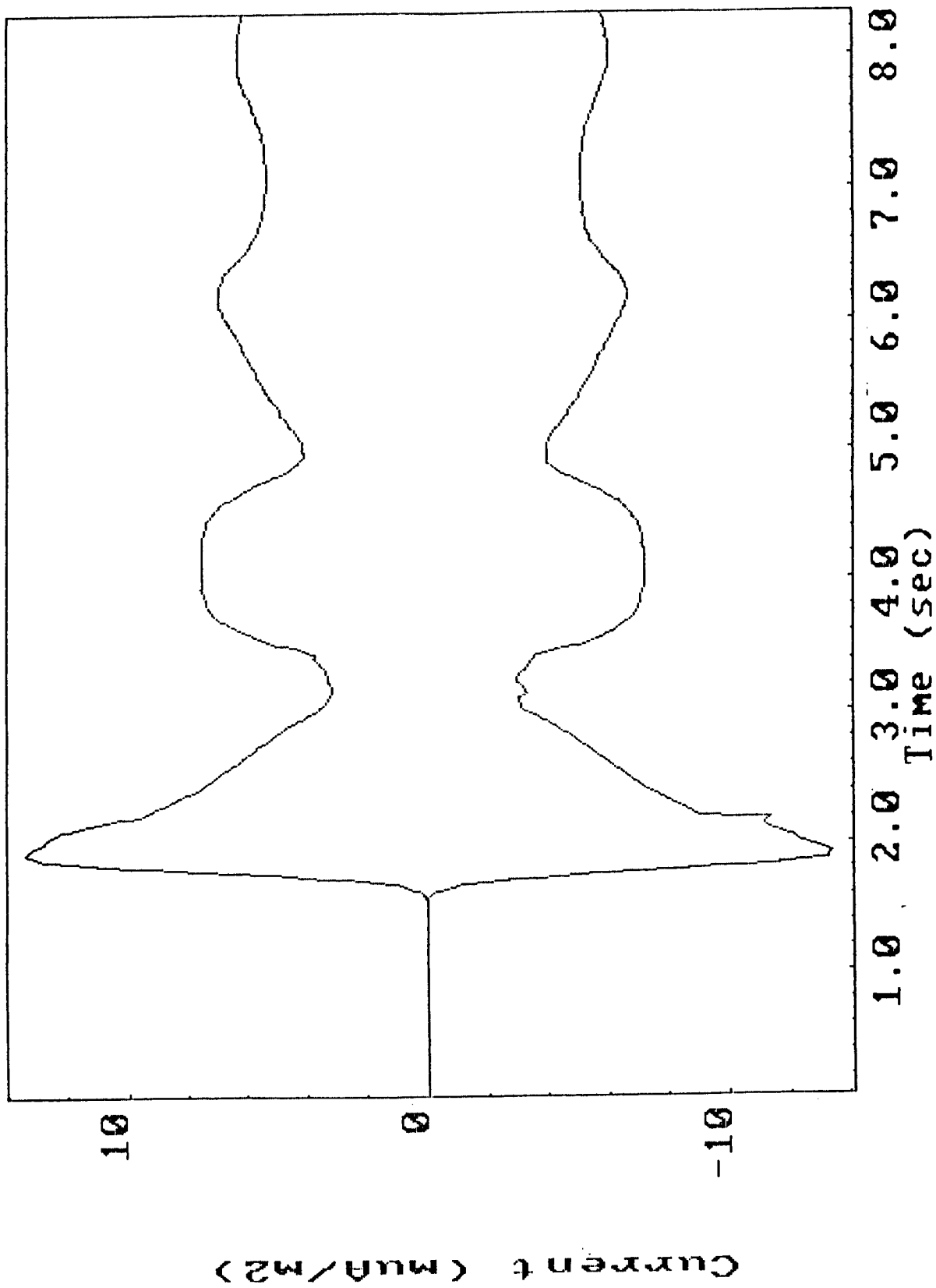
Figure 7. Similar to Figures 5 and 6 but including a nonlinear resistivity. The maximum current is drastically reduced due to the diffusion of the current structure to 6 $\mu A/m^2$.

162
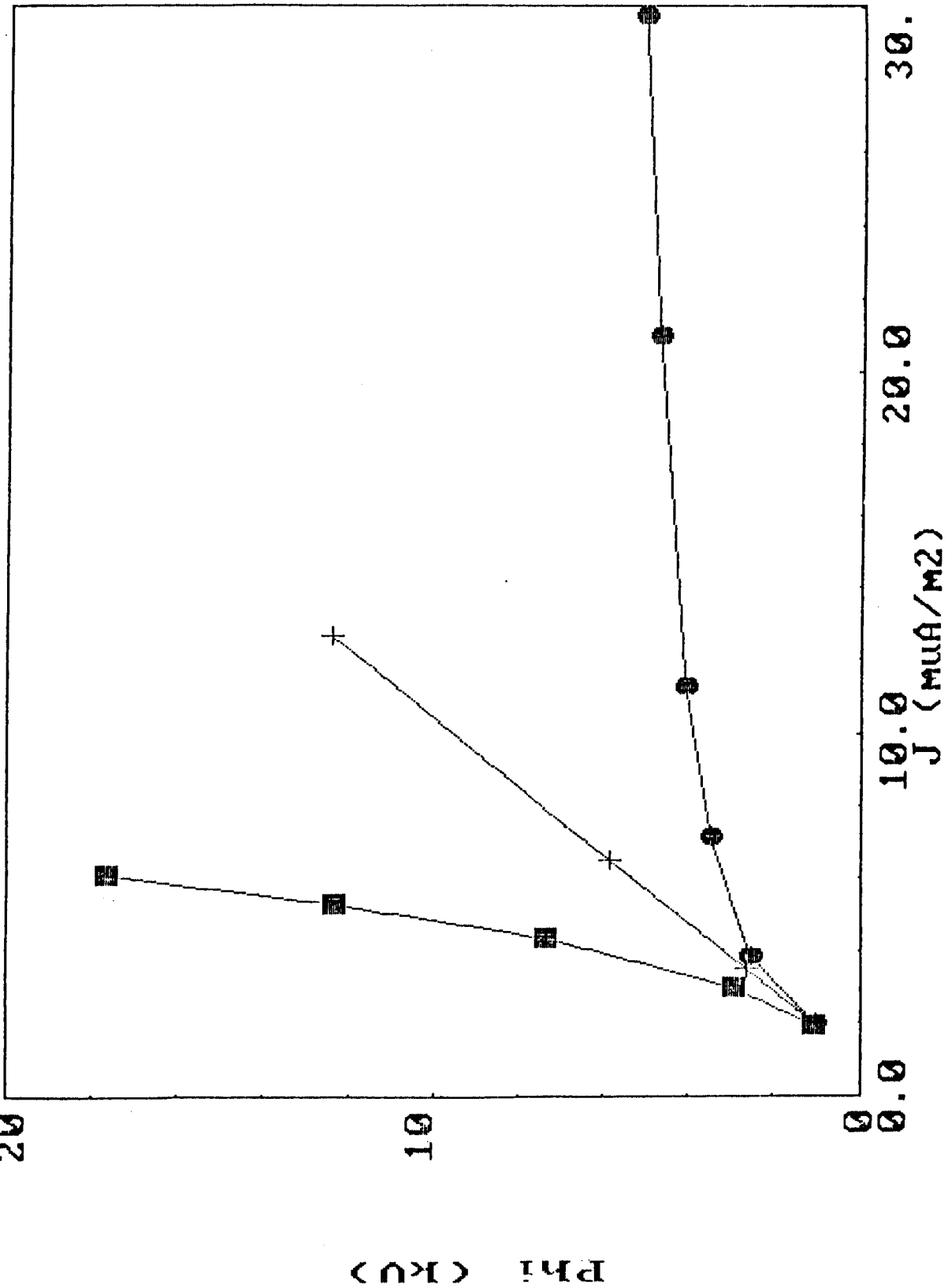
Figure 8. Current-voltage characteristics for a set of runs comparing the double layer model (dots), linear resistivity model (crosses), and the nonlinear resistivity model (squares).

163
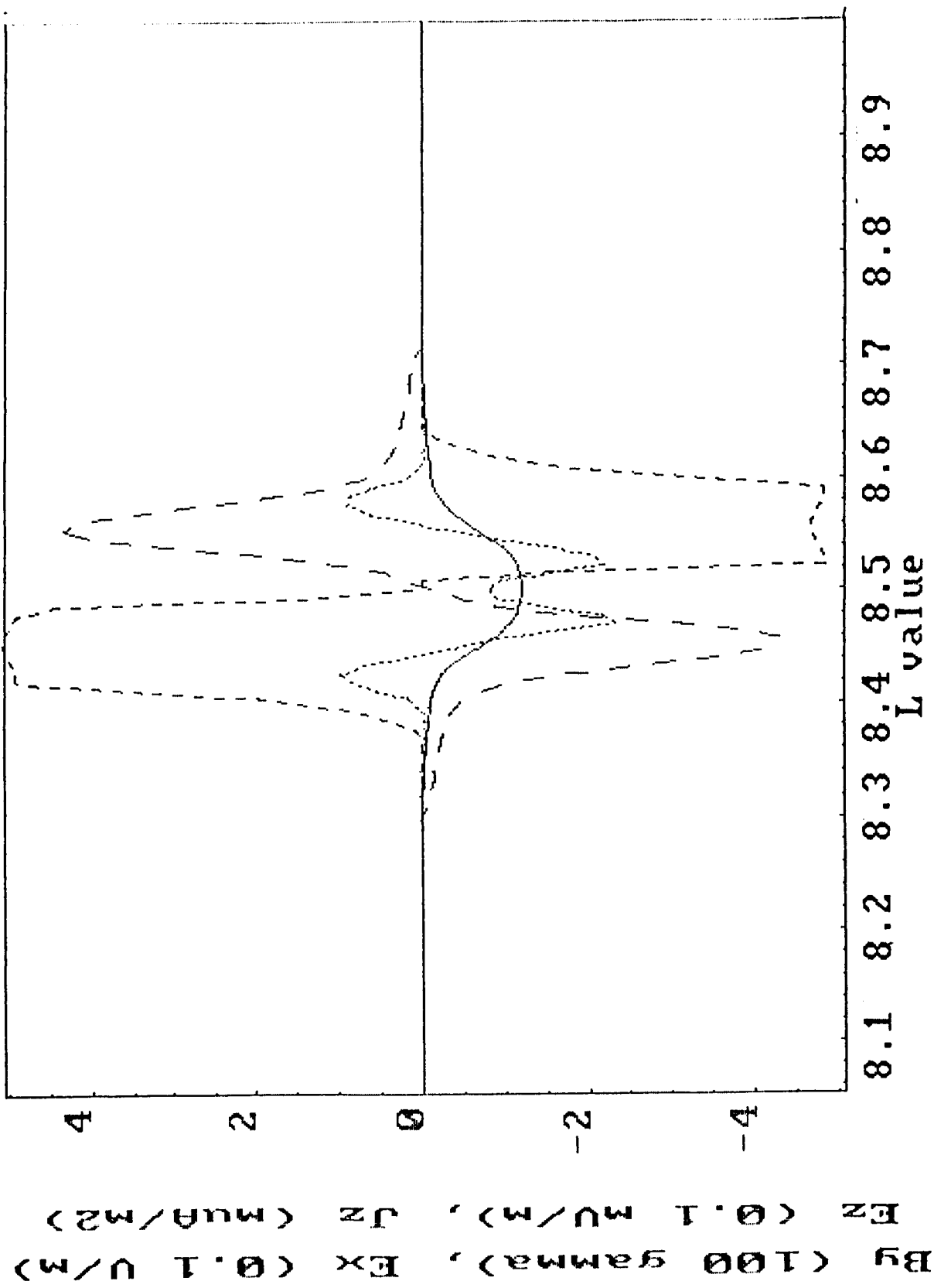
Figure 9. Field profiles at 2 R_E for the double layer run of Figure 6. The solid line gives the magnetic perturbation, the dotted line the perpendicular electric field, the short dashed line the parallel electric field, and the long dashed line the field-aligned current. These fields are in units of 100 γ, 0.1 V/m, 0.1 mV/m, and μA/m^2, respectively.
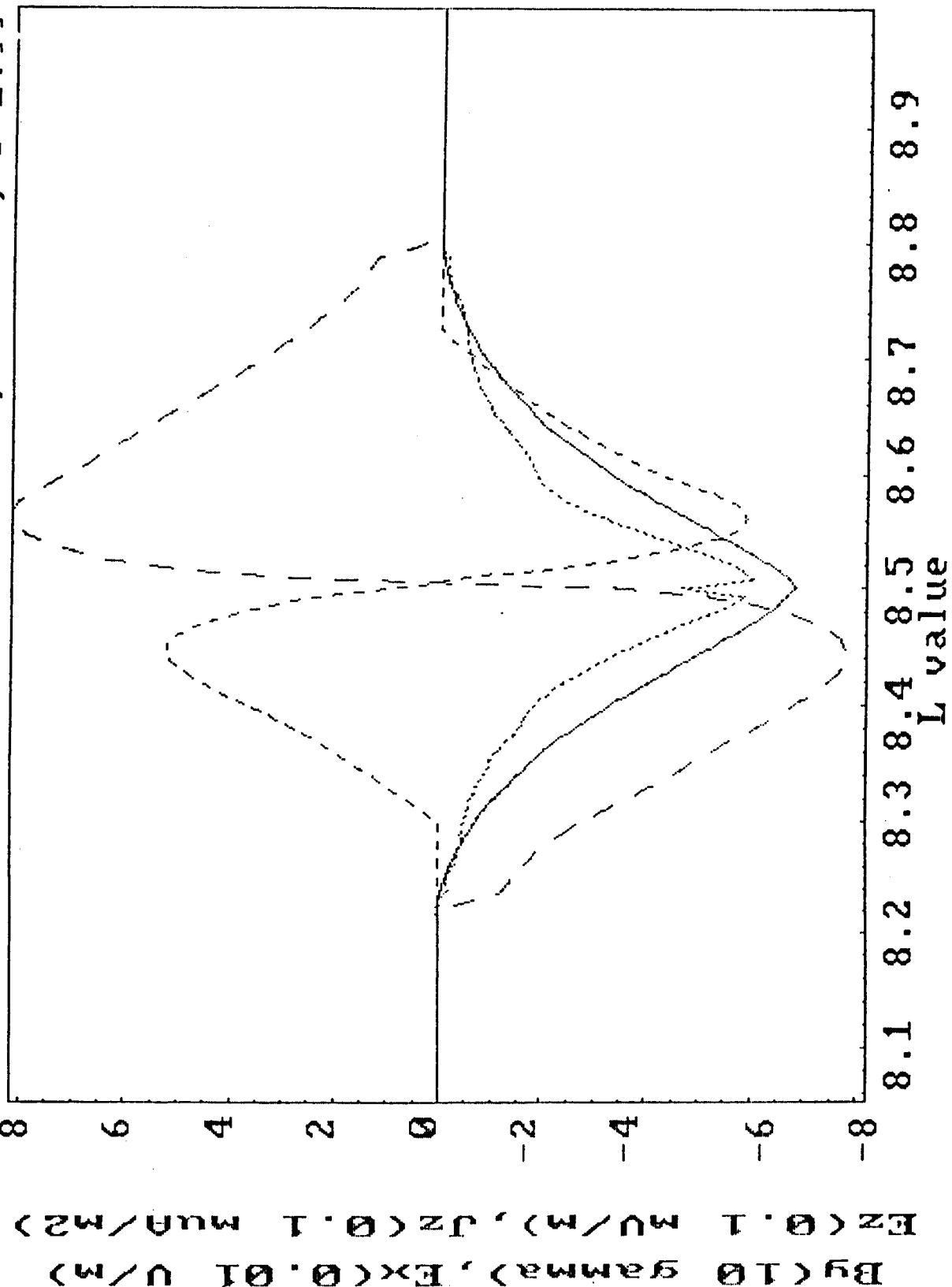
Figure 10. Same as Figure 9 but for the nonlinear resistivity run of Figure 7. The units in this case are 10 γ, 0.01 V/m, 0.1 mV/m, and 0.1 μA/m² for B_y, E_x, E_z, and J_z, respectively.
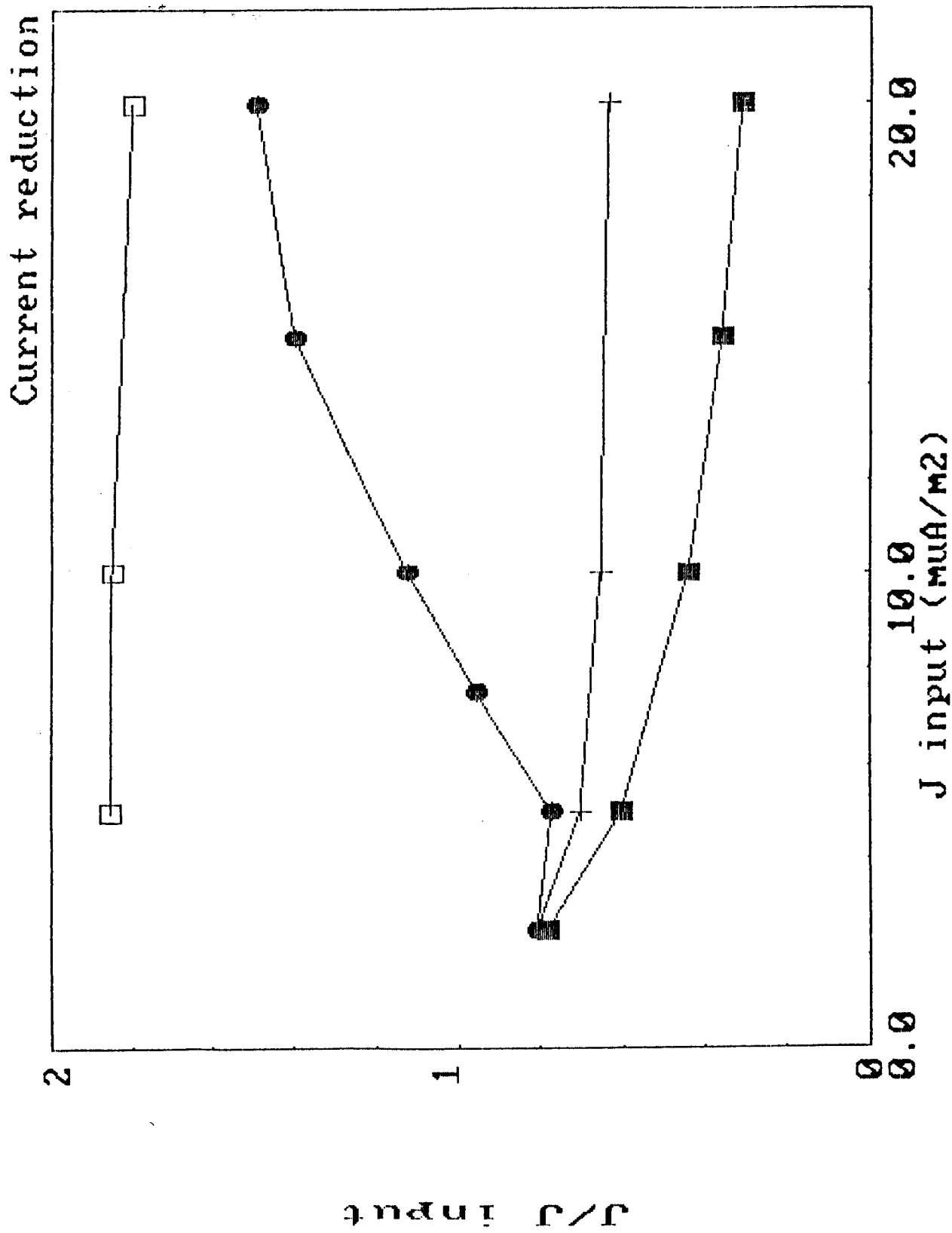
Figure 11. A comparison of the final currents to the injected currents for the runs of Figure 8, using the same symbols. In addition, runs in which no parallel electric fields were included are indicated by open squares.

CURRENT DRIVEN WEAK DOUBLE LAYERS

Gérard Chanteur

CRPE/CNET, 92131 Issy-les-Moulineaux, France

ABSTRACT

Double layers in plasmas can be created by different means. For example, a potential difference forms between two plasmas with different temperatures (Hultqvist, 1971; Ishiguro et al., 1985), in a plasma jet flowing along a converging magnetic field (Serizawa and Sato, 1984), in a quiescent plasma submitted to an external difference of potential, or in a turbulent plasma carrying an electric current. The first three cases can be current-free, but not necessarily, although the numerical simulations have been made under such conditions for the first two points (Ishiguro et al., 1985; Serizawa and Sato, 1984). Apart from the third case, which is mainly of interest for laboratory experiments, these double layers are good candidates for accelerating the auroral electrons to the few kiloelectron volts observed.

I. INTRODUCTION

This paper is devoted to the fourth case, i.e., to weak double layers driven by an electric current. Two papers have triggered the studies in this field: DeGroot et al. (1977) showed the formation of localized potential jumps in an homogeneous plasma with a suprathermal electron drift; later, Sato and Okuda (1980) gave evidence for the formation of small double layers under ion-acoustic instability conditions, i.e., a large electron-to-ion temperature ratio and a subthermal electron drift. Our present understanding of weak double layers built by electric currents has mainly grown from the analysis of numerical simulations with either superthermal (DeGroot et al., 1977; Singh et al., 1985; Singh and Schunk, 1984) or subthermal (Sato and Okuda, 1980, 1981; Kindel et al., 1981; Hudson and Potter, 1981; Okuda and Ashour-Abdalla, 1982; Hasegawa and Sato, 1982; Nishihara et al., 1982; Chanteur et al., 1983; Chanteur, 1984, 1986; Barnes et al., 1985) electron drifts, but always in linearly unstable conditions. The formation mechanism seems to be different in these two cases; furthermore, it is likely to be sensitive to the boundary conditions in the superthermal case. The basic mechanism which produces weak ion-acoustic double layers is a current interruption caused by a negative potential spike. This fact was primarily recognized in one-dimensional periodic simulations (Sato and Okuda, 1981; Kindel et al., 1981; Hasegawa and Sato, 1982; Nishihara et al., 1982; Chanteur et al., 1983) and has been recently confirmed in the two-dimensional case with a strong magnetic field and under various boundary conditions (Barnes et al., 1985). The theoretical explanation given to the appearance and the growth of a double layer (Hasegawa and Sato, 1982; Nishihara et al., 1982; Chanteur et al., 1983; Chanteur, 1984) turns out to be more or less independent of the linear instability. The goal of this paper is to specify this point, and it will be shown that small and localized differences of potential can be built by a partial current interruption under linearly stable conditions. It has been demonstrated (Dupree, 1983; Berman et al., 1985; Pécseli, 1984) that phase space holes can be unstable for electron drifts less than the critical value which destabilizes the ion-acoustic modes. Although different from our work in many respects, it invokes the same physical basis, i.e., the reflection of the current carrying electrons by coherent structures. Section II gives an account of the formation of weak ion-acoustic double layers under linearly unstable conditions. Section III is a first presentation of recent simulations demonstrating that small double layers can be produced by a localized current interruption in a marginally stable plasma. A more thorough presentation of these numerical experiments is in preparation (Verga et al., 1986).

II. UNSTABLE CASE

Most of the numerical studies concerning ion-acoustic double layers have been made with electrostatic particle codes that allow for the existence of thermal fluctuations. Indeed, the relatively small number of particles per Debye length (usually a few 10^1 or 10^2) gives rise to an artifically high level of thermal fluctuations. Besides, the probability of "big" fluctuations of the electric potential increases with the length of the system and should not be dismissed. Since ion-acoustic waves are weakly dispersive, we can argue that a big and negative potential spike present in the "initial" condition has a coherence time long enough to interact resonantly with the electrons. The word "initial" deserves a short explanation: a particle run is usually started with particles regularly distributed in space and attributing each particle a velocity given by a random number generator. The electric field usually taken equal to zero everywhere at t = 0 is built self-consistently by the thermal motion of the particles in a few tens of time steps. It appears that the "initial" condition on the field is determined by the microscopic details of the loading of the particles. The longer the system, the greater the probability to find a negative potential spike sufficiently above the thermal level to produce a persistent interruption of the current by reflecting the electrons. In a short and periodic system without any externally applied electric field, this current interruption goes on for the transit time of the electron flow through the system and a stable BGK state results with a large fraction of trapped electrons. If the system is long enough for the establishment of this BGK state to be delayed and if the negative spike is not too close downstream of another big spike, the evolution will be qualitatively different, giving rise to a weak and transient double layer, as will be seen below. Increasing the length of the system, we increasee the probability of the large fluctuations and delay the appearance of the BGK state; the combination of these two facts is likely to explain both the reason why double layers have never been observed in short periodic systems and the reason for the mean distance between double layers in very long systems. Instead, open boundary conditions not only provide a continuous input of energy into the system but new potential fluctuations are usually created near the input boundary (i.e., where the incoming flux of electrons is greater) and propagate through the system, giving rise to the observed temporal recurrence of double layers even in short open systems (Barnes et al., 1985). Consequently, the spatial and temporal recurrences of double layers in open systems are mainly governed by the chosen injection process of the particles at the boundaries. On the other hand, it has been shown (Barnes et al., 1985) that the formation mechanism of a weak double layer reported in detail in Nishihara et al. (1982), Chanteur et al. (1983), Chanteur (1984, 1986), and Barnes et al. (1985) is independent of the boundary conditions. Let us now recall the main features of this process.

In a system driven unstable by an electric current, the perturbations propagating against the electron flow are strongly damped, and the perturbations close to the most unstable wave number are rapidly selected among the other ones. On the basis of the linear instability theory for an homogeneous plasma, we expect the turbulence to develop homogeneously. Instead, it is observed that the evolution of long systems is dominated by one or few coherent structures, as was shown initially by Sato and Okuda (1980). For example, Figure 1 shows a negative potential spike (the figure in fact represents the potential energy of an electron), with $e\phi/T_e \sim 1$ which has emerged from the thermal noise in a one-dimensional electrostatic and periodic particle simulation with the following parameters: length $L = 512 \lambda_D$, ion-to-electron mass ratio $m_i/m_e = 100$, electron-to-ion temperture ratio $T_e/T_i = 20$, and electron drift to thermal speed ratio $V_d/V_{th} = 0.8$. As previously discussed, this pulse originates in a thermal fluctuation present in the "initial" condition. This negative spike of potential is initially amplified by the linear instability taken over by the nonlinear instability discussed in Nishihara et al. (1982) and Chanteur (1983). The electrons having a kinetic energy less than the height of the potential barrier are reflected on both sides of the pulse; yet, due to the current, more electrons impinge on the left side of the barrier than on the right side and, consequently, more electrons are reflected upstream of the barrier than downstream. This simple fact has important implications. First, the resulting charge separation in the vicinity of the barrier develops a difference of potential between the two sides of the pulse, as can be seen around $x = 120 \lambda_D$ in Figue 1, the low electric potential being on the upstream side of the barrier (upstream with respect to the electron drift). Second, quasi-neutrality of the plasma being preserved outside of the pulse, the electron density in excess on the upstream side is compensated for by an increased ion

density. Thus, the deep density trough associated with the potential pulse separates the upstream region of inflated plasma density from the depleted downstream region. Third, taking into account the velocity of the barrier, the mechanism of the instability can be easily understood. Let $\vec{V}_o$ be the velocity of the barrier and $\vec{V}$ the velocity of an incoming electron in the frame of reference moving with the barrier; assuming that the potential does not change during the interaction with this electron (a reasonable assumption considering the time scales in the numerical experiments), the collision is elastic and the particle leaves with a velocity $-\vec{V}$. The kinetic energy of the particle in the laboratory frame has changed from $1/2 \; m_e(\vec{V}_o + \vec{V})^2$ to $1/2 \; m_e(\vec{V}_o - \vec{V})^2$; i.e., an energy $2m_e \; \vec{V}_o.\vec{V}$ has been transferred to the barrier. The potential barrier moving primarily in the direction of the electron flow receives more energy from the electrons impinging on the upstream side than it gives the downstream side, and the field energy locally grows! Detailed energy and momentum balances have been made theoretically (Nishihara et al., 1982; Chanteur et al., 1983; Pecseli, 1984) and checked in the simulations (Chanteur et al., 1983).

Due to the relatively small number of particles per Debye length, local diagnostics in phase space (for example the distribution function of electrons at a given location) are poorly done in particle simulations. Instead, Vlasov simulations are free of this limitation, but in return suffer, at least for this study, from the absence of thermal noise. Starting with an initial condition strictly independent of x, a good Vlasov code can be run a long time before truncation and round-off errors seed a potential instability. An initial perturbation has to be put, whether random or not, in the system; an account of weak double layer formation under such circumstances has been given in Chanteur (1984). For the present discussion, we just recall the simulation presented in Chanteur et al. (1983). This Vlasov run was initialized with the same physical parameters as the aforementioned particle run, the initial perturbation being a localized 10 percent density depression on both species. Although qualified "perhaps unphysical" in Borovsky (1984), this initial condition reproduces what is built from the exaggerated thermal noise present in particle simulations. In fact, the potential energy of an electron shown versus x and t in Figure 2 is strinkingly similar to the result of the particle simulation (see Fig. 1). This temporal evolution of the system is not an artifact of the periodic boundary conditions; doubling the length of the system while keeping the same physical parameters does not change anything. On the other hand, this behavior is also observed in bounded systems and for different physical parameters (Barnes et al., 1985). Thus, it is not due either to some numerical coincidence for a magic set of parameters; in turn, the boomerange motion of the localized wave seems to be an artifact of one-dimensionality (Barnes et al., 1985). Figure 3 displays the electron phase space in the vicinity of the double layer at three different times during its propagation in the direction of the electron flow. The reflections of the electrons are clearly visible on both sides of the structure, and the electron holes are seen to be formed in the depleted downstream region [see also Chanteur (1984) and Barnes et al. (1985)].

The slowing down and the late evolution of the weak double layer cannot be understood without taking into account the ion dynamics (Chanteur et al., 1983; Chanteur, 1984). Figures 4a and b are local representations of the ion phase space just around the double layer for the above-mentioned particle and Vlasov simulations, respectively. It again emphasizes the similarity of the two runs. In the beginning, the negative pulse of potential is moving subsonically ($\sim 0.8 \; c_s$) toward the right in Figures 1 and 2, consistently with the negative velocity perturbation seen at times 320 and 340 in Figures 4a and b.. The pulse first undergoes a very faint slowing down (Chanteur et al., 1983) of purely hydrodynamic origin because of the extremely small number of resonant ions. It has been emphasized in Chanteur (1986) that resonant ions are by no means responsible for this slowing down and the point can be stated in the following way. Weakly nonlinear ion-acoustic waves in a stable plasma with a large electron-to-ion temperature ratio are well accounted for by assuming a cold fluid behavior of the ions and a Boltzmannian distribution of the electrons in the electrostatic potential. The evolution of the potential is then determined by a Korteweg-de Vries (KdV) equation, and the numerical integration of this evolution equation shows that a localized and rarefactive ion-acoustic wave is very slightly slowed down, and simultaneously weakly damped by the radiation of a dispersive tail on its trailing edge (Nishihara et al., 1982; Fornberg and Whitham, 1978; Okutsu and Nakamura, 1979). In the unstable case presently under investigation, the alteration of the pulse by the reflection of the electrons has been incorporated in a dissipative KdV equation (Nishihara et al., 1982; Chanteur et al., 1983). The resulting amplification strengthens the deceleration of the pulse caused by the quadratic nonlinearity $\phi \; (\partial\phi/\partial x)$ of the evolution equation (Nishihara et al., 1982). Of course, the validity of this dissipative KdV equation relying on a fluid description of the ions progressively breaks down with the onset of the ion trapping. The growth of the potential

pulse occurs on a time scale comparable to the transit time of the ion through the pulse; thus, the closer to resonance the ions, the greater the non-adiabatic effect they suffer (which eventually traps them inside the pulse). The onset of the trapping is visible in Figures 4a and b at times 448 and 512, respectively. The transfer of momentum to these ions enhances the slowing down of the pulse, which in turn makes the trapping more efficient as the pulse velocity moves toward the central part of the ion distribution, as shown in Figures 4a and b where the pulse velocity is indicated at each time by a heavy horizontal line. The trapping is completed when the pulse velocity comes to zero, at times around 600 in both simulations; yet, the trapped ions are not phase-mixed inside the pulse, and the highly asymmetric trapped population is responsible for the backward acceleration of the pulse with the subsequent detrapping of the ions. The burst of ions accelerated up to C_s is formed during this process (Fig. 4b) in the downstream region. Such bursts up to 2 C_s are commonly observed in Vlasov simulations started with random initial conditions (Chanteur, 1986). In a two-dimensional system, the trapping acts differently since the ions can enter sideways the potential well, which leads to a trapped population much more symmetric than in one dimension. Barnes et al. (1985) actually observed in two-dimensional simulations that the pulse does not move backward after it has stopped. We can thus conclude that the observed boomerang motion of the structure is an artifact of one-dimensionality.

Except for this rather secondary point, one- and two-dimensional simulations agree on the basic process responsible for the formation of weak double layers driven by the ion-acoustic instability. This process recently received an experimental confirmation in the laboratory experiment done by Sekar and Saxena (1985).

III. AROUND THE MARGINAL STABILITY

It has been suggested in Chanteur (1986) and Pecseli (1984) that the formation mechanism discussed at length in Section II can work with electron drift velocities unable to destabilize the ion-acoustic mode. A series of Vlasov simulations have been done to check that point. More generally, we have studied both subthermal and superthermal drift cases, but always near or below the marginal stability of the plasma. The marginal stability condition referred to is the classical one computed for an infinitesimal harmonic perturbation of the plasma and thus, strictly speaking, is not of concern for the initial condition used to start the simulations. Nevertheless, it indicates that the thermal noise, absent in the Vlasov simulation, would be marginally stable. We chose the same initial condition previously used in Chanteur et al. (1983) and Chanteur (1984) and reported to in the preceding section, i.e., a 10 percent density dip on both species. The drift motion of the electrons relative to the ions rapidly creates a potential trough, the depth of which strongly depends on the drift velocity V_d and on the initial amplitude of the density dip. It is worth noticing that the weak double layers triggered by initial density dips almost vanish when the initial amplitude of these dips is reduced to 1 percent. Thus, under marginally stable conditions, the formation mechanism of weak double layers needs a rather strong initial depression of the plasma density to be effective. In this respect, the linear instability helps a lot in the unstable case. In the present case, the initial density dip has to be produced by other means. The length of the system has been chosen equal to 1024 λ_D and 2048 λ_D in some cases to prevent an early influence of the periodic boundary conditions in the circulating electrons. As said in the introduction, we only present a small sample of our simulation results. A full account of these results will be given in the paper by Verga et al. (1986), presently under preparation. The physical parameters of the five selected runs are listed in Table 1. Figures 5 to 8 illustrate runs 1 to 4, respectively, each figure being composed of an upper panel for the electric potential (averaged over two plasma periods) in unit T_e/e, and of a lower panel for the electron phase space. The results are conveniently organized with respect to the ion-to-electron temperature ratio.

TABLE 1. PHYSICAL PARAMETERS OF THE SELECTED RUNS

Run Number	T_i/T_e	V_c/V_{th}	V_d/V_{th}	Linearly Stable?	System Length (λ_D)
1	0.30	0.55	0.50	yes	1024
2	0.30	0.55	0.60	no	1024
3	0.50	0.88	0.85	yes	1024
4	1.00	1.44	1.25	yes	1024
5	1.00	1.44	1.50	no	2048

Note: The mass ratio is $m_i/me_e = 100$ for the five runs, and V_c is the critical electron drift which destabilizes the plasma.

The case of relatively cold ions ($T_i/T_e = 0.30$) is illustrated by runs 1 and 2, which are linearly stable and unstable, respectively, but both marginally, as appears from Table 1. The two upper panels in Figures 5 and 6 show that the electric potential in the vicinity of the moving density depression has the same spatial variation as the one discussed in Section II for strongly unstable cases. Only quantitative differences occur; the amplitude of the negative pulse and the difference of potential between the downstream (on the right of the figures) and upstream sides which were of the order of one in the Section II cases are now reduced to 0.05 for run 1 and 0.10 for run 2. It is worth noticing that the linear instability, although weak, helps building a difference of potential which is twice the one of the stable case. The electron phase spaces drawn with the same contour levels (lower panels in Figs. 5 and 6) show the same enhancement of the structure; moreover, tiny electron holes are formed downstream of the double layer in run 2. These electron holes can be associated one to one with the small positive pulses seen on the high potential side (Fig. 6, upper part). Run 3 for $T_i/T_e = 0.50$ differs from run 1 by the formation of electron holes, which are even deeper than in run 2, as shown by the phase space (Fig. 7, lower part) and the associated pulses of potential, also more pronounced than in case 2. The potential trough and jump have values twice those of the corresponding values in run 1. Going on to higher ion temperature with $T_i/T_e = 1$, a superthermal drift velocity is now required to get the marginal stability of the plasma, and differences with the colder ion cases can be seen both on the potential and in the electron phase space. First, the potential trough is not as sharp as in the previous cases. Second, the difference of potential, although greater than previously, is much less steep, apart from the large pulses associated with very deep electron holes. Correspondingly, the acceleration region of the electrons in the vicinity of the potential well (see Fig. 8, lower part) is not as well defined as in the cold ion case. To briefly summarize the observations, we can say that, except for very weak drift velocities, electron holes moving at velocities close to 0.5 V_{th} are recurrently formed in the density depression which moves subsonically. The region of high potential extends between the density depression and the leading electron hole.

Run 5 differs from run 4 by the initial condition, which is now made of two identical density depressions separated by 512 λ_D. Snapshots of the averaged potential presented in Figure 9 show that the two structures evolve independently, as long as they are disconnected, yet a blowup of the potential occurs when the two depleted regions join together. This behavior has not yet been investigated in detail and needs to be confirmed for other sets of parameters.

IV. CONCLUSION

The physics of the formation of weak double layers by current interruption seems now to be satisfactorily understood after a few years of both theoretical and numerical work. We have presented the first evidence of weak double layer formation in stable conditions: they share conditions, except for those associated to the ion dynamics. Their weakness explains why they have almost no effect in the ion phase space. An interesting point associated with these structures is the recurrent formation of electron holes; we believe that it deserves further work, as well as the blowup of the field observed during the coalescence of two depleted regions.

REFERENCES

Barnes, C., M. K. Hudson, and W. Lotko, *Phys. Fluids, 28,* 1055 (1985).

Berman, R. H., D. J. Tretault, and T. H. Dupree, *Phys. Fluids, 28,* 155 (1985).

Borovsky, J. E., in *Second Symposium on Plasma Double Layers,* edited by R. Schrittwieser and G. Eder, University of Innsbruck, p. 33, 1984.

Chanteur, G., in *Computer Simulation of Space Plasmas,* edited by H. Matsumoto and T. Sato, Terra Scientific Publ Co., p. 279, 1984.

Chanteur, G., in *Proceedings of the International Conference on Comparative Study of Magnetospheric Systems,* Cepadues Editions, Toulouse, to appear, 1986.

Chanteur, G., J. C. Adam, R. Pellat, and A. S. Volokhitin, *Phys. Fluids, 26,* 1584 (1983).

DeGroot, J. S., C. Barnes, A. E. Walstead, and O. Buneman, *Phys. Rev. Lett., 38,* 1283 (1977).

Dupree, T. H., *Phys. Fluids, 26,* 2460 (1983).

Fornberg, B., and G. B. Whitham, *Phil Trans. Roy Soc. London, A, 289,* 373 (1978).

Hasegawa, A., and T. Sato, *Phys. Fluids, 25,* 632 (1982).

Hudson, M. K., and D. Potter, in *Physics of Auroral Arc Formation,* Geophys. Monogr. Series #25 (American Geophysical Union: Washington, D.C.), p. 260 (1981).

Hultqvist, B., *Planet. Space Sci., 19,* 749 (1971).

Ishiguro, S., T. Kamimura, and T. Sato, *Phys. Fluids, 28,* 2100 (1985).

Kindel, J. M., C. Barnes, and D. W. Forslund, in *Physics of Auroral Arc Formation,* Geophys. Monogr. Series #25 (American Geophysical Union: Washington, D.C.), p. 296, 1981.

Nishihara, K., H. Sakagami, T. Taniuti, and A. Hasegawa, in *First Symposium on Plasma Double Layers,* edited by P. Michelsen and J. J. Rasmussen, p. 41, Risoe National Laboratory, Denmark, 1982.

Okuda, H., and M. Ashour-Abdalla, *Phys. Fluids, 25,* 1564 (1982).

Okutsu, E., and Y. Nakamura, *Plasma Physics, 21,* 1053 (1979).

Pécseli, H., in *Second Symposium on Plasma Double Layers,* edited by R. Schrittwieser and G. Eder, University of Innsbruck, p. 81, 1984.

Sato, T., and H. Okuda, *Phys. Rev. Lett., 44,* 740 (1980).

Sato, T., and H. Okuda, *J. Geophys. Res., 86,* 3357 (1981).

Sekar, A. N., and Y. C. Saxena, *Plasma Physics and Controlled Fusion, 27,* 181 (1985).

Serizawa Y., and T. Sato, *Geophys. Res. Lett., 11,* 595 (1984).

Singh, N., and R. W. Schunk, in *Second Symposium on Plasma Double Layers,* edited by R. Schrittwieser and G. Eder, University of Innsbruck, p. 364, 1984.

Singh, N., H. Thiemann, and R. W. Schunk, *J. Geophys. Res., 90,* 5173 (1985).

Verga, A., G. Chanteur, and R. Pellat, in preparation (1986).
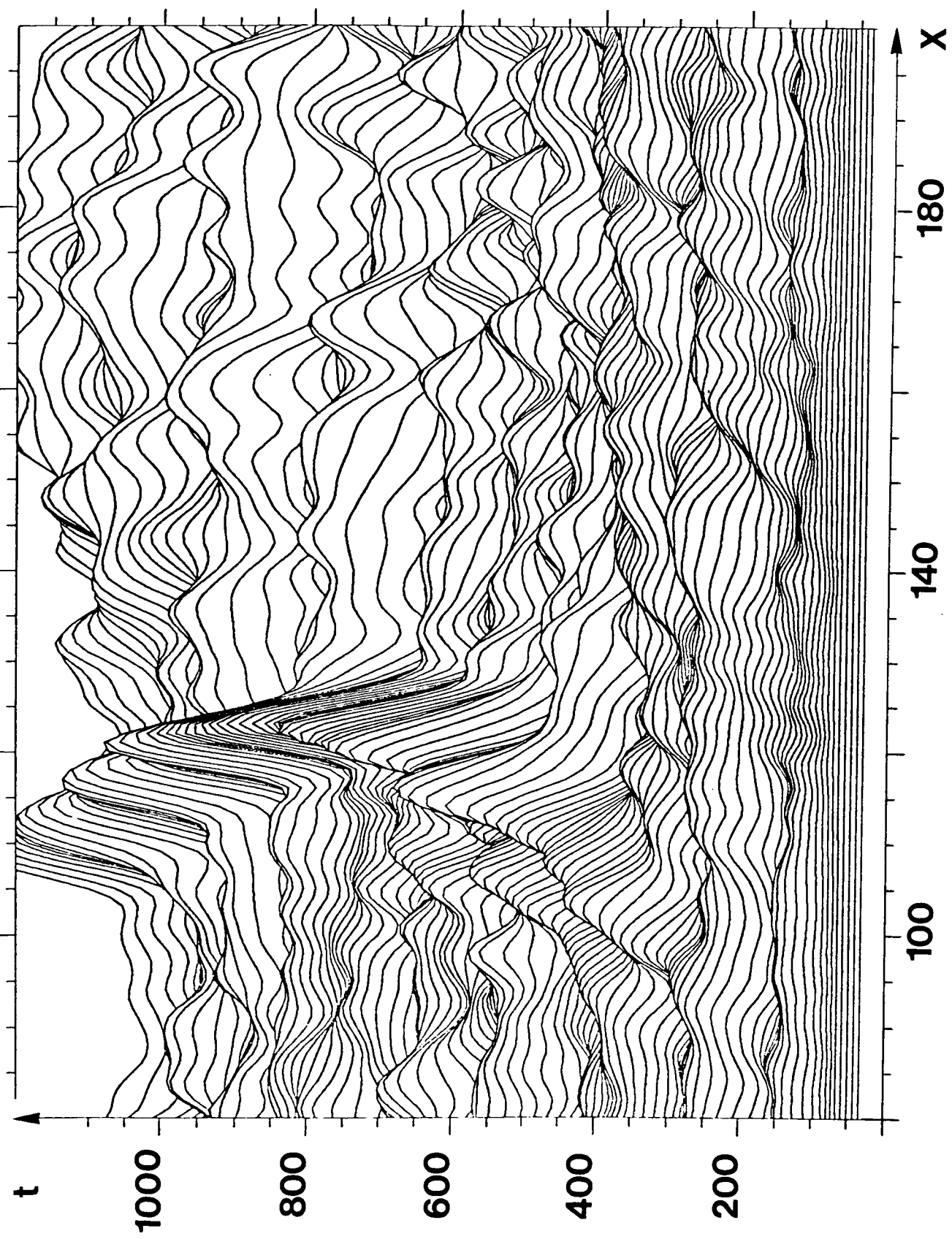
Figure 1. Potential energy of an electron versus x and t in the vicinity of the moving density dip (particle simulation).
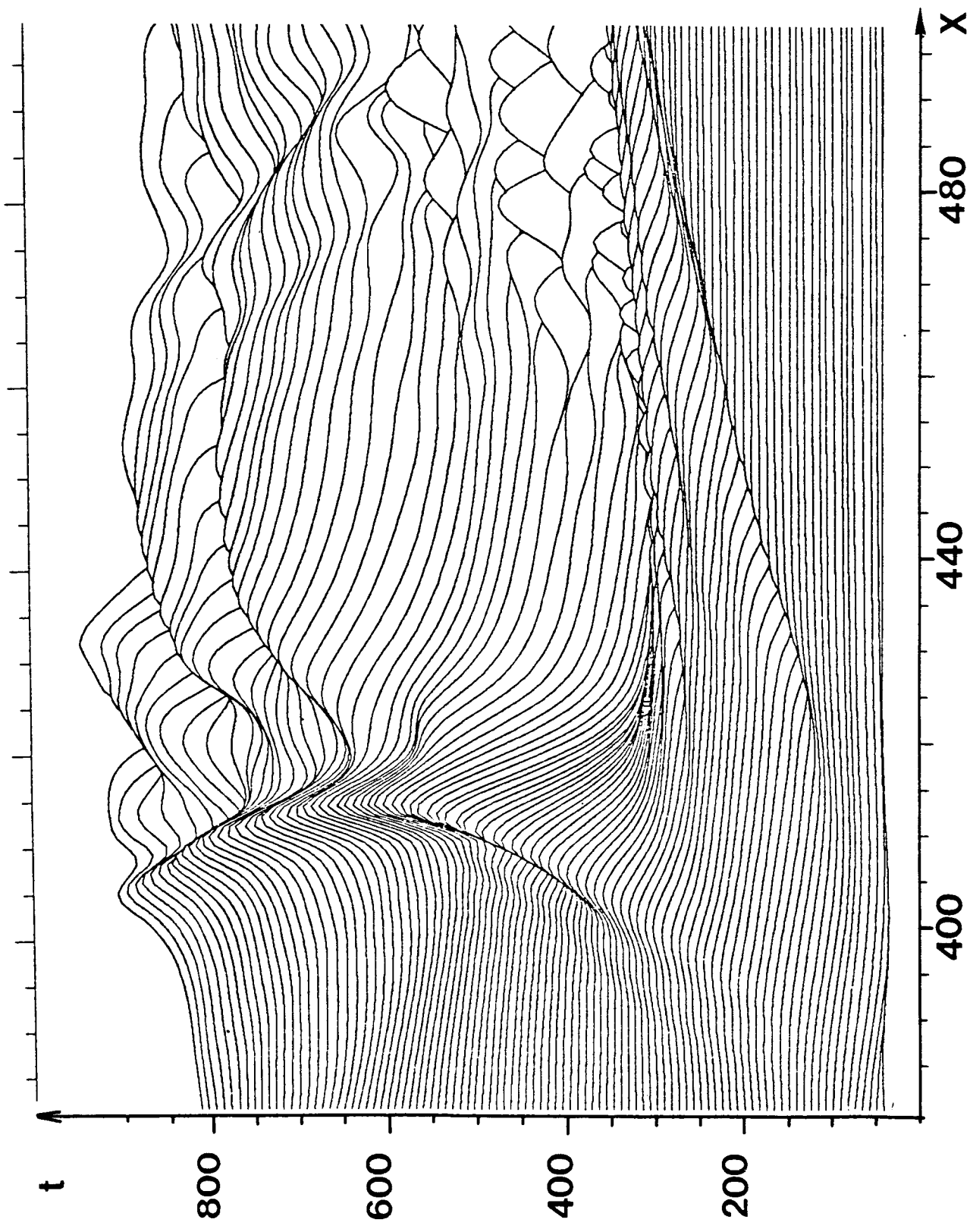
Figure 2. Same as Figure 1 but for the Vlasov simulation.

174
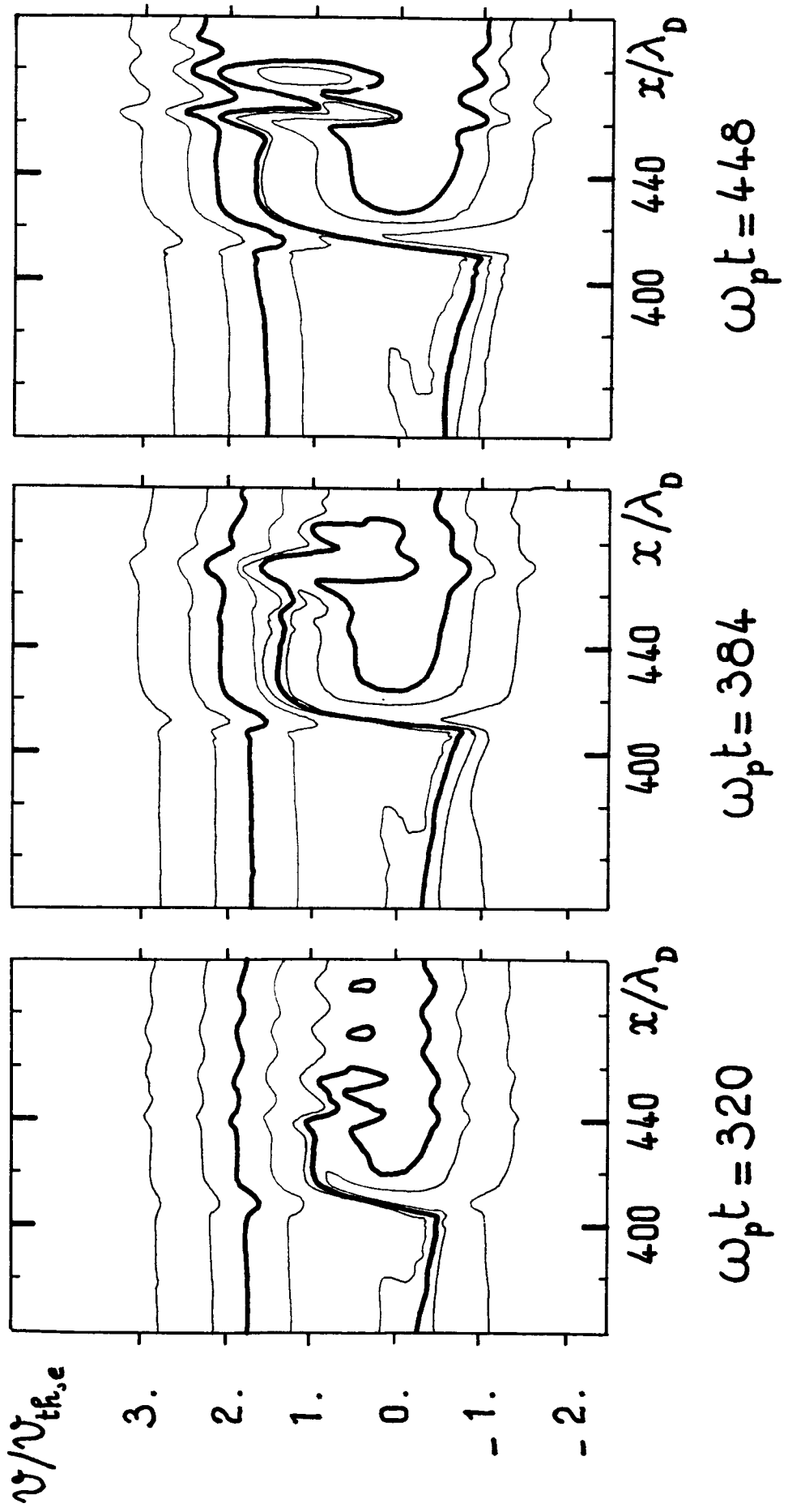
Figure 3. Electron phase space at three different times in the vicinity of the double layer at three different times (Vlasvos simulation).
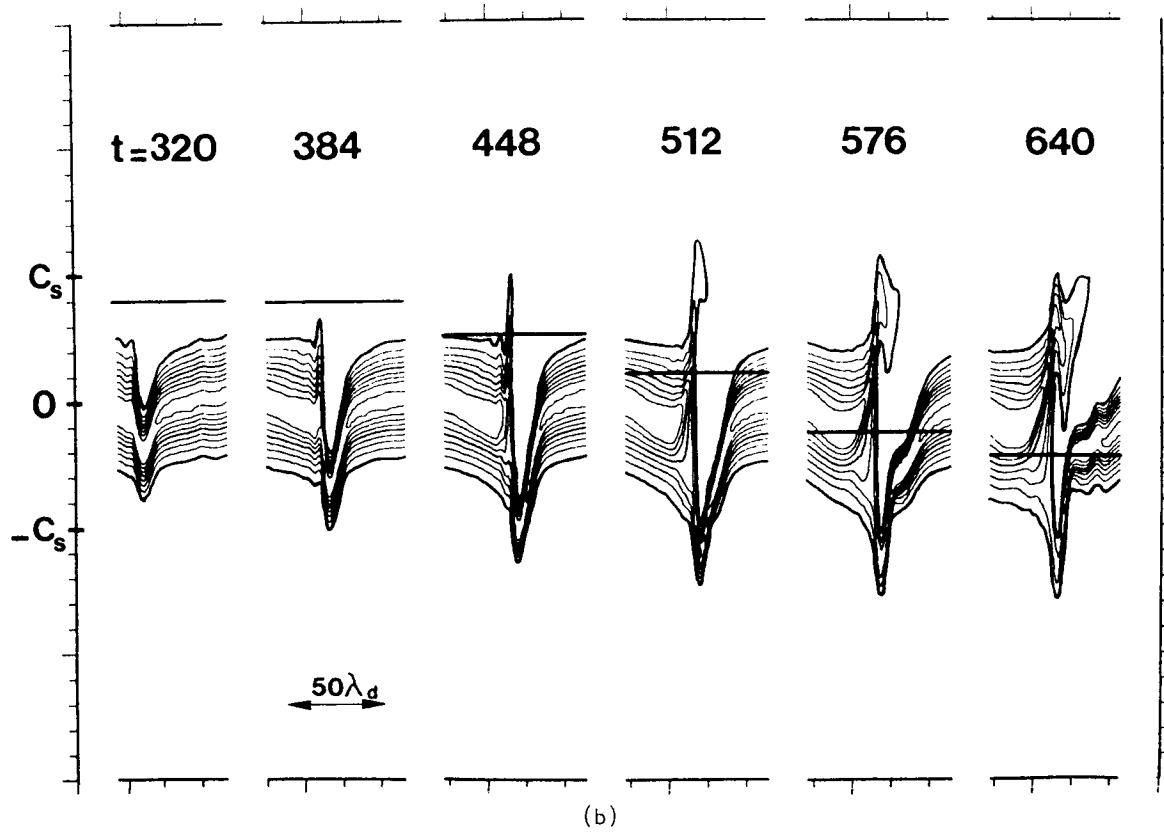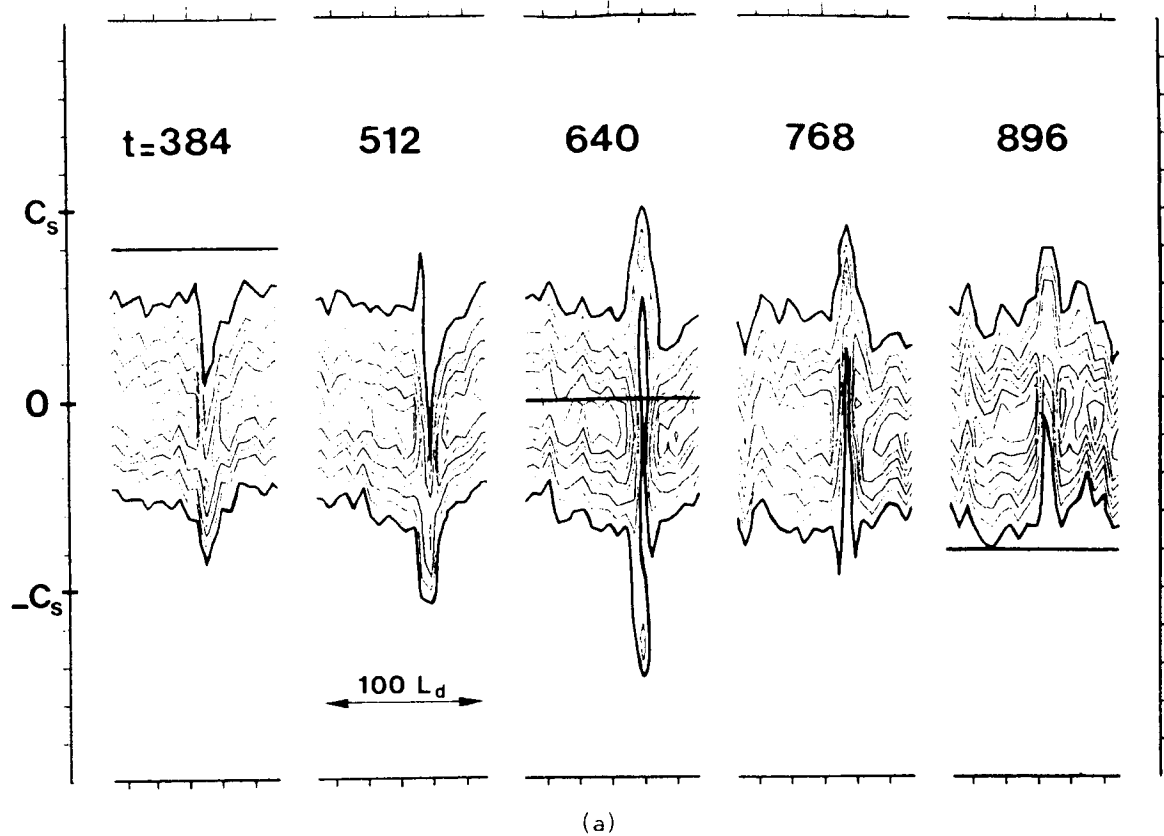
Figure 4. Ion phase spaces around the double layer at different times. (a) Particle simulation; (b) Vlasov simulation. The heavy horizontal line indictes the velocity of the localized wave.

AVERAGED POTENTIAL (over $4\pi/\omega_p$)
vd/vt=0.50   ti/te=0.30   mi/me=100.

PHI

1.00

0.75

0.50

0.25

0.00   0.0

-.25

200.   400.   600.   800.   1000.

X/Ld

DRHO = -0.10
NX   = 1024
DX   = 1.00
NT   = 2048
DT   = 0.50
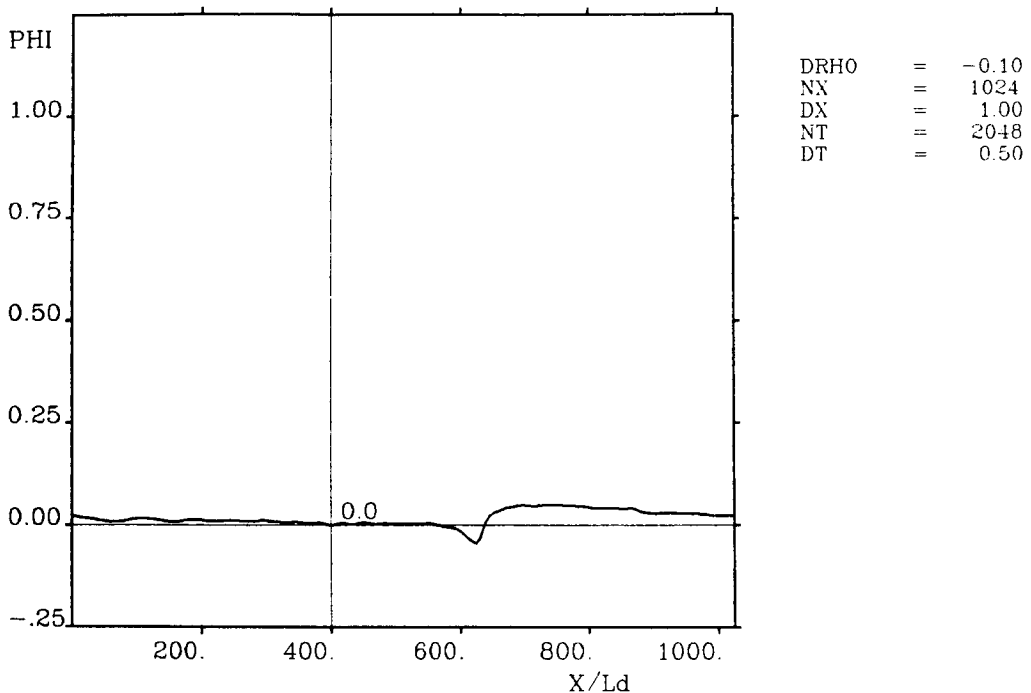
ELECTRON PHASE SPACE   vlasov code
vd/vt=0.50   ti/te=0.30   mi/me=100.

V/Vt

2.0

1.0

0.0

-1.0

-3.0

150.   300.   450.   600.   750.   900.

X/Ld

TIME 1024

DRHO = -0.10
NX   = 1024
DX   = 1.00
VMIN = -4.00
VMAX = +6.00

+0.350

+0.325

+0.300

+0.275

+0.200

+0.100

+0.010
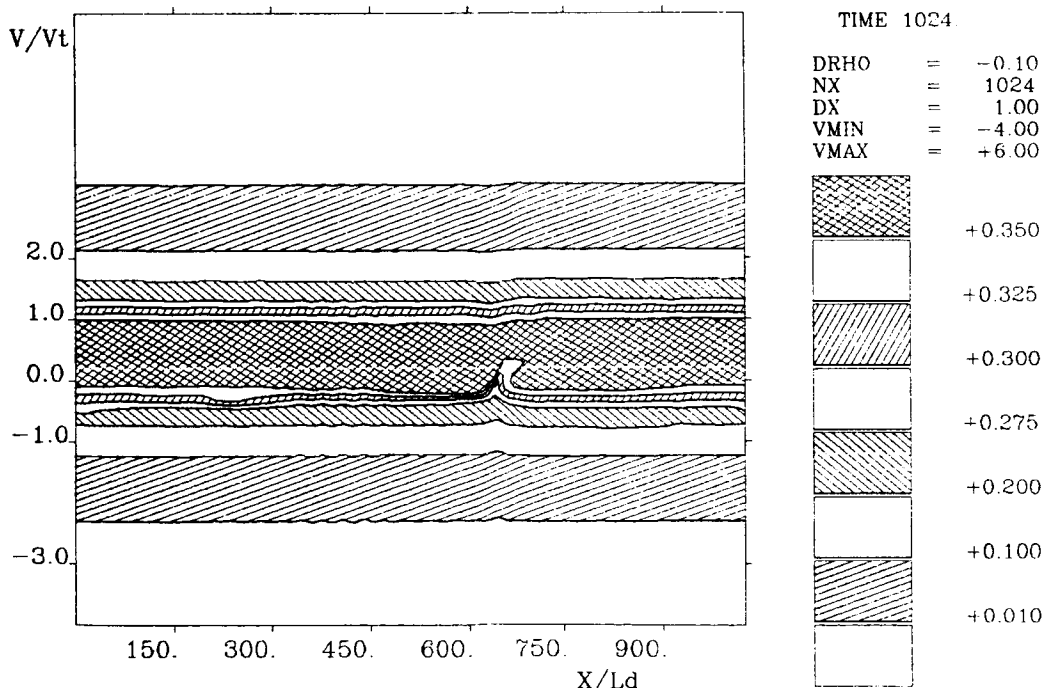
Figure 5. Upper: averaged electrostatic potential around t = 1024 for run 1 of Table 1.
Lower: corresponding electron phase space.

177

AVERAGED POTENTIAL (over $4\pi/\omega_p$)
vd/vt=0.60   ti/te=0.30   mi/me=100.

DRHO = −0.10
NX   =   1024
DX   =   1.00
NT   =   2048
DT   =   0.50
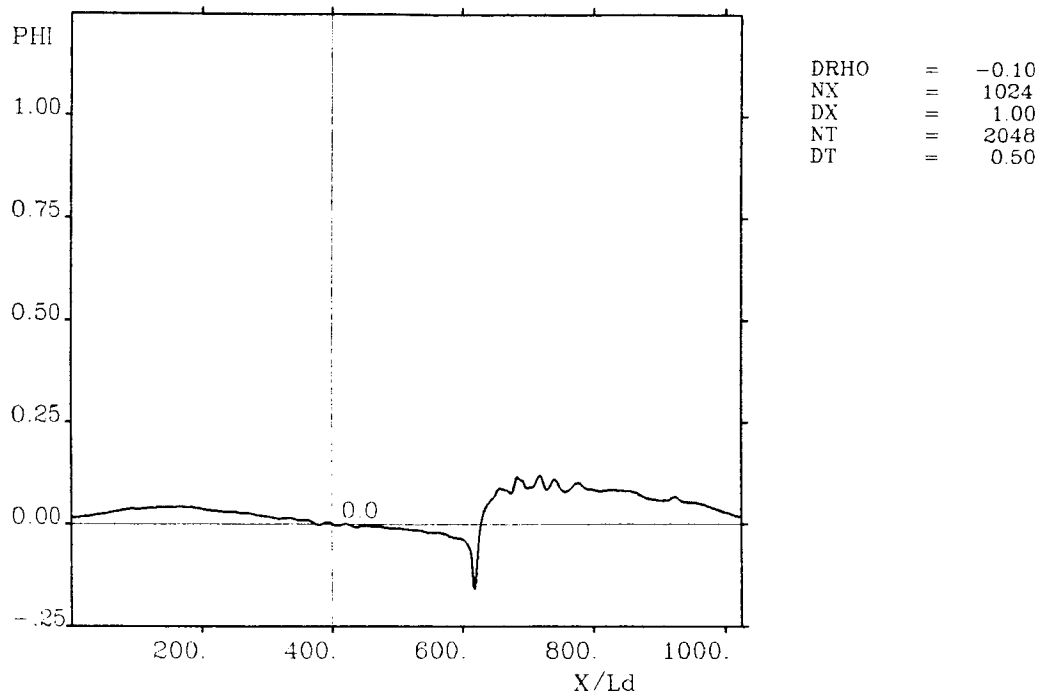
ELECTRON PHASE SPACE   vlasov code
vd/vt=0.60   ti/te=0.30   mi/me=100.

TIME 1024.

DRHO = −0.10
NX   =   1024
DX   =   1.00
VMIN = −4.00
VMAX = +6.00

+0.350
+0.325
+0.300
+0.275
+0.200
+0.100
+0.010
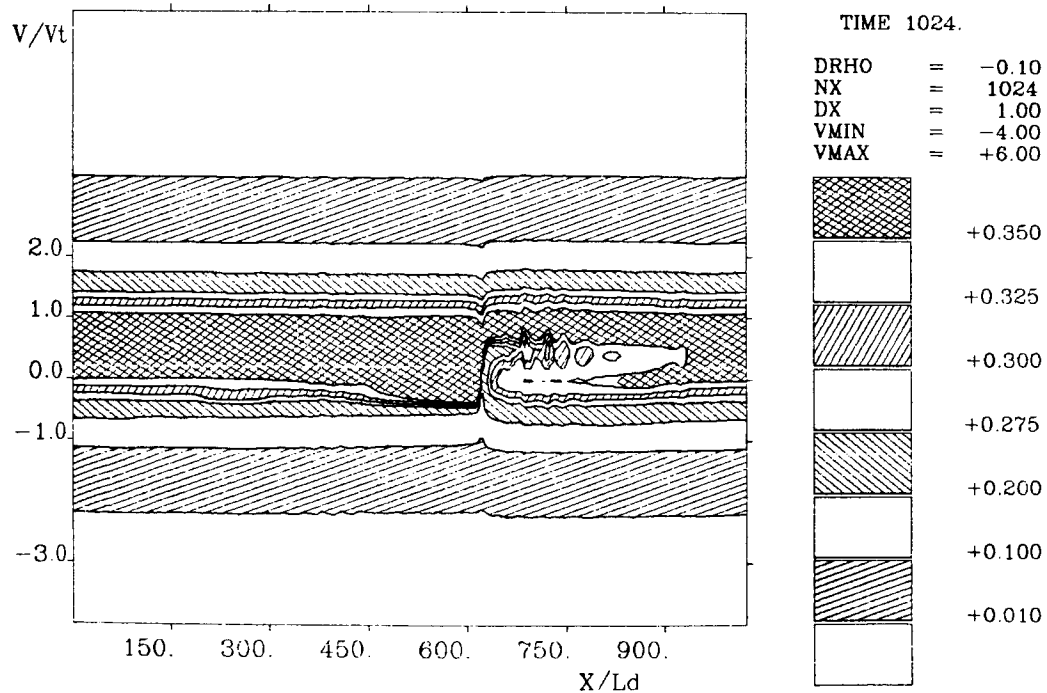
Figure 6. Same as Figure 5 for run 2.

AVERAGED POTENTIAL (over $4\pi/\omega_p$)
vd/vt=0.85   ti/te=0.50   mi/me=100.

PHI

1.00

0.75

0.50

0.25

0.00

-.25

0.0

200.   400.   600.   800.   1000.
X/Ld

DRHO	=	-0.10
NX	=	1024
DX	=	1.00
NT	=	2048
DT	=	0.50
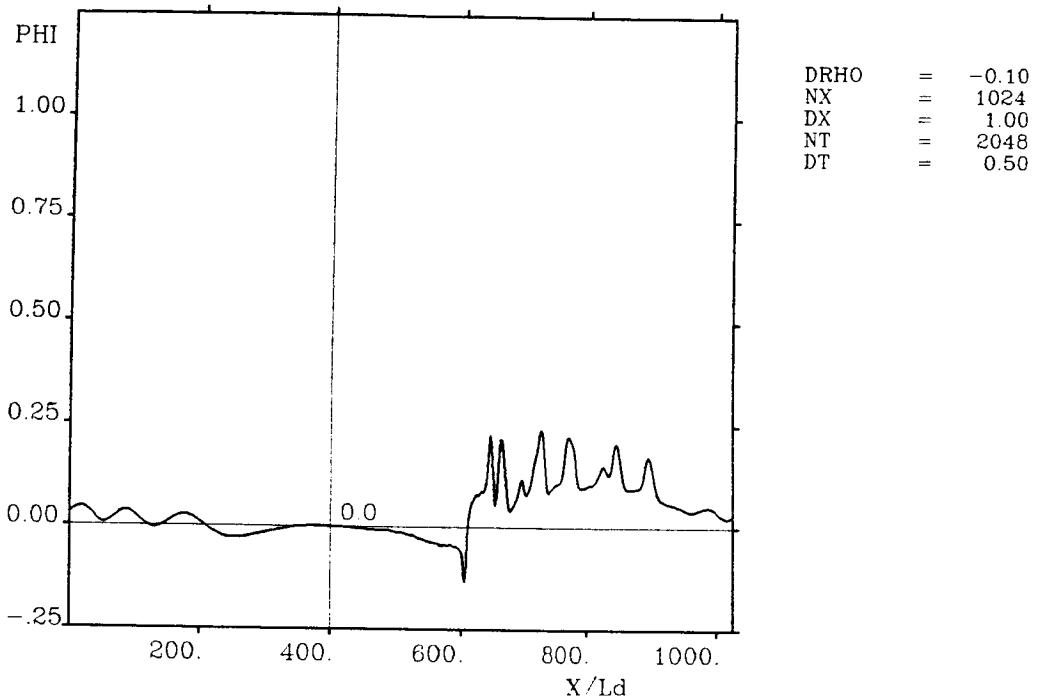
ELECTRON PHASE SPACE   vlasov code
vd/vt=0.85   ti/te=0.50   mi/me=100.

V/Vt

2.0

1.0

0.0

-1.0

-3.0

150.   300.   450.   600.   750.   900.
X/Ld

TIME 1024.

DRHO	=	-0.10
NX	=	1024
DX	=	1.00
VMIN	=	-4.00
VMAX	=	+6.00

+0.350

+0.325

+0.300

+0.275

+0.200

+0.100

+0.010
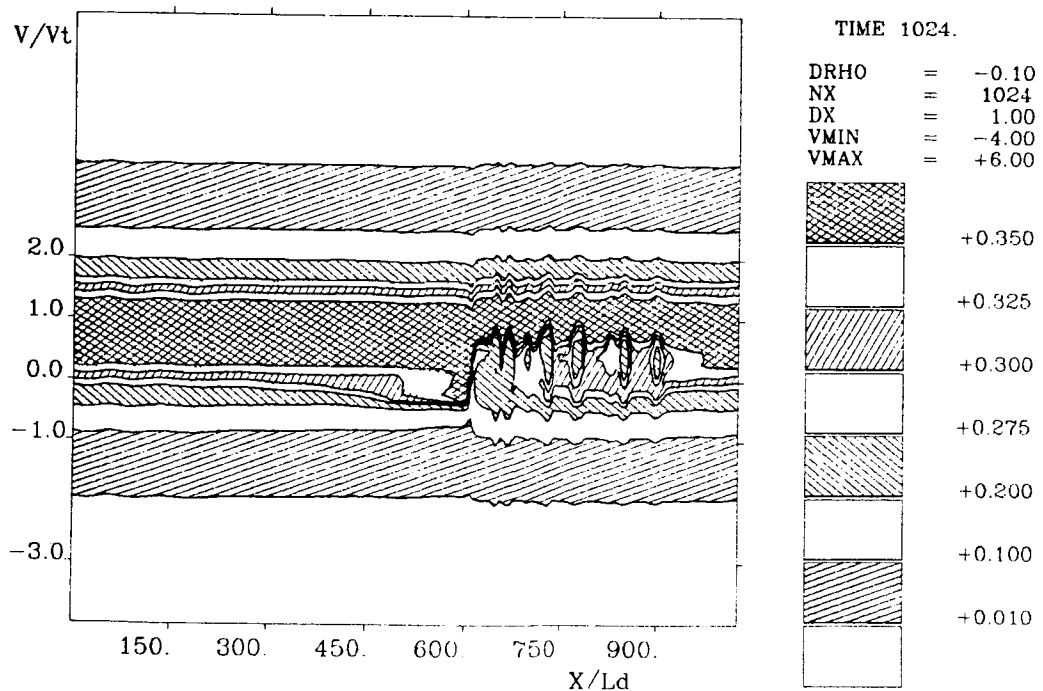
Figure 7. Same as Figure 5 for run 3.

179

AVERAGED POTENTIAL (over $4\pi/\omega_p$)
vd/vt=1.25   ti/te=1.00   mi/me=100.

PHI

DRHO   =   -0.10
NX   =   1024
DX   =   1.00
NT   =   2048
DT   =   0.50

X/Ld
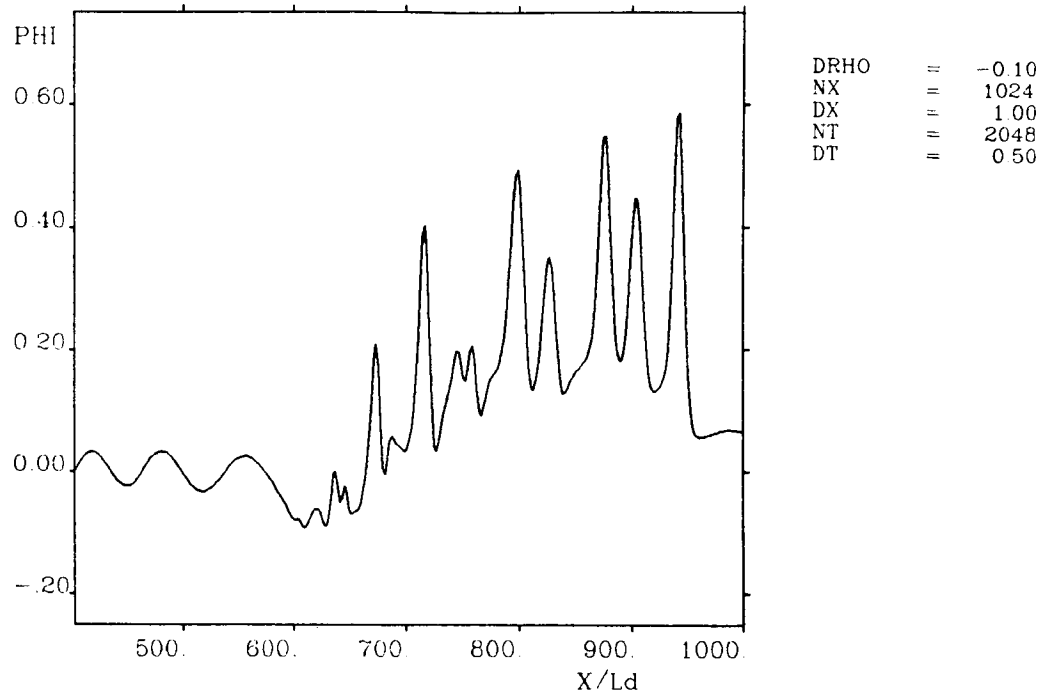
ELECTRON PHASE SPACE   vlasov code
vd/vt=1.25   ti/te=1.00   mi/me=100.

TIME 1024.

DRHO   =   -0.10
NX   =   1024
DX   =   1.00
VMIN   =   -4.00
VMAX   =   +6.00

+0.350
+0.300
+0.275
+0.250
+0.225
+0.200
+0.100

X/Ld
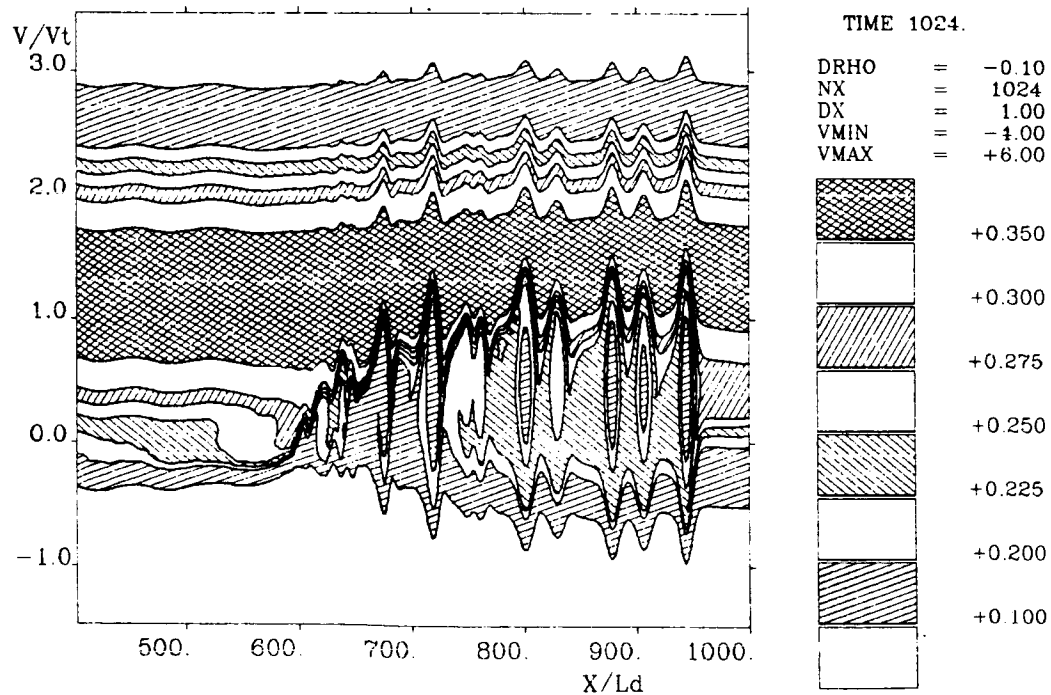
Figure 8. Same as Figure 5 for run 4.

180
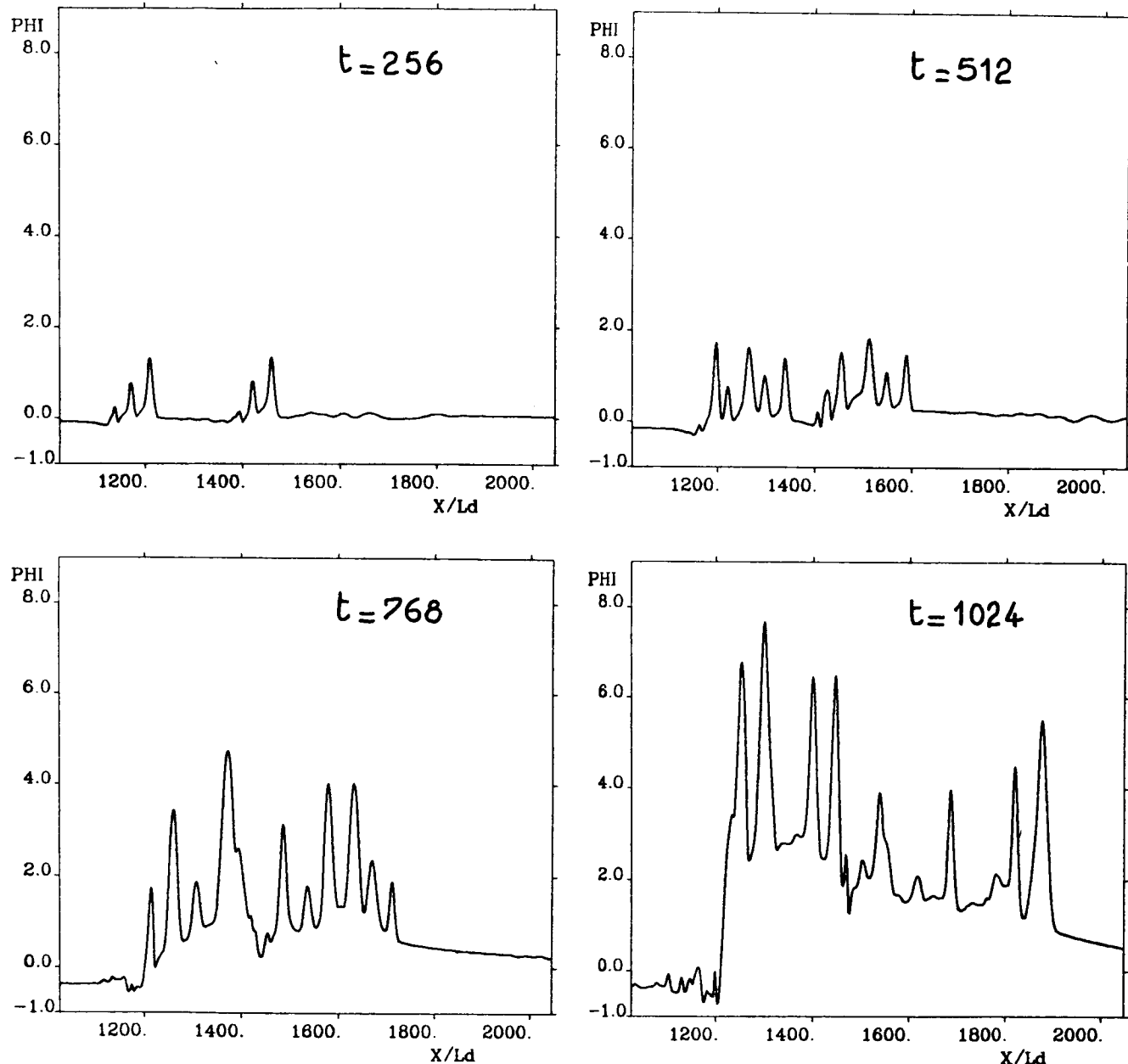
Figure 9. Averaged electric potential at times 256, 512, 768, and 1024 ω_{pe}^{-1} for run 5. Notice the blowup of the potential after time 768.

ELECTRIC FIELDS AND DOUBLE LAYERS IN PLASMAS

Nagendra Singh, H. Thiemann, and R. W. Schunk
Center for Atmospheric and Space Sciences
Utah State University
Logan, Utah 84322-3400, U.S.A.

ABSTRACT

Various mechanisms for driving double layers in plasmas are briefly described, including applied potential drops, currents, contact potentials, and plasma expansions. Some dynamical features of the double layers are discussed. These features, as seen in simulations, laboratory experiments, and theory, indicate that double layers and the currents through them undergo slow oscillations which are determined by the ion transit time across an effective length of the system in which the double layers form. It is shown that a localized potential dip forms at the low potential end of a double layer, which interrupts the electron current through it according to the Langmuir criterion, whenever the ion flux into the double is disrupted. The generation of electric fields perpendicular to the ambient magnetic field by contact potentials is also discussed. Two different situations have been considered; in one, a low-density hot plasma is sandwiched between high-density cold plasmas, while in the other a high-density current sheet permeates a low-density background plasma. Perpendicular electric fields develop near the contact surfaces. In the case of the current sheet, the creation of parallel electric fields and the formation of double layers are also discussed when the current sheet thickness is varied. Finally, the generation of electric fields (parallel to an ambient magnetic field) and double layers in an expanding plasmas is discussed.

I. INTRODUCTION

Since the early days of double layer (DL) research (e.g., Block, 1972), considerable progress has been made in the understanding of the formation of DL's and their dynamical features. The purpose of this summary is to highlight some of the major findings on the generation of electric fields in collisionless plasmas and on the formation, dynamics, and structure of double layers. We define double layers as electrostatic potential structures that can support localized electric fields in collisionless plasmas. The nomenclature "double layer" is derived from the fact that the electric field is primarily supported by two layers of charges (positive and negative). Such potential structures can form in current carrying plasmas as well as in the absence of a current.

Figure 1 shows a summary of the various mechanisms that can create double layers in a plasma. Broadly speaking, the mechanisms can be categorized as follows:

1. Applied potential drop across a plasma

2. Current through a plasma

3. Contact potentials

4. Plasma expansion.

These mechanisms are not as distinct from each other as it may appear. For example, when a potential drop is applied across a plasma, a current develops (Singh, 1980, 1982; Singh and Schunk, 1982a), or when a current is drawn through a plasma, a potential drop develops (Singh and Schunk, 1982b, 1984a). The characteristics of double layers driven by an applied potential drop and by a current through the plasma have been compared, and they have been shown to be very similar (Singh and Schunk, 1983a).

Contact potentials develop when plasmas with different properties come into contact. The difference in the ion and electron gyroradii plays an important role in creating perpendicular electric fields when the contact surfaces are parallel to the ambient magnetic field. Typically, the scale length of such electric fields is of the order of the ion Larmor radius. The potential structures associated with such electric fields appear as perpendicular or oblique double layers. When the perpendicular electric fields are shorted out at some location away from the source region, it is possible to generate two-dimensional potential structures with electric fields parallel to the ambient magnetic field. Such two-dimensional potential structures are known to play an important role in auroral electrodynamics. It is worth mentioning that the generation of a parallel potential drop by shorting out the perpendicular electric fields away from their source region is, in a sense, equivalent to applying a potential drop. Here, the perpendicular potential drop becomes a parallel potential drop due to the conducting boundary condition.

Current sheets or filaments of a finite thickness in plasmas are examples where the plasma processes driven by both the contact potential and the current take place. Multi-dimensional double layers form in such cases (Singh et al., 1983, 1984, 1985, 1986).

When a high-density plasma expands along an ambient magnetic field into a low-density plasma or into a vacuum, electric fields are set up. Near the expansion front, a double-layer type-charge separation occurs. Thus, currentless double layers form in expanding plasmas (Singh annd Schunk, 1984b).

The purpose of this paper is to present a summary of our studies on the above mechanisms for generating electric fields and double layers. These studies have been performed either with a one-dimensional Vlasov-Poisson solver (Singh, 1980) or with a two-dimensional particle-in-cell (PIC) code (Singh et al., 1983, 1985).

II. APPLIED POTENTIAL DROP

Basically, the process of DL formation is creating a potential drop. Thus, the application of a potential drop across a collisionless plasma may drive a double layer along with a host of other plasma processes (Singh and Schunk, 1982a). There are several laboratory experiments (Coakley and Hershkowitz, 1979; Iizuka et al., 1983, 1985) and numerical simulations (Joyce and Hubbard, 1978; Singh, 1980, 1982; Singh and Thiemann, 1980a,b; Singh and Schunk, 1982a,c, 1983a; Johnson, 1980) in which DL's have been driven by applied potential drops. Some of these experiments and simulations (Singh, 1982; Singh and Schunk, 1982a, 1983a) show remarkable similarities in both the processes leading to the formation of a DL and its dynamics. It is found that these processes are cyclic; the DL formation leads to current interruption, as the DL moves the currents recuperate, leading to the reformation of a new DL. In connection with several space and cosmic plasma phenomena, Alfvén (1982) has invoked the role of exploding double layers, which are cyclic. Thus, it is relevant here to discuss the cyclic behavior of double layers as seen in laboratory experiments and simulations.

Here we illustrate some important plasma processes taking place during recurring DL formation by presenting results from one-dimensional Vlasov simulations (Singh, 1982; Singh and Schunk, 1982a,c, 1983a) in which the dynamics of the plasma of length $0 \leq x \leq d$ is followed by solving the Vlasov and Poisson equations after a potential drop $\Delta \phi_0$ is applied across the plasma. In Figure 2 we present a summary of a simulation in which $d = 100$ λ_0 and $\Delta \phi_0 = 30 \, k_B T_0/e$, where λ_0 is the plasma Debye length with T_0 as the electron and ion temperature.

Applying a potential drop across a quasi-neutral plasma is equivalent to applying a uniform electric field E_0 (see the potential profile at $t = 0$ in Figure 2a), whose strength depends on the applied drop $\Delta\phi_0$ and the length of the system; $E_0 \simeq \Delta\phi_0/d$ (Fig. 2a). This field accelerates electrons and ions in opposite directions. However, during very early time ion acceleration is not important, but the electrons are accelerted to the extent that a current is set up in the plasma which may exceed the current at the cathode boundary, $x = 0$ (Fig. 2b). When this happens a positive space charge appears near the cathode ($x = 0$, in Fig. 2) modifying greatly the initial linear potential profile (Fig. 2a). This potential perturbation evolves into an electron hole in the form of a positive potential pulse which propagates in the direction of the initial electric field (Fig. 2a) and it is destroyed when it reaches the anode end. During the phase of the electron hole propagation, counterstreaming electron beams form (Singh, 1982). After this phase the plasma is subject to a strong high frequency turbulence, which modifies the plasma greatly. One important modification is the expulsion of the plasma and creation of plasma cavity. In simulations with very short lengths (Singh, 1980) ($\ell <$ 100 λ_{do}), the formation of an extended cavity is not seen. However, as the system length increases, the extended cavity becomes an important feature of the plasma (Singh, 1982; Singh and Schunk, 1982a). Also, the ion flux into the plasma from the anode boundary is totally disrupted; as a matter of fact, an outflux of ions occurs.

The potential step near the cathode evolves into a double layer (Figs. 2a, c, and d) self-consistently modifying the electron and ion velocity distribution functions. Soon after its formation, the DL develops a potential dip (potential profiles marked with "A" in Fig. 2e) at its low potential end which interrupts the electron current (bottom panel in Fig. 2e) and it moves toward the anode (compare potential profiles "A" and "B" in Fig. 2e). The moving double layer sits on an expanding plasma density front moving approximately at the ion-acoustic speed (Singh and Schunk, 1982b). The expanding plasma and the ion acceleration by the double layer produce counterstreaming ion beams near the low potential end of the DL (Singh and Schunk, 1982a). In the frame of reference of the moving double layer, the electron and ion current continuity conditions are maintained (Singh and Schunk, 1982a).

As the double layer moves, the ion flux (current) at the anode reverses from outflux to influx (Fig. 2e). As the ion current through the DL recuperates, so does the electron current approximately satisfying the Langmuir condition (Singh and Schunk, 1982c). In the presence of the ion beam and the electron current on the low potential side, any positive potential perturbation near the cathode triggers the reformation of the double layer and the above plasma processes repeat in a cyclic fashion (Fig. 2e). The time constant of this cyclic process is the ion transit time (τ_i) across the system or equivalently the transit time of the double layer across the system. The above cyclic phenomenon of DL formation is summarized in Figure 3. The cyclic reformation of double layers has been seen in simulations with applied potential drops reported by other authors (Joyce and Hubbard, 1978; Borovsky and Joyce, 1983).

Some of the cyclic processes seen in the simulations have also been seen in laboratory experiments (Iizuka et al., 1983, 1985). These experiments were carried out in a Q machine with both single- and double-ended operations. In the single-ended operation only the cathode plasma source was operative. On the other hand, in the double-ended operation both the cathode and anode plasma sources were operative. Iizuka et al. (1983) clearly show that in both types of operations, cyclic behaviors were seen, but there were some differences between them as discussed below. With the single-ended operation, the double layer formed near the cathode and subsequently moved toward the anode and disappeared there, and with the applied potential drop persisting, a new double layer formed near the cathode and moved away from it. Thus, the double layer appears to show a forward (toward anode) and backward motion. However, the backward motion (toward cathode) was found to be so fast that the details of the plasma processes during this phase could not be resolved in the experiments. From our simulations we find that the time scale of the rise in the potential at the low potential end of the double layer, which eventually leads to the formation of a new double layer (Fig. 2f), is roughly $\tau_r < 100\ \omega_{po}^{-1}$. For the plasma densities ($\sim 10^8\ cm^{-3}$) in the experiment, $\tau_r \simeq 0.1\ \mu s$ which is much smaller than the temporal resolution of about 1 μs in the experiments.

C - 3

In double-ended operations, Iizuka et al. did not see the motion of the whole double layer; instead, a back and forth motion of the low potential end of the double layer was seen. In agreement with the single-ended operation, the backward motion was found to be so fast that it could not be resolved in the experiment while the forward motion was slow. These motions were correlated with the oscillation in the current at a frequency determined by the transit time of the low potential end during its forward motion. Such features of double layers seen in the Q machine with the double-ended operations are common in simulations with very short system lengths (Singh, 1980; Singh and Thiemann, 1980a).

The cyclic behavior seen in the simulations and laboratory experiments driven by applied potential drops has also been seen in simulations (Singh and Schunk, 1982b, 1983a, 1984a) and experiments (Leung et al., 1980) in which double layers were driven by current injections.

It is important to assert here that the cyclic behavior seen in the simulations and experiments do not appear to be an artifact of the boundary conditions. The primary cause of the cyclic behavior appears to be the fundamentally different time scales associated with the electron and ion dynamics. The plasma processes which lead to the double layer formation interrupt the ion flux into the double layer. Due to the lack of the ion flux, the double layer moves and also the current through it disrupts according to the Langmuir condition (Singh and Schunk, 1982c). When the ion flux recuperates slowly, so does the electron current. Some plasma fluctuations on the low potential side, after the current recovery, start the process of double layer reformation. In the simulations, the fluctuations are found to be growing electron holes, which appear to be caused by the rarefaction instability (Carlqvist, 1972; Block, 1972; Singh, 1982).

The cyclic oscillations discussed above appear to be in accord with the theoretical work of Silevitch (1981), who showed that in an unbounded plasma, strong double layers have a negative dynamic resistance. Thus, only when the system (circuit), of which the double layer is a part, is sufficiently "lossy," it is possible to create a steady double layer. Otherwise, the double layer oscillates with a frequency determined by an effective ion transit time (Silevitch, 1981).

It is worthwhile to mention that Smith (this proceedings) draws quite different conclusions from those drawn here regarding the cyclic behavior of double layers as seen in simulations and experiments. His discussion on the experimental results with the double-ended operation of the Q machine and the comparison of the results from experiments (Iizuka et al., 1983) with those from simulations (Singh and Schunk, 1982a,c) are misleading.

The cyclic behaviors of the double layer and the current through it, as discussed here, may be relevant to some space and cosmic plasma phenomena such as magnetic storms, solar flashes, and solar flares, which are found to be repetitive (Alfvén, 1982). It has been suggested that these phenomena may be caused by exploding double layers (Alfvén, 1982) which are caused by the inductive effects in the current systems in the plasma. When the double layer forms, the current interrupts. The decreasing current may induce large voltages which add to the double layers. The repetitive feature appears because of the subsequent current recovery. The time scale (τ_c) of such recovery may be determined by the circuit properties. If $\tau_c \ll \tau_i$, the current recovery through a DL is dictated by the time scale of the ion transit time. Otherwise ($\tau_c \gg \tau_i$), the repetition time is determined by τ_c. For a given space or cosmic situation it is possible to make rough estimates of τ_i (Singh and Schunk, 1982c), but it is difficult to estimate τ_c because of the distributed nature of the circuit properties associated with the currents.

As an illustrative example, let us consider the auroral circuit. If we assume that circuit length parallel to the geomagnetic field is $\ell_\parallel \simeq R_e$, the Earth radius, the transit time of an ionospheric hydrogen ion with thermal energy $\sim$ 1 eV is $\tau_i \simeq 500$ s. For an auroral circuit, Alfvén (1982) estimated the inductance $L \simeq 30$ H. Assuming the resistance in the circuit to be $R \simeq 0.1$ ohm, $\tau_c = 300$ s. However, we note that these numbers are highly tentative. It is not even certain that for the auroral double layer, which exists in extended auroral cavity, the transit times across or along the field lines are relevant (Singh and Schunk, 1982c).

III. CURRENT INJECTION

The above cyclic process leading to double layer reformation has been seen in laboratory experiments (Leung et al., 1980) and simulations (Singh and Schunk, 1982b, 1984a) when electron current is injected into the plasma. However, there are some important differences in the formation processes of the double layers driven by current injection or applied potential drop. In the former case when the electron drift velocity is sufficiently large the Buneman instability leads to the double layer formation. In the early stage of the Buneman mode relatively small scale waves grow (see early time ($\bar{t} < 1920$) plots Fig. 4a). During the nonlinear stage of the instability the small scale oscillations transform into long wavelength ones ($1920 < \bar{t} < 2000$; Fig. 4a). Further evolution of the waves leads to formation of solitary pulses ($t \gtrsim 2000$; Fig. 4a). The double layers evolve from these pulses by self-consistent modification of the electron and ion distributions.

IV. DOUBLE LAYER STRUCTURE

During their temporal evolution, double layers undergo considerable modification in their potential distribution which critically depends on the current through the double layers. In this section we illustrate this through an example in which the plasma was driven by a current as discussed in Section III. However, it is important to note that the features discussed here are quite general. Figure 4b shows the temporal evolution of the double layer potential profile after the initial evolution shown in Figure 4a. The corresponding temporal evolutions of the average electron drift ($\bar{V}_{de}$), electron thermal velocity ($\bar{V}_{te}$), electron current ($\bar{J}_e$), and electron temperature ($\bar{T}_e$), all quantities being on the low potential side ($\bar{x} = 50$), are given in Figure 4c. At early time ($\bar{t} < 2340$), when the current density is large ($|\bar{J}_e| > 1.5$), multiple double layer formations with typical double layer dimension $\ell_{DL} \simeq 20 \, \lambda_{do}$ are seen. On the other hand, when the current interrupts suddenly at $\bar{t} = 2345$, the double layer develops a localized potential dip at its low potential side. At such times $\bar{V}_{de} < \bar{V}_{te}$. The sudden electron current interruption is seen to be accompanied by a disruption in the ion influx caused by the strong solitary pulse at $\bar{t} = 2345$. Figure 4d shows the structure of the double layers with a dip by plotting the electron and ion density profiles along with the potential profile. Considering the charge separation (Fig. 4d) we note that the potential distribution is a triple layer. However, its predominant nature, as determined by the large electric field, is still of double layer type. The dip plays the role of a current interruptor to adjust the electron current in accordance with the ion influx so that the Langmuir condition is met.

The formation of a dip at the low potential end of a weak ion-acoustic (IA) double layer has been known since its first observation in numerical simulations (Sato and Okuda, 1981). The interesting fact to note is that the formation of an IA double layer itself depends on such dips (Hasegawa and Sato, 1982). On the other hand, we have shown here that in the case of an already existing double, whether weak or strong (Singh et al., 1985), the current interruptions lead to the formation of such dips.

V. DOUBLE LAYER SCALE LENGTHS

Several simulations and laboratory experiments have indicated that for strong double layers the scale length L is given by (Joyce and Hubbard, 1978, Singh, 1980),

$$L \simeq 6 \; (e\Delta\phi_{DL}/k_B T_o)^{1/2} \quad . \tag{1}$$

This scaling has been empirically derived from simulations based on applied potential drops. We find that when double layers evolve from waves or wavelets, such as the electron holes (Fig. 4b), the double layer scale length is typically of the order of the scale length of the perturbations from which the DL evolves.

VI. CONTACT BETWEEN DIFFERENT PLASMAS

The existence of contact potentials (electric fields) near the contact surface between two materials having different electrical properties is a well-known phenomenon. In plasmas, the existence of such potentials has been investigated in connection with plasma confinement (e.g., see Sestero, 1964). In space plasmas, the studies related to the structure of the magnetopause indicate that this is a region where contact potentials can develop (e.g., see Whipple et al., 1984 and references therein). Several years ago, Hultqvist (1971) suggested that the contact between the hot plasma in the plasma sheet and the cold ionospheric plasma may create magnetic field-aligned (parallel) electric fields which could account for the observed precipitating energetic ions along the auroral field lines. More recently, Barakat and Schunk (1984) suggested that the contact between the cold polar wind electrons and the hot polar rain electrons may create parallel electric fields.

It is now clear that electric fields perpendicular to the geomagnetic field are an important feature of the auroral plasma. However, the mechanisms for creating such fields have not been well established. It is possible that they are supported by discontinuities in the plasma properties (such as particle temperatures and densities) across magnetic field lines. Such discontinuities, in which the normals to the plane of the discontinuities are perpendicular to the magnetic field lines, are known as tangential discontinuities.

Even though the existence of perpendicular electric fields in the auroral plasma is well established, the nature of the plasma discontinuities (associated with the fields), if they exist, remains virtually unexplored. Recently, however, Evans et al. (1986) have presented observational evidence that tangential discontinuities do occur in association with discrete auroral arcs. They also conducted one-dimensional steady-state calculations on the generation of perpendicular electric fields through the contact of a high-density hot plasma with a low-density relatively cold plasma. They obtained electric fields having scale lengths of both the electron and ion Larmor radii. This is expected because in their model the electrons were not highly magnetized; they used $\Omega_e/\omega_{pe} < 1/3$, where Ω_e and ω_{pe} are the electron-cyclotron and electron-plasma frequencies, respectively. However, in the auroral plasma, where the large perpendicular electric fields have been observed, typically $\Omega_e >> \omega_{pe}$, implying highly magnetized electrons.

Motivated by the observations of large perpendicular electric fields in the auroral plasma, we have pursued two different approaches for creating perpendicular fields by contact potentials as follows:

1. When a low-density containing sufficiently hot ions is sandwiched by high-density cold plasmas, it is possible to generate electric fields having strengths comparable to those observed in the auroral plasma. In such a situation the electric fields occur near the edges of a cavity in the plasma density as it is sometimes the case in the auroral plasma (Mozer and Temerin, 1983).

2. Upward field-aligned currents are a well-known phenomenon in the auroral plasma. These currents can occur in the form of thin sheets or filaments. We study such a situation by driving currents through a background plasma. The currents flow in sheets of finite thicknesses. The contact between the plasmas inside and outside the sheet produces perpendicular electric fields.

By means of numerical simulations, we have studied the above mechanisms for the generation of perpendicular electric fields. We briefly summarize our studies in the following two subsections.

A. Perpendicular Electric Fields Near the Contact Surface Between Hot and Cold Plasmas

Figure 5 shows the geometrical scheme of our simulations. Using a standard particle-in-cell code (Morse, 1970), we simulate a two-dimensional plasma of size $L_x \times L_y$. The magnetic field $\mathbf{B}$ is along the y-axis. It is assumed that all field quantities and plasma properties are invariant along the z-axis. In order to study the generation of the perpendicular electric fields, the plasma is stratified along the x-axis. The simulation plasma is divided into regions I, II, and III, which are initially (time t = 0) filled with plasmas with different properties. For this study, the plasmas are as follows. In region I, $n_{i1} = n_{e1} = n_o$, where n denotes density and subscripts e, i, and 1 refer to electrons, ions, and region I, respectively; the electron temperature $T_{e1} = T_0$ and the ion temperature T_{i1} is varied in the different simulations. In regions II and III, the plasma properties are the same: $n_{i2} = n_{e2} = n_{i3} = n_{e3}$ and $T_{i2} = T_{e2} = T_{i3} = T_{e3} = T_c$. The temporal evolution of the plasmas for t > 0 is followed by calculating the particle dynamics with the self-consistent electric fields.

In our simulations we use the electrostatic approximation. Thus, the electric fields are calculated by solving the Poissson equation with the following boundary conditions: $\phi(x = -L_x/2, y) = \phi(x = L_x/2, y) = 0$. Note that these are the Dirichlet conditions on the electric potential ϕ. Along y we use a periodic boundary condition, implying $\phi(x, y = 0) = \phi(x, y = L_y)$. The electric field $\mathbf{E}$ is obtained from $\mathbf{E} = -\nabla\phi$.

In the simulations described here, we ignore the magnetic fields generated by the plasma currents, which flow near the plasma interfaces. Thus, the ambient magnetic field remains unperturbed. Such an assumption appears justified at altitudes up to a few Earth radii, where the geomagnetic field is strong and the particle pressures are much smaller than the magnetic pressure.

We use the following definitions and normalizations: density $\tilde{n} = n/n_o$; temperture $\tilde{T} = T/T_o$, where n_o and T_o are the initial (time t = 0) density and electron temperature in region I; distance $\tilde{x} = x/\lambda_{do}$; velocity $\tilde{V} = V/V_{to}$; time $\tilde{t} = t\omega_{po}$; electric potential $\tilde{\phi} = e\phi/k_B T_o$; electric field $\tilde{E} = E/E_o$; current $\tilde{J} = J/(n_o e V_{to})$, where $V_{to} = (k_B T_o/m_e)^{1/2}$, $\omega_{po} = n_o e^2/m_e \varepsilon_o$, $\lambda_{do} = V_{to}/\omega_{po}$, $E_o = k_B T_o/e\lambda_{do}$, k_B is Boltzmann's constant, and m_e is the electron mass. In the simulations we use an artificial ion mass, $m_i = 64 m_e$.

The results described in the following sections are taken from simulations in which $L_x \times L_y = 64 \times 64 \lambda_{do}^2$, $d = 32 \lambda_{do}$, $\Omega_e/\omega_{po} = 4$, where Ω_e is the electron cyclotron frequency, and where the number of electrons and ions per cell of dimension λ_{do}^2 was 4 in region I and 16 in regions II and III.

When the plasma properties change along a direction perpendicular to the magnetic field, as in Figure 5, the ions play a crucial role in creating the contact potential near the interfaces between the different plasmas. As long as the ion temperature $T_i > (m_e/m_i)^{1/2} T_e$, where T_e is the electron temperature, the ion Larmor radius $\rho_i > \rho_e$, the electron Larmor radius. Thus, ions from the neighboring plasmas penetrate the interface more effectively than do the electrons. Thus, depending on the relative densities and the ion temperatures in the neighboring plasmas, a contact potential may develop.

There are numerous possibilities for choosing the relative densities and temperatures in region I to III of Figure 5. In this study, we were primarily motivated by the observations of perpendicular electric fields near the edges of density cavities (Mozer and Temerin, 1983). Thus, we chose $\tilde{n}_2 = \tilde{n}_3 = 4$ and $\tilde{n}_1 = 1$. We assumed that the dense plasmas in regions II and III were cold and that they had the same temperature $T_c < T_o$. On the other hand, the electrons and ions in region I were assumed to be warmer than those in the other two regions. We present results on the effect of the variation of the warm ion temperature on the perpendicular electric fields that developed near the contact surfaces.

Figure 6 shows the distributions of the electric potential, the perpendicular electric field, and the plasma density as functions of $\bar{x}$ at $\bar{t} = 100$ for $T_c = 0.2\,T_o$, and $T_{i1} = 20\,T_o$. Recall that $T_{e1} = T_o$. Thus, in the low-density plasma of region I, the ions are hotter than the cold ions in regions II and III by a factor of 100. We note that the average Larmor radius of the hot ions $\rho_H \simeq 9\,\lambda_{do}$. The quantities shown in Figure 2 are time-averaged over a time interval of $\Delta\bar{t} = 50$ centered at $\bar{t} = 100$.

Figure 6a shows that a negative potential valley develops in region I ($|\bar{x}| < 16$). The large perpendicular electric fields develop near the contact surfaces, where sharp gradients occur in the density (Fig. 6b). The maximum magnitude of the electric fields is approximately $\bar{E}_\perp \simeq 0.6$ and the scale length of the electric field near each interface is about $\rho_H \simeq 9\,\lambda_{do}$.

We find that such large electric fields develop only when the ions in region I are sufficiently warm. In order to show this we carried out simulations by varying the hot ion temperature T_{i1}. For $T_{i1} = T_o$, we did not find any enhancement in $E_\perp$ near the interfaces. As the ion temperature T_{i_1} was increased, bipolar electric fields developed near the interfaces; for $T_{i1}/T_o = 5$, $E_{\perp max} \sim 0.2$. It was found that for $T_{i1}/T_o > 10$, $E_{\perp max}$ does not increase indefinitely, but for the parameters used in the simulation it is limited to about $\bar{E}_{\perp max} \lesssim 0.6$.

A noteworthy feature was found that is that the electric fields maximize just inside the low-density plasma and not at the interface (Fig. 6). This happens because the gyrating cold ions in the high-density plasmas of regions II and III partially neutralize the space charges created by the hot gyrating ions near the interfaces. In Figure 6 the magnitude of the hot ion Larmor radius ρ_H is indicated. The electric fields at the interfaces have scale lengths of the order of the Larmor radius.

The temporal evolution of the potential drop $\Delta\phi = \phi(x = 0)$ in the simulations show that at early times ($\bar{t} < 20$) the potential drop grows and afterward undergoes a slow oscillation, with time-averaged values depending on the hot ion temperature T_{i1}. It is worth mentioning that the time constant (τ_{cont}) for the development of the contact potential ($\Delta\phi$) is approximately given by

$$\tau_{cont} \sim 20\,\omega_{po}^{-1} \sim \Omega_i^{-1} \quad , \tag{2}$$

where Ω_i is the ion-cyclotron frequency ($\Omega_i \simeq eB/m_i$). By varying Ω_e/ω_{po}, we found that the above scaling of τ_{cont} with Ω_i is generally valid. Thus, the contact potential sets up with a time constant that is associated with the ion cyclotron motion.

The slow oscillations occur at the ion-plasma frequencies of the plasmas in regions I and II. Comparing the relative amplitudes of $E_\perp$ and $E_\parallel$ associated with the oscillations, we find that $E_\perp \gg E_\parallel$. Thus, these oscillations are not of the ion-acoustic type, but are associated with the lower hybrid frequencies in regions I to II.

It is important to note that the geometry of our simulations does not allow the excitation of drift modes propagating in the direction of the diamagnetic currents near the interfaces at $x = \pm d/2$. These currents flow along the z-axis. We have assumed in our simulations that all physical quantities are invariant with respect to z. Thus, no wave modes are allowed to propagate in this direction.

The contact potential develops because the hot ions in region I, while gyrating, penetrate into the neighboring plasmas of regions II and III. In order to show this, the ion velocity distribution function (F) is plotted in Figure 7 as a function of the x-component of the ion energy, $W_x = 1/2\,m_i V_x^2 = 32\,\bar{V}_x^2 k_B T_o$, at several locations for the simulation with $T_{i1}/T_o = 15$. The distribution at $x = 0$ (center of region I) clearly matches the initial Maxwellian distribution with a temperature $\bar{T}_{i1} = 15$, as shown by the asymptote marked with this temperature. On the other

hand, at $\bar{x} = 32$ (near the end of region III) the ion population is cold. At $\bar{x} = 24$, we see that the hot and cold ions have mixed together. The average ion Larmor radius for the hot ions in region I for $\bar{T}_{i1} = 15$ is $\tilde{\rho}_H \simeq 8$. Thus, we expect the penetration of a large number of hot ions from region I($|\bar{x}| < 16$) into region III up to a distance of about $\bar{x} \simeq 24$. This is verified by the distribution function at $\bar{x} = 24$. The distribution at $\bar{x} = 16$ is near the initial interface, where we see that compared to the numbers of ions in the cold and hot populations at $\bar{x} = 24$, the number of ions in the cold population has decreased, while that in the hot population has increased.

We summarize this section by noting that when a low-density plasma containing hot ions comes into contact with a high-density cold plasma with the contact surface being parallel to the magnetic field, it is possible to create perpendicular electric fields. The time constant for creating such fields is roughly Ω_i^{-1} and the scale length is approximately ρ_H, the Larmor radius of the hot ions.

The above results indicate that when the hot ion temperature $T_{i1} > 10\,T_o$, a rough estimate of the strength of the perpendicular electric field is

$$E_\perp \sim 0.5\,E_o \quad , \tag{3}$$

where the normalizing electric field E_o critically depends on n_o and T_o. When n_o varies from 1 to 10 cm^{-3} and T_o varies from 1 to 100 eV, the strength of $E_\perp$ ranges from several tens to several hundreds of mV/m. Satellite observations indicate that the electric fields associated with electrostatic shocks (Mozer et al., 1980) have a similar strength. For example, if we assume that the hot plasma in region I is of plasma sheet origin and the electron temperature $T_o = 100$ eV, then it is possible to create perpendicular electric fields of several hundreds of mV/m if the hot ion temperature $T_{i1} > 1$ keV, which is common in the plasma sheet. For $T_o = 100$ eV, the cold plasma temperature assumed in our simulations is $T_c = 20$ eV. We find that when T_c is reduced below $0.2\,T_o$, as assumed here, this does not significantly affect the electric fields. Thus, the cold plasma may originate in the ionosphere.

However, the question of how the stratification of the plasma assumed in our simulations (Fig. 5) is created in space plasmas still needs to be answered. It now appears that plasma blobs and clouds are created in the magnetotail region. When these blobs of plasma move closer to the Earth where a colder plasma exists, the stratification of the plasma assumed in our simulations may be created.

In this section we were mainly concerned with the generation of perpendicular electric fields. In the near future we will study the creation of parallel electric fields, the formation of double layers, the parallel acceleration of electrons and ions, and the generation of parallel currents that occurs when the perpendicular electric fields generated by contact potentials are shorted out by a conducting boundary. Such studies will complement our previous studies on current sheets as summarized in the next section.

B. Double Layer Structures Associated with Current Filaments or Sheets

There are evidences that the current systems in space and cosmic plasmas are filamented (e.g., see Alfvén, 1982 and references therein). Thus, there is a need to study double layer structure in filamentary currents. The available temporal and spatial resolutions for the plasma measurements in the auroral region indicate that the field-aligned currents are highly structured in the form of current sheets with north-south thicknesses of a few kilometers (Dubinin et al., 1985). Probably even thinner sheets exist but they have not been resolved.

Here we briefly summarize our recent efforts on simulations of double layers driven by current sheets (Singh et al., 1983, 1984, 1985; Thiemann et al., 1984). Figure 8 shows our simulation scheme. A two-dimensional

plasma of size $L_x \times L_y$ is driven by a magnetic field-aligned current sheet having a current density J_o. Initially the simulation region is filled with a plasma of density n_o and temperature T_o. At later times, particles are injected both at the top and lower boundaries. Electrons and ions injected at the top boundaries have temperature T_o and T_{iu} (T_H) while those at the lower boundary $T_{i\ell}$ and $T_{e\ell}$. Various simulations were performed by varying these temperatures using a standard particle-in-cell (PIC) code. The electron current is set up in the sheet by injecting electrons at the top of the current sheet at rates to produce desired current (flux) densities. These electrons were also given a downward drift V_{de}. Overall, charge neutrality of the simulation plasma was maintained by counting the number of electrons and ions and injecting an appropriate number of the deficient particles at the lower boundary. The electrostatic boundary conditions are as follows; the plane $y = 0$ is assumed to be conducting, $\phi(x, y = 0) = 0$; at the top boundary we set $E_y(x, y = L_y) = 0$ and a periodic boundary condition was used in x.

We use the following definitions: λ_{do} is the Debye length based on the temperature T_o and on the initial density of $n_o = 4$ particles per cell, Ω_e is the electron-cyclotron frequency and $\omega_{po}^2 = n_o e^2/m\varepsilon_o$, where ε_o is the permittivity of free space and m is the electron mass. The ion-electron mass ratio was chosen to be $M/m = 64$. In the analysis that follows, we use the following normalizations: distance $\bar{y} = y/\lambda_{do}$, time $\bar{t} = t\omega_{po}$, velocity $\bar{V} = V/V_{to}$, potential $\tilde{\phi} = e\phi/k_B T_o$, electric field $\bar{E} = E/E_o$, $E_o = (k_B T_o/e\lambda_{do})$, and current density $\bar{J} = J/(en_o V_{to})$, where $V_{to} = (k_B T_o/m_e)^{1/2}$. The numerical technique used here has been previously described in much greater detail by Singh et al. (1985).

Figure 9 shows an example of the potential structure as seen in a simulation in which $\ell = 12\lambda_{do}$, $\rho_H = 9\lambda_{do}$, $\rho_{i\ell} = 4\lambda_{do}$, $\Omega_e/\omega_{po} = 2$, $\bar{J}_o = 1.25$, $T_H/T_o = 5$, $T_{e\ell} = T_{i\ell} = T_o$, and $L_x \times L_y = 64 \times 128\lambda_{do}^2$, where ρ_H and $\rho_{i\ell}$ are the Larmor radii of the ions injected at the top and bottom of the simulation plasma, respectively. The potential structure is illustrated by plotting (a) equipotential surfaces, (b) contours of constant $E_\perp$, the component of the electric field perpendicular to the magnetic field, and (c) contours of constant $E_\parallel$, in x – y plane. The current sheet edges are indicated by the arrows at the bottom of each panel. The solid and broken line contours show positive and negative values of the quantities. A V-shaped potential structure is evident from panel (a); a negative potential valley develops in the upper portion of the current sheet. Panel (b) shows the occurrence of a large bipolar perpendicular electric field near the edges of the current sheet at the top of the simulation plasma. The perpendicular electric fields develop due to the contact between the high-density plasma inside the sheet with a low-density plasma around it (Kan and Akasofu, 1979; Wagner et al., 1980; Singh et al., 1983). The hot ion Larmor radius determines the perpendicular scale length of the electric fields. The V-shaped potential structure develops when the perpendicular electric fields originating near the top of the simulation plasma are shorted out by the conducting surface at y = 0, thus, creating a parallel potential drop.

Panel (c) of Figure 10 shows the localized parallel upward electric fields as indicated by the "H" inside the current sheet. These parallel fields are of double layer type. There are three double layers stacked on top of each other inside the current sheet. The existence of these double layers can also be inferred from the equipotential surfaces in Figure 9a. Typically the maximum electric field strength in the double layers is about $\bar{E} = 0.25$. The scale length of the double layers along the magnetic field is found to be about $10\lambda_{do}$ while they fill the entire width of the current sheet.

The double layers shown here are not dc, but they undergo considerable temporal variations at time scales ranging from electron to ion-plasma periods. Figure 10a shows the temporal variation in the double layer potential profile after averaging out the fast electron oscillations. Note the considerable changes in the potential profile and as well as in the magnitude of the net potential drop across the double layer. The temporal variations in $E_\parallel$ and $E_\perp$ at the point (0, 100) in the region of double layer formation, are shown in Figure 10b. Even at the times when $E_\parallel$ has a dc component, there are considerable fluctuations in both $E_\parallel$ and $E_\perp$. These fluctuations appear to have frequencies ranging from below the ion-cyclotron frequency to above the lower hybrid frequency. In addition, $E_\parallel$ is found to have high frequency oscillations up to electron-plasma frequency and its harmonic which are averaged out in Figure 10b. The high frequency oscillations are not seen in $E_\perp$.

192

In a narrow current sheet, as discusssed above in context of Figures 9 and 10, it is difficult to distinguish clearly between the double layers inside the current sheet and the large perpendicular electric fields occurring near the edges of the sheet. On the other hand, in wide sheets ($\ell \gg \rho_H$), the double layers inside the current sheets are well separated from the large $E_\perp$ occurring near the edges. Figure 11 shows an example of a potential structure associated with a current sheet of thickness $\ell = 32\,\lambda_{do}$, and $\ell/\rho_H \simeq 10$. Panel (a) shows the equipotential surfaces in the $x - y$ plane, panel (b) shows the perpendicular distributions of $E_\perp(x)$ and $\phi(x)$ at $y = 120\,\lambda_{do}$, and panel (c) shows the perpendicular distribution of $J_\parallel(x)$ at $y = 120\,\lambda_{do}$. In this simulation maximum possible value of the upward current in the sheet is $J_o \simeq 0.6\,n_o e V_{to}$. Note that only weak potentials ($\sim k_B T_o/e$) develop inside the sheet, and the regions exterior to the sheet near the top (panel a) are highly positive. The perpendicular potential profile in the sheet is quite flat (panel b). Thus, $E_\perp$ is mostly confined near the edges. In the region of large $E_\perp$ near the edges we find that $E_\perp \gg E_\parallel$, which is an important feature of the electrostatic shocks observed in the auroral plasma (Mozer et al., 1980). On the other hand, inside a wide sheet where double layers from $E_\perp \sim E_\parallel$ and both $E_\perp$ and $E_\parallel$ are considerably smaller than the perpendicular electric field near the edges. It is found that near the edges

$$E_\perp \sim E_{\perp m} \sim E_o \quad . \tag{4}$$

We note that E_o depends on n_o and T_o; when n_o varies from 1 to 10 cm^{-3} and T_o from 1 to 100 eV, E_o ranges from about 100 to 1300 mV/m. Thus, the large perpendicular electric fields occurring near the edges of the current sheets resemble the phenomenon of electrostatic shocks observed in the auroral plasma Mozer et al. (1980).

Whether or not the double layers are well separated from the large $E_\perp$ near the current sheet edges, it is found that

$$E_{\parallel DL} \ll E_o \quad . \tag{5}$$

Depending on n_o and T_o, $E_{\parallel DL}$ may range from a few mV/m to several tens of mV/m. So far only weak double layers ($E_\parallel < 15$ mV/m) have been observed in space plasmas (Temerin et al., 1982).

We find that in the case of wide sheets it is possible to develop relatively large downward parallel electric fields outside the current sheets (panel a, Fig. 11). These fields drive downward return currents (panel c).

In these simulations we have seen both parallel and perpendicular accelerations of ions (Singh et al., 1986). Most energetic ions are seen to be at pitch angles near 90°. Ion beams are seen only in narrow sheets with thicknesses $\ell \lesssim \rho_H$.

It is found that the double layers play a key role in electron acceleration, even though, all the features of the accelerated electrons cannot be explained by a simple picture of electron acceleration by dc double layers. The double layers act as a trigger mechanism for a host of plasma processes, which determines the velocity distribution function of the accelerated electrons.

VII. PLASMA EXPANSION

Plasma expansions have been studied since the pioneering work of Gurevich et al. (1966), who studied the expansion of a plasma into a vacuum using the quasi-neutrality approximation. In this case the plasma equations allow self-similar solutions. However, this approximation breaks down in the low-density region where the local plasma Debye length becomes comparable to the scale length in the density gradient. Thus, a positive-negative charge separation occurs like in a double layer (Singh and Schunk, 1984b). However, it is worth noting that there is no current through such a double layer. The charge separation is supported by a relative smooth variation in the electron density while the ion density has a sharp density jump creating an ion density front. The plasma expansion is preceded by such a density front, behind which the self-similar solutions are found to be valid.

When a high-density (n_I) plasma expands into a plasma of low density (n_{II}), the expansion properties critically depend on the density ratio $R = n_I/n_{II}$ (Mason, 1971). An example of such a dependence is shown in Figure 12, in which we have compared the potential profiles associated with expanding plasmas as the ratio R is varied from R = 0.001 to 0.2. The potential profiles shown in this figure are obtained as follows. We consider that initially (time t = 0) the high- and low-density plasmas occupy the regions I $(x \leqslant 300 \lambda_{di})$ and II, respectively. At times t > 0, the expansion is studied solving Vlasov equations for the ions in a self-consistent electric field obtained by solving the Poisson equation. The electrons are assumed to obey the Boltzmann law. In the calculations presented here we assume that the electron temperature $T_e = 10 T_i$, where T_i is the initial ion temperature in regions I and II. The potential profiles shown in Figure 12 are at $t = 60 \omega_{pi}^{-1}$, where ω_{pi} is the ion-plasma frequency in region I and $\lambda_{di} = V_{ti}/\omega_{pi}$ with V_{ti} being the ion thermal velocity. The different curves shown in Figure 12 are for different values of R as marked.

The noteworthy feature of the potential profile shown in Figure 12 is that as the density in region II is increased, the potential profiles steepen over a localized region in the expansion zone. When R is increased from 0.001 to 0.01, we note the formation of a "knee" in the potential profile near $x \sim 625 \lambda_{di}$. When R is increased further this "knee" steepens and for n = 0.1 and 0.2 we note the presence of two sharp transitions in the potential profiles; one occurs in region I in which the rarefaction wave propagates in the backward direction, and the other occurs in the expansion region II. Near the transitions localized electric fields, like that in a double layer, occur. It is important to note that the sharp transitions in the potential profiles (double layers) occurring in regions I and II move in opposite directions. With increasing time the potential profile in region I becomes less and less steep while that near the sharp transition in region II maintains its profile giving a localized electric field nearly constant with time. The features associated with occurrence of localized electric fields also occur when a multi-ion plasma expands into a vacuum (Singh and Schunk, 1983b).

VIII. CONCLUSION

We have presented a brief summary of our studies related to the generation of electric fields in plasmas. Some of the mechanisms we discussed are as follows. When a potential drop is applied across a plasma, localized electric fields in the form of double layers occur. Double layers also form when a current is drawn through a plasma. The dynamical feature of such a double layer shows a cyclic behavior with a frequency determined by the transit time of the ions across an effective length of the system, in which the double layer forms. The formation of a potential dip at the low potential end of a DL and the current interruption are intimately related phenomena.

We have also discussed the generation of electric fields perpendicular to the ambient magnetic field in a plasma. Such fields can be generated by contact potentials near discontinuities in plasma properties. It was found that ion gyration plays an important role in generating the fields. The cases presented indicate that the scale length of the perpendicular electric field is of the order of the ion Larmor radius. Two complementary situations, in which perpendicular electric fields can be generated, were discussed. In one situation, we considered a low-density hot plasma sandwiched between high-density cold plasmas. It was shown that even if the hot ion density is low these ions are effective in creating electric fields of the magnitude observed in the auroral plasma. In the other situation, we considered a current sheet in a plasma. The density gradient across the sheet created the perpendicular electric fields. The formation of double layers in the sheet were studied.

The generation of electric fields in expanding plasmas was briefly discussed. It was shown that when a high-density plasma expands into a low-density plasma, the nature of the spatial distribution of the electric field critically depends on the density ratio of the two plasmas. A currentless double layer forms near the expanding plasma front.

REFERENCES

Alfvén, H., *Cosmic Plasma*, Reidel, Dordrecht, 1982.

Barakat, A. R., and R. W. Schunk, *J. Geophys. Res., 89,* 9771 (1984).

Block, L. P., *Cosmic Electrodyn., 3,* 349 (1972).

Borovsky, J. E., and G. Joyce, *J. Geophys. Res., 88,* 3116 (1983).

Carlqvist, P., *Cosmic Electrodyn., 3,* 377 (1972).

Coakley, P., and N. Hershkowitz, *Phys. Fluids, 22,* 1171 (1979).

Dubinin, E. M., et al., *Kosm. Issled, 23,* 466 (1985).

Evans, D. S., M. Roth, and S. Lemaire, "Electrical potential distribution at the inference between plasma sheet clouds," Presented at the Workshop on Double Layers in Astrophysics, Marshall Space Flight Center, Huntsville, Alabama, March 17-19, 1986.

Gurevich, A. V., L.-V. Pariiskaya, and L. P. Pitaevskii, *Sov. Phys. JETP, Eng. Transl., 22,* 449 (1966).

Hasegawa, A., and T. Sato, *Phys. Fluids, 25,* 632 (1982).

Hultqvist, B., *Planet. Space. Sci., 19,* 749 (1971).

Iizuka, S., P. Michelsen, J. J. Rasmussen, R. Schrittwieser, R. Hatakeyama, K. Saeki, and N. Sato, *Riso Report-M-2414,* Riso National Laboratory, Denmark, 1983.

Iizuka, S., P. Michelsen, J. J. Rasmussen, R. Schrittwieser, R. Hatakeyama, K. Saeki, and N. Sato, *J. Phys. Soc. (Japan), 54,* 2516 (1985).

Johnson, L. E., *J. Plasma Phys., 23,* 433 (1980).

Joyce, G., and R. F. Hubbard, *J. Plasma Phys., 20,* 391 (1978).

Kan, J. R., and S.-I. Akasofu, *J. Geophys. Res., 84,* 507 (1979).

Leung, P., A. Y. Wang, and B. H. Quon, *Phys. Fluids, 23,* 952 (1980).

Mason, R. J., *Phys. Fluids, 14,* 1943 (1971).

Morse, R. L., in *Computational Physics,* edited by Alder, Fernbach, and Rotinberg, Vol. 9, p. 213, Academic Press, New York, 1970.

Mozer, F. S., C. D. Cattell, M. K. Hudson, R. L. Lysak, M. Temerin, and R. B. Torbert, *Space Sci. Rev., 27,* 155 (1980).

Mozer, F. S., and M. Temerin, in *High-Latitude Space Plasma Physics,* edited by B. Hultqvist and T. Hagfers, p. 43, Plenum, New York, 1983.

Sato, T., and H. Okuda, *J. Geophys. Res., 86,* 3357 (1981).

Sestero, A., *Phys. Fluids, 7,* 44 (1964).

Silevitch, M. B., *J. Geophys. Res., 86,* 3573 (1981).

Singh, N., *Plasma Phys., 22,* 1 (1980).

Singh, N., *Plasma Phys., 24,* 639 (1982).

Singh, N., and R. W. Schunk, *J. Geophys. Res., 87,* 3561 (1982a).

Singh, N., and R. W. Schunk, *Geophys. Res. Lett., 9,* 1345 (1982b).

Singh, N., and R. W. Schunk, *Geophys. Res. Lett., 9,* 446 (1982c).

Singh, N., and R. W. Schunk, *J. Geophys. Res., 88,* 10081 (1983a).

Singh, N., and R. W. Schunk, *Phys. Fluids, 26,* 1123 (1983b).

Singh, N., and R. W. Schunk, *Plasma Phys. Controlled Fus., 26,* 859 (1984a).

Singh, N., and R. W. Schunk, in *Second Symposium on Plasma Double Layers and Related Topics,* edited by R. Schrittwieser and G. Eder, p. 272, University of Innsbruck, 1984b.

Singh, N., and H. Thiemann, *Geophys. Res. Lett., 8,* 737 (1980a).

Singh, N., and H. Thiemann, *Phys. Rev. Lett., 76A,* 383 (1980b).

Singh, N., H. Thiemann, and R. W. Schunk, *Geophys. Res. Lett., 10,* 745 (1983).

Singh, N., R. W. Schunk, and H. Thiemann, *Adv. Space Res., 4,* 481-490 (1984).

Singh, N., H. Thiemann, and R. W. Schunk, *J. Geophys. Res., 90,* 5173 (1985).

Singh, N., H. Thiemann, and R. W. Schunk, in *Ion Acceleration in the Magnetosphere and Ionosphere, Geophysical Monograph, 38,* edited by Tom Chang, pp. 343-347, AGU, Washington, D.C., 1986.

Temerin, M., K. Cerny, W. Lotko, and F. S. Mozer, *Phys. Rev. Lett., 48,* 1175 (1982).

Thiemann, H., N. Singh, and R. W. Schunk, *Adv. Space Res., 4,* 511 (1984).

Wagner, J. S., T. Tajima, J. R. Kan, J. N. Leboeuf, and J. M. Dawson, *Phys. Rev. Lett., 45,* 803 (1980).

Whipple, E. C., J. R. Hill, and J. D. Nichols, *J. Geophys. Res., 89,* 1508 (1984).

DOUBLE LAYER FORMATION

Creation of Potential Drop (Electric Field)
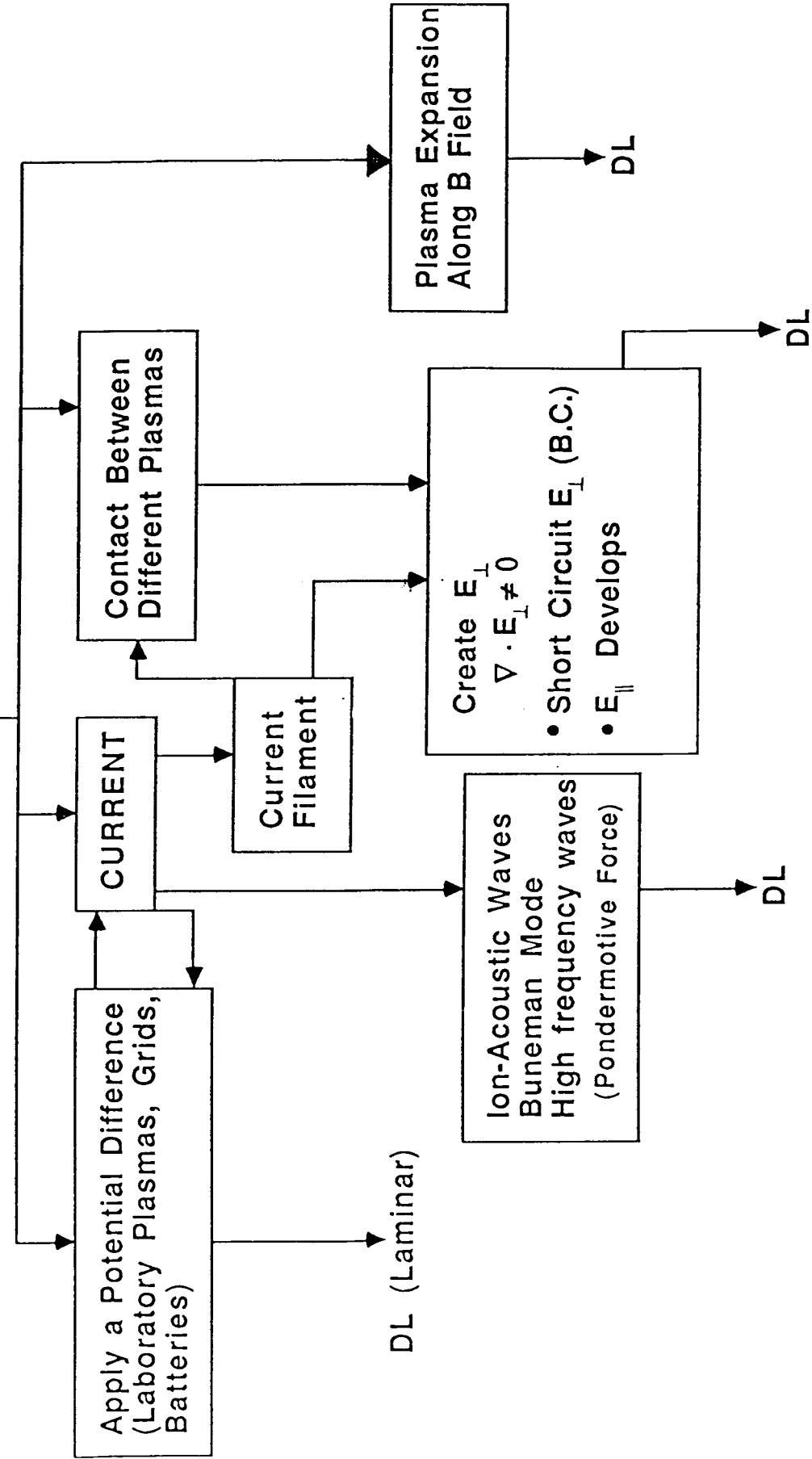
Figure 1. Summary of mechanisms for driving double layers.

197
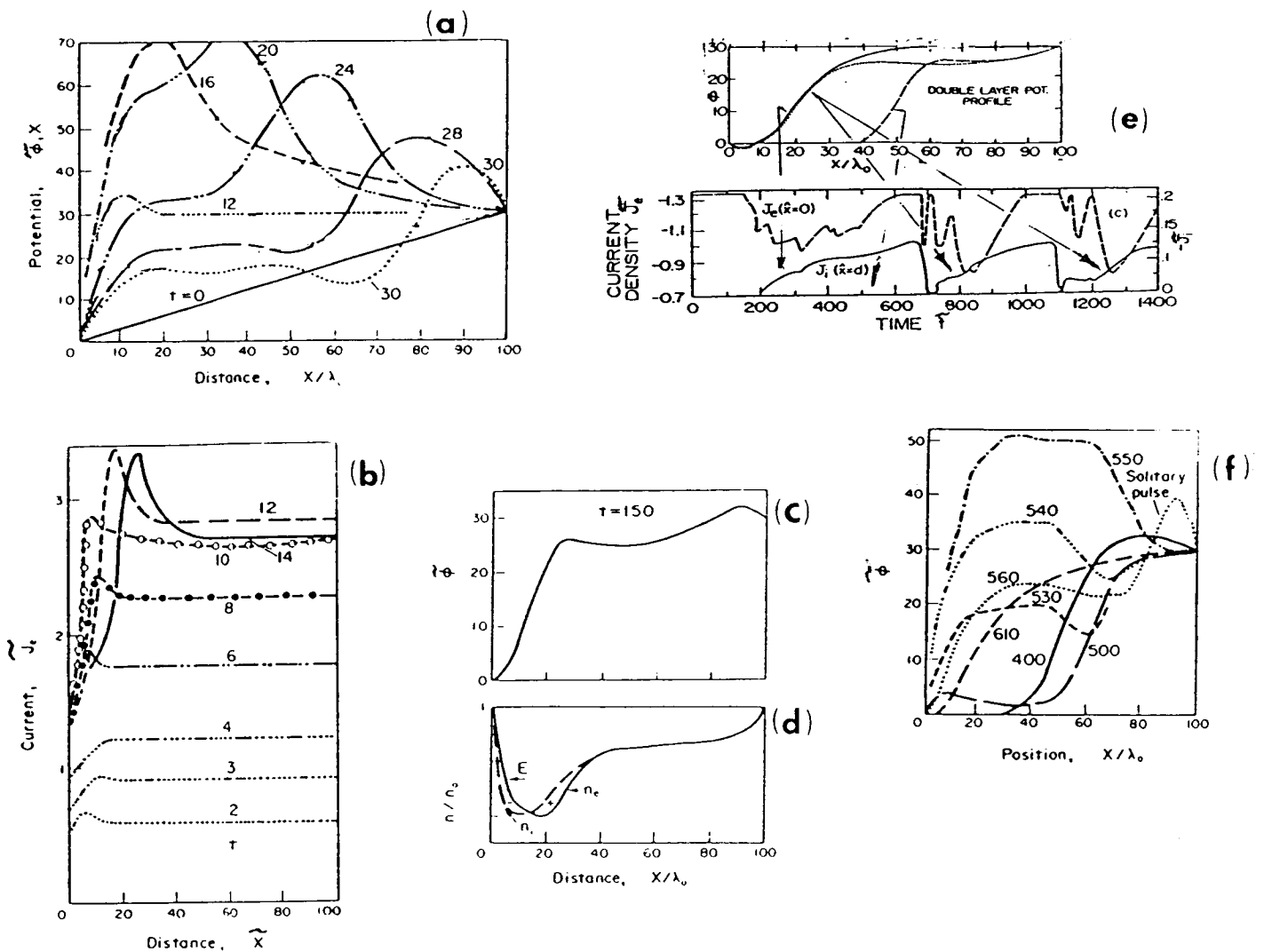
Figure 2. Double layer formation and dynamics as seen in one-dimensional Vlasov simulations. In the simulation, the plasma occupied the region $0 \leqslant x \leqslant 100 \lambda_0$, where λ_0 is the Debye length in the initial plasma ($t = 0$) across which a potential drop of $\Delta\phi_0 = 30(k_B T_0/e)$ was applied, where T_0 is the initial plasma temperature. We used the following normalizations: $\bar{x} = x/\lambda_0$, velocity $\bar{V} = V/V_{t0}$, time $\hat{t} = t\omega_{po}$, temperature $\hat{T} = T/T_0$, potential $\tilde{\phi} = e\phi/k_B T_0$, current $\hat{J} = J/n_0 e V_{t0}$, where $V_{t0} = (k_B T_0/m_e)^{1/2}$, ω_{po} is the electron plasma frequency with the initial density n_0, k_B is the Boltzmann constant, m_e is the electron mass, and $m_i/m_e = 64$, with m_i the ion mass; (a) temporal evolution of the potential profile, (b) temporal evolution of the current density profile, $\bar{J}_e(\bar{x})$, (c) double layer potential profile at $\hat{t} = 150$, (d) density profiles and space charges supporting the DL in (c), and (e) recurring DL formation (top) and electron and ion current interruptions and recovery (bottom). The arrows indicate the times of the potential profiles; the arrows originating from the potential profiles marked with "A" indicate that these profiles correspond to the early stages of the electron current interruptions and to the beginning of the ion influx into the double layer during the three cycles of the double layer formation. Note the dip at the low potential end. The potential profile marked with "B" corresponds to the current recovery stage during the first cycle. (f) Potential profiles during a reformation of the DL; at $\hat{t} = 400$ there is a DL, a positive potential perturbation near $x = 0$ is seen at $\hat{t} = 500$; at later times this perturbation grows and eventually a new DL forms at $\hat{t} \sim 610$.

Apply a Potential Drop

⇓

Uniform Electric Field

⇓

Accelerate Electrons (early time)

⇓

$J_p > J_0$ (near cathode boundary)

⇓

Positive Spacecharge Near Cathode Boundary

⇓

Electron Hole & Propagation
Counterstreaming Electrons
Plasma Modification/Expulsion
Cavity Formation
Distruption of Ion Flux from the Anode Boundary

⇓

DOUBLE LAYER (DL)

⇓

DL Propagation/Plasma Expansion from Cathode

⇓

Potential dip Formation at the Low Potential Side

⇓

Ion Influx Resumption at Anode (Ion or DL Transit Time Effect)

⇓

Current Recovery

⇓

Instabilities on the Low Potential Side

⇓

Positive Potential Perturbation near the Cathode

Figure 3. Summary of the various plasma processes occurring during the formation and reformation of a DL when a potential drop is applied across a plasma.
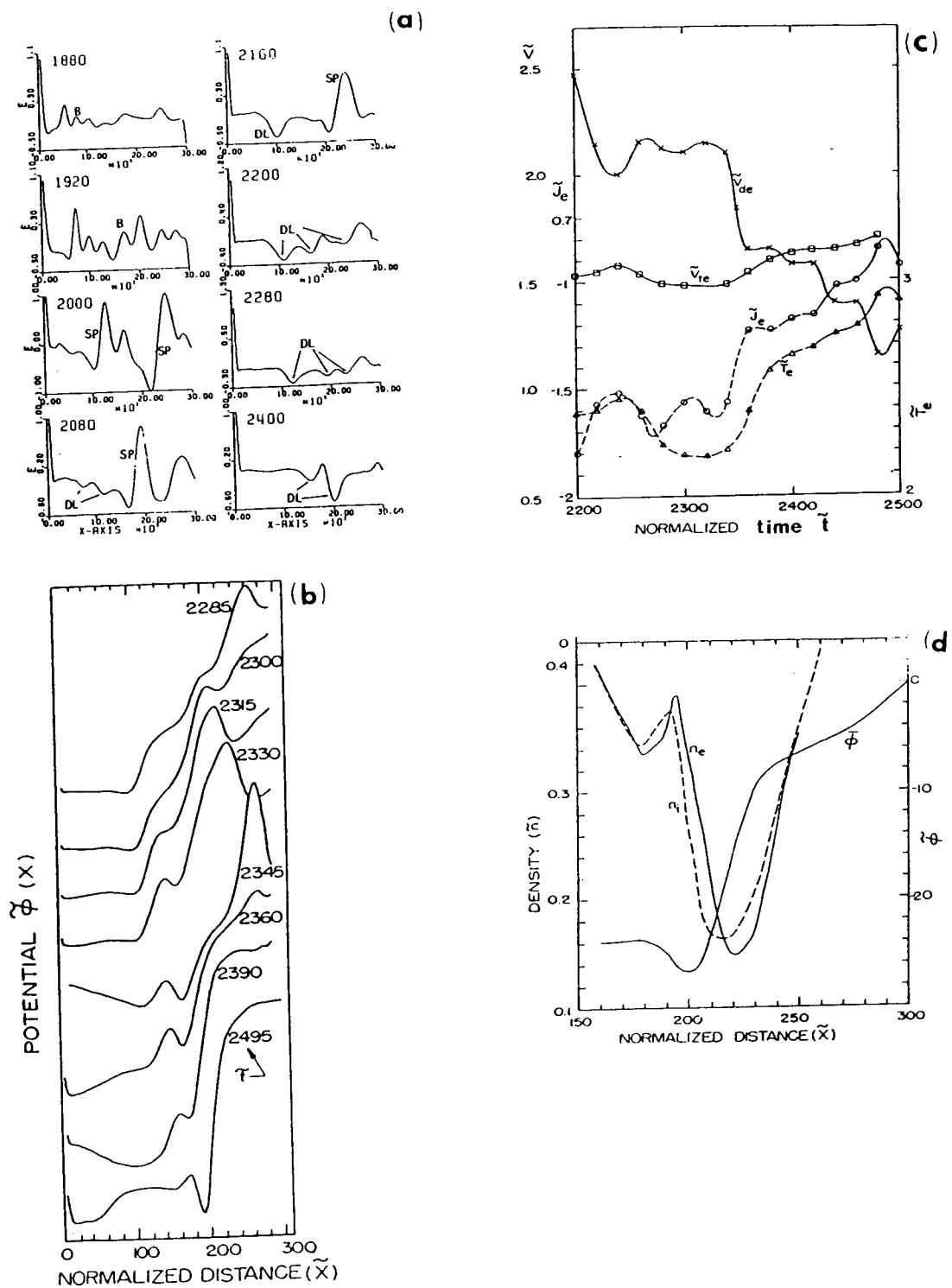
Figure 4. (a) Double layer evolution from the Buneman instability. Spatial profiles of the electric field E are shown at different times. At early times, $1880 < \tilde{t} < 2000$, small wavelength waves grow. At later times, in the nonlinear regime, these waves coalesce into long wavelength oscillations, which evolve into solitary pulses and double layers. (b) Temporal evolution of the double layer potential profile, (c) the corresponding temporal evolutions of the electron current J_e, electron drift velocity V_{de}, thermal velocity V_{te}, and temperature T_e at $\tilde{x} = 50$, and (d) spatial profiles of the electron and ion densities and the potential profile for a DL with a dip at its low potential end. The charge separation indicates the presence of a triple charge layer.

200
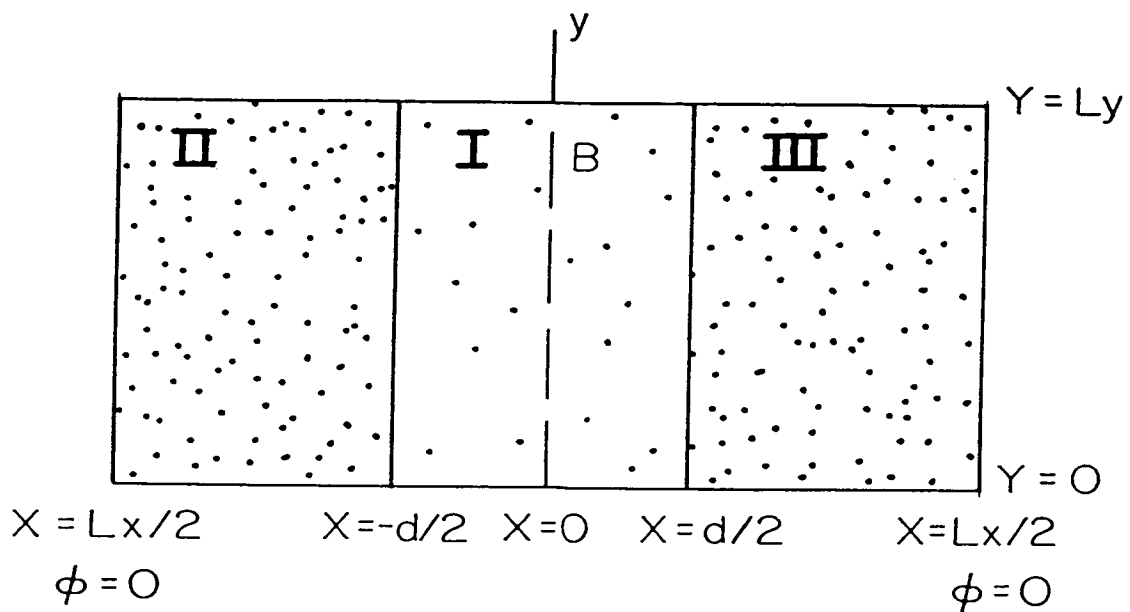
Figure 5. Geometry of the simulation scheme. A two-dimensional plasma of size $L_x \times L_y$ is simulated. Initially (t = 0), regions I to III are filled with plasmas. In the simulations described in this paper, the plasma in region I ($-d/2 < x < d/2$) is assumed to be hot, while the plasmas in regions II and III ($|x| > d/2$) are assumed to be cold and have similar properties. The **B** field is along the y-axis. The particles leaving the simulation plasmas at y = 0 and L_y are recirculated according to a periodic boundary condition, while those leaving at $x = \pm L_x/2$ are replaced from plasma reservoirs at the boundaries.
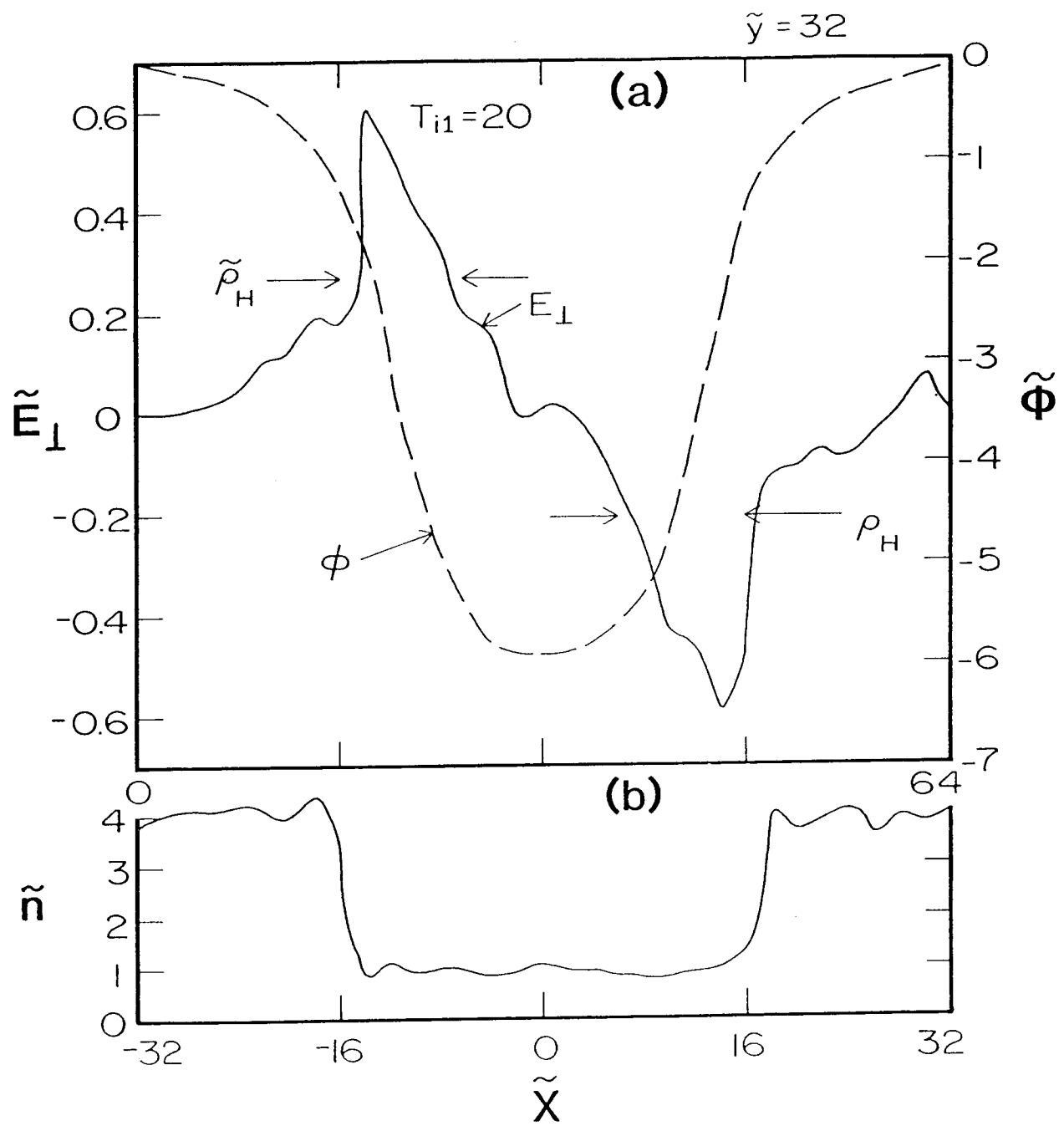
Figure 6. Variations of (a) electric potential and perpendicular electric field, and (b) plasma density as a function of x from a simulation with $\tilde{T}_{i1} = 20$. The average value of the hot in Larmor radius ρ_H is indicated in (a).

202
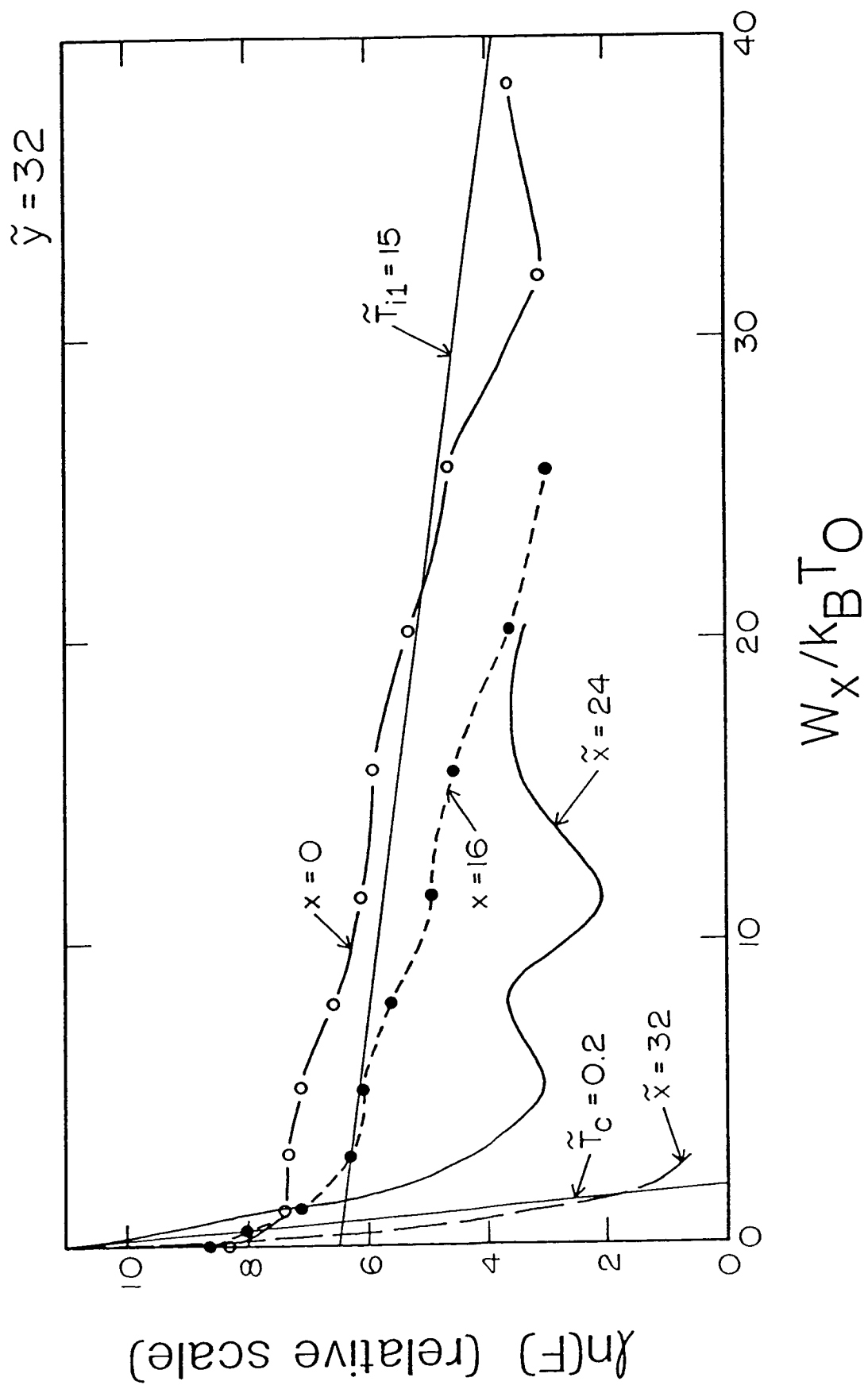
Figure 7. Ion energy distribution function $F(W_x = 1/2\, m_i V_x^2)$ at several locations for $x \geq 0$. The distribution functions for $x < 0$ are nearly the same. Note that the two asymptotes marked with $\tilde{T}_{i1} = 15$ and $\tilde{T}_c \simeq 0.2$ show the initial Maxwellian distributions.
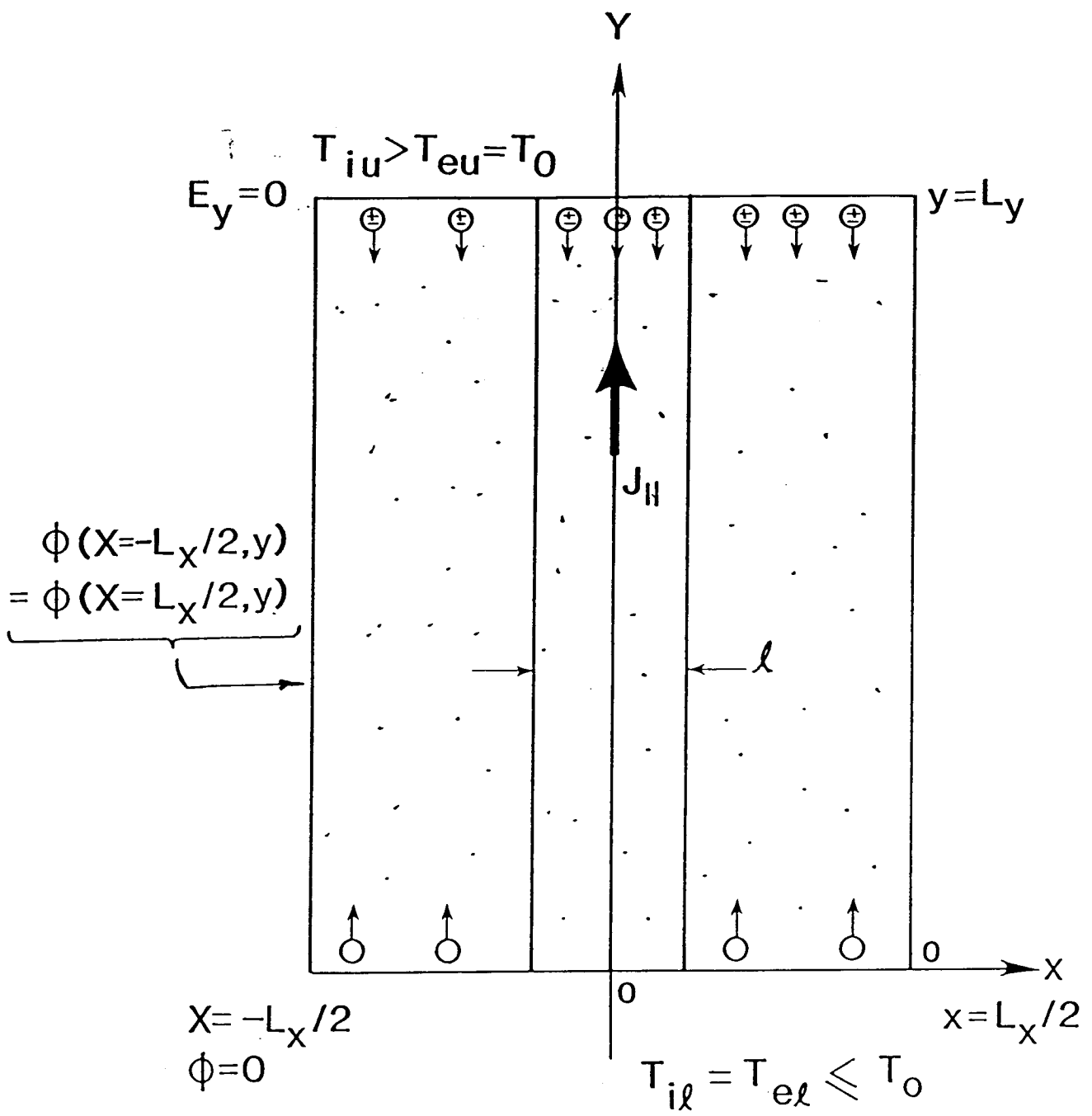
Figure 8. Scheme for simulating double layers driven by a current sheet.
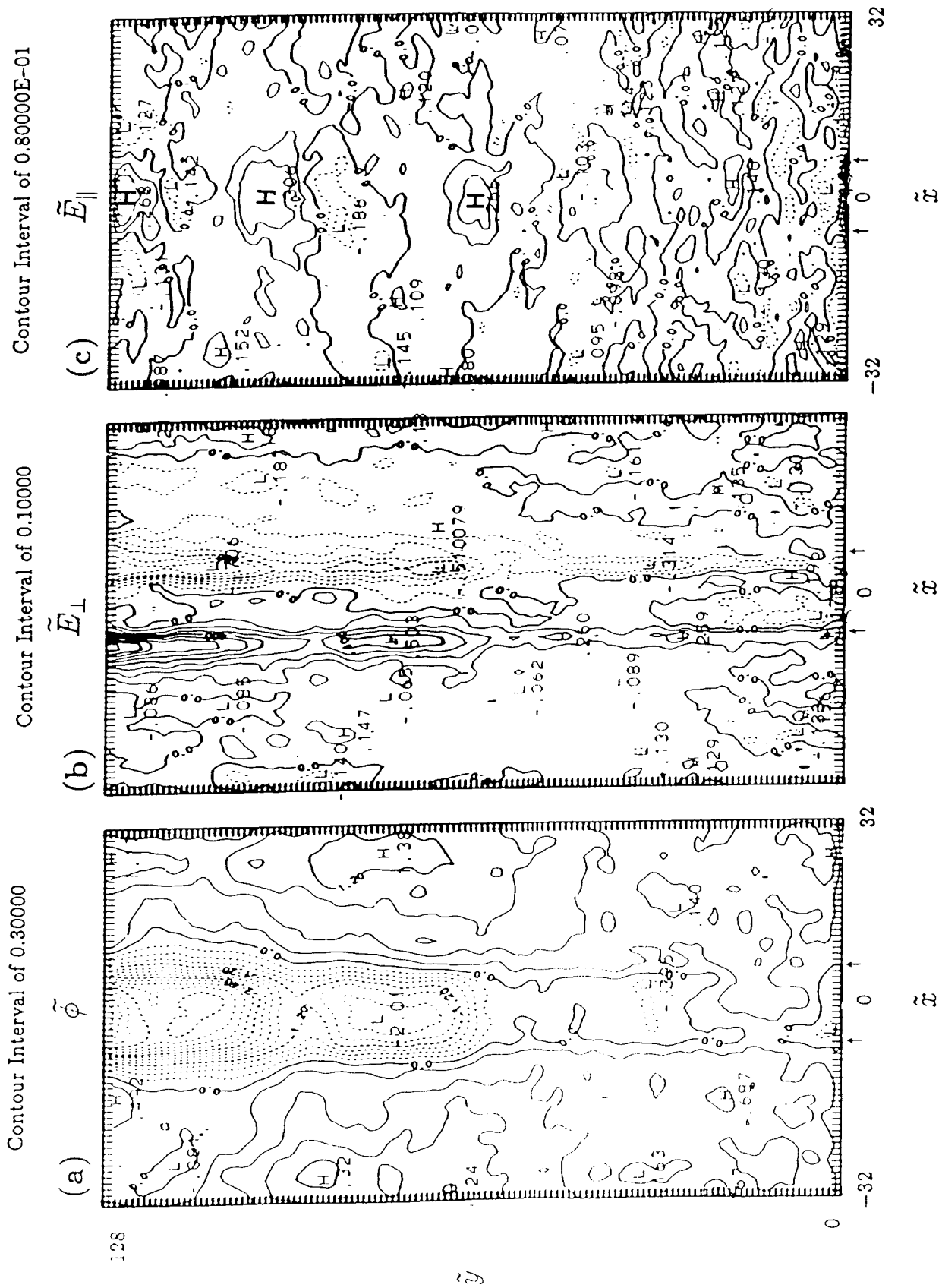
Figure 9. Potential structure driven by a current sheet with $\ell = 12\,\lambda_{do}$, $\rho_H = 9\,\lambda_{do}$, $J_o = 1.25\,en_oV_{to}$; (a) equipotential surfaces, (b) contours of constant $E_\perp$, and (c) contours of cosntant $E_\parallel$. The contour intervals are indicated on the top of the panels. The edges of the sheet are indicated by the arrows at the bottom of the panels.

205
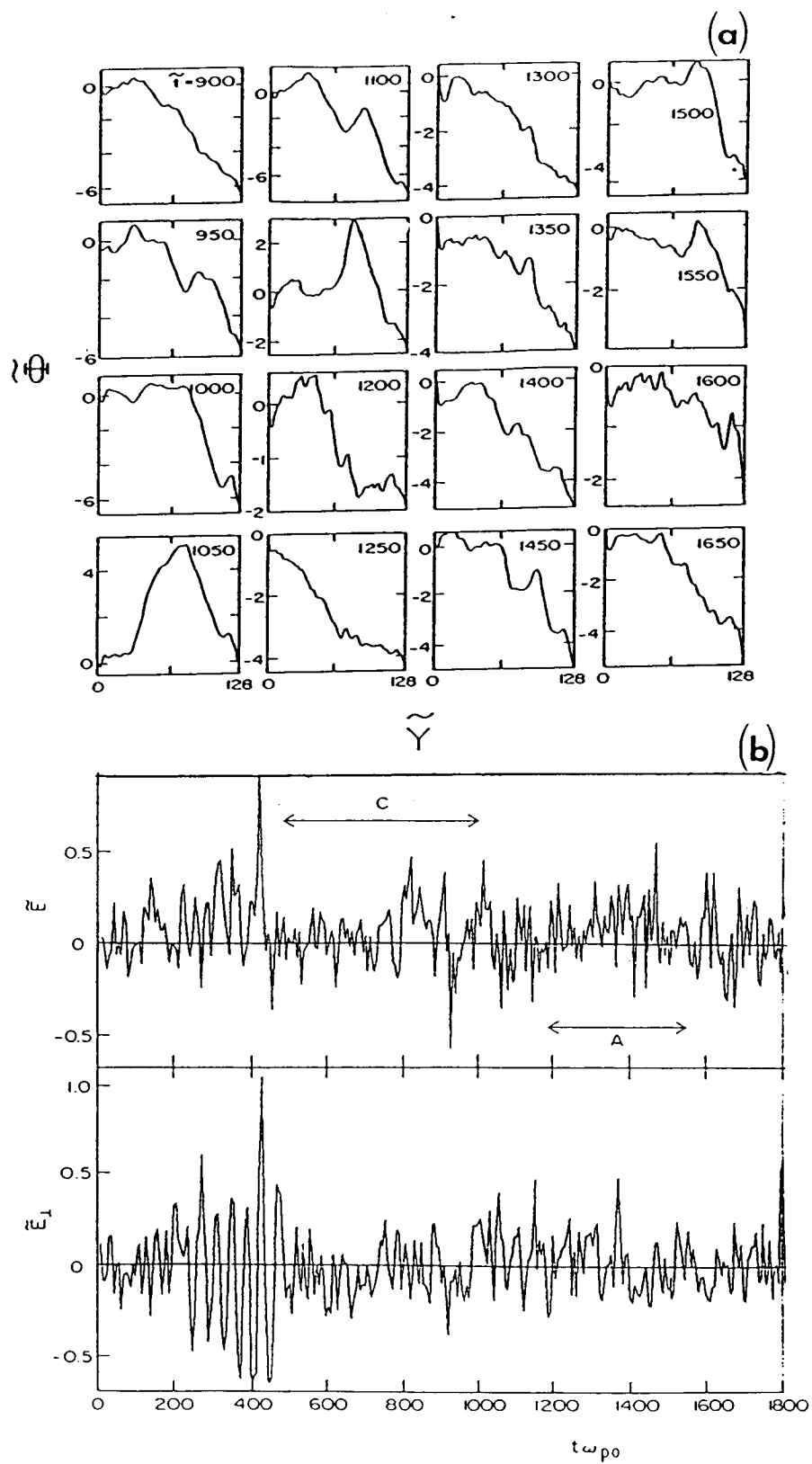
Figure 10. (a) Temporal evolution of the double layer potential profile along the axis of the current shown in Figure 8 and (b) fluctuations in $E_\parallel$ and $E_\perp$ in the region of the DL formation.

206
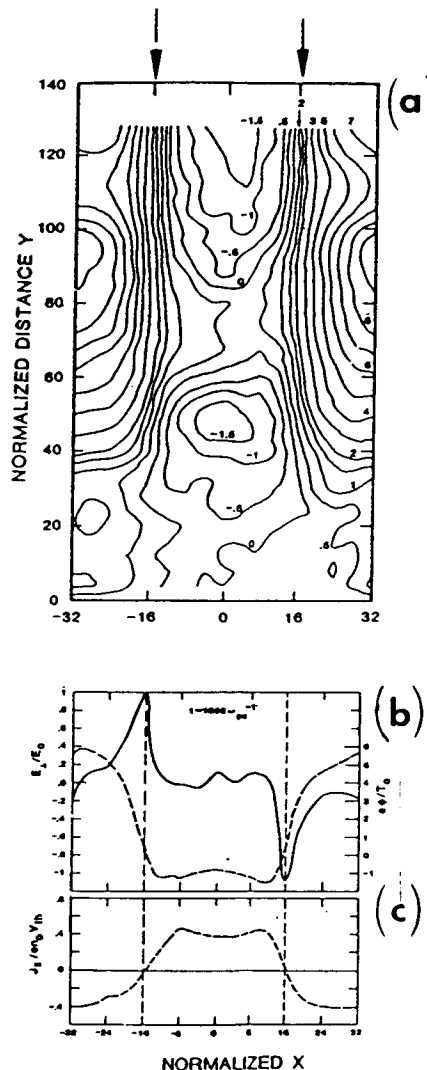
Figure 11. (a) Potential structure associated with a wide current sheet, with $\ell = 32\,\lambda_{do}$, $\rho_H = 3\,\lambda_{do}$, and $J_o = 0.6$ $n_o e V_{to}$. The current sheet edges are indicated by the arrows at the top of the panel. Equipotential surfaces are shown. (b) Perpendicular distribution of $E_\perp$ and ϕ near the top ($\bar{y} = 1120$) of the potential structure in (a). Note that $E_\perp$ is primarily confined near the edges of the current sheet. (c) Perpendicular distribution of the parallel current density $J_\parallel$; note the positive (upward) current inside the sheet, while outside the sheet the current is negative (downward). The downward current is caused by the upward acceleration of the electrons by the downward (parallel) electric field (see the potential distribution outside the sheet in (a)).
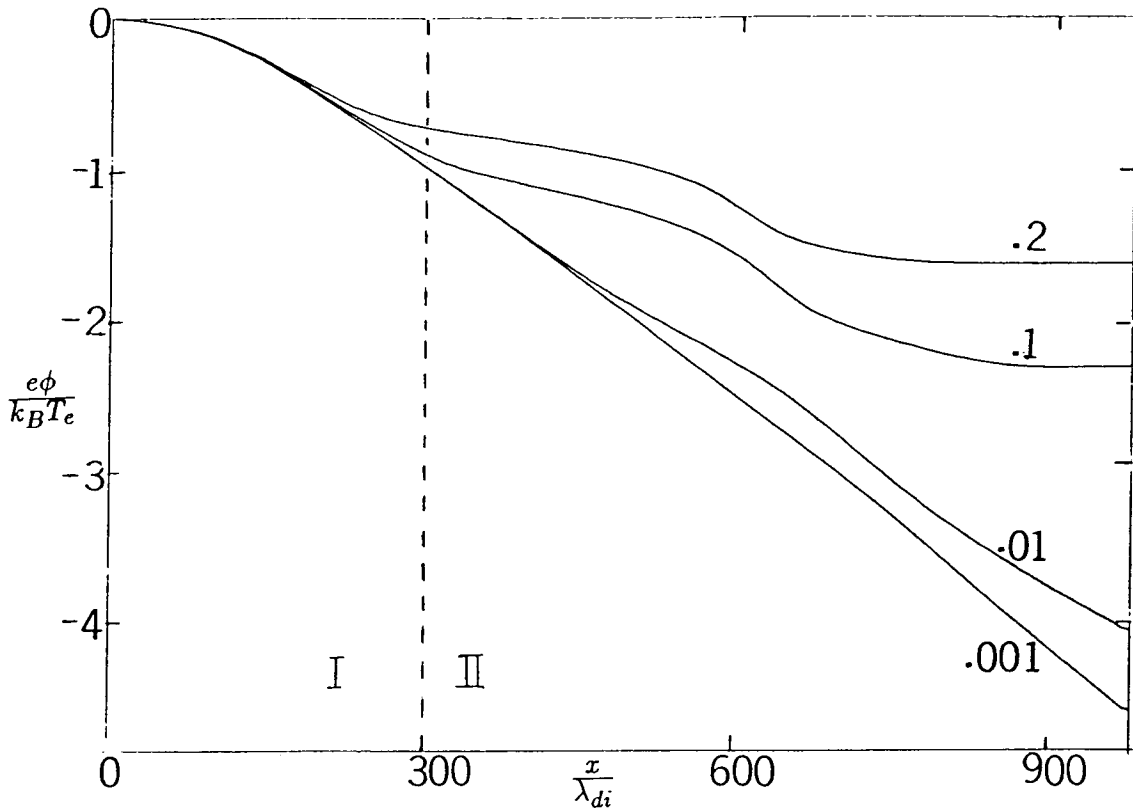
Figure 12. Snapshot (t = 60 ω_{po}^{-1}) of the potential profile associated with the expansion of a high-density plasma into region II. The different profiles are for different values of the density ratio n_I/n_{II}, as indicated.

ELECTRON ACCELERATION IN STOCHASTIC DOUBLE LAYERS

William Lotko
Dartmouth College, Hanover, New Hampshire 03755, U.S.A.

ABSTRACT

Transversely localized double layers evolve randomly in turbulent regions of strongly magnetized plasma carrying current along the magnetic field. Results from numerical simulations and spacecraft observations in the auroral plasma indicate that the parallel electric field in such regions is microscopically intermittent or stochastic. The implications of stochastic double layer fields on electron acceleration will be discussed here in terms of a statistical process involving ensemble averages over test particle motion. A Fokker-Planck equation can be derived for the electron phase space density, which depends on the mean and rms amplitudes of the double layers, the mean double layer density, and the initial electron velocity distribution. It is shown that the resulting electron acceleration is very sensitive to the ratio of the initial electron energy to the rms double layer amplitude. When this ratio is large, the acceleration process differs little from that expected in a dc electric field. When it is small, stochastic "heating" competes with directed acceleration. Evidence for both cases can be found in the auroral ionosphere in association with so-called inverted-V precipitation and collimated edge precipitation.

ANOMALOUS TRANSPORT IN DISCRETE ARCS AND SIMULATION OF DOUBLE LAYERS IN A MODEL AURORAL CIRCUIT

Robert A. Smith

Plasma Physics Division
Science Applications International Corporation
McLean, Virginia 22102, U.S.A.

ABSTRACT

The evolution and long-time stability of a double layer (DL) in a discrete auroral arc requires that the parallel current in the arc, which may be considered uniform at the source, be diverted within the arc to charge the flanks of the U-shaped double layer potential structure. A simple model is presented in which this current redistribution is effected by anomalous transport based on electrostatic lower hybrid waves driven by the flank structure itself. This process provides the limiting constraint on the double layer potential. The flank charging may be represented as that of a nonlinear transmission line. A simplified model circuit, in which the transmission line is represented by a nonlinear impedance in parallel with a variable resistor, is incorporated in a one-dimensional simulation model to give the current density at the DL boundaries. Results are presented for the scaling of the DL potential as a function of the width of the arc and the saturation efficiency of the lower hybrid instability mechanism.

I. INTRODUCTION

A vast body of ground-based, rocket, and satellite observations reveals that auroral-zone acceleration processes occur in a hierarchy of latitudinal scale widths. On the scale of the inverted-V region ($\Delta\Lambda > 1°$) parallel electric fields are observed in narrow, soliton-like structures interpreted as weak or ion-acoustic double layers (DL's) (Temerin et al., 1982). Assuming statistical homogeneity of the distribution of these weak DL's over an altitude range comparable to 1 R_e, one infers a total potential drop of up to a few kV, typical of the inverted-V region. On smaller spatial scales ($\Delta\Lambda < 0.1°$) more energetic precipitation is observed in discrete arcs, which have projected widths ~ 1 km in the ionosphere. Discrete arcs (DA's) are associated with electrostatic shocks (Torbert and Mozer, 1978; Kletzing et al., 1983). We adopt the hypothesis that electrostatic shocks constitute the nearly field-aligned "flanks" of the paradigmatic U-shaped potential structure of a strong double layer. Although this hypothesis seems plausible, many questions exist concerning the conditions under which DL's may exist in space, their dynamics, and their structure. These questions are vital for understanding the complex observational morphology of fields and particles in the auroral zone. At present, investigations of such questions must to a large extent be motivated by and proceed from consideration of the fast-growing literature on experiments and simulations, although usually the applicability of these situations to DL's in space is indirect (Smith, 1985, 1986a).

In this paper, we first discuss theoretically the question of what limits the potential of DL's in auroral arcs, and report results of recent simulations of DL's in a model circuit. Somewhat more detailed expositions are given by Smith (1986b, c).

II. THEORY

Experiments and simulations (Goertz and Joyce, 1975; Coakley and Hershkowitz, 1979) reveal a scaling law for the DL potential in terms of its length ℓ_{DL} and the electron density n_{eK} on the low potential (cathode:K) side; we write this law as

$$\phi_{DL}(kV) \simeq 300 \left(\frac{n_{eK}}{10^2 \text{ cm}^{-3}}\right)\left(\frac{\ell_{DL}}{1 \text{ km}}\right)^2 \qquad , \qquad (1)$$

where $\ell_{DL} \equiv \phi_{DL}/\max|E_{\parallel}|$. In space, ℓ_{DL} is not limited a priori and, absent other constraints, equation (1) implies that the potential may grow to much larger values than the observed limit on the auroral precipitation energy, which is a few tens of keV.

This dilemma is resolved by considering how the field-aligned flanks of the arc become charged during the evolution of the DL's. We adopt as a starting point the basic idea of the recent MHD models discussed by Haerendel (1983) and Goertz (1985, 1986) in which the DL evolves in the parallel current sheet of a kinetic Alfvén wave. This scenario limits the thickness of the sheet a priori to a few times the ion gyroradius at an energy representative of the distant plasma population in the generator region. Taking this energy to be ~ 1 keV, we may estimate $j_{\parallel}$ by

$$j_{\parallel} = neU_{ei} \sim \frac{c}{4\pi} \frac{\delta B_{\perp}}{R_i}$$

Using $n \sim 10^2$ cm^3, $B_0 \sim 0.05$ G, $\delta B_{\perp} \sim 10^{-3}$ G, and assuming a current sheet of a few kilometers thick, this equation gives a relative drift velocity U_{ei} greater than the electron thermal velocity V_e. At such a relative drift velocity, the current sheet is unstable to a variety of instabilities, including the ion cyclotron and Buneman instabilities. We expect the instability to be triggered at some altitude z_* where the density and magnetic field profiles first combine such that U_{ei} exceeds the threshold drift. In addition, experiments reveal that the U-shaped structure, with the field-aligned flanks curved toward the low potential side as is required for Earthward-directed Poynting flux (Smith, 1986a), requires $\omega_e < \Omega_e$, where ω_e and Ω_e are the electron plasma frequency and gyrofrequency, respectively. This is just the condition for strong magnetization ($\omega_e/\Omega_e = R_e/\lambda_e$), and is fulfilled in a limited altitude range along the auroral field lines (Gurnett, 1974).

Simulations show that DL's evolve from current-driven instabilities when the current is interrupted by trapping (Smith, 1982a, b). Trapping creates local regions of macroscopic non-neutrality; in the finite-thickness current sheet, the plasma tends to expel charge in the transverse direction in an attempt to neutralize the local electric field (Fig. 1). Electrons are tightly magnetized and cannot be expelled very far, but the ion motion is essentially ballistic (the evolution time scale is $<\Omega_i^{-1}$), and ions are accelerated in the transverse direction out to some distance greater than their gyroradius. Owing to mirror forces, the expelled charge spreads upward, providing the initial charging of the flanks.

The charging mechanism described above operates in the transient phase. The characteristic time scale of the evolution is $\tau_{DL} \sim \ell_{DL}/U_{iA}$, where $U_{iA} > C_s$ the ion inflow velocity in the frame of the DL. The charge spreads along the flank at velocity $c/\sqrt{\epsilon_{\perp}}$, where $\epsilon_{\perp}$ is the dielectric constant. In the MHD limit, $\epsilon_{\perp} \simeq c^2/V_A^2$, but we shall see later that $\epsilon_{\perp} < c^2/V_A^2$ in the DL flank. In any case, however, we find that the time $\tau_{ind} = \int ds c/\sqrt{\epsilon_{\perp}}^{1/2}/c$ for the charge to spread along the field lines back to the generator region (Fig. 2) is long compared to $\tau_{DL} < t < \tau_{ind}$, the spreading

charge would thin out along **B** and the flank would not sustain the DL potential; then the DL would discharge. This would occur in a time short compared with the typical lifetime of discrete arcs. Therefore, asymptotic stability of the DA requires a transport mechanism producing a cross-field current density $J_x(\phi)$, which persists as $\partial\phi_{DL}/\partial t \to 0$.

If such a mechanism exists, then in the time-asymptotic regime, the density n_{eK} in equation (1) is determined by current continuity and is of the form

$$n_{eK}(z_*) = n_{e\infty} - g \int_{z_*}^{\infty} dz\, J_x(\phi,z) \quad , \tag{2}$$

where g is a constant. Substituted in equation (1), equation (2) provides the physical constraint on the DL potential, which is transparently self-stabilizing for J_x, a monotonically increasing function of ϕ.

A mechanism to maintain a distributed J_x in the time-asymptotic regime is discussed by Smith (1986b). The mechanism is based on anomalous transport due to lower hybrid waves which are driven by the inhomogeneous structure of the flank itself. The discussion above implies that the initial scale length ℓ_f of the perpendicular electric field E_x in the flank is $\ell_f > R_i$. As this field is established along **B**, the electrons acquire the local polarization drift velocity cE_x/B_0. The ions, however, encounter an inhomogeneous electric field over the scale of their gyroradius, and so their drift orbit is modified by finite-Larmor-radius (FLR) effects. For $\ell_f > R_i$, the ion drift speed is approximately given by the first non-vanishing order of the phase-averaged FLR correction:

$$V_{Di} \simeq (1 + \frac{1}{4} R_i^2 \nabla^2) \frac{cE_x}{B_0} \simeq \left(1 - \frac{R_i^2}{4\ell_f^2}\right) \frac{c\phi}{B_0 \ell_f} \tag{3}$$

Then there is a relative drift

$$U_{ei} = V_{De} - V_{Di} \simeq \frac{R_i^2}{4\ell_f^2} \left(\frac{c\phi}{B_0 \ell_f}\right) \quad ;$$

if $U_{ei} > V_i$, this relative drift drives the electrostatic modified two-stream instability (MTSI) studied by McBride et al. (1972). (Other instabilities are also possible, of course, but for simplicity we consider only the MTSI.) The most unstable mode has frequency $\omega \sim \omega_{LH} = \omega_i/(1 + \omega_e^2/\Omega_e^2)^{1/2}$, with growth rate $\gamma \sim \omega_{LH}$, and parallel wave number $k_\parallel \sim (m/M)^{1/2} k_\perp$.

The salient property of the MTSI for our purposes is that it saturates by trapping ions in the perpendicular drift direction and electrons in the parallel direction; in the saturation process, the ions and electrons are heated to a fraction α^2 of the relative drift energy:

$$T_{\perp i} \simeq T_{\parallel e} \simeq \alpha^2 M U_{ei}^2/2 \ .$$

From simulations, McBride et al. (1972) find $\alpha \simeq 0.5$, with a wave energy density W at saturation of $W/nMU_{ei}^2 \sim$ a few percent.

Motivated by these results, Smith (1986b) postulates a self-scaling model in which the flank is assumed to be always at saturation (marginal instability) with respect to an instability such as the MTSI. The model characterizes the instability by two parameters α, β, defined by

$$V_{\perp i} = \alpha \, (cE_x/B_o) \quad ; \quad U_{ei} = \beta \, (cE_x/B_o) \quad , \tag{4}$$

where U_{ei} is now the threshold drift speed and $E_x \sim \phi/\ell_f$. Using equations (3) and (4), we find the self-similar scalings

$$R_i^2/\ell_f^2 = \alpha\beta \quad ; \quad T_{\perp i}/T_{eo} = (\alpha^3\beta)^{1/2} \, (e\phi_{DL}/T_{eo}) \quad ;$$

$$V_{De} \equiv \frac{cE_x}{B_o} = \left(\frac{\beta}{\alpha}\right)^{1/4}\left(\frac{m}{M}\right)^{1/2}\left(\frac{e\phi_{DL}}{T_{eo}}\right)^{1/2} \quad ; \qquad \left(\frac{\alpha}{\beta}\right)^{1/4}\left(\frac{M}{m}\right)^{1/2}\left(\frac{\omega_{eo}}{\Omega_{eo}}\right)\left(\frac{e\phi_{DL}}{T_{eo}}\right)^{1/2} \quad ; \tag{5}$$

where λ_{eo}, T_{eo}, and ω_{eo} are reference values of the electron Debye length, temperature, and plasma frequency.

Owing to momentum conservation, there is a wave-modulated friction between the electrons and ions, which may be described by an anomalous collision frequency (Davidson and Krall, 1977) $\nu_* \simeq \epsilon\omega_{LH}$, where $\epsilon \equiv W/nMU_{ei}^2$. Thus, the electron and ion fluids are acted on by volume forces $F_{yi} = -F_{ye}$, leading to an $\mathbf{F} \times \mathbf{B}$ drift velocity in the x-direction, i.e., opposite to E_x (the coordinate system is defined by Fig. 3). This drift velocity is given by $V_{xe} = V_{xi} \equiv V_x \, (n_e, \phi_{DL})$, where

$$V_x = \epsilon \, (\alpha^3\beta^5)^{1/4}\left(\frac{m}{M}\right)^{1/2}\frac{\omega_{LH}}{\Omega_i}\left(\frac{e\phi_{DL}}{T_{eo}}\right)^{1/2} V_{eo} \quad , \tag{6}$$

and $V_{eo} = (T_{eo}/m)^{1/2}$. Thus, above the DL, plasma is transported from the center of the arc to the flanks, concentrating the parallel current there (Fig. 3). Although $V_{xe} = V_{xi}$, there is a net current J_x because above the region of strong $E_\parallel$ in the DL, we expect an extended region of small charge density ρ which sustains a weak parallel density field $E_\parallel$ driven by beam-plasma instabilities. Then the continuity equation is

$$\partial J_z/\partial z \simeq -\partial J_x/\partial x \simeq -\partial(\rho V_x)/\partial x \quad ,$$

Upon solving and integrating along the field line, we obtain (Smith, 1986b)

$$J_z(\infty) - J_z(0) \simeq C(\alpha,\beta) \, (\phi_{DL}/\ell_a^2)^{5/8} \tag{7}$$

where $C(\alpha,\beta)$ is a constant and ℓ_a is the perpendicular scale length of the arc (Fig. 3). The RHS of equation (7) is just the term $\int J_x dz$ in equation (2). Assuming $J_z(0) \ll J_z(\infty)$, equation (7) gives a scaling law

$$\phi_{DL} \lesssim (J_z(\infty)/c)^{8/5} \, \ell_a^2 \quad . \tag{8}$$

For typical auroral-zone parameters equation (8) yields $\phi_{DL} \sim 10\,kV$ for $\ell_a \sim 1\,km$, in general accord with observations.

III. SIMULATION

In the context of the above discussion, the flank may be modeled as a transmission line with local potential $\phi = E_x \ell_f$, where $\ell_f \sim \phi^{1/2}$. Once the DL potential has reached a threshold value ϕ_* required to drive the MTSI, the transmission line is charged by the distributed (in z) perpendicular current $J_x = \rho V_x$ of equation (7). We shall report elsewhere on simulations in which the transmission-line equations (Smith, 1986c) are solved simultaneously with a one-dimensional simulation of the DL evolution; this procedure provides the necessary self-consistent boundary condition on the current density $J_{DL}(t)$ at the simulation boundaries. In this paper, we replace the transmission line with a simple model circuit.

If the flank were uniform between the DL ($z = z_* \equiv 0$) and the generator, the transmission line would appear to the DL as a pure impedance over the evolution time of the DL, with value $Z_T = (L_T/C_T)^{1/2}$, where $L_T = \ell_f/4\pi c^2$, $C_T = 4\pi\epsilon_\perp/\ell_f$. We model the impedance by the same form, with variable $\ell_f(\phi)$. We thus adopt the model circuit shown in Figure 4 where the diode symbol represents the DL and the variable resistor $R(\phi)$ represents leakage current in the flank; this term is modeled by using the same form for J_x as derived above, but over the perpendicular scale length ℓ_f instead of ℓ_a, by integrating $J_x \sim n^{1/2}(z)$ over the length $z_K(t) = ct/\sqrt{\epsilon_\perp}$. The dielectric constant is defined by

$$\epsilon_\perp = 1 + (\omega_{eo}^2/\Omega_e^2) + (\omega_{io}^2/\Omega_i^2)\,[(1-\alpha\beta)^2 + \alpha^2(1+\gamma_e)] \quad , \tag{9}$$

where $\gamma_e \equiv T_{\|e}/T_{\perp i}$.

The heuristic definition [equation (9)] is such that the total energy stored in the dielectric is $\epsilon_\perp E_x^2/8\pi$: the first term in [] represents the reduced ion drift speed, while the second term accounts for ion and electron heating by saturation of the self-scaled modified two-stream instability.

For the purpose of testing the scaling of ϕ_{DL} with ℓ_a and α, we adopt the philosophy that owing to the separation between the perpendicular scale lengths ℓ_a and ℓ_f, the flank may be represented by these circuit elements while the DL will evolve in an essentially one-dimensional fashion in the central region of the arc. The DL evolution is simulated with the one-dimensional Vlasov code described by Smith (1982b), replacing the circuit used there by that of Figure 4. The boundary condition on the current density $J_{DL}(t)$ is then given by

$$J_{DL}(t) = \frac{I_S}{\ell_a} - \frac{\phi_{DL}(t)}{\ell_a}\left[\frac{1}{Z_T(\phi_{DL})} + \frac{1}{R(\phi_{DL})}\right] \quad , \tag{10}$$

where I_S is the constant source current and

$$Z_T = [\alpha/\beta]^{1/4}\,(Y/\epsilon_\perp^{1/2})\,(V_{eo}/c)\,(\ell_a/\mu^{1/2})\,\phi_{DL}^{1/2} \quad , \tag{11}$$

215

$$R = \left(\frac{\mu}{2}\frac{T_{eo}}{T_{\parallel i}}\right)^{1/2}\frac{(Y\ell_a)^{2/3}}{(\alpha^7\beta)^{1/8}}\frac{\phi_{DL}^{1/4}}{[1-\exp(-K_2 Z_K(t))/2]}\tag{12}$$

$\mu = m/M$, K_2 is defined in Smith (1986b) $Y = \omega_{eo}/\Omega_{eo}$, $V_{eo} = \omega_{eo}\lambda_{eo}$, and all lengths and time scales are normalized to the nominal upstream quantities λ_{eo} and ω_{eo}, respectively; also $\phi_{DL} \rightarrow e\phi_{DL}/T_{eo}$. The term in [] in equation (10) replaces the physically derived I_x of equation (8). This term is valid only after the threshold potential ϕ_* has been attained, and so is turned on adiabatically for $\phi > \phi_*$. Therefore, the circuit model does not accurately describe the initial dynamics in the linear instability phase of the evolution. In addition, the lumped circuit of Figure 4 cannot represent the distributed nature of the flank charging, and so we cannot construct a circuit topology that allows for inductive fields. Therefore, we cannot model the acceleration of the inflowing (injected) distributions by inductive effects.

For the parameters we use (see below), we estimate that the effect of neglecting inductive effects is small. As for the first limitation, the transient charging mechanism vanishes as $\partial\phi_{DL}/\partial t \rightarrow 0$. Thus, we expect the model to be adequate for our present objective of studying time-asymptotic scalings.

We show results for five runs. For all cases, the injected distributions are drifting Maxwellians with drift speeds in the simulation frame of $U_e = 2 V_{eo}$, $U_i = -0.5 V_{eo}$. The forms of these distributions are held fixed (up to normalization). The threshold drift parameter β is held equal to 2, and $M/m = 16$. Holding $\ell_a/\lambda_e = 60$, we use values of $\alpha = 0.05, 0.02, 0.50$. Fixing $\alpha = 0.50$, we use $\ell_a/\lambda_e = 20, 40, 60$. Initialization and other implementations are as described by Smith (1982b).

Figure 5 shows the scaling of ϕ_{DL} with α, the fundamental parameter of the self-scaling marginal stability model of the MTSI discussed earlier. In the circuit equation (10), the principal effect of α is contained in the dependence of the impedance Z_T on the dielectric constant $\epsilon_\perp$. In terms of the circuit equation (10), the DL scaling law equation (1) becomes in dimensionless notation

$$\phi_{DL} = G\ell_{DL}^2 J_s\left[1 - \frac{\phi_{DL}^{1/2}}{Z_o J_s} - \frac{\phi_{DL}^{3/4}}{R_o J_s}\right],\tag{13}$$

where $Z_T(\phi) = Z_o\phi^{1/2}$, $R(\phi) = R_o\phi^{1/4}$. The RHS (13) has the form of a large factor $GJ_s\ell_{DL}^2$ times a small factor [...], and the upper bound for ϕ_{DL} is obtained from setting [...] = 0. Because $Z_o << R_o$, equation (13) implies $\phi_{DL} \sim Z_o^2$. In Figure 5 we also plot the dependence of Z_o^2 on α, which agrees well with the plotted points.

Figure 6 confirms the scaling $\phi_{DL} \sim \ell_a^2$ found above. Again, this result is contained in equation (13) through the dependence $\phi_{DL} \sim Z_o^2$ (the results of Fig. 6 are all for $\alpha = 0.5$, where $Z_o << R_o$).

Because the speed of light c is introduced in the impedance, the choice of V_{eo}/c yields a physical scaling of velocities. Because $Y = \omega_{eo}/\Omega_{eo}$ is a parameter, we obtain physical values of the length scales for an assumed value of either B_o or n_{eo}. All runs discussed here are for $T_{eo} = T_{io} = 1$ keV, typical of the plasma sheet population (note ϕ_{DL} scales independently of T_{eo}). The scaled ϕ_{DL} is then given in kV as shown in the right-hand scale of Figure 6. Similarly, if we adopt a nominal value of $B_o = 0.05$ G ($f_{ce} = 250$ kHz) for the acceleration region, the top scale of Figure 6 gives arc thickness projected into the ionosphere of the order 1 km, which is the correct order of magnitude.

216

The power flows ($I\phi$) through the various parts of the circuit are shown for one case in Figure 7; for this case $\phi_{DL} = 42.5$ kV. In the steady state, only 10 percent of the power flows goes through the DL, and about 90 percent goes into charging the flanks. The physical scale on the right shows the power dissipated per 1000 km extent of the arc in the E-W direction. Arcs are generally observed in systems of parallel bands, quasi-periodic in the N-S direction; for the parameters of this example, each DA in such a system would dissipate about 10^{11} W, compared with a typical substorm power of $\sim 10^{12}$ W.

The scalings in α and ℓ_a have straightforward physical intepretations. The increase of ϕ_{DL} with α has two related aspects. First, the efficacy of the anomalous transport mechanism reported in Smith (1986b) increases with α, which is a measure of the strength of the MTSI. Second, in this self-scaling model the ratio $R_i(\phi)/\ell_f(\phi) \sim \alpha^{1/2}$, so that as α increases, finite-Larmor radius effects lead to decreasing ion drift speed; hence, a higher ratio of electrostatic to kinetic energy is stored in the flank "dielectric" for a given charge. The factor ℓ_a in Z_o [equation (6)] originates in the current balance ($I_s = J_s\ell_a$), and because the flank is charged from the interior of the arc the charge available increases with ℓ_a. The quadratic scaling $\phi_{DL} \sim \ell_a^2$ derives from the self-scaling of the transport model because $\ell_f \sim \phi^{1/2}$.

IV. DISCUSSION

We have shown that basic considerations of DL evolution and stability require anomalous transport processes to divert the uniform upstream current to the flanks of a DA even after the parallel electric field has evolved to a steady state. The transport model we have discussed, albeit highly simplified, yields an estimate [equation (8)] for the arc potential in general accord with observations. Other important consequences of the model are also in accord with satellite and rocket observations of DA's and laboratory DL experiments. These include: (1) the density in a DA is substantially depleted relative to the ambient density (Benson and Calvert, 1979; Alport et al., 1986); and (2) concomitant with the depletion of the arc is that the current is diverted to the flanks, so that the highest current density is at the edges (Bruning, 1983; Burke, 1984).

Besides the simple transport mechanism discussed here, there are many other mechanisms which are probably important in DA's. We are presently investigating models including ion-cyclotron modes.

In terms of the simple circuit model, the potentials, perpendicular length scales, and power flows physically scale to correct orders of magnitude. For the nominal parameters we have chosen, the potential ranges from 5 to 42 kV, while the length scales are consistent with the observational bound of ≈ 3 km on the latitudinal scale projected in the ionosphere (Boehm and Mozer, 1981). These quantities scale as n_{eo} and $n_{eo}^{-1/2}$, respectively. We adopted $B_o = 0.05$ to correspond to the frequency of peak intensity of the auroral kilometric radiation, and chose ω_{eo}/Ω_{eo} as the marginal limit of strong magnetization ($\omega_e/\Omega_e = R_e/\lambda_e$), which experiments reveal to be a requisite for strong DL formation with Earthward-directed Poynting flux (Smith, 1986a). (Recall that n_{eo} is the ambient density before DL formation, not that of the evacuated arc.) Thus, our choice of $\omega_{eo} = \Omega_{eo}$ is an upper bound; smaller values lead to lower potential, larger widths, and lower power flows.

In future publications we shall report on refinements and extensions of the simulation concept, including a model in which the simplified circuit used here is replaced by the transmission-line equations.

REFERENCES

Alport, M. J., S. L. Cartier, and R. L. Merlino, *J. Geophys. Res., 91,* 1599-1608 (1986).

Benson, R. F. and W. Calvert, *Geophys. Res. Lett., 6,* 479-482 (1979).

Boehm, M. H. and F. S. Mozer, *Geophys. Res. Lett., 8,* 607-610 (1981).

Bruning, K., Dissertation, Univ. of Munster, 1983.

Burke, W. J., in *Magnetospheric Currents,* edited by T. A. Potemra, Amer. Geophys. Union, Washington, D.C., pp. 294-303, 1984.

Coakley, P. and N. Hershkowitz, *Phys. Fluids, 22,* 1171-1181 (1979).

Davidson, R. C. and N. A. Krall, *Nuclear Fusion, 17,* 1313-1372 (1977).

Goertz, C. K., *Space Sci. Rev., 42,* 499-513 (1985).

Goertz, C. K., in *Comparative Study of Magnetospheric Systems,* edited by B. M. Pedersen, D. Le Queau, A. Roux, and A. Sant-Marc, CNRS, Toulouse, France, pp. 357-370, 1986.

Goertz, C. K. and G. Joyce, *Astrophys. Space Sci., 32,* 165-173 (1975).

Gurnett, D. A., *J. Geophys. Res., 79,* 4227-4238 (1974).

Haerendel, G., in *High-Latitude Space Plasma Physics,* edited by B. Hultqvist and T. Hagfors, Plenum, New York, pp. 515-535, 1983.

Kletzing, C., C. Cattell, F. S. Mozer, S.-I. Akasofu, and K. Makita, *J. Geophys. Res., 88,* 4105-4113 (1983).

McBride, J. B., E. Ott, J. P. Boris, and J. H. Orens, *Phys. Fluids, 15,* 2367-2383 (1972).

Smith, R. A., *Physica Scripta, 25,* 413-415 (1982a).

Smith, R. A., *Physica Scripta, T2,* 238-251 (1982b).

Smith, R. A., in *Unstable Current Systems and Plasma Instabilities in Astrophysics,* edited by M. R. Kundu and G. D. Holman, Reidel, Dordrecht, pp. 113-123, 1985.

Smith, R. A., in *Comparative Study of Magnetospheric Systems,* edited by B. M. Pedersen, D. Le Queau, A. Roux, and A. Saint-Marc, CNRS, Toulouse, France, pp. 327-350, 1986a.

Smith, R. A., *Geophys. Res. Lett.,* submitted, 1986b.

Smith, R. A., *Geophys. Res. Lett.,* submitted, 1986c.

Temerin, M., K. Cerny, W. Lotko, and F. S. Mozer, *Phys. Rev. Lett., 48,* 1175-1179 (1982).

Torbert, R. B. and F. S. Mozer, *Geophys. Res. Lett., 5,* 135-138 (1978).
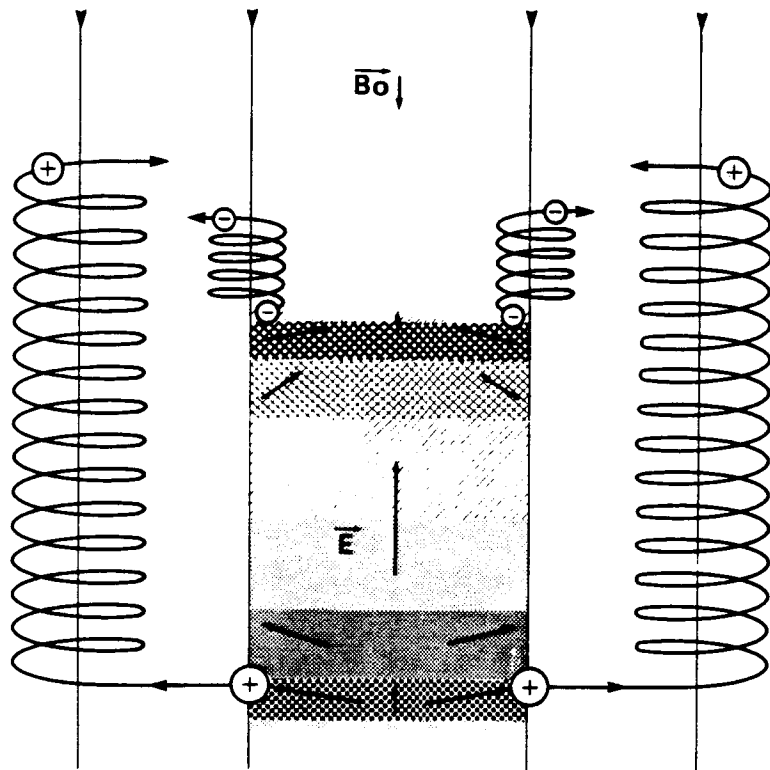
Figure 1. Schematic illustration of initial charging of the DL flanks by expulsion of charge from the localized, rapidly changing non-neutral region (shaded: stippled region $\rho > 0$, cross-hatched $\rho < 0$) where onset of current-driven instabilities occurs in the parallel sheet of a kinetic Alfvén wave.
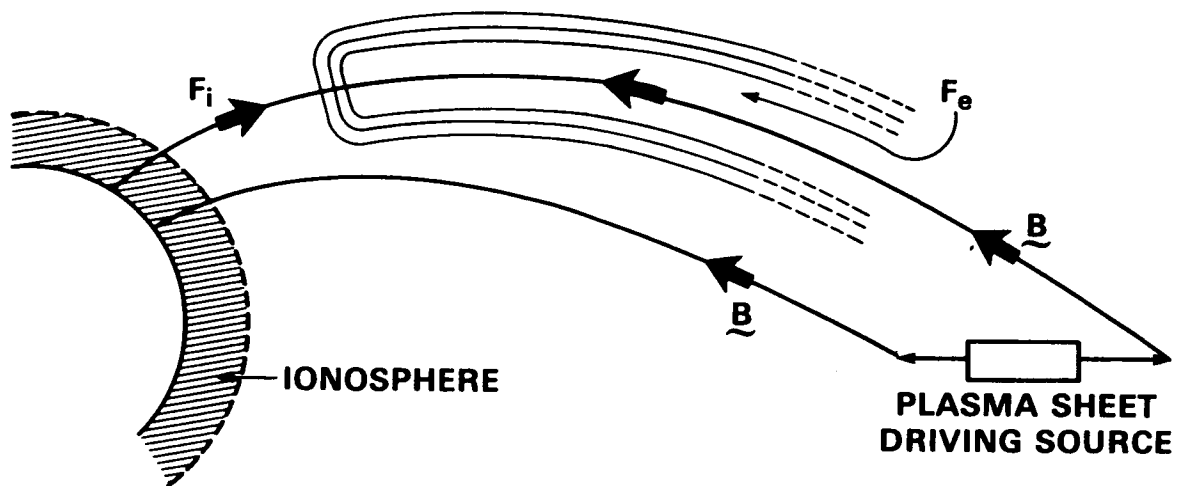
Figure 2. Schematic of the double layer flank spreading along **B** from the double layer toward the generator (here for illustration taken to be in the plasma sheet).
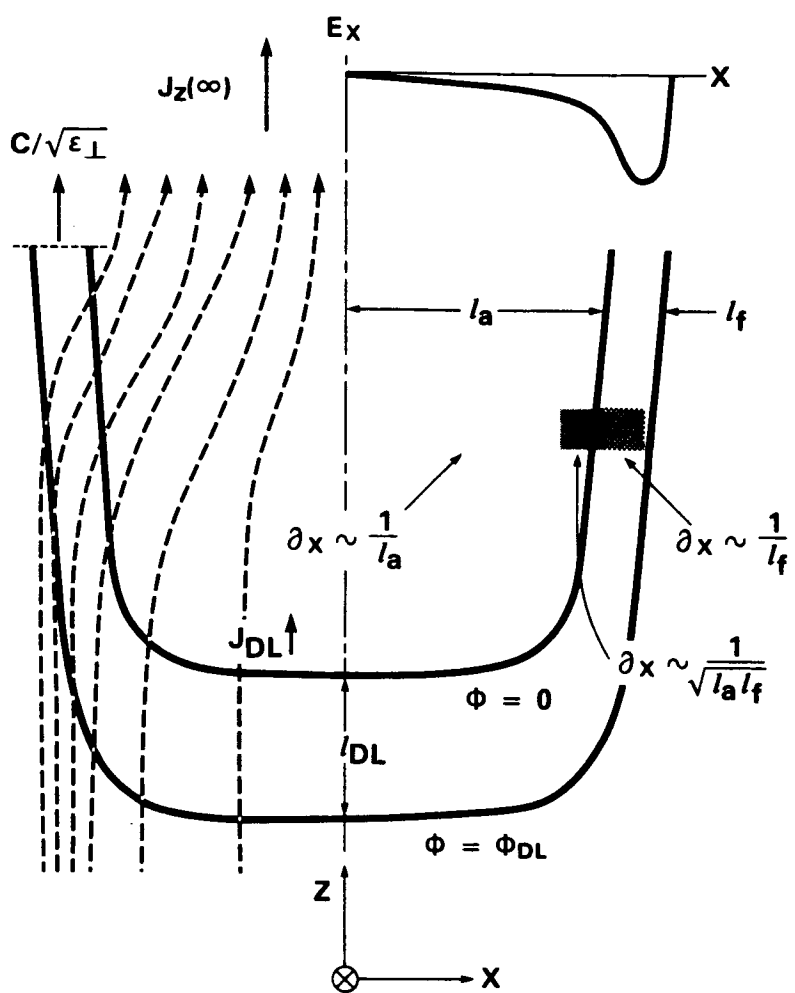
Figure 3. Left side: Schematic of the current diversion in the discrete arc. Right side: Definition of the scale lengths of the arc (ℓ_a) and flank (ℓ_f) and the associated scale factors which are used in the text to replace perpendicular derivatives. Also shown is a sketch of the inhomogeneous electric field E_x, which produces relative drift between the electrons and ions owing to finite-Larmor-radius effects, and the definition of the xyz coordinate system. The magnetic field $\mathbf{B_o} = -B_o\mathbf{e_z}$.
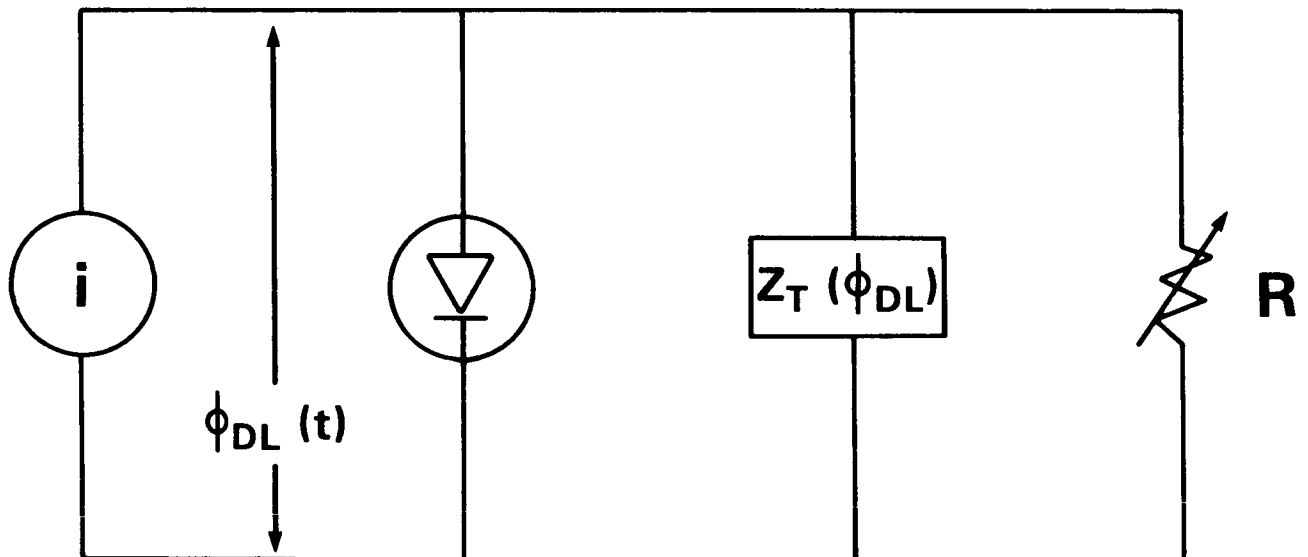
Figure 4. Model circuit used to provide the current density boundary condition in one-dimensional DL simulation.
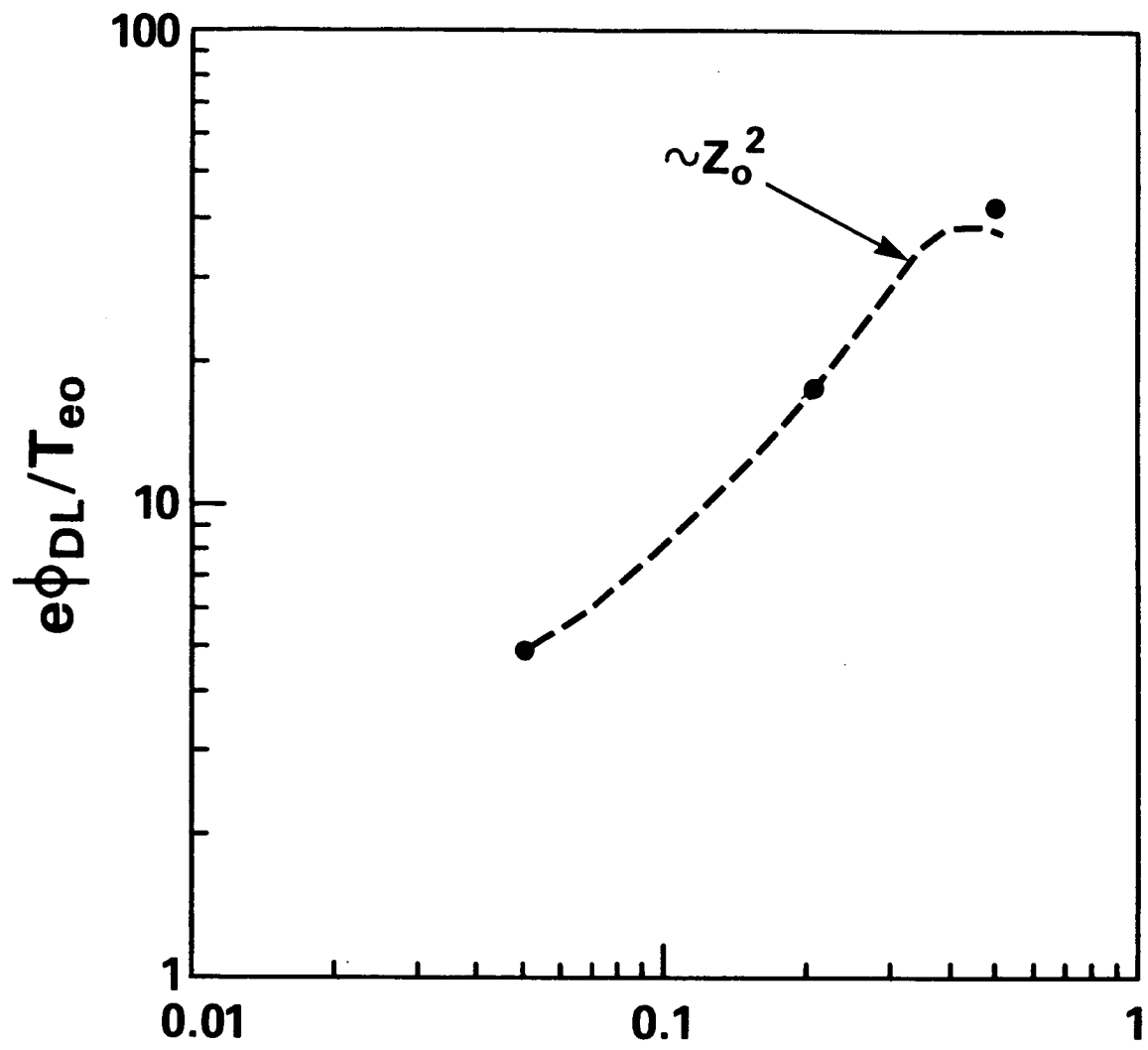
Figure 5. Scaling of the DL potential ϕ_{DL} with the fundamental parameter α of the anomalous transport mechanism. The dashed curve is arbitrarily normalized to the point at $\alpha = 0.2$.
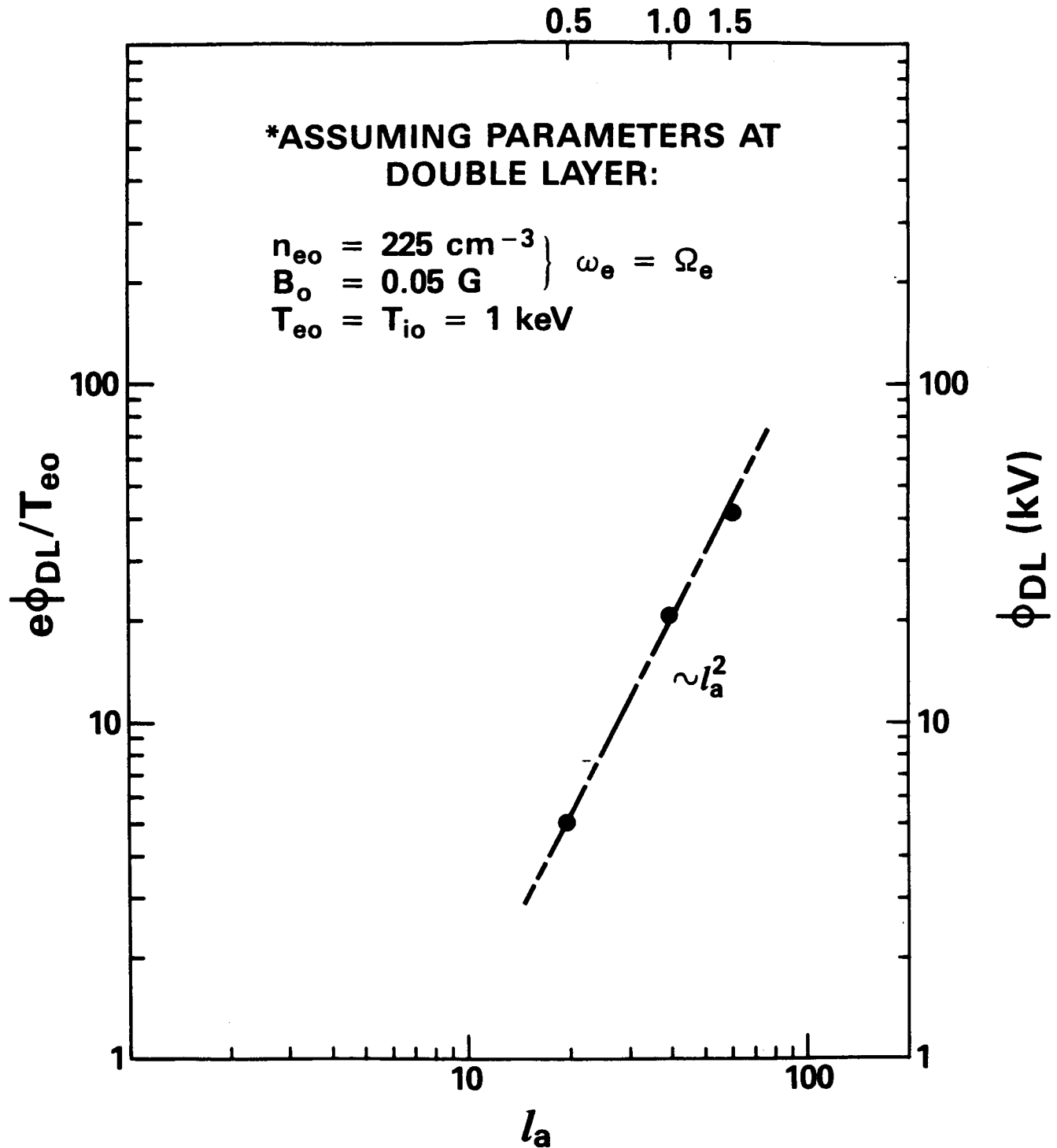
Figure 6. Scaling of ϕ_{DL} with the perpendicular scale width ℓ_a of the arc model. The bottom and left scales are dimensionless. The right scale shows the potential in kV for assumed $T_{eo} = 1$ keV; the top scale shows the arc dimension ($2\ell_a$) projected into the ionosphere, for the given ambient parameters (before DL formation).
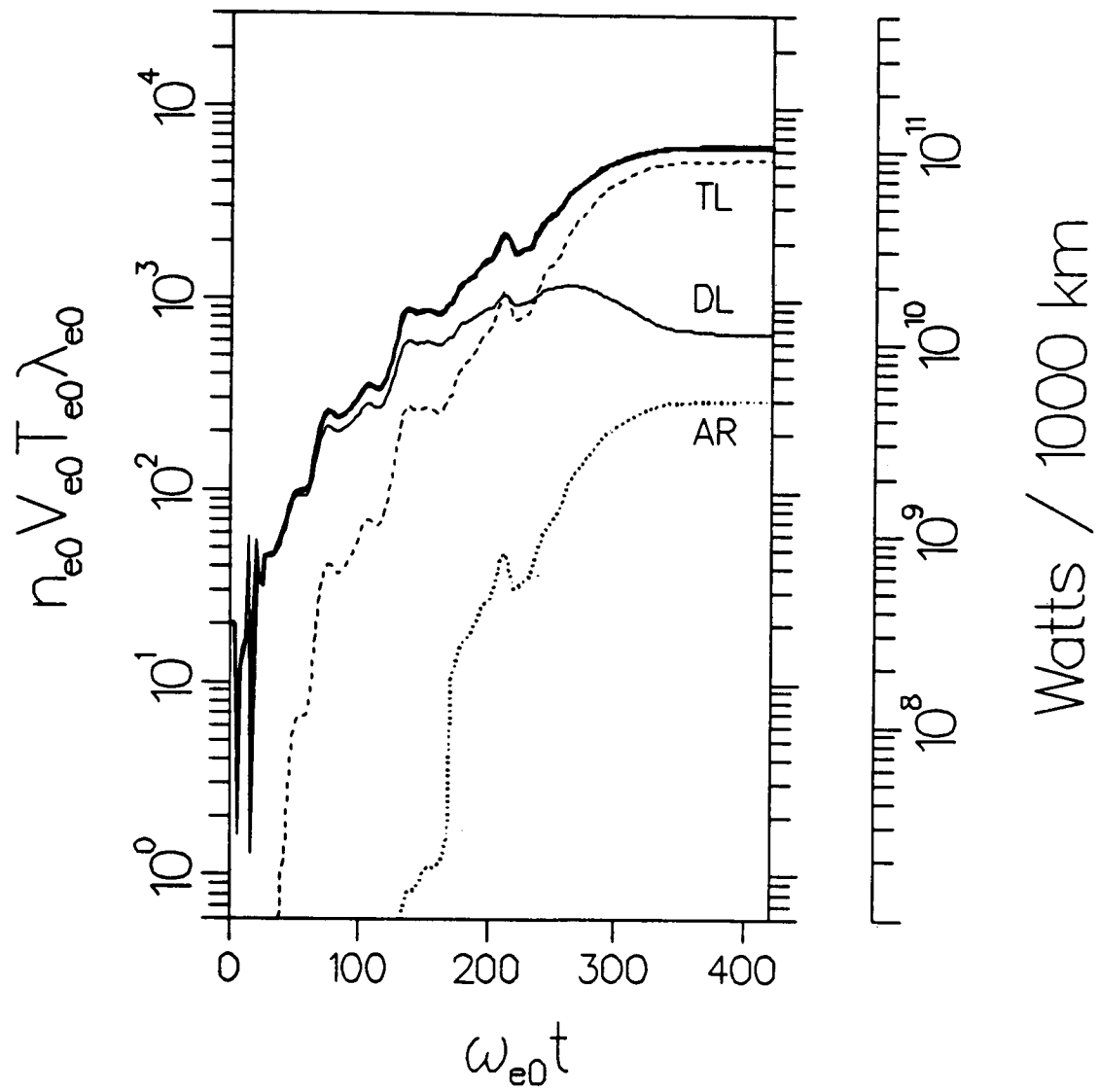
Figure 7. Time history of power flows through the various circuit elements for run 8606 ($e\phi_{DL}/T_{eo} = 42.5$). TL – transmission line (flank) impedance; DL – double layer; AR – anomalous resistivity (leakage) in flank. The right-hand scale shows the physically scaled power for an arc extended 1000 km in the E-W direction.

WEAK DOUBLE LAYERS IN THE AURORAL IONOSPHERE

M. K. Hudson, T. L. Crystal, and W. Lotko
Physics and Astronomy Department
Dartmouth College
Hanover, New Hampshire 03755, U.S.A.

and

C. Barnes
Los Alamos National Laboratory
Los Alamos, New Mexico 87545, U.S.A.

ABSTRACT

Previous work on the evolution of weak double layers in a hydrogen plasma has been extended to include H^+ and O^+ with relative drift. It has been shown (Bergmann and Lotko, 1986) that the relative drift between hydrogen and oxygen ions due to a quasi-static parallel electric field gives rise to a strong linear fluid instability which dominates the ion-acoustic mode at the bottom of the auroral acceleration region. This ion-ion instability can modify ion distributions at lower altitudes and the subsequent nonlinear evolution of weak double layers at higher altitudes in the ion-acoustic regime. We have found that ion hole formation can occur for smaller relative electron-ion drifts than seen in previous simulations, due to the hydrogen-oxygen two-stream instability. This results in local modification of the ion distributions in phase space, and a partial filling of the valley between the hydrogen and oxygen peaks, which would be expected at higher altitudes on auroral field lines. It is shown that the observed velocity diffusion does not necessarily preclude ion hole and double layer formation in hydrogen in the ion-acoustic regime. These simulation results are consistent with the experimentally measured persistence of separate hydrogen and oxygen peaks, and the observation of weak double layers above an altitude of 3000 km on auroral field lines.

I. INTRODUCTION

Weak double layers with potential jumps comparable to the electron thermal energy have been observed to form in one-dimensional (Sato and Okuda, 1980) and two-dimensional (Barnes et al., 1985) electrostatic particle simulations; the double layer formation is driven by an electron drift relative to ions which is unstable to the ion-acoustic mode but is less than the electron thermal speed. Such weak double layers have been observed in space in the auroral particle acceleration region (Temerin et al., 1982), and in laboratory plasmas (Chan et al., 1984; Sekar and Saxena, 1985; Chan, 1986). Thus far, theoretical efforts at understanding weak double layer formation have focussed on a single ion species, while it is known from space observations that weak double layers occur in regions of upward flowing hydrogen and oxygen of ionospheric origin. A quasi-static parallel electric field has been postulated to explain the observed particle distributions (Chiu and Schulz, 1978; Lyons, 1980). While the existence of such a field will remain a zeroeth order assumption in the present paper, we will also examine non-adiabatic modifications of the particle distributions at the bottom of the acceleration region which may affect weak double layer evolution further up the field line, and the stability of the assumed quasi-static field.

We will first briefly review previous work on weak double layer evolution in a hydrogen plasma, and then extend our simulations to include a relative drift between hydrogen, oxygen, and electrons which occurs, for example, in a mirror-supported parallel electric field. Our purpose is to examine the nonlinear effects of the resulting hydrogen-oxygen two-stream instability (Bergmann and Lotko, 1986) on the particle distributions, and consequences for double layer formation further up the field line.

225

III. WEAK DOUBLE LAYER FORMATION IN A HYDROGEN PLASMA

Barnes et al. (1985) showed in a series of one- and two-dimensional, bounded and periodic particle simulations that weak double layers with potential jumps comparable to the electron thermal energy form when the system is driven by an electron drift relative to ions which is less than the electron thermal speed, e.g., $V_d = 0.5 - 0.7 \, a_e$, and an electron to ion temperature ratio $T_e/T_i >> 1$. The electron drift was maintained by injection of electrons from the boundaries at a continuous rate in bounded runs, and by applying a weak electric field uniformly across the system in periodic runs.

Sato and Okuda (1980) first studied the occurrence of weak double layers in a one-dimensional periodic system in which electrons are given an initial drift that subsequently decays. They found that it was necessary to use a long system, $L > 256 \, \lambda_D$ (Debye lengths), in order for weak double layers to form in periodic runs. Our subsequent interpretation (Barnes et al., 1985) is that long periodic systems are required to prevent electron recycling from the low to high potential side, which neutralizes the double layer. Electron injection boundary conditions eliminate this problem in bounded simulation runs, and a weak applied electric field acts to impede electron recycling in periodic runs; both of these simulation techniques allow shorter system lengths.

Figure 1 from Barnes et al. (1985) shows the temporal evolution and recurrence of weak double layers in a one-dimensional system with electron injection boundaries. Ion-acoustic turbulence evolves, for $V_H = 0.5 \, a_e$ and $T_e/T_i = 50$, into a discrete localized pulse which propagates into the system initially at the sound speed. The pulse is characterized by a negative potential dip which amplifies by momentum exchange with reflected electrons (Lotko, 1983; Chanteur et al., 1983); the asymmetic reflection of electrons results in a potential jump downstream. As the negative potential dip grows, it traps ions, slowing down the pulse via mass loading until an effective Bohm criterion for existence of the double layer potential jump is no longer met. The latter requires that ions flow into the high potential side at or near the sound speed (Chen, 1974), achieved here by motion of the pulse in the ion frame. The potential jump then decays and ion holes (Chan, 1986) or ion-acoustic solitons (Sato and Okuda, 1981) propagate away from the high potential side to seed new double layer formation. The decaying ion hole, still apparent in phase space, recoils backward as it moves downward through the ion distribution.

Barnes et al. (1985) examined the persistence of weak double layers in two-dimensional magnetized simulations. Electron injection boundary conditions produce one-dimensional double layers which are roughly uniform across the system in the direction perpendicular to **B**. To examine the transverse scale, a doubly periodic system with a weak electric field imposed uniformly along **B** was employed. The magnitude of the electric field was such that the corresponding potential drop across the system was less than the electron thermal energy, or $eE_o/T_e = 0.6/160 \, \lambda_D$. Figure 2 shows transverse localization of weak double layers for strongly magnetized electrons ($\omega_{ce}/\omega_{pe} = 3$ is the ratio of electron gyro to plasma frequency). The transverse dimension appears to decrease with increasing magnetic field strength, scaling with $\sqrt{\lambda_D^2 + \rho_s^2}$, where λ_D is the Debye length and ρ_s is the ion gyroradius at the electron temperature. The parallel scale length remains the order of tens of Debye lengths, as in one-dimensionality. Ion-acoustic turbulence becomes homogeneous and does not evolve into localized weak double layers in weakly magnetized ($\omega_{ce}/\omega_{pe} < 1$) periodic systems. One therefore might expect to see such structures in the auroral acceleration region, but not, for example, in the solar wind.

226

IV. ION HOLES IN MULTIPLE ION SPECIES PLASMAS

To the double layer evolution problem we would now like to add the effects of multiple ion species, H^+ and O^+, with relative drift. This introduces an important complication noted by Bergmann and Lotko (1986). A quasi-static parallel electric field produces a relative drift between ionospheric hydrogen and oxygen ions which have been accelerated through the same potential drop, such that $V_H/V_O = \sqrt{M_O/M_H} = 4$. This situation is fluid unstable for parallel propagating modes when the relative H^+-O^+ drift exceeds a minimum, determined primarily by ion Landau damping, up to a maximum value that is less than about twice the hydrogen sound speed $C_s = \sqrt{T_e/M_H}$. This indicates that the ion two-stream instability (for parallel propagating waves) will be confined to the bottom of the acceleration region, since at higher altitudes the relative drift will exceed the upper bound for instability. It is likely, although it has not yet been demonstrated, that obliquely propagating modes may still be unstable for drifts exceeding this upper bound. The growth rate for the ion two-stream instability is larger than that for typical (electron-ion) current-driven instabilities, and one might expect significant modifications of the hydrogen and oxygen distributions to occur. In particular, the unstable ion two-stream waves have phase velocities lying between the hydrogen and oxygen distributions, and one might expect some quasi-linear filling, that is to say, formation of tails on the high and low velocity sides of oxygen and hydrogen, respectively. This quasi-linear filling could, in turn, affect the ion-acoustic instability and double layer evolution at higher altitudes, when ion drifts relative to electrons become a significant fraction of the electron thermal speed, as required for double layer formation in hydrogen plasma simulations. The instability analysis and simulations require knowledge or assumptions about the electron distribution in the region of interest. Bergmann and Lotko (1986) have integrated the electron distribution functions, $F(v_\parallel, v_\perp)$, in the Chiu-Schulz (1978) equilibrium model of a mirror-supported electric field to obtain an effective one-dimensional distribution, $f(v_\parallel)$. These electron populations include precipitating magnetospheric electrons, primary and secondary backscattered electrons, and those electrons which are trapped between the magnetic mirror below and retarding electrostatic potential above. At an altitude relevant to the ion two-stream instability, the bulk of ionospheric electrons has been retarded at lower altitudes by the potential drop which produces the relative ion drifts. The sum of the remaining electron populations, shown in Figure 3, is essentially a stationary Maxwellian with a precipitating electron tail. Also shown in the figure is a Maxwellian fit for the first three moments as described by Bergmann and Lotko.

We would like to examine the spatial evolution of the ion distribution functions along the geomagnetic field line at various distances above the bottom of the acceleration region (nominally at an altitude of 2000 km in Chiu and Schulz, 1978), including the ion two-stream unstable regime near the bottom on up to altitudes where the ion drifts become comparable to the electron thermal speed, and where double layers have been observed (>3000 km altitude). Since our computer resources limit the simulation system to lengths less than or the order of 1000 Debye lengths, we examine instead a temporal evolution problem which differs from the spatial evolution problem in at least one respect. In the spatial evolution case, the ratio of the H^+/O^+ bulk drift velocity is $\sqrt{M_O/M_H}$, as oxygen and hydrogen are accelerated to the same energy as a function of potential at a given altitude. In steady state at a fixed altitude there will be a continuous flow of oxygen and hydrogen whose drifts differ by a factor of 1 to 4, respectively, but the hydrogen and oxygen ions passing that altitude at a fixed time will not leave the bottom of the acceleration region simultaneously, since hydrogen flows up the field line faster. This follows from the relation

$$e\phi = 1/2\, M_H V_H^2 = 1/2\, M_O V_O^2 \quad ,$$

(1)

which holds at any given altitude where the potential is $e\phi$. Alternatively, in a simulation system evolving in time with a uniformly applied E_o, the ion velocity varies as

$$V_i = \frac{eE_o t}{M_i}$$

which results in an H^+–O^+ velocity of M_O/M_H, rather than $(M_O/M_H)^{1/2}$. Furthermore, depending on the strength of the applied electric field E_o, the ions may accelerate so rapidly that the upper limit on the relative drift for the ion two-stream instability may be exceeded before nonlinear saturation can occur. In such a case, we would not see the full effects of wave-particle interactions on the ion distributions.

With these caveats in mind, we performed a series of one-dimensional electrostatic simulations using the particle code ES1 (Birdsall and Langdon, 1984), in a periodic system of length 240 λ_D, using 16,000 hydrogen and 16,000 oxygen ions and 32,000 electrons. We varied the uniform applied electric field from $eE_o/T_e = 0$, $1.2/240 \lambda_D$ to $2.4/240 \lambda_D$ and applied it only to the ions in order to simulate the approximately stationary electron Maxwellian (Fig. 3) through which the outflowing ions accelerate. We did initial value runs with $V_H = V_O = O$ at $t = O$ and runs which were initiated with V_H and V_O in the range where the ion two-stream growth rate peaks.

Figure 4 shows the nonlinear evolution of the ion two-stream instability for initial drifts $V_H = 1.2\, C_s$ and $V_O = 0.3\, C_s$ and a uniform applied electric field $eE_o/T_e = 2.4/240 \lambda_D$. The electron-to-ion temperature ratio is $T_e/T_i = 20$ and the mass ratios are $M_H/M_e = 50$ and $M_O/M_H = 8$. The choice of drifts $V_H/V_O = 4$ is intermediate between the spatial evolution case where $V_H/V_O = \sqrt{M_O/M_H} = 2\sqrt{2}$ and the temporal evolution case where $V_H/V_O = M_O/M_H = 8$ for our mass ratio. Variations about this set of parameters are discussed below. One observes the formation of a localized fluctuation in the potential similar to that seen in the previously described (single ion) simulations at a time when the hydrogen drift relative to electrons is $V_H = 0.2$-$0.3\, a_e$. This drift is smaller by a factor of 2 than in the single ion runs previously shown. The localized wave is a result of the nonlinear evolution of the ion two-stream instability which occurs at lower relative drifts (V_H-V_O) than the current-driven, ion-acoustic instability. The potential pulse is subsonic in the ion frame, and appears to propagate with the ions out the right-hand boundary and re-enter on the left. Periodicity of the system allows one to see that the pulse is continuous from the right through the left boundary of an adjacent frame, since the pulse has not moved much from frame to frame. (The frames are separated in time by 60 ω_{pe}^{-1}.) A significant localized potential jump $e\phi/T_e \gtrsim 1$ develops, but does not persist as far downstream as in cases where the relative electron-ion drift is larger (Fig. 11). We therefore hesitate to call this structure a double layer when the system is in the ion two-stream unstable regime, although its features are very similar to those shown in Figure 1, when translated to a frame in which electrons are stationary and ions drift. One sees trapping of hydrogen and oxygen on the sides of the distribution functions corresponding to the phase velocities of the (ion two-stream) unstable waves, namely the low velocity side of hydrogen and the high velocity side of oxygen. It seems appropriate to call this structure an ion hole.

We observed ion hole formation in the ion two-stream unstable regime for a range of parameters summarized in Table 1. The ion two-stream instability was observed over a broader range of parameters (Bergmann and Lotko, 1986) than was ion hole formation, which apparently requires large amplitude waves and occurs only for sufficiently rapid linear instability. Recall that the ion two-stream instability is limited in duration as the electric field accelerates ions into and out of the range of linearly unstable drifts. Ion hole formation did not occur in runs 2-4 until the hydrogen bulk was accelerated to 0.2-0.3 a_e. In run 6, with no applied electric field but the same initial drifts as run 3, ion hole formation was not observed. In run 7, also with no electric field, but with initial drifts in the range produced by the electric field in run 3 at the time ion hole formation was observed, an ion hole forms. Sato and Okuda (1980) saw weak double layer formation in a system 256 λ_D long but not in one 128 λ_D long. Our system length of 240 λ_D is marginally long enough to allow a double layer to form in the absence of an applied electric field before periodic electron cycling neutralizes the evolving double layer space charge. We also did a run (8) using a bounded one-dimensional electrostatic code, PDW1 (Lawson, 1984), with constant particle injection maintained by an external circuit and floating potential at both ends of the system, but with parameters otherwise the same as in run 7. Ion hole formation in runs 7 and 8 is comparable, as shown in Figure 5.

In order to address the temporal evolution question, we performed two runs (9 and 10) with two different values of the applied electric field, $eE_0/T_e = 1.2, 2.4/240 \lambda_D$, no initial ion drifts, and periodic boundary conditions. Ion hole formation was evident but weaker for the larger electric field (run 9) than in the initial drift case (e.g., run 3), and absent for the weaker electric field (run 10) when compared at time such that $C_s < V_H\text{-}V_O < 2 C_s$. Some ion heating occurs in the initial value runs (9 and 10) before the relative drifts are comparable to the initial drift runs, i.e., optimum for ion two-stream instability. In initial value runs the hydrogen and oxygen ion distributions separate more quickly than in the case of spatial evolution, and so spend less time in the range of unstable relative drifts, $V_H - V_O \lesssim 2 C_s$. The maximum growth rate of the two ion-stream instability is the order of $\gamma/\omega_{pe} \sim 10^{-2}$ (Bergmann and Lotko, 1986, Fig. 3) for the k modes in our simulation system of length $240 \lambda_D$ and grid size $0.5 \lambda_D$. Both initial value (run 9) and initial drift (run 3) cases remain in the range of unstable drifts $V_H\text{-}V_O \sim 1.2\text{-}2 C_s$ a number of e-folding times, but there appears to be some difference between initializing the system in the linearly unstable regime and evolving through it. In the auroral problem, one expects spatial evolution and weaker electric fields, discussed below, to separate the drifts more slowly relative to the linear growth time.

The question arises whether ion heating by the ion two-stream instability, evident in Figure 4, will affect double layer evolution at higher altitudes where the ion drift relative to electrons is larger. Figure 6 shows the initial ion and electron distributions for runs 9 and 10. Figure 7 shows the same distributions for run 9 at the time an ion hole is beginning to form, while Figure 8 shows the same distributions at a later time when the hydrogen drift is becoming significant relative to electrons. Figure 9 shows the particle distributions in the weaker electric field case at a time when the drift is the same as Figure 7. We would conclude from this set of figures tht there is no major modification of the hydrogen and oxygen distributions by the ion two-stream instability, which is present in runs 9 and 10. There is some heating on the low velocity side of hydrogen and the high velocity side of oxygen, as expected, in the range of unstable ion two-stream phase velocities. Figure 10, a similar plot for run 3 which showed ion hole formation at large trapping amplitudes ($e\phi/T_e \sim 1$), indicates more heating between the hydrogen and oxygen distributions. This plot exhibits distribution functions which are spatially averaged across the whole system, and it is the case that the plateau evident in hydrogen (and oxygen) is due primarily to the spatially localized ion hole evident in Figure 3. It is questionable to call this heating versus localized ion trapping since it is not uniform across the system. It therefore seems reasonable to conclude that in our simulation system the hydrogen and oxygen average distributions are not so greatly modified by the ion two-stream instability as to preclude ion-acoustic instability and double layer formation at larger ion drifts relative to electrons.

IV. ION-ACOUSTIC DOUBLE LAYERS IN AN O^+-H^+ PLASMA

As hydrogen and oxygen continue to accelerate up the geomagnetic field line out of the region of ion two-stream instability, hydrogen eventually acquires a drift relative to electrons comparable to the electron thermal speed. If the hydrogen velocity distribution has not been too greatly modified by the ion two-stream instability, as our preceding results indicate, we might expect double layers to evolve from the electron-hydrogen acoustic instability, as described by Barnes et al. (1985), as long as oxygen and hydrogen remain well separted. To test this, we did a series of simulations at large electron drifts ($0.7\text{-}0.9\, a_e$) in the oxygen frame with hydrogen drifting at -0.2 C_s. Electron injection boundary conditions were employed as in Barnes et al. (1985), in a system 512 λ_D long, containing 8000 ions of each species and 16,000 electrons. More realistic mass ratios, $M_H/M_e = 1000$ and $M_O/M_H = 10$, were used. Oxygen was kept cold relative to electrons, $T_e/T_O = 100$, and two cases were examined for hydrogen: $T_e/T_H = 20$ corresponding to no significant heating of hydrogen by the ion two-stream instability at lower altitudes, and $T_e/T_H = 2$ where significant heating has occurred. The assumption that electrons are hotter than ions is justified by the altitude where weak double layers have been observed (>3000 km), since the large scale parallel electric field restricts colder electrons to lower altitudes. No electric field was applied in these bounded runs.

Figure 11 shows the hydrogen and oxygen distributions and potential at a time when one and possibly a second double layer are forming with hole(s) evident in hydrogen phase space. Oxygen responds more slowly and appears to play a passive role in the double layer formation, but eventually forms a hole in ion-phase space by the time hydrogen has undergone significant heating and the double layer is disappearing (Fig. 12). In a similar run with $T_e/T_H = 2$, a hole does not appear to form in hydrogen but is evident in oxygen at later times. This result is consistent with Schamel's (1982) criterion that ion holes do not form for $T_e/T_i < 3.5$ (see also Hudson et al., 1983). An oxygen ion hole and weak double layer appear to form when the hydrogen is heated too much to support such a structure. Should the hydrogen be significantly heated and the oxygen remain cool, a hole can still form in oxygen in association with an electron -O^+ drift instability at phase velocities between the electron and O^+ peaks.

V. APPLICATION TO THE AURORAL REGION

A number of caveats are in order before applying the foregoing simulation results to the auroral particle acceleration region. We have examined separately two regimes: (1) where the two ion-stream instability operates at low relative ion drifts (<2 C_s) produced by a quasi-static parallel electric field near the bottom of the acceleration region, and (2) ion-acoustic double layer formation at higher altitudes where relative electron-ion drifts are larger and the ion distributions will have undergone some heating at lower altitudes. We have restricted our analysis to parallel propagating modes and one-dimensional simulations in the present paper. It is likely that oblique modes will affect the ion distributions. Kaufmann et al. (1986) have examined the stability of hydrogen and oxygen beams measured by the S3-3 and DE 1 satellites and concluded that oblique modes are unstable. It may also be the case that the upper limit on relative drift for the ion two-stream instability is relaxed for oblique modes, since $\hat{k} \cdot (V_H - V_O) < 2$ C_s for larger relative ion drifts when k is oblique. The linear instability of oblique modes is under investigation by Bergmann (private communication, 1986). Barnes et al. (1985) showed that ion-acoustic double layers evolve in the presence of oblique (EIC) modes in two-dimensionality with behavior similar to the one-dimensional case. We plan to extend the present multi-ion studies to two-dimensional in the future.

Another qualification to our conclusions is the strength of the electric field used in the initial value simulations. The values of $eE_o/T_e = 1.2$-$2.4/240$ λ_D correspond to 5-10 mV/m for $\lambda_D = 10$ m, $T_e = 10$ eV, and $n_e = 10$ cm^{-3}. These are not large parallel electric fields compared with observations in the acceleration region (Temerin, private communication, 1986), but are larger than the mirror-supported fields calculated by Chiu and Schulz (1978) which maximize at $E_o < 0.5$ mV/m near the bottom of the acceleration region.

It is somewhat difficult to extrapolate from the temporal evolution approach taken in this paper to the spatial evolution of ion distributions along auroral field lines. Nonetheless, with the neglect of oblique modes and use of somewhat large electric fields, and/or initializing the simulations with unstable drifts, and preheated ions in the ion acoustic regime, we find the following:

1. Ion holes form in the ion two-stream unstable regime at relatively low drifts compared with those required to form ion-acoustic double layers. They occur in systems with and without an applied electric field, but over a narrow range of relative hydrogen-oxygen drifts.

2. The ion two-stream instability does not appear to greatly modify the ion distributions, except locally in the presence of a large amplitude ($e\phi/T_e \sim 1$) ion hole.

3. Double layer evolution should proceed at higher altitudes as previously described in the ion-acoustic regime, with holes forming in hydrogen, and oxygen responding passively.

230

There are two pieces of experimental evidence supporting our conclusion that hydrogen and oxygen distributions are not so greatly modified at lower altitudes by the ion two-stream instability as to preclude double layer formation at higher altitudes.The first is the set of particle measurements from the S3-3 and DE 1 satellites analyzed by Kaufmann et al. (1986) showing well separated H^+ and O^+ peaks, with a slight filling in between the two. The second is the observation of what have been identified as weak double layers by Temerin et al. (1982), also Temerin and Mozer (1986), at altitudes >3000 km in regions of upward ion flows. These observations indicate that the heating of the ion distributions that occurs at lower altitudes is not as great as the relative acceleration, nor enough to make $T_e/T_i \sim 1$, which would preclude ion-acoustic double layer formation.

A number of questions remain to be addressed: Can one design a temporal evolution simulation which better models the spatial evolution problem within the constraints of computer time and memory, e.g., by moving one ion species with an electric field which differs from the other by $\sqrt{M_H/M_O}$ to mimic the spatial case in an initial value problem? What effects do oblique modes and two-dimensionality introduce in the problem? Is it possible to use weaker electric fields and follow the evolution from the ion two-stream through the ion-acoustic double layer regime. These and other questions remain to be addressed in future work on the evolution of weak double layers in the multi-species auroral plasma.

TABLE 1. ION HOLE FORMATION IN THE ION TWO-STREAM
UNSTABLE REGIME

Run	$V_O(0)$ (a_e)	$V_H(0)$ (a_e)	V_H-V_O (C_s)	eE_o/T_e	bc	t (ω_{pe}^{-1})	hole
1	0	0.17	1.2	2.4	per	0	no
2	0.035	0.17	0.95	2.4	per	0	yes
3	0.042	0.17	0.91	2.4	per	0	yes
4	0.049	0.17	0.86	2.4	per	0	yes
5	0.06	0.17	0.78	2.4	per	0	no
6	0.042	0.17	0.91	0	per	0	no
7	0.06	0.30	1.7	0	per	0	yes
8	0.06	0.30	1.7	0	bnd	0	yes
9	0	0	0	2.4	per	0	marginal
10	0	0	0	1.2	per	0	no

Note: Units of eE_o/T_e are $(240 \lambda_D)^{-1}$; bnd and per refer to bounded and periodic boundary conditions (bc).

REFERENCES

Barnes, C., M. K. Hudson, and W. Lotko, *Phys. Fluids, 28,* 1055 (1985).

Bergmann, R. A., and W. Lotko, *J. Geophys. Res.,* in press, 1986.

Birdsall, C. K., and A. B. Langdon, *Plasma Physics via Computer Simulations,* McGraw Hill, New York, 1984.

Chan, C., these proceedings, 1986.

Chan, C., M. H. Cho, N. Hershkowitz,, and T. Intrator, *Phys. Rev. Lett., 52,* 1782 (1984).

Chanteur, G. J., C. Adam, R. Pellat, and A. S. Volokhitin, *Phys. Fluids, 26,* 1584 (1983).

Chen, F. F., *Introduction to Plasma Physics,* Plenum, New York, 1974.

Chiu, Y. T., and M. Schulz, *J. Geophys. Res., 83,* 629 (1978).

Hudson, M. K., W. Lotko, I. Roth, and E. Witt, *J. Geophys. Res., 88,* 916 (1983).

Kaufmann, R. L., G. R. Ludlow, H. L. Collin, W. K. Peterson, and J. L. Burch, *J. Geophys. Res.,* submitted, 1986.

Lawson, W. S., *PDW1 Users Manual,* Memorandum No. UCB/ERL M84/37, University of California, Berkeley, 1984.

Lotko, W., *Phys. Fluids, 26,* 1771 (1983).

Lyons, L. R., *J. Geophys. Res., 85,* 17 (1980).

Sato, T., and H. Okuda, *Phys. Rev. Lett., 44,* 740 (1980).

Sato, T., and H. Okuda, *J. Geophys. Res., 86,* 3357 (1981).

Schamel, H., *Symposium on Plasma Double Layers,* Riso (1982).

Sekar, A. N., and Y. C. Saxena, *Plasma Phys. and Cont. Fusion, 27,* 181 (1985).

Temerin, M., and F. S. Mozer, these proceedings, 1986.

Temerin, M., K. Cerny, W. Lotko, and F. S. Mozer, *Phys. Rev. Lett., 48,* 1175 (1982).
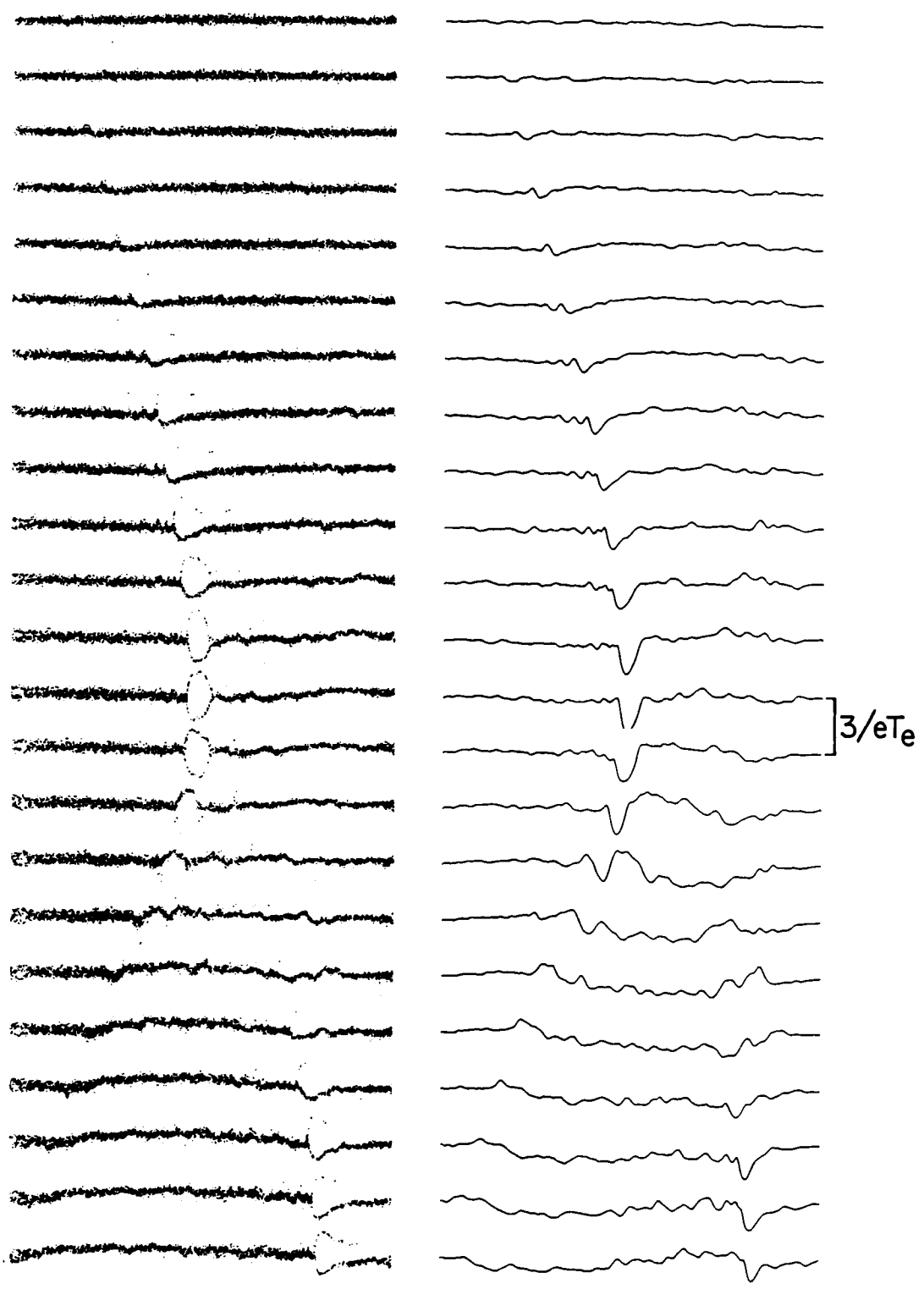
Figure 1. Time series plots of ion-phase space (left) and electrostatic potential (right) for a bounded one-dimensional run with $M/m = 2000$, $T_e/T_i = 50$, and $V_H = 0.5\ a_e$. The snapshots are taken at intervals of 360 ω_{pe}^{-1} (8 ω_{pi}^{-1}) beginning at 1080 ω_{pe}^{-1} (24 ω_{pi}^{-1}) (from Barnes et al., 1985).
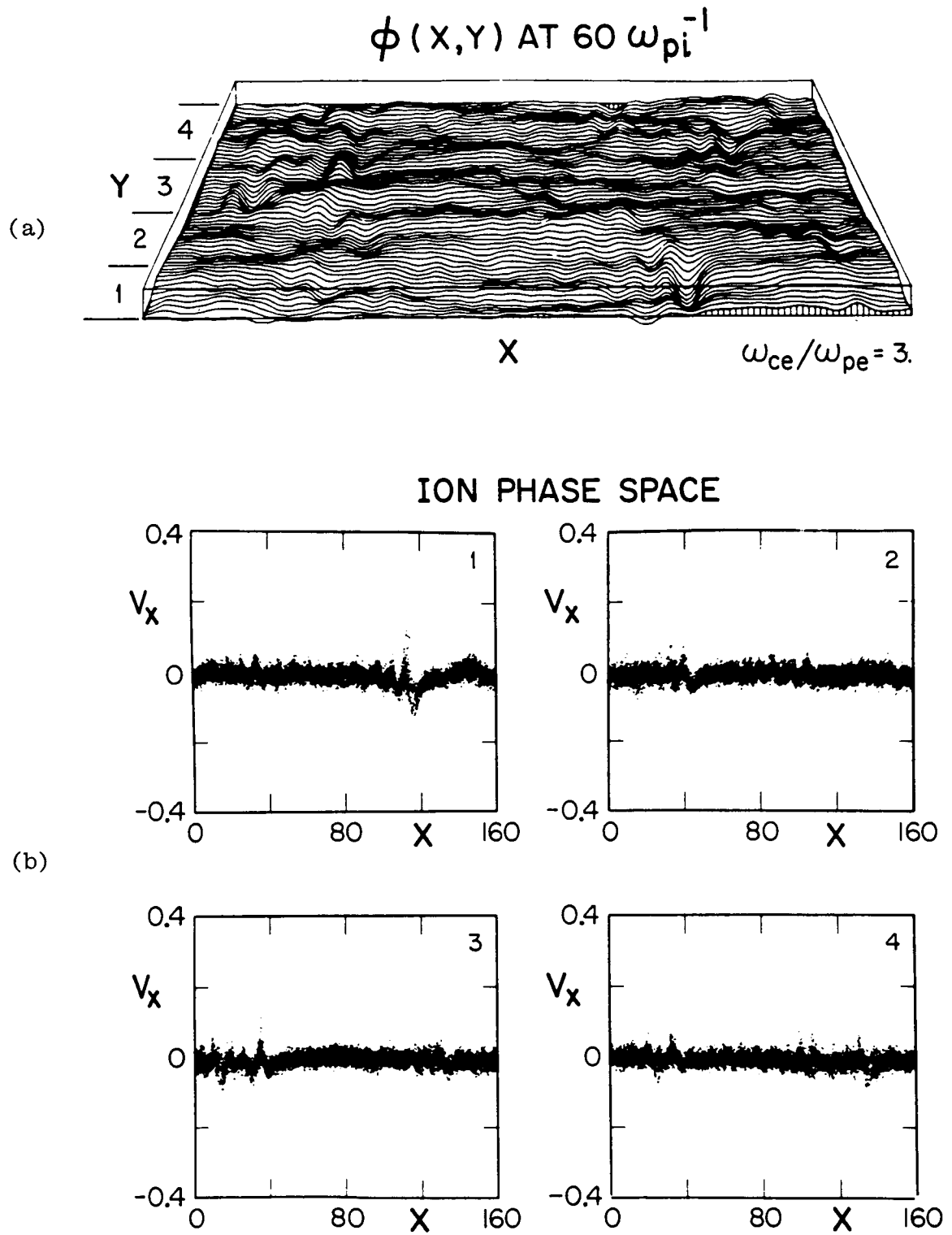
Figure 2. Magnetized doubly periodic system with $\omega_{ce}/\omega_{pe} = 3$ and a weak uniform applied electric field pointing to the left, $eE_o/T_e = 0.6/160 \lambda_d$. (a) Potential profiles are averaged over 4 ω_{pi}^{-1}; (b) ion-phase space v_x versus x is displayed in each of four bands in y. v_x is in units of a_e. The most prominent double layers are in band 1 at $x \approx 120 \lambda_D$ and band 3 at $x \approx 40 \lambda_D$.
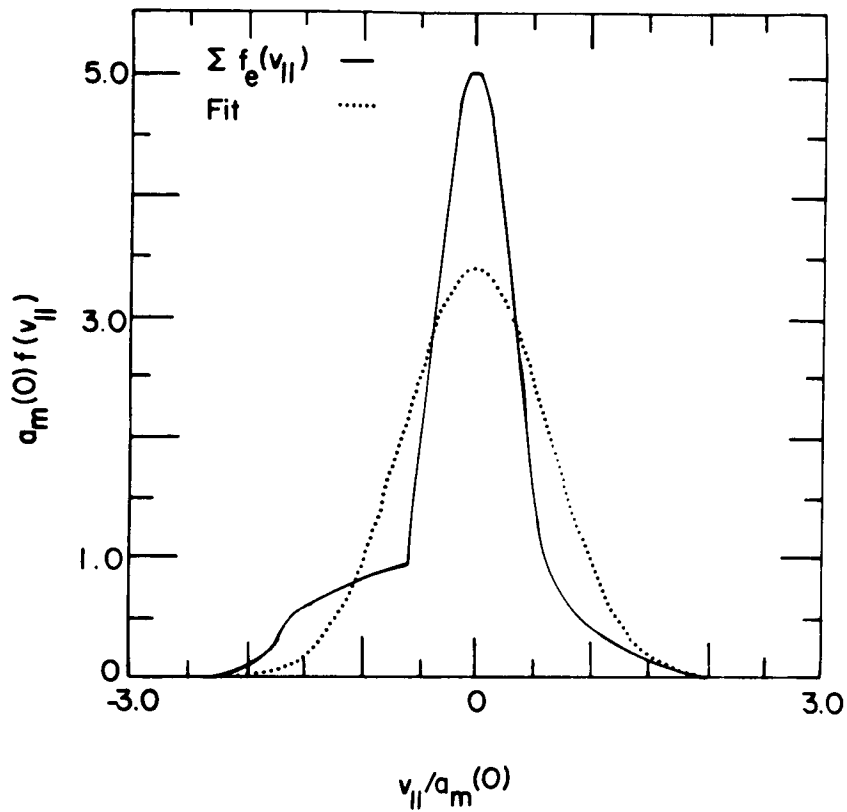
Figure 3. Reduced electron distribution function f(V) for Chiu and Schulz (1978) Model W, at $e\phi/T_c = 110$, where T_c is the cold ionospheric electron temperature. This represents a sum of contributions from magnetospheric, primary and secondary backscattered and trapped electrons, with ionospheric electrons negligible at this value of the mirror potential measured from zero at an altitude of 2000 km (adapted from Bergmann and Lotko, 1986).
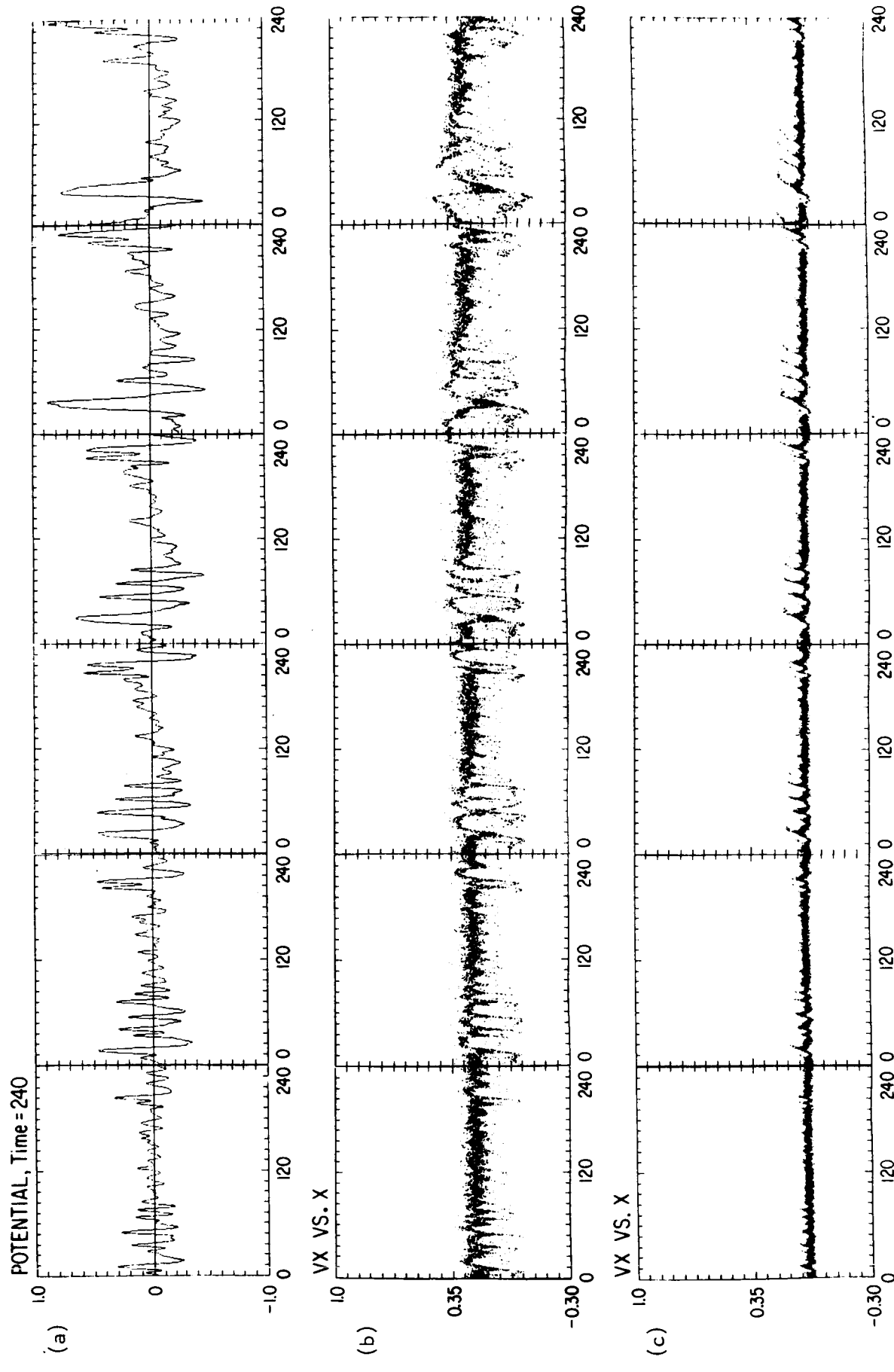
Figure 4. Run 3, Table 1. Time evolution from left to right of (a) the electrostatic potential every $60 \, \omega_{pe}^{-1}$ averaged over $30 \, \omega_{pe}^{-1}$ from $240\text{-}900 \, \omega_{pe}^{-1}$; (b) corresponding hydrogen; and (c) oxygen phase space. The system is $240 \, \lambda_D$ long; timestep $\omega_{pe} \, \Delta t = 0.2$ and other parameters are given in the text.

Figure 4. (Concluded)

POTENTIAL, Time=900

(a)

AVE. POT., T=900

(b)
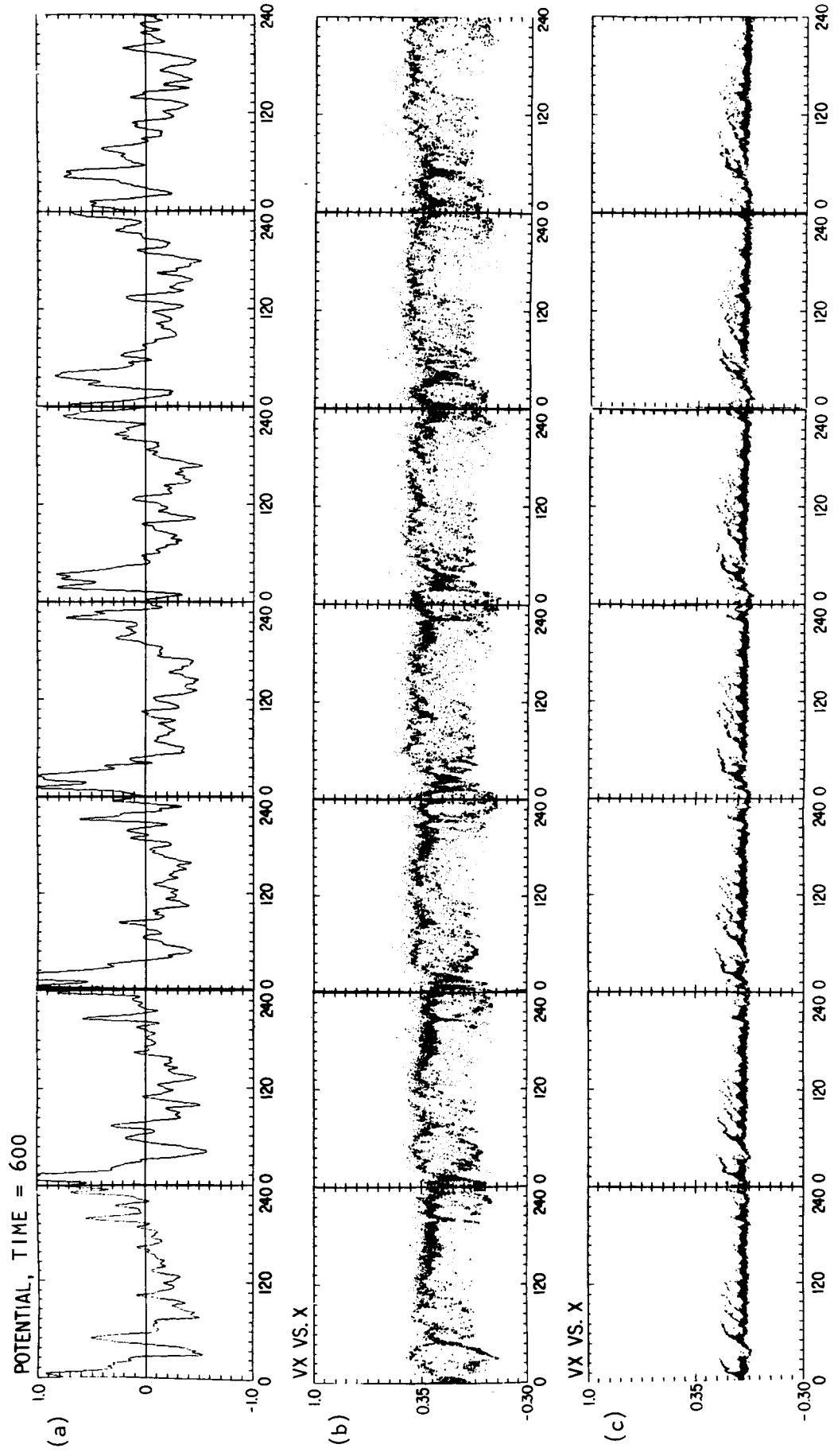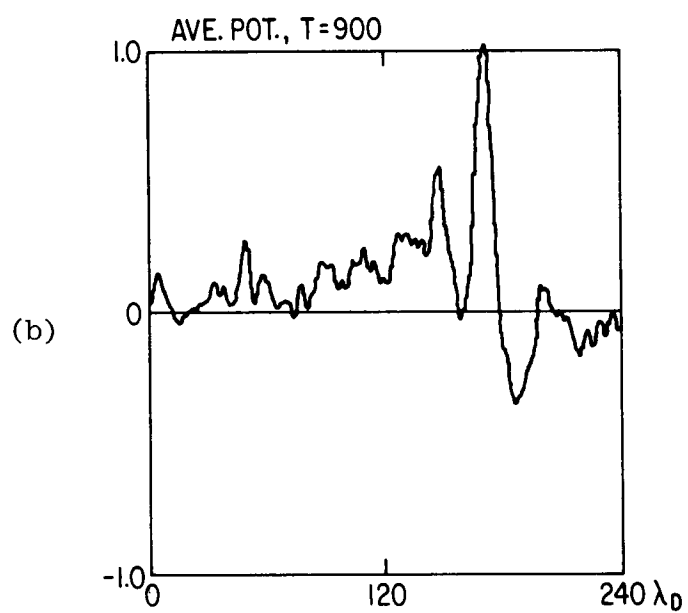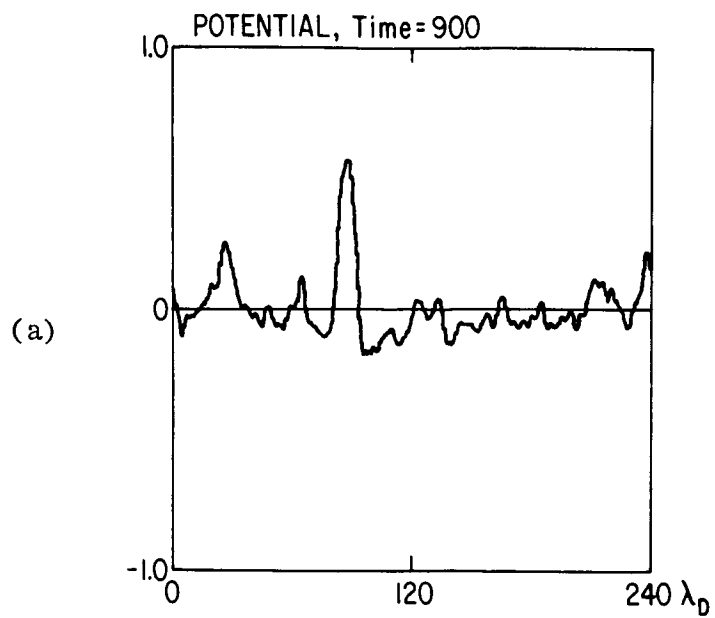
Figure 5. (a) Potential for run 7 at $\omega_{pe} \Delta t = 900$; (b) Potential for run 8 at $\omega_{pe} \Delta t = 900$. Parameters in (a) and (b) are the same, except that (a) was periodic, using ES1, and (b) was bounded using PDW1, with particle injection maintained constant as initialized ($V_H = 0.30$, $V_O = 0.06$, $V_e = 0$ in units of a_e) by an external circuit. All potential plots shown are averaged over 30 ω_{pe}^{-1}.

238
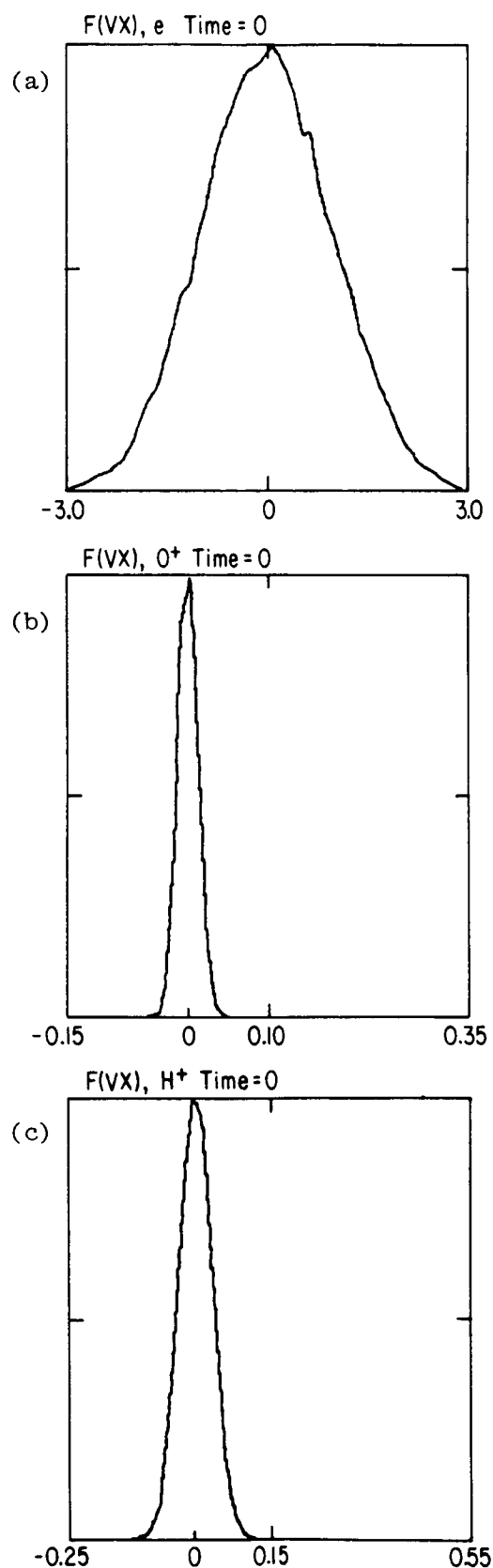
Figure 6. Initial (a) electron, (b) hydrogen, and (c) oxygen distribution functions for runs 9 and 10.
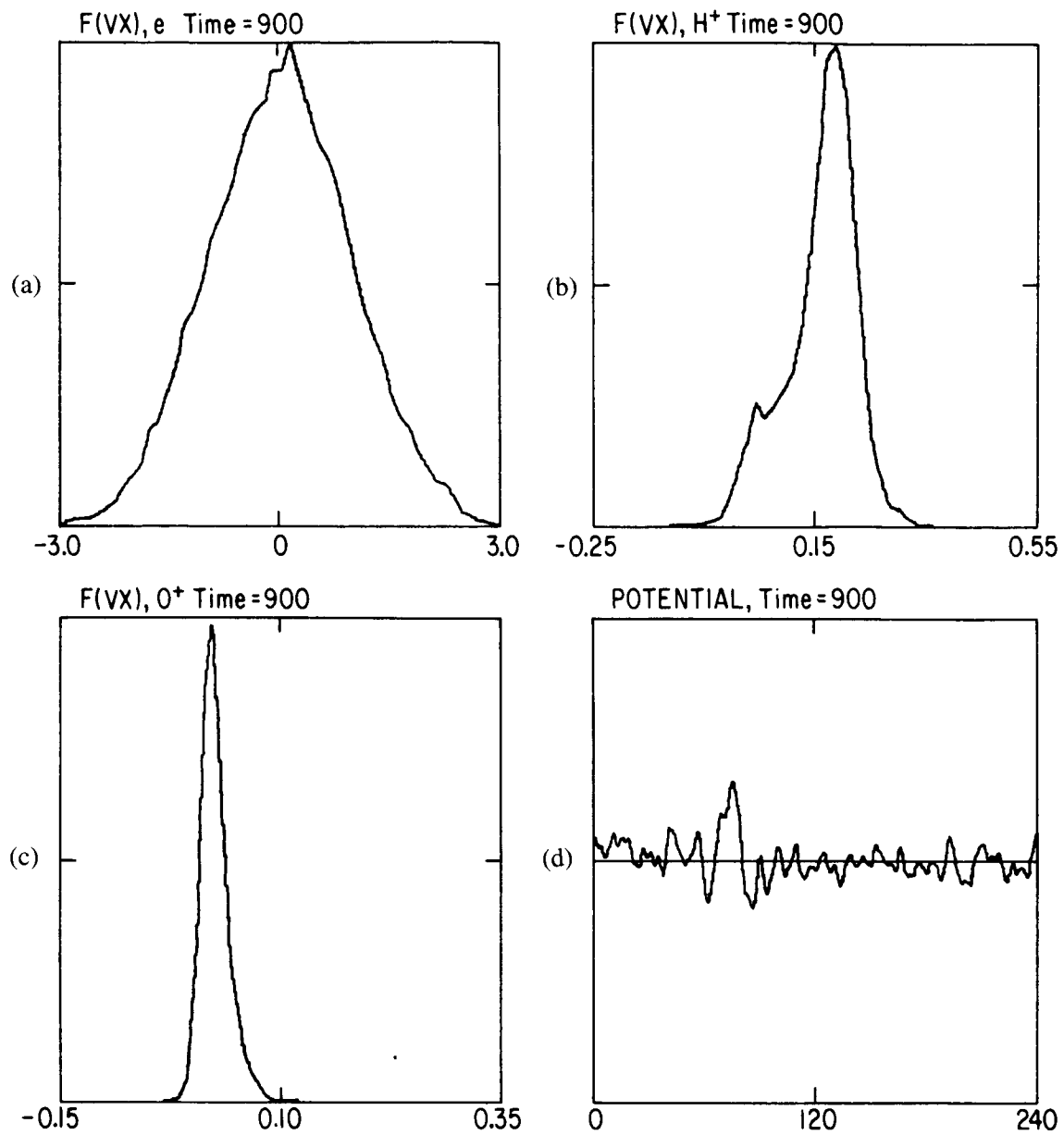
Figure 7. Same plots as Figure 6 for the stronger electric field case $eE_o/T_e = 2.4/240 \lambda_D$, at the time an ion hole is beginning to form, $\omega_{pe} \Delta t = 900$. The potential averaged over 30 ω_{pe}^{-1} is also shown in (d).
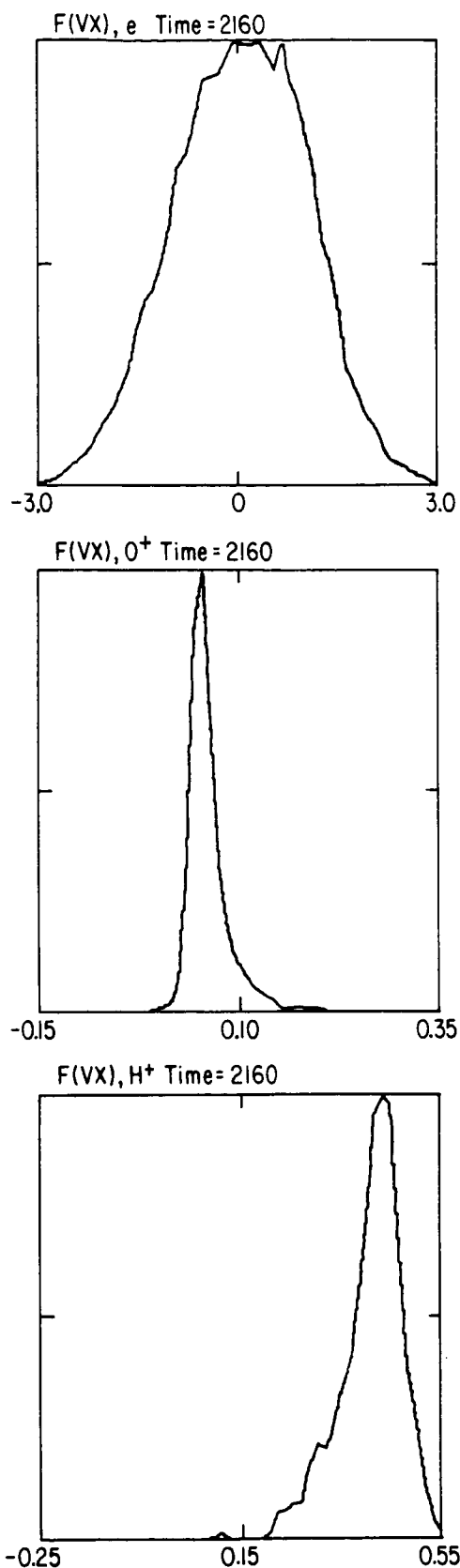
Figure 8. Same plots as Figure 6 for run 9 at $\omega_{pe} \Delta t = 2160$ when $V_H = 0.44\ a_e$ is becoming comparable to Figure 1.
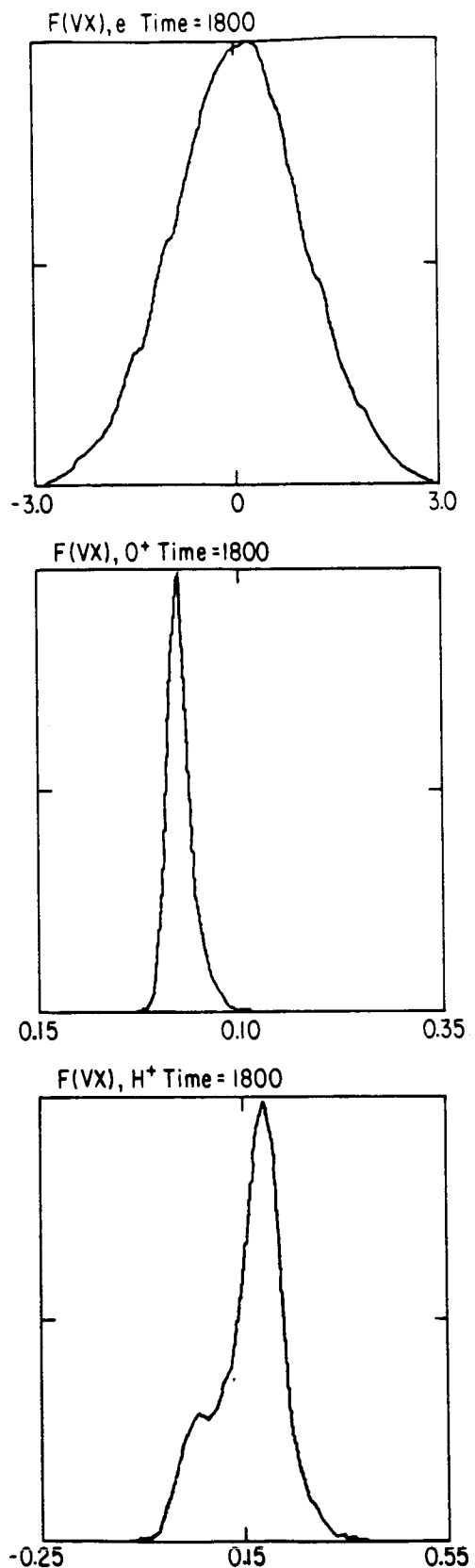
Figure 9. Same plots as Figure 6 for the weaker electric field case, run 10, with $eE_0/T_e = 1.2/240 \lambda_D$, at $\omega_{pe} \Delta t = 1800$, corresponding to the same amount of ion acceleration as Figure 7.

242

F(VX), e Time = 960

-3.0   0   3.0

F(VX), O⁺ Time = 960

-0.15   0.10   0.35

F(VX), H⁺ Time = 960

-0.25   0.15   0.55
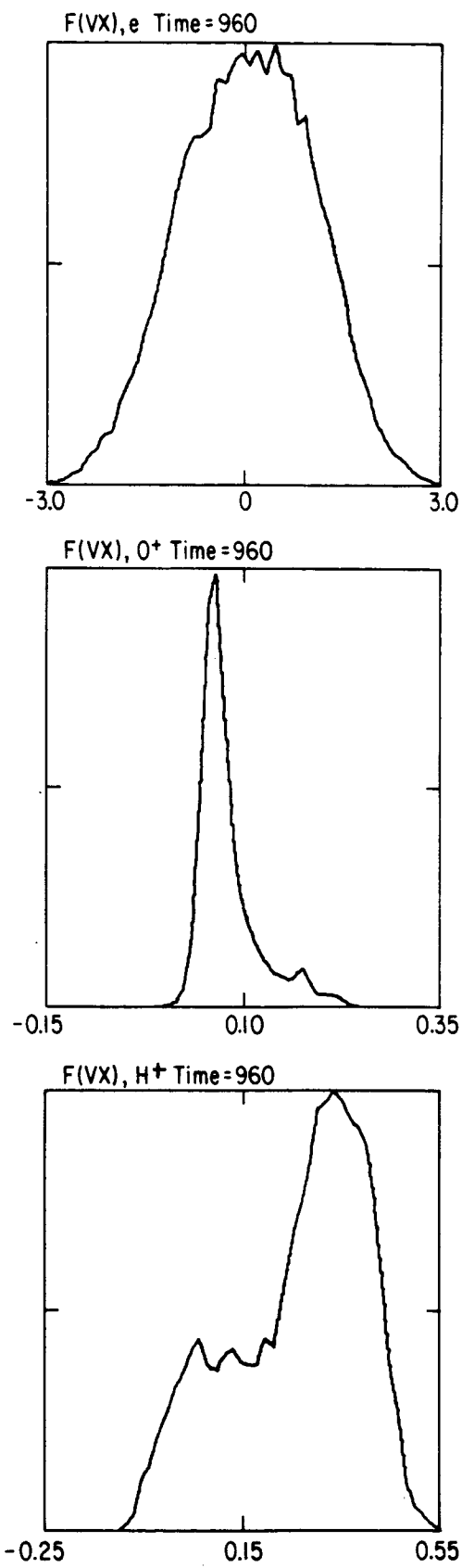
Figure 10. Same plots as Figure 6 for run 3, at the end of the time series shown in Figure 4.
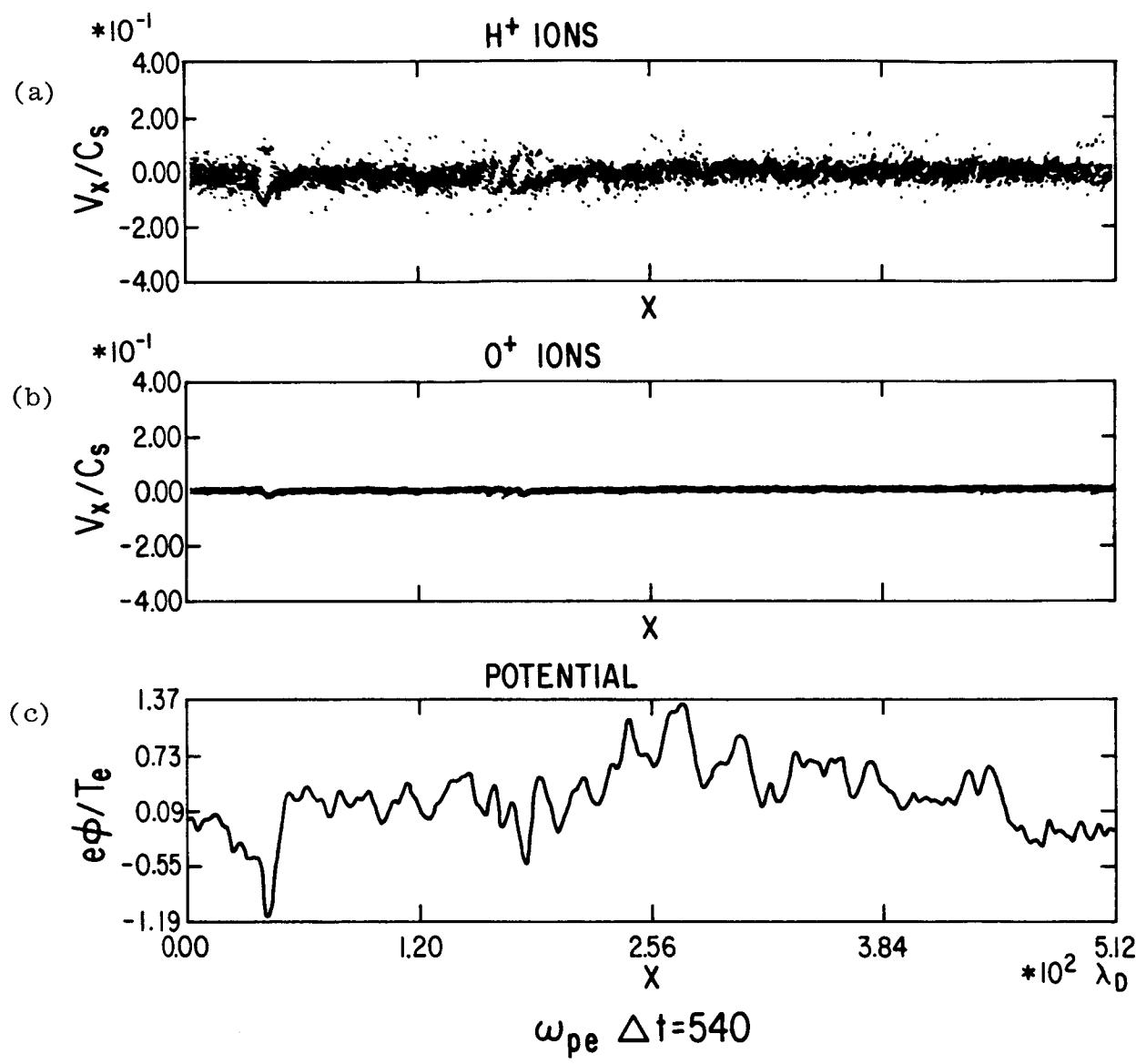
Figure 11. (a) Hydrogen and (b) oxygen distributions, and (c) potential averaged over 67.5 ω_{pe}^{-1} at $\omega_{pe} \Delta t = 540$. One or more double layers are apparent.
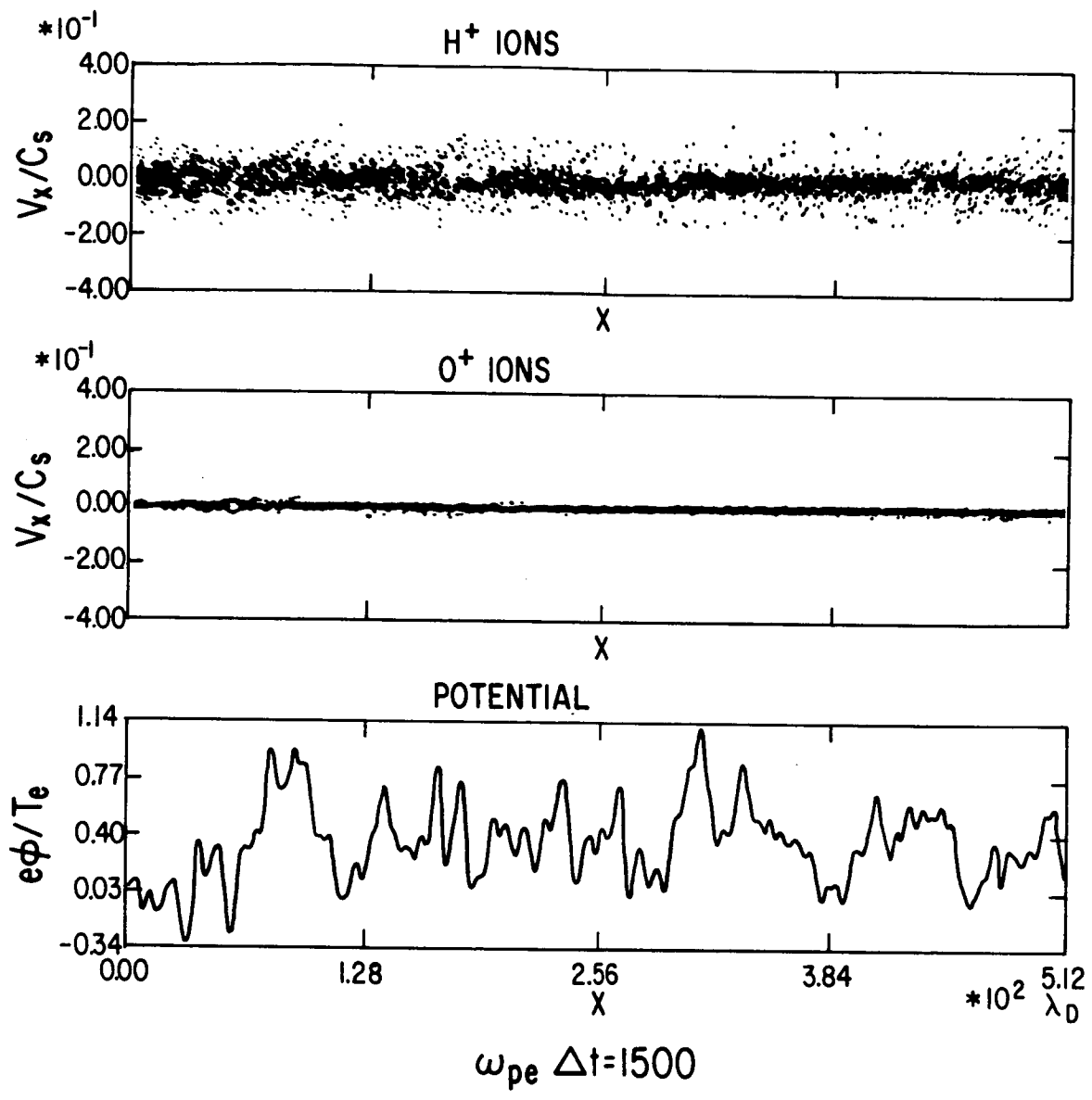
Figure 12. Same as Figure 11 at a later time $\omega_{pe}\,\Delta t\,=\,1500$.

PARTICLE SIMULATION OF AURORAL DOUBLE LAYERS

Bruce L. Smith* and Hideo Okuda
Princeton Plasma Physics Laboratory
Princeton, New Jersey 08544, U.S.A.

ABSTRACT

We report on our work to simulate auroral double layers (DL's) with "realistic" particle-in-cell models. An early model simulated weak DL's formed in a self-consistent circuit but under conditions subject to the ion-acoustic instability. More recent work has focused on strong DL's formed when currentless jets are injected into a dipole magnetic field.

INTRODUCTION

For several years we have been simulating space plasmas using "realistic" models. These models have included both numerical MHD and particle-in-cell (PIC) codes. Here we discuss two PIC models that simulate auroral double layers (DL's).

An early analysis of DL's was performed by Block (1972). In his model four species of particles, reflecting/passing electrons/ions, were incident upon a strong (eV >> kT) DL. The two fluid equations, an adiabatic equation of state and Poisson's equation, led to two criteria on the drift velocities of ions and electrons incident on the high and low field sides of the DL, respectively. These are called the Bohm criteria in analogy with the similar criterion on ions in a plasma sheath (Bohm, 1949). In Block's model the drifts necessary to sustain the DL result in a net current.

Using these criteria as a recipe, one could easily simulate a DL. Such simulations only required fixed potentials at the boundaries to drive the necessary current or a floating potential (or even periodic boundary conditions) with large enough drifts (i.e., a current) to satisfy the criteria. Although these conditions permit DL's, in auroral regions, where DL's have been observed (Temerin and Mozer, 1984), such conditions may not be present.

Sato and Okuda (1980, 1981) performed a series of simulations with "more realistic" conditions. In one of these simulations they assumed:

1. $U_{\text{drift } e} < v_{\text{the}}$

2. $T_e >> T_i$

3. Floating self-consistent potentials.

This is the range of parameters for ion-acoustic instabilities, but avoids the large relative drifts which may cause the two-stream instability.

Their model was that of the polar region field lines in a self-consistent circuit. Initial conditions included a driving potential and an initial current. The subseuent potential and current were related by a fixed resistance consistent with the initial conditions. One of the results shown in Figure 1 was obtained for $v_{de}/v_{te} = 0.6$, $M/m = 100$,

---

* Now at Air Force Office of Scientific Research.

$n\lambda_D = 100$, $w_{pe}\Delta t = 0.2$. As is apparent, the simulation resulted in multiple weak (eV $\lesssim$ kT) DL's about 1000 λ_D apart and with scale lengths $\ell \sim 50 \lambda_D$. These DL's are unstable and propagate at near the ion-acoustic velocity but recur at a rate such that approximately the same number of DL's are always present.

Hasegawa and Sato (1982) provided the mechanism for such DL's. Basically an ion hole is created which cuts off the electron current. Formation of an adjacent electron hole follows. This yields a DL which decays on the ion time scale.

Other authors have found different ways to relax the constraints imposed by the Bohm criteria. In particular, Kan and Lee (1980) concluded that the condition on the electron velocity was unnecessary if trapped electrons were present. Similarly Perkins and Sun (1981) demonstrated that even currentless DL's could exist. Incidentally, their analysis contrasts with that of Chiu and Schulz (1978) who computed the potential along a mirror magnetic field due to multiple species of ions and electrons using the condition of charge neutrality.

A recent experiment further indicated the possibility for modifying the conditions necessary for creation of DL's. Stenzel et al. (1981) conducted an experiment with a dipole B-field which reflected an incident ion beam. This experiment resulted in strong DL's for varying magnetic field strengths. These, too, were inherently current-less DL's.

The previous investigations compelled us to simulate a flowing neutral plasma injected along a (fully) dipole magnetic field. This model is meant to simulate the storm-generated flow from the reconnection region to the polar auroral regions. Of course, such a flow would cause ions and electrons of the same temperature to have different turning points. As the ions overshoot the electrons, a space charge potential could form and a DL would be present. This model then substantiates a source of energetic electrons for an aurora.

Parameters for the region through which such substorms are supposed to develop are n = 10-1000 cm^{-3}, B = 10^3-10^4 γ, and $T_e \lesssim T_i \sim$ 100's eV. These values yield $w_{pe} \sim w_{ce} \sim 10^5$-$10^6$ rad/s and $\beta \ll 1$. In this parameter regime the electrostatic approximation is appropriate (Krall and Trivelpiece, 1973).

RESULTS

Results for a one-dimensional PIC simulation with $L/\lambda_D = N_g = 1024$, M/m = 25, $w_{pe}\Delta t = 0.25$, and $B_{max}/B_{min} \simeq 25$ are shown. For boundary conditions we chose V = 0 at z = 0 (the "ionosphere") and using symmetry, dV/dz = 0 at z = L (the "magnetosphere"). Figures 2a-c show the injection of plasma at approximately 0.8 v_{the}. As the plasma drifts into the dipole field, a double layer is evidenced by the acceleration of ions and electrons and by their relative charges at L = 600 λ_D for w_{pe} t = 1900 and L = 800 λ_D for w_{pe}t = 2600. One notes that the DL is unstable by the modulation (with $\lambda \sim 25 \lambda_D$) and the fact that the DL moves at a velocity 200 λ_D/700/w_{pe} = 2/7 v_{the}. This value is on the order of the ion-acoustic velocity.

The f-spectrum for different positions (Fig. 3) shows the presence of a mode at w = 0.15-0.2 $w_{pe} \lesssim w_{pi}$ and at w = 0.05-0.1 $w_{pe} \ll w_{pi}$. Similarly the mode structure (Fig. 4) gives wavelengths most strongly peaked at λ = 0 and λ = 60 λ_D. The data are consistent with a two-stream instability (with w $\ll w_{pi}$). Finally the scale length of the DL is kT/eE $\sim$ 50 $\lambda_D \gg \lambda_D$.

In the next panels (Figs. 5 a-d) are shown $f(v_+)$-$f(v_-)$ for both electrons and ions at different positions. If there were simply a B-field with no other interaction we would expect a snapshot of the loss cone for such a comparison. Instead the panels clearly show that the electrons accelerate from $w_{pe}t = 1000$ to $w_{pe}t = 2800$ as they pass over the DL. Similarly the ions slow down and cool during this same time. (This cooling of ions may allow an ion-acoustic instability.)

In the final panels (Fig. 6) we show the measured energies from the simulation. As can be seen in the first panel, total energy is conserved to within less than 1 percent. One also sees that the ion kinetic energy is converted to electron kinetic energy until the two are approximately equal. Surprisingly, the collective potential energy is a small fraction of the total.

A theory for this model was derived by Serizawa and Sato (unpublished manuscript). Using an adiabatic approximation, their kinetic analysis showed that $eV \approx KE_i/(1 + T_i/T_e)$ with small variations predicted for mass ratios $m/M \ll 1$ and mirror ratios $B_{max}/B_{min} \gg 1$. A plot of eV versus KE_i for varying KE_i confirms the linear relation between these quantities (Fig. 7).

Similar results for ions and electrons streamed from both ends are obtained.

CONCLUSION

In conclusion, simulations have been undertaken to model aurorae under realistic conditions. The simulation of ion acoustic DL's in a self-consistent circuit showed multiple DL's with $eV/kT \lesssim 1$. Currentless DL's with $eV \gg kT$ have been demonstrated. Although not discussed here, these simulations furthered the theory of Fourier transforms for bounded systems and successfully demonstrated the utility of a guiding center code for electrons. Currently two-dimensional codes are being tested to verify the one-dimensional results and to study two-dimensional instability mechanisms.

REFERENCES

Block, L. P., *Cosmic Electrodynamics, 3,* 349 (1972).
Bohm, D., in *The Characteristics of Electrical Discharges in Magnetic Fields,* edited by A. Guthrie and R. K. Wakerling, p. 77, McGraw-Hill, New York, 1949.
Chiu, Y. T., and M. Schulz, *J. Geophys. Res., 83,* 629 (1978).
Hasegawa, A., and T. Sato, *Phys. Fluids, 25,* 632 (1982).
Kan, J. R., and L. C. Lee, *J. Geophys. Res., 85,* 788 (1980).
Krall, N. A., and A. W. Trivelpiece, in *Principles of Plasma Physics,* p. 427, McGraw-Hill, New York, 1973.
Perkins, F. W., and Y. C. Sun, *Phys. Rev. Lett., 46,* 115 (1981).
Sato, T., and H. Okuda, *Phys. Rev. Lett., 44,* 740 (1980).
Sato, T., and H. Okuda, *J. Geophys. Res., 86,* 3357 (1981).
Serizawa, Y., and T. Sato, unpublished report on "Generation of Large Scale Potential Difference by Currentless Plasma Jets Along the Mirror Field."
Stenzel, R. L., M. Ooyama, and Y. Nakamura, *Phys. Fluids, 24,* 708 (1981).
Temerin, M., and F. Mozer, in *Second Symposium on Plasma Double Layers and Related Topics,* edited by R. Schrittwieser and G. Eder, p. 119, University of Innsbruck, 1984.
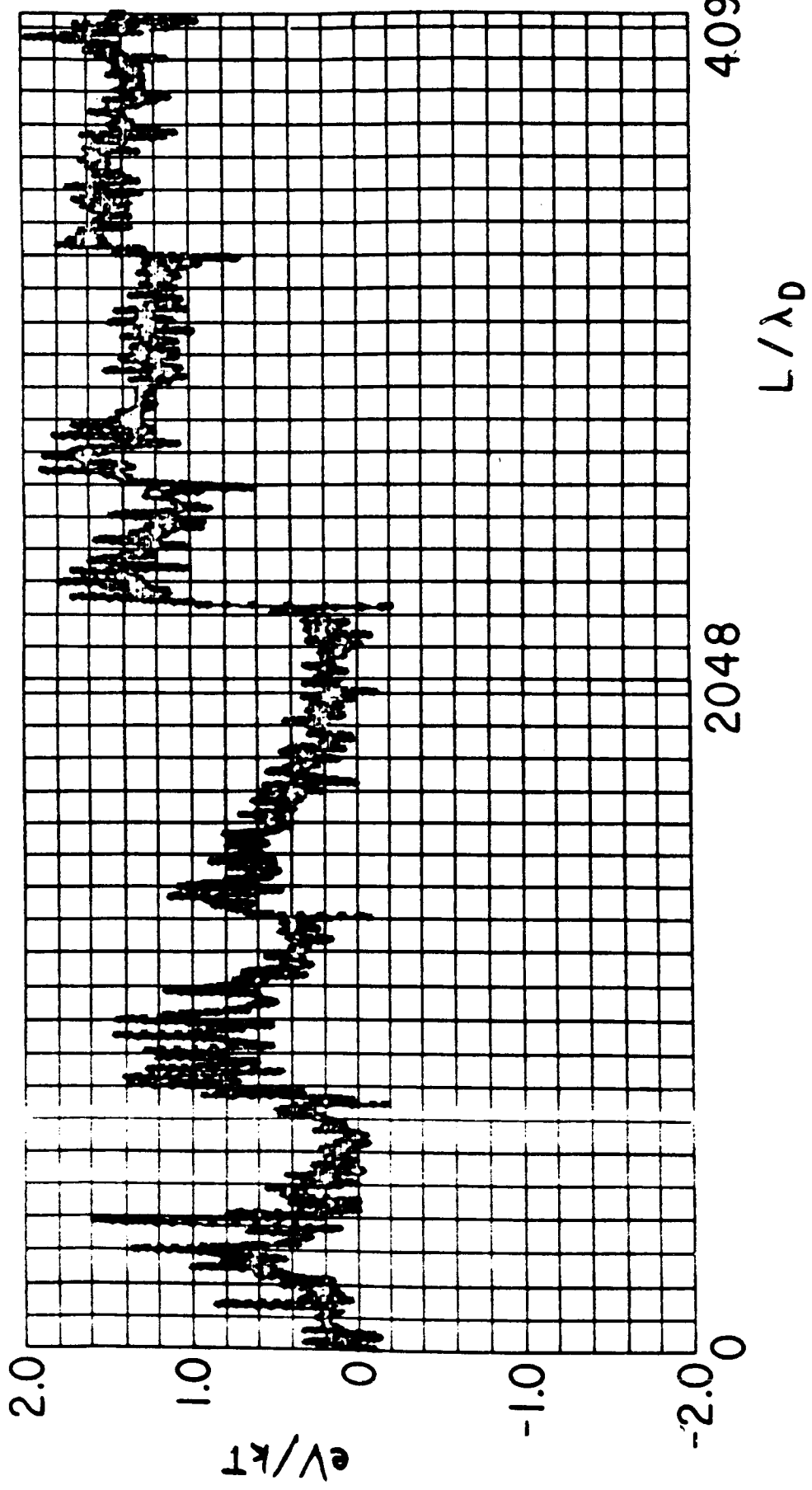
Figure 1. The electric potential as a function of position showing the formation of multiple weak double layers. The simulation results here are due to Sato and Okuda (1980, 1981).
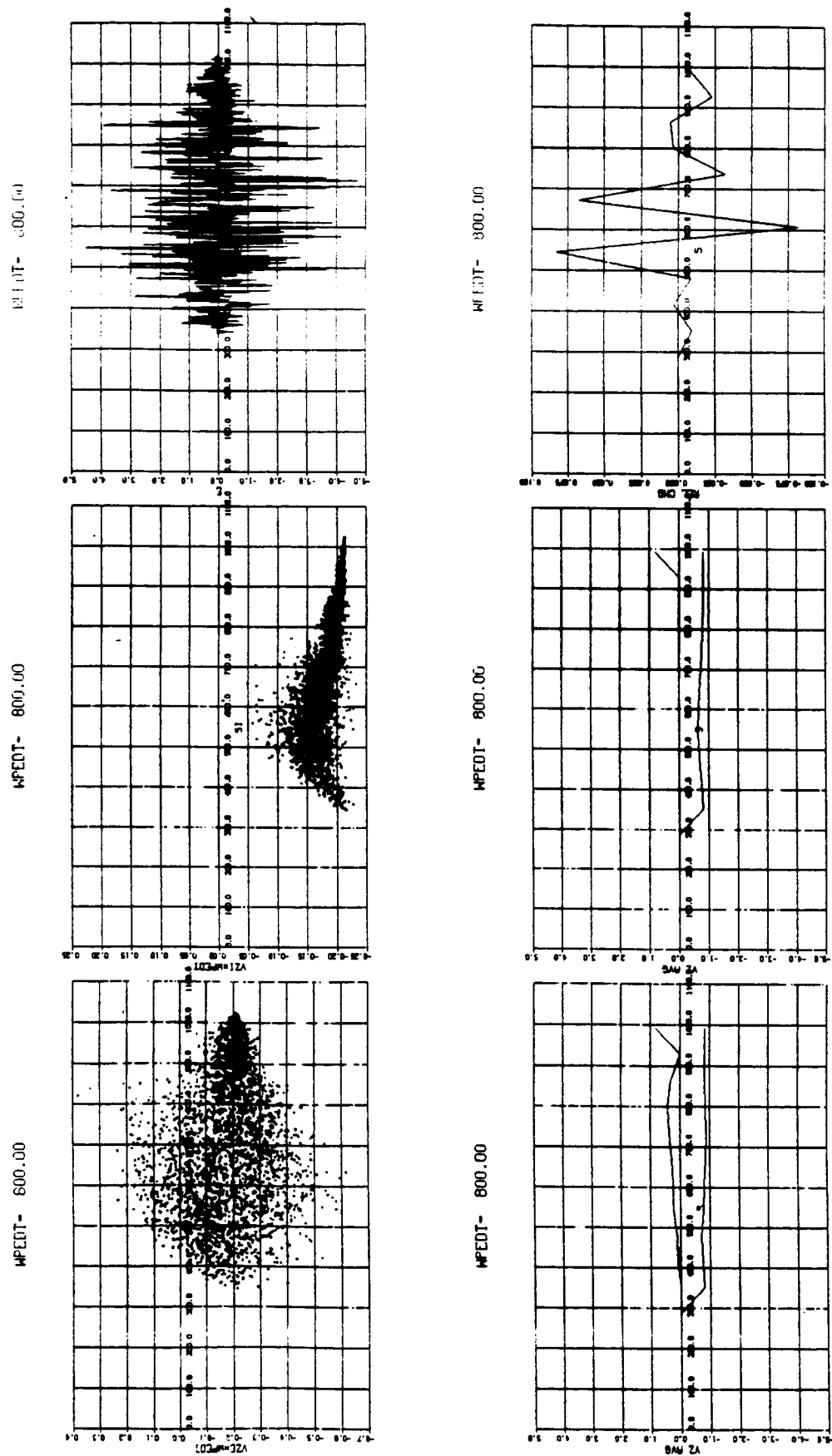
Figure 2. Results for a one-dimensional simulation with $L/\lambda_0 = Ng = 1024$, $M/m = 25$, $B_{max}/B_{min} \cong 25$, and $w_{pe}\Delta t$ as indicated by the value of WPEDT in the figures.

251
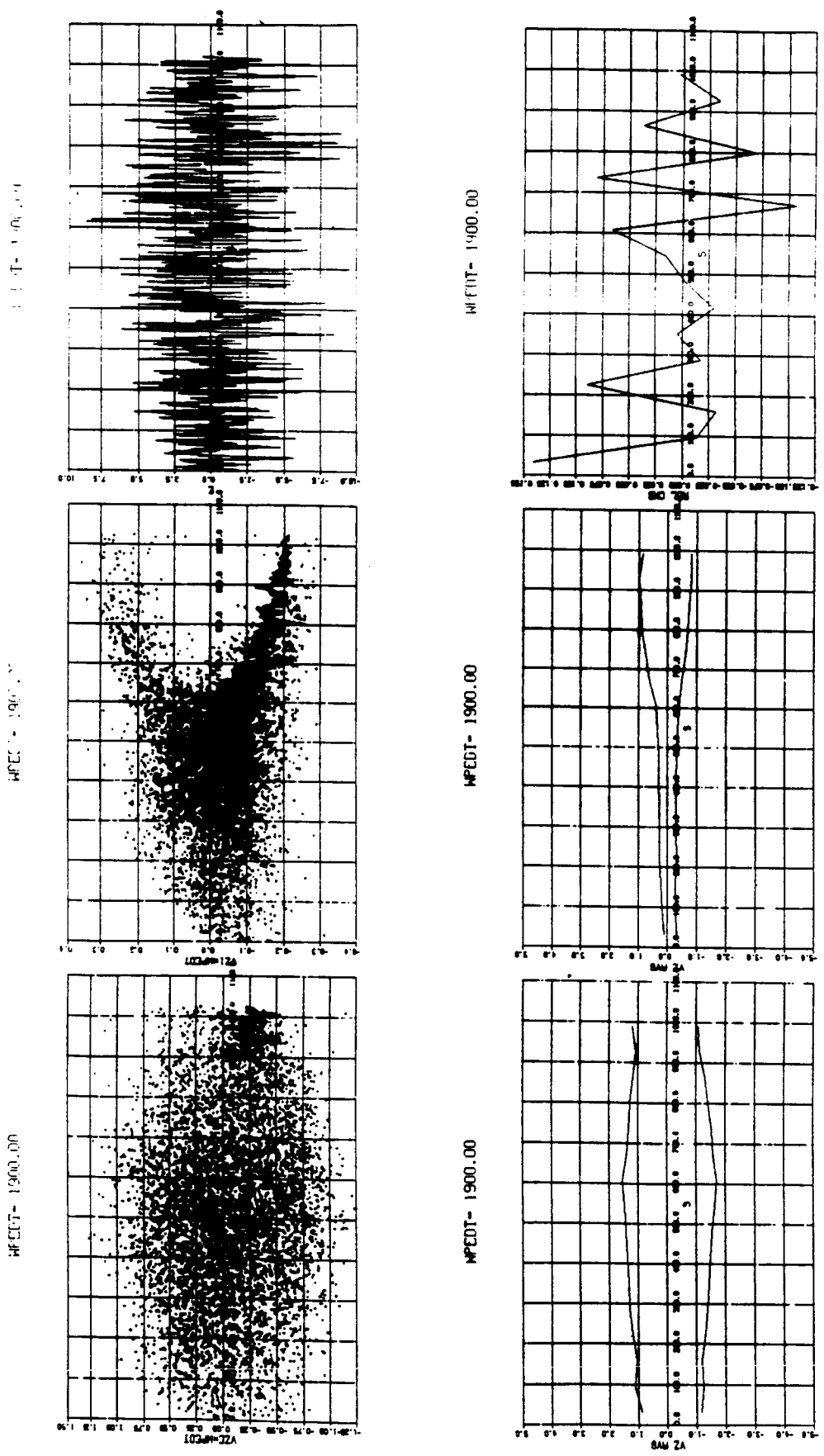
Figure 2. (Continued)
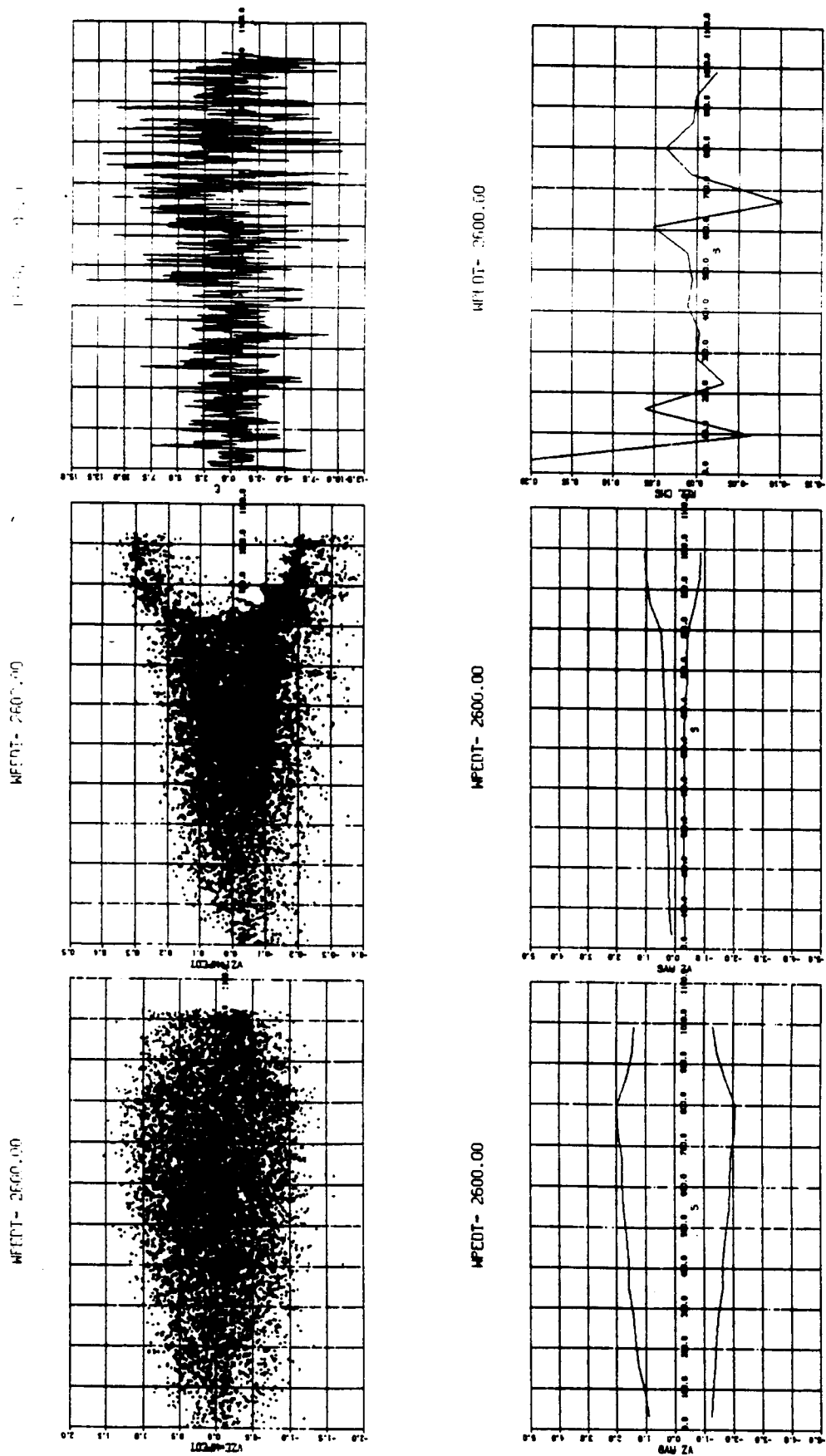
Figure 2. (Concluded)
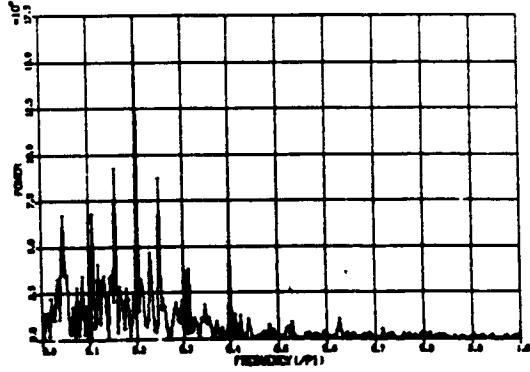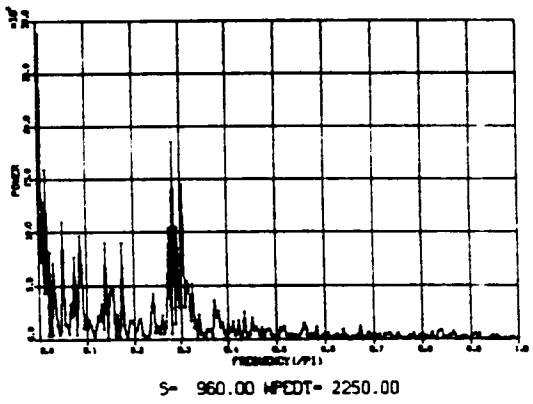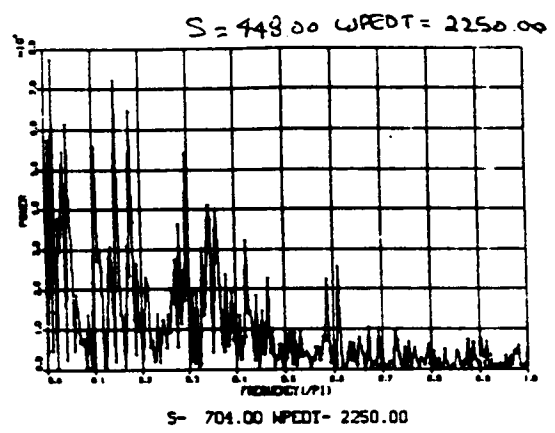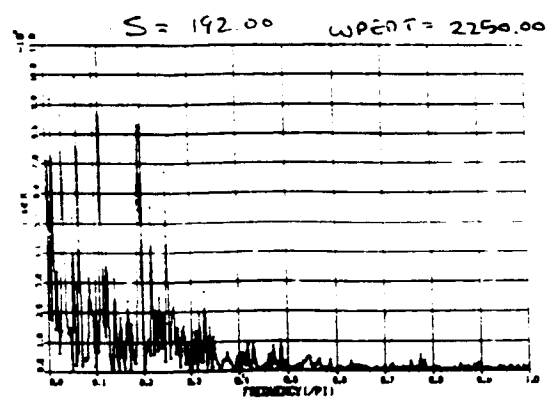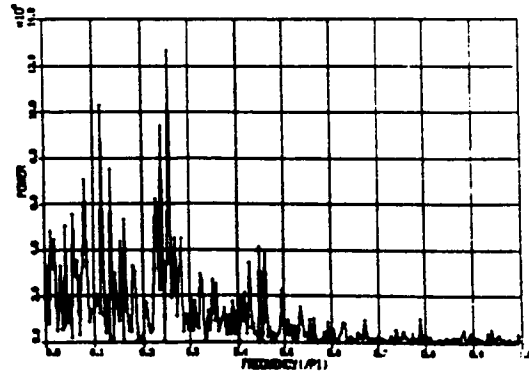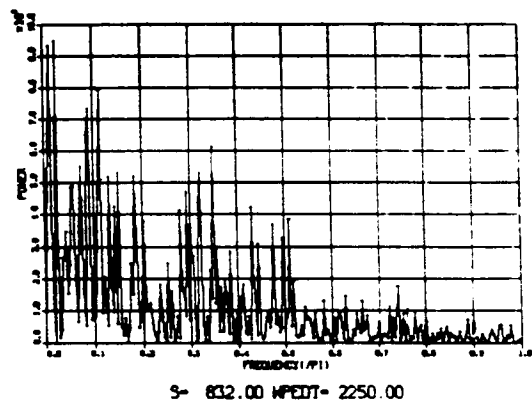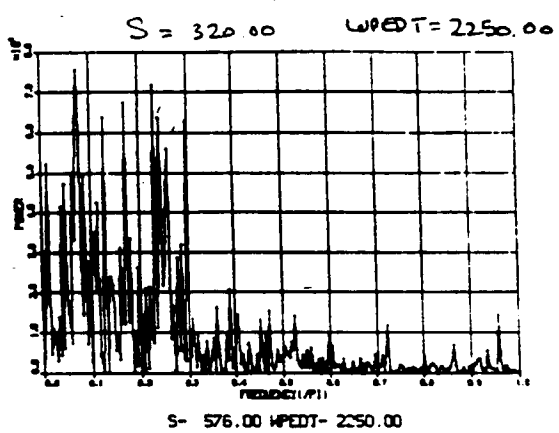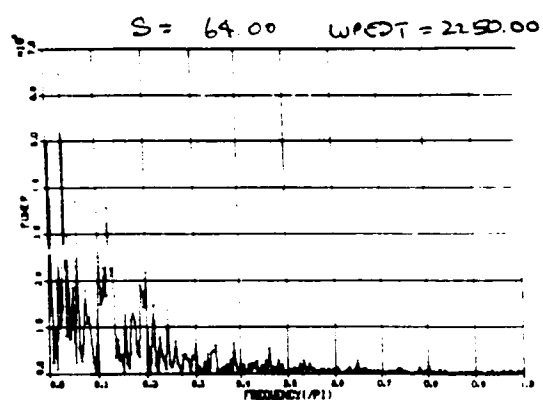
Figure 3. The frequency spectrum for different positions with $w_{pe}\Delta t = 2250$.

TIME- 2250.00(/WPE)   TIME- 2250.00(/WPE) $k = \frac{1}{\lambda_D}$
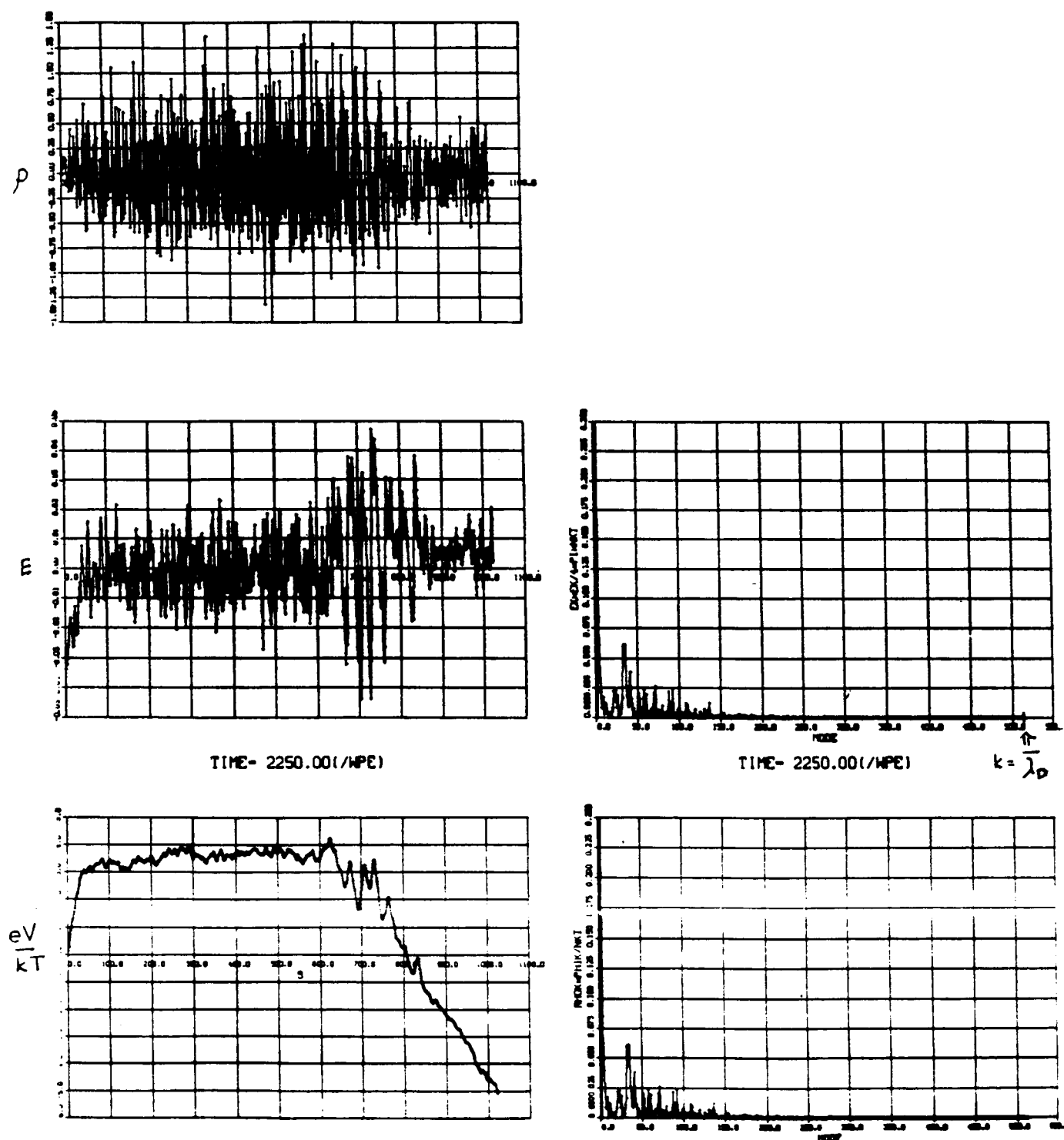
Figure 4. The charge density, electric potential, electric field intensity, and mode structure
from the simulations of Figure 3.

255
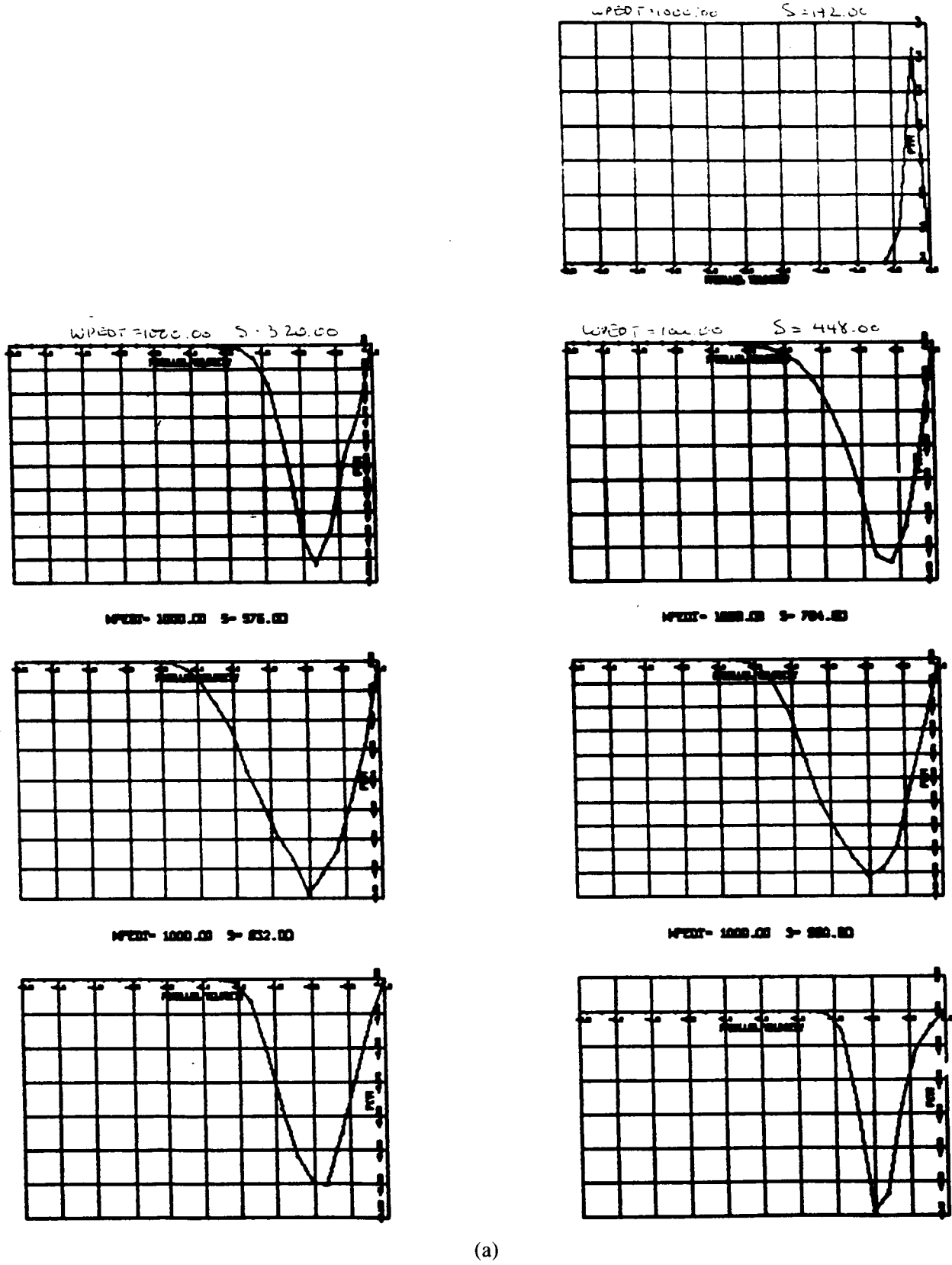
Figure 5. A plot of f(v$_+$) - f(v$_-$) for the electrons and ions at various positions.
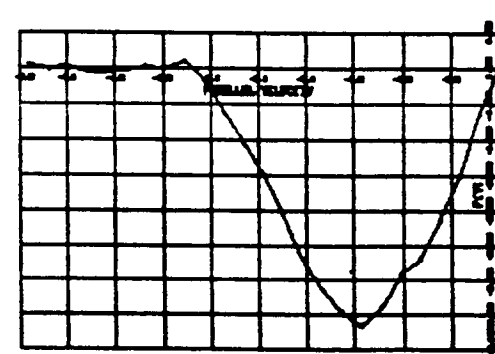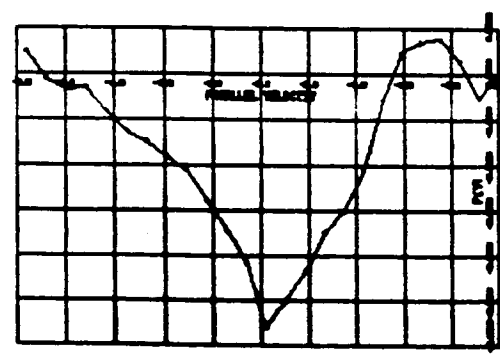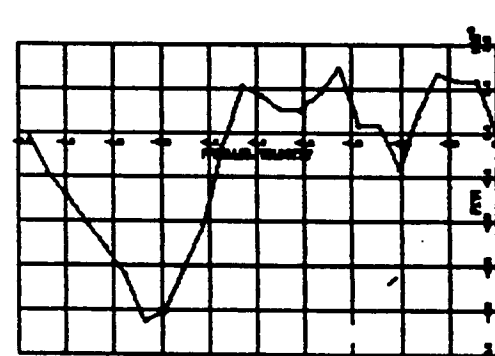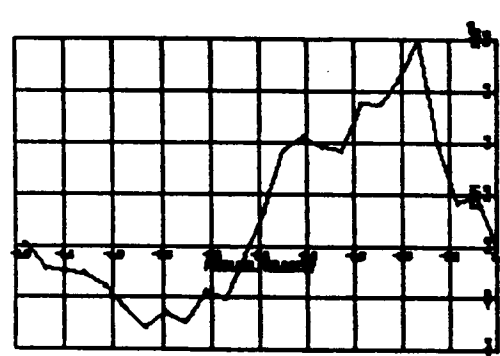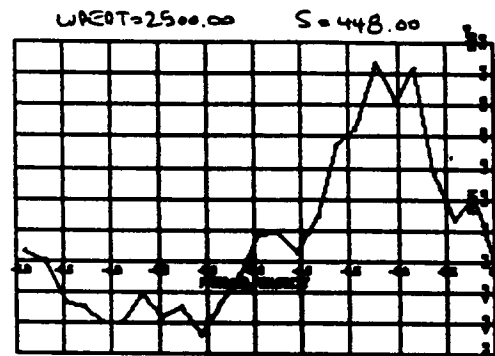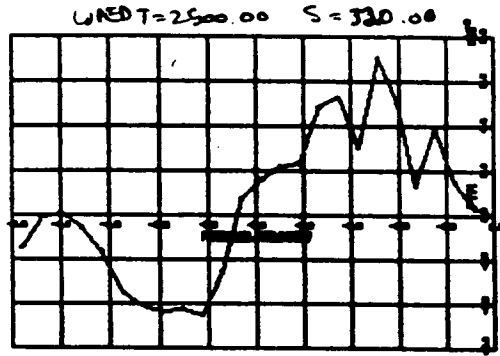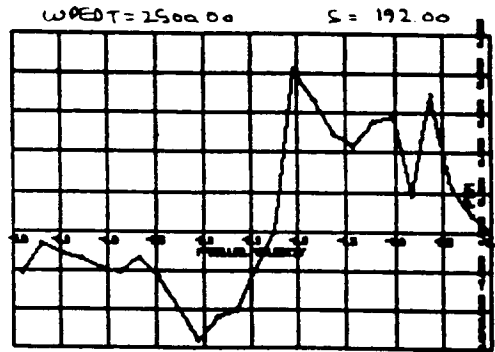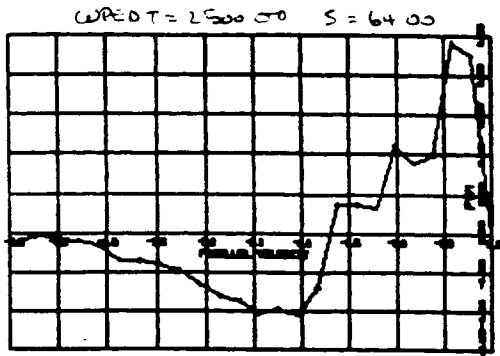
(a)

Figure 5. (Continued)

(b)

(c)
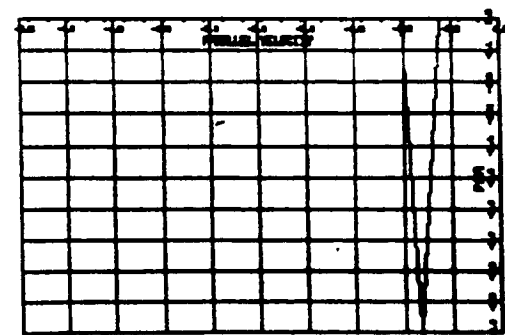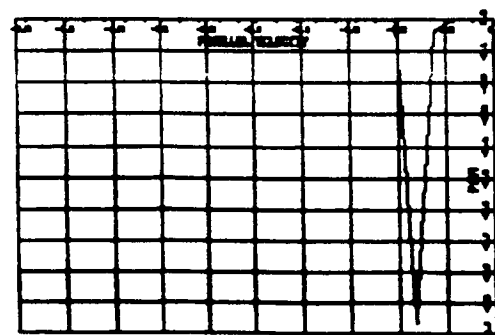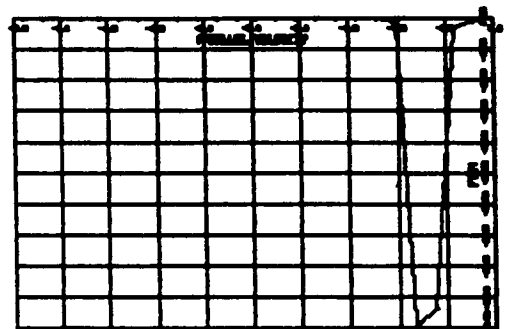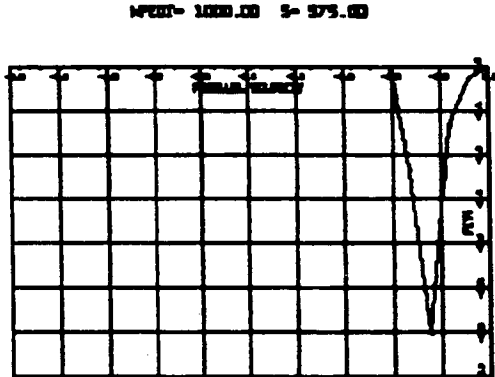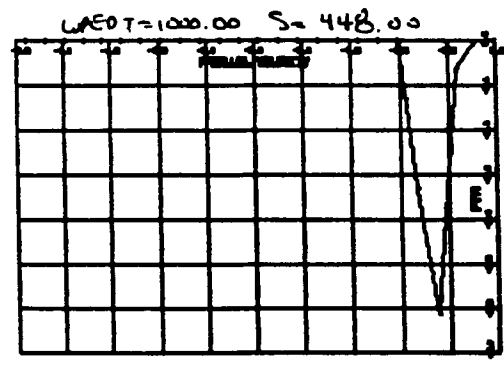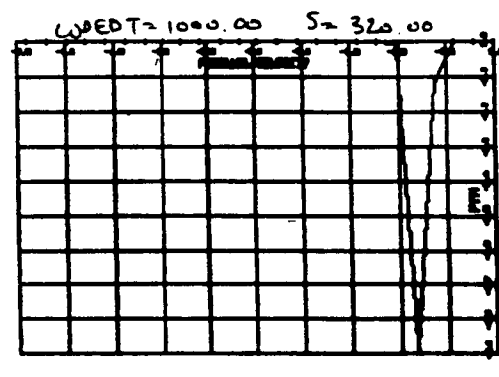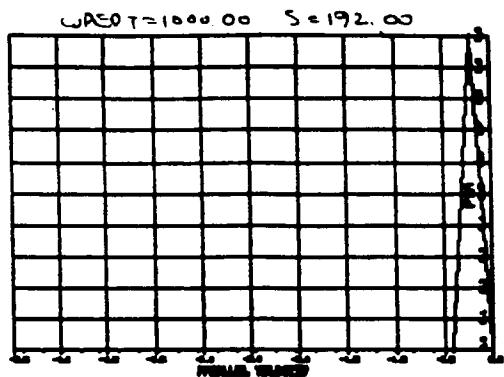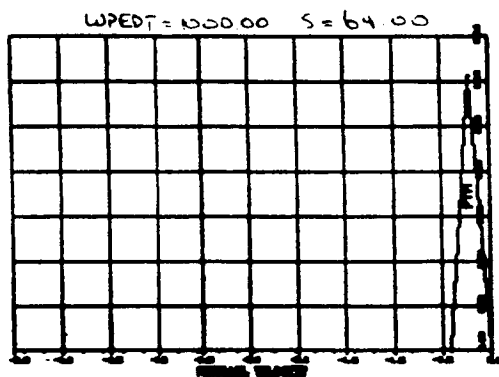
Figure 5. (Continued)
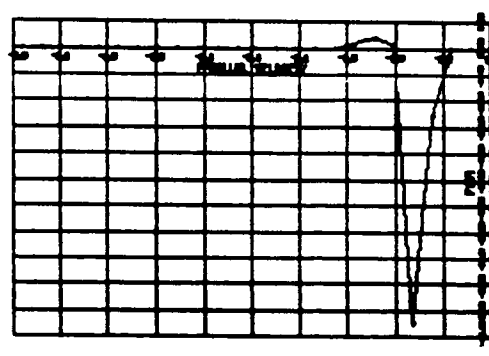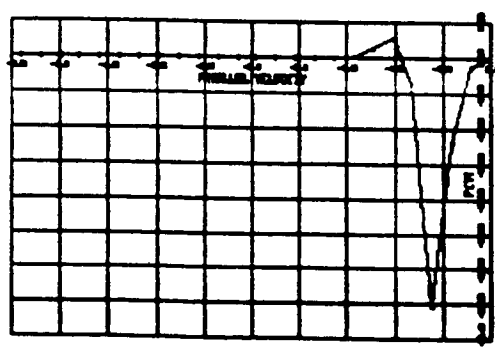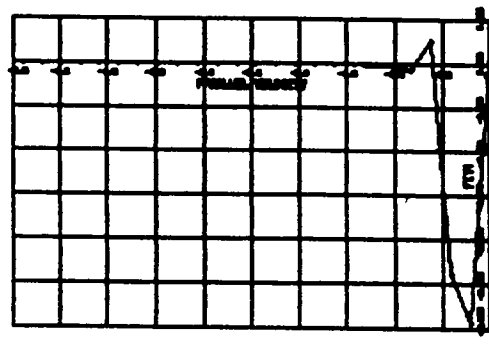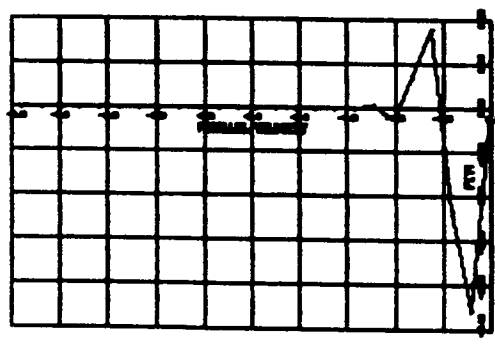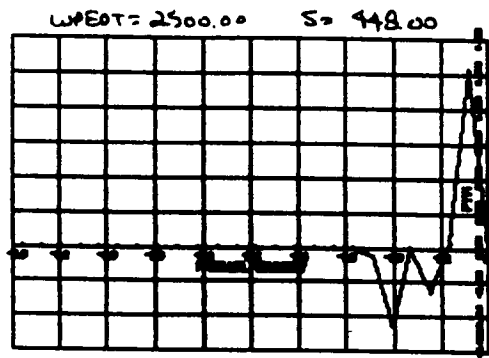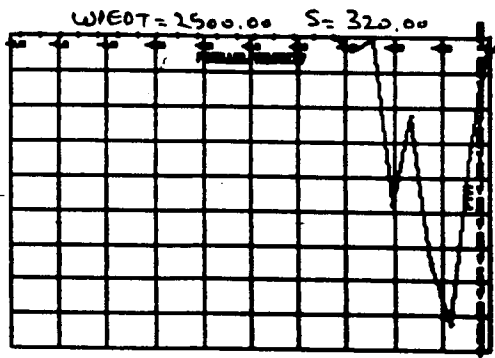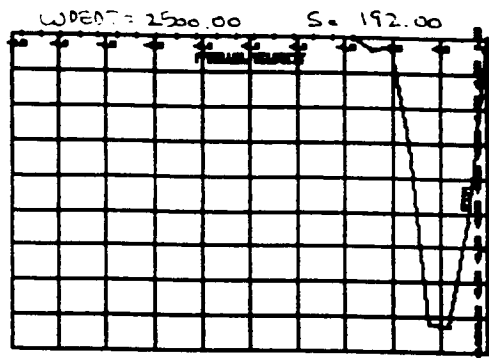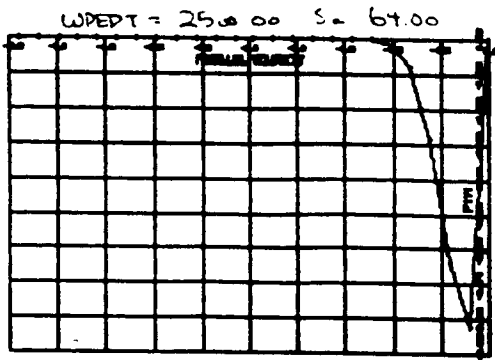
(d)

Figure 5.   (Concluded)
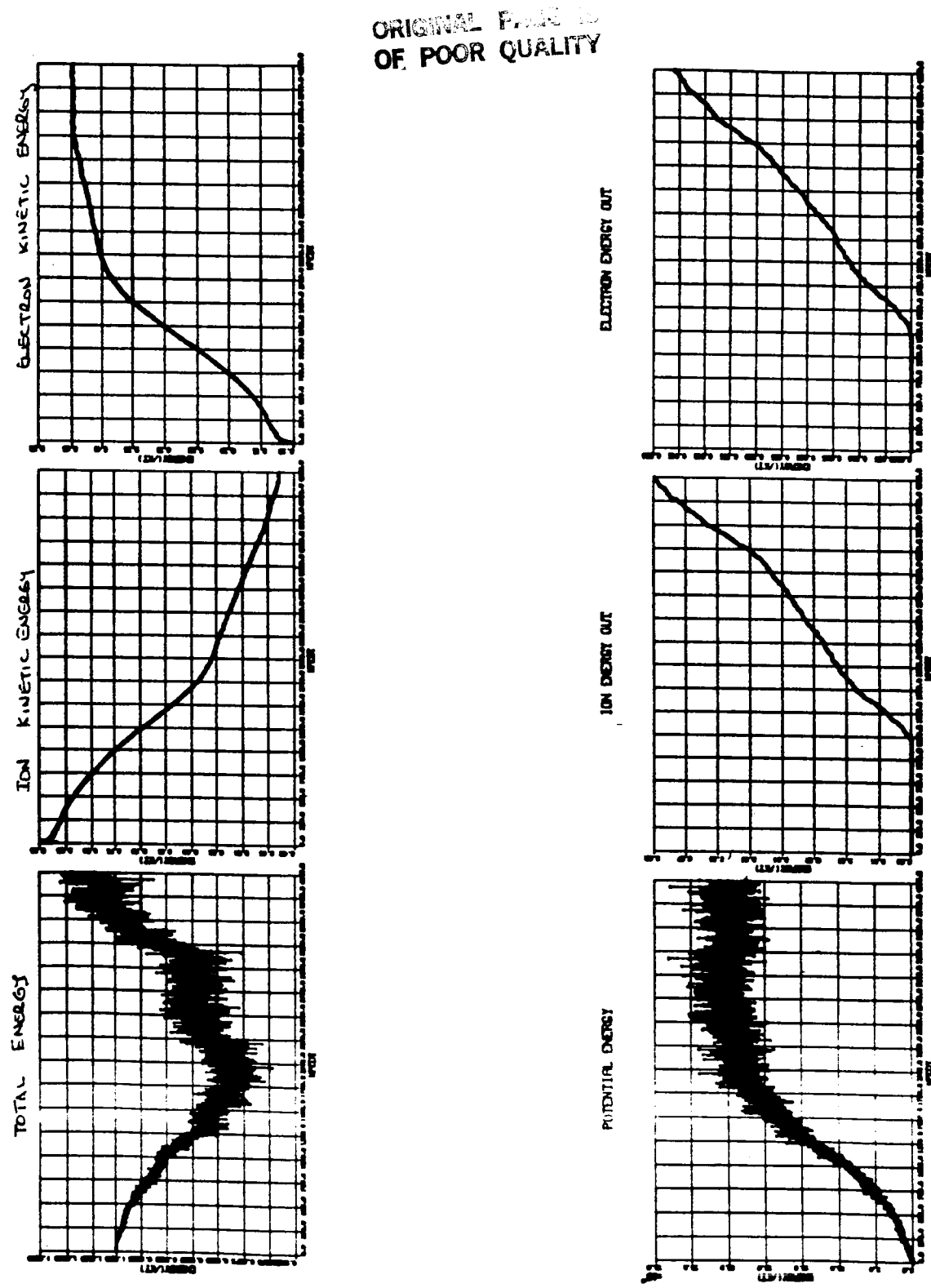
Figure 6. The calculated energies implicit in the simulation results.
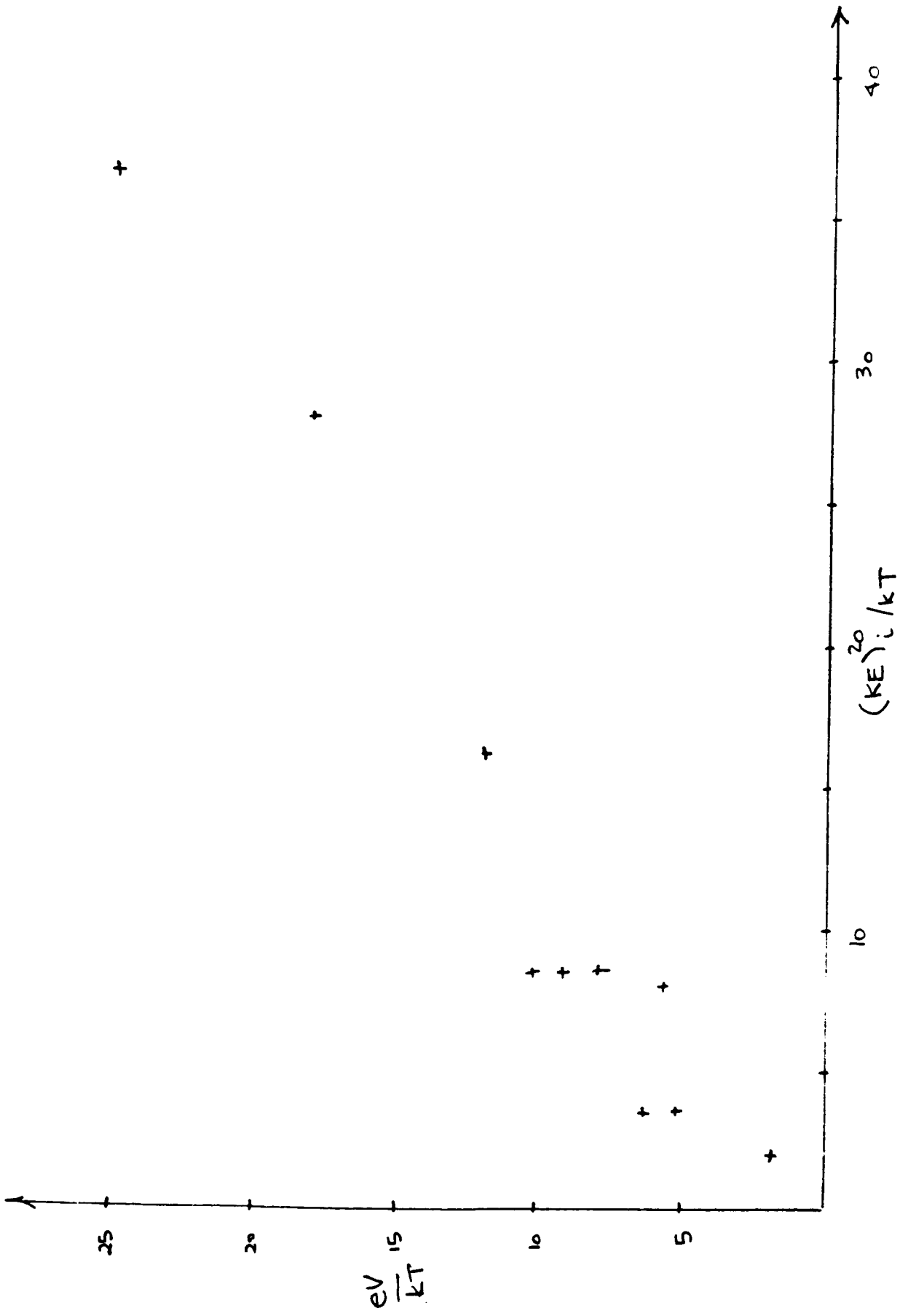
Figure 7. A plot of the double layer potential eV versus the ions kinetic energy.

III. SPACE APPLICATIONS

CONDITIONS FOR DOUBLE LAYERS IN THE EARTH'S MAGNETOSPHERE AND PERHAPS IN OTHER ASTROPHYSICAL OBJECTS

L. R. Lyons
Space Sciences Laboratory, M2-260
The Aerospace Corporation
P.O. Box 92957
Los Angeles, California 90009, U.S.A.

ABSTRACT

Double layers (i.e., electric fields parallel to $\mathbf{B}$) form along auroral field lines in the Earth's magnetosphere. They form in order to maintain current continuity in the ionosphere in the presence of a magnetospheric electric field $\mathbf{E}$ with $\nabla \cdot \mathbf{E} \neq 0$. Features which govern the formation of the double layers are: (1) the divergence of $\mathbf{E}$, (2) the conductivity of the ionosphere, and (3) the current-voltage characteristics of auroral magnetic field lines. Astrophysical situations where $\nabla \cdot \mathbf{E} \neq 0$ is applied to a conducting plasma similar to the Earth's ionosphere are potential candidates for the formation of double layers. The region with $\nabla \cdot \mathbf{E} \neq 0$ can be generated within, or along field lines connected to, the conducting plasma. In addition to $\nabla \cdot \mathbf{E}$, shear neutral flow in the conducting plasma can also form double layers.

I. INTRODUCTION

Here I describe the large-scale, electrodynamical phenomena that give rise to the formation of double layers in the Earth's magnetosphere. I point out what I believe are the important features which might be found in association with other astrophysical objects, and which could produce double layers analogous to those associated with the Earth.

In the laboratory, double layers form if one tries to drive a current through a plasma that is greater than that which can be carried by the available charge particles in a plasma. The same situation occurs along auroral magnetic field lines. When the magnetosphere-ionosphere system tries to drive a current with a density greater than can be carried by the plasma available to flow along field lines, a field-aligned potential drop $V_{\parallel}$ forms. This $V_{\parallel}$ accelerates electrons toward the atmosphere, and the accelerated electrons form discrete auroral arcs.

In this discussion, I do not distinguish between double layers, where large $V_{\parallel}$'s occur across short distances, and smoothly varying potentials, where $V_{\parallel}$'s are distributed over large distances along field lines. The overall electrodynamics is the same for both situations.

II. CONDITIONS FOR DOUBLE LAYERS

Three critical features of the Earth's magnetosphere-ionosphere system are involved in the formation of significant ($\gtrsim 1$ kV) $V_{\parallel}$'s along auroral magnetic field lines. These are listed in Figure 1.

First, it is necessary to drive a current with a non-zero divergence. In the magnetosphere, the large-scale, convection electric $\mathbf{E}$ has $\nabla \cdot \mathbf{E} \neq 0$ across auroral field lines. This divergence in $\mathbf{E}$ maps along field lines to the ionosphere.

Second, the ionosphere has a layer of high conductivity perpendicular to the magnetic field $\mathbf{B}$. This conductivity results from collisions between ionospheric particles and the neutral atmospheric particles. Thus, an electric field with $\nabla \cdot \mathbf{E} \neq 0$ in the ionosphere drives Pedersen (parallel to $\mathbf{E}$) currents $\mathbf{I_P}$ in the ionosphere with $\nabla \cdot \mathbf{I_P} \neq 0$. This divergence in $\mathbf{I_P}$ must be balanced by field-aligned currents to maintain current continuity in the ionosphere.

Third, if the intensity of the required field-aligned current density $j_{||}$ exceeds that which can be carried by plasma flowing along field lines with $V_{||} = 0$, then a $V_{||} \neq 0$ must form.

Any astrophysical situation where an electric field drives a current $\mathbf{I}$ perpendicular to $\mathbf{B}$, with $\nabla \cdot \mathbf{I} \neq 0$, has the potential for forming $V_{||}$'s along $\mathbf{B}$. A layer with significant conductivity perpendicular to $\mathbf{B}$ would be an attractive candidate for having currents with $\nabla \cdot \mathbf{I} \neq 0$.

To determine whether a $V_{||}$ will form, we must evaluate the $j_{||}$ versus $V_{||}$ characteristics of magnetic field lines for $j_{||}$'s of the magnitude expected from $\nabla \cdot \mathbf{I}$. Currents associated with aurora on the Earth typically have $j_{||} \sim 1\text{-}10$ $\mu A/m^2$. Two particle populations can contribute to this current: the ionospheric plasma moving up along field lines, and magnetospheric plasma (from the plasmasheet) which precipitates into the atmosphere. Only magnetospheric particles within the loss cone contribute to $j_{||}$, since particles outside the loss cone mirror above the atmosphere.

Downward $j_{||}$'s can result from ionospheric electrons moving upward and from the precipitation of magnetospheric ions. However, ionospheric electrons can generally supply a $j_{||} > 10$ $\mu A/m^2$ to a downward $j_{||}$, so that $V_{||}$'s do not generally form for downward $j_{||}$'s.

On the other hand, the maximum $j_{||}$ that can be carried by ionospheric ions is generally < 1 $\mu A/m^2$. Thus, the precipitation of magnetospheric electrons must be considered for upward $j_{||}$'s. For typical parameters of plasmasheet electrons, the maximum $j_{||}$ that can be supplied by the precipitation of magnetospheric electrons is ~ 1 $\mu A/m^2$ for $V_{||} = 0$. However, increasing $V_{||}$ increases $j_{||}$ by enhancing the flux of electrons in the loss cone. The relation between $j_{||}$ and $V_{||}$ along auroral field lines was obtained by Knight (1973), and is shown in Figure 2.

Figure 2 shows $j_{||}$ versus $V_{||}$ for an electron density $n = 1$ cm^{-3} and an electron thermal energy $K_{th} = 1$ keV, values which are reasonable for the plasmasheet. Results for other values of n and K_{th} can be obtained from the normalizations given in the figure. Curves are shown for various values of the ratio between the magnetic field in the ionosphere B_i and the magnetic field $B_{V_{||}}$ at the top of the region where significant potential variation exists along field lines. Satellite obsevations (Gorney et al., 1981) indicate that $B_i/B_{V_{||}} \approx 30$ is reasonable. Notice from Figure 2 that upward $j_{||}$'s $\sim 1\text{-}10$ $\mu A/m^2$ require the existence of $V_{||}$'s $\sim 1\text{-}10$ kV. Such $V_{||}$'s are of the magnitude observed over auroras.

Figure 3 illustrates a way in which an $\mathbf{E}$ with $\nabla \cdot \mathbf{E} \neq 0$ develops in the Earth's magnetosphere. Both open, polar-cap field lines connected with the interplanetary field and closed, lower latitude field lines are shown. Solar wind flow across the open polar cap field lines forms a dawn-to-dusk electric field across the open field line region, and the electric field changes direction across the boundary between open and closed field lines. The boundary is thus charged as indicated in the figure. Mapping the electric field to the ionosphere gives $\nabla \cdot \mathbf{I_P} < 0$ and upward $j_{||}$'s on the dusk side, and $\nabla \cdot \mathbf{I_P} > 0$ and downward $j_{||}$'s on the dawn side. The magnitude of $\nabla \cdot \mathbf{I_P}$ gives large enough $j_{||}$'s on the dusk side to require a $V_{||} > 0$.

Similar situations as shown in Figure 3 should occur in the magnetospheres of other magnetized, solar system planets, and could exist in association with other magnetized, astrophysical objects. Also, regions of $\nabla \cdot \mathbf{E} \neq 0$ can be formed by plasma sources, such as Io, that move across field lines within a magnetosphere.

Figure 4 shows that the observed change in $\mathbf{E}$ across the dusk auroral zone can account for the observed magnitude of auroral $V_{||}$'s and precipitation intensities. The observations (Gurnett and Frank, 1973) were from a low-altitude satellite. An electric field of 0.12 V/m was observed across the auroral region, and the equation for

current continuity in the ionosphere was solved (Lyons, 1980) for an electric field of magnitude 0.06 V/m on each side of the reversal. The resulting values of $V_\parallel$ and precipitating electron energy fluxes are shown in Figure 4 as a function of latitudinal distance. These can be seen to compare well in magnitude with values obtained from electron observations on the satellite. The auroral observations in Figure 4 have more structure than that obtained from the simple solution to the current continuity equation. However, this type of structure, which is typical of discrete auroral arcs, can be explained as a result of more detailed structure in the magnetospheric electric field (Lyons, 1981; Chiu et al., 1981).

So far, the discussion here has been under the assumption that the velocity V_n of neutrals in the conducting layer is zero. Including V_n, I_P may be written as the difference between the electric field drift velocity V_E and V_n:

$$I_P = \Sigma_P \, (-V_E + V_n) \times B \quad,$$

where Σ_P is the layer-integrated Pedersen conductivity. Since $j_\parallel = -\nabla \cdot I_P$, the above relation shows that shears in V_n, as well as shears in V_E, can cause field-aligned currents within a conducting layer.

Generally, thermospheric neutral winds in the conducting region of the Earth's ionosphere are not sufficiently large to generate $V_\parallel$'s. However, this is not necessarily always the case. Recently, Lyons and Walterscheid (1985) proposed that neutral wind shear can drive waves of aurora (omega bands), with $V_\parallel > 0$, that occasionally occur on the poleward boundary of the post-midnight, diffuse aurora. In addition it has been proposed the neutral winds in the photosphere and lower chromosphere of the Sun can generate $V_\parallel$'s (e.g., Kan et al., 1983).

III. SUMMARY

Figure 5 summarizes conditions that might exist in other astrophysical objects and which could lead to the formation of significant $V_\parallel$'s in a manner analogous to what occurs in the Earth's auroral zones. A conducting layer carrying current I perpendicular to B with $\nabla \cdot I \neq 0$ will force field-aligned currents. If the required field-aligned current density $j_\parallel$ exceeds the maximum $j_\parallel$ that can be carried along field lines by the available plasma with $V_\parallel = 0$, then a $V_\parallel > 0$ will form.

Two processes can drive Pedersen currents with $\nabla \cdot I_P \neq 0$ within a collisional, conducting layer. The first is sheared plasma flow (i.e., $\nabla \cdot E \neq 0$) applied anywhere along the magnetic field lines connected to the conducting layer. In this case, the sheared plasma flow will map along field lines to the conducting layer. The second process is a neutral flow with shear within the conducting layer. Such flow can drive divergent Pedersen currents without an electric field being applied to the system.

REFERENCES

Chiu,Y. T., A. L. Newman, and J. M. Cornwall, *J. Geophys. Res.*, *86*, 10,029 (1981).

Gorney, D. J., A. Clarke, D. Croley, J. Fennell, J. Luhmann, and P. Mizera, *J. Geophys. Res.*, *86*, 83 (1981).

Gurnett, D. A., and L. A. Frank, *J. Geophys. Res.*, *78*, 145 (1973).

Kan, J. R., S.-I. Akasofu, and L. C. Lee, *Solar Phys.*, *84*, 153 (1983).

Knight, L., *Planet. Space Sci.*, *21*, 741 (1973).

Lyons, L. R., *J. Geophys. Res.*, *85*, 17 (1980).

Lyons, L. R., *J. Geophys. Res.*, *86*, 1 (1981).

Lyons, L. R., and R. L. Walterscheid, *J. Geophys. Res.*, *90*, 12,321 (1985).

THREE ASPECTS OF MAGNETOSPHERE – IONOSPHERE SYSTEM INVOLVED IN FORMATION OF DISCRETE AURORAL ARCS

1. DIVERGENCE OF MAGNETOSPHERIC ELECTRIC FIELD

   A. DIVERGENCE REQUIRED TO DRIVE THE ARCS

2. CONDUCTIVITY OF THE IONOSPHERE

   A. WITHOUT CONDUCTING IONOSPHERE, THERE WOULD BE NO ARCS

3. CURRENT-VOLTAGE CHARACTERISTICS OF AURORAL FIELD LINES

Figure 1. Critical features of the Earth's magnetosphere-ionosphere system involved in the formation of significant $V_{\parallel}$'s.
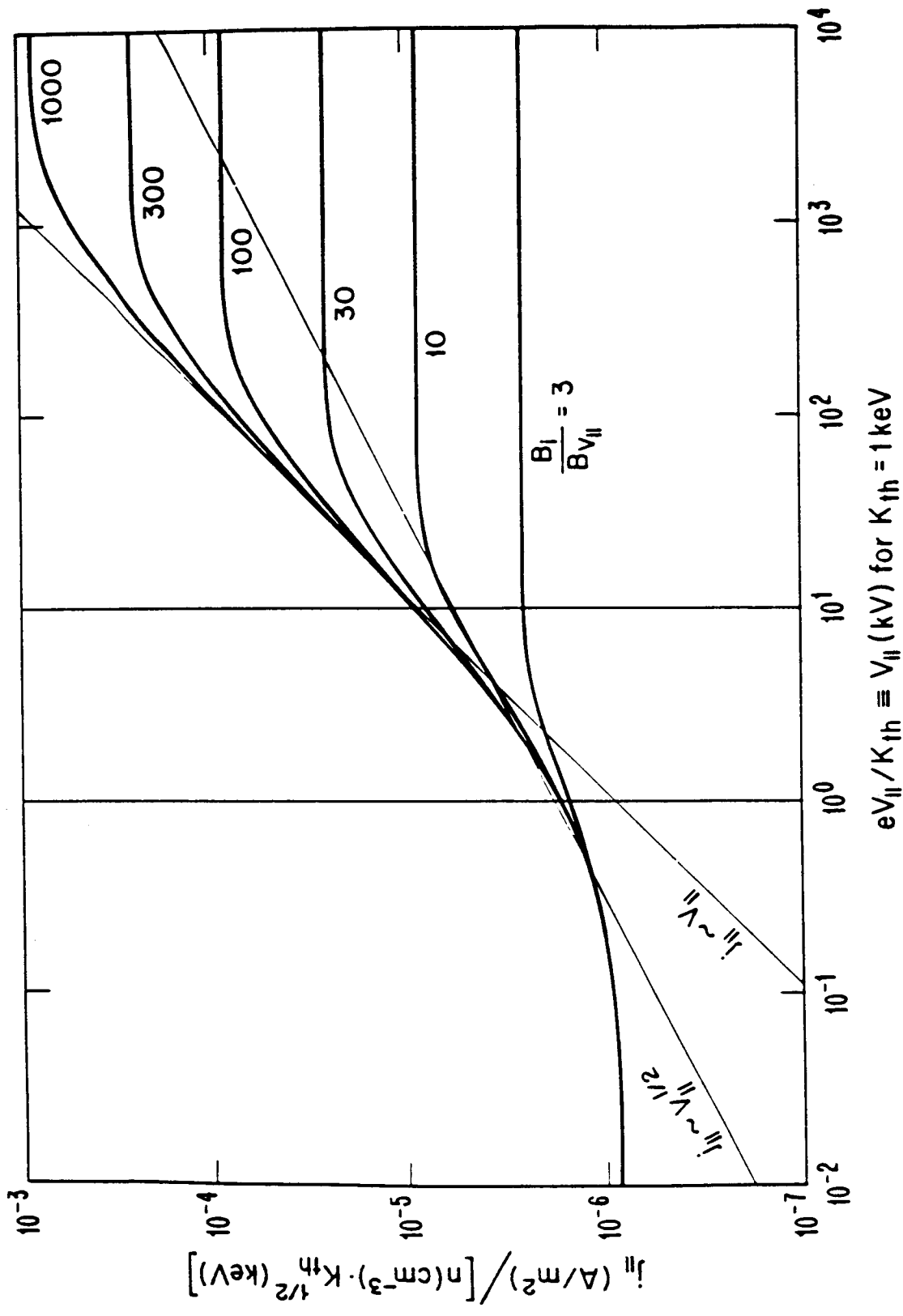
Figure 2. The $j_{\parallel}$ and $V_{\parallel}$ relation for uninhibited, single-particle motion along field lines for a high-altitude electron plasma with $n = 1$ cm^{-3} and $K_{th} = 1$ keV. Results for other values of n and K_{th} can be obtained by multiplying the current densities on the vertical axis by n(cm^{-3}). $K_{th}^{1/2}$ (keV) and the potential differences on the horizontal axis by K_{th} (keV). Curves are shown for $B_i/B_{V_{\parallel}}$ from 3 to 1000. Lines for $j_{\parallel} \sim V_{\parallel}^{1/2}$ and $V_{\parallel}$ and for $eV_{\parallel}/K_{th} = 1$ and 10 are shown for reference.

DUSK

DAWN

EVENING AURORAL ZONE

v$_{SW}$ SOLAR WIND VELOCITY

v$_E$ ELECTRIC FIELD DRIFT ACROSS CLOSED FIELD LINES

j$_{||}$ FIELD-ALIGNED CURRENT
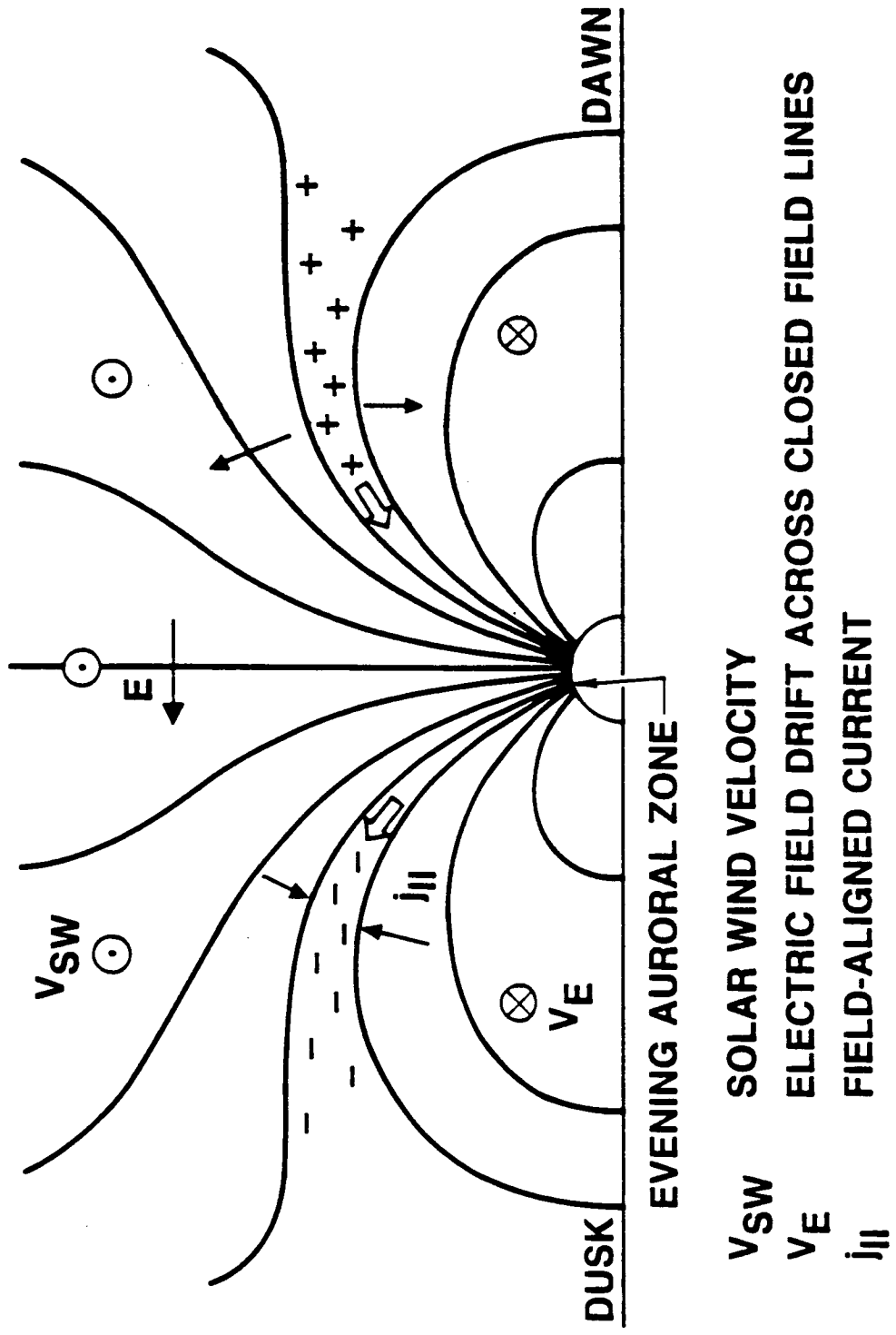
Figure 3. Schematic illustration of generation of **E**, with $\nabla \cdot \mathbf{V} \neq 0$, by the solar wind flow across the Earth's polar-cap field lines.
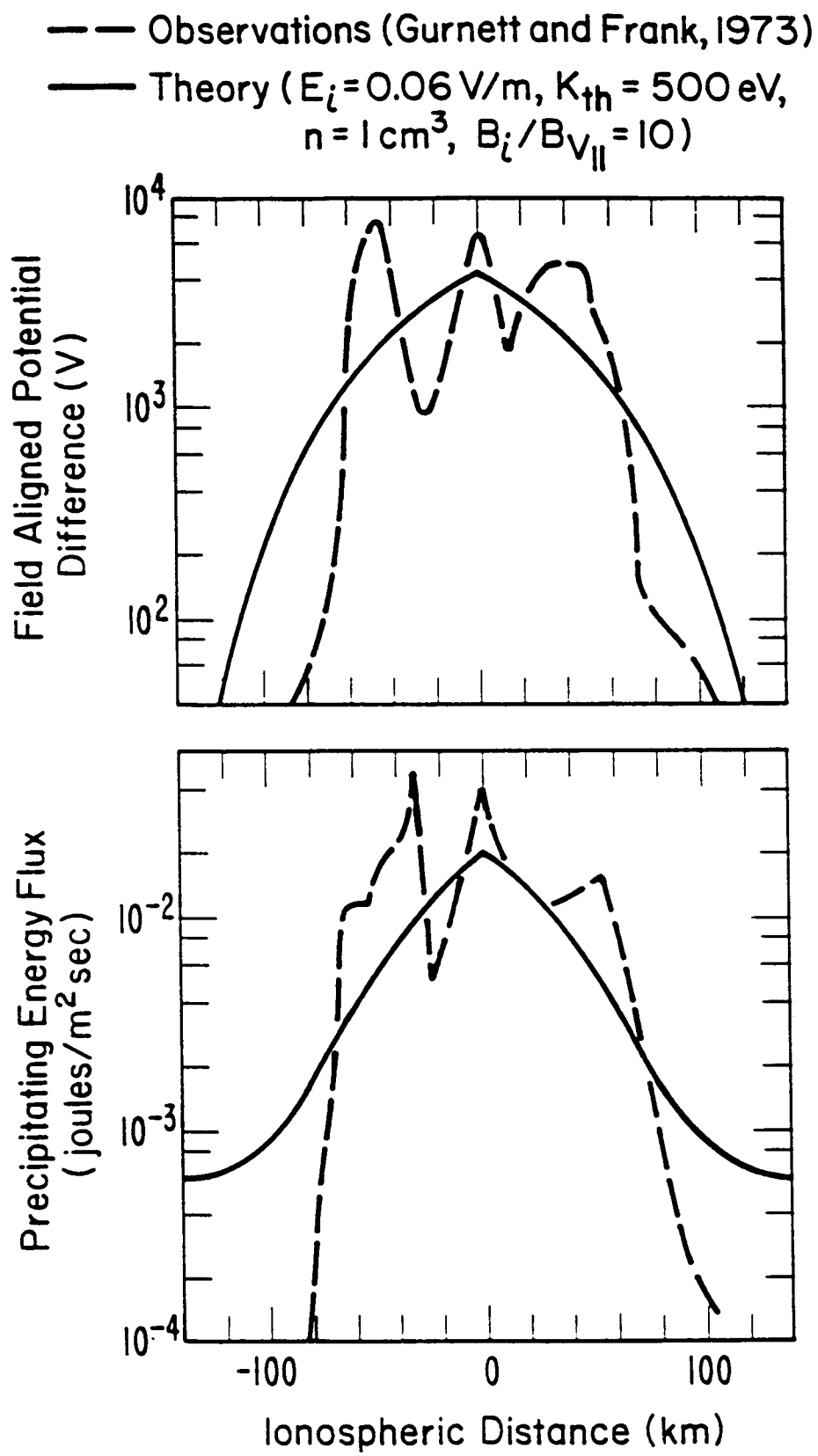
Figure 4. Comparison of the solution to the ionospheric current continuity equation (Lyons, 1980) with observations. The observations (Gurnett and Frank, 1973) were obtained over the auroral zone from a low-altitude satellite near 1800 LT.
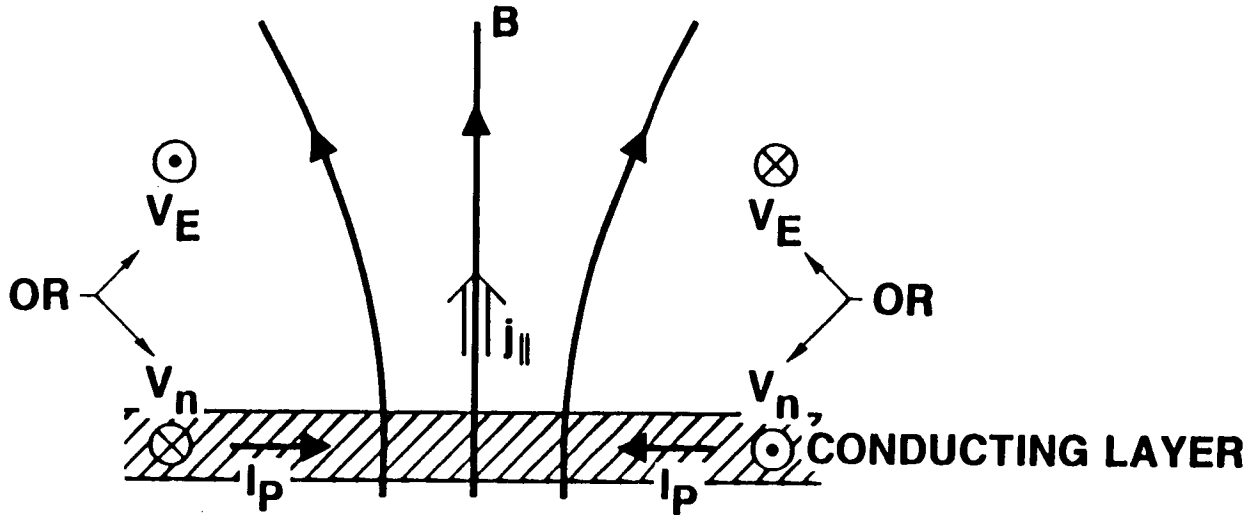
- ● **CONVERGING I$_p$ CAN BE DRIVEN BY:**

  1. **SHEARED PLASMA FLOW V$_E$ APPLIED ANYWHERE ALONG B**

  2. **SHEARED NEUTRAL FLOW V$_n$ APPLIED IN CONDUCTING LAYER**

- ● **IF j$_\parallel$ > CRITICAL j$_\parallel$, GET V$_\parallel$**

Figure 5. Summary of conditions that could lead to the formation of significant V$_\parallel$'s in a manner analogous to what occurs in the Earth's auroral zones.

SOME ASPECTS OF DOUBLE LAYER FORMATION IN A PLASMA CONSTRAINED BY A MAGNETIC MIRROR

W. Lennartsson
Lockheed Palo Alto Research Laboratory
Palo Alto, California 94304, U.S.A.

ABSTRACT

The discussion of parallel electric fields in the Earth's magnetosphere has undergone a notable shift of emphasis in recent years, away from wave-generated anomalous resistivity toward the more large-scale effects of magnetic confinement of current carrying plasmas. This shift has been inspired in large part by the more extensive data on auroral particle distribution functions that have been made available, data that may often seem consistent with a dissipation-free acceleration of auroral electrons over an extended altitude range.

Efforts to interpret these data have brought new vigor to the concept that a smooth and static electric field can be self-consistently generated by suitable pitch angle anisotropies among the high-altitude particle populations, different for electrons and ions, and that such an electric field is both necessary and sufficient to maintain the plasma in a quasi-neutral steady state. This paper reviews and criticizes certain aspects of this concept, both from a general theoretical standpoint and from the standpoint of what we know about the magnetospheric environment. It is argued that this concept has flaws and that the actual physical problem is considerably more complicated, requiring a more complex electric field, possibly including double layer structures.

I. INTRODUCTION

Few topics in space plasma physics have been as controversial as that of "parallel electric fields," that is electric fields with a static or quasi-static component aligned along the Earth's magnetic field lines and strong enough to substantially alter the velocity distribution of the charged particles. Much of this controversy has centered on the interpretation of auroral particle data, especially the data on precipitating electrons, and has evolved along with developments in measurement technology (e.g., Swift, 1965; Block, 1967; O'Brien, 1970; Evans, 1974; Lennartsson, 1976; Papadopoulos, 1977; Hudson et al., 1978; Chiu and Schulz, 1978; Goertz, 1979; Lyons et al., 1979; Smith, 1982; and references therein).

Possibly the first truly compelling evidence of parallel electric field was presented by Evans (1974), who was able to account in a rather convincing fashion for the different parts of a typical auroral electron spectrum. The type of data presented by Evans is illustrated in a condensed form in Figure 1, which is taken from a more recent study by Kaufmann and Ludlow (1981). The two principal parts of this spectrum are a virtually isotropic low-energy part, including the central peak and most of the plateau, and a high-energy part on the flanks, which is essentially isotropic in the downward hemisphere (positive $v_\parallel$) but strongly reduced in the upward hemisphere (negative $v_\parallel$). According to Evans' interpretation, only the high-energy part in the downward hemisphere consists of precipitating primary electrons, accelerated by an upward parallel electric field at higher altitude. Only these primary electrons can contribute to a field-aligned (upward) current at this point in space. The low-energy part consists of back-scattered and energy-degraded primary electrons and of electrons of atmospheric origin, many of which are secondary electrons generated by the impact of primary electrons. All of these low-energy electrons are trapped below the electric field and cannot contribute to the field-aligned current. Any additional contribution must be from upward-moving ions.

As noted by Evans (and by other investigators before him) the primary electrons ("p") on the downward flanks of the distribution typically have a velocity distribution f_p that is reminiscent of a Maxwell-Boltzmann distribution that has been displaced in energy:

$$f_p(\vec{v}) \approx C \exp[-(m|\vec{v}|^2/2 - U)/kT] \quad , \tag{1}$$

where C is a normalization constant, m the electron mass, kT a thermal energy, and the positive quantity U is independent of $\vec{v}$ and may be equated to a certain difference in electric potential energy eV:

$$U = e\Delta V \quad . \tag{2}$$

This quantity corresponds to the kinetic energy of the electrons on the downward edge of the plateau in Figure 1 and, by inference, corresponds to primary electrons with zero initial energy (at high altitude).

If the distribution in Figure 1 is integrated in terms of a net field-aligned current density $i_\parallel$, only the electrons on the flanks make a significant contribution because of the near isotropy at energies smaller than U. If the distribution of these flank electrons f_p ("primary electrons") is approximated by (1) at pitch angles $\alpha \leq \alpha_{max}$ (where α_{max} is slightly larger than 90° in this figure) and approximated by zero at $\alpha > \alpha_{max}$, then the integration of $-ef_p(\vec{v})v\cos\alpha$ readily yields:

$$i_\parallel \approx -eC2\pi(kT/m)^2\sin^2\alpha_{max} (1 + U/kT) \quad , \tag{3}$$

which is a linear function of U for constant values of C, kT, and α_{max} (the latter corresponding to a local atmospheric "loss cone" angle of 180° $-\alpha_{max}$). Some comparisons of auroral electron spectra with the associated field-aligned currents (inferred from other data) have confirmed that the precipitating primary electrons do in fact account for a large or dominant portion of upward field-aligned currents, and the current density is sometimes fairly well approximated by (3) (Burch et al., 1976; Lyons, 1981; Yeh and Hill, 1981).

Although the right-hand side in (3) can be derived on purely empirical grounds, as an approximation of observed electron fluxes, the same type of expression can also be "predicted" if the primary electrons are assumed to originate at high altitude (a few Earth radii, or more), with an isotropic Maxwell-Boltzmann distribution with a temperature T, and fall through a static parallel electric field with a total potential difference $\Delta V = U/e$ (e.g., Knight, 1973; Lemaire and Scherer, 1974; Lennartsson, 1976, 1980; Lyons et al., 1979, Lyons, 1981; Chiu and Schulz, 1978; Chiu and Cornwall, 1980; Stern, 1981). The electric field distribution is not uniquely defined by (3), but to assure the maximum degree of isotropy of the precipitating electrons at low altitude, in accordance with Figure 1, and thus the closest approximation of a linear dependence between $i_\parallel$ and ΔV, it is necessary to assume that the electric potential V varies with the magnetic field strength B in such a fashion that

$$V(B) - V(B_o) \geq (B-B_o) \Delta V/\Delta B \quad , \tag{4}$$

where o refers to the high-altitude origin of the electrons and ΔB refers to the total difference in magnetic field strength between this origin and the low-altitude point of observation (Lennartsson, 1977, 1980). Among the possible solutions of (4) are various double layer configurations, single or multiple.

276

The fact that (3) can be derived under such simple assumptions and yet give a fair approximation of upward field-aligned currents, at least in some studies, has helped in focusing attention on the subject of magnetic confinement of current carrying plasmas. The theoretical implications of this fact are still obscure, however, and there is no consensus yet on the actual properties of the parallel electric field. This paper reviews a few aspects of this complex problem, including the possible role of double layers.

II. NATURAL BOUNDARY CONDITIONS

A rather traditional approach to magnetospheric plasma dynamics at non-relativistic energies is to consider adiabatic single-particle motion, assuming that at least the first adiabatic invariant is preserved for both ions and electrons. This approach has proved fruitful in numerous applications but does have intrinsic problems in many others. To illustrate the latter it is assumed that the particle dynamics is dominated by magnetic and electric force fields, $\vec{B}$ and $\vec{E}$, respectively. To save space the symbols M and Q are used for the mass and charge, respectively, of either ions or electrons. The first invariant (in MKS units) can thus be expressed as

$$\mu = M v_g^2/2/B \approx \text{constant} \quad , \tag{5}$$

where the gyro velocity v_g equals $|\vec{v}_\perp - \vec{E} \times \vec{B}/B^2|$, apart from a small perturbations velocity $\vec{v}_\perp'$ defined by:

$$\vec{v}_\perp' = (M/Q/B^2)(d\vec{E}_\perp/dt + v_g^2(\vec{B} \times \nabla B)/2/B + v_\parallel^2 \vec{B} \times (1/B)\vec{B}\cdot\nabla(\vec{B}/B) \quad , \tag{6}$$

where the time derivative is taken in the frame of reference of the moving particle (e.g., Alfvén and Fälthammar, 1963; Longmire, 1963). This velocity represents the mass and charge dependent part of the gyro center drift, which is added to the common $\vec{E} \times \vec{B}$ drift. The parallel velocity is likewise defined by

$$M (d\vec{v}/dt)_\parallel \approx QE_\parallel - M v_g^2(\vec{B}\cdot\nabla B)/2/B^2 \quad . \tag{7}$$

The intrinsic problem in these equations lies in the second and third terms on the right-hand side of (6), which have opposite directions for ions and electrons and are generally non-zero in the Earth inhomogeneous magnetosphere. These terms thus translate into electric currents which flow across the magnetic field lines and must be part of closed current loops in a stationary state. Otherwise the assumption in (5) cannot be a valid description of the particle dynamics.

As far as (5) is valid, equations (6) and (7) should provide a valid description of the interaction between the solar wind plasma and the Earth's magnetic field. In this case the currents associated with (6) can, at least in principle, close through the Earth's ionosphere, as indicated schematically in Figure 2. The field-aligned portions of such a current loop may be carried in part by terrestrial particles, but the flow density of these particles is limited by the maximum possible escape rates (e.g., Lemaire and Scherer, 1974). This restriction is less severe for the downward current, since the terrestrial electrons may escape at a higher rate than the ions if allowed to flow freely.

If the demand for upward current exceeds the flow rate of terrestrial ions, the additional contribution must be carried by precipitating solar electrons. The flow density of these electrons is on the other hand limited by the "magnetic mirror" force on the right-hand side of (7), and can only be increased by a parallel electric field. In fact, if these electrons have a Maxwell-Boltzmann distribution with a temperature T and density n, the flow density is limited by (3), where $U = e\Delta V$ and $C = n\sqrt{kT/(2\pi m)}$ (Lennartsson, 1980). This approach thus leads in a natural fashion to the subject of magnetic confinement. The fact that auroral electrons are observed to have a significantly higher temperature than solar electrons (cf. Fig. 1), may suggest, however, that (5) is not entirely valid.

III. A "CLASSICAL" APPROACH TO MAGNETIC CONFINEMENT

Since particles with different pitch angles mirror at different locations in an inhomogeneous static magnetic field, the number density n of these particles is a function of B, unless the velocity distribution is completely isotropic (according to Liouville's theorem). If the magnetic field strength has a single minimum B_o and increases monotonically away from this minimum, in at least one direction, then the density n is known at any $B > B_o$, if the distribution function is known at B_o. This is still true in the presence of a parallel electric field (assuming a one-dimensional geometry), provided the electric field is also time independent:

$$dE/dt = 0 \quad , \tag{8}$$

and the electric potential is sufficiently monotonic, for example (Chiu and Schulz, 1978):

$$dV/dB > 0 \tag{9}$$

$$d^2V/dB^2 \leq 0 \quad . \tag{10}$$

The last condition is much stronger than (4); it precludes double layer structures and implies that the electron and ion densities are very nearly equal at all points. Under these three conditions, and assuming that (5) holds and the ions are all positive and singly charged, the quasi-neutrality may be expressed in a somewhat "classical" form as:

$$n_e (V,B,f_{eo}) \approx n_i (V,B,f_{io}) \quad , \tag{11}$$

where f_{eo} and f_{io} are the electron and ion distribution functions, respectively, at B_o. With a careful selection of f_{eo} and f_{io} this relation will yield a solution for V in the form $V = V$ (B) (e.g., Alfvén and Fälthammar, 1963; Persson, 1963, 1966; Block, 1967; Lemaire and Scherer, 1974; Chiu and Schulz, 1978; Stern, 1981). Whether this also yields a self-consistent solution of Poisson's equation is a rather intricate question, however.

A comparatively simple and analytically tractable case is illustrated in Figure 3, which is adapted from the works of Persson (1966) and Block (1967). The shaded areas repesent the only populated regions of velocity space. Within these regions the particle distributions are assumed to be isotropic but may have arbitrary functional dependence on the energy and may be different for electrons and ions. The ions are also assumed to have energies

278

larger than $e(V_a - V(B))$, which ensures that no part of the ion energy distribution is entirely excluded from low altitude ($B \approx B_a$). The electron energies are only limited by the acceleration ellipsoid and by the loss hyperboloid. As discussed by Persson and Block, these ion and electron populations can be made to have equal densities everywhere, $n_i = n_e$, if and only if:

$$E_{\parallel} = -((V_a - V_o)/(B_a - B_o))dB/ds \quad , \tag{12}$$

where s is a distance coordinate running along $\vec{B}$ (downward). The conventional physical interpretation of this case is the following (cf. Persson and Block): Since the ion distribution at $B = B_o$ includes smaller pitch angles than the electron distribution, the ion density tends to exceed the electron density at $B > B_o$, thereby creating an upward electric field that drags the electrons along, modifies the electron and ion distributions, and maintains $n_i \approx n_e$ at all $B_o \leq B < B_a$ (and $n_i = n_e = 0$ at $B \geq B_a$).

Although this case may be considered more of a textbook example than a description of typical magnetospheric conditions, it has generally been thought to illustrate a sound physical principle. However, on closer inspection this physical principle may not seem entirely sound. If the right-hand side in (12) is differentiated once more with respect to s, assuming the magnetic field is a dipole field, it follows that:

$$dE_{\parallel}/ds < 0 \quad . \tag{13}$$

Hence, the small net charge required to maintain $n_i \approx n_e$ cannot be provided by the ions. In fact, there is no net positive charge at any location along the magnetic field line where $n_i > 0$, and there are no ions to support the electric stress at $B \geq B_a$. It can thus be argued that this simple case rather illustrates the difficulty of satisfying all of the conditions in (8)-(11) at the same time.

A much more elaborate and perhaps more realistic case has been presented by Chiu and Schulz (1978) and Chiu and Cornwall (1980). Their case also considers an ion population at high altitude which is isotropic outside of the loss hyperboloids in Figure 3, but the corresponding electron population is required to be anisotropic, with a wider distribution in $v_{\perp}$ and in $v_{\parallel}$ (bi-Maxwellian). Their case further includes particles within the loss hyperboloids, some of which have a terrestrial origin, and thus includes a net current. They reach the condition in (11) not by analytical methods alone, but by iterative numerical approximations, and their solution is far too complex to be evaluated here. A few comments with bearing on their case will be made below, however.

IV. POSSIBLE ROLE OF DOUBLE LAYERS

The studies of quasi-neutrality in a model magnetic mirror configuration show that it is mathematically possible to satisfy $n_i \approx n_e$ in a time-independent parallel electric field that extends over large distances and does not contain any double layer structures, provided the particle distribution functions are carefully designed. It is not clear from these studies, however, that such electric fields are realistic, or even physically possible. One argument to that effect was made in the preceding section, applied to a simple case where all particles are trapped by the combined electric and magnetic fields. Other arguments to the same effect may be applied to the more general case where the loss hyperboloids are also populated, and thus a current flows (e.g., Chiu and Schulz, 1978). In that case it can be argued, for instance, that the parallel electric field is made subject to potentially conflicting conditions; on one hand

the model electric field is designed to satisfy $n_i \approx n_e$ everywhere, based on the entire pitch angle distributions of all particles, while on the other hand the electric field in reality must also be subject to the external condition that the current be of the appropriate magnitude, and the current only involves particles within the loss hyperboloids.

The aforementioned studies, however, do point to an unambiguous condition for the non-existence of electric fields; in order for the parallel electric field to vanish over a large distance along a magnetic flux tube, the pitch angle distributions of ions and electrons, when integrated over all energies, must be identical (cf. Persson, 1963). As a consequence, it may not be possible, given realistic particle distributions, to have the electric field entirely contained within a single stable double layer, or even within multiple double layers. The double layers naturally generate different pitch angle distributions for the ions and the electrons, and these in turn will affect the quasi-neutrality at all other altitudes. In other words, a stable double layer may not be nature's replacement for an extended electric field, but may perhaps be part of it (cf. Stern, 1981). Such a configuration cannot be modeled, however, if the condition in (10) is part of the assumptions.

A possibly fundamental shortcoming of the classical approach to magnetic confinement is its disallowance of temporal variations in the electric field, including rapid and small-scale fluctuations. The assumption in (8) is needed to make a tractable problem, but may not be supported by data. Close scrutiny of Figure 1, for example, fails to produce the sharp boundaries of Figure 3 (with $B \approx B_a$). This and other published illustrations of auroral electron spectra have in fact a rather blurred appearance, suggesting that the electrons have traversed a "turbulent" electric field. Numerous reports of intense plasma wave turbulence at various altitudes along auroral magnetic field lines (e.g., Fredricks et al., 1973; Gurnett and Frank, 1977; Mozer et al., 1980; and references therein) lend additional support to that kind of interpretation.

Allowing the electric field to have temporal fluctuations of a small scale size may render an untractable computational problem, but provides for a more realistic description of the collective behavior of the particles. From a qualitative point of view this may also seem to make the magnetic mirror a more favorable environment for the formation of double layers, as illustrated schematically in Figure 4. This figure assumes that the increase in kinetic energy of individual electrons is not a unique function of location in space, but varies somewhat randomly about an average increase, due to temporal fluctuations in the electric field. Only the average increase is a function of location and has the sharp boundaries in velocity space. An electron that has a kinetic energy slightly inside of the acceleration boundary when passing point P, either on the way down or after mirroring in the magnetic field below, is likely to be trapped by the average electric field on the way up, thereby adding to the local concentration of negative charge (during part of its oscillation), at the expense of the negative charge at higher altitude. This in turn further widens the acceleration boundary in the transverse direction, enabling electrons with a larger perpendicular energy to be trapped as well. Electrons inside the acceleration boundary may be removed again after a slight increase in the energy, but the net diffusion is assumed inward as long as the density of particles is higher on the outside. A conceivable end result may be some form of double layer, thin enough to harbor a significant charge imbalance in a stable fashion (cf. Lennartsson, 1980).

Whether trapping of electrons between magnetic and electric mirror points will produce a stable double layer, or merely add to the plasma turbulence, cannot be decided from this simplistic exercise alone. A redistribution of the electric field from higher to lower altitude carries with it a redistribution of the ion density as well, and that is not considered. It is worth noting, however, that the shape and size of the electron acceleration boundary depends on the angle of the double layer, and is the smallest for a double layer with the electric field nearly perpendicular to $\vec{B}$. In that case the boundary may be almost circular (cf. Figure 3 with $B >> B_o$), and can trap the fewest number of electrons. This kind of structure is perhaps the most likely to materialize and is, in fact, reminiscent of the "electrostatic shocks" commonly observed in the auroral regions (e.g., Mozer et al., 1977; see also Swift, 1979; Lennartsson, 1980; Borovsky and Joyce, 1983). It also has a favorable geometry for satisfying (4), thus producing a large electron current.

280

REFERENCES

Alfvén, H., and C.-G. Fälthammar, *Cosmical Electrodynamics, Fundamental Principles,* Clarendon Press, Oxford, 1963.

Block, L. P., *Space Sci. Rev., 7,* 198 (1967).

Burch, J. L., W. Lennartsson, W. B. Hanson, R. A. Heelis, J. H. Hoffman, and R. A. Hoffman, *J. Geophys. Res., 81,* 3886 (1976).

Borovsky, J. E., and G. Joyce, *J. Geophys. Res., 88,* 3116 (1983).

Chiu, Y. T., and M. Schulz, *J. Geophys. Res., 83,* 629 (1978).

Chiu, Y. T., and J. M. Cornwall, *J. Geophys. Res., 85,* 543 (1980).

Evans, D. S., *J. Geophys. Res., 79,* 2853 (1974).

Fredricks, R. W., F. L. Scarf, and C. T. Russell, *J. Geophys. Res., 78,* 2133 (1973).

Goertz, C. K., *Rev. Geophys. Space Phys., 17,* 418 (1979).

Gurnett, D. A., and L. A. Frank, *J. Geophys. Res., 82,* 1031 (1977).

Hudson, M. K., R. L. Lysak, and F. S. Mozer, *Geophys. Res. Lett., 5,* 143 (1978).

Kaufmann, R. L., and G. R. Ludlow, *J. Geophys. Res., 86,* 7577 (1981).

Knight, S., *Planet. Space Sci., 21,* 741 (1973).

Lemaire, J., and M. Scherer, *Planet. Space Sci., 22,* 1485 (1974).

Lennartsson, W., *J. Geophys. Res., 81,* 5583 (1976).

Lennartsson, W., *Astrophys. Space Sci., 51,* 461 (1977).

Lennartsson, W., *Planet. Space Sci., 28,* 135 (1980).

Longmire, C. L., *Elementary Plasma Physics,* John Wiley and Sons, Inc., New York, London, 1963.

Lyons, L. R., D. S. Evans, and R. Lundin, *J. Geophys. Res., 84,* 457 (1979).

Lyons, L. R., *J. Geophys. Res., 86,* 1 (1981).

Mozer, F. S., M. K. Hudson, R. B. Torbert, B. Parady, and J. Yatteau, *Phys. Rev. Lett., 38,* 292 (1977).

Mozer, F. S., C. A. Cattell, M. K. Hudson, R. L. Lysak, M. Temerin, and R. B. Torbert, *Space Sci. Rev., 27,* 155 (1980).

O'Brien, B. J., *Planet. Space Sci., 18,* 1821 (1970).

Papadopoulos, K., *Rev. Geophys. Space Phys., 15,* 113 (1977).

Persson, H., *Phys. Fluids, 6,* 1756 (1963).

Persson, H., *Phys. Fluids, 9,* 1090 (1966).

Smith, R. A., *Physica Scripta, 25,* 413 (1982).

Stern, D. P., *J. Geophys. Res., 86,* 5839 (1981).

Swift, D. W., *J. Geophys. Res., 70,* 3061 (1965).

Swift, D. W., *J. Geophys. Res., 84,* 6427 (1979).

Yeh, H.-C., and T. W. Hill, *J. Geophys. Res., 86,* 6706 (1981).
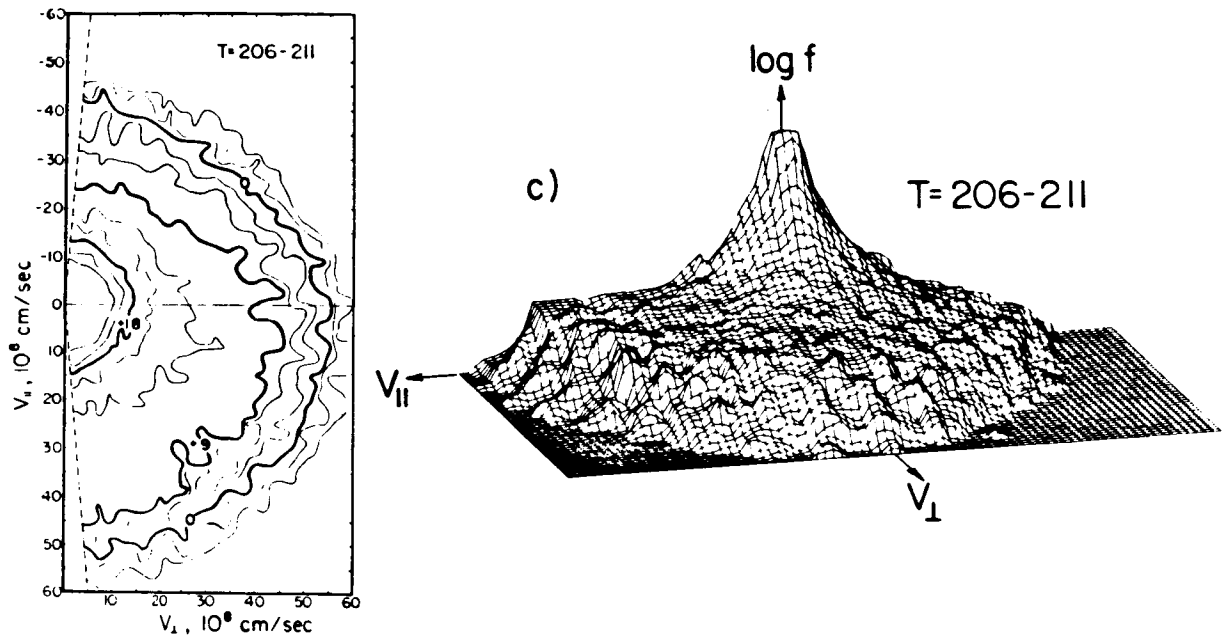
Figure 1. Contour and three-dimensional plot of auroral electron distribution function, in the energy range 25eV to 15 keV, measured from a rocket at about 240 km altitude. Downgoing electrons have positive $v_{\parallel}$. Curves of constant $f(\vec{v})$ on the contour plot are labeled by the common logarithm of $f(\vec{v})$ in s^3/km^6. This distribution is typical of electrons producing discrete auroral arcs (from Kaufmann and Ludlow, 1981).

C-4
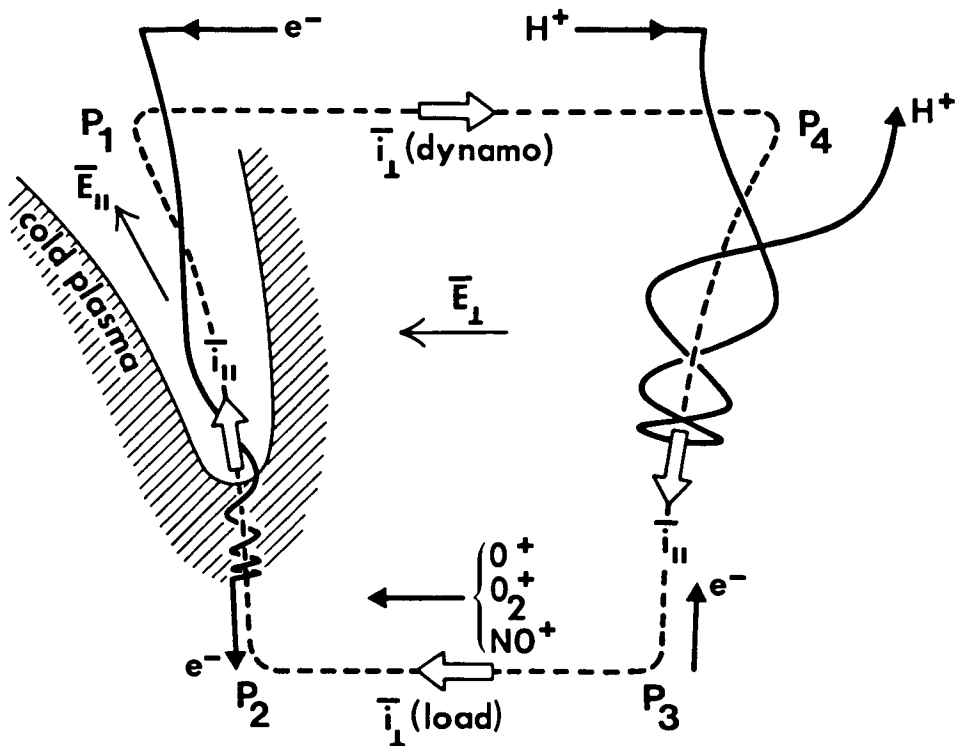
Figure 2. Schematic magnetosphere-ionosphere current system. The dynamo current $P_1 - P_4$ is assumed to be caused by the differential drift of hot protons and electrons. The downward parallel current $P_4 - P_3$ may be carried mainly by escaping ionospheric electrons, while the upward parallel current $P_2 - P_1$ is carried to a large extent by downflowing hot electrons. Point P_2 is at a high positive potential with respect to point P_1, which enables the downflowing electrons to overcome the magnetic mirror. The current $P_3 - P_2$ is a Pedersen current (from Lennartsson, 1976).

ELECTRONS
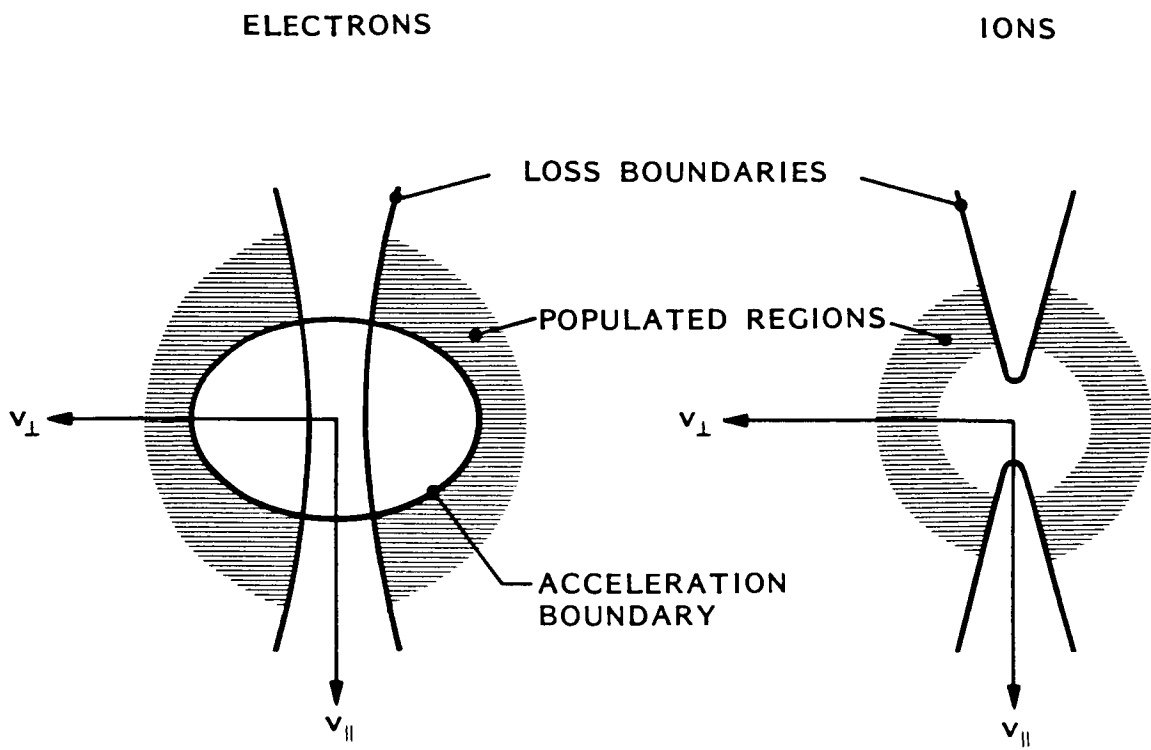
IONS

Figue 3. Hypothetical case of plasma confinement by a magnetic mirror in the presence of a parallel electric field, directed away from the magnetic mirror (upward). Only the shaded regions are assumed populated (see text). The loss boundaries (hyperboloids) are defined by $(B_a/B - 1)v_\perp^2 - v_\parallel^2 = 2H (V_a - V)$, where the subscript a refers to atmospheric (loss) altitude and $H = e/m_e$ for electrons and $H = -e/m_i$ for ions. The acceleration boundary (ellipsoid) is defined by $(1 - B_o/B)v_\perp^2 + v_\parallel^2 = 2 (e/m_e) (V - V_o)$, where the subscript o refers to a high altitude ($B_o <$ B) (adapted from Persson, 1966).
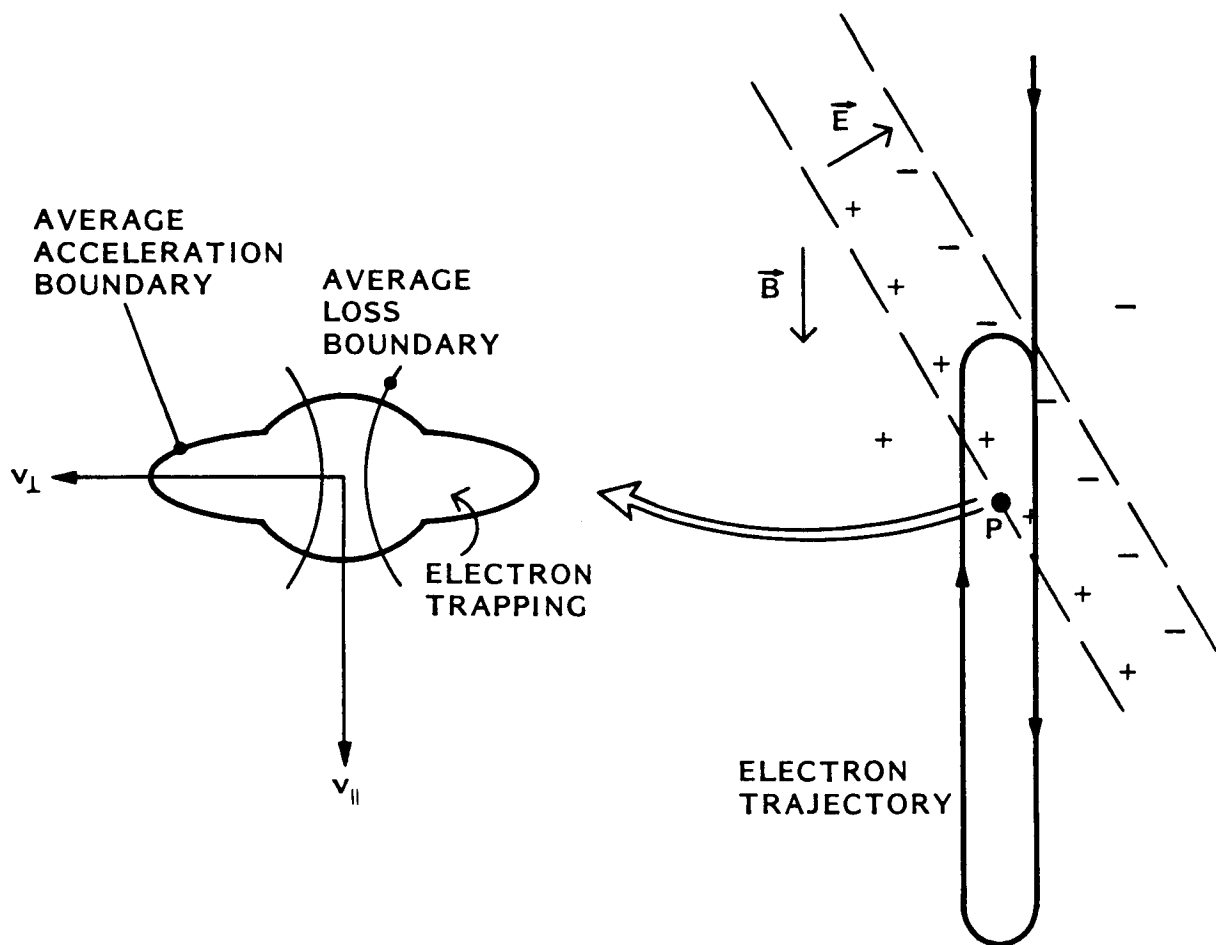
Figure 4. Hypothetical case of electron trapping by a locally enhanced electric field (right panel), associated with diffusion in velocity space (left panel). The diffusion is assumed to result from small-scale fluctuations in the electric field. The acceleration boundary at point P refers to an average acceleration and is the combined effect of the weak electric field at higher altitudes and the stronger field nearby (see text) (adapted from Lennartsson, 1980).

ELECTRIC POTENTIAL DISTRIBUTIONS AT THE INTERFACE
BETWEEN PLASMASHEET CLOUDS

D. S. Evans
NOAA/SEL
325 Broadway
Boulder, Colorado 80303, U.S.A.

and

M. Roth and J. Lemaire
Institut d'Aéronomie Spatiale de Belgique
3 av. Circulaire
B-1180 Bruxelles, Belgium

ABSTRACT

At the interface between two plasma clouds with different densities, temperatures, and/or bulk velocities, there are large charge separation electric fields which can be modeled in the framework of a collisionless theory for tangential discontinuities (see Lemaire and Burlaga, 1976; Roth, 1980; Botticher et al., 1983).

Two different classes of layers have been identified: the first one corresponds to (stable) ion layers which are thicker than one ion Larmor radius; the second one corresponds to (unstable) electron layers which are only a few electron Larmor radii thick.

We suggest that these thin electron layers with large electric potential gradients (up to 400 mV/m) are the regions where large-amplitude electrostatic waves are spontaneously generated. These waves scatter the pitch angles of the ambient plasmasheet electron into the atmospheric loss cone. The unstable electrons layers can therefore be considered as the seat of strong pitch angle scattering for the primary auroral electrons.

I. INTRODUCTION

Lyons and Evans (1984) found direct evidence from coordinated auroral and magnetospheric particle observations that discrete auroral arcs are located along geomagnetic field lines mapping in plasmasheet regions where significant spatial gradients in the magnetospheric particles velocity distribution are observed.

These observations as well as earlier theoretical calculations by Lemaire and Burlaga (1976) and Roth (1976, 1978, 1979, 1980) have motivated the present application of kinetic plasma theory to thin layers separating a hot plasmasheet cloud from a cooler background or another cloud which is populated with ions and electrons of different densities and temperatures. However, we do not simulate the magnetic field reversal region in the neutral sheet of the magnetotail.

We briefly recall the basic features of the kinetic model as well as the boundary conditions in the next section. The numerical results are presented in Section III; the discussion of this solution is given in the last section with the conclusions.

II. FORMULATION OF THE MODEL AND BOUNDARY CONDITIONS

The kinetic model used below is an extension of that proposed by Sestero (1964) to describe collisionless plasma sheaths in the laboratory. Although the plasmasheet is rarely in a stationary state, we assume that its structure does not change significantly over the characteristic period of time required for an Alfvén wave to traverse the transition layer.

Furthermore, it is assumed that the radius of curvature of the plasma sheath is much larger than its characteristic thickness, which is of the order of a few ion gyroradii. Under these circumstances the plasma layer can be considered as planar. Every physical quantity depends then on one space coordinate only, say x.

Since in general the magnetic field direction at the interface between plasmasheet diamagnetic irregularities does not vary by more than 10° or 20°, we consider that the direction of $\mathbf{B}$, does not change nor reverse across the transition layer, but that $\mathbf{B}$ remains always parallel to the z-axis. The partial electric current densities ($j^{+,-}$) of the ions (+) and electrons (-) are then necessarily parallel to the y-axis. The electric field (as spatial gradient of the potential ϕ) is in the x-direction. Indeed we assume that, in a frame of reference fixed with respect to the plasma layer, there is no mass flow across nor toward the surface of discontinuity ($v_x = 0$).

In our kinetic model the ions and electrons from the left-hand side (i.e., side 1) have velocity distributions ($f_1^{+,-}$) which tend to an isotropic Maxwellian at x = -∞. The zero-order moment (i.e., the density: $n_1^{+,-}$) of these distribution functions tends to an asymptotic density $N_1 = N_1^- = 0.5 \, cm^{-3}$, at x = -∞. The temperature of the ions and electrons $\theta_1^{+,-}$ from side 1 is determined by the second-order moments of $f_1^{+,-}$. When x tends to -∞, $\theta_1^+(x)$ tends to $T_1^+ = 12 \, keV$, and $\theta_1^-(x)$ tends to $T_1^- = 2.5 \, keV$.

When x varies from -∞ to +∞ we expect $n_1^{+,-}$ to decrease to zero, and the velocity distributions $f_1^{+,-}$ to become depleted in the domain of the velocity space which is not accessible to the particles from side 1, i.e., for those particles with the smallest velocities and therefore the smallest gyroradii.

In absence of Coulomb collisions and wave-particle interactions, these velocity distributions are solutions to the collisionless Boltzmann-Vlasov equation. Any function of the constants of motion is then a solution. Following Sestero (1964) we choose for $f_1^{+,-}$ truncated distributions which tend to isotropic Maxwellians at x = -∞, where $n_1^{+,-}$ and $\theta_1^{+,-}$ tend to the above given values for the densities and temperatures ($N_1^{+,-}$ and $T_1^{+,-}$), respectively.

When x tends to +∞ the domains of the velocity space where $f_1^{+,-}$ differs from zero become vanishingly small; $n_1^{+,-}$ decreases then asymptotically to zero, as expected, because a smaller and smaller fraction of ions and electrons from side 1 has large enough gyroradius to penetrate deep into region 2 on the opposite side of the transition layer. For details see Roth et al. (1986).

Region 2 is populated with electrons and ions of a different origin, i.e., with different temperature distributions $\theta_2^{+,-}(x)$ and different density distributions $n_2^{+,-}(x)$. In our numerical calculation we have taken the following boundary conditions: $\theta_2^{+,-}(\infty) = T_2^{+,-}$ with $T_2^+ = 3 \, keV$ and $T_2^- = 0.8 \, keV$; $n_2^{+,-}(\infty) = N_2^{+,-} = 0$, 15 cm^{-3} and $n_2^{+,-}(-\infty) = 0$.

The velocity distributions $f_2^{+,-}$ of the ions and electrons originating from region 2 can again be any function of the constants of motion. As above, truncated Maxwellian velocity distributions are adopted. They tend to isotropic Maxwellians at x = +∞, with densities and temperatures, respectively, equal to $N_2^{+,-}$ and $T_2^{+,-}$. When x tends to -∞, $f_2^{+,-} \neq 0$ only for a decreasing number of particles from side 2 which has large enough velocities (and gyroradii) to penetrate deep inside region 1.

288

Note that the asymptotic behavior of the plasma distribution depends only on the asymptotic form of $f_{1,2}^{+,-}$ when x goes to $\pm\infty$. The form of $f_{1,2}^{+,-}$ for any other x in between is responsible for the shape of the transition profiles. Thus, the state of the plasma at one end of the transition region (or at both ends in our case) does not uniquely determine the plasma and field variation within the transition. This results from the collisionless and adiabatic nature of the interaction between the plasma particles. In a collision-dominated plasma when irreversible processes are important, this would not, however, be the case; the transition profile is then uniquely determined by the boundary conditions.

The moments of $f_{1,2}^{+,-}$ are integrals over the domain of velocity space where $f_{1,2}^{+,-}$ is not equal to zero. The densities $n_{1,2}^{+,-}(x)$ are the zero-order moments of $f_{1,2}^{+,-}$; the partial current densities $(j_{1,2}^{+,-} = eZ^{+,-} n_{1,2}^{+,-} \cdot v_{1,2}^{+,-})$ are first-order moments, etc. These moments are analytical expressions depending on x through the electric potential $\phi(x)$ and the magnetic vector potential $a(x)$. Indeed, both $\phi(x)$ and $a(x)$ appear explicitly in the constants of motion and consequently in $f_{1,2}^{+,-}$. The analytic expressions for $n_{1,2}^{+,-}$ and $j_{1,2}^{+,-}$ are similar to those derived by Sestero (1964, 1966). They are given in the more detailed article by Roth et al. (1986).

The electric potential $\phi(x)$ must satisfy Poisson's equation. However, in non-relativistic plasmas, where the thermal velocity of the ions and electrons is much smaller than the speed of light, Sestero (1966) has shown that a satisfactory first approximation for $\phi(x)$ is obtained by solving, iteratively, the charge-neutral approximation of Poisson's equation, i.e.,

$$n_1^+ + n_2^+ = n_1^- + n_2^- \quad . \tag{1}$$

Once $\phi(x)$ has been determined for all x, the charge separation electric field, $E(x)$, can also be evaluated as $-d\phi/dx$. Finally, the Laplacian of $\phi(x)$ (i.e., $d^2\phi/dx^2$) can be calculated to estimate the value of the electric charge density $e(n^+ - n^-)$ associated with $\phi(x)$. It is shown, a posteriori, that the actual charge separation relative density $(n^+ - n^-)/n^+$ is indeed a small quantity throughout the whole plasma sheath; i.e., that (1) is a valid first approximation and substitute for Poisson's equation.

In the next section we present numerical results corresponding to a solution of equation (1) for which the electric potential ϕ_1 at $x = -\infty$ is equal to ϕ_2 at $x = +\infty$. A wider family of solutions for which $\phi_2 - \phi_1 = 0$ is discussed in Roth et al. (1986).

The partial current densities $(j_{1,2}^{+,-})$ carried by the ions and electrons drifting in the electric field $E(x)$ and magnetic fields $B(x)$ are also analytical expressions of $\phi(x)$ and $a(x)$. The currents produce diamagnetic effects which determine the variation of $a(x)$ and consequently of $B_z(x)$, the z-component of curl a. The vector potential $a(x)$ is solution of Maxwell's euations:

$$B_z = da/dx \text{ and } dB_z/dx = -\mu_o(j_1^+ + j_2^+ - j_1^- + j_2^-) \quad . \tag{2}$$

The standard predictor-corrector Hamin method for numerical integration of equation (2) can be used to obtain the value of $a(x)$ for all x, across the diamagnetic plasma layer (Ralston and Wilf, 1965). Since the magnetic field does not change direction, $a(x)$ is an increasing function of x; it varies from $a = -\infty$ at $x = -\infty$ to $a = +\infty$ at $x = +\infty$.

III. NUMERICAL RESULTS

Figures 1a and 1b show the distributions of $n_{1,2}^{+,-}$, the partial ion and electron density distributions as a function of x. The upper horizontal scale represents x in kilometers. The lower scale of the left-hand panels corresponds to x in units of proton gyroradii. The x's in the lower scale of the right-hand panels are expressed in electron gyroradii. Note in the left-hand side panels the smooth variation of the densities over distances of 2-3 ion Larmor gyroradii, i.e., 500-800 km. In the middle of this broad transition region near x = 0, there is a much sharper transition where all densities change significantly over distances of 2-3 electron Larmor gyroradii, i.e., 6-9 km (see enlargement in the right-hand side panels).

Panels c1 and c2 in Figure 1 show the total ion density, $n^+ = n_1^+ = n_2^+$, which according to the charge neutral equation (1), is equal to the total electron density $n^- = n_1^- + n_2^-$.

Panels d1 and d2 illustrate how $\theta^{+,-}$, the total ion and electron temperatures vary in the transition region: $\theta^{+,-}$ $= (n_1^{+,-}\theta_1^{+,-} + n_2^{+,-}\theta_2^{+,-})/(n_1^{+,-} + n_2^{+,-})$. Note again the broader scale of variation in the left-hand side panels and the much sharper decrease of θ^- near x = , illustrated in the right-hand side panel.

The distribution of the magnetic field $B_z(x)$ is shown in panels e1 and e2. The magnetic field intensity is equal to 40 nT at x = $-\infty$; this is a typical value of B in the plasmasheet chosen as boundary condition on side 1 at x = $-\infty$. The value of $B_z(x)$ increases to 66.4 nT at x = $+\infty$ with an enhanced variation near x = 0 due to the diamagnetic current contributed by the electrons in the thin electron sheath. It could be shown that the sum of the magnetic pressure and kinetic pressure is precisely a constant throughout the plasma layer.

The electric potential distribution shown in panels f1 and f2 is a continuous function of x. The potential difference between x = $-\infty$ and x = $+\infty$ is equal to zero in the case considered. But similar continuous solutions have been obtained for positive and negative values of $\phi_2 - \phi_1$ of the order of $\pm k T_{1,2}^{+,-}/e$ (see Roth et al. 1986). The gradient of the electric potential has a different direction in the electron layer near x = 0 than on both sides in the proton layer. This is also illustrated in the next panels (g1 and g2) showing the electric field intensity which is perpendicular to the surface of the plasma layer: E_x has a large negative value of -220 mV/m in the middle of the thin electron layer. This charge separation electric field accelerates the hotter and more numerous electrons from side 1 toward region 2. On both sides of the electron layer E_x has smaller positive values, not exceeding 2.5 mV/m. This electric field tends to accelerate the hotter and more numerous protons of side 1 toward the cooler and less dense region 2.

The relative electric space charge density deduced from $d^2\phi/dx^2$ is given in panels h1 and h2. It can be seen that $|n^+ - n^-|/n^+$ is smaller than 2 percent within the electron layer; it is smaller than 3 x 10^{-6} in the ion layer. This confirms a posteriori that charge-neutrality is satisfied to a very good approximation. This confirms also that the solution of equation (1) gives a satisfactory approximation $\phi(x)$ for the electric potential distribution throughout the whole transition.

The average bulk speed of the protons and electrons is given in kilometers per second in the panels i1 and i2: $V^{+,-} = (n_1^{+,-}V_1^{+,-} + n_2^{+,-}V_2^{+,-})/(n_1^{+,-} + n_2^{+,-})$. In the left-hand panel note the large ion jet velocity of more than 500 km/s. V^+ is parallel to the plasma layer and perpendicular to the magnetic field direction. These large ion jets (or ion beams) are spread over a distance of several hundred kilometers. Even more surprising is the narrow jet sheath of electrons with a velocity of the order of 10,000 km/s near x = 0 (see panel i2). These bulk speeds result from the acceleration of charges by the inhomogeneous electric field E(x) and from their deflection in opposite direction by the non-uniform magnetic field B(x).

Panels j1 and j2 give the value of $A = (V^+ - V^-)/U^+$ across the plasma layer; U^+ is the average thermal ion speed. When A is larger than unity, the plasma is unstable. Indeed $A = 1$ corresponds to the threshold for the modified two-stream instability (McBride et al., 1972) also called the lower-hybrid drift instability. It can be seen that in the ionic layer, outside the thin electron layer, $A < 1$; therefore, the parts of the plasma layer on both sides of the electron layer are stable, at least with respect to the modified two-stream instability. However, the thin electron sheath near $x = 0$ is highly unstable and consequently is a potential source for large-amplitude electrostatic waves. These waves can then interact with the electrons, change their pitch angles, and fill the atmospheric loss cone.

As a result of wave-particle interactions, the initially anisotropic (truncated) electron velocity distribution becomes more isotropic until A is equal to or lower than unity: the instability is then quenched. However, as long as the velocity distributions of the electrons have not become isotropic everywhere between $x = -\infty$ and $x = +\infty$, unstable electrons layers will form and generate electrostatic noise.

IV. DISCUSSION AND CONCLUSIONS

The results of the stationary kinetic model illustrated in this paper indicate a number of features pertinent to the study of plasma layers which are associated with discrete auroral arcs.

1. First of all, for the boundary conditions considered (i.e., different densities and temperatures of the electrons and ions on both sides of the plasma layer), the electric potential $\phi(x)$ is not constant, although $\phi(-\infty)$ and $\phi(+\infty)$ are imposed to be equal to zero at $x = \pm\infty$. This indicates that a plasma layer like that studied by Harris (1962) and Alpers (1969), where it is assumed that $\phi(x) = 0$, is by no means a unique nor a general solution.

2. The characteristic scales of variation of the plasma and field variables are the average ion Larmor radius for the broadest structure and the average electron Larmor radius for the thinner embedded electron sheath. If the wider scale of variation is typically 500-800 km in the equatorial plane of the magnetosphere at $L = 10$, its extent projected in the ionosphere is 30 times smaller, i.e., 15-30 km. This corresponds almost to the extent of inverted-V regions near discrete auroral arcs. It corresponds also to the region over which auroral field-aligned potential differences vary significantly.

3. Superimposed on these broad regions of potential variation are often much narrower ones (only a few hundred meters in extent) where sharp potential gradients are observed. We suggest that these thin regions with large electric field intensities are associated with electron layers in the magnetosphere like that found in our kinetic model calculation. The minimum thickness of these electron layers is 5-9 km in the plasmasheet. One can imagine velocity distributions for which there are several electron sheaths embedded in one broader ion structure. The thickness of 5-9 km is a minimum one; indeed electron sheaths are unstable with respect to the modified two-stream instability or lower-hybrid drift instability. Therefore, pitch angle scattering or diffusion of the electrons as a result of wave-particle interactions within these regions eventually tend to make the electron velocity distribution more isotropic. As a consequence the electron sheath tends to broaden and eventually to disappear when the velocity distribution of electrons has become isotropic within the plasma cloud and in the ambient background plasma.

4. Although in our one-dimensional model there is no proper atmospheric loss cone for the plasmasheet electrons, one can easily imagine that for a three-dimensional plasma layer in the magnetosphere the modified two-stream instability can similarly be a source for pitch angle scattering of the electrons and for filling of the atmospheric loss cone. To aliment this source of auroral electron precipitation it is necessary, however, to maintain the electron sheath unstable for the whole lifetime of the discrete auroral arc. Therefore, the plasma layer must constantly be reforming for instance by convection of the plasma cloud "surfing" earthward in the ambient plasmasheet background.

5. The peak value of -200 mV/m for the electric field intensity obtained in our kinetic model calculation is probably excessive. Indeed, the wave-particle diffusion mechanism mentioned above, will smooth irreversibly any too large electric potential gradient. Furthermore, such large perpendicular magnetospheric electric fields (EMF), when mapped down at ionospheric altitudes, must drive very large Pedersen and Hall electric currents through the resistive ionosphere. The Joule dissipation of these currents increases the local plasma temperature. But the local ionization density is then enhanced not only by the increased plasma temperature but also by primary auroral electron bombardment. All these effects concur to enhance the local electric conductivity and to short-circuit the ionospheric load. The large potential gradients applied across the magnetospheric plasma sheath are then discharged as the ionospheric resistance becomes vanishingly small. Magnetospheric potential differences (EMF) perpendicular to magnetic field lines then become field-aligned potential differences accelerating auroral electrons downward along auroral arc magnetic field lines.

6. Ion beams streaming earthward and/or tailward are typical features in the plasmasheet boundary layer adjacent to the tail lobe. These ion beams are observed from high energies of tens of keV to low energies of tens of eV (Lui et al., 1983). Occasionally, these ion beams are found within the plasma sheet proper, near its outer boundary where irregular magnetic field intensities are generally observed. Sugiura et al. (1970) have interpreted these irregular B-field variations as being diamagnetic signatures of spatial plasma clouds for which β is of the order of unity or larger (see also Meng and Mihalov, 1972). Both the ion beam streaming and the change in the magnetic field intensities are inherent in the kinetic model illustrated in Figure 1. It is suggested that ion beam streaming observed at the outer edge of the plasmasheet results from the electric field acceleration and magnetic field deflection of charge particles in plasma layers separating a hot plasma cloud and the cooler ambient plasmasheet or two adjacent diamagnetic plasma clouds of different densities, different temperatures, and different magnetizations, as in our kinetic model.

7. Changing boundary conditions at $x = \pm\infty$ ($N_{1,2}^{+,-}$, $T_{12,,}^{+,-}$) and the choice of the velocity distributions $f_{1,2}^{+,-}$, one can generate a wide variety of different plasma and field distributions within the plasma layer. The plasma layer shown in Figure 1 is only an illustrative example for a magnetospheric EMF source. From this case study one can deduce orders of magnitudes for maximum electric potential gradients (i.e., charge separation electric field), as well as for the maximum velocity of ion beams or jets expected in such plasma layers. By adjusting these boundary conditions and by adequately choosing $f_{1,2}^{+,-}$, it is likely that such kinetic model calculations will be able to simulate a variety of detailed plasma and field measurements across plasma layers or boundaries when available from instruments with high enough time resolution.

The temperature $\theta(x)$ and density $n(x)$ of each plasma species vary across the potential layer separating the hot plasmasheet cloud at $x = -\infty$ from the cooler background magnetotail plasma at $x = +\infty$. The layers considered here [for different values of $\phi_2 - \phi_1 = \phi(+\infty)$] have boundary conditions listed in Table 1. B_{sh} denotes the value of the magnetic field at $x = -\infty$, i.e., deeply inside the plasmasheet cloud. The lower indices sh and t refer to the plasmasheet cloud and background magnetotail particles, respectively, while the upper indices (-) and (+) refer to electrons and protons, respectively. The following notations are assumed: $n_{sh}^{+,-}(-\infty) = N_{sh}^{+,-}$; $\theta_{sh}^{+,-}(-\infty) = T_{sh}^{+,-}$; $n_t^{+,-}(+\infty) = N_t^{+,-}$; $\theta_t^{+,-}(+\infty) = T_t^{+,-}$.

The plasma boundary conditions given in Table 1 correspond to two interpenetrated hydrogen plasmas with different characteristics. Therefore, $n_{sh}^{+,-}(+\infty) = 0$ and $n_t^{+,-}(-\infty) = 0$.

TABLE 1. BOUNDARY CONDITIONS

N_{sh}^- cm^{-3}	T_{sh}^- keV	N_{sh}^+ cm^{-3}	T_{sh}^+ keV	N_t^- cm^{-3}	T_t^- keV	N_t^+ cm^{-3}	T_t^+ keV	B_{sh} nT
0.5	2.5	0.5	12	0.15	0.8	0.15	3	40

292

REFERENCES

Alpers, W., *Astrophys. Space Sci.*, *5*, 425-537 (1969).

Botticher, W., H. Wank, and E. Schulz-Gulde (editors), *Proceedings of International Conference on Phenomena in Ionized Gases*, Dusseldorf, August 29-September 2, 1983, pp. 139-147, 1983.

Harris, E. G., *Nuovo Cimento, 23,* 115-121 (1962).

Lemaire, J., and L. F. Burlaga, *Astrophys. Space Sci., 45,* 303-325 (1976).

Lui, A. T. Y., T. E. Eastman, D. J. Williams, and L. A. Frank, Preprint APL/JHU 83-22, 1983.

Lyons, L. R., and D. S. Evans, *J. Geophys. Res., 89,* 2395-2400 (1984).

McBride, J. E., E. Ott, J. P. Boris, and J. H. Orens, *Phys. Fluids, 15,* 2367-2383 (1972).

Meng, C. I., and J.D. Mihalov, *J. Geophys. Res., 77,* 4661-4669 (1972).

Ralston, A., and H. S. Wilf, *Méthodes Mathématiques Pour Calculateurs Arithmétiques,* Dunod, Paris, 482 pp., 1965.

Roth, M., *J. Atmos. Terr. Phys., 38,* 1065-1070 (1976).

Roth, M., *J. Atmos. Terr. Phys., 40,* 323-329 (1978).

Roth, M., in *Proceedings of Magnetospheric Boundary Layers Conference, Alpbach, 11-15 June 1979,* ESA SP-148, edited by B. Battrick and J. Mort, pp. 295-309, ESTEC, Norrdwijk, The Netherlands, 1979.

Roth, M., Ph.D. Thesis, ULB, Brussels, 1980; *Aeronomica Acta A, 221* (1980) (also *Académie Royale de Belgique, Mémoire de la Classe des Sciences,* Collection in 8° - 2e série, T XLIV - Fascicule 7 et dernier, 1984).

Roth, M., D. S. Evans, and J. Lemaire, *J. Geophys. Res.,* submitted, 1986.

Sestero, A., *Phys. Fluids, 7,* 44-51 (1964).

Sestero, A., *Phys. Fluids, 9,* 2006-2013 (1966).

Sugiura, M., T. L. Skillman, B. G. Ledley, and J. P. Heppner, in *Particles and Fields in the Magnetosphere,* edited by B. M. McCormac, pp. 165-170, D. Reidel Publishing Company, Hingham, Massachusetts, 1970.
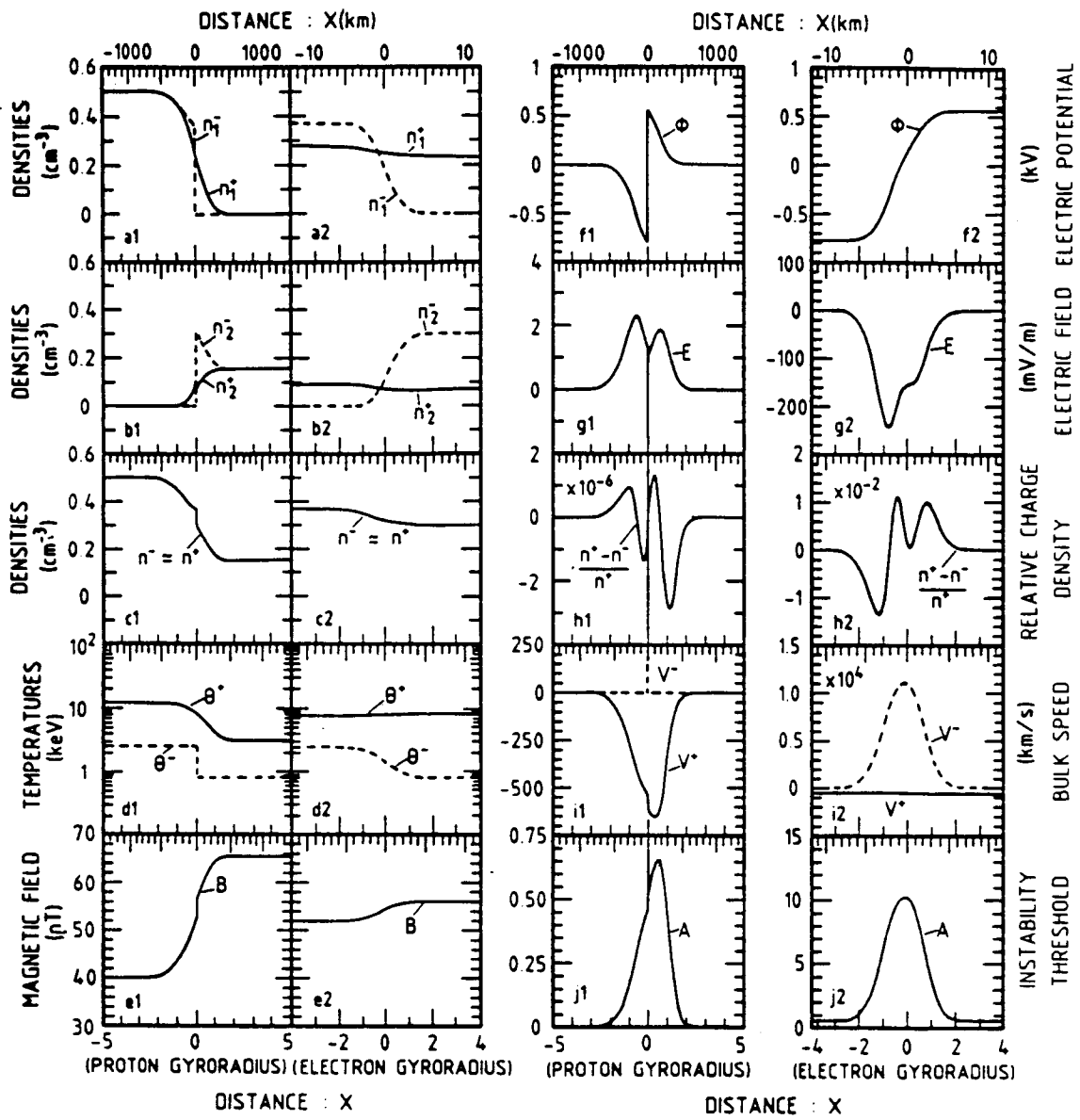
Figure 1. Plasma and field distributions across a plasma layer with boundary conditions typical in the plasmasheet. $\phi(x)$ and $B(x)$ are the electric potential and magnetic field intensity, respectively: ϕ varies from $\phi(-\infty) = 0$ to $\phi(+\infty) = 0$ (see panels f1 and f2); the gradient of ϕ determines the charge separation electric field E which is normal to the surface of the plasma layer (see panels g1 and g2); the relative electric space charge density remains small (see panels h1 and h2); the proton (+) and electron (-) densities $n_{1,2}^{+,-}$ from side 1 (i.e., $x = -\infty$) and from side 2 (i.e., $x = +\infty$) vary across the layer from $n_1^{+,-} = 0.5$ cm^{-3}, $n_2^{+,-} = 0$ at $x = -\infty$ to $n_1^{+,-} = 0$, $n_2^{+,-} = 0,15$ cm^{-3} at $x = +\infty$ (see panels a1, a2, b1, b2, c1, c2); the proton (+) and electron (-) temperatures $\theta^{+,-}$ vary from $\theta_1^+ = 12$ keV, $\theta_1^- = 2.5$ keV at $x = -\infty$ to $\theta_2^+ = 3$ keV, $\theta_2^- = 0,8$ keV at $x = +\infty$ (see panels d1 and d2); the proton (+) and electron (-) bulk velocities $V^{+,-}$ have large peak values in the middle of the composite plasma layer (see panels i1 and i2). Note the very thin electron layer embedded near $x = 0$ within the broader ion layer extending over 4 average ion Larmor gyroradii (see lower scales of left-hand side panels). Expanded views of the narrow electron layer (only 3 or 4 average electron Larmor gyroradii in extent) are shown in the right-hand side panels. The distance x across the planar surface of interface is also shown in kilometers by the upper scales. The thin electron layer is unstable with respect to the modified two-stream instability. Indeed the instability threshold A (see panel j2) exceeds unity in this narrow region where extremely large (and unstable) E-fields are generated.

294

DOUBLE LAYERS ABOVE THE AURORA

M. Temerin and F. S. Mozer
Space Sciences Laboratory and Physics Department
University of California, Berkeley, California 94720, U.S.A.

ABSTRACT

Two different kinds of double layers have been found in association with auroral precipitation. One of these is the so-called "electrostatic shock," which is oriented at an oblique angle to the magnetic field in such a way that the perpendicular electric field is much larger than the parallel electric field. This type of double layer is often found at the edges of regions of upflowing ion beams and the direction of the electric field in the shock points toward the ion beam. The potential drop through the shock can be several kV and is comparable to the total potential needed to produce auroral acceleration. Instabilities associated with the shock may generate obliquely propagating Alfvén waves, which may accelerate electrons to produce flickering aurora. The flickering aurora provides evidence that the electrostatic shock may have large temporal fluctuations.

The other kind of double layer is the small-amplitude double layer found in regions of upward flowing ion beams, often in association with electrostatic ion cyclotron waves. The parallel and perpendicular electric fields in these structures are comparable in magnitude. The associated potentials are a few eV, which is substantially less than the energy of the measured particles. However, since many such double layers are found in regions of upward flowing ion beams, the combined potential drop through a set of these double layers can be substantial.

Some important questions concerning double layers and their relation to parallel electric fields in the aurora are:

1. What is the relation between small-amplitude double layers and electrostatic shocks?

2. What is the relation between electrostatic shocks and discrete arcs?

3. Are there strong double layers in the aurora?

4. What is the relation between ion conics and electrostatic shocks?

5. What are the parallel electric field magnitudes on auroral field lines?

6. Are there large parallel electric fields in the return current region?

7. How important are the dynamic properties of the parallel electric field on auroral field lines?

Here are some answers:

1. What is the relation between small-amplitude double layers and electrostatic shocks?

Small-amplitude double layers and electrostatic shocks are distinctly different phenomena. Electrostatic shocks are large, greater than about 100 mV/m, mostly perpendicular electric fields that vary discontinuously when measured at the 0.125 s resolution of the dc electric field detector on the S3-3 satellite below 8000 km altitude (Mozer et al., 1977, 1980) (see Fig. 1 for examples). Small-amplitude double layers are several mV/m, mostly

parallel electric fields lasting for a few milliseconds as measured by the S3-3 satellite (Temerin et al., 1982; Mozer and Temerin, 1983; Temerin and Mozer, 1984a,b) (Fig. 2). Electrostatic shocks occur in both upward and downward current regions (Cattell et al., 1979) in association with both upflowing ion beams and ion conics (Redsun et al., 1985) (Figs. 3 and 4). The electrostatic shocks associated with upflowing ion beams typically occur at the edges of energetic (>1 keV) upflowing ion beams (Temerin et al., 1981; Bennett et al., 1983; Temerin and Mozer, 1984a; Redsun et al., 1985), and the potential drop through the electrostatic shock corresponds fairly well to the energy of the upflowing ion beam. Small-amplitude double layers, on the other hand, occur within regions of less energetic upflowing ion beams, and the potential drop through many small double layers may correspond to the total potential drop along the field line. It is often difficult to determine on the basis of the S3-3 wave data whether small-amplitude double layers occur in more energetic ion beams because of detector saturation problems associated with the large-amplitude wave turbulence that occurs in the more energetic events.

2. What is the relation between electrostatic shocks and discrete arcs?

It has previously been argued that electrostatic shocks are associated with discrete arcs (Torbert and Mozer, 1978; Kletzing et al., 1983). It is clear from the data that, as described in 1 above, some electrostatic shocks are associated with upflowing ion beams and inverted-V events. Other electrostatic shocks are associated with conics and counterstreaming and field-aligned electron events (Temerin and Mozer, 1984a). These latter electrostatic shocks would then not be associated with discrete arcs. It should be noted that upflowing ion beams and inverted-V electron events associated with electrostatic shocks have the ~10 km to over 200 km latitudinal width normally associated with inverted-V electron events (Lin and Hoffman, 1979a; Redsun et al., 1985). This is typically larger than the latitudinal width of the electrostatic shock and implies that the electrostatic shock makes an oblique angle with respect to the magnetic field over part of its altitudinal extent.

3. Are there strong double layers in the aurora?

Whether there are strong double layers in the aurora depends to some extent on one's definition of a strong double layer. If by a strong double layer one means a potential drop the order of a significant fraction of the total auroral zone potential drop over a few Debye lengths, then the parallel electric field should be in excess of 1 V/m. Boehm and Mozer (1981) searched the S3-3 electric field data and found no convinncing parallel electric fields greater than 250 mV/m in association with inverted-V events. They concluded that strong double layers are not associated with inverted-V events but could be associated with narrow discrete auroral arcs since the statistics were not good enough to rule out strong double layers if they were confined to narrow regions. This begs the question of whether there is any qualitative difference between narrow discrete arcs and inverted-V electron events with respect to the auroral potential structure. The problem of narrow discrete arc scales was raised by Maggs and Davis (1968) who reported that discrete arcs had scales down to 70 m. It has become popular to contrast such scales with inverted-V scales which are known to be much larger. However, the observation of 70 m scales was made by image orthicon television cameras that tend to emphasize small contrasts (Davis, 1978). Rocket observations indicate that typically the smallest gradients in the downward auroral electron energy flux are an order of magnitude larger (D. Evans, private communication). One should also keep in mind that inverted-V scales can be quite small. Lin and Hoffman (1979a), using AE-D data, reported that the largest number of inverted-V events had scales close to the minimum resolution of 0.2° or about 20 km in the ionosphere. The smallest paired electrostatic shock structure, which includes the region of smaller electric field between the large electric fields of the paired shock, and the smallest resolvable inverted-V structure on S3-3 map to about 5 km in the ionosphere (e.g., the first paired shock structure in orbit 209 in Fig. 1). In addition, one should keep in mind that smaller scale structures, such as field-aligned electron fluxes at the edges of inverted-V events (Arnoldy et al., 1985; McFadden et al., 1986) and field-aligned electron structures within inverted-V events, do not seem to correspond to larger overall potential as measured by the monoenergetic peak in the electron distribution function (Lin and Hoffman, 1979b). Thus, it seems consistent to regard narrow discrete arcs as narrow inverted-V events with the smallest scale structure within the arc as either due to relatively small changes in the field-aligned potential or enhanced field-aligned electron fluxes not directly related to changes in the potential. If this is the case, it could be that there are no strong double layers associated with the aurora. More data are needed to answer the question definitively.

4. What is the relation between ion conic and electrostatic shocks?

It has been proposed that electrostatic shocks produce ion conics (Yang and Kan, 1983; Greenspan, 1984; Borovsky, 1984). Figures 3 and 4 show that many electrostatic shocks are indeed associated with ion conics. However, the idea that electrostatic shocks produce conics does not explain the clear distinction between electrostatic shocks associated with ion beams and electrostatic shocks associated with ion conics, nor does it explain the production of conics in regions where there are no electrostatic shocks. Even in regions where there are electrostatic shocks, the conic occurs in a much broader region than the electrostatic shock. Models for the generation of ion conics by electrostatic shocks show that the thickness of the electrostatic shock and the angle it makes with the magnetic field determine the relative perpendicular and parallel acceleration. One would then expect a continuous transition between conics and ion beams. In fact there is almost always at S3-3 altitudes (<8000 km) a clear distinction between ion beams and ion conics, and, except for some general heating of the ion distribution, ion beams are consistent with acceleration purely parallel to the magnetic field while ion conics are consistent with acceleration purely perpendicular to the magnetic field. As mentioned previously, energetic ion beams are clearly associated with electrostatic shock. This implies that electrostatic shocks associated with ion beams are quasi-static on the ion transit time scale but that electrostatic shocks associated with ion conics are not. A more correct model of ion conic acceleration in regions of electrostatic shocks would need to take account of the fluctuations in the electric field and the general electric field turbulence in the region surrounding the electrostatic shocks. In regions of ion conics "electrostatic shocks" are not necessarily electrostatic (Temerin and Mozer, 1984a).

5. What are the parallel electric field magnitudes on auroral field lines?

The parallel electric field can be measured directly or inferred from particle measurements. Measurements of ion beams and electron loss cones indicate that potential drops of 10 kV or larger can sometimes occur below the S3-3 satellite at altitudes of 6000 to 8000 km. Since the upward pointing electric field region has never been observed on S3-3 to extend below 3000 km and is usually limited to above 5000 km, the average parallel electric field in an inverted-V acceleration region must at least sometimes be the order of 5 to 10 mV/m and the maximum parallel electric field should be substantially larger since it is not likely that the electric field is uniform throughout the region. Direct measurements in electrostatic shocks indicate parallel electric fields up to about 100 mV/m (Mozer et al., 1980; Mozer, 1980). However, in most cases, the parallel electric field is less than 25 mV/m even in electrostatic shocks associated with upward flowing ion beams (Temerin and Mozer, 1984a).

6. Are there large parallel electric fields in the return current region?

There are also large potential drops in the return current region. The electric field points down, which is in the direction to accelerate ions into the ionosphere and electrons into the magnetosphere. Some of the best evidence for downward pointing electric fields is shown in Figure 5, which displays some recent rocket data, courtesy of C. Carlson, J. McFadden, and M. Boehm. At 760 s into the flight, there was an almost complete dropout in the energetic electrons correlated with an enhancement in the precipitating ions flux over a narrow energy range at energies between 5 and 10 keV. At the same time, the eastward component of the magnetometer was consistent with a downward field-aligned current. These data imply a potential drop in the return current region in excess of 5 kV. Large downward electric fields can also be inferred from the observations of black aurora (Davis, 1978). Black aurora appear as narrow streaks of dark sky in regions of otherwise diffuse illumination. Broader regions of weaker parallel electric fields can be inferred from the S3-3 and DE 1 observations of upward flowing field-aligned electrons. One would expect that the narrow regions of downward pointing electric fields would correspond to paired electrostatic shocks with the electric fields in the paired shock pointing away from the region of parallel acceleration. Examples of such events are, however, comparatively rare in the S3-3 data.

7. How important are the dynamic properties of the parallel electric field on auroral field lines?

On the ion transit time scale the fluctuating portion of the parallel electric field must be several times larger than the dc portion. This is clear from the parallel velocity distribution of the upflowing ion beam. Typically, there is observable flux in an ion beam at energies four times larger than the energy of the maximum flux. This implies that in the frame of reference moving with the energetic ion the electric field is four times larger than the average field. These fields may be provided by the small-amplitude double layers and the parallel electric field components of the electrostatic ion cyclotron waves that are associated with the upflowing ion beams.

Another interesting dynamic property of auroral acceleration is flickering aurora. Recent data and theoretical models (Temerin et al., 1986) show that an obliquely propagating ion cyclotron wave, which may be produced by an oscillating double layer or oscillating parallel electric field, can produce the oscillating field-aligned electron flux in the flickering aurora.

REFERENCES

Arnoldy, R. L., T. E. Moore, and L. H. Cahill, Jr., *J. Geophys. Res.*, *90*, 8445 (1985).

Bennett, E. L., M. Temerin, and F. S. Mozer, *J. Geophys. Res.*, *88*, 7107 (1983).

Boehm, M. H., and F. S. Mozer, *Geophys. Res. Lett.*, *8*, 607 (1981).

Borovsky, J. E., *J. Geophys. Res.*, *89*, 2251 (1984).

Cattell, C. A., R. L. Lysak, R. B. Torbert, and F. S. Mozer, *Geophys. Res. Lett.*, *6*, 621 (1979).

Davis, T. N., *Space Sci. Rev.*, *22*, 77 (1978).

Greenspan, M. E., *J. Geophys. Res.*, *89*, 2842 (1984).

Kletzing, C., C. Cattell, F. S. Mozer, S.-I. Akasofu, and K. Makita, *J. Geophys. Res.*, *84*, 4105 (1983).

Lin, C. S., and R. A. Hoffman, *J. Geophys. Res.*, *84*, 1514 (1979a).

Lin, C. S., and R. A. Hoffman, *J. Geophys. Res.*, *84*, 6547 (1979b).

Maggs, J. E., and T. N. Davis, *Planet. Space Sci.*, *16*, 205 (1968).

McFadden, J. P., C. W. Carlson, and M. H. Boehm, *J. Geophys. Res.*, *91*, 1723 (1986).

Mozer, F. S., *Geophys. Res. Lett.*, *7*, 1097 (1980).

Mozer, F. S., and M. Temerin, in *High-Latitude Space Plasma Physics*, edited by B. Hultqvist and T. Hagfors, Plenum, New York, 1983.

Mozer, F. S., C. W. Carlson, M. K. Hudson, R. B. Torbert, B. Parady, J. Yatteau, and M. C. Kelley, *Phys. Rev. Lett.*, *38*, 292 (1977).

Mozer, F. S., C. A. Cattell, R. L. Lysak, M. K. Hudson, M. Temerin, and R. B. Torbert, *Space Sci. Rev.*, *27*, 15 (1980).

Redsun, M. S., M. Temerin, and F. S. Mozer, *J. Geophys. Res.*, *90*, 9615 (1985).

Temerin, M., and F. S. Mozer, *Proc. Indian Acad. Sci.*, *93*, 227 (1984a).

Temerin, M., and F. S. Mozer, in *Second Symposium on Plasma Double Layers and Related Topics*, edited by R. Schrittwieser and G. Eder, University of Innsbruck, 1984b.

Temerin, M., M. H. Boehm, and F. S. Mozer, *Geophys. Res. Lett.*, *8*, 799 (1981).

Temerin, M., K. Cerny, W. Lotko, and F. S. Mozer, *Phys. Rev. Lett.*, *48*, 1175 (1982).

Temerin, M., J. McFadden, M. Boehm, and C. W. Carlson, *J. Geophys. Res.*, in press, 1986.

Torbert, R. B., and F. S. Mozer, *Geophys. Res. Lett.*, *5*, 135 (1978).

Yang, W. H., and J. R. Kan, *J. Geophys. Res.*, *88*, 465 (1983).
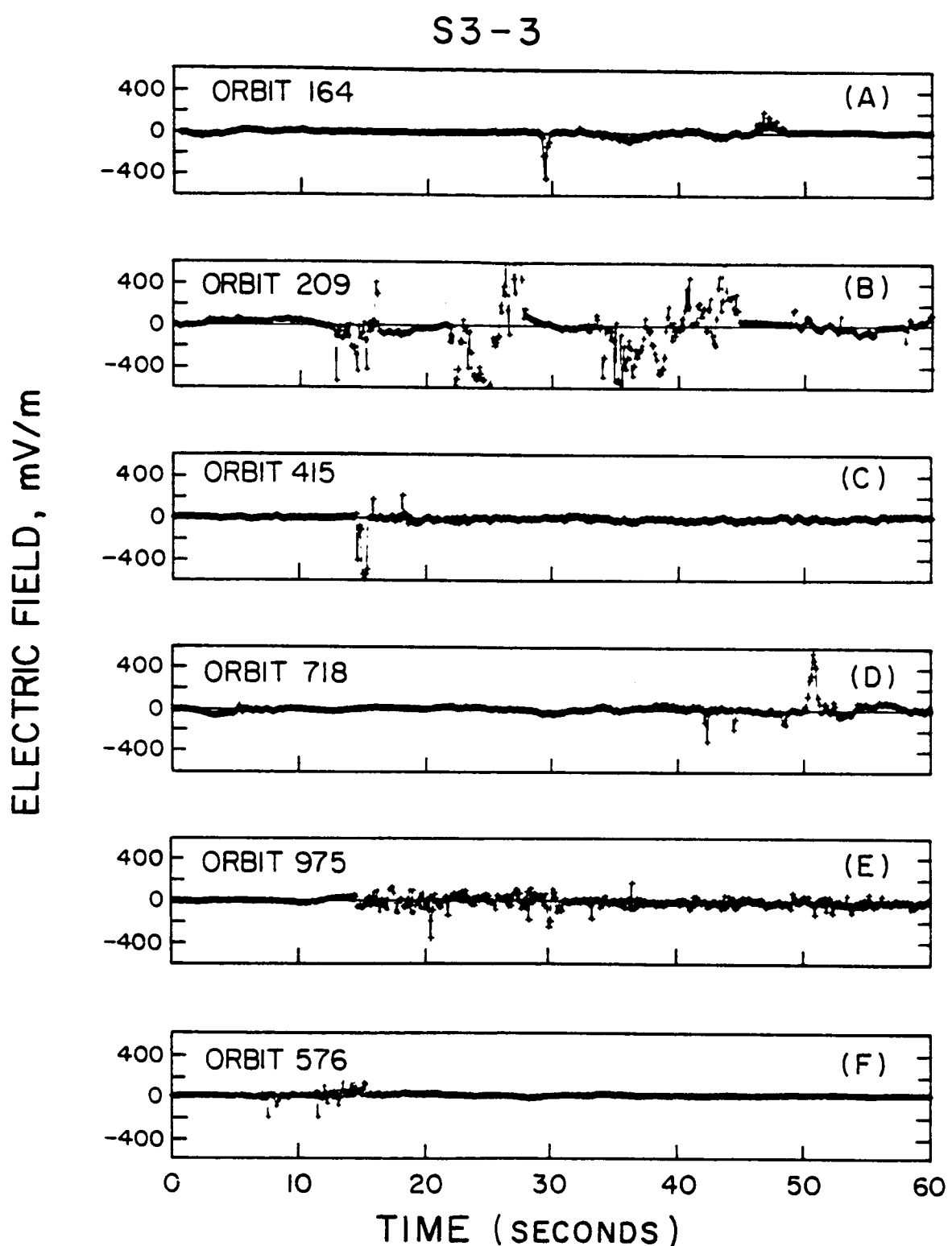
Figure 1. Examples of electrostatic shocks measured by the S3-3 satellite
at altitudes below 8000 km.
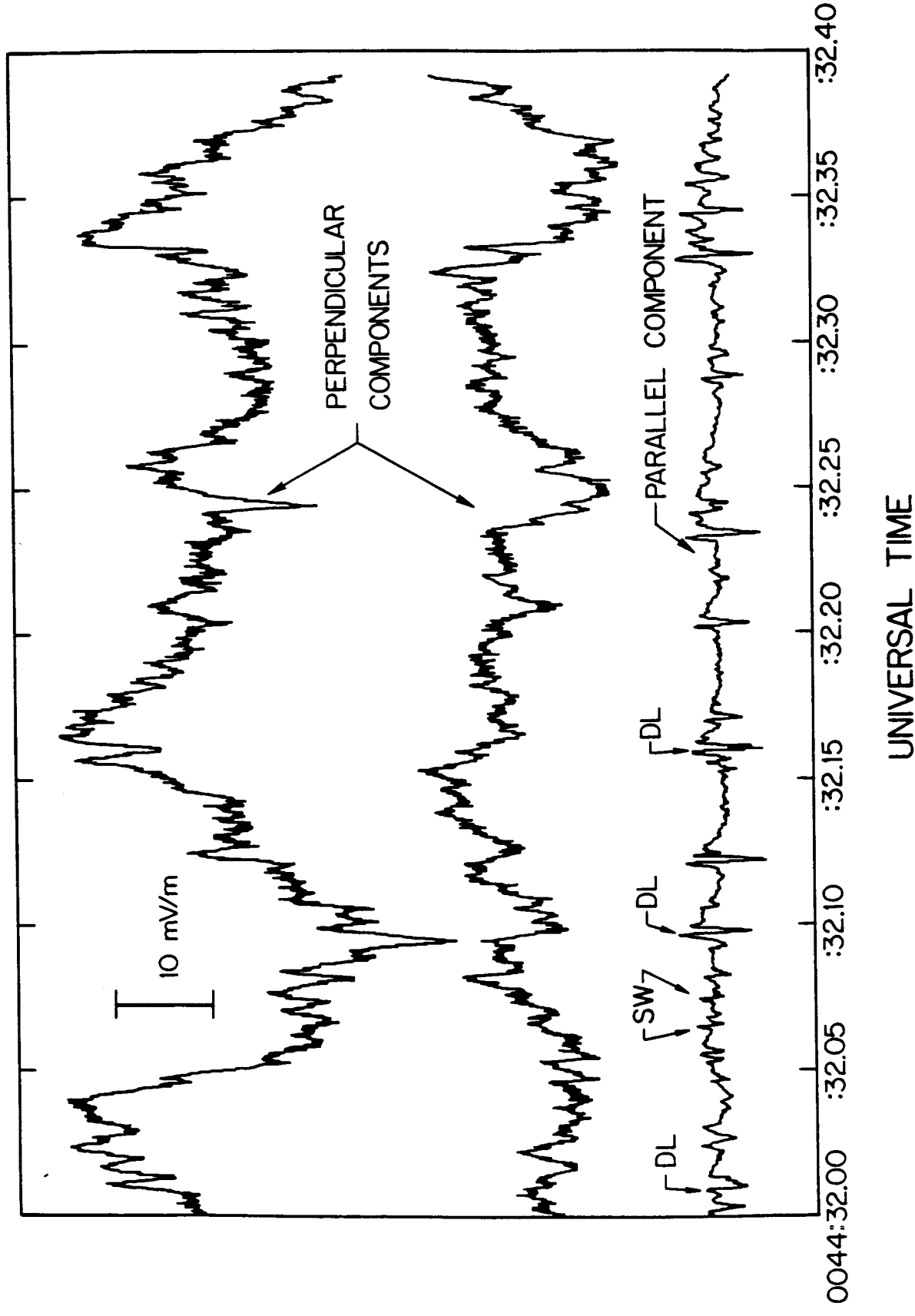
Figure 2. Examples of small-amplitude double layers measured by the S3-3 satellite. The noteworthy aspect of small-amplitude double layers is the significant parallel electric field (from Temerin et al., 1982).
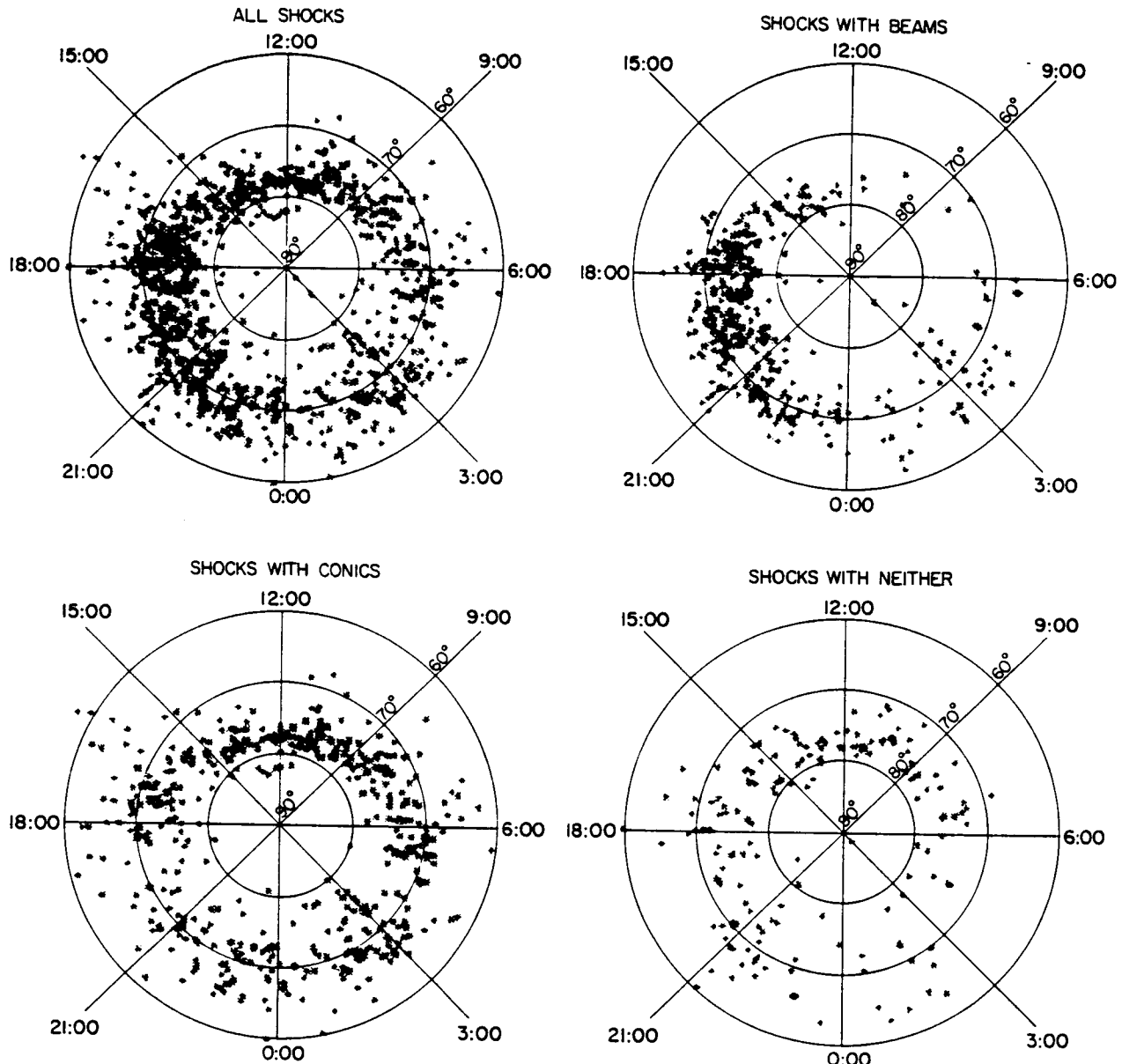
Figure 3. The distribution of electrostatic shocks as a function of invariant
latitude and magnetic local time (from Redsun et al., 1985).

301
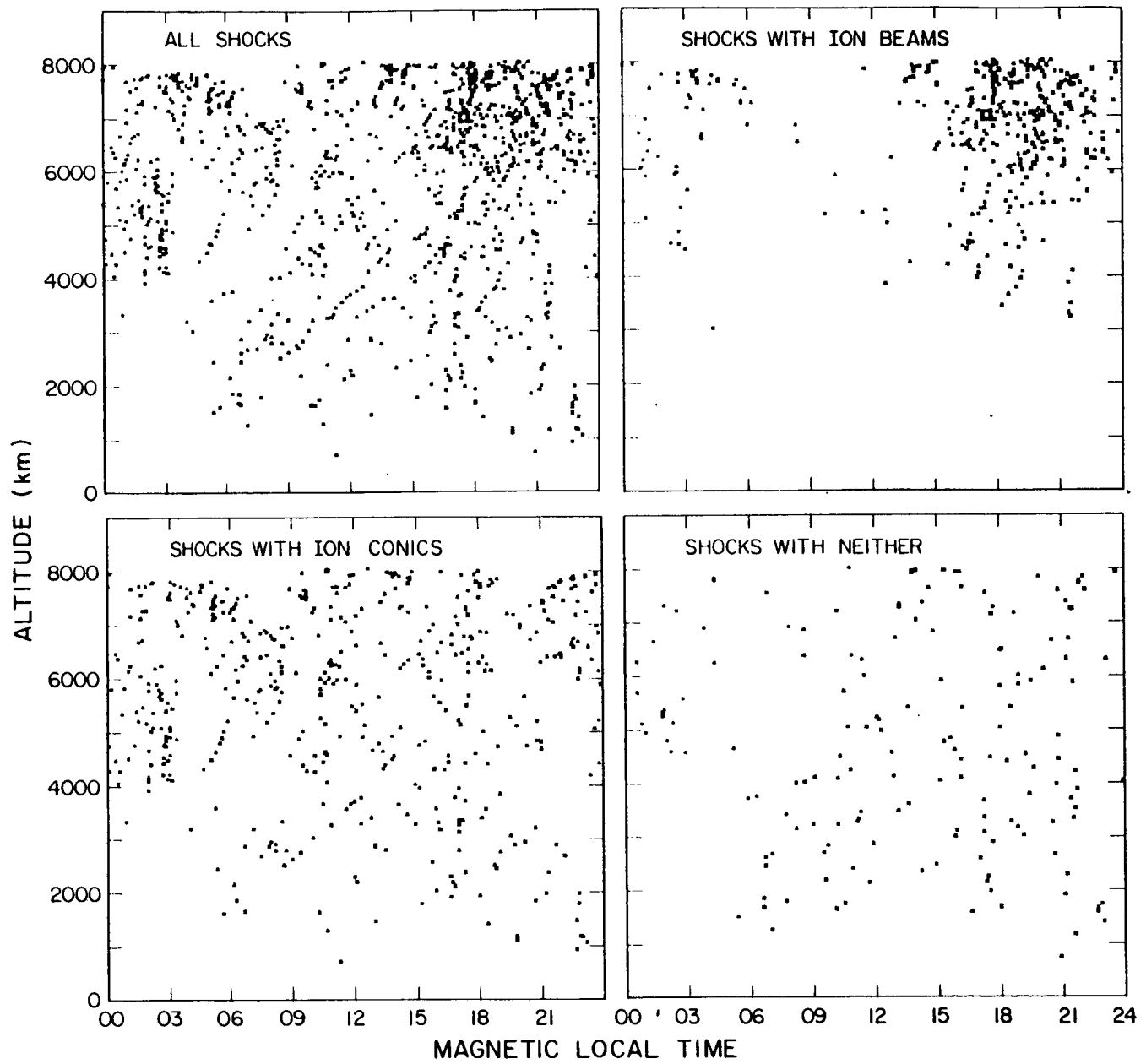
Figure 4. The distribution of electrostatic shocks as a function of altitude
and magnetic local time (from Redsun et al., 1985).
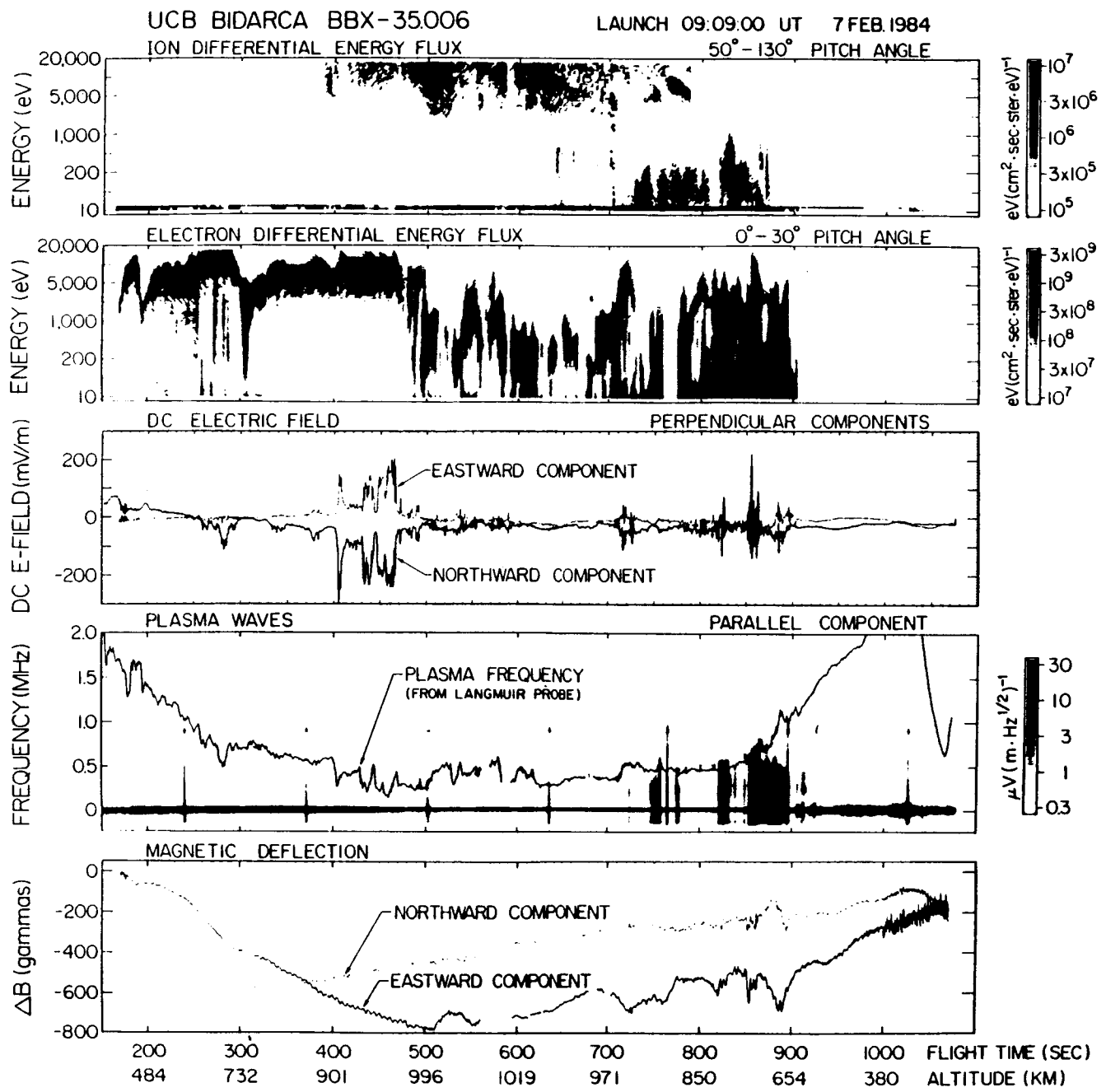
Figure 5. Recent rocket data. Example of anticorrelation of electron and ion fluxes can be seen at 760 s flight time. (Data courtesy of C. Carlson, J. McFadden and M. Boehm.)

BEAMED EMISSION FROM GAMMA-RAY BURST SOURCES

R. Epstein
Los Alamos National Laboratory
Los Alamos, New Mexico 87545, U.S.A.

Gamma-ray bursts are intense fluxes of radiation in the 100 keV to several MeV energy range which typically persist for between a fraction of a second and several seconds. The observed spectral shapes of these bursts suggest that the radiation is emitted as highly collimated beams emanating from neutron stars. This inference is based on the lack of significant gamma-gamma absorption (which indicates that photon paths do not cross at large angles) and by the dirth of x-ray energy photons (which are produced when gamma rays interact with stellar surfaces). The gamma-ray beams may be a consequence of particle acceleration in double layers in neutron star magnetospheres.

DOUBLE LAYERS AND PLASMA-WAVE RESISTIVITY IN EXTRAGALACTIC JETS: CAVITY FORMATION AND RADIO-WAVE EMISSION

Joseph E. Borovsky
Space Plasma Physics Group
Los Alamos National Laboratory
Los Alamos, New Mexico 87545, U.S.A.

ABSTRACT

For estimated values of the currents carried by extragalactic jets, current-driven electrostatic-wave- and electromagnetic-wave-produced resistivities do not occur. Strong plasma double layers, however, may exist within self-maintained density cavities, the relativistic double-layer-emitted electron, and ion beams driving plasma-wave resistivities in the low- and high-potential plasma adjacent to the double layers. The double-layer-emitted electron beams may also emit polarized radio waves via a collective bremsstrahlung process mediated by electrostatic two-stream instabilities.

I. INTRODUCTION

Extragalactic jets are collimated radio-luminous plasmas that are thought to be supersonic outflows from the nuclei of elliptical galaxies, the jet plasma traveling long distances through the intergalactic medium before being stopped (Begelman et al., 1984). Often, the length of a jet is much larger than the size of its parent galaxy.

The internal plasma pressures of some extragalactic jets are thought to exceed the plasma pressures in the external media. This had led to the hypothesis that these jet plasmas are radially confined via electric-current pinching, the electrical current flowing axially through the column of jet plasmas (Alfvén, 1977, 1978; Benford, 1978), as depicted in Figure 1. The hypothesis that jets carry currents is also supported by electrodynamic models of jet-plasma acceleration (Lovelace, 1976). The presence of currents opens the important possibility that large amounts of energy are being transported down the jets via electrical processes. If electrical currents are in fact present, then electric fields are also expected to be present.

In this report, a model of the electric field that may reside within an extragalactic jet is described. The model involves a plasma double layer or a multiple of plasma double layers in series, each one residing within a density cavity that is created by the action of the double-layer-emitted particle beams.

In section II, the properties of extragalactic jets are reviewed and the Coulomb-collision resistivities and the plasma-wave resistivities within the jets are discussed. In Section III, the double layer model is described. In Section IV, some consequences of the double layer model are discussed, including radio-wave emission from the double-layer-emitted electron beams via a collective bremsstrahlung process, and in Section V, some double layer topics that need further research are pointed out.

II. COLLISIONAL AND PLASMA-WAVE RESISTIVITIES IN JETS

Subject to great uncertainties, extragalactic jets and the plasmas within them have the following properties (Begelman et al., 1984). The lengths of the jets vary from L $\sim 10^4$ Pc to L $\sim 10^6$ Pc, where 1 Pc $= 3.1 \times 10^{18}$ cm, and the radii of the jets vary from r $\sim 10^2$ Pc close to the galactic centers to r $\sim 10^3$ Pc further out; typical diameters of galaxies are 10^4 to 10^5 Pc. The jet plasma is believed to be of low density, n $\sim 10^{-6} - 10^{-4}$ cm^{-3} and warm $T_e \sim T_i$ 10^5 K, with an additional population of relativistic synchrotron-emitting electrons. The luminosity of the jet plasma is non-uniform, implying higher densities of relativistic electrons and/or stronger magnetic fields in localized hot spots. Estimates of the magnetic field strength yield B $\sim 10^{-5} - 10^{-4}$ gauss. For a few jets that reside in the centers of clusters of galaxies, the ambient plasma is detectable via its x-ray bremsstrahlung, and pressure estimates for these ambient media can be obtained. In some of these instances, the pressures of the jet plasmas are believed to exceed the pressures of the ambient plasmas, and z-pinching of the jets by electrical currents may be acting to confine the jets. Estimates of the total amount of current needed to z-pinch the jets are I $\sim 10^{17}-10^{18}$ Amp, implying current densities j $\sim 10^{-23}-10^{-21}$ Amp/m^2. If these currents are carried by drifts between the ion and electron distributions, then typical drift velocities are $10^{-5}-10^{-2}$ cm/s.

These jet plasmas are very nearly collisionless; for a plasma with n $= 10^{-4}$ cm^{-3} and T $= 10^5$ K, the Coulomb-collision conductivity is $\sigma_\parallel \simeq 1.8 \times 10^{13}$ s^{-1}. For a current density $j_\parallel = 1.0 \times 10^{-21}$ Amp m^{-2}, the electric field along the jet required to drive the current is $E_\parallel = 4.9 \times 10^{-7}$ V/cm. For a jet 10^5 Pc in length, this amounts to a total potential drop $\Delta\phi$ of a mere 1.5×10^{-3} V. By almost all standards, the jet is a perfect conductor.

Electrostatic plasma-wave instabilities that are driven by relative drifts between Maxwellian ions and electrons require an electron-ion relative drift velocity v_o that is comparable to v_{te} (Papadopalous, 1977). As mentioned above, the relative drift within an extragalactic jet is typically $v_o \sim 10^{-5}-10^{-2}$ cm/s. This drift speed is orders of magnitude lower than the electron thermal velocity. Thus, electrostatic microinstabilities driven by electron-ion relative drifts will not provide electrical resistivities in current-carrying extragalactic jets.

Neither will electromagnetic plasma-wave instabilities that are driven by relative drifts between Maxwellian ions and electrons produce resistivity in extragalactic jets. For a uniform-current-density z-pinched jet in equilibrium, no electromagnetic waves with wavelengths shorter than the jet diameter are unstable (Borovsky, 1986). Hence, no resistivity can be produced.

Note that since anomalous-resistivity processess might not occur in the jet plasma, the jet plasmas might be truely ohmic, at least for the current densities envisioned to z-pinch the jets.

III. THE DOUBLE LAYER MODEL

Some of the properties of strong plasma double layers are as follows (Michelsen and Rasmussen, 1982; Schrittwieser and Eder, 1984). The thicknesses of double layers are $\Delta L \sim 10^1-10^5 \lambda^D$, the double layers being thicker if the potential jump $\Delta\phi$ across them is greater. The current density within and near the double layer is independent of the local electric field strength; therefore, the plasma containing the double layer is non-ohmic. Ions that drift into the high potential edge of the double layer are accelerated to form a fast, cold beam in the low potential plasma, and electrons that drift into the low potential edge of the double layer are accelerated to form a fast, cold beam in the high potential plasma. The efficiency of turning electrical energy into the kinetic energy of high-energy particles in the double layer is 100 percent. These beams drive space charge waves in the adjacent plasmas (Borovsky and Joyce, 1983), the electron beam drives Langmuir waves and electrostatic electron-cyclotron waves in the high potential plasma, and the ion beam drives ion-acoustic and electrostatic and ion-cyclotron waves in the low potential plasma. If the double layer has a large enough potential drop $\Delta\phi$, then Langmuir waves and electrostatic electron-cyclotron waves will also be driven by the ion beam in the low potential plasma.

Double layers are also characterized by Bohm criteria at their high and low potential edges. For steady-state double layers, these criteria require the ion-inflow drift velocity to exceed C_s and the electron-inflow drift velocity to exceed v_{te}. As was the case for electrostatic plasma-wave instabilities, these required inflow velocities imply large current densities. However, the Bohm criteria may be satisfied without large current densities if a density cavity is formed by the action of the double-layer-emitted beams. When the potential drop $\Delta\phi$ of a double layer is large enough to produce highly relativistic electron beams, the growth length for two-stream electrostatic waves in the high potential plasma is

$$\lambda_{growth}/\lambda_{De} = 2.1 \times 10^{-3}\, T_e^{4/3}(e\Delta\phi/k_BT) ,$$

and if the potenial jump is large enough to produce a highly relativistic ion beam, then the growth length for high-frequency electrostatic plasma waves in the low potential plasma is

$$\lambda_{growth}/\lambda_{De} = 4.8 \times 10^{-5}\, T_e^{4/3}(e\Delta\phi/k_BT)$$

(Borovsky, 1986). Because the phase and group velocities of the growing waves are in the direction of the beams, these waves will propagate away from the double layer, leaving regions of calm plasma near the double layer. Beyond these calm regions, however, plasma waves will be present with very large amplitudes (Fig. 2). In the fields of waves on either side of the double layer, the effective collision frequency may approach ω_{pe}. Since the mobilities of charged particles in these regions are small, they require long periods of time to transit to the double layer; accordingly, their number densities are high within these regions. When a particle leaks out of one of these turbulent regions and passes into a calm region near the double layer, it drifts without scattering; this drift being at the thermal velocity, the number density is low (see Fig. 3, top and middle). Thus, the double layer produces electron and ion beams which create two regions of plasma turbulence removed from the double layer itself, these regions acting to keep the plasma density high away from the double layer and creating a cavity around the double layer. It is in this density-cavity region that the Bohm criteria for the double layer can be met; these high drift velocities do not produce high current densities because they occur only in regions where the particle density is low. The current density is conserved throughout the region (Fig. 3, bottom). This cavity production can also be described as the outwardly directed double-layer-emitted beams driving plasma waves that transfer the beam momentum to the ambient plasma, pushing open a cavity and maintaining it with beam pressure.

In order for current to be driven through the regions of electrostatic turbulence near the double layer, resistive electric fields will arise, adding to the potential of the double layer. Note that in this model the anomalous resistivity regions are required, not for their resistive potential drops, but for the reduction of the particle mobility that they cause.

A laboratory example of a double-layer-driven cavity is contained in Figures 9 and 10 of Guyot and Hollenstein (1983), reproduced here as Figure 4. In the first panel of Figure 4, the double layer is clearly visible at $x \simeq 50$ cm. Note also that there is a region of resistive potential drop in the high potential plasma adjacent to the double layer. In the second panel, a density cavity around the double layer is visible. In the bottom panel, the electron drift speed is seen to increase within the cavity. Electrostatic turbulence is detected on both sides of the double layer. Another example of a cavity formed around a laboratory double layer appears in Figure 3 of Sato et al. (1981).

Multiple double layers may occur in a series, each double layer surrounded by regions of beam-driven turbulence that maintains density cavities. The double layers must be separated by distances large enough for their emitted electron and ion beams to thermalize, the thermalized beam particles constituting plasma sources between the double layers.

IV. CONSEQUENCES OF THE MODEL

If they are of relativistic energies, the double-layer-produced beams of electrons will undoubtedly emit synchrotron radiation, making the high potential plasmas near double layers radio luminous. More important, however, the relativistic electron beams will rapidly emit polarized radio waves via a collective-bremsstrahlung process (Kato et al., 1983). The electron-electron two-stream instability that produces the electrostatic waves in the high potential plasma causes the beam electrons to bunch up and the background-plasma electrons to bunch up. The beam electrons are accelerated by random electric fields as they pass through the charge-bunched background plasma, causing them to emit electromagnetic radiation. Because the beam electrons are charge-bunched, they emit coherently. Thus, this emission is like a collective bremsstrahlung, with charge clumps in the beam radiating as they scatter off charge clumps in the background plasma. As observed in the laboratory, the electron beams emit electromagnetic waves with frequencies of approximately $\gamma^2 \omega_{pe}$ (Kato et al., 1983), where γ is the relativistic factor of the beam.

It is reasonable to anticipate that a radio hot spot would be associated with a double layer or a series of double layers within a jet, since most of the energy dissipated by the double layer appears as an energetic electron beam that is capable of radiating. Further, if multiple double layers are separated by distances great enough, then the individual radio striations in the jet might be resolvable.

A model that proves to be very similar to this model was developed by Langmuir (1929) to describe the current flows in partially ionized gases. In that model, the inflow of plasma to a double layer was described as an ambipolar diffusion down density gradients. A similar approach may be taken in the present model, with only a change in the nature of the diffusion coefficient.

The double layers envisioned here have many features in common with auroral zone double layers (Shawhan, 1978; Borovsky, 1984). Auroral double layers accelerate electrons to energies of 1–10 keV, the electrons following the terrestrial magnetic field lines to the upper atmosphere where they produce visible auroral arcs. The auroral double layers also accelerate ions upward where they are believed to drive the large-amplitude electrostatic ion-cyclotron waves. The energetic beam electrons are believed to drive Langmuir and electrostatic electron-cyclotron waves, and are also believed to drive collective radio emissions (Anderson, 1983).

V. FUTURE RESEARCH IN DOUBLE LAYERS

There are many topics that must be researched before the double layer model discussed in Sections III and IV is complete.

Two topics important to this model are relativistic double layers and double layers in finite-β plasmas, the stability and dynamics of both types of double layers having yet to be examined. For relativistic double layers, stability factors may favor particular values for the potential jump, such as $e\Delta\phi = m_e c^2$ or $e\Delta\phi = m_i c^2$. For finite-β double layers, beam-driven electromagnetic-wave turbulence may provide another cavity-forming mechanism. Laboratory diagnostics will be difficult to construct for relativistic double layers, and very large plasma chambers will be required to magnetize the particles for finite-β double layer experiments.

Another important topic is the dynamics of multiple double layers. In most laboratory devices, the system potential drops are limited to the ionization potentials of the gases used, and the ions are Coulomb-collisional. To investigate multiple double layers via computer simulation, very large numerical systems must be used to resolve the large-scale phenomena (beam thermalization), the small-scale phenomena (double layers), the fast time scales (Langmuir waves), and the slow time scales (beam evolution). A further goal would be to understand the pre-sheaths at the edges of the double layers. Unfortunately for the theoretical approach, pre-sheaths in collisionless plasmas probably involve electric field fluctuations, and, unfortunately for laboratory experiments, these weak electric field structures are very difficult to observe.

In order to understand the inflow of plasma through the regions of electrostatic turbulence, diffusive flows driven by density gradients and fluctuating electric fields need to be studied.

The spatial evolution of double-layer-emitted electron beams is also a topic for future study. Since these electrons scatter and lose energy as they travel, there will be a spatial dependence of the collective bremsstrahlung spectra. A knowledge of this spectral evolution matched against the spectra of radio hot spots will provide a direct test for the presence of double layer energy dissipation within jets.

REFERENCES

Alfvén, H., *Rev. Geophys. Space Phys., 15,* 271 (1977).

Alfvén, H., *Astrophys. Space Sci., 54,* 279 (1978).

Anderson, R. R., *Rev. Geophys. Space Phys., 21,* 474 (1983).

Begelman, M. C., R. D. Blandford, and M. J. Rees, *Rev. Mod. Phys., 56,* 255 (1984).

Benford, G., *Mon. Not. Roy. Astron. Soc., 183,* 29 (1978).

Borovsky, J. E., *J. Geophys. Res., 89,* 2251 (1984).

Borovsky, J. E., *Astrophys. J.,* in press, 1986.

Borovsky, J. E., and G. Joyce, *J. Plasma Phys., 29,* 45 (1983).

Guyot, M., and G. Hollenstein, *Phys. Fluids, 26,* 1596 (1983).

Kato, K. G., G. Benford, and D. Tzach, *Phys. Fluids, 26,* 3636 (1983).

Langmuir, I., *Phys. Rev., 33,* 954 (1929).

Lovelace, R.V.E., *Nature, 262,* 649 (1976).

Michelsen, P., and J. J. Rasmussen (editors), *First Symposium on Plasma Double Layers,* Riso National Laboratory, Denmark, Document Riso-R-472, 1982.

Papadopalous, K., *Rev. Geophys. Space Phys., 15,* 113 (1977).

Sato, N., R. Hatakeyama, S. Iizuka, T. Mieno, K. Saeki, J. J. Rasmussen, and P. Michelsen, *Phys. Rev. Lett., 46,* 1330 (1981).

Schrittwieser, R., and G. Eder (editors), *Second Symposium on Plasma Double Layers and Related Topics,* University of Innsbruck, 1984.

Shawhan, S. D., C.-G. Fälthammar, and L. P. Block, *J. Geophys. Res., 83,* 1049 (1978).
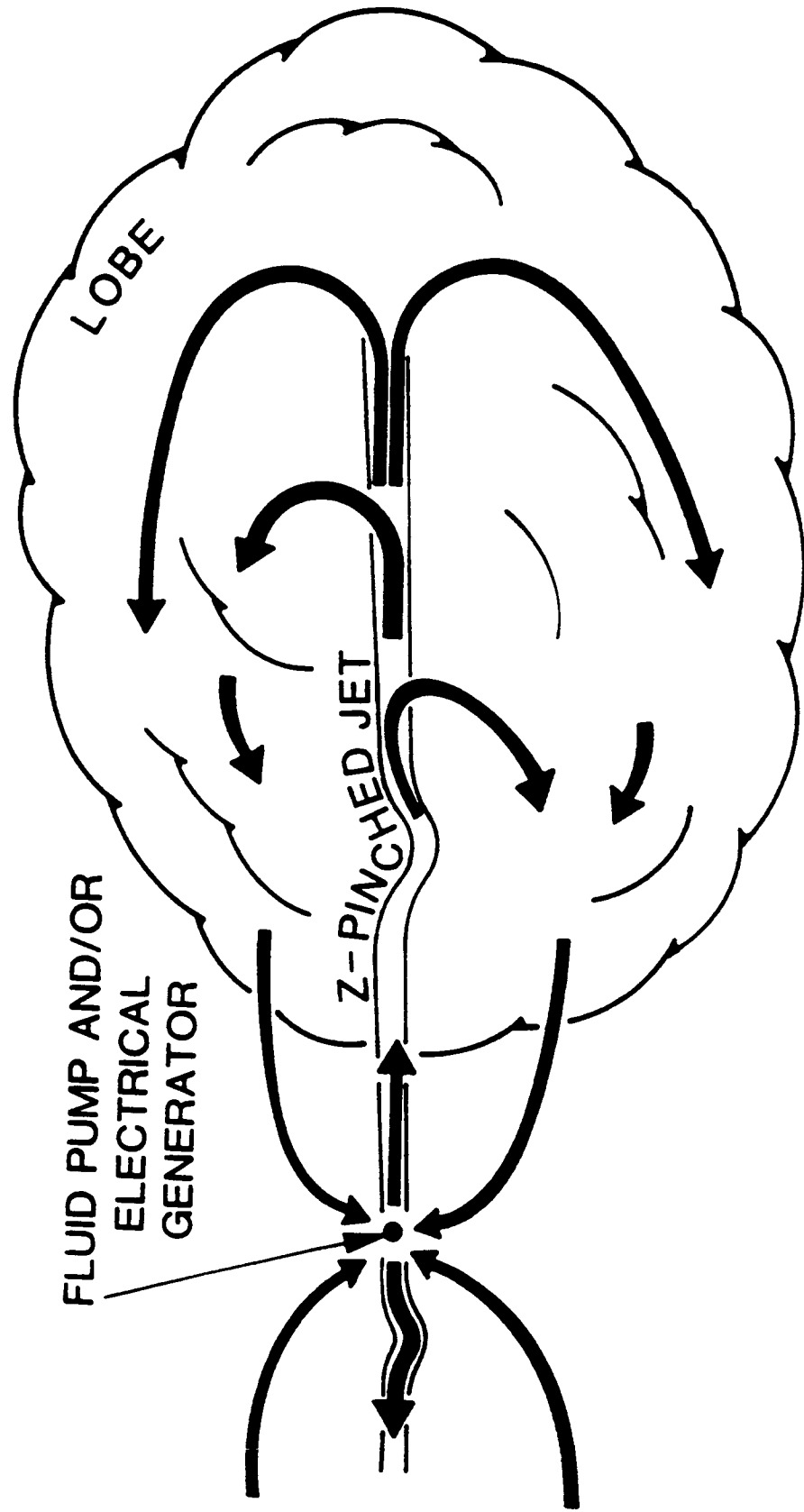
Figure 1. Schematic of an extragalactic jet carrying current within a collimated jet plasma.

LOBE

Z–PINCHED JET

FLUID PUMP AND/OR ELECTRICAL GENERATOR
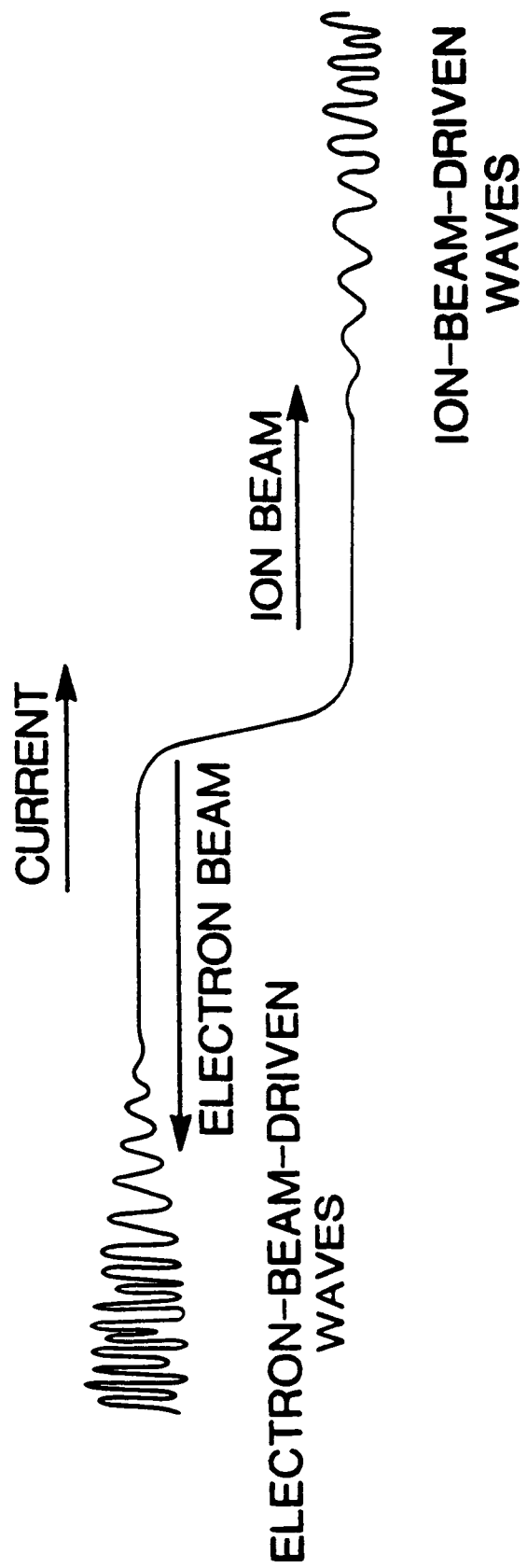
Figure 2. Schematic of a plasma double layer and the waves that the double-layer-emitted electron and ion beams produce.
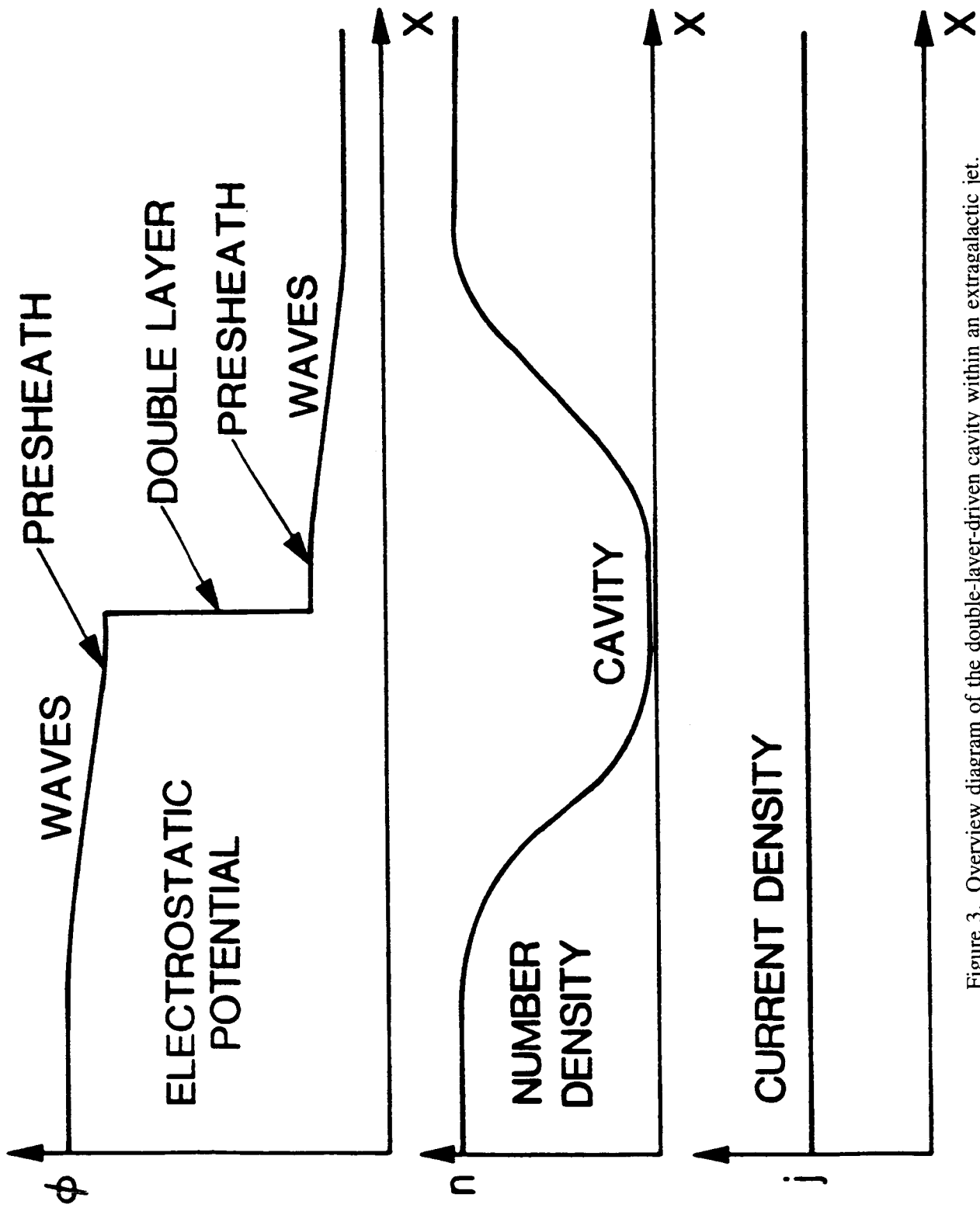
Figure 3. Overview diagram of the double-layer-driven cavity within an extragalactic jet. In the top panel the electrostatic potential is depicted, in the middle panel the particle density is depicted, and in the bottom panel the current density is depicted, all as functions of the distance along the jet.
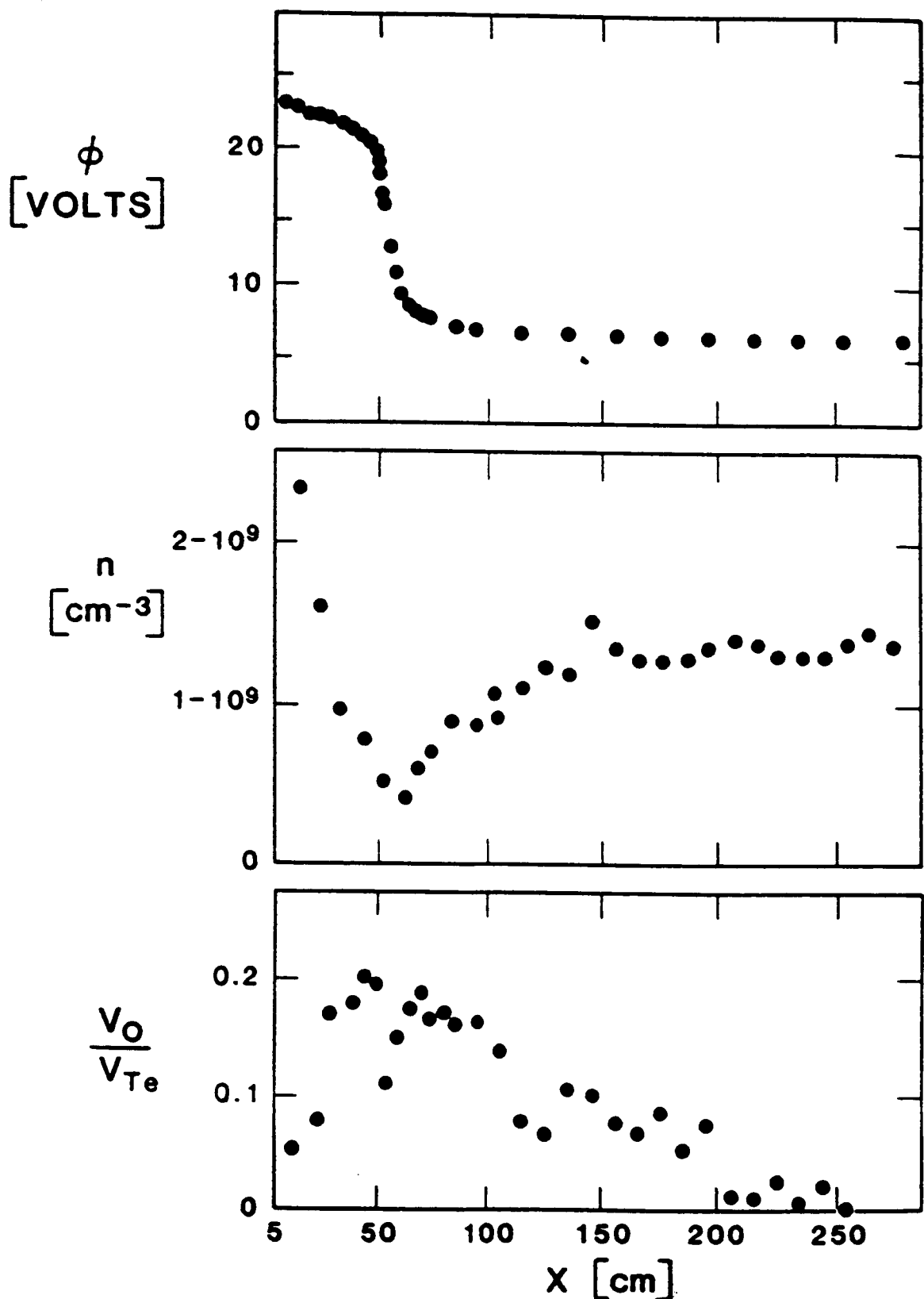
Figure 4. After Figures 9 and 10 of Guyot and Hollenstein (1983), the experimentally measured electrostatic potential ϕ, the number density n, and the electron drift velocity v_o are plotted as functions of distance in the top, middle, and bottom panels, respectively.

ACCRETION ONTO NEUTRON STARS WITH THE PRESENCE OF A DOUBLE LAYER

A. C. Williams, M. C. Weisskopf, R. F. Elsner, and W. Darbro
Space Science Laboratory
NASA Marshall Space Flight Center
Huntsville, Alabama 35812 U.S.A.

and

P. G. Sutherland
Department of Physics, McMaster University
Hamilton, Ontario L8S4M1, Canada

It is known, from laboratory experiments, that double layers will form in plasmas, usually in the presence of an electric current. In this paper we argue that a double layer may be present in the accretion column of a neutron star in a binary system. We suggest that the double layer may be the predominant deceleration mechanism for the accreting ions, especially for sources with x-ray luminosities of less than about 10^{37} erg s^{-1}. Previous models have involved either a collisionless shock or an assumed gradual deceleration of the accreting ions to thermalize the energy of the infalling matter.

THE FORMATION OF A DOUBLE LAYER LEADING TO THE CRITICAL VELOCITY PHENOMENON

A. C. Williams
Space Science Laboratory
NASA Marshall Space Flight Center
Huntsville, Alabama 35812, U.S.A.

ABSTRACT

The formation of a double layer is proposed as the mechanism which produces the critical velocity phenomenon. We examine this hypothesis, qualitatively, and find that the double layer can be a very efficient mechanism for transferring the kinetic energy of the neutral gas into the kinetic energy of electrons which, in turn, will ionize the neutral gas if the critical velocity has been reached or exceeded.

I. INTRODUCTION

In a study of the mass distribution of secondary bodies in the solar system, Alfvén (1954) noted that these bodies were arranged in discrete bands surrounding the central object. The particular location of the band in which each body appeared was found to be dependent upon the chemical composition of the dominant elements of the body. To explain this band structure, Alfvén proposed that a strong coupling suddenly occurs between a neutral gas and a magnetized plasma whenever their relative velocity reaches the critical velocity, v_{crit}, given by

$$v_{crit} = (2 e V_i/m_n)^{1/2} \quad .$$

(1)

Here, V_i is the ionization potential of the neutral gas and m_n is the mass of one of the neutral particles. The proposed interaction has to have the effect of prohibiting the relative velocity from exceeding this critical velocity in order to explain the band structure.

In the rest frame of the plasma, equation (1) implies that when the kinetic energy of the neutral particles is equal to the ionization potential, a strong coupling occurs between the neutral gas and the plasma. Such a coupling would be expected if, for example, the gas suddenly begins to be ionized at this relative velocity. Then the magnetic field, which is threading the plasma, will interact strongly with the newly formed ions and electrons. However, ionization is not expected to become prominent when the relative velocity is equal to the critical velocity because the cross section for ionization due to binary collisions between neutral particles and plasma ions is essentially zero for the energy transfer needed at this relative velocity (assuming negligible random kinetic energy). For equal mass particles the maximum energy transfer is one-half the kinetic energy. Furthermore, the energy of electrons with a velocity equal to the critical velocity is orders of magnitude smaller than the ionization energy.

Hence, traditional classical plasma physics seems to be unable to explain why an enhanced interaction should occur between a neutral gas and a magnetized plasma when the relative velocity reaches the critical value. However, laboratory experiments have verified the critical velocity phenomenon and the validity of equation (1) (see Danielsson, 1973, and Raadu, 1981, for reviews). Subsequently, theories have been proposed to explain the

experiments (see Sherman, 1973, and Raadu, 1978, for reviews). The present theoretical situation, nevertheless, is that there is no one theory that satisfactorily explains the phenomenon over the wide range of parameters (magnetic field, density of the gas, etc.) that have been demonstrated in the laboratory. Hence, the general consensus has been that different physical processes occur, depending upon the parameters, to give the one result – the critical velocity phenomenon.

In this paper, however, a simple mechanism is proposed to explain the critical velocity phenomenon. This mechanism appears to be applicable over the entire range of experimental parameters examined to date. This mechanism invokes the formation of a double layer. Double layers form in a plasma, usually when a current exceeding a certain threshold value is passed through the plasma (see Block, 1978, for a review).

II. THE FORMATION OF A DOUBLE LAYER

On a macroscopic level, a double layer can be defined as a local discontinuity surface in a plasma; but, microscopically, it consists of two equal but oppositely charged space-charge layers. The electric field within the double layer is very strong, but it is essentially zero outside this region. The spatial extent of the double layer is roughly of the order of the Debye length, although experimental results have shown that the double layer can be as thick as 1000 Debye lengths (Chan et al., 1984; Sato and Okuda, 1981). The electric potential for the type of double layer that we will be considering (the strong double layer) is monotonic and has the general form as that shown in Figure 1.

The double layer, once formed, separates the plasma into two sections with a potential difference across them. Years of laboratory research on the formation and stability of double layers have revealed that they form easily either by utilizing density gradients or by introducing a potential difference across the plasma (or across a segment of the plasma by inserting a charged electrode), or by some other method. Regardless of how the double layer is formed, the determining factor as to whether it will remain depends upon the distribution functions of the various types of charged particles that will be accelerated, decelerated, or reflected by the double layer.

To understand why a double layer should be expected to form when a neutral gas is incident upon a magnetized plasma, consider Figure 2. Here, the neutral gas is incident from the left. The magnetic field of the plasma, for simplicity, is assumed to be uniform, and in order to simulate the experimental situations where the critical velocity phenomenon has been observed, the magnetic field is taken to be almost perpendicular to the incoming neutral beam velocity vector. Even before the velocity of the neutral atoms reaches the critical velocity, a limited amount of ionization will naturally take place due mainly to impact and charge exchange collisions. Suppose that an atom is ionized at point O in Figure 2. The electron and ion will then be influenced by the magnetic field which is threading the plasma. Because of differences in magnetic moments, the ions will penetrate more deeply into the plasma than the electrons; i.e., both will spiral about the field lines but the ions with much large radii. This will result in a charge separation in the plasma which, in turn, will force the plasma to react in order to maintain charge neutrality. We expect the plasma to respond through the formation of a double layer, just as in the laboratory. The potential difference across the double layer will be essentially the kinetic energy of the newly formed ions since it is these ions that must be stopped in order to maintain charge neutrality. These ions, though, will have approximately the same energy as the original neutral atoms. Hence, the potential energy of the double layer is expected to be equal to the kinetic energy of the neutral gas.

This scenario also dictates the length scale of the double layer. It must have a width which is intermediate between the electron and the ion gyro radius. This is precisely the scale length associated with the leaky ionization fronts which have been observed in the experimental investigations of the critical velocity phenomenon (see e.g. Petelski, 1981).

The double layer will decelerate the newly formed ions. It will also accelerate the newly formed electrons as well as any electrons of the background plasma which drift into the double layer region. On the high potential side of the double layer, then, there will be some energetic electrons moving anti-parallel to the magnetic field. These electrons will be available for ionizing more neutral atoms through impact collisions. This process, in turn, will tend to establish a second double layer. This process could then be repeated and result in a series of double layers in the plasma. However, as mentioned previously, the charged particle distributions determine whether the double layers are stable. Although it may be possible that the conditions are favorable for the formation of several double layers, we speculate these double layers dissipate after they are formed. In this case, we have the equivalent to a single double layer moving through the plasma. Moving double layers are observed to occur in laboratory plasmas when the particle fluxes do not satisfy what is referred to as the Langmuir condition for a stable double layer (Block, 1978). In the laboratory, these moving double layers propagate to the end of the physical system confining the plasma where they disappear, and a new double layer appears at the opposite end.

The process described above may take place whenever a neutral gas beam is incident upon a magnetized plasma, regardless of the relative velocity of the beam. Laboratory experiments, as well as theoretical considerations, indicate that the thermal speed of the plasma particles makes the formation of a double layer possible. However, when the relative velocity becomes equal to the critical velocity, the picture we have presented leads to the conclusion that predicts a strong interaction should occur. This follows from the fact that the potential energy difference across the double layer and, hence, the energy of the accelerated electrons, is equal to the kinetic energy of the neutral atoms. When this energy is equal to the ionization energy of the atoms, the electrons will then have precisely the amount of energy needed to ionize the atoms. Consequently, when the relative velocity is equal to, or higher than, the critical velocity, the effect of the moving double layer (or a stationary double layer if appropriate) is to establish an ionization front which ionizes the neutral beam. This explains the observed connection between the critical velocity and ionization. This also implies that energetic electrons will be produced with velocity vectors directed anti-parallel to the magnetic field. This conclusion, in turn, is consistent with laboratory studies of the critical velocity phenomenon (see e.g. Danielsson and Brenning, 1975).

III. THE ORIENTATION OF THE MAGNETIC FIELD

In all of the laboratory experiments that have studied the critical velocity phenomena, the magnetic field has been more or less perpendicular to the velocity vector of the incoming neutral beam. In our explanation of the critical velocity phenomenon, we must require that the angle between the two vectors is not precisely 90°. This requirement is necessary in order to have both a component of the electron's velocity parallel to the magnetic field line and also traverse through the double layer region. In Figure 3, this departure from 90° is given by the angle δ. To examine the minimum value that δ may have, we consider the experimental arrangement of Danielsson and Brenning (1975). The effective physical confines of the plasma region in this experiment was 5 cm × 5 cm. Therefore the length (along an equipotential surface) of the double layer was 5 cm. The width of the double layer, of course, can be no more than 5 cm, but its value will be determined mainly by the electron and ion gyro radii. The width, a, of the double layer satisfies the condition

$$r_e \ll a \ll r_i \quad , \qquad\qquad\qquad\qquad (2)$$

where r_e and r_i are the corresponding gyro radii of the electrons and ions. The exact value of a, of course, depends upon the particle densities. For the Danielsson and Brenning experiment, typical parameters were B = 0.18 T and v = 400 km/s, resulting in $r_e \simeq 13$ μm and $r_i \simeq 10$ cm. Hence, the width of the double layer, a, was of the order of 1 mm. For this value of a, Figure 3 implies that the minimum value of δ is 1.2°, which is hardly a stringent requirement. Hence, it can be concluded that the magnetic field vector can be essentially perpendicular to the relative velocity vector within our model.

321

IV. COMPARISON WITH OTHER THEORIES

Some theorists have examined the consequences of building up space charge by the trapping of electrons by the magnetic field. In particular, Piel et al. (1980) proposed the formation of a sheath similar to the double layer, but they considered only the $E \times B$ drift motion in the sheath. They considered the possibility that the drift motion would lead to a modified two-stream instability which, in turn, would heat the electrons. This would then provide a feedback mechanism to produce the ionization, and thus explain the critical velocity phenomenon. As is the case with essentially all of the theoretical models, this particular approach explains a subset of the experimental observations of the phenomenon, but it fails in other cases (see e.g. Haerendel, 1982).

Lehnert (1967) analytically examined the potential structure that could form consistent with the Vlasov and Poisson equations. Assuming that collisions are negligible over scale lengths, of the order of the ions gyro radius, and a potential gradient in the plasma, he found that an oscillatory-type potential structure could be supported. The spatial extent of each cycle in the potential, naturally, turned out to be comparable to the gyro radius of the ions. The formation mechanism for this charge separation, however, requires that the electric field within the sheath be directed in the same direction as the velocity vector of the incoming neutral beam. This is precisely in the opposite direction of the field of the double layer in our picture. Because of the direction of the electric field in Lehnert's model, it is difficult for him to utilize it to energize the electrons. He, thus, relies on collisions to accomplish this (Danielsson and Brenning, 1975). Nevertheless, if the particle distributions in the plasma are such that a series of double layers would be stable, then the potential structure of the present model would be similar to Lehnert's model except for the oppositely directed electric field. The electric field of the present model is properly oriented for direct electron acceleration.

Varma (1978) also examined a possible consequence of charge separation upon the ionization of a marginal amount of the neutral gas. However, his analysis was directed mainly at explaining the direct interaction experiments (Danielsson, 1970, 1973; Danielsson and Brenning, 1975). Since these experiments provided evidence for electron acceleration parallel to the magnetic field, Varma suggested that a density gradient in the direction parallel to the magnetic field, due to the finite size of the experimental apparatus, would cause a potential well to form which could accelerate the electrons in the required direction. Again, this is a theoretical model which is very dependent upon the experimental parameters. Hence, it does not explain the general critical velocity phenomenon.

V. SUMMARY

In this paper, we have proposed that the formation of a double layer leads to the critical velocity phenomenon. The role of the double layer is to transfer the energy of the neutral particles to electrons which, in turn, ionize the neutral particles when the critical velocity is reached or exceeded. This mechanism is expected to operate under a wide variety of conditions as has been verified by double layer observations in the laboratory.

Although we have only described the model qualitatively here, it is evident that such a mechanism is a viable candidate for explaining the critical velocity phenomenon. It remains for future work to carry out computer simulation studies to investigate the formation and stability of double layers under the conditions where the critical velocity phenomenon has been observed.

REFERENCES

Alfvén, H., *On the Origin of the Solar System*, Oxford University Press, Oxford, 1954.

Block, L. P., *Ap. Space Sci.*, *55*, 59 (1978).

Chan, C., M. H. Cho, N. Hershkowitz, and T. Intrator, *Phys. Rev. Lett.*, *52*, 1782 (1984).

Danielsson, L., *Phys. Fluids*, *13*, 2288 (1970).

Danielsson, L., *Ap. Space Sci.*, *24*, 459 (1973).

Danielsson, L., and N. Brenning, *Phys. Fluids*, *18*, 661 (1975).

Haerendel, G., *Z. Naturforsch.*, *371*, 728 (1982).

Lehnert, B., *Phys. Fluids*, *10*, 2216 (1967).

Petelski, E. F., in *Relations Between Laboratory and Space Plasmas*, p. 23, D. Reidel, Dordrecht, 1981.

Piel, A., E. Möbius, and G. Himmel, *Ap. Space Sci.*, *72*, 211 (1980).

Raadu, M. A., *Ap. Space Sci.*, *55*, 125 (1978).

Raadu, M. A., in *Relations Between Laboratory and Space Plasmas*, p. 13, D. Reidel, Dordrecht, 1981.

Sato, T., and H. Okuda, *J. Geophys. Res.*, *86*, 3357 (1981).

Sherman, J. C., *Ap. Space Sci.*, *24*, 487 (1973).

Varma, R. K., *Ap. Space Sci.*, *55*, 113 (1978).
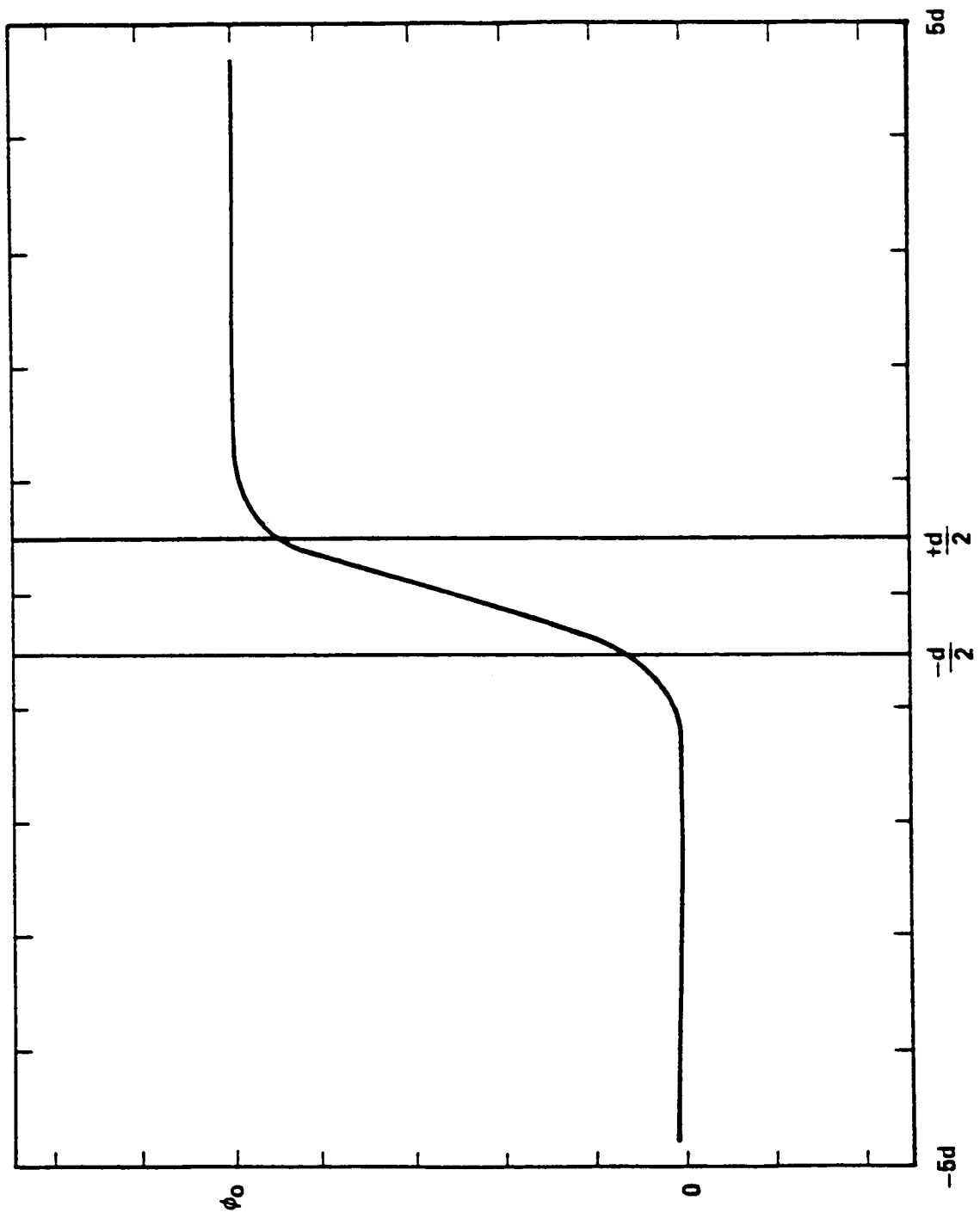
Figure 1. The general shape of the electric potential of a strong double layer as a function of position. The strength of the double layer is ϕ_0 and its effective width is d.
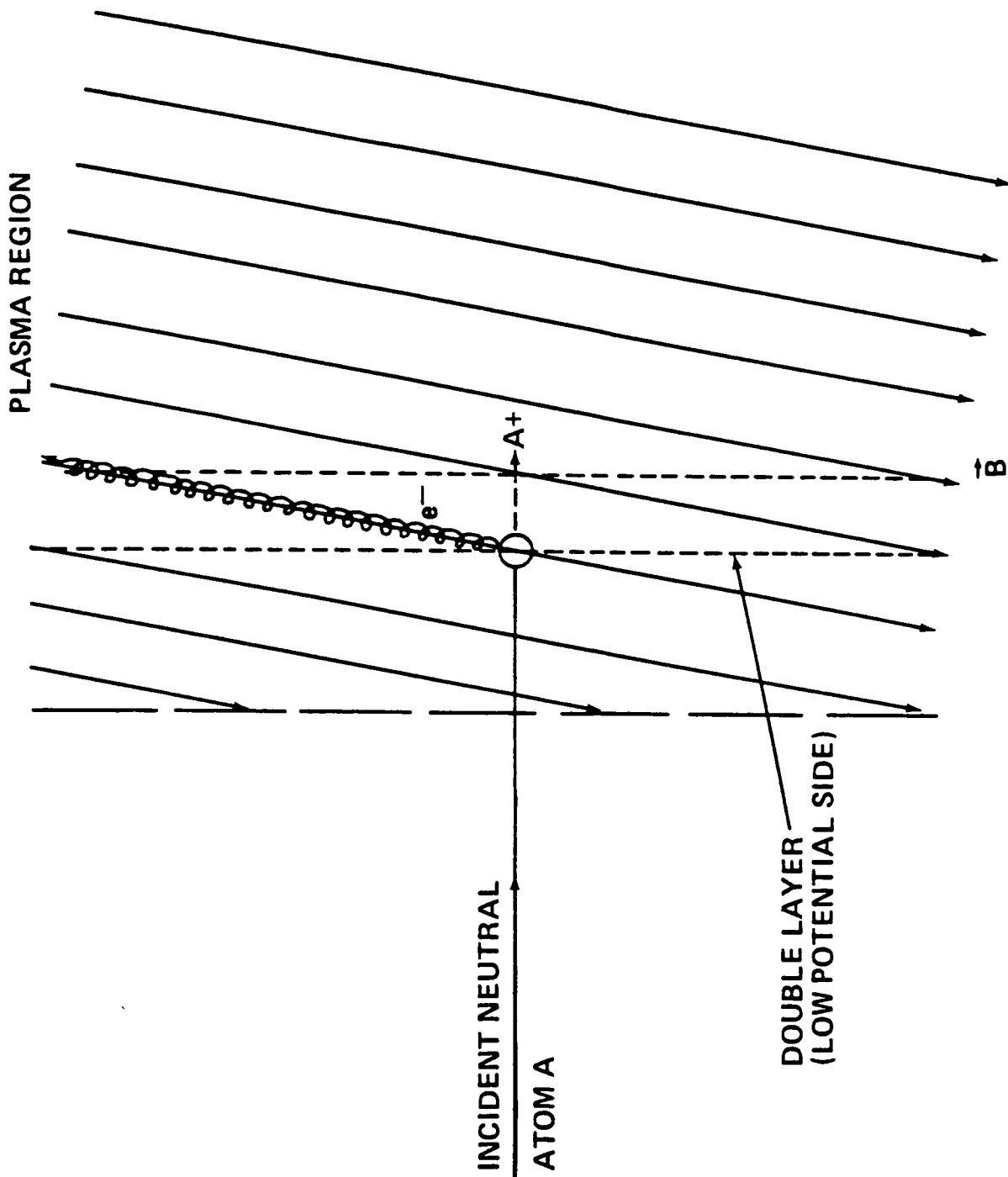
Figure 2. The interaction of a neutral gas beam with a magnetized plasma.
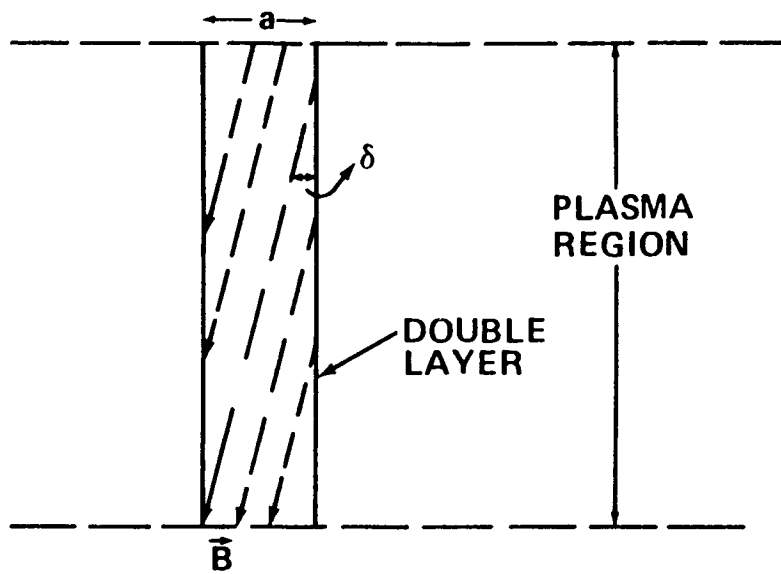
Figure 3. The orientation of the magnetic field vector of the plasma with respect to the equipotential surfaces of the double layer.

RECOMMENDATIONS

One noteworthy outcome of the symposium was the adoption of a circuit symbol for the double layer. This symbol was proposed by H. Alfvén, and the participants agreed to adopt it and use it in future papers dealing with double layers. The symbol is shown in Figure 1. An example of a circuit with a double layer is the prominence-solar flare circuit where an exploding double layer is assumed to be responsible for the flare. Such a circuit was presented at the symposium by Alfvén and is shown in Figure 2.

Although it is possible to have a plasma double layer without a net current, many applications will have a net current. In these applications the "L" in the double layer symbol would be most appropriately oriented so as to show the direction of the current. This is illustrated in Figure 3.

Since the double layer will accelerate and decelerate particles depending upon their charge and direction of travel, power will be delivered to, as well as taken from, charged particles passing through it. The net power delivered to the charged particles passing through the double layer is the equation

$$P = I\Delta V$$

where I is the net current and ΔV is the potential difference across the double layer. In the case of no net current, the double layer simply serves as an energy transfer mechanism. It transfers energy from one species of charged particles to another. Applications of this type of double layer were discussed in the symposium by Williams.

It is hoped that researchers in this field, as well as all who refer to the double layer, will join with the participants of the symposium in adopting the double layer symbol in Figure 1 in all future references.

RESISTANCE　　DOUBLE
　　　　　　　　LAYER
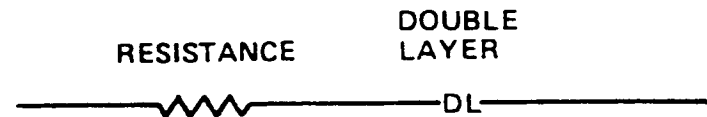
Figure 1. A diagram showing the adopted electrical symbol for the double layer when represented in a circuit.


SUN
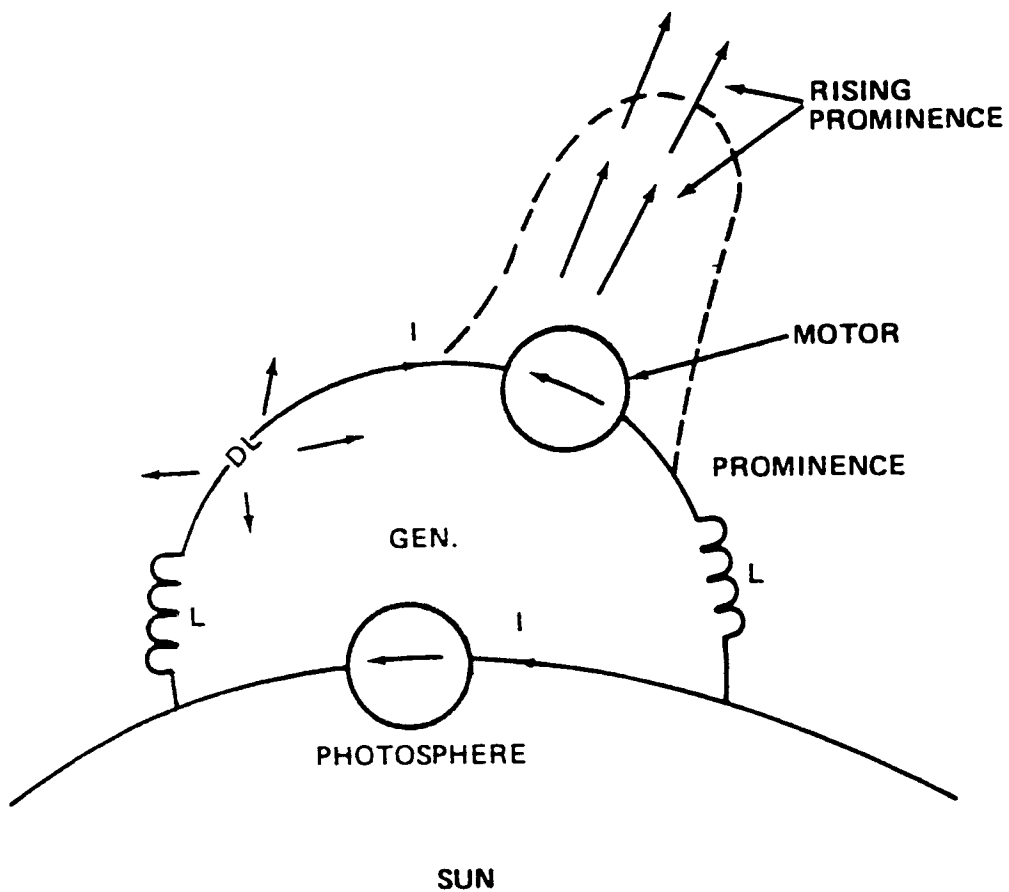
Figure 2. An example of an astrophysical circuit where a double layer plays a role – the solar prominence/flare circuit.
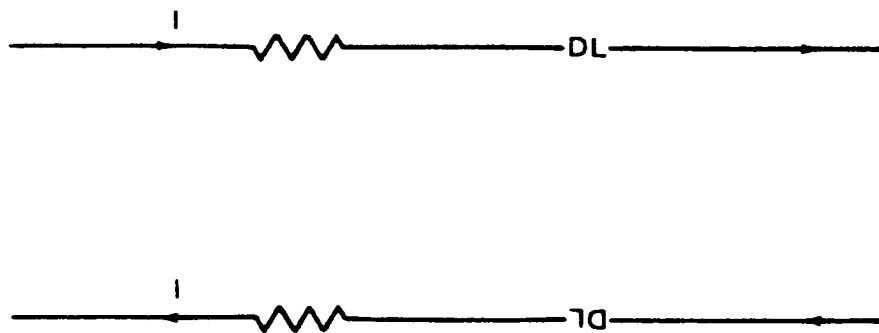

Figure 3. A diagram showing how the double layer symbol can indicate the direction of the current.

328

1. REPORT NO. NASA CP-2469	2. GOVERNMENT ACCESSION NO.	3. RECIPIENT'S CATALOG NO.
4. TITLE AND SUBTITLE Double Layers in Astrophysics		5. REPORT DATE May 1987
		6. PERFORMING ORGANIZATION CODE ES65/ES01
7. AUTHOR(S) Alton C. Williams and Tauna W. Moorehead, Editors		8. PERFORMING ORGANIZATION REPORT #
9. PERFORMING ORGANIZATION NAME AND ADDRESS George C. Marshall Space Flight Center Marshall Space Flight Center, Alabama 35812		10. WORK UNIT NO. M-560
		11. CONTRACT OR GRANT NO.
		13. TYPE OF REPORT & PERIOD COVERED
12. SPONSORING AGENCY NAME AND ADDRESS National Aeronautics and Space Administration Washington, D.C. 20546		Conference Publication
		14. SPONSORING AGENCY CODE

15. SUPPLEMENTARY NOTES
Sponsored, in part, by the Universities Space Research Association, Washington, D.C.

16. ABSTRACT

   This report contains results of a workshop held on March 17-19, 1986, at the Space Science Laboratory of NASA/Marshall Space Flight Center, Huntsville, Alabama. The contents of this report are divided as follows:

   o   Double Layers in the Laboratory
   o   Theory and Simulation of Double Layers
   o   Space Applications

17. KEY WORDS Double Layers, X-Ray Astrophysics, Gamma Ray Astronomy, Magnetospheric Physics	18. DISTRIBUTION STATEMENT Unclassified—Unlimited Subject Category 88		
19. SECURITY CLASSIF. (of this report) Unclassified	20. SECURITY CLASSIF. (of this page) Unclassified	21. NO. OF PAGES 339	22. PRICE A15